IN SPECTRAL

ANALYSIS

Sponsored by

Office of Naval Research

and

Science Foundation

MENTATION PAGE

Form Approved
OMB No. 0704-0188

	AD-A215 849	1b. RESTRICTIVE MARKINGS			
		3. DISTRIBUTION/AVAILABILITY OF REPORT			
2b. DECLASSIFICATION/DOWNGRADING SCHEDULE		UNLIMITED			
4. PERFORMING ORGANIZATION REPORT NUMBER(S)		5. MONITORING ORGANIZATION REPORT NUMBER(S)			
Final Project Report		N00014-88-J-1143			

6a. NAME OF PERFORMING ORGANIZATION	6b. OFFICE SYMBOL (If applicable)	7a. NAME OF MONITORING ORGANIZATION
Univ. of Southern California		Office of Naval Research

6c. ADDRESS (City, State, and ZIP Code)	7b. ADDRESS (City, State, and ZIP Code)
Dept. of Elec. Engineering-Systems SAL 300, MC-0781, University Park Los Angeles, CA 90089-0781	c/o Dr. Neil Gerr, Code 1111SP 800 N. Quincy Street Arlington, VA 22217-6000

8a. NAME OF FUNDING/SPONSORING ORGANIZATION	8b. OFFICE SYMBOL (If applicable)	9. PROCUREMENT INSTRUMENT IDENTIFICATION NUMBER
Office of Naval Research		

8c. ADDRESS (City, State, and ZIP Code)	10. SOURCE OF FUNDING NUMBERS			
c/o Dr. Neil Gerr, Code 1111SP 800 N. Quincy Street Arlington, VA 22217-6000	PROGRAM ELEMENT NO.	PROJECT NO.	TASK NO.	WORK UNIT ACCESSION NO.

11. TITLE (Include Security Classification)
Workshop on Higher-Order Spectral Analysis (UNCLASSIFIED)

12. PERSONAL AUTHOR(S)
C. L. Nikias and J. M. Mendel

13a. TYPE OF REPORT	13b. TIME COVERED	14. DATE OF REPORT (Year, Month, Day)	15. PAGE COUNT
FINAL PROJECT	FROM 06/01/88 TO 09/30/89	1989 NOV 28	8

16. SUPPLEMENTARY NOTATION

COSATI CODES			18. SUBJECT TERMS (Continue on reverse if necessary and identify by block number)
FIELD	GROUP	SUB-GROUP	

19. ABSTRACT (Continue on reverse if necessary and identify by block number)

A Workshop on Higher-Order Spectral Analysis was held in Vail, CO, from
June 28-30, 1989. This Workshop, which was sponsored by ONR and NSF, had
two tutorial sessions, two keynote speakers, and 10 sessions of invited papers.
This final report describes all of this.

ELECTE
DEC 12 1989
S B D

89 12 11 112

DISTRIBUTION STATEMENT A
Approved for public release;
Distribution Unlimited

20. DISTRIBUTION/AVAILABILITY OF ABSTRACT	21. ABSTRACT SECURITY CLASSIFICATION
☒ UNCLASSIFIED/UNLIMITED ☐ SAME AS RPT ☐ DTIC USERS	
22a. NAME OF RESPONSIBLE INDIVIDUAL	22b. TELEPHONE (Include Area Code)	22c. OFFICE SYMBOL

DD Form 1473, JUN 86
Previous editions are obsolete.
SECURITY CLASSIFICATION OF THIS PAGE
UNCLASSIFIED

DISCLAIMER NOTICE
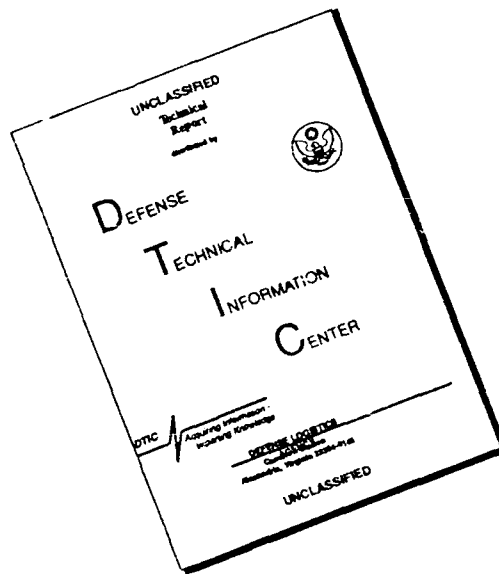
THIS DOCUMENT IS BEST QUALITY AVAILABLE. THE COPY FURNISHED TO DTIC CONTAINED A SIGNIFICANT NUMBER OF PAGES WHICH DO NOT REPRODUCE LEGIBLY.

FINAL PROJECT REPORT

Workshop on Higher-Order Spectral Analysis

Jerry M. Mendel
University of Southern California
Dept. of Elec. Engineering-Systems
Los Angeles, CA   90089-0781
U. S. A.

Signature of Principal Investigator

Jerry M. Mendel
Professor and Chairman
Dept. of Elec. Engineering-Systems
(213) 743-5534

WORKSHOP ON HIGHER-ORDER SPECTRAL ANALYSIS

June 28-30, 1989

Vail, Colorado

SUMMARY

by

C. L. Nikias and J. M. Mendel

About 123 attendees from the United States, France, United Kingdom, Italy, Japan, and Israel participated in the Workshop on Higher-Order Spectral Analysis. Held in Vail, Colorado, the three day event turned out to be very successful in terms of participation and quality of contributions. The objective of the workshop was to provide a forum for discussion of new theories and methods for processing signals that are based on Higher-Order Spectra. The overwhelming response to its announcement, as well as the breadth and depth of contributions and informal discussions among participants, clearly established that higher-order spectra is a new and emerging technology in signal processing and is expanding rapidly.

The workshop featured two tutorial sessions, two keynote addresses, one panel discussion and ten technical sessions. Total of fifty papers were presented. There were no parallel sessions at the workshop. The technical program was truly outstanding. In addition, the workshop provided a very relaxing atmosphere where many informal discussions took place.

The workshop was sponsored by the Office of Naval Research and the National Science Foundation. Their support allowed the allocation of travel grants for keynote speakers, as well as post-doctorals and graduate students to participate and present their most recent work on higher-order spectra. The IEEE Societies on Acoustics, Speech and Signal Processing, Control Systems and Geoscience and Remote Sensing cooperated towards the success of the workshop.

The workshop was organized and co-chaired by Chrysostomos L. Nikias of Northeastern University and Jerry M. Mendel of the University of Southern California. A number of individuals put forth outstanding efforts to make this workshop a success: Kevin M. Buckley (Local Arrangements),

Richard Leahy (Treasurer/Registration), Georgios Giannakis (Proceedings) and Mysore Raghuveer (Publicity).

The following sessions were held:

TUTORIAL SESSIONS

The workshop featured two tutorial sessions, one and one-half hours each. The first one was given by Chrysostomos L. Nikias on **Higher-Order Spectra in Signal Processing**. This tutorial seminar: introduced the motivation, definitions and properties of moments, cumulants and higher-order spectra in a digital signal processing framework; discussed detection, parameter estimation and signal reconstruction application problems that can directly benefit from the use of higher-order spectra: and, motivated further research and developments in this area. The second tutorial seminar was delivered by Jerry M. Mendel on **Nonminimum Phase System Identification**. Many new cumulant- based methods for identifying MA, AR and ARMA models just from noisy output measurements were described. The tutorial also covered reasons for using more than just second-order statistics, theoretical aspects of the methods, their potential strengths and weaknesses, and their interrelationships.

KEYNOTE ADDRESSES

David R. Brillinger delivered the first keynote address of the workshop on **Higher-Order Moments and Spectra: some history, some applications, some extensions and some comparative aspects.** The usefulness of higher-order moments was emphasized for phase estimation, removal of Gaussian or certain types of non-Gaussian noise, linear and nonlinear system identification, and, improved parameter estimation. A specific example was presented to demonstrate that the quality of parameter estimates can be improved by combining second- and third-order statistics. It was concluded that methods based on higher-order moments will be useful for generating initial estimates of maximum likelihood iterative methods. The second keynote address was deliverd by J. Chris Dainty on **Bispectrum Imaging Through Turbulence.** The radioimage reconstruction problem was explained and the limitations of autocorrelation-based methods discussed. The prob-

2

lem of bispectral imaging through turbulence was then reviewed by giving particular attention to the effect of turbulence on the bispectrum, signal-to-noise and computational aspects of low-light-level images. Computer algorithms were also presented for two-dimensional signal reconstruction from magnitude bispectrum.

PANEL DISCUSSION

(Moderator: C. L. Nikias)

A very stimulating two-hour panel discussion on **Higher-Order Spectra: Where is the Field Heading?** took place the first evening of the workshop. The first issue that was debated concerned the major limitations of higher- order spectra in signal processing. Workshop participants mentioned: high computational-complexity graphics, (i.e., the difficulties of displaying and interpreting multidimensional functions conveniently), the need for long data records, and, the need to connect statistical properties of higher-order spectra to real physical models. However, the panel discussion participants also pointed out to the big payoffs that have already occurred using higher order spectra in signal processing. These are: (i) detection and estimation of transients in low SNR environments, (ii) the bispectrum is now a standard technique in ocean wave work and radioastronomy, (iii) bispectra have shed a lot of new light on plasma physics and turbulence, (iv) volumes of EEG data have been analyzed via bispectrum/trispectrum since power spectra don't tell us anything about this data, (v) detection and characterization of nonlinearities, (vi) blind equalization in communications, and (vii) suppression of additive colored noise in sonar/radar signals.

The third issue that was debated concerned the question whether there are any other properties of higher-order spectra we don't know yet, or any generalizations that can help us solve new problems. Two possible generalizations were pointed out: the use of multispectra of which higher-order spectra are special cases, and, the use of other inverting functions than the natural logarithm of the characteristic function in defining higher- order statistics. The panel discussion concluded with the question: "Do we need another workshop?" The answer was unanimous: "Yes, in two years."

IDENTIFICATION OF NONMINIMUM PHASE SYSTEMS I

(Chairman: D. J. Thomson)

The first paper of this session *An Iterative Approach to Nonminimun Phase AR Identification* presented by G. Jacovitti was interesting in that it discussed moments of nonlinear transformations of the data instead of simple moments. The second paper *AR Identifiability using Cumulants* by A. Swami and J. Mendel was interesting in providing conditions for consistant estimates and in giving simple examples where single slice estimators fail. *On the Use of Second- and Higher-Order Inverse Statistics* by M. Rangussi and G. Giannakis extended Cleveland's ideas of inverse autocorrelations to the polyspectra. As in the usual case the inverse swaps the AR and MA parts of the model. *Approaches to FIR System Identification with Noisy Data using Higher-Order Statistics* by J. K. Tugnait was valuable in giving a Monte-Carlo comparisons of four competitive algorithms.

BISPECTRAL ANALYSIS

(Chairman: E. J. Powers)

In the paper *Multi-Window Bispectrum Estimates* D. J. Thomson described a non-parametric multiple-window method for computing consistant estimates of the bispectrum from short data segments of a process. H. Sakai in his paper *A Composite Linear Model Generating a Stationary Stochastic Process with Given Bispectrum* presented a composite linear model capable of generating a stationary stochastic process with a given bispectrum. His approaches are based on the fact that a certain linear system with a non-Gaussian, i.i.d., input process provides an output stationary process whose third-order cumulant vanishes except for special combination of two time lags. In the paper *Estimation of Frequency Response and Intermodulation Distortion from Bispectrum* by M. R. Raghuveer the properties of the bispectrum and the second-order Volterra model are utilized to quantify intermodulation distortion introduced by quadratically nonlinear systems. The approach facilitates measurement of the intermodulation distortion at more frequency points in the frequency plane than does the conventional two-tone test.

SONAR AND RADAR APPLICATIONS

(Chairman: J. Smith)

Four papers were presented in this session that spanned detection and classification functions of applied systems for transient and image signal types. The first paper by George Ioup presented an evaluation of cross- correlation and bicorrelation processing for detecting acoustic transient signals. Three example transient signals were analyzed. In the second paper Roger Dwyer showed the analysis of a doppler-shifted target echo from an amplitude modulated transmitted pulse. It was shown that the fourth-order spectra could be used to extract range and doppler from the echo signal. Under the same conditions the target information was unabtainable from the power spectrum processing.

A. C. Dubey presented examples of sonar and optical images in the third paper of the session. Individual seam lines of the images were used to reduce the 2-D problem to a 1-D problem. The complex cepstrum of higher-order cumulants (bicepstrum) was used to estimate the nonminimum phase of the impulse response of the backscatter medium and to reduce the noise in the sonar data. The data represented early results of using the bicepstrum methods. The fourth paper of the session showed the application of bispectrum methods to the analysis of the scattered field of radar targets. The paper was presented by I. Young. Radar scattering data from scale models of commercial transport aircraft was used to show the multiple reflection interactions of target scattering components. The bispectral plots clearly showed the phase interactions of features of different aircraft that might be used as signature classification discriminants.

NONLINEAR SYSTEM ANALYSIS

(Chairman: R. R. Mohler)

A nice combination of higher-order moments, polyspectra and functional-series method were included in this session. The first paper by B. Picinbono considered the parameter linearity property of the Volterra kernels to derive nonlinear detection and filter algorithms by geometrical arguments. This can be compared with an approach which uses a canonical decomposition of linear systems with

5

multipliers. Tests for linearity and Gaussianity, formerly derived by D. Hinich from the bispectrum, are supplemented conveniently by means of the new trispectrum test presented by D. Molle and M. Hinich. In the third paper, E. J. Powers and his associates estimate the three-wave coupling coefficients from turbulent data for fluids and plasmas. System dynamics of a cascade of two-linear minimum-phase subsystems separated by a zero-memory, monotonic nonlinearity are identified by means of the appropriate third-order moment or bispectrum.

HARMONIC RETRIEVAL AND DETECTION

(Chairman: J. L. LaCoume)

In this session two papers were related to the retrieval of harmonics, one to transient estimation and the last to detection using higher-order statistics. K. Lii and T. Tsou developed new statistics for the detection of periodicities using slices of the bispectrum and/or trispectrum. G. Volovitz and G. Scarano introduced hybrid moments constructed with nonlinear transforms of the data. They extended to these hybrid nonlinear moments the methods of spectral estimation. In a very close topic C. K. Papadopoulos and C. L. Nikias extended the Prony method to higher-order statistics. Their presentation contains the definition of *higher-order statistics like* operators for deterministic signals and established the validity of the proposed generalized Prony method. Finally, D. Kletter and H. Messer gave the structure of a detector of non- Gaussian signals in Gaussian noise using higher-order (reward) statistics.

MULTIDIMENSIONAL SIGNAL PROCESSING

(Chairman: B. Picinbono)

The lead paper entitled *Texture Discrimination via Higher-Order Statistics* was presented by G. Ramponi. The second paper addressed image sequence analysis and reconstruction from the bispectrum and was presented by B. M. Sadler. M. R. Raghuveer gave a stimulating talk on two-dimensional nonminimum phase signal processing. T. E. Hall presented predictive image coding techniques using parametric models and cumulants. His talk was followed by K. Jhang who introduced a third velocity field tomography method using higher-order correlations. An

interesting presentation was given by Y. Hu who showed how to reconstruct the autocorrelation from sixth-order moments in optics.

BIOMEDICAL SIGNAL ANALYSIS

(Chairman: R. Leahy)

The session presented some work on the application of the bispectrum to EEG and other biomedical signals. D. L. Sherman provided new results in EEG data analysis via eigenstructure based bispectra and P. K. Pearson demonstrated the usefulness of bispectral analysis to rat EEG. T. Ning presented results on the detection of quadratic phase coupling in EEG data and K. Yana demonstrated the effectiveness of bispectral analysis to bioelectric phenomena.

ARRAY PROCESSING

(Chairman: M. Hinich)

The lead paper was presented by J. LaCoume who formulated the array processing problem as an optimization problem where fourth-order cumulants are minimized under non-linear constraints. R. Mohler presented a new method based on higher-order statistics and J. Cardoso demonstrated a new eigenstructure based method using fourth-order cumulants. C. L. Nikias presented an extension of the ESPRIT algorithm to the trispectrum domain and C. Weigel discussed the performance of time delay estimation methods based on the bispectrum. The final talk was given by P. Comon on *Separation of Stochastic Processes when a Linear Mixture is Observed.*

IDENTIFICATION OF NONMINIMUM PHASE SYSTEMS, II

(Chairman: K. S. Lii)

The paper by Y. Inouye and T. Matsui describe a procedure for estimating the coefficient matrices of multichannel nonminimum phase ARMA models based on third-order cumulants. A recursive algorithm for AR model was proposed for the computation. The paper by A. M. Tekalp and A. T. Erdem discussed the necessary and sufficient conditions for the existence of a stable LTI system such that its output matches a given nth-order spectrum. Deeming's paper discussed a few

methods for seismic deconvolution. It considered a continuous time linear system model for the seismic wavelet and approximated it by an ARMA model. Fourth-order statistics were used to estimate the AR part of the wavelets.

APPLICATIONS

(Chairman: J. K. Tugnait)

There were six papers in the session. E. J. Powers used bispectral analysis to estimate a second-order Volterra system to predict the response of tethered offshore structures to random seas. The theoretical results were confirmed by a scale-model physical experiment. S. Elgar used bispectral analysis to explain some aspects of the nonlinear dynamics of shoaling ocean surface waves. The presence of quadratic phase coupling was confirmed. G. Sebert presented the results of extensive Monte-Carlo simulations to estimate the statistics of the estimates of bicoherence and biphase of time-series consisting of various triads of sinusoids. The results were then used to interpret the results of bispectral analysis of shallow water surface gravity waves.

G. B. Giannakis used a triple cross-correlation approach to noise cancelling and related signal processing tasks, in lieu of the usual LMS approach. K. Sasaki proposed and analyzed two higher-order spectral analysis based passive imaging systems for reconstruction of acoustic noise source distributions. Finally, I. J. Clarke developed a "near optimal" efficient maximum likelihood algorithm for second-order spectral analysis applications to array processing.

WORKSHOP ON HIGHER-ORDER SPECTRAL ANALYSIS

Sponsored by
Office of Naval Research
and
National Science Foundation

In cooperation with the IEEE Societies:
Control Systems;
Geoscience and Remote Sensing;
Acoustics, Speech and Signal Processing

The Lodge at Vail
Vail, Colorado
June 28-30, 1989

89 12 11 1 1

Greetings From The Chairmen

It is our pleasure to welcome you to the Workshop on Higher-Order Spectral Analysis. We are extremely excited about both the breadth and the depth that the first workshop on this topic has obtained. Your overwhelming response to its announcement allowed us to assemble a truly outstanding technical program consisting of two tutorial sessions, two keynote addresses and ten technical sessions. The workshop program promises to provide a forum for discussion of new theories and methods for processing signals that are based on Higher-Order Spectra. We are also confident that you will enjoy your stay in Vail.

We take this opportunity to thank the Office of Naval Research and the National Science Foundation for sponsoring this event. Their support allowed us to provide travel grants for keynote speakers, as well as post-doctorals and graduate students to participate and present their most recent work on higher-order spectra. We would also like to thank the IEEE Societies on Acoustics, Speech and Signal Processing, Control Systems, and Geoscience and Remote Sensing for cooperating towards the success of the workshop.

A number of individuals put forth outstanding efforts to make this Workshop a success. We would like to thank the Workshop Committee Members who have been indispensable in arranging local details, publications, registration and finances, and publicity. Special thanks to the various session chairmen and to Anna Aleska, Gloria Bullock, Cathy Montagna, and Linda Varilla. We are also indebted to David Dobson of McGregor and Werner.

We thank you for your participation, and we look forward to meeting you personally.

Chrysostomos L. Nikias   Jerry M. Mendel

WORKSHOP ON HIGHER-ORDER SPECTRAL ANALYSIS

Sponsored by the Office of Naval Research and National Science Foundation and in Cooperation with the IEEE Societies: Acoustics, Speech and Signal Processing; Control Systems; and Geoscience and Remote Sensing

The Lodge at Vail
Vail, Colorado
June 28-30, 1989

Higher-order spectra of a signal contain important information that is not present in its power spectrum, e.g., nonminimum phase information, as well as information due to deviations from Gaussianity and types of nonlinearity. The purpose of this workshop is to provide a forum for discussion of new theories and methods for processing signals to extract information that are based on higher-order spectra or cumulants.

- Emphasis on Technology Transfer Issues

- Two Tutorial Sessions (1½ hours each)

- Two Keynote Addresses

- Ten Technical Sessions

WORKSHOP COMMITTEE

Organizers and Co-Chairmen

Chrysostomos L. Nikias
CDSP Research Center
Dana Research Building
Northeastern University
360 Huntington Avenue
Boston, MA 02115
Tel.

Jerry M. Mendel
Department of Electrical
Engineering Systems
University of Southern California
University Park
Los Angeles, CA 90089
Tel.

Local Arrangements

Kevin M. Buckley
Department of Electrical Engineering
123 Church Street, S.E.
University of Minnesota
Minneapolis, MN 55455
Tel.

Proceedings

Georgios B. Giannakis
Department of Electrical Engineering
Thornton Hall
University of Virginia
Charlottesville, VA 22901
Tel.

Treasurer Registration

Richard Leahy
Department of Electrical
Engineering Systems
University of Southern California
University Park
Los Angeles, CA 90089
Tel.

Publicity

TUTORIAL SESSIONS

1. Higher-Order Spectra in Signal Processing

by Chrysostomos L. Nikias, Northeastern University, Boston, MA

This tutorial seminar introduces the motivation, definitions and properties of moments, cumulants and higher-order spectra in a digital signal processing framework, discusses detection, parameter estimation and signal reconstruction application problems that can directly benefit from the use of higher-order spectra, and motivates further research and developments in this area.

2. Nonminimum Phase System Identification

by Jerry M. Mendel, University of Southern California, Los Angeles, CA

This tutorial seminar describes many new cumulant-based methods for identifying MA, AR and ARMA models just from noisy output measurements. It covers reasons for using more than just second-order statistics, theoretical aspects of the methods, their potential strengths and weaknesses, and their interrelationships.

Attendees will receive the full set of viewgraphs for each tutorial.

KEYNOTE ADDRESSES

1. Higher-Order Moments and Spectra: Some History, Some Applications, Some Extensions and Some Comparative Aspects

by David R. Brillinger, University of California, Berkeley, CA

Higher-Order moments and spectra have been employed for the description and analysis of random processes since the mid-thirties. These parameters go hand in hand with nonlinear transformations of processes. They are useful in problems of system identification and of examining the basic structure of processes. In some cases they have basic interpretations. They may be defined for: time series, point, generalized, spatial, vector and particle processes among others. They may be estimated in a variety of fashions. They have been used successfully in practice, particularly in the presence of a physical description of the circumstance. As well as illustrating the preceding remarks there will be detailed examination of the particular case of a bilinear system involving a comparison of linear, quadratic and maximum likelihood analysis.

2. Bispectrum Imaging Through Turbulence

by J.Chris Dainty, Imperial College, London, U.K.

The resolution of conventional optical images formed through atmospheric turbulence is usually limited by the turbulence rather than the optical system. Diffraction-limited information can be retained by averaging spatial correlation functions of the image intensity, rather than the image intensity itself. It is difficult, or perhaps impossible, to reconstruct a map of the object from its spatial autocorrelation, but an unique map can be found from the triple correlation or the bispectrum. In this talk some aspects of bispectral imaging through turbulence are reviewed. Particular attention will be given to: the effect of turbulence on the bispectrum, signal-to-noise and computational aspects of low light level (photon) images, and computer algorithms for two dimensional data.

TECHNICAL SESSIONS

- Identification of Nonminimum Phase System, I
- Bispectral Analysis
- Sonar and Radar Applications
- Nonlinear System Analysis
- Harmonic Retrieval and Detection

- Multidimensional Signal Processing
- Biomedical Signal Processing
- Array Processing
- Identification of Nonminimum Phase Systems II
- Applications

GENERAL INFORMATION

How to Reach Vail from Denver Airport

Vail is a 2 - 2.5 hour drive west from Denver, on Interstate 70. To get there from Stapleton Airport by rent-a-car, take the only airport exit to Quebec Street. Go right on Quebec Street and follow it for 1.6 miles (to I-70). At the I-70 intersection, take 70 West (you exit Quebec Street from the left lane). Take I-70 west 102 miles to the Vail exit. VANS TO VAIL provides a shuttle between Denver Airport and Vail. Departing Times: 10:00 AM, 2:00 PM, 7:00 PM. For further information call 1-800-222-2112 or (303) 476-4467.

Workshop Site

The Workshop will be held at THE LODGE AT VAIL, 174 East Gore Creek Drive, Vail, CO 81657. Tel. (303) 476-5011 or (800) 237-1236. Guest rooms for the Workshop are priced at $80 per night plus tax, single or double occupancy per bedroom however long you wish to stay.

Registration

• Participation is limited to 100 attendees including authors. If you have not registered by June 1, 1989 and wish to attend, please call Ms. Gloria Bullock at (213) 743-5515 to confirm availability of space.

• Please pick up your registration package Tuesday evening, June 27, 1989, 5:30 PM - 8:00 PM or Wednesday, June 28, 1989, starting 7:30 AM.

Social Functions

• Ice-Breaker Reception
  Tuesday, June 27, 1989 from 6:300 PM to 8:30 PM

• Luncheon
  Wednesday, June 28, 1989 from 12:00 PM to 2:00 PM

• Dinner Party
  Thursday, June 29, 1989, starting at 7:00 PM

TABLE OF CONTENTS

4:00 PM-5:30 PM — June 30, 1989
Applications
J.K. Tugnait, Exxon Production Research Co.,
Houston, TX; *K. Sasaki*, University of Tsukuba,
Japan

† Manuscript unavailable for publication.

Author Index

AR IDENTIFIABILITY USING CUMULANTS

Ananthram Swami and Jerry M. Mendel

Signal and Image Processing Institute
Department of Electrical Engineering-Systems
University of Southern California
Los Angeles, CA 90089-0781

Abstract. We address the problem of estimating the AR order and the AR parameters of a causal, stable, SISO ARMA(p,q) model, excited by an unobservable i.i.d. process; the observed output is corrupted by additive colored Gaussian noise. The ARMA model may be mixed-phase, and have inherent all-pass factors and repeated poles. We show that consistent AR parameter estimates can be obtained via the normal equations based on $(p+1)$ 1-D slices of the m-th order $(m \geq 2)$ cumulant. We show via counter-examples that consistent AR estimates cannot, in general, be obtained from a single 1-D slice of the cumulant. Necessary and sufficient conditions for the existence of a full-rank slice are also derived. Extensions to the multi-dimensional, multi-channel and non-causal cases are discussed briefly.

Model and Assumptions

Consider the causal SISO ARMA(p,q) model.

$$\sum_{k=0}^{p} a(k) y(n-k) = \sum_{k=0}^{q} b(k) u(n-k) \tag{1}$$

with transfer function

$$H(z) = \frac{\prod_{i=1}^{q}(1 - \beta_i z^{-1})}{\prod_{i=1}^{p}(1 - \alpha_i z^{-1})} \tag{2}$$

We assume that

AS1. There are no pole-zero cancellations in $H(z)$: $a(p) \neq 0$, $b(q) \neq 0$; $a(0) = b(0) = h(0) = 1$.

AS2. The poles of $H(z)$ lie strictly within the unit circle.

AS3. Input, $u(n)$, is i.i.d., non-Gaussian, and has finite non-zero m-th order cumulant.

Note that we do not assume $q < p$ or $q \leq p$ as is usually done.

The correlation based normal equations are given by

$$\sum_{i=0}^{p} a(i) C_{2,y}(m-i) = 0, \quad m > q \tag{3}$$

If the system has no inherent all-pass factors, then, consistent estimates of the AR parameters can be obtained from (3), with $m = q + 1, \ldots, q + p + 1$. Gersch's result leads to the SVD-based AR order determination techniques. In practice, over-determined, and weighted least squares solutions of (3) are used.

Cumulant-based AR estimation is indicated if the input is non-Gaussian, and the model has inherent all-pass factors, or if the additive noise is colored Gaussian of unknown power spectral density. The Brillinger-Rosenblatt summation formula relates the m-th order cumulant to the impulse response via

$$C_{m,y}(i_1, \ldots, i_{m-1}) = \sum_{n} \prod_{k=0}^{m-1} h(n + i_k) \tag{4}$$

where $i_0 = 0$. Hence, the cumulant-based normal equations for the causal model in (1) are readily obtained as, (see [3, 6, 14], for example),

$$\sum_{k=0}^{p} a(k) C_{m,y}(\tau - k, i_2, \ldots, i_{m-1}) = 0, \quad \tau > q \tag{5}$$

Since the m-th order cumulant is a $(m-1)$-dimensional statistic, several algorithms based on 1-D slices of the cumulant have been proposed, [2, 4, 6, 8, 9].

Collecting (5) for $\tau = q + 1, \ldots, q + p + 1$, we obtain

$$C_T(\tau) \bar{\mathbf{a}} = \underline{\mathbf{b}}(\tau) \tag{6}$$

where $C_T(\tau)$ is a Toeplitz matrix with (i, j) entry $C_{m,y}(\tau - i + j, i_2, \ldots, i_{m-1})$, $\tau \geq q$, $\bar{\mathbf{a}} = [a(1), \ldots, a(p)]^T$, and vector $\underline{\mathbf{b}}(\tau)$ has $C_{m,y}(\tau + j, i_2, \ldots, i_{m-1})$ as its i-th element. If matrix $C_T(\tau)$ has rank p, then consistent AR parameter estimates can be obtained via (5) from the 1-D slice, parametrized by the fixed lags $i_2, \ldots, i_{m-1}$; we will call such a slice a *full-rank* slice. If the rank of $C_T(\tau)$ is p, we will call the 1-D slice a rank p slice. The existence of a full-rank slice is usually assumed implicitly or explicitly, [2, 4, 6, 9, 13].

The *objectives* of this paper are to establish that consistent AR parameter estimates can be obtained from the 'normal' equations, i.e., (5), based on a specific set of $(p+1)$ 1-D slices. Additionally, we will show via an example, that consistent parameter estimates cannot be obtained from a smaller set of 1-D slices. Since the m-th order cumulant is a function of $(m-1)$ lag variables, the examples and the Theorems in subsequent sections establish that for ARMA processes, cumulants may be treated as $1\frac{1}{2}$-D sequences, a phrase first coined in [3]. Necessary and sufficient conditions for the existence of a full-rank slice, for ARMA(p,q) models, are also derived.

The Z-transform of a 1-D cumulant slice

Define the 1-D slice, parametrized by the lag variable k_o, of the m-th order cumulant by,

$$C_{m,y}(\tau;k_o) = C_{m,y}(\tau,k_o,0,\ldots,0) = C_{m,y}(\tau+k_o,\tau,\ldots,\tau) \quad (7)$$

where the second equality follows from the stationarity of $y(n)$. The (two-sided) Z-transform of the 1-D slice is given by,

$$C_{m,y}(z;k_o) = \sum_{\tau=-\infty}^{\infty} C_{m,y}(\tau;k_o)z^{-\tau}$$

$$= H_{m-1}(z;k_o)H(z^{-1}) \quad (8)$$

where we have used (4), $m \geq 3$, $H_2(z;0) = H(z)$, and

$$H_{m-1}(z;k_o) = z^{k_o}H(z) * H(z) * \cdots * H(z) \quad (9)$$

$$= z^{k_o}H(z) * H_{m-2}(z;0) \quad (10)$$

where $*$ denotes complex convolution. $H_{m-1}(z;k_o)$ is the Z-transform of the sequence $h_{m-1}(n;k_o) = h^{m-2}(n)h(n+k_o)$.

The complex convolution in (10) may be written as

$$H_{m-1}(z;k_o)$$

$$= \frac{1}{2\pi\sqrt{-1}} \oint u^{k_o-1} H(u)H_{m-2}(zu^{-1};0)\,du \quad (11)$$

$$= \frac{1}{2\pi\sqrt{-1}} \oint u^{k_o-p+q-1} \frac{\prod_{i=1}^{q}(u-\beta_i)}{\prod_{i=1}^{p}(u-\alpha_i)} H_{m-2}(zu^{-1};0)\,du$$

Evaluating the complex convolution via the Cauchy Residue Theorem [7, pp 52-53 and 63-66], we obtain

$$H_{m-1}(z;k_o) = \sum_{j=1}^{p} c_j\alpha_j^{k_o}H_{m-2}(z\alpha_j^{-1};0) + c_0\delta(k_o-p-q) \quad (12)$$

where $k_o-p-q \leq 0$, and

$$c_0 = \frac{\prod_{i=1}^{q}-\beta_i}{\prod_{i=1}^{p}-\alpha_i} = \frac{b(q)}{a(p)} \neq 0 \quad (13)$$

$$c_j = \frac{\prod_{i=1}^{q}(1-\beta_i\alpha_j^{-1})}{\prod_{i\neq j}^{p}(1-\alpha_i\alpha_j^{-1})}, \quad j = 1,\ldots,p \quad (14)$$

The relation $c_0 \neq 0$ follows from (AS1). *In deriving (12), we assumed that the poles are simple;* repeated poles will be considered later. We have excluded the case $n = k_o-p-q < 0$, since this leads to multiple poles at the origin and, hence, additional terms on the right-hand side of (12) given by $\sum_{n}^{-1} d_{in}z^{-1}$. Equation (12) was also derived in [2] for the $k_o = 0$, $q < p$, $m = 3$ case.

We note for later use that, if $H(z)$ has p_d distinct poles, α_i, of multiplicity s_i, $i = 1,\ldots,p_d$, $\sum_{i=1}^{p_d} s_i = p$, then,

$$H(z) = \sum_{i=0}^{q-p} d_i z^{-i} + \sum_{i=1}^{p_d}\left(\sum_{k=1}^{s_i}\frac{c_{ik}}{(1-\alpha_i z^{-1})^k}\right) \quad (15)$$

where

$$c_{ik} = \frac{1}{(s_i-k)!}\left\{\frac{d^{s_i-k}}{dz^{s_i-k}}(1-\alpha_i z^{-1})^{s_i}H(z)\right\}_{z=\alpha_i} \quad (16)$$

If $q \leq p$ and the poles are simple, then,

$$H(z) = c_0\delta(p-q) + \sum_{j=1}^{p}c_j/(z-\alpha_j) \quad (17)$$

which may be written in the time-domain as

$$h(n) = c_0\delta(n)\delta(p-q) + \sum_{j=1}^{p}c_j\alpha_j^{n}, \quad n \geq 0 \quad (18)$$

Equation (8) may be written as

$$C_{m,y}(z;k_o)A(z^{-1}) = H_{m-1}(z;k_o)B(z^{-1}) \quad (19)$$

or in the lag-domain, as

$$\sum_{k=0}^{p} a(k)C_{m,y}(k-\tau;k_o) = \sum_{k=0}^{q} b(k)h_{m-1}(k-\tau;k_o)$$

$$= \sum_{k=0}^{q} b(k)h^{m-2}(k-\tau)h(k-\tau+k_o)$$

$$= 0 \quad \tau > q \quad (20)$$

Equation (20) states that any 1-D cumulant slice satisfies an AR recursion of maximum order p. Concatenating the last equation for $\tau = q+1,\ldots,q+p+M$, $M \geq 0$, we obtain a possibly over-determined set of equations, $\mathcal{H}(k_o)\mathbf{a} = \mathbf{0}$, where $\mathbf{a} = [1, a(1),\ldots,a(p)]^T$. If $\mathcal{H}(k_o)$ has rank p, then the corresponding 1-D slice (parametrized by k_o) of the m-th order cumulant is a *full-rank* slice. From (19), we note that the recursion in (20) will hold with minimal order p (equivalently, $\mathcal{H}(k_o)$ will have rank p) if and only if $A(z^{-1})$ and the numerator of $H_{m-1}(z;k_o)$ have no common factors. We note that the simple derivation leading to (5) does not reveal the possibility of pole-zero cancellations, and minimal recursions of order less than p.

Is every 1-D slice a full-rank slice ?

Example 1. Consider the ARMA(1,1) model $H(z) = (z-b)/(z-a)$. From (8) and (12), we obtain

$$C_{3,y}(z;0) = \frac{z^{-1}-b}{z^{-1}-a}\cdot\frac{z-b(2a-b)}{z-a^2} \quad (21)$$

If $ab(2a-b) = 1$, i.e., $b = a\pm\sqrt{a^2-1}/a$, then the pole at $z = a^{-1}$ gets canceled by the zero at $z = b(2a-b)$; i.e., $C_{3,y}(z;0) = (bz-1)/a(z-a^2)$; hence, $C_{3,y}(n;0)$ is zero for all $n < 0$. From the discussion following (20), we note that matrix $\mathcal{H}(0)$ has all zero entries; the AR parameters cannot be determined in this case. The condition $ab(2a-b) = 1$ includes an all-pass model with $a = -1/2$ (denoted by an 'x' in Fig. 1), as well as a family of *minimum-phase models* (depicted by the upper curve in Fig. 1, for $-1 < a < -0.5$), which are identifiable using only output correlation. However, we also note that for the conditions of Fig. 1, the slices $C_{3,y}(\tau;k_o)$, $k_o \neq 0$, are full-rank slices. Similarly, it can be shown, that the 1-D slice, $C_{4,y}(n;0,0)$, is a zero-rank slice, if $b = a+(1/a-a^3)^{1/3}$, $0 < a < 1$ (see Fig. 2).

Example 2. Consider the AR(2) model, $H(z) = 1/(1-\rho^2 z^{-2})$, with impulse response, $h(2n) = \rho^{2n}$, $h(2n+1) = 0$, $n \geq 0$. From (4), it follows immediately that $C_{3,y}(\tau_1,\tau_2) = 0$, if τ_2 is odd; thus, these slices are zero rank.

Example 3. The slices $C_{3,y}(\tau,k_o)$, $k_0 \neq mp$, of the AR(p) model with poles at $z = \exp(j2\pi n/p)$, $n = 0,\ldots,p-1$, are all zero-rank slices.

From the above examples, we conclude that **every 1-D slice need not be a full-rank slice.**

Does there exist a full-rank slice ?

The existence of a full-rank slice has been implicitly or explicitly assumed in [2-4], [6, 8, 9, 13]. The assumption that a given 1-D cumulant slice has full-rank, may be appropriate for *modeling* where the unknown impulse response is approximated by an ARMA model, but not for *identification*, where $H(z)$ is assumed to be an ARMA model.

Example 4. Consider a maximum-phase ARMA(2,2) model, with $\beta_i = 1$, $\alpha_i \alpha_1$, $i = 1, 2$, i.e.,

$$H(z) = \frac{(z - \alpha_1^{-1})(z - \alpha_2^{-1}\alpha_2^{-1})}{(z - \alpha_1)(z - \alpha_2)} .$$

For this model, it is easily shown that for $k_o \neq 0$,

$$C_{3y}(-\tau; k_o) \quad \alpha_2 C_{3y}(1 - \tau; k_o) = 0, \quad \tau > 1 \qquad (22)$$

Hence, the recursion in (20) has minimal order 1. The 1-D slices $C(\tau; k_o)$, $k_o \neq 0$ have rank 1: the AR recursion based on these slices leads to consistent estimates of α_2, but cannot reveal the presence of the pole at $z = \alpha_1$.

Can we find a pair (α_1, α_2) such that the numerator of $H_2(z; 0)$ has the factor $z - \alpha_2$? If such a pair exists, then, the slice $C_{3y}(\tau; 0)$ will also have rank 1. In order to find such a pair, we set $H_2(z; 0)|_{z = \alpha_2} = 0$: this leads to

$$\alpha_1^4 - \alpha_1^2(1 - \alpha_2^3 - \alpha_2^2 - 1 - \alpha_2) - \alpha_2 - 0$$

which is a quadratic equation in α_1^2. For $-1 < \alpha_2 < 0.49$, one of the two solutions for α_1^2 is real and satisfies $0 < \alpha_1^2 < 1$. Figure 3 shows the combinations of α_1, α_2 for which the $k_o = 0$ slice cannot be used to identify the pole at $z = \alpha_2$. Hence, for this example, all slices are of rank 1. There does not exist a full-rank slice for this example.

Example 5. More generally, the 1-D slices, $C_{3y}(\tau, k_o)$, of the maximum-phase ARMA(p,p) model, with zeros at $\beta_j = \alpha_l \alpha_j^{-1}$, $j = 1, \ldots, p$, and l fixed, have rank $p - 1$, for $k_o \neq 0$ [see [8] and [12]]. As in the ARMA(2,2) example just considered, the slice at $k_o = 0$ will also have only rank $p - 1$ for various combinations of the α_j's.

From these examples, we conclude that **A full-rank slice may not exist.**

When does a full-rank slice exist?

The 1-D slice, $C_{my}(\tau, i_2, \ldots, i_m)$, is a full-rank slice provided that the Toeplitz matrix in (6) has rank p. Assume $q < p$, and substitute (18) into (4), to obtain

$$c(\tau) := C_{my}(\tau, i_2, \ldots, i_m)$$

$$= \sum_{n_1=0}^{\infty} \prod_{j=0}^{m-1} h(n - i_j) \sum_{n_1=0}^{\infty} \prod_{j=0}^{m-1} \left(\sum_{k=1}^{p} c_k \alpha_k^{n-i_j} \right)$$

$$\sum_{k=1}^{p} \alpha_k^{-\tau} c_k S(k; i_2, \ldots, i_{m-1}) \qquad (23)$$

where $i_0 = 0$, and $i_1 = \tau$, and

$$S(k; i_2, \ldots, i_{m-1}) := \sum_{i=1}^{p} c_i \left(\prod_{l=2}^{m-1} \sum_{j_l=1}^{p} \frac{c_{j_l} \alpha_{j_l}^{i_l}}{1 - \alpha_k \alpha_i \prod_{n=2}^{m-1} \alpha_{j_n}} \right) \qquad (24)$$

The elements of the Toeplitz matrix C_T in (6) are given by (23). Hence, we obtain

$$C_T = V_1 D V_2 \qquad (25)$$

where the Vandermonde matrices V_1 and V_2 have (i, j) entries given by α_j^{i-1} and α_i^{-j+1}, $i, j = 1, \ldots, p$. Matrix D is a diagonal matrix with entries $D(k, k) = c_k \alpha_k^{-\tau} S(k; i_2, \ldots, i_{m-1})$. Since the poles α_i are distinct, matrices V_1 and V_2 have full rank p. Therefore, matrix C_T will have full rank p if and only if $D(k, k) \neq 0$, $k = 1, \ldots, p$. Hence, we obtain:

Theorem 1. If $q < p$, and the poles of $H(z)$ are simple, then a necessary and sufficient condition for the 1-D slice, $C_{my}(\tau, i_2, \ldots, i_{m-1})$, to be a full-rank slice is given by

$$S(k; i_2, \ldots, i_{m-1}) \neq 0, \quad k = 1, \ldots, p, \qquad (26)$$

where $S(k; i_2, \ldots, i_{m-1})$ is given by (24).

We note that this condition appears to be very restrictive, i.e., in general, we cannot expect a 1-D slice to be a full-rank slice. Theorem 1 can be extended to the $q > p$ and repeated roots cases. A condition similar to (26) is obtained; however, (24) has to be modified. These extensions will be discussed later.

Special case: $k = 3$ (Third-order cumulants)

For convenience let us define,

$$C_{3y}(\tau, 0): \quad \sum_n h(n) h^*(n) h(n - \tau) \qquad (27)$$

Since we are dealing with real processes, $h(n)$ is real, and the last equation is identical to the Brillinger-Rosenblatt formula. Mimicking the development leading to Theorem 1, we obtain

$$C_{3y}(\tau, 0) = \sum_{k=1}^{p} c_k \alpha_k^{-\tau} S(k; 0) \qquad (28)$$

$$S(k; 0) = \sum_{i=1}^{p} \sum_{j=1}^{p} \frac{c_i c_j^*}{1 - \alpha_k \alpha_i^* \alpha_k} \quad c^H M_k c \qquad (29)$$

where $M_k(i, j) = (1 - \alpha_i \alpha_j^* \alpha_k)^{-1}$, the superscript H denotes conjugate transpose, and $c = [c_1, \ldots, c_p]^T$. $C_{3y}(\tau, 0)$ is a full-rank slice iff $S(k; 0) = c^H M_k c \neq 0$, $k = 1, \ldots, p$ (Theorem 1). For α_k real, M_k is Hermitian symmetric. If M_k is non-singular, then $S(k; 0) \neq 0$. Assume that α_k is complex; since pole-pairs occur in complex conjugate pairs, we need both $S(k) \neq 0$ and $S^*(k) \neq 0$. Hence, a sufficient condition is that the Hermitian symmetric matrix $M_k - M_k^H$ be non-singular. Collecting both cases together, we obtain:

Corollary 1. If the Hermitian matrices $N_k = M_k - M_k^H$, $k = 1, \ldots, p$, where $M_k(i, j) = (1 - \alpha_i \alpha_j^* \alpha_k)^{-1}$, are non-singular, $q < p$, and α_i are distinct, then $C_{3y}(\tau, 0)$ is a full-rank slice.

How many 1-D slices are required ?

Since the conditions for the existence of a full-rank slice appear to be restrictive, we naturally ask ourselves whether a finite set

of 1-D slices are sufficient to obtain consistent AR parameter estimates.

In (20), let $\tau = q + 1,...,q + p + M$, $M \geq 0$, and $k_a = q + p,...,q$; we obtain the system of equations

$$R_a\, \underline{a} = \underline{0}. \tag{30}$$

Note that we have used $(p+1)$ 1-D slices of the m-th order cumulant. If the matrix R has rank p, then consistent AR parameter estimates can be obtained via (30).

From (19), we note that the rank of the matrix R in (30) will be p, if and only if $H_{m-2}(z;k_a)$ does not have a zero at $z = \alpha_j^{-1}$ for every $j = 1,...,p$ and every $k_a = q+p,...,q$; i.e., if $k_a = q+p,...,q$ such that α_j^{-1} is not a zero of $H_{m-2}(z;k_a)$.

Lemma 1. Assume that conditions (AS1) and (AS2) hold. Also assume that the poles of $H(z)$ are simple. Then α_j^{-1} cannot be a zero of $H_{m-2}(z;k_a)$ for every $k_a = q+p,...,q$.

Proof. Let

$$H_{m-2}(z;k_a) = \sum_j c_j \alpha_j^{(m)} z^{-j}, \quad j = 1,...,p \tag{31}$$

Assume that $z = \alpha_j^{-1}$ is a zero of $H_{m-2}(z;k_a)$ for $k_a = q+p,...,q$. Then, we obtain from (31)

$$\sum_j c_j \alpha_j^{k_a}(k_a + p - q) = 0, \quad k_a = q+p,...,q \tag{32}$$

which may be written as

$$\begin{bmatrix} \cdots \\ \cdots \\ \cdots \\ \cdots \end{bmatrix} \begin{bmatrix} c_1 \\ \vdots \\ c_p \end{bmatrix} = \begin{bmatrix} 0 \\ 0 \\ \vdots \\ 0 \end{bmatrix} \tag{33}$$

or in matrix form as

$$V\, \underline{c} = \underline{0} \tag{34}$$

By assumption, the α_j's are distinct; hence, the Vandermonde matrix V is non-singular. Hence, (34) implies that $c_j = 0$, $j = 1,...,p$ and $c_0 = 0$. From (13), and also discussion following (14), this means that $q = 0$, which violates assumption (AS1).

Hence (32) cannot hold. Consequently, $k_a = q+p,...,q$ such that α_j^{-1} is not a root of $H_{m-2}(z;k_a)$. □

Corollary 2. Assume that (AS1) and (AS2) hold. Then α_j^{-1} cannot be a zero of $H_{m-2}(z;k_a)$ for every $k_a = q+p,...,q$.

Proof. Assume that $H(z)$ has a pole of multiplicity s at $z = \alpha_{p_d}$, $d = 1,...,s$, and all other roots are simple. In evaluating the contour integral in (11), the residue at the multiple pole is given by (12), pp. 52-53,

$$c_j = \frac{1}{(s-1)!} \lim_{z \to \alpha_{p_d}} \frac{d^{s-1}}{dz^{s-1}}[H(z)(1 - \alpha_{p_d} z)^s H_{m-2}(z;k_a)z^{k_a}]$$

This residue may be written as

$$\sum_j c_j = \prod_j (k_a + p - q + 1) \cdots [L_a]$$

where the terms in parentheses are to be interpreted as in (36), and where the F_j's do not depend on z. Equation (32) now becomes

Corollary 3. Under assumptions (AS1)-(AS2), the AR parameters can be identified from the 1-D slices $C_{m,y}(\tau;k_a)$, $k_a = 0,\max(1, q-q); via (30), provided $c_q \neq 0$. Additionally, if $q > p$, then $k_a = 0,\max(p-q,1), q$ suffices.

Proof. The first part of the Corollary follows immediately from Theorem 2 and the identity

of 1-D slices are sufficient to obtain consistent AR parameter estimates.

In (20), let $\tau = q + 1,...,q + p + M$, $M \geq 0$, and $k_a = q + p,...,q$; we obtain the system of equations

$$R_a\, \underline{a} = \underline{0}. \tag{30}$$

Note that we have used $(p+1)$ 1-D slices of the m-th order cumulant. If the matrix R has rank p, then consistent AR parameter estimates can be obtained via (30).

From (19), we note that the rank of the matrix R in (30) will be p, if and only if $H_{m-2}(z;k_a)$ does not have a zero at $z = \alpha_j^{-1}$ for every $j = 1,...,p$ and every $k_a = q+p,...,q$; i.e., if $k_a = q+p,...,q$ such that α_j^{-1} is not a zero of $H_{m-2}(z;k_a)$.

Lemma 1. Assume that conditions (AS1) and (AS2) hold. Also assume that the poles of $H(z)$ are simple. Then α_j^{-1} cannot be a zero of $H_{m-2}(z;k_a)$ for every $k_a = q+p,...,q$.

Proof. Let

$$H_{m-2}(z;k_a) = \sum_j c_j \alpha_j^{(m)} z^{-j}, \quad j = 1,...,p \tag{31}$$

Assume that $z = \alpha_j^{-1}$ is a zero of $H_{m-2}(z;k_a)$ for $k_a = q+p,...,q$. Then, we obtain from (31)

$$\sum_j c_j \alpha_j^{k_a}(k_a + p - q) = 0, \quad k_a = q+p,...,q \tag{32}$$

which may be written as

$$\begin{bmatrix} \cdots \\ \cdots \\ \cdots \\ \cdots \end{bmatrix} \begin{bmatrix} c_1 \\ \vdots \\ c_p \end{bmatrix} = \begin{bmatrix} 0 \\ 0 \\ \vdots \\ 0 \end{bmatrix} \tag{33}$$

or in matrix form as

$$V\, \underline{c} = \underline{0} \tag{34}$$

By assumption, the α_j's are distinct; hence, the Vandermonde matrix V is non-singular. Hence, (34) implies that $c_j = 0$, $j = 1,...,p$ and $c_0 = 0$. From (13), and also discussion following (14), this means that $q = 0$, which violates assumption (AS1).

Hence (32) cannot hold. Consequently, $k_a = q+p,...,q$ such that α_j^{-1} is not a root of $H_{m-2}(z;k_a)$. □

Corollary 2. Assume that (AS1) and (AS2) hold. Then α_j^{-1} cannot be a zero of $H_{m-2}(z;k_a)$ for every $k_a = q+p,...,q$.

Proof. Assume that $H(z)$ has a pole of multiplicity s at $z = \alpha_{p_d}$, $d = 1,...,s$, and all other roots are simple. In evaluating the contour integral in (11), the residue at the multiple pole is given by (12), pp. 52-53,

$$\frac{1}{(s-1)!} \lim_{z \to \alpha_{p_d}} \frac{d^{s-1}}{dz^{s-1}}\left[H(z)(1 - \alpha_{p_d}z)^s H_{m-2}(z;k_a)z^{k_a} \right]$$

This residue may be written as

$$\sum_j c_j = \prod_j (k_a + p - q + 1) \cdots [L_a]$$

where the terms in parentheses are to be interpreted as in (36), and where the F_j's do not depend on z. Equation (32) now becomes

$$H_{m-2}(z;k_a) = \sum_{j=1}^{p-s} c_j \alpha_j^k H_{m-2}(z\alpha_j^{-1};0)$$

$$+ \sum_{k=1}^{s} d_k(k_a)\alpha_{p_d}^{k+p-q-k} F_k(z)$$

$$= c_0 \delta(k_a + p - q), \quad k_a + p - q \geq 0 \tag{35}$$

where c_j, $j = 0,1,...,p-s$ are given by (13) and (14), and

$$d_s(k_a) = \prod_j^{s-1}(k_a + p - q + i), \quad d_1(k_a) = 1 \tag{36}$$

Let c_j, $j = 1,...,p-s$ be defined by (31) in Lemma 1, and let

$$v_{p-s+j} = \alpha_{p_d}^{p-q+j} F_j(\alpha_j^{-1}), \quad j = 1,...,s.$$

Assume that $z = \alpha_j^{-1}$ is a zero of $H_{m-2}(z;k_a)$, for $k_a = q+p,...,q$. Following the development in Lemma 1, we obtain

$$\sum_j^{p-s} c_j \alpha_j^k v_{p-j} + \sum_j^{s} v_{p-s+j}\alpha_{p_d}^k d_j(k_a) = c_0 \delta(k_a + p - q) = 0 \tag{37}$$

which may be written as

$$V_1 U_1\, \underline{v} = \underline{0} \tag{38}$$

where V_1 is the $(p+1)$-by-$(p+1-s)$ leading submatrix of V in (34); since α_j, $j = 1,...,p-s$, are distinct, matrix V_1 has rank $p+1-s$. The $(p+1)$-by-s matrix U_1 may be written as $U_1 = \mathrm{diag}(\alpha_{p_d}^{q},...,\alpha_{p_d}^{q})D$, where $D(i,j) = d_j(q-p-1+i) = \prod_l^{j-1}(i-l)$, $i = 1,...,p+1$, $j = 1,...,s$. Matrix D is the permutation of a lower triangular matrix with diagonal elements $(i-1)!$; hence, matrices D and U_1 are of full (column) rank s. Additionally, it is easily verified that the columns of U_1 are linearly independent of the columns of V_1. Hence, arguing as in the proof of the Lemma, we conclude that (38) can hold only if $c_0 = 0$, which contradicts assumption (AS2). The proof is readily extended to multiple repeated roots. □

As a consequence of the Lemma, and the preceding discussion, we obtain a useful result:

Theorem 2. Under assumptions (AS1)-(AS2), the AR parameters can be identified from $(p + 1)$ 1-D slices of the m-th order cumulant $C_{m,y}(\tau;k_a)$, $\tau = q+1,...,q+p+M$, $M \geq 0$, and $k_a = q+p,...,q$, via (30).

It is interesting that the Lemma is stated in terms of the MA order, q, and the relative order, $q - p$. Lemma 1 specifies the set of $p+1$ slices; it may not hold for an arbitrary set of slices, e.g., $k_a = q+1,...,p+q+1$; see Examples 4 and 5.

Theorem 2 establishes the sufficiency of $p+1$ slices in special cases; for example, when a full-rank slice exists, a smaller number of slices may be sufficient, e.g., the $k_a = 0$ slice in Example 1.

Corollary 3. Under assumptions (AS1)-(AS2), the AR parameters can be identified from the 1-D slices $C_{m,y}(\tau;k_a)$, $k_a = 0,\max(1, q-q)$, via (30), provided $c_q \neq 0$. Additionally, if $q > p$, then $k_a = 0,\max(p-q,1), q$ suffices.

Proof. The first part of the Corollary follows immediately from Theorem 2 and the identity

$$C_{2,y}(z_1 k_{z_1}) = C_{3,y}(z_1 \cdots k_{z_2} z^2) \qquad (39)$$

For the second part ($q \leq p$ case), use the slices $k_0 = q - p + 1, q$, and obtain, as in the proof of Lemma 1, $s_{x,i} = 0, i = 1, \ldots, p$ there is no reference but this implies that $H(z)$ has p zeros at $a_i^{-1} a_i^{-1}$, $j = 1, \ldots, i$, contradicting the assumption $q > p$. Finally, use (29) to establish the sufficiency of the slices $k_0 = 0, \max(q, p) - q + 1$.

Corollary 4. If all the poles of $H(z)$ lie strictly outside the unit circle (replacing assumption (AS2)), then, Lemma 1, Theorem 2 and Corollary 3 hold.

Proof. Strictly anti-causal systems may be made causal by "time reversal". Hence, the corollary follows immediately.

How does Theorem 2 relate to past work?

The existence of a full-rank slice, in particular the diagonal slice, has usually been assumed in cumulant-based AR estimation.

Lemma 1 was stated for the $q \leq p, m = 3$, simple roots case and Corollary 3 was proved in [14] using the theory of block Hankel matrices.

The $m = 4$ case was studied in [15] where the theory of block Hankel matrices is again used to establish the sufficiency of the set of $m = 4, (m + 2)(2 D)$ slices, $C_{4,y}(m; k_1, k_2) = 0 \leq k_1 \leq k_2 = \max(q, p) - 1$, under the assumption of simple roots.

In [5], it is claimed that, if a full-rank slice $C_{3,y}(m; k_i)$ exists and $q > p$, then, there exists a full-rank slice $C_{3,y}(m; k_0)$ with $k_0 = q-p$. Corollary 3 shows that a smaller set of slices suffices. Further, in Theorem 1 we have established the necessary and sufficient conditions for the existence of a full rank slice. It is also claimed in [5] that the AR order and parameters can be estimated from $C_{3,y}(m; k_0, k_1) = q - p, q$, or from $C_{4,y}(m; k_0, k_1)$, $k_1, k_2 = q - p, q$, as appropriate. Note that **our results are much stronger**.

What about non-causal ARMA models?

The preceding development does not hold for non-causal ARMA models, i.e., we cannot write normal equations of the form (5). Hence, another approach is required. For causal ARMA processes in AWGN with no inherent all-pass factors, it is well-known that all the poles can be identified using the correlation. One approach would be to: a) estimate the spectrally-equivalent minimum phase (SEMP) system, using prediction-error approaches; and b) compute the innovations corresponding to the estimated SEMP model [2, 3]. Now the innovations sequence is an all-pass (AP) process, with all its poles lying outside the unit circle, and is corrupted by colored Gaussian noise. For the AP system, $q_i = p_i$; hence, the required order is more (q, p). The true order is usually not known, but we usually know an upper bound for it, say P_0. We could augment [?] based on $r = 0, P_0$; then, use the SVD to determine the effective rank p_0. This procedure is also applicable to non-causal AR systems, and to non-causal ARMA systems with all zeros inside the unit circle, because the resulting AP system has linear poles outside the unit circle.

The two-step SEMP-AP approach may be practical, because sample estimates of the correlation usually show less variance than sample estimates of the cumulant: but if cumulant

are used to estimate all the poles, then $p + 1$, rather than $p_q + 1$, cumulant slices would be required; hence, the SEMP-AP decomposition is computationally attractive; and, c) for non-causal systems, the usual normal equations do not hold. However, the innovations sequence has to be computed; and the procedure will not work if the additive noise is colored Gaussian. In the latter case, all the poles should be estimated using cumulants. See [5] for alternative methods.

Extensions to the multichannel, multi-dimensional and non-causal cases are discussed in [12], [11] and [5].

In [5], non-conventional cumulant-based normal equations are derived as follows. The bispectrum satisfies

$$C(z_1, z_2) = \gamma_{3e} \frac{B(z_1) B(z_2) B(z_1^{-1} z_2^{-1})}{A(z_1) A(z_2) A(z_1^{-1} z_2^{-1})} \qquad (40)$$

where $H(z) = B(z)/A(z)$ may be non-causal.

Multiplying both sides of (40) by $A(z_1) A(z_2) A(z_1^{-1} z_2^{-1})$, and evaluating the 2-D inverse Z-transform leads to

$$\sum_{i=-p}^{p} \sum_{j=-p}^{p} \alpha(i,j) C_{3,y}(m-i,n-j) = \beta(m,n) \qquad (41)$$

where

$$\alpha(i,j) = \sum_{k=0}^{p} a(k) a(k-i) a(k+j) \qquad (42)$$

$$\beta(i,j) = \sum_{k=0}^{q} b(k) b(k-i) b(k+j) \qquad (43)$$

$\alpha(i,j)$ ($\beta(i,j)$) are non-zero only over the hexagonal region, $N(p)$ ($N(q)$), where $N(p)$ is bounded by the lines $j = p, i = p$, $i = j - p, j = -p, i = -p$, and $i = j - p$; $N(q)$ is defined similarly. $\alpha(i,j)$ ($\beta(i,j)$) enjoy all the properties of the cumulants of a MA(p) (MA(q)) process. From (41), we note that $C_{3,y}(m,n)$ is the impulse response of a 2D-ARMA model. Thus, in order to establish the sufficiency of a finite set of 1-D cumulant slices for AR parameter estimation, we can appeal to 2-D deterministic realization theory; i.e., how many slices of the IR are required to estimate the ARMA parameters? Since $\alpha(z_1, z_2) = A(z_1) A(z_2) A(z_1^{-1} z_2^{-1})$, the model is not separable, but is non-causal symmetric. Extensions of this procedure to higher-order cumulants are obvious.

Conclusion

We showed via counter-examples that 1) every 1-D slice may not be a full-rank slice, and 2) a full-rank slice may not exist. Necessary and sufficient conditions for the existence of a full-rank slice were established in Theorem 1. For strictly causal or strictly anti-causal ARMA(p,q) models, which may have repeated poles, Theorem 2 assures us that consistent estimates of the AR parameters may be obtained via the 'normal' equations based on a set of $(q + 1)$ 1-D slices of the m-th order cumulant, $C_{m,y}(m; k_0, 0, \ldots, 0, k_0) = q - p, q$. Theorem 2 generalizes Giannakis' identifiability results, and suggests a practical SVD based procedure for AR order determination. A two-step approach (the SEMP-AP decomposition) that yields consistent estimates of the AR parameters of non-causal ARMA processes, with zeros inside the unit circle, observed in AWGN was discussed. Finally,

if the moments of a deterministic signal are defined as

$$M_{ky}(\tau_1, \dots, \tau_{k-1}) = \sum_n y(n)y(n-\tau_1)\cdots y(n-\tau_{k-1}),$$

then, Theorems 1 and 2 hold for the moments of deterministic signals, modeled as the impulse response of an ARMA model. If the observed signal is corrupted with additive colored Gaussian noise, additional processing is required to estimate M_{ky} from the noisy output. Procedures for doing this, for the $k = 3$ and $k = 4$ cases, are discussed in [10]. Using the definitions of cumulants of complex processes, given in [10], the results in this paper may be readily extended to complex processes as well.

References

[1] W. Gersch, "Estimation of the AR Parameters of a Mixed ARMA Time Series", *IEEE Trans. Auto. Control*, 583-587, 1970.

[2] G.B. Giannakis and J.M. Mendel "Stochastic Realization of Non-Minimum Phase Systems", in *Proc. Amer. Control Conf.*, v.2, 1254-59, Seattle, WA, 1986.

[3] G.B. Giannakis and J.M. Mendel, "Identification of Non-Minimum Phase Systems Using Higher-Order Statistics", *IEEE Trans. on ASSP*, March 1989.

[4] G.B. Giannakis, J.M. Mendel and W. Wang, "Modeling Using Cumulant and Autocorrelation Statistics", in *Proc. ICASSP-87*, v.1, 61-64, Dallas, 1987.

[5] G. Giannakis and A. Swami, "On Estimating Non-Causal Non-Minimum Phase ARMA Models of Non-Gaussian Processes", in *Proc. IV IEEE ASSP Workshop on Spectrum Estimation and Modeling*, 187-192, Minneapolis, MN, 187-192, Aug. 1988.

[6] C.L. Nikias and M. Raghuveer, "Bispectrum Estimation: A Digital Signal Processing Framework", *Proc. IEEE*, v.75, 869-891, 1987.

[7] A.V. Oppenheim and R.W. Schafer, *Digital Signal Processing*, Englewood Cliffs, NJ: Prentice-Hall, 1975.

[8] M. Raghuveer, "Multichannel Bispectrum Estimation", in *Proc. III IEEE ASSP Workshop on Spectral Estimation and Modeling*, 21-24, Boston, 1986.

[9] M.S. Raghuveer and C.L. Nikias, "Bispectrum Estimation: a Parametric Approach", *IEEE Trans. on ASSP*, v.33, 1213-30, 1985.

[10] A. Swami, "System Identification Using Cumulants", *Ph.D. Dissertation*, Dept. of EE-Systems, University of Southern California, Los Angeles, CA, Oct. 1988.

[11] A. Swami, G.B. Giannakis and J.M. Mendel, "Modeling of Multidimensional Non-Gaussian Processes Using Cumulants", submitted to *IEEE Proc.*, Jan 1989; see also *Proc. ICASSP-88*, New York, NY, 729-33, April 1988.

[12] A. Swami, G. Giannakis and J.M. Mendel, "Multi-channel ARMA Parameter Estimation Using Cumulants", to be presented at *IEEE ICASSP-89*, Glasgow, Scotland, 1989.

[13] J.K. Tugnait, "Identification of Nonminimum Phase Linear Stochastic Systems", in *Proc. 23rd IEEE Conf. Decision and Control*, 342-347, Las Vegas, 1984, also in *Automatica*, v.22 457-464, 1986.

[14] J.K. Tugnait, "On Selection of Maximum Cumulant Lags for Non-causal Autoregressive Model Fitting", in *Proc. ICASSP-88*, New York, NY, 2372-5, April 1988.

[15] J.K. Tugnait, "Recovering the Poles From Fourth-Order Cumulants of System Output", in *Proc. Amer. Contr. Conf.*, 2090-3, Atlanta, GA, June 1988.
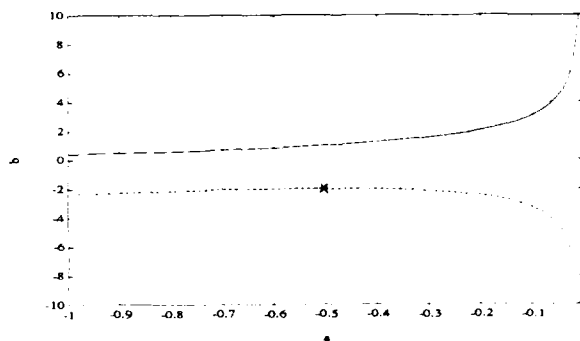
Figure 1: A family of ARMA(1,1) models, $H(z) = (z-b)/(z-a)$, for which $C_{3,y}(n,0)$ is not a full-rank slice.
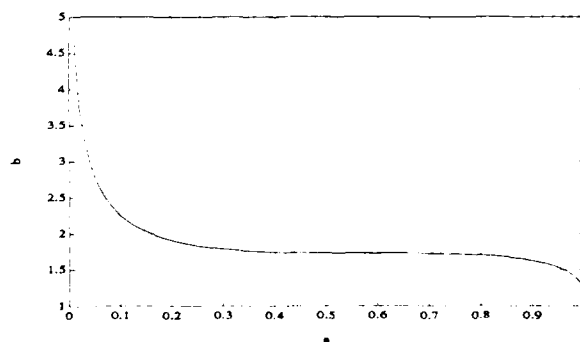
Figure 2: A family of ARMA(1,1) models, $H(z) = (z-b)/(z-a)$, for which $C_{4,y}(n,0,0)$ is not a full-rank slice.
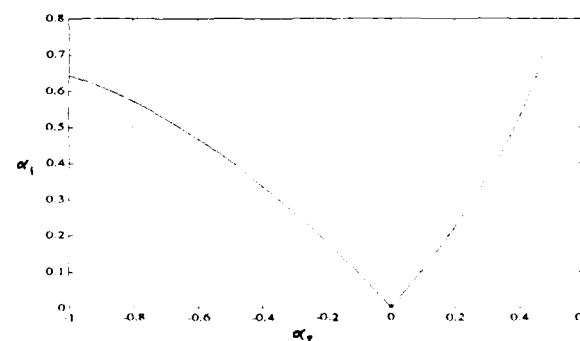
Figure 3: A family of maximum-phase ARMA(2,2) models, $H(z) = (z-1/\alpha_1^2)(z-1/\alpha_2)/(z-\alpha_1)(z-\alpha_2)$, which have no full-rank slices.

ON THE USE OF SECOND- AND HIGHER-ORDER INVERSE STATISTICS

Maria Rangoussi and Georgios B. Giannakis

Dept. of Electrical Engineering
University of Virginia
Charlottesville, VA 22901

Abstract

Inverse higher-order statistics of non-Gaussian, stationary random processes are introduced in this paper, as an extension of their 2nd- order counterparts, known as *inverse correlations*. Their use in system identification, and specifically in model order determination and parameter estimation problems, is investigated. Estimation procedures are proposed for obtaining sample estimates of inverse statistics and the corresponding (poly)spectra. The algorithms derived are illustrated by simulation examples, involving inverse 2nd- and 3rd-order statistics.

I. Introduction

Inverse higher- than- 2nd-order *statistics*, along with their Fourier-domain pairs, *inverse polyspectra*, constitute a natural extension of inverse correlations and spectra, in a higher- than- 2nd-order domain. Inverse correlations and inverse spectra were introduced by Cleveland, [5], and studied in [4], [2], and [1]. Overview discussion on inverse correlations can also be found in [16], and [14].

The *duality* property between inverse and direct spectra, offers one the flexibility to interchange the roles of AR and MA parts in ARMA modeling. Thus, MA parameters can be estimated via linear equations, if inverse correlations are employed, [5]. Several procedures for the estimation of inverse correlations have been proposed, [1], [5], and asymptotic analysis of their sample estimators is reported in [2].

Autocorrelation and spectral estimates perform poorly in the presence of additive, Gaussian noise of unknown covariance (AGN/UC). Additionally, they are insensitive to phase information. Thus, minimum phase, causality, and white Gaussian noise assumptions, become necessary when 2nd-order statistics are employed.

On the other hand, higher- than- 2nd-order statistics, known as *cumulants*, and their Fourier pairs, *polyspectra*, are both sensitive to phase information, and insensitive to AGN/UC. A detailed treatment of *k*th-order cumulants and

polyspectra, along with a wide range of applications, can be found in [3], [10], [13], [8].

Motivated by the existing work on 2nd-order inverse statistics, we introduce here inverse *k*th-order statistics, in a perspective of combining the advantages of both the inverse statistics and the *k*th-order cumulant domain. The algorithms presented in the following sections, focus on the use of inverse 3rd-order cumulants and bispectra for order determination and parameter estimation. In addition, we propose the use of inverse correlations for model order selection using rank determination criteria.

In what follows, definitions of inverse statistics along with some basic background results, are included in Section II; procedures for sample estimation of inverse statistics are proposed in Section III; inverse correlation-based algorithms for the model order selection problem are given in Section IV. Section V includes the proposed algorithms that use inverse statistics in sysem identification, and Section VI contains simulation results.

II. Definitions - Background

Let $\{x(t)\}$ be a non-Gaussian, stationary, zero-mean, discrete random process, with finite moments, and let the *k*th-order cumulant of $\{x(t)\}$, denoted by $c_{kx}(m_1,...,m_{k-1})$, be absolutely summable. Then, the *k*th-order spectrum C_{kx}, the *k*th-order inverse spectrum CI_{kx}, and the *k*th-order inverse cumulant ci_{kx} are respectively defined as

$$C_{kx}(\omega_1,...,\omega_{k-1}) = \sum_{m_1,...,m_{k-1}} c_{kx}(m_1,...,m_{k-1})e^{-j(\omega_1 m_1 + ... + \omega_{k-1} m_{k-1})}, \quad (1)$$

$$CI_{kx}(\omega_1,...,\omega_{k-1}) = \frac{1}{C_{kx}(\omega_1,...,\omega_{k-1})}$$

$$= \sum_{m_1,...,m_{k-1}} ci_{kx}(m_1,...,m_{k-1})e^{-j(\omega_1 m_1 + ... + \omega_{k-1} m_{k-1})}, \quad (2)$$

where it is assumed that $C_{kx}(\omega_1,...,\omega_{k-1}) \neq 0$, $|\omega_1,...,\omega_{k-1}| \leq \pi$, and that $CI_{kx}(\omega_1,...,\omega_{k-1})$ admits a $(k-1)$-dimensional Fourier series expansion.

It should be noted here that the first of the above assumptions imposes the restriction that the corresponding model of $x(t)$ have no zeroes on the unit circle. Note also that, for $k=2$, the above general definitions reduce to the ordinary inverse correlations/spectra definitions of [5].

In the following, we will focus on the $k=3$ case, where the above definitions reduce to

$$CI_{3x}(\omega_1,\omega_2) \equiv \sum_{m,n=-\infty}^{\infty} ci_{3x}(m,n) e^{-j(\omega_1 m + \omega_2 n)} \quad (3a)$$

$$= \frac{1}{C_{3x}(\omega_1,\omega_2)} = \frac{1}{\sum_{m,n=-\infty}^{\infty} c_{3x}(m,n) e^{-j(\omega_1 m + \omega_2 n)}} , \quad (3b)$$

where $c_{3x}(m,n) \equiv E[x(t)x(t+m)x(t+n)]$.

A useful result, established by the stationarity of $\{x(t)\}$, is that several symmetries hold for the lags of c_{kx} and ci_{kx}, [3]. These symmetries will be used later on, to reduce the dimensionality of systems of equations involving direct and inverse cumulants.

Now, let $y(t)$ be a linear process, expressed as $x(t) = \sum_i h(t-i)w(i)$, where $\{w(t)\}$ is a non-Gaussian, stationary, zero-mean, i.i.d. process, with $0 < \sigma_w^2, |\gamma_{3w}| < \infty$; $h(t)$ is exponentially stable, and $\{y(t)\}$ is the observed output process, corrupted by additive noise $\{v(t)\}$, independent of $\{w(t)\}$. Then, it can be proved that

$$c_{3y}(m,n) = c_{3x}(m,n) + c_{3v}(m,n) = h_3(m,n)^* c_{3w}(m,n) + c_{3v}(m,n) \quad (4a)$$

$$h_3(m,n) \equiv \sum_i h(i)h(i+m)h(i+n) . \quad (4b)$$

If the noise is AGN/GC, then $c_{3y}(m,n) \equiv c_{3x}(m,n)$, and furthermore, if $\{w(t)\}$ is i.i.d.,

$$c_{3x}(m,n) = \gamma_{3w} h_3(m,n) , \quad C_{3x}(\omega_1,\omega_2) = \gamma_{3w} H_3(\omega_1,\omega_2) , \quad (5a)$$

$$H_3(\omega_1,\omega_2) = H(\omega_1)H(\omega_2)H(-\omega_1-\omega_2), \quad H(\omega) = \sum_i h(i)e^{-j\omega i} . \quad (5b)$$

III. Sample estimates of inverse cumulants and polyspectra

If $x(t)$ corresponds to an ARMA(p,q) model $x(t) = \sum ... = \sum ... B_q / A_p ...$, then (3b) yields

$$CI_{3x}(\omega_1,\omega_2) = \sigma_w^2 \frac{A_p(...)}{B_q(...)} \quad (6)$$

which shows that $CI_{3x}(\omega_1,\omega_2)$ corresponds to the bispectrum of the "inverse" ARMA(q,p) model $HI(z) = A_p(z)/B_q(z)$; in general, inverse statistics of $\{x(t)\}$ coincide with the direct statistics of $HI(z)$.

The following four procedures are discussed in [1], [5], for estimating inverse correlations: (i) *orthogonality* approach, (ii) *windowed periodogram* approach, (iii) *long AR approximation* approach, and, (iv) best *linear interpolator* approach. Here, we use the extension of (i) and (ii) for sample estimation of kth-order inverse cumulants.

IIIa. Frequency-domain approach

The proposed algorithm is based on the definition of inverse cumulants and polyspectra, and includes the following steps :

step 1 : Segmentation of the zero-mean (or zero-mean compensated) process $\{x(t)\}$ in L (possibly overlapping) segments, each M points long.

step 2 : (a) Estimation of the kth-order spectrum $\hat{C}_{kx}^{(l)}(n_1,...,n_{k-1}) = \hat{C}_{kx}^{(l)}(\omega_1,...,\omega_{k-1}) |_{\omega_i = \frac{2\pi}{M} n_i}$, $1 \leq l \leq L$ at M discrete frequency points.

(b) Averaging of $\hat{C}_{kx}^{(l)}(n_1,...,n_{k-1})$ over the L segments :
$\hat{C}_{kx}(n_1,...,n_{k-1}) = \frac{1}{L}\sum_{l=1}^{L} \hat{C}_{kx}^{(l)}(n_1,...,n_{k-1})$.

step 3 : Estimation of the inverse kth-order spectrum using $\hat{CI}_{kx}(n_1,...,n_{k-1}) = 1/[\hat{C}_{kx}(n_1,...,n_{k-1})]$.

step 4 : If the intended application involves inverse cumulants, use $(k-1)$-D inverse FFT to obtain $\hat{ci}_{kx}(m_1,...,m_{k-1})$, from $\hat{CI}_{kx}(n_1,...,n_{k-1})$.

Several remarks are appropriate at this point :

(i) The estimation of the kth-order spectrum (step 2a) can be done in two ways, that both yield consistent estimates :

- The kth-order *periodogram* alternative amounts to calculating

$$\hat{C}_{kx}^{(l)}(n_1,...,n_{k-1}) = \frac{1}{N} X(n_1)...X(n_{k-1})X(-n_1-...-n_{k-1}),$$

where $X(n)$ denotes the FFT of $\{x(t)\}$. For $k=2$, the above procedure reduces to the (windowed) *periodogram* estimation method of [5]. This fast approach is appropriate for frequency-domain approaches, where the DFT of a model rather than its coefficients are sought.

- The kth-order *correlogram* alternative amounts to calculating

$$\hat{C}_{kx}(n_1,...,n_{k-1}) = FFT_{(k-1)D}\{\hat{c}_{kx}(m_1,...,m_{k-1})\} .$$

where $\hat{c}_{kx}^{(l)}(m_1,...,m_{k-1})$ is now estimated from the l th data segment.

(ii) Besides data segmentation, windowing of either the data $\{x(t)\}$, or, the kth-order spectrum $\hat{C}_{kx}^{(l)}(n_1,...,n_{k-1})$ usually yields smooth estimates. In [17], the following optimal (in the m.s.e. sense) 2-D frequency-domain window is proposed for smoothing the bispectrum estimate

$$K(\omega_1,\omega_2) = \frac{3^{1.3}}{\pi^3}[1 - \pi^{-2}(\omega_1^2 + \omega_2^2 + \omega_1\omega_2)], \quad \omega_1^2 + \omega_2^2 + \omega_1\omega_2 \le \pi^2,$$

$$= 0, \qquad\qquad\qquad\text{else}.$$

Other windows can be employed trading off reduced variance for increased bias of the $\hat{C}_{kx}(\omega_1,\omega_2)$ estimators, [17].

(iii) The zero-mean assumption on $\{x(t)\}$ is necessary to guarantee that the additive noise will be canceled in the cumulant domain.

IIIb. Cumulant-domain approach

The time-domain equivalent of (3b) is the kth-dimensional *orthogonality* property

$$\sum_{l_1,...,l_{k-1}=-\infty}^{\infty} ci_{kx}(l_1,...,l_{k-1})c_{kx}(m_1-l_1,...,m_{k-1}-l_{k-1}) = \delta(m_1,...,m_{k-1}). \quad (7)$$

For $k = 2$, (7) yields the *orthogonality* estimates of [1],

$$\sum_{l=-\infty}^{\infty} ci_{2x}(l)c_{2x}(m-l) = \delta(m). \quad (8a)$$

Using eq. (7) for $k = 3$, we obtain

$$\sum_{l_1,l_2=-\infty}^{\infty} ci_{3x}(l_1,l_2)c_{3x}(m_1-l_1,m_2-l_2) = \delta(m_1,m_2). \quad (8b)$$

For different values of (m) and (m_1,m_2), eqs. (8a) and (8b) yield infinite-dimensional systems which are linear in the unknown inverse statistics. Hence, if $\{x(t)\}$ is generally an IIR linear process, it is necessary to truncate the infinite summations at points $[-M,M]$. Depending on the pole-zero locations of the specific model, i.e., on the point at which the statistics of the model effectively die out, the approximation imposed by truncation may, or may not, yield acceptable estimates.

However, if $\{x(t)\}$ corresponds to an AR(p) model of order p, then the inverse statistics correspond to an MA(p) model of order p, i.e., $ci_{2x}(m) = p$, and $ci_{3x}(m_1,m_2) = 0$, for $|m_1,m_2| > p$. In this case, the summation $\dots$ is bounded at points $\pm p$, and for $|m_1,m_2| > p,$ $\dots$ can be written in matrix form as

$$R \, ci_{2x} = e, \quad C \, ci_{3x} = e, \quad (9)$$

where e is a $\dots$ vector, $e_{2x}[e_{3x}]$ is a

$(2p+1)\times1$ $[(2p+1)^2\times1]$ zero vector with an 1 in the middle position, and R [C] is a $(2q+1)\times(2q+1)$ $[(2q+1)^2\times(2q+1)^2]$ Toeplitz symmetric [block Toeplitz] matrix.

Note that, contrary to the approach described in [12], the derivation of (9) does not include any approximation, i.e., eq. (9) will yield the true ci_{2x},ci_{3x}, if the true c_{2x},c_{3x} are used to form the two matrices.

Several comments should be made at this point:

(i) This estimation method is more suitable if the intended application of inverse statistics involves explicitly ci_{2x} and ci_{3x}, and not the corresponding inverse spectra.

(ii) If we exploit the symmetries in autocorrelations and cumulants, then the dimensionality of the R [C] system reduces to q $[q(q+3)/2]$.

(iii) For the case discussed here, ci_{2x} [ci_{3x}] are the 2nd- [3rd-] order correlation of the AR(p) model parameters $\{a(i)\}_{i=0}^{p}$, [9].

(iv) In practice, both R and C matrices are composed of sample statistics, thus yielding sample estimates $\hat{ci_2}$ and $\hat{ci_3}$, of the true inverse statistics. Overdeterminancy of the resulting system matrices usually improves the accuracy of the estimates.

(v) If $\{x(t)\}$ corresponds to an MA(q) model, the inverse statistics correspond to an AR(q) model. In this case, the neat linear system of eqs. (9) cannot be obtained, since any finite number of equations involves twice as many unknowns. An approximation of the AR order by M, i.e., a truncation at point M, is then necessary, incurring the risks discussed earlier in this section. Nevertheless, MA parameter estimation algorithms are available, using direct cumulant statistics, [8],[15].

(vi) Because $\hat{c}_{2x}$ and $\hat{c}_{3x}$ are consistent estimators, and the estimation procedure proposed is linear, it follows that the $\hat{ci_{2x}}$ and $\hat{ci_{3x}}$ estimators are also consistent. Asymptotic analysis and variance expressions for the $\hat{ci_{3x}}$ estimator will be reported elsewhere.

(vii) There exists a finite number of equations (8b) [not necessarily the ones used in (9)] which guarantee uniqueness when solving for ci_{3x}. The latter holds true because otherwise, two inverse processes coming from two different models, would satisfy the same infinite set of equations. Consequently, they would correspond to the same kth order spectrum, which is a contradiction, given the one-to-one correspondence between IIR models and their kth order spectra. [10]

IV. Model order selection using inverse correlations

If $\{x(t)\}$ corresponds to an MA(q) model, then the inverse statistics $\dots$ Due to the property $\dots$

posed in [5] to estimate the order p of an AR(p) process, by calculating its inverse correlation sequence $ci_{2x}(m)$, and checking (by visual inspection) the lag beyond which $ci_{2x}(m)$ is effectively zero.

Here, we propose the use of inverse correlations to solve the "inverse" problem. If the process $\{x(t)\}$ corresponds to an ARMA(p,q) model $B_q(z)/A_p(z)$, of unknown MA order q, then using the *extended Yule-Walker* equations, a qth-order recursion can be established for the inverse correlation lags, [14]

$$\sum_{l=0}^{q} b(l) ci_{2x}(m-l) = 0 , \quad m > p , \tag{10}$$

where $p = 0$ corresponds to the pure MA case. The proposed algorithm proceeds as follows :

step 1 : Obtain $\hat{ci}_{2x}(m)$ using any of the methods presented in *Section III*.

step 2 : Given an upper bound $\bar{p}(\bar{q})$ on the order of the AR (MA) part of the original process, form the $\bar{p} \times \bar{p}$ Hankel matrix $\hat{H}_{ri}$, with elements $\{ci_{2x}(\bar{p}-\bar{q}+i+j-1)\}_{i,j=1}^{\bar{q}}$.

step 3 : Perform Singular Value Decomposition (SVD) on $\hat{H}_{ri}$, to specify the order q as the number of the first effectively zero singular values.

The numerically robust, SVD-based approach uses the entire $ci_{2x}(m)$ [and hence $\hat{c}_{2x}(m)$] sequence, and as such, it is expected to outperform the visual inspection method, which determines the MA order based on a single point estimate.

Note that, as far as our concern is order determination, the MA part can be non-minimum phase (NMP), since recursion (10) holds true even for NMP models which are free of all-pass factors. However, $ci_{2x}(m)$ lags now correspond to a process $x'(t)$, that is spectrally equivalent to $\{x(t)\}$. Consequently, (10) should not be used for parameter estimation, unless $\{x(t)\}$ is minimum phase.

An alternative, when the minimum-phase and causality assumptions are satisfied, is to use a recursion similar to (9) derived for inverse 3rd-order cumulants

$$\sum_{l=0}^{i} b(l) ci_{3x}(m-l,n) = 0, \quad m=p+1,...,p+q, \quad n=p-q,...,p , \tag{11}$$

and form the corresponding block-Hankel matrix $\hat{H}_{ci}$, whose rank q is then specified using SVD, [7]. In the general case, however, inverse correlations suffice for model order determination, as long as no all-pass factors are included in the model. A cumulant-based alternative for the general case, is currently under investigation.

V. Parameter estimation using inverse cumulants

The flexibility of handling the MA part of a general ARMA (p,q) model via inverse statistics, as if it were an AR one, is exploited here. This is because AR parameter estimation requires the solution of a linear system of equations, while MA parameter estimation traditionally requires non-linear minimization procedures.

When $\{x(t)\}$ comes from a minimum phase MA(q) model, the use of inverse correlations was proposed in [5] for estimating the parameters $\{b(i)\}_{i=0}^{q}$ using normal equations. In [8], an algorithm was introduced for the solution of the generally non-minimum phase problem, using both autocorrelations and 3rd-order cumulants (see also [15]).

In the case of *non-causal AR models*, (NC AR), however, the parameter estimation problem can only be faced in the kth-order statistics domain, and only through a considerably raised dimensionality of systems and matrices [9]. The latter prompted us to approach the NC AR parameter estimation problem as a NMP MA one. The algorithm uses 3rd-order inverse cumulants and includes the following steps :

step 1 : Estimate $\hat{ci}_{2x}$ and $\hat{ci}_{3x}$, corresponding to the known order AR(p) model $H(z) = 1/A_p(z)$, using one of the approaches described in Section III.

step 2 : The estimated inverse statistics correspond to a NMP MA(p) model, $HI(z) = A(z)$. Hence, we can employ the algorithm of [8], to estimate $\{a(i)\}_{i=1}^{P}$ solving the system of linear equations :

$$\left[\tilde{ci}_3 \mid \tilde{ci}_2 \right] \left[\bar{a} \right] = \left[\bar{e} \right] . \tag{12}$$

This system is derived by modifying the basic equation of [8] as in [15], so that it can be applied to the inverse model

$$\sum_{l=0}^{p} a(l) ci_3(m-l,m+m_0-l) = \frac{\sigma_w^2}{\gamma_{3w}} \sum_{l=0}^{p} a(l) a(l+m_0) ci_2(m-l), \quad -p \le m \le 2p.$$

step 3 (optional): Further improvement of the estimates $\{a(i)\}_{i=0}^{P}$ is achieved, if the estimates derived in step 2 are used as a starting point for the *weighted least-squares* algorithm of [15]. In general, any algorithm for MA parameter estimation can be implemented in step 2.

An *alternative* to this approach is the *frequency-domain reconstruction* algorithm, [6], implemented as follows :

step 1 : Estimate the bispectrum $C_{3x}(\omega_1,\omega_2)$ [assuming that $\{x(t)\}$ is an AR(p) model, with parameters $\{a(i)\}_{i=0}^{P}$], and compute the inverse bispectrum $CI_{3x}(\omega_1,\omega_2)$ as in (3b).

step 2 : Reconstruct the Fourier transform $A(k)$ of $\{a(i)\}^P_{i=0}$, from the inverse bispectrum, using the frequency-domain reconstruction algorithm described in [6]. This algorithm recursively calculates the values of $A(k)$ at discrete frequency points, based on the recursion :

$$A(k) = \frac{1}{[k/2]} \sum_{i=0}^{[k/2]} \frac{CI_x(k,0)}{A(0)\,CI_{3x}(k-l,l)} A(l) A(k-l), \quad k=2,3,...,(p+1)/2.$$

A phase correction step integrates the $A(k)$ reconstruction, [6].

step 3 : Use inverse FFT to obtain the parameters $\{a(i)\}^P_{i=0}$ from the reconstructed FFT $A(k)$.

A second *alternative* for step 2 of the above algorithm generalizes the least-squares reconstruction approach proposed in [11]. Specifically, the following relations for the magnitude and the phase of the inverse bispectrum can be derived

$$\ln|CI_{3x}(n_1,n_2)| = \ln|\gamma_{3w}| + \ln|A(n_1)| + \ln|A(n_2)|$$

$$+ \ln|A^*(n_1+n_2)|, \tag{13}$$

$$\psi_{I3x}(n_1,n_2) = \phi_A(n_1) + \phi_A(n_2) - \phi_A(n_1+n_2), \tag{14}$$

where $\psi_{I3x}(n_1,n_2)[\phi_A(n)]$ denotes the phase of $CI_{3x}(n_1,n_2)[A(n)]$, and (n_1,n_2) are taken from the non-redundant region of $CI_{3x}(n_1,n_2)$.

Concatenating the equations resulting from (13) and (14), two linear systems of equations can be solved, one for the magnitude $|A(k)|$, and one for the phase $\phi_A(k)$. Analogously to the asymptotically optimal approach of [15], quadratic matching and *weighted least-squares* solution of (13) and (14), appear to be feasible using the bispectral amplitude and phase variance expressions derived in [10]. Performance evaluation of the approach based on (13) and (14) remains to be tested.

VI. Simulation Results

Examples illustrating the model order selection algorithm described in Section IV, are shown in Figs. 1,2 and 3. The four more significant singular values of the 16×16 matrix $\hat{H}_{ri}$ are shown in Figs. 1 and 2, versus five different SNR levels of AWGN, with zero-mean and unit variance. Fig. 1, (Fig. 2) corresponds to the MP (NMP/spectrally equivalent) MA(2) model with coefficients [1, -0.17, 0.72], ([1, -0.2361, 1.3889]). The results shown are averages over 30 Monte Carlo experiments, each involving an 1024-point long data record segmented in 4 non-overlapping segments. Sample inverse correlation estimates were computed using the periodogram alternative of Section IIIa. As the SNR level raises from left to right (see Figs. 1,2), the gap between the 2nd and the 3rd singular

values becomes more pronounced, thus determining the correct order 2 as the estimated order.

The same conclusion can be drawn from Fig. 3, where the first four singular values of an ARMA(1,2) model are plotted. The AR and MA parameter vectors were [1,-0.17, 0.72], and [1, -0.5] respectively. Thirty Monte Carlo experiments are averaged here, each involving a 2048-point long data record, driven by WGN and segmented in 8 non-overlapping segments.

Tables I and II show the parameters of the models in Figs. 1 and 2, estimated using eq. (16). As expected, in the NMP MA model case, the autocorrelation-based method of eq. (10) yields estimated parameters of the spectrally equivalent model.

Results of the implementation of the algorithm described in Section V for parameter estimation, are shown in Tables III and IV. Table III (Table IV) corresponds to a causal (NC) AR(2) model with coefficients [1, -1.25, 0.375] ([1, -2.1333, 1.0667]). The values shown are averages over 50 Monte Carlo experiments, driven by an exponentially distributed noise process, each involving a 1024-point long data record, segmented in 4 non-overlapping segments. The last row of these tables includes the results of the asymptotically optimal WLS algorithm, initialized by the previously derived estimates. The expected improvement of the estimates towards the true values, is exhibited only in the NC AR case, though.

VII. Conclusions

Inverse higher- than- 2nd-order statistics were introduced here, and algorithms for both their estimation and application in the model identification problem were proposed and implemented. Further potential applications, as well as performance analysis, of inverse statistics in batch or recursive form are interesting future research topics.

REFERENCES

[1] F. Battaglia, "On the estimation of the inverse correlation function," *Journal of Time Ser. Anal.*, v. 9, pp. 1-10, 1988.

[2] R. J. Bhansali, "Autoregressive and window estimates of the inverse correlation function," *J. Time Ser. Anal*., pp. 137-162, 1983.

[3] D.R. Brillinger and M. Rosenblatt, "Computation and interpretation of kth-order spectra," in *Spectral Analysis of Time Series*, pp. 189-232, B. Harris, Ed., New York, Wiley, 1967.

[4] C. Chatfield, "Inverse correlations," *J. Roy. Statist. Ser. A*, pp. 363-377, 1979.

[5] W.S. Clevelant, "The inverse autocorrelations of a time-series and their applications," *Technometrics*, v. 14, pp. 277-293, 1972.

[6] G. B. Giannakis, "Signal reconstruction from multiple correlations: Frequency- and time-domain approaches," *Journal of the Optical Society of America*, May 1989.

[7] G. B. Giannakis, "Wavelet parameter and phase estimation using cumulant slices," *IEEE Trans. on Geosc. and Remote Sensing*, June 1989.

[8] G. B. Giannakis, and J. M. Mendel, "Identification of Non-Minimum Phase Systems using Higher-Order Statistics," *IEEE Trans. on ASSP*, v. 37, pp. 360-377, March 1989.

[9] G.B. Giannakis, and A. Swami, "On estimating non-causal ARMA non-Gaussian processes," *Proc. 4th ASSP Workshop on Spec. Est. & Model.*, pp. 187-192, Minneapolis, MN, August 1988.

[10] K.S. Lii and M. Rosenblatt, "Deconvolution and estimation of transfer function phase and coefficients for non-Gaussian linear processes," *Ann. Stat.*, pp. 1195-1208, 1982.

[11] T. Matsuoka and T.J. Ulrych, "Phase Estimation using the Bispectrum," *IEEE Proc.*, pp. 1403-1411, 1984.

[12] C. L. Nikias and Hsing-Hsing Chiang, "Non-causal autoregressive bispectrum estimation and deconvolution," *IEEE Trans. ASSP*, v. 36, pp. 1911-1913, 1988.

[13] C. L. Nikias and M. R. Raghuveer, "Bispectrum estimation: A digital signal processing framework," *Proc. of IEEE*, pp. 869-891, 1987.

[14] E. Parzen, "Some recent advances in time-series modeling," *IEEE Trans. on Auto. Control*, v. AC-19, pp. 723-730, 1974.

[15] B. Porat, and B. Friedlander, "Optimal estimates of MA and ARMA parameters of non-Gaussian processes from higher-order cumulants," *Proc. 4th ASSP Workshop on Spec. Est. & Model.*, pp. 208-212, Minneapolis, MN, August 1988.

[16] M. Priestley, "Spectral analysis and time series," *Academic Press*, London, 1981.

[17] T. Subba Rao, and M. M. Gabr, *An Introduction to Bispectal Analysis and Bilinear Time Series Models*, Lecture Notes in Statistics; Ed. D. Brillinger etal, Springer Verlag, 1984.

Table I

MP MA(2) Parameters (mean ± var)			
	b_0	b_1	b_2
True values	1	-0.1700	0.7200
Section IV alg.	1	-0.1708±0.0012	0.6982±0.0022

Table II

NMP MA(2) Parameters (mean ± var)			
	b_0	b_1	b_2
True values	1	-0.2361	1.3889
Section IV alg.	1	0.1748±0.0013	0.7043±0.0015

Table III

Causal AR(2) Parameters (mean ± var)			
		a_1	a_2
True values	1	1.2500	0.3750
Section V alg.	1	1.2539±0.0013	0.3625±0.0086
Opt. WLS	1	1.2537±0.1125	0.3571±0.0576

Table IV

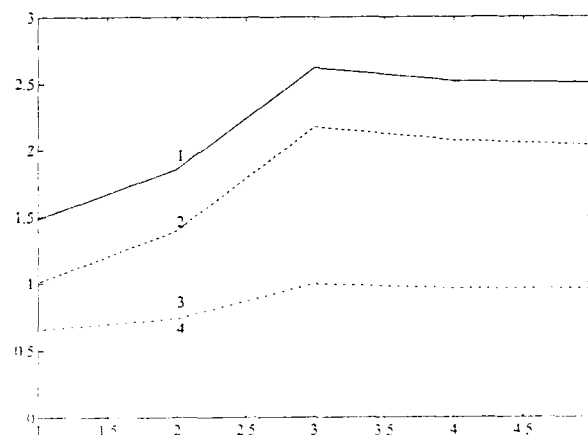| Non-Causal AR(2) Parameters (mean ± var)			
	a_0	a_1	a_2
True values	1	-2.3333	1.0667
Section V alg.	1	-2.4172±0.1719	1.0936±0.0150
Opt. WLS	1	-2.4028±0.1109	1.0810±0.0076
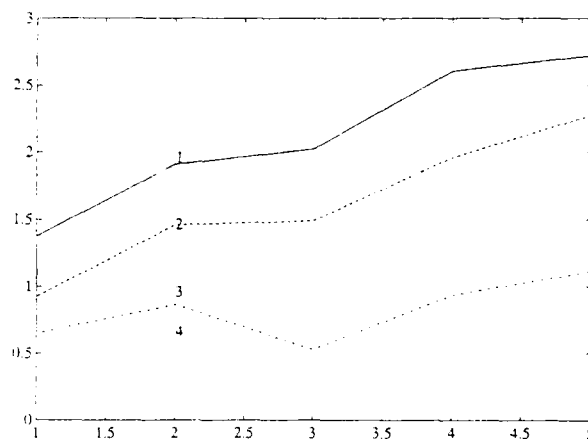
FIG 1: MA(2), SNR(db) of AWGN = 0,10,20,30,inf.

FIG 2: NMP-MA(2), SNR(db) of AWGN = 0,10,20,30,inf.

APPROACHES TO F.I.R. SYSTEM IDENTIFICATION WITH NOISY DATA
USING HIGHER-ORDER STATISTICS

Jitendra K. Tugnait

Exxon Production Research Company
P.O. Box 2189
Houston, TX 77252-2189

ABSTRACT

In this paper we address the problem of estimating the parameters of a *moving average* (MA) *model given the noisy observations of the system output*. The system is driven by an i.i.d. (independent and identically distributed) non-Gaussian sequence that is not observed. The noise is additive, i.i.d. and possibly non-Gaussian. We first briefly review the existing linear parametric approaches to this problem. Chief among these are: the linear least-squares solution due to Giannakis and Mendel (GM) (ICASSP 1987), the ARMA modeling approach due to Nikias (IEEE Trans. ASSP, April 1988), and the solution due to Giannakis (IEEE Proc., Sept. 1987). We observe that in the presence of the non-Gaussian measurement noise the Nikias' solution may be biased. In the presence of any measurement noise the GM approach yields biased solutions. Both the Nikias' and the Giannakis' solutions neglect the second-order statistics. The Giannakis' solution yields high-variance estimates, and is unstable under order mismatch. We focus on the GM approach and show that following their basic approach, several other useful linear relations may be obtained between the system parameters and the output statistics. Using these relations we modify the GM solution to obtain consistent parameter estimates in measurement noise. Finally, we investigate the direct, nonlinear least-squares solution to the simultaneous second- and higher-order cumulant matching problem. Simulations show that this approach yields the most accurate estimates.

I. INTRODUCTION

Consider the following finite impulse response (FIR) signal model

$$x(t) = \sum_{i=0}^{q} b(i) \, w(t-i) \qquad (1.1)$$

where the observations of the signal $x(t)$ are, in general, noisy:

$$y(t) = x(t) + v(t). \qquad (1.2)$$

In the above equations, the driving noise sequence $\{w(t)\}$ is not observed. Moreover, the sequence $\{w(t)\}$ is assumed to be i.i.d., non-Gaussian and zero-mean with its third cumulant nonzero. The measurement noise sequence $\{v(t)\}$ is also assumed to be i.i.d., possibly non-Gaussian, zero-mean and independent of $\{w(t)\}$. Let σ_w^2 and σ_v^2 denote the variances of $w(t)$ and $v(t)$, respectively. Also, let γ_{3w} and γ_{3v} denote the third cumulants of $w(t)$ and $v(t)$, respectively. The focus of this paper is the problem of recovering the coefficients $b(i)$'s given a sample function of the observations over N consecutive instants. This problem is of considerable interest in geophysical signal processing [12], digital communications [13], and astronomical signal processing [14].

In this paper we are concerned with the situation where the system (1.1) is allowed to be nonminimum phase. A vast majority of the literature deals with minimum phase systems only.

Approaches to the above problem of nonminimum phase FIR system identification may be divided into two broad categories: nonparametric and parametric. This paper is concerned with the parametric approaches. For some possible advantages of parametric approaches over the nonparametric solutions, we refer the reader to [11].

Within the class of parametric approaches, we have three broad classes, the distinguishing feature among them being the choice of the optimization criterion. All of the criteria involve (more or less) a least-squares error measure. The error definition differs, however, as follows:

(i) *Inverse filter error :* Filter $x(t)$ in (1.1) by an inverse filter (inverse of the MA(q) model) to obtain an estimate $\hat{w}(t)$ of $w(t)$ and then minimize some functional of $\hat{w}(t)$. The approaches of Donoho [15] and Benveniste et al. [13],[16] fall in this category. [The prediction error minimization criterion for minimum phase systems also belongs to this category.] The theory fails when data is noisy, i.e., when one works with $y(t)$ instead of $x(t)$. This class of solutions results in a nonlinear optimization problem, in general.

(ii) *Fitting error :* Match the model statistics to estimated statistics in a least-squares sense, as in [10] and [17] for example. This approach allows consideration of noisy observations. In general, it results in a nonlinear optimization problem.

(iii) *Equation error :* It is based on minimizing the "equation error" in some equation which is satisfied ideally. A common example is the Yule-Walker equations. The approaches of [3], [4], [11] and [20] fall in this category. In general, this class of approaches results in a linear solution.

The area of parametric modeling via cumulant statistics [18] has attracted considerable attention in the past few years; for a tutorial and two surveys see [1] and [8]-[9], respectively, where further references may be found. In this paper we concentrate on fitting error and equation error approaches to nonminimum phase FIR system identification. We review, analyze, extend and compare some of the existing approaches. We do not consider the inverse-filter-error-based approaches since they do not *explicitly* exploit the cumulant statistics. The main emphasis in this paper is on approaches that yield explicit estimates of the FIR system parameters, as for example in [3], [4] and [17]. The approaches of [11] and [20] lead to "implicit" parameter estimates, they do not directly estimate $b(i)$'s. Moreover, we do not also consider IIR (infinite impulse response) systems which are also of significant practical and theoretical interest.

II. EXPLICIT PARAMETER ESTIMATION VIA EQUATION ERROR FORMULATION

In this section we analyze the approaches of [2],[3],[4] and [14], and offer some extensions and generalizations. It is shown that the recursive version of the approach of [2]-[3] does not necessarily imply the consistency of their least-squares version, and more significantly, the least-squares version as formulated in [2]-[3] (and as further analyzed and recursified in [6] and [7]) leads to *biased* estimates in the presence of i.i.d. measurement noise. We show the various ways to augment the linear equations in the least-squares approach of [2],[3] to obtain *unbiased* parameter estimates. Finally, we show that the approach of Lohmann et al. [14] that has been mimicked in [4], can be derived via the generalizations/extensions discussed here.

II.A Fundamental Relations

For the system (1.1) we have

$$c_{1x}(\tau, \tau+m) := E\{x(t)x(t+\tau)x(t+\tau+m)\}$$

$$= \gamma_{3w} \sum_{k=0}^{q} b(k)b(k+\tau)b(k+\tau+m) = \gamma_{3w} \sum_{k=0}^{q} b(k)g(k+\tau;m) \quad (2.1)$$

where

$$g(k;m) = b(k)b(k+m), \quad (2.2)$$

$\gamma_{3w} := E\{w^3(k)\}$, and m is an integer constant. Let $G(z;m)$ denote the z-transform of the sequence $\{g(k;m)\}$, and let $C_{3x}(z;m)$ denote the z-transform of the third-order cumulant sequence $\{c_{3x}(\tau,\tau+m)\}$. Then it is easy to establish that

$$C_{3x}(z;m) = \gamma_{3w} B(z^{-1}) G(z;m) \quad (2.3)$$

$$G(z;m) := B(z) * [z^m B(z)] = \sum_{k=0}^{q} g(k;m) z^{-k}; \quad B(z) = \sum_{k=0}^{q} b(k) z^{-k}.$$

The autocorrelation function is given by

$$r_x(\tau) = E\{x(t)x(t+\tau)\} = \sigma_w^2 \sum_{k=0}^{q} b(k)b(k+\tau) \quad (2.4)$$

and its z-transform is

$$S_x(z) = \sigma_w^2 B(z) B(z^{-1}). \quad (2.5)$$

Using (2.3) and (2.5) with m=0, the following relationship (for m=0) was discovered in [2],[3]. Eliminate $B(z^{-1})$ from (2.3) and (2.5) to get

$$B(z^{-1}) = S_x(z)[\sigma_w^2 B(z)]^{-1} = C_{3x}(z;m)[\gamma_{3w}G(z;m)]^{-1}$$

$$=> G(z;m)S_x(z) = \varepsilon B(z)C_{3x}(z;m) \quad (2.6)$$

where $\varepsilon := \sigma_w^2 \gamma_{3w}^{-1}$. In the time-domain, for m=0 (2.6) becomes

$$\sum_{k=0}^{q} b^2(k) r_x(\tau-k) = \varepsilon \sum_{k=0}^{q} b(k) c_{3x}(\tau-k,\tau-k). \quad (2.7)$$

Clearly, there is no reason to restrict oneself to m=0 as has been done in [2],[3]. For m≠0, (2.6) becomes

$$\sum_{k=0}^{q} b(k)b(k+m) r_x(\tau-k) = \varepsilon \sum_{k=0}^{q} b(k)c_{3x}(\tau-k,\tau-k+m). \quad (2.8)$$

Without loss of any generality, we take (as in [2],[3]) b(0):=1. Then (2.8) has, when viewed as an equation linear in the unknown parameters, (q-m+1) unknowns b(k)b(k+m) and (q+1) unknowns εb(k).

Another basic set of recursions (not to be found in [2],[3]) results when we look at the interrelationships between two different 1-D cumulant slices. Consider (2.3) for two different values of m to obtain

$$\gamma_{3w} B(z^{-1}) = C_{3x}(z;m_0)[G(z;m_0)]^{-1} = C_{3x}(z;m_1)[G(z;m_1)] \quad (2.9)$$

from which it follows that ($m_0 \neq m_1$):

$$\sum_{k=0}^{q} g(k;m_1) c_{3x}(\tau-k,\tau-k+m_0) = \sum_{k=0}^{q} g(k;m_0) c_{3x}(\tau-k,\tau-k+m_1)$$

$$=> \sum_{k=0}^{q} b(k)b(k+m_1) c_{3x}(\tau-k,\tau-k+m_0)$$

$$= \sum_{k=0}^{q} b(k)b(k+m_0) c_{3x}(\tau-k,\tau-k+m_1). \quad (2.10)$$

Remark 2.1. As is seen by (1.2), one does not observe x(t) directly. Therefore, in (2.8) and (2.10), we have to replace $c_{3x}(\tau_1,\tau_2)$ and $r_x(\tau)$ by $c_{3y}(\tau_1,\tau_2)$ and $r_y(\tau)$, respectively. In the presence of the measurement noise, we have $r_x(\tau)=r_y(\tau)$ only for τ≠0, and $c_{3x}(\tau_1,\tau_2)=c_{3y}(\tau_1,\tau_2)$ only if $\tau_i \neq 0$ for at least either i=1 or i=2. [Note that $r_y(\tau)=r_x(\tau)+\sigma_v^2\delta(\tau)$ and $c_{3y}(\tau_1,\tau_2)=c_{3x}(\tau_1,\tau_2)+\gamma_{3v}\delta(\tau_1)\delta(\tau_2)$ where δ(τ) is the Kronecker delta.] This restriction must be honored for (2.8) and (2.10) to be valid when the statistics of {x(t)} are replaced with the statistics of {y(t)}. This, in turn, implies that (2.8) and (2.10) cannot be used for certain values of lags. □

Remark 2.2. In practice where only a sample sequence of the noisy data is available, we replace the "true" cumulants by their sample averages. It is easy to show that the sampled cumulants converge with probability one (w.p.1) to the true cumulants as N→∞. □

In the sequel, (2.8) and (2.10) will be used, for a variety of values of m, m_0 and m_1, to derive several *linear, consistent* parameter estimation algorithms.

II.B Alternative Derivations of the Algorithms of [4],[14]

A recursive method and then a least-squares version of it has been presented in [2] and [3] based on the relations (2.8) with m=0. Later a different closed-form solution was proposed in [4] based on entirely different arguments. It turns out that the results of [4] were already available in [14]. The approach of [4] mimics the approach of [14]. We now present two different derivations of the results of [4] and [14]: one based on (2.8) and the other based on (2.10). The point is that the relations (2.8) and (2.10) are "rich" enough to yield several interesting results. Use of (2.8) and (2.10) leads to a unified approach to the algorithms of [2]-[4] and [14].

It has been shown in [4] and [14] that

$$b(k) = c_{3x}(q,k)/c_{3x}(q,0), \quad k=0,1,\cdots,q. \quad (2.11)$$

To derive these relations via (2.8), consider (2.8) with τ=−q and let m take values in the interval [0,q]. Then we have from (2.8)

$$b(0)b(m)r_x(-q) = \varepsilon b(0)c_{3x}(-q,-q+m)$$

leading to

$$b(m) = \frac{\varepsilon c_{3x}(-q,-q+m)}{r_x(-q)} \quad (m=0,1,\cdots,q). \quad (2.12)$$

If we assume b(0)=1 (as in [4]), then $\varepsilon=r_x(-q)[c_{3x}(-q,-q)]^{-1}$. Substitute this value of ε in (2.12) to obtain

$$b(m) = \frac{c_{3x}(-q,-q+m)}{c_{3x}(-q,-q)} = \frac{c_{3x}(q,m)}{c_{3x}(q,0)}.$$

which is exactly as (2.11).

Now we derive (2.11) via (2.10). Take $m_0=0$, $m_1=m$ and τ=−q in (2.10) to obtain

$$b(0)b(m)c_{3x}(-q,-q) = b^2(0)c_{3x}(-q,-q+m)$$

leading to (b(0):=1)

$$b(m) = \frac{c_{3x}(-q,-q+m)}{c_{3x}(-q,-q)} = \frac{c_{3x}(q,m)}{c_{3x}(q,0)}$$

which is exactly as (2.11). Alternatively, set τ=2q in (2.10) to obtain

$$b(q)b(q+m_1)c_{3x}(q,q+m_0) = b(q)b(q+m_0)c_{3x}(q,q+m_1)$$

leading to

$$b(q+m_1)c_{3x}(-q,m_0) = b(q+m_0)c_{3x}(-q,m_1).$$

The above equation will yield (2.11) for appropriate selection of the values for m_0 and m_1.

In the presence of i.i.d. measurement noise, by Remark 2.1, (2.11) holds true when $c_{3x}(q,m)$ is replaced with $c_{3y}(q,m)$.

II.C An Algorithm based on Autocorrelations and c(q,k)

The relations (2.11) do not exploit the second-order statistics. We now present an algorithm that uses both $r_y(\tau)$ and $c_{3y}(q,\tau)$, 0≤τ≤q. In the presence of i.i.d. measurement noise, we exclude $r_y(0)$ and still obtain consistent solution. This algorithm is new. It is offered as an alternative to the approach of Section II.B when one wishes to use the second-order statistics also.

The basis of this algorithm is (2.8). Set m=q in (2.8) to obtain

$$b(0)b(q)r_x(\tau) = \varepsilon \sum_{k=0}^{q} b(k)c_{3x}(\tau-k,\tau-k+q).$$

With b(0):=1, we rewrite the above relations as

$$\sum_{k=1}^{q} b(k)c_{3x}(\tau-k,\tau-k+q) - \varepsilon' r_x(\tau) = -c_{3x}(\tau,\tau+q) \quad (2.13)$$

where $\varepsilon':=b(q)/\varepsilon$. We let −q≤τ≤q in (2.13) if v(t)≡0 in (1.2) else take −q≤τ≤−1 and 1≤τ≤q. We have q+1 unknowns b(1), b(2), ..., b(q), and ε', and 2q (or, 2q+1) equations. The solution can be obtained either in closed-form by utilizing q equations, or by least-squares by using all of the 2q equations.

Closed-Form Solution : Set τ=−q in (2.13) to obtain

$$-\varepsilon' r_x(-q) = -c_{3x}(-q,0) => \varepsilon' = \frac{c_{3x}(-q,0)}{r_x(q)}. \quad (2.14)$$

Next set $\tau=-q+1$ in (2.13) and use (2.14) to obtain

$$b(1)c_{3x}(-q,0) - \varepsilon' r_x(-q+1) = -c_{3x}(-q+1,1)$$

$$\Rightarrow \quad b(1) = [\varepsilon' r_x(-q+1) - c_{3x}(-q+1,1)]/c_{3x}(-q,0). \quad (2.15)$$

Continuing this way we can successively obtain $b(k)$ $(1 \le k \le q)$ by using the previously obtained $b(m)$ for $1 \le m \le k-1$ and ε', and (2.13) with $\tau=-q+k$. The solution so obtained is well-conditioned in that the only division done is done through $c_{3x}(-q,0)$ which is nonzero for an MA(q) model. Finally, we obtain $b(q)$ by use of (2.13) with $\tau=q$.

Least-Squares Solution : We can rewrite (2.13) in the matrix form as (for $-q \le \tau \le -1$ and $1 \le \tau \le q$)

$$\mathbf{A}\, \mathbf{b} = \mathbf{c} \quad (2.16)$$

where

$\mathbf{b} = [\ \varepsilon'\ b(1)\ b(2)\ \cdots\ b(q)\ ]^T = (q+1)$–column vector

$\mathbf{c} = [\ c_{3x}(-q,0)\ c_{3x}(-q,-1)\ \cdots\ c_{3x}(-q,-q+1)\ 0\ \cdots\ 0\ ]^T$

$\mathbf{A} = 2q \times (q+1)$ matrix appropriately defined.

The above equation yields a unique solution as can be seen by the earlier closed-form solution.

It is interesting to observe that the above least-squares solution utilizes the same slice of the third-order cumulants, namely, $c_{3x}(q,k)$ $(0 \le k \le q)$ (or, equivalently, $c_{3x}(-q,-q+k)$ $(0 \le k \le q)$) as that used by the algorithm of Section II.B. In addition, it also uses the autocorrelations $r_x(\tau)$ $(1 \le \tau \le q)$. Besides, we have redun¹ancy in that we have $q+1$ unknowns and $2q$ equations. Intuitively, use of extra information (second-order statistics) and of overdetermined set of equations should lead to more accurate parameter estimates compared to the approach of [4],[14].

It ought to be emphasized that the above approaches (Sections II.B and II.C) will work well only if one knows the exact value of q. If the true value of q is overestimated, then $c_{3x}(q,k) \equiv 0$ for $q > q_0$ (=true value) leading to totally erroneous estimates.

II.D. On the Approach of [2],[3]

An algorithm that has attracted considerable attention recently is now discussed. It has been proposed in [2],[3], and analyzed in [6] and recursified in [7]. This approach is based on utilizing the statistics $r_y(\tau)$ $(0 \le \tau \le q)$ and $c_{3y}(\tau,\tau)$ $(-q \le \tau \le q)$.

In [2],[3] a recursive, closed-form solution for parameter estimation for MA models has been presented by use of the autocorrelations and the "diagonal" third-order cumulant slice. We note that the closed-form solution as given in [2] does not always work in that it involves division by zero for some choices of the FIR models. Also, the approach does not extend to the 4th- (and higher-) order statistics. Subsequently in [2], the closed-form, recursive solution has been used to justify the consistency (uniqueness) of the solution to a least-squares version of the same problem. We show that the consistency of the closed-form solution does not necessarily imply consistency of the least-squares solution. We also show that the least-squares version will yield *biased* solution in the presence of the measurement noise whereas the recursive, closed-form solution is unbiased (whenever it yields unique solution).

As noted earlier, the basis of this algorithm is (2.8) with m=0 leading to

$$r_x(\tau) + \sum_{k=1}^{q} b^2(k) r_x(\tau-k) = \varepsilon\, c_{3x}(\tau,\tau) + \sum_{k=1}^{q} [\varepsilon b(k)] c_{3x}(\tau-k,\tau-k) \quad (2.17)$$

where we have used the fact that b(0):=1. In the least-squares version of [2],[3], (2.17) is parametrized with $2q+1$ unknowns: ε, $b^2(k)$ and $\varepsilon b(k)$ $(1 \le k \le q)$, and (2.17) is used with $-q \le \tau \le 2q$ ($3q+1$ equations). In contrast, the recursive closed-form solution parametrizes (2.17) with $q+1$ unknowns: ε and b(k) $(1 \le k \le q)$, and it also uses (2.4) in addition to (2.17). Therefore, it is difficult to see why the consistency of the closed-form version would imply the consistency of the least-squares version, as claimed in [2],[3].

Here is a counterexample in the support of the above assertion. Consider an MA(1) model:

$$q=1, \quad b(0) = 1 = b(1), \quad v(t) \equiv 0.$$

For this example, the least-squares approach to solving (2.17) fails. To see this, following [2],[3], we solve (2.17) for three variables ε, $b^2(1)$, and $\varepsilon b(1)$ using (2.17) for $-1 \le \tau \le 2$:

$$\begin{bmatrix} c_{3x}(-1,-1) & 0 & 0 \\ c_{3x}(0,0) & c_{3x}(-1,-1) & -r_x(1) \\ c_{3x}(1,1) & c_{3x}(0,0) & -r_x(0) \\ 0 & c_{3x}(1,1) & -r_x(1) \end{bmatrix} \begin{bmatrix} \varepsilon \\ \varepsilon b(1) \\ b^2(1) \end{bmatrix} = \begin{bmatrix} r_x(-1) \\ r_x(0) \\ r_x(1) \\ 0 \end{bmatrix} \quad (2.18)$$

Assume (without loss of any generality) that $\sigma_w^2 = \gamma_{3w} = 1$ so that true ε is 1. Then (2.18) becomes

$$\begin{bmatrix} 1 & 0 & 0 \\ 2 & 1 & -1 \\ 1 & 2 & -2 \\ 0 & 1 & -1 \end{bmatrix} \begin{bmatrix} \varepsilon \\ \varepsilon b(1) \\ b^2(1) \end{bmatrix} = \begin{bmatrix} 1 \\ 2 \\ 1 \\ 0 \end{bmatrix}. \quad (2.19)$$

Now it is easy to see that (2.19) does not have a unique solution since the rank of the matrix on the left side of (2.19) is two instead of three as claimed in [2],[3]. The solution to (2.19) is $\varepsilon=1$, and $\varepsilon b(1)=b^2(1)=$ arbitrary finite real number. The minimum-norm solution is $\varepsilon=1$ and $b(1)=0$ -- an inconsistent solution. On the other hand, it is straightforward to use the closed-form, recursive solution of [2] to obtain

$$\hat{\varepsilon} = \text{estimate of } \varepsilon = \frac{r_x(q)}{c_{3x}(-q)} = \frac{r_x(1)}{c_{3x}(-1)} = 1 = \text{true value of } \varepsilon,$$

$$\hat{b}(q) = \hat{b}(1) = \text{estimate of } b(1) = \frac{c_{3x}(1)}{c_{3x}(-1)} = 1 = \text{true value of } b(1).$$

In the following we will restrict ourselves to the least-squares version because that is what has been found to be practical (see [2], [3], [6] and [7], for example) compared to the recursive, closed-form solution which is numerically ill-conditioned.

We will now consider noisy observations. From (1.2), $r_y(\tau)=r_x(\tau)$ only if $\tau \ne 0$, in the presence of i.i.d. measurement noise. Returning to (2.17), it follows that we can use it only for $-q \le \tau \le -1$ and $q+1 \le \tau \le 2q$ since (2.17) involves $r_x(0)$ for $0 \le \tau \le q$. Therefore, in the noisy data case, we end up with 2q equations and $2q+1$ unknowns ! That is, we have an *underdetermined* system. This leads to inconsistency, contrary to the claims of [2] and [3].

In [3] several examples have been presented with Gaussian measurement noise. Presumably, they have been executed by replacing $r_x(\tau)$ with $r_y(\tau)$ in (2.17) and by using (2.17) for $-q \le \tau \le 2q$. We now consider an example to investigate the asymptotic bias introduced owing to the lack of availability of $r_x(0)$. We assume that the true statistics are available, i.e., N (record length) $\rightarrow \infty$.

Consider the system

$$x(k) = w(k) + 1.5w(k-1) - 0.75w(k-2) + 0.5w(k-3) \quad (2.20)$$

$$y(k) = x(k) + v(k)$$

Take $E\{w(k)\}=0$, $E\{w^2(k)\}=1$, and $E\{w^3(k)\}=2$ ($\{w(k)\}$ is one-sided exponential). Take $\{v(k)\}$ to be zero-mean, i.i.d. Gaussian. The true output statistics were computed by use of (2.1) and (2.4). The following solutions were obtained for different values of the signal-to-noise ratios (SNR) by use of the procedure of [2],[3]:

True Values: $\varepsilon = 0.500$, $b(1) = 1.500$, $b(2) = -0.750$, $b(3) = 0.500$

Estimates at SNR=∞ : $\hat{\varepsilon} = 0.500$, $\hat{b}(1) = 1.500$, $\hat{b}(2) = -0.750$, $\hat{b}(3) = 0.500$

Estimates at SNR=100 : $\hat{\varepsilon} = 0.505$, $\hat{b}(1) = 1.461$, $\hat{b}(2) = -0.732$, $\hat{b}(3) = 0.490$

Estimates at SNR=10 : $\hat{\varepsilon} = 0.541$. Estimates of b(i)'s "failed" because the estimate of $b^2(3)$ turned out to be negative (-0.010698).

[Recall that, in [3], $\hat{b}(i):=[\text{sign } \widehat{\varepsilon b(i)}/\hat{\varepsilon}]\, \{(\widehat{\varepsilon b(i)}/\hat{\varepsilon}) + \widehat{b^2(i)}\}^{0.5} .]$

Next we turn to the problem of "fixing" the algorithm of [2],[3] to obtain unbiased estimates.

II.E. Modifications to the Approach of [2],[3]

The basic premise here is that we wish to retain the use of (2.17) and still obtain consistent parameter estimates (under the assumption that the model order q is known). As discussed in Section II.D, after deletion of equations involving $r_y(0)$ and $c_{3y}(0,0)$ (see also Remark 2.1), one is left with 2q equations and $2q+1$ unknowns. Thus, we have to augment (2.17) with some additional set of equations. We now suggest a method; note that several are possible.

Consider (2.10) with $m_1=0$ and $m_0=q$ leading to

$$b(q)c_{3x}(\tau,\tau) - \sum_{i=1}^{q} b^2(i)c_{3x}(\tau-i,\tau-i+q) = c_{3x}(\tau,\tau+q). \qquad (2.21)$$

Consider (2.21) for $-q\leq\tau\leq-1$ and $1\leq\tau\leq q$ in conjunction with (2.17) for $-q\leq\tau\leq-1$ and $q+1\leq\tau\leq2q$. Then we have $4q$ equations and $2q+2$ unknowns: ε, $b^2(i)$, $\varepsilon b(i)$ ($1\leq i\leq q$), and $b(q)$. We can solve (2.21) and (2.17) recursively for the given lags without using the constraints $b^2(i)=(\varepsilon b(i)/\varepsilon)^2$, etc. For example, set $\tau=-q$ in (2.21) to obtain

$$b(q) = \frac{c_{3x}(-q,0)}{c_{3x}(-q,-q)} = \frac{c_{3y}(-q,0)}{c_{3y}(-q,-q)}. \qquad (2.22)$$

Next set $\tau=-q+1$ in (2.21) and use (2.22) to obtain

$$b^2(1)c_{3x}(-q,-q) = c_{3x}(-q+1,1) - b(q)c_{3x}(-q+1,-q+1)$$

$$\Rightarrow b^2(1) = [c_{3x}(-q+1,1) - b(q)c_{3x}(-q+1,-q+1)]/c_{3x}(-q,-q) (2.23)$$

Continuing this way we can successively obtain $b^2(i)$ ($1\leq i\leq q$) by using the previously obtained $b(q)$ and $b^2(m)$ ($1\leq m\leq i-1$). The solution so obtained is well-conditioned in that the only division done is done through $c_{3x}(-q,-q)$ which is nonzero for an MA(q) model. Next consider (2.17). Since $b^2(k)$ have been obtained by the above procedure, we can now recursively peel off ε and $\varepsilon b(k)$ by use of $\tau=-q,-q+1,\cdots$

The above recursive solution justifies the uniqueness of a least-squares solution to (2.21) and (2.17) with the lag values as stated earlier. As discussed in [2] and [3], one would prefer a least-squares formulation from a numerical viewpoint.

III. IMPLICIT PARAMETER ESTIMATION VIA EQUATION ERROR FORMULATION

In this section we take a brief look at the approaches of Nikias and his associates; see [1], [11], [20] and references therein. Their approaches involve ARMA or AR modeling of an FIR model. As is the case for the approaches discussed in Section II, the approaches of Nikias et al. yield closed-form "global" solution. Moreover, unlike [2]-[4], they make use of more than a single slice of the cumulants. On the other hand the second-order statistics are not used for parameter estimation. More importantly, the solution is not obtained in terms of the MA parameters ($b(i)$'s in (1.1)); rather one solves for the "autoregressive parameters" of an "(asymptotically) equivalent" noncausal AR model [20], or an "(asymptotically) equivalent" ARMA model [11]. This is clearly inefficient (non-parsimonious) if the main objective is to estimate the MA parameters, particularly if some of the system zeros are close to the unit circle. As we show below, in the presence of the non-Gaussian measurement noise, the approaches of Nikias et al. will yield biased estimates of the "implicit" parameters (i.e., the parameters of the ARMA/noncausal AR models).

Consider the noisy measurements as given by (1.2). In this case the equations (14) and (16) of [11] are not necessarily valid for the third-order cumulants of the noisy observations. As discussed in Remark 2.1, one must exclude the zero-lag cumulants in (14) and (16) of [11] for them to remain valid. Now if this is not done then we will obtain biased estimates since $c_{3x}(0,0)\neq c_{3y}(0,0)$. If we exclude all the equations (14) and (16) of [11] that involve these zero-lag cumulants then we may get an underdetermined system of equations (as in Section II.D). We show this by a simple example.

Let $q=1$ in (1.1) and let the single zero lie inside the unit circle. Then in the notation of [11] we have $L_1=1$ and $L_2=0$. Suppose that we take $p=10$ in [11,Eqn. (10)], i.e., we choose to model the MA(1) model by a stable ARMA(10,0) (i.e., AR(10)) model. The approach of [11] consists of estimating these AR parameters from the third-order cumulants of the observations. We rewrite [11,Eqn. (14)] as

$$\sum_{i=1}^{p} a_i c_{3x}(-\tau+i,-\rho+i) = -c_{3x}(-\tau,-\rho) \text{ for } \tau \text{ or } \rho > L_2 \qquad (3.1)$$

where a_i's are the desired AR parameters and $p=10$. The following approach has been suggested in [11]. Take the lag pairs (τ,ρ) for $\tau=L_2+k$ ($1\leq k\leq p$) and $\rho=\tau-j+1$ ($j=1,2,\cdots,L_1+L_2$). For the MA(1) model under consideration this reduces to $\tau=\rho=1,2,\cdots,10$. Now none of these values can be used in (3.1) without also using $c_{3y}(0,0)$! Thus we have a system of zero equations and ten unknowns if we desire to exclude the zero-lag cumulant.

The approach of [20] also suffers from the above deficiency since it follows the basic approach of [11] as applied to noncausal AR models.

Remark 3.1. In light of the above example, a closer examination of the approach of [11] reveals that it may be possible to fix the above problem. We suggest that in [11,Sect. III.A] one should take $i=1,2,\cdots,L_1+L_2+1$ in (16) instead of $i=1,2,\cdots,L_1+L_2$ as suggested in [11]. That is, we should also use an additional set of equations. In the noisy data case, take $i=2,3,\cdots,L_1+L_2+1$ in (16) which would exclude the zero-lag cumulants. Similar modification applies to [11,Eqn. (24)]. This modification when applied to the MA(1) model considered above, leads to the recursion

$$\sum_{i=1}^{p} a_i c_{3x}(-\tau+i,-\tau+1+i) = -c_{3x}(-\tau,-\tau+1) \text{ for } \tau=1,2,\cdots,p. \quad (3.2)$$

Now one can solve for a_i's, at least in principle. □

Since the ARMA/AR modeling of FIR models does not lead directly to the estimates of the MA parameters which is the objective of this paper, we will not further consider this class of approaches.

IV. PARAMETER ESTIMATION VIA FITTING ERROR FORMULATION

In this section we briefly review and analyze the approaches of [10] and [17]. The basic approach is to estimate the model parameters by matching (in a least squares sense) the estimated data statistics with the model statistics. The approaches considered in this section differ only in the set of statistics chosen for the purpose of nonlinear least squares matching.

The most general approach is that of [17] which we now outline. Define the ($q+4$)-vector θ of the unknown model parameters as

$$\theta := (b(1) \quad b(2) \quad \cdots \quad b(q) \quad \sigma_w^2 \quad \gamma_{3w} \quad \sigma_v^2 \quad \gamma_{3v}). \qquad (4.1)$$

Choose θ to minimize the cost

$$J_N(\theta) = J_{1N}(\theta) + \lambda J_{2N}(\theta) \qquad (4.2)$$

where $\lambda>0$ is scalar and

$$J_{1N}(\theta) = 0.5 \sum_{t=-q}^{0} [r_y(t|\theta) - \hat{r}_y(t)]^2 \qquad (4.3)$$

$$J_{2N}(\theta) = 0.5 \sum_{t_1=-q}^{0} \sum_{t_2=t_1}^{0} [c_{3y}(t_1,t_2|\theta) - \hat{c}_{3y}(t_1,t_2)]^2 \qquad (4.4)$$

$$r_y(t|\theta) = E\{y(k)y(k+t)|\theta\} \qquad (4.5)$$

$$\hat{r}_y(t) = (1/N) \sum_{k=-t+1}^{N} y(k)y(k+t) \quad (t\leq0) \qquad (4.6)$$

$$c_{3y}(t_1,t_2|\theta) = E\{y(k)(k+t_1)y(k+t_2)|\theta\} \qquad (4.7)$$

$$\hat{c}_{3y}(t_1,t_2) = (1/N) \sum_{k=N_1}^{N_2} y(k)y(k+t_1)y(k+t_2) \qquad (4.8)$$

$$N_1 = \max(1,-t_1,-t_2), \quad N_2 = \min(N,N+t_1,N+t_2). \qquad (4.9)$$

Note that $\hat{r}_y(t)$ and $\hat{c}_{3y}(t_1,t_2)$ are the sampled autocorrelation and third-order autocumulant functions, respectively, of the given observations $\{y(k), 1\leq k\leq N\}$.

The positive scalar λ acts as a weight that maintains a balance between the contributions of the second- and the third- order cumulants. We choose λ as follows

$$\lambda = \lambda_0 \left\{ \sum_{t=-q}^{0} [\hat{r}_y(t)]^2 \right\} \left\{ \sum_{t_1=-q}^{0} \sum_{t_2=t_1}^{0} [\hat{c}_{3y}(t_1,t_2)]^2 \right\}^{-1} \qquad (4.10)$$

with the "nominal" value of $\lambda_0=1$. The above choice is motivated by the desire to equally penalize errors in matching the estimated (sampled) correlation and cumulant functions, respectively. Note that the above choice also makes the relative matching errors invariant to any scaling of the data.

The cost function (4.2) was first proposed in [17] for ARMA model fitting following the approaches involving correlation matching (see references [28]-[30] in [17]). As was shown by means of a simulation example in [17], the cost function is also suitable for FIR model identification; (the analysis of [17] also goes through with some simple modifications.) Earlier, in [10], a different version of (4.2) had been proposed. In [10], it has been suggested that the unknown parameters $b(i)$'s ($1\leq i\leq q$) and γ_{3w} be selected to minimize

$$\sum_{t=-q}^{q} |\hat{c}_{3y}(t,t) - c_{3y}(t,t|\theta)|^2 \tag{4.11}$$

where θ is now a $(q+1)$-vector. The performance of this estimator has never been illustrated either through simulations or through analysis. Moreover, consistency of the resulting estimator has also not been shown. In contrast, the consistency of the parameter estimator resulting from criterion (4.2) is very easy to establish: for example, use the results of discussed in Section II.

In Section V we compare these two approaches via a simulation example after modifying (4.11) to include the measurement noise cumulant term. The optimization approach that was used for the results presented in Section V is the same as outlined in [17] (see also [19]).

Remark 4.1. We note that the two-step approach discussed in [10] and [17] will not work for noisy MA models. The two-step approach involves fitting a minimum-phase MA model in the first step. It is well-known that MA signal-plus-noise models are *not identifiable* from the second-order statistics. Therefore, the first-step fails for noisy models; hence, the two-step approach fails. This is in marked contrast to the cases of AR and (strictly proper) ARMA models where the first-step of the two-step approach always works [17]. □

V. SIMULATION EXAMPLE

Consider the following MA(5) signal-in-noise model:

$$x(t) = w(t) + 0.1\,w(t-1) - 1.87\,w(t-2) + 3.02\,w(t-3)$$
$$- 1.435\,w(t-4) + 0.49\,w(t-5) \tag{5.1}$$

$$y(t) = x(t) + v(t) \tag{5.2}$$

In terms of (1.1) we have $b(0)=1$, $b(1)=0.1$, $b(2)=-1.87$, $b(3)=3.02$, $b(4)=-1.435$ and $b(5)=0.49$. The sequences $\{w(t)\}$ and $\{v(t)\}$ consist of mutually independent, zero-mean, i.i.d. exponential random variables with $\sigma_w^2=1$. and $\gamma_{3w}=2.0$. The statistics of $v(t)$ were chosen to generate two sets of observations: one with the signal-to-noise ratio (SNR) of ∞ (i.e., $v(t)\equiv0$) and the other with SNR=10. ($\sigma_v^2=1.5927$ and $\gamma_{3v}=4.0199$).

We have compared the GM approach [2],[3] with the approach given in [4] and with the fitting error based approaches of [17] (criterion (4.2) with $\lambda_0=1$) and of Lii and Rosenblatt [10] (criterion (4.11)). Ten independent realizations of the signal were generated with record length of N=1024 for each realization. As stated earlier, two sets of observations were generated: to one set no observation noise was added, and to the other set exponential noise was added to yield an SNR=10.

Tables 1 and 2 show the results of our simulations. We show the arithmetic mean and one standard deviation of the parameter estimates averaged over 10 Monte Carlo runs for each approach. Table 1 depicts the results for SNR=∞ and Table 2 shows the results for SNR=10. The initial guesses for the fitting error based approaches were chosen as follows for each of the 10 runs:

$$\hat{b}(i) = 0. \quad (1\le i\le5), \quad \hat{b}(0)=1., \quad \hat{\sigma}_w^2 = \hat{\gamma}_{3w} = 1.0, \quad \hat{\sigma}_v^2 = \hat{\gamma}_{3v} = 0.1.$$

For the GM approach, we calculated the estimates as recommended in [2] and [3] unless we had $b^2(i)<0$, in which case we took $b(i)=\epsilon b(i)/\hat{\epsilon}$.

It is seen from the two tables that the approach of [17] outperforms that of [10]. This is intuitively not surprising since the criterion (4.2) uses all the relevant statistics whereas the criterion (4.11) does not use the second-order statistics and it also restricts itself to the 1-D "diagonal" cumulants $c_{3y}(t,t)$. The GM approach ([2],[3]) yields very high variance estimates. Note that the GM approach uses both the second-order statistics as well as the diagonal cumulants whereas [10] utilizes only the diagonal cumulants. Yet the approach based on the criterion (4.11) outperforms the GM by a very wide margin! Replacement of (2.1) (with m=0) and (2.4) with a single equation (2.8) (with m=0) has clearly resulted in a severe loss of accuracy.

VI. CONCLUSIONS

We have reviewed, analyzed, extended and compared certain approaches to explicit identification of the parameters of an FIR system given noisy observations of the system output. The simulation example presented in Section V suggests that the fitting error approach of [17] involving simultaneous matching of the second- and higher- order statistics of the data, yields the most accurate estimates. Unfortunately, it is also computationally the most demanding.

Although we dealt with only the third-order statistics, the material presented in this paper goes through for the fourth (and higher) order cumulants with "obvious" modifications.

We did not address the problem of system order selection which is of utmost importance for any practical application of the results of this paper. Standard methods that utilize only the second-order statistics may be used for system order selection; see, e.g., [11] and [17].

Finally, for large-order systems, an IIR system may provide a more parsimonious description of the observed series. For some existing approaches, see [1]-[3], [7]-[9], [17] and [21]-[25].

REFERENCES

[1] C.L. Nikias and M.R. Raghuveer, "Bispectrum estimation: A digital signal processing framework," *IEEE Proc.*, vol. 75, pp. 869-891, July 1987.

[2] G.B. Giannakis, "Signal processing via higher-order statistics," Ph.D. Dissertation, Dept. of Electrical Eng., Univ. of Southern California, July 1986.

[3] G.B. Giannakis, J.M. Mendel, and W. Wang, "ARMA modeling using cumulant and autocorrelation statistics," in *Proc. 1987 ICASSP*, pp. 61-64, Dallas, TX, April 1987. (Also in *IEEE Trans. ASSP*, March 1989.)

[4] G.B. Giannakis, "Cumulants: A powerful tool in signal processing," *Proc. IEEE (Lett.)*, vol. 75, pp. 1333-1334, Sept. 1987.

[5] J.K. Tugnait, "Comments on: 'Cumulants: A powerful tool in signal processing'," *Proc. IEEE (Lett.)*, vol. 77, 1989 (to appear).

[6] B. Porat and B. Friedlander, "Performance analysis of parameter estimation algorithms based on high-order moments," *Intern. J. Adaptive Control Signal Proc.* appear in 1989. (See also *Proc. 1988 ICASSP*, pp. 2412-2415, April 1988.)

[7] B. Friedlander and B. Porat, "Adaptive IIR algorithms based on high-order statistics," in *Proc. 21st Asilomar Conf. Circuits, Systems, Computers*, Pacific Grove, CA, Nov. 1987.

[8] J.M. Mendel, "Use of higher-order statistics in signal processing and system theory: A short perspective," presented at the *1987 MTNS Conf.*, Phoenix, AZ, June 15-19, 1987.

[9] J.M. Mendel, "Use of higher-order statistics in signal processing and system theory: An update," presented at *SPIE Conf. Advanced Algorithms Architectures for Signal Processing III*, San Diego, CA, Aug. 1988.

[10] K.S. Lii and M. Rosenblatt, "Deconvolution and estimation of transfer function phase and coefficients for nongaussian linear processes," *Annals of Statistics*, vol. 10, pp. 1195-1208, 1982.

[11] C.L. Nikias, "ARMA bispectrum approach to nonminimum phase system identification," *IEEE Trans. Acoustics, Speech, Signal Processing*, vol. ASSP-36, pp. 513-524, April 1988.

[12] D.G. Stone, "Wavelet estimation," *Proc. IEEE*, vol. 72, pp. 1394-1402, Oct. 1984.

[13] A. Benveniste and M. Goursat, "Blind equalizers," *IEEE Trans. Communications*, vol. COM-32, pp. 871-883, Aug. 1984.

[14] A.W. Lohmann, G. Weigelt and B. Wirnitzer, "Speckle masking in astronomy: Triple correlation theory and applications," *Applied Optics*, vol. 22, pp. 4028-4037, 1983.

[15] D. Donoho, "On minimum entropy deconvolution," in *Applied Time Series Analysis, II*, D.F. Findley, Ed. New York: Academic, 1981.

[16] A. Benveniste, M. Goursat, and G. Ruget, "Robust identification of a nonminimum phase system: Blind adjustment of linear equalizer in data communications," *IEEE Trans. Automatic Control*, vol. AC-25, pp. 385-398, June 1980.

[17] J.K. Tugnait, "Identification of linear stochastic systems via second-and fourth- order cumulant matching," *IEEE Trans. Information Theory*, vol. IT-33, pp. 393-407, May 1987.

[18] M. Rosenblatt, *Stationary sequences and random fields*. Boston, MA: Birkhäuser, 1985.

[19] J.E. Dennis, Jr. and R.B. Schnabel, *Numerical Methods for Unconstrained Optimization and Nonlinear Equations*. Englewood Cliffs, NJ: Prentice-Hall, Sect. 10.3, 1983.

[20] C.L. Nikias and H.-H. Chiang, "Higher-order spectrum estimation via noncausal autoregressive modeling and deconvolution," *IEEE Trans. Acoustics, Speech, Signal Processing*, vol. ASSP-36, pp. 1911-1913, Dec. 1988.

[21] J.K. Tugnait, "Identification of nonminimum phase linear stochastic systems," *Automatica*, vol. 22, pp. 457-464, July 1986.

[22] J.K. Tugnait, "Fitting noncausal autoregressive signal plus noise models to noisy non-Gaussian linear processes," *IEEE Trans. Automatic Control*. vol. AC-32, pp. 547-552, June 1987.

[23] J.K. Tugnait, "On selection of maximum cumulant lags for noncausal autoregressive model fitting," in *Proc. IEEE Intern. Conf. Acoustics, Speech, Signal Proc.*, pp. 2372-2375, New York, NY, April 11-14, 1988.

[24] J.K. Tugnait, "Recovering the poles from fourth-order cumulants of system output," in *Proc. 1988 American Control Conf.*, pp. 2090-2095, Atlanta, GA, June 1988.

[25] J.K. Tugnait, "Recovering the poles from third-order cumulants of system output," *IEEE Trans. Automatic Control*, vol. AC-34, scheduled to appear in Aug. 1989.

TABLE 1

Parameter Estimates : SNR = ∞ , b(0):=1, 10 Monte Carlo runs, N = 1024 = data length in each run.

Parameter Estimates					
parameter	true value	Approach of [17] mean (std. dev.)	Approach of [10] mean (std. dev.)	Approach of [3] mean (std. dev.)	Approach of [4] mean (std. dev.)
b(1)	0.1000	0.1150 (0.1060)	0.1758 (0.3030)	2.0552 (17.7030)	-1.3469 (2.1266)
b(2)	-1.8700	-1.9062 (0.3082)	-2.0303 (0.7337)	-7.3755 (26.7141)	2.1431 (4.0095)
b(3)	3.0200	3.0627 (0.4217)	3.2694 (0.8669)	10.9016 (29.4864)	-1.6281 (3.8538)
b(4)	-1.4350	-1.4709 (0.2679)	-1.5712 (0.7666)	-7.5998 (20.3394)	-2.1412 (5.6231)
b(5)	0.4900	0.4987 (0.1419)	0.5343 (0.3788)	2.4662 (5.7858)	2.104 (7.8522)
σ_w^2	1.0000	0.9449 (0.2490)			
γ_{3w}	2.0000	1.8266 (0.5521)	1.6472 (0.7290)		
σ_v^2	0.0000	0.2521 (0.2314)			
γ_{3v}	0.0000	-0.3060 (1.5887)	1.8773 (0.9586)		

TABLE 2

Parameter Estimates : SNR = 10., b(0):=1, 10 Monte Carlo runs, N = 1024 = data length in each run.

Parameter Estimates					
parameter	true value	Approach of [17] mean (std. dev.)	Approach of [10] mean (std. dev.)	Approach of [3] mean (std. dev.)	Approach of [4] mean (std. dev.)
b(1)	0.1000	0.1170 (0.1271)	0.2910 (0.5639)	10.4659 (81.1747)	1.0639 (4.486)
b(2)	-1.8700	-1.9774 (0.3934)	-2.2879 (1.4675)	-34.2444 (126.3142)	-1.0639 (4.4860)
b(3)	3.0200	3.1866 (0.5904)	3.9071 (1.7930)	34.9123 (118.3546)	-1.0831 (5.4915)
b(4)	-1.4350	-1.4956 (0.3456)	-1.7932 (1.5246)	-21.0983 (57.2785)	1.9312 (5.7471)
b(5)	0.4900	0.4772 (0.1651)	0.6025 (0.7262)	2.5711 (6.9135)	-0.7919 (2.0247)
σ_w^2	1.0000	0.9223 (0.3033)			
γ_{3w}	2.0000	1.7891 (0.7082)	1.5783 (0.9991)		
σ_v^2	1.5727	1.6310 (0.7356)			
γ	0.0000	3.5217 (1.8007)	1.6912 (1.0438)		

Multi-Window Bispectrum Estimates

David J. Thomson

AT&T Bell Laboratories
Murray Hill, New Jersey 07974

Abstract

In many applications where the use of higher-order spectra is desirable, use of conventional methods is hampered by lack of data or, equivalently, by the evolutionary nature of the process. Here we describe a multiple-window method for computing consistent estimates of the bispectrum from a short segment of the process. In multiple-window methods the information in a narrow band is summarized by the coefficients of its expansion in Slepian sequences (discrete prolate spheroidal sequences). Bispectrum estimates are then formed either by averaging what are effectively complex demodulates over time, or by averaging products of such expansions centered at frequencies f_1, f_2, and $-f_1 - f_2$ over a three-dimensional element of the frequency domain. Either choice reduces to a weighted average of products of the expansion coefficients.

1. Introduction

Higher-order spectra, or polyspectra, are used for the statistical characterization of stationary non-Gaussian stochastic processes, see *e.g.* Haubrich [1965] or Nikias & Raghuveer [1987]. Of these, the simplest is the bispectrum, which is a frequency domain expansion of the third moments of the process. In this paper we propose a non-parametric multiple-window estimate of bispectra.

We assume a stationary, discrete-time process with unit sampling time, and consequently a Cramér, or spectral, representation of the data

$$x(t) = \int_{-\frac{1}{2}}^{\frac{1}{2}} e^{i2\pi ft} \, dX(f)$$

with frequency, f, regarded as a continuous variable on $[-\frac{1}{2}, \frac{1}{2}]$ and extended periodically. The spectral density is defined to be

$$S(f_1) \, df_1 = E\{ \, dX(f_1) \, dX(f_2) \} \tag{1}$$

for $(f_1 + f_2) \bmod 1 = 0$ and zero otherwise. The spectrum, via the Wiener-Khintchine theorem, is a frequency-domain decomposition of the second moments of the process

$$E\{ x(t) x(t+\tau) \} = \int_{-\frac{1}{2}}^{\frac{1}{2}} e^{i2\pi f\tau} S(f) \, df$$

Similarly, the bispectrum is defined to be

$$B(f_1, f_2) df_1 \, df_2 = E\{ dX(f_1) dX(f_2) dX(f_3) \} \tag{2}$$

for $(f_1 + f_2 + f_3) \bmod 1 = 0$ and zero otherwise. In analogy with the Wiener-Khintchine theorem, the bispectrum is an expansion of the third moments

$$E\{x(t)x(t+\tau_1)x(t+\tau_2)\} = \int_{-\frac{1}{2}}^{\frac{1}{2}} \int_{-\frac{1}{2}}^{\frac{1}{2}} B(f_1, f_2)$$
$$e^{i2\pi(f_1\tau_1 + f_2\tau_2)} \, df_1 df_2 \ .$$

Unfortunately, while such analytic properties of polyspectra are well known and, as shown by Hasselmann *et.al.* [1963], are similar to second-order theory, statistical properties of estimates of polyspectra are not well understood and do not resemble those of the second-order theory. The fundamental problem is that the estimate mimicking (2) is *anticonsistent*, that is it's variance *increases* with sample size. Specifically, given a sample $\{x(0), \cdots, x(N-1)\}$ of N observations from a process with a "simple" spectrum and their discrete Fourier transform

$$y(f) = \sum_{n=0}^{N-1} x(n) \, e^{-i2\pi fn}$$

the estimation analog of (1), the *periodogram*,

$$P_1(f_1) = \frac{1}{N} y(f_1) y(f_2)$$

again for $(f_1 + f_2)$ mod $1 = 0$, is an asymptotically unbiased estimate of the spectrum. For $\{x_n\}$ Gaussian the variance of the periodogram, $1 \cdot S(f_1)S(f_2)$, is independent of the sample size N so the estimate is inconsistent.

Similarly, the analog of (2), the *biperiodogram*,

$$P_2(f_1, f_2) = \frac{1}{N} y(f_1)y(f_2)y(f_3)$$

again for $(f_1 + f_2 + f_3)$ mod $1 = 0$, is an asymptotically unbiased estimate of the bispectrum. For Gaussian data and distinct frequencies the variance of the biperiodogram is $N \cdot S(f_1)S(f_2)S(f_3)$, that is the variance is proportional to sample size, so the estimator is anticonsistent.

The property of anticonsistency in an estimator suggests that one should find a better estimator. Because the variance of the simple biperiodogram is proportional to sample size, an obvious approach is to divide the sample into J smaller subsamples of length L, estimate a biperiodogram on each subsample, and average the results. The variance of the average is then proportional to L / J. The disadvantage of this approach is that frequency resolution is also reduced from $1 / N$ to $1 / L$. "Subdivide and average" estimates of the bispectrum have traditionally been calculated by three related methods: weighted Fourier transforms of sample third moments, e.g. Rao and Gabr [1984]; frequency-domain averages, e.g. Lii, Rosenblatt, and Van Atta [1976]; and time averages of complex demodulates, e.g. Hinich and Clay [1968] or Godfrey [1965]; plus combinations of these. While these methods are asymptotically equivalent, their sample properties can be dramatically different as described by in Huber et al [1971]; "all the pitfalls known from ordinary spectrum analysis occur here too, some of them with new twists." As usual, these problems are more serious when only a short data record is available and are exacerbated if the spectrum has a large dynamic range or has a complicated frequency dependence. Moreover, estimates of higher moments are susceptibility to both outliers and legitimate extreme values. These are far more common, and serious, in the non-Gaussian data where polyspectral estimates are needed than they are with Gaussian processes. These effects, combined with a dirth of robust estimators for bispectra, may be responsible for the poor reputation of bispectra and the generally pessimistic conclusion in Brillinger [1965].

2. Multiple-Window Estimation of Bispectra

In the following we give two multiple window bispectrum estimates; the first is a time-average of products of complex demodulates, the second is an average over a cube in three-dimensional frequency space of products of the best local least-squares approximations to dX. In the former, the use of Slepian sequences allows one to generate a complex demodulate for the entire length of the series; it is consequently more efficient than filter forms whose output sequence is shorter than the length of the original series by the duration of the filter's impulse response. In the latter, the three-dimensional integral is done subject to the usual bispectrum requirement that the three frequencies sum to zero, so the integration reduces to two dimensions.

As above, we assume a sample $\{x(0), \cdots, x(N-1)\}$ with sample size N finite. We *choose* a frequency resolution W, $0 < W < \frac{1}{2}$ and assume that the spectrum and bispectrum do not depart significantly from linear functions of frequency over bandwidths of less than W, which typically is in the range $3/N$ to $20/N$. We also assume that the *first* moment of $dX(f)$ is zero or that the process contains no periodic components. We denote the number of expansion coefficients necessary to describe the information in a band $(f - W, f + W)$ by K with $K = \lfloor 2 N W \rfloor$. We use the notation of Slepian's [1978] paper in the following and refer to the nth equation of that paper as S[n]. Thus the kth discrete prolate spheroidal sequence, or *Slepian sequence*, defined in S[18] is $v_n^{(k)}(N, W)$. We define the corresponding wave function $V_k(f)$ by

$$V_k(f) = \sum_{n=0}^{N-1} v_n^{(k)}(N,W) \, e^{-i2\pi nf} \, , \qquad (3)$$

which is a complex version of S[10] with

$$V_k(f) = \frac{1}{\varepsilon_k} e^{-i2\pi f(\frac{N-1}{2})} U_k(-f) \, .$$

The Fourier transform (3) has two inverses:

$$v_n^{(j)}(N,W) = \frac{1}{\lambda_j} \int_{-W}^{W} V_j(\xi) \, e^{i2\pi\xi} \, d\xi \qquad (4)$$

following S[29], with the eigenvalues λ_k defined in S[18], and

$$v_n^{(j)}(N,W) = \int_{-\frac{1}{2}}^{\frac{1}{2}} V_j(\xi) \, e^{i2\pi\xi} \, d\xi \qquad (5)$$

as in S[28].

Multiple-window methods, Thomson [1982], isolate the energy in a band $(f - W, f + W)$ and express it as an orthogonal expansion of Slepian functions. As is well known, this has approximate dimensionality $K = 2NW$ and is the best possible L_2 approximation to the bandlimiting projection operator on the given time span. For a narrow band of width W about a frequency f we form an estimate of the *observable* part of the Cramér representation

$$d\hat{X}(f + v) = \sum_{k=0}^{K-1} \frac{1}{\lambda_k} \hat{x}_k(f) V_k(v) dv \qquad (6)$$

for $|v| < W$. The expansion coefficients $\hat{x}_k(f)$ are estimated by weighting the raw eigencoefficients

$$y_k(f) = \sum_{n=0}^{N-1} e^{-i2\pi f n} v_n^{(k)}(N, W) x(n) \qquad (7)$$

for $k = 0, 1, \cdots, K - 1$ as described in Thomson [1982], that is $\hat{x}_k(f) = d_k(f) y_k(f)$. As will be seen in the following, obtaining low variance bispectrum estimates requires that large time-bandwidth products be used. Consequently, the eigenvalues and weights are both nearly 1 so differences between the x_k's and y_k's can be safely ignored, as can terms in $1 - \lambda_k$. The time series corresponding to (6), the "complex demodulate," is

$$x(f;t) = e^{i2\pi f t} \int_{-W}^{W} e^{i2\pi v t} d\hat{X}(f + v)$$

or

$$= e^{i2\pi f t} \sum_{k=0}^{K-1} \hat{x}_k(f) v_t^{(k)}(N, W). \qquad (8)$$

"Time Average" Multiple-Window Estimates

Consider estimating the bispectrum by averaging products of the complex demodulates (8) over time

$$\hat{B}(f_1, f_2) = \frac{1}{\gamma} \sum_{n=0}^{N-1} x(f_1;n) x(f_2;n) x(f_3;n)$$

where, as usual, $(f_1 + f_2 + f_3) \bmod 1 = 0$, and γ is a normalizing constant defined below in (12). Using representation (8) for the complex demodulates, this becomes

$$\hat{B}(f_1, f_2) = \frac{1}{\gamma} \sum_{j,k,l=0}^{K-1} \hat{x}_j(f_1) \hat{x}_k(f_2)$$

$$\hat{x}_l(f_3) P(j,k,l) \qquad (9)$$

where

$$P(j,k,l) = \sum_{n=0}^{N-1} v_n^{(j)}(N,W) v_n^{(k)}(N,W) v_n^{(l)}(N,W)$$

Integral representations for P are in the appendix, and some statistics of the estimate (9) are derived below.

"Frequency Average" Estimates

Taking the inverse estimate of the orthogonal increment process (6) in the three bands and integrating over a volume element concentrated on $|\eta_j| < W$, another estimate of the bispectrum is

$$\hat{B}_f(f_1, f_2) = \int_{-W}^{W} \int_{-W}^{W} \int_{-W}^{W} d\hat{X}(f_1 + \eta_1) d\hat{X}(f_2 + \eta_2)$$

$$d\hat{X}(f_3 + \eta_3) C(\eta_1, \eta_2, \eta_3) \qquad (10)$$

where C is a symmetric weight function of its three arguments. Substituting (6) in (10), and interchanging orders of integration and summation, this estimate may be written in the same form as (9), that is as a triple sum of the eigencoefficients times the integral of a weighted product of the three Slepian functions. Taking uniform weighting throughout the volume and integrating subject to the constraint $(eta_1 + \eta_2 + \eta_3) \bmod 1 = 0$ shows the latter, via the appendix, to be equivalent to (9).

Standardization and Variance

To find the expected value of these estimates it is useful to write (7) as

$$y_j(f) = \int_{-\frac{1}{2}}^{\frac{1}{2}} V_j(\xi) \, dX(f - \xi) \tag{11}$$

Substituting (11) in (9) gives

$$\hat{B}(f_1, f_2) = \frac{1}{\gamma} \sum_{j,k,l=0}^{K-1} P(j,k,l) \int_{-\frac{1}{2}}^{\frac{1}{2}} \int_{-\frac{1}{2}}^{\frac{1}{2}} \int_{-\frac{1}{2}}^{\frac{1}{2}} V_j(\xi_1) V_k(\xi_2)$$

$$\overline{V_l(\xi_3)} \, dX(f_1 - \xi_1) \, dX(f_2 - \xi_2) \overline{dX(f_1 + f_2 - \xi_3)}$$

The expected value of the product of the three dX's is, by the definition of the bispectrum (2),

$$B(f_1 - \xi_1, f_2 - \xi_2) \, \delta(\xi_1 + \xi_2 - \xi_3) \, d^3\xi$$

so

$$E\{\hat{B}(f_1, f_2)\} = \frac{1}{\gamma} \sum_{j,k,l=0}^{K-1} P(j,k,l) \int_{-\frac{1}{2}}^{\frac{1}{2}} \int_{-\frac{1}{2}}^{\frac{1}{2}} V_j(\xi_1)$$

$$V_k(\xi_2) \overline{V_l(\xi_1 + \xi_2)} B(f_1 - \xi_1, f_2 - \xi_2) d\xi^2$$

If, as assumed, the bispectrum varies slowly within the bandwidth W, the integral becomes $B(f_1, f_2)$ times

$$\int_{-\frac{1}{2}}^{\frac{1}{2}} \int_{-\frac{1}{2}}^{\frac{1}{2}} V_j(\xi_1) V_k(\xi_2) \overline{V_l(\xi_1 + \xi_2)} \, d\xi_1 \, d\xi_2 \, ,$$

the integral representation (A7) for P. Defining

$$\gamma = \sum_{j,k,l=0}^{K-1} P^2(j,k,l) \tag{12}$$

gives $E\{\hat{B}(f_1, f_2)\} \approx B(f_1, f_2)$ so the estimate is approximately unbiased.

The variance of (9) for Gaussian data and distinct frequencies, using (1), is approximately

$$\mathbf{E_G}\{|\hat{B}(f_1, f_2)|^2\} = \gamma^{-2} S(f_1) S(f_2) S(f_3) \cdot \tag{13}$$

$$\left\{ \sum_{n,m=0}^{N-1} \left[\sum_{j=0}^{K-1} v_n^{(j)} v_m^{(j)} \right]^3 \right\}$$

if the spectrum varies slowly within a bandwidth W of the three frequencies. Noting that the terms in brackets { } of (12) sum to γ gives

$$\mathbf{E_G}\{|\hat{B}(f_1, f_2)|^2\} \approx \frac{1}{\gamma} S(f_1) S(f_2) S(f_3) \, .$$

Approximating the inner sum in (13) by Mercer's theorem, rotating coordinates, and crudely approximating the outer sums by integrals, one obtains

$$\mathbf{E_G}\{|\hat{B}(f_1, f_2)|^2\} \approx \frac{1}{3NW^2} S(f_1) S(f_2) S(f_3) \tag{14}$$

so, for fixed W, the estimate is consistent.

Even though (9) is an unbiased consistent estimator of the bispectrum, the W^2 term in the denominator of (14) may cause the variance to be very large. Moreover, because the bispectrum of Gaussian processes is identically zero, it is unreasonable to expect a variance as small as predicted by (14) in cases where the bispectrum is of interest; further, the estimates should be expected to have a "long tailed" distribution, and consequently robust estimation procedures are essential. These may be constructed from the consistent estimators given here, by, for example, using M estimates on the results from overlapping subsections.

Appendix: Integral Representations of $P(j,k,l)$

Beginning with the basic definition of the P coefficient

$$P(j,k,l) = \sum_{n=0}^{N-1} v_n^{(j)}(N,W)\, v_n^{(k)}(N,W)\, v_n^{(l)}(N,W)$$

one may use either of the representations (4) or (5) for each of the three Slepian sequences. Using (4) gives

$$P(j,k,l) = \frac{1}{\lambda_j \lambda_k \lambda_l} \int_{-W}^{W}\int_{-W}^{W}\int_{-W}^{W} V_j(\xi_1) V_k(\xi_2)$$

$$V_l(\xi_3)\, K_N(-(\xi_1+\xi_2+\xi_3))\, d\xi^3$$

where the kernel K_N is the sum of exponentials

$$K_N(-(\xi_1+\xi_2+\xi_3)) = \sum_{n=0}^{N-1} e^{i2\pi n(\xi_1+\xi_2+\xi_3)}$$

Again there is a choice of which integration to do first; we choose that over ξ_3. Recalling the basic integral equation of the Slepian functions,

$$\lambda_k V_k(f) = \int_{-W}^{W} K_N(f-v)\, V_k(v)\, dv$$

one obtains

$$P(j,k,l) = \int_{-W}^{W}\int_{-W}^{W} \frac{V_j(\xi_1)}{\lambda_j} \frac{V_k(\xi_2)}{\lambda_k} \overline{V_l(\xi_1+\xi_2)}\, d\xi^2$$

where we have used the fact that $V_l(-\xi) = \overline{V_l(\xi)}$. With integrals over $[-\tfrac{1}{2}, \tfrac{1}{2})$ one uses the identity

$$V_k(f) = \int_{-\frac{1}{2}}^{\frac{1}{2}} K_N(f-v)\, V_k(v)\, dv$$

in place of the integral equation to obtain

$$P(j,k,l) = \int_{-\frac{1}{2}}^{\frac{1}{2}}\int_{-\frac{1}{2}}^{\frac{1}{2}} V_j(\xi_1) V_k(\xi_2) \overline{V_l(\xi_1+\xi_2)}\, d\xi^2 .$$

Using (4) and (5) together gives a third form. Note that if $j + k + l$ is odd P is zero by symmetry and also that $P(j,k,l)$ is symmetric in its arguments. Thus there are 6 combinations for j, k, and l distinct, and 3 if two are equal. Consequently it is only necessary to compute P for $0 \le j < K$, $j \le k < K$, and $k \le l < K$ so, for example, with $K = 10$ only 110 distinct terms of the 1000 are needed.

References

Brillinger, D.R., [1965] *An Introduction to Polyspectra*, Ann. Math. Statist. **36**, pp 1351-74.

Godfrey, M.D. [1965], *An Exploratory Study of the Bi-Spectrum of Economic Time Series*, Appl. Statist. **14**, pp 48-69.

Hasselmann, K., W. Munk, and G. MacDonald, *Bispectra of Ocean Waves*, pp 125-39 of **Time Series Analysis**, M. Rosenblatt, Ed., J. Wiley & Sons, 1963.

Haubrich, R.A. [1965], *Earth Noise, 5 to 500 Millicycles per Second, 1: Spectral Stationarity, Normality, and Nonlinearity*, J. Geophys. Res. **70**, pp 1415-27.

Hinich, M.J. and C.S. Clay [1968], *The Application of the Discrete Fourier Transform in the Estimation of Power Spectra, Coherence, and Bispectra of Geophysical Data*, Rev. of Geophysics **6**, pp 347-63.

Huber, P.J., B. Kleiner, T. Gasser, and G. Dumermuth [1971], *Statistical Methods for Investigating Phase Relations in Stationary Stochastic Processes*, IEEE Trans. on Audio and Electroacoustics **AU-19**, pp 78-86.

Nikias, C.L. & M.R.Raghuveer [1987], *Bispectrum Estimation: A Digital Signal Processing Framework*, Proc. IEEE **75**, pp 869-91.

Lii, K.S., M. Rosenblatt, and C. Van Atta, *Bispectral measurements in turbulence*, J. Fluid Mech., vol 77, part I, pp 45-62, 1976.

Rao, T.S. & M.M. Gabr [1984], **An Introduction to Bispectral Analysis and Bilinear Time Series Models**, Springer-Verlag, New York.

Slepian, D. [1978] *Prolate Spheroidal Wave Functions, Fourier Analysis, and Uncertainty- V: The Discrete Case*, Bell System Tech. J., vol **57**, pp 1371-1430.

Thomson, D.J. [1982] *Spectrum Estimation and Harmonic Analysis*, Proc. IEEE, vol **70**, pp 1055-96.

A COMPOSITE LINEAR MODEL GENERATING A STATIONARY STOCHASTIC PROCESS WITH GIVEN BISPECTRUM

Fuminori Sakaguchi[*]   and   Hideaki Sakai[**]

* Faculty of Humanities and Social Sciences,
  Mie University, Tsu 514, Japan

**Department of Applied Mathematics and Physics,
  Faculty of Engineering, Kyoto University, Kyoto 606, Japan

ABSTRACT

A composite linear model is proposed, which converts from non-Gaussian i.i.d. processes into a non-Gaussian stationary stochastic processes with given third-order cumulant spectrum and with white power spectrum. The design for the model is based on the fact that a type of finite-impulse-response linear system with non-Gaussian i.i.d. input process makes an output process whose third order autocorrelations exist only for special time lags. Arbitrary third order autocorrelation function can be obtained by some superposition of independent output processes of this type. Results of numerical experiments confirm this fact. This model requires at most $2L^2+4L+1$ input i.i.d. processes independent of one another, for the third order autocorrelation function with the largest time lag L. With sufficient large L, a process with desired bispectrum can be made by this model.

INTRODUCTION

There are various phenomena whose time evolutions can not be modelled as Gaussian processes, and the study for non-Gaussian processes is important. The third order statistics are often treated for analyses on non-Gaussian stationary stochastic processes ([1] - [8] and many other papers). Some works treated only the third order moment or the third order cumulant of the stochastic variable on a single time instant ([9] etc.). Other works investigated the third order statistics for dynamic characteristics of stochastic processes, such as the third order autocorrelation function, the third order cumulant function (for three time instants) and the bispectrum. These statistics are easily translated from one to another.

In these works, some kind of models generating non-Gaussian processes has been used. The lineae model which assumes a linear system with a non-Gaussian i.i.d. input process, has been frequently used ([4],[5], [10] - [13] etc.) This model is a direct extension of the Gaussian linear model which generates a stochastic process with given power spectrum from an i.i.d. process. It is very simple and convenient, and many tools for Gaussian case is directly applicable there. Moreover, the analysis of the third order statistics is an analogous one to the second order statistics for the linear model. However, the bispectrum of this model is in a form of triple product of the transfer function of the linear system [3], [6] , which is of a very restricted class. In general, the variety of bispectra is greater, and more general model are required. Several non-linear models have been tried. Subba Rao [14] and Gabr [15] investigatedthe bispectra of the processes made by a cretain bilinear model. Mao & Lin [16] and Toda & Usui [17] did non-linear autoregressive models. Earlier, Brillinger ([3], pp.40-41) derived a general expression for the bispectrum of the processes generated by the Volterra functional expansion model, though it is too complicated to solve the inverse problem which find out appropriate parameters for a prescribed bispectrum. As another trial, the authors studied for Markovian-switched two Gaussian processes, but this model produced only a very special type of bispectra.
Here we consider the problem whether there exists any simple model which produces stationary processes with arbitrary bispectrum or not. In general, nonlinear models have a grater possibility for making wider class of processes. However, they often make the problem much complicated, and the inverse problem from given third order statistics to parameters seems to be hardly solvable. In this study, we try to seek one of its solution in a class of composite linear models. A certain linear system with an non-Gaussian i.i.d. input process makes an output stationary process whose third order cumulant vanishes except for special combinations of two time lags. This fact enables us to construct a composite linear model which produces arbitrary bispectrum, by a superpositions of many independent such output processes.

In the following sections, the contruction of the composite linear model is explained. It is also shown that the processes made by this model are not distingished from white noises only by their power spectrum. Finally, some results of numerical experiments are given.

Some precise and comprehensive reviews for the higher order statistics of stationary processes have been made in [1] – [3] and [18,pp.210-226]. Here we mention only some necessities about the third order ones very briefly.

Let $\{x_t\}$ be a stationary discrete-time stochastic process. The third order autocorrelation function (or moment function) and the third order cumulant function are defined as

$$R_3(\tau_1,\tau_2) \triangleq E\left[x_t\, x_{t+\tau_1}\, x_{t+\tau_2} \right] \qquad , \qquad r_3(\tau_1,\tau_2) \triangleq \text{cum}(\, x_t,\, x_{t+\tau_1},\, x_{t+\tau_2}\,) \qquad (1,2)$$

respectively. Because of the stationarity, both are not dependent on t, but only on two time lags τ_1, τ_2.

If $E\{x_t\}=0$, then they are identical to each other. For simplicity, in the following sections we will consider only such cases, so that we need not distinguish one from the other. From the definition, they have the following symmetry. (Similarly for the cumulant function (2).)

$$R_3(\tau_1,\tau_2) = R_3(\tau_2-\tau_1,-\tau_1) = R_3(-\tau_2,\tau_1-\tau_2) = R_3(\tau_2,\tau_1) = R_3(\tau_1-\tau_2,-\tau_2) = R_3(-\tau_1,\tau_2-\tau_1) \qquad (3)$$

The symmetry shows that the third order autocorrelation function is completely specified by the values only on the octant plane such that $0\le\tau_1\le\tau_2$. When the third order autocorrelations exist only within a finite region of time lags where the largest absolute value of time lag is L, then it is shown from the symmetry that it vanishes at least outside the hexagon configulated by the six lines

$$\tau_1=\pm L, \quad \tau_2=\pm L, \quad \tau_2-\tau_1=\pm L \quad . \qquad (4)$$

When the third order cumulant function (2) satisfy some conditions ([1],[2]), its discrete- time Fourier transform exists and is called bispectrum.

$$f_3(\omega_1,\omega_2) \triangleq \sum_{\tau_1=-\infty}^{\infty} \sum_{\tau_2=-\infty}^{\infty} r_3(\tau_1,\tau_2)\, e^{-j\omega_1\tau_1-j\omega_2\tau_2} \qquad (\, j^2=-1\,) \qquad (5)$$

It is 2π-periodic both for ω_1 and ω_2, and it has the following symmetry.

$$f_3(\omega_1,\omega_2) = f_3(\omega_2,-\omega_1-\omega_2) = f_3(-\omega_1-\omega_2,\omega_1) = f_3(\omega_2,\omega_1) = f_3(\omega_1,-\omega_1-\omega_2) = f_3(-\omega_1-\omega_2,\omega_2) \qquad (6)$$

When a linear system is treated, the bispectra have the following convenient relation. Let $f_3^i(\omega_1,\omega_2)$ be the bispectrum of the input, $f_3^o(\omega_1,\omega_2)$ be that of the output and $H(\omega)$ be the transfer function of the linear system, then

$$f_3^o(\omega_1,\omega_2) = H(\omega_1)\, H(\omega_2)\, H(\omega_3)\, f_3^i(\omega_1,\omega_2) \qquad \text{where } \omega_3 \triangleq -\omega_1-\omega_2 \qquad (7,8)$$

BASIC LINEAR SYSTEMS USED IN THE MODEL

Now we introduce two types of linear systems $H^{(+,d)}$ and $H^{(-,d)}$, whose impulse responses are

$$h_t^{(+,d)} = \begin{cases} 1 & (\text{if } t=0 \text{ or } t=d) \\ 0 & (\text{otherwise}) \end{cases} \qquad , \qquad h_t^{(-,d)} = \begin{cases} 1 & (\text{if } t=0) \\ -1 & (\text{if } t=d) \\ 0 & (\text{otherwise}) \end{cases} \qquad (9,10)$$

Their transfer functions are

$$H^{(+,d)}(\omega) = 1 + z^d \qquad , \qquad H^{(-,d)}(\omega) = 1 - z^d \qquad (11,12)$$

respectively, where $z \triangleq \exp(-j\omega)$. $\qquad (13)$

Here we consider the cases where the input of these linear systems are non-Gaussian i.i.d. processes. Let $\{\varepsilon_t\}$ be an i.i.d. process with $E\{\varepsilon_t\}=0$, $E\{\varepsilon_t^2\}=\sigma^2$ and $E\{\varepsilon_t^3\}=\kappa_3$, then its bispectrum is a constant, i.e.

$$\frac{\kappa_3}{2\pi} \triangleq \gamma_0 \qquad (14)$$

Then, the trispectrum of the output of the system $H^{(+,d)}$ with the input $\{\varepsilon_t\}$ is

$$f_3^{(+,d)}(\omega_1,\omega_2) = H^{(+,d)}(\omega_1)\, H^{(+,d)}(\omega_2)\, H^{(+,d)}(\omega_3) = 2\gamma_0 \left[1 + \cos d\omega_1 + \cos d\omega_2 + \cos d\omega_3 \right] \qquad (15)$$

where ω_3 has been defined in (8). Similarly, the system $H^{(-,d)}$ with the input $\{\varepsilon_t\}$ makes an output whose bispectrum is

$$f_3^{(-,d)}(\omega_1,\omega_2) = H^{(-,d)}(\omega_1)\, H^{(-,d)}(\omega_2)\, H^{(-,d)}(\omega_3) = -2j\gamma_0 \left[\sin d\omega_1 + \sin d\omega_2 + \sin d\omega_3 \right] \qquad . \qquad (16)$$

These systems with independent i.i.d. input processes now are combined as follows(with '*' denoting the convolution operatitor);

$$y_t^{(r,s)} = h_t^{(+,r)} * h_t^{(+,s)} * u_t^{(+,r,+,s)} - h_t^{(+,r)} * h_t^{(-,s)} * u_t^{(+,r,-,s)}$$
$$- h_t^{(-,r)} * h_t^{(+,s)} * u_t^{(-,r,+,s)} + h_t^{(-,r)} * h_t^{(-,s)} * u_t^{(-,r,-,s)} \qquad (17)$$

$$z_t^{(d)} = h_t^{(+,d)} * v_t^{(+,d)} - h_t^{(-,d)} * v_t^{(-,d)} \qquad (18)$$

where $\{u_t^{(+,r,+,s)}\}$, $\{u_t^{(+,r,+,s)}\}$, $\{u_t^{(-,r,+,s)}\}$, $\{u_t^{(-,r,-,s)}\}$ (r,s:integers, respectively) , $\{v_t^{(+,d)}\}$, and $\{v_t^{(-,d)}\}$ (d:integer, respectively) are non-Gaussian i.i.d. processes independent of one another and have the common mean 0, common variance σ^2 and the common third order cumulant $\mathbf{K}_3$. The bispectrum of the outputs of these combined 'units' are the following. For $\{v_t^{(r,s)}\}$

$$f_3^{y(r,s)}(\omega_1,\omega_2) = 4Q \left[\sum_{m=1}^{3} \sum_{n=1}^{3} z_m^r z_n^s + \sum_{m=1}^{3} (z_m^r + z_m^s) + 1 \right] \qquad (19)$$

and for $z_t^{(d)}$

$$f_3^{z(d)}(\omega_1,\omega_2) = 2Q \left[\sum_{m=1}^{3} z_m^d + 1 \right] \qquad (20)$$

where

$$z_1 \triangleq \exp(-j\omega_1) \; , \qquad z_2 \triangleq \exp(-j\omega_2) \; , \qquad z_3 \triangleq \exp(j\omega_1+j\omega_2) \; . \qquad (21,22,23)$$

The inverse discrete time Fourier transforms of (19) and (20) become the third order autocorrelation function of the output processes if these 'units'. When any of r, s and d is not zero, we have

$$R_3^{y(r,s)}(\tau_1,\tau_2) = \begin{cases} 8\mathbf{K}_3 & (\text{ if } r=s \text{ and } (\tau_1,\tau_2) \in S_{1a}(r) \;) \\ 4\mathbf{K}_3 & (\text{ if } r=s \text{ and } (\tau_1,\tau_2) \in S_{1b}(r) \;) \\ 4\mathbf{K}_3 & (\text{ if } r \neq s \text{ and } (\tau_1,\tau_2) \in S_2(r,s) \;) \\ 0 & (\text{ otherwise }) \end{cases} \qquad (24)$$

$$R_3^{z(d)}(\tau_1,\tau_2) = \begin{cases} 2\mathbf{K}_3 & (\text{ if } (\tau_1,\tau_2) \in S_3(d) \;) \\ 0 & (\text{ otherwise }) \end{cases} \qquad (25)$$

where

$$S_{1a}(r) \triangleq \{ (r,r), (-r,0), (0,-r), (0,r), (r,0), (-r,-r) \} \qquad (26)$$

$$S_{1b}(r) \triangleq \{ (0,0), (-2r,-2r), (2r,0), (0,2r) \} \qquad (27)$$

$$S_2(r,s) \triangleq \{ (0,0), (0,r), (r,0), (-r,-r), (0,s), (s,0), (-s,-s), (r+s,0), (0,r+s), (-r-s,-r-s),$$
$$(r,s), (s,r), (-s,r-s), (-r,s-r), (s-r,-r), (r-s,-s) \} \qquad (28)$$

$$S_3(d) \triangleq \{ (0,0), (0,d), (d,0), (-d,-d) \} \qquad (29)$$

These show that the outputs $\{y_t^{(r,s)}\}$ and $\{z_t^{(d)}\}$ have the third order autocorrelations only at several respective specific combinations of two time lags. This fact suggests us an possibility that some superposition of the se independent process make an arbitrary bispectrum. For latter convenience, here we define another non-Gaussian i.i.d. process w_t with th mean 0, the variance σ^2 and the third order cumulant $\mathbf{K}_3$, which is independent of $\{u_t^{(\pm,r,\pm,s)}\}$'s (r,s.integers) and $\{v_t^{(\pm,d)}\}$'s (d;integer). Its third order autocorrelation function is obviously

$$R_3^w(\tau_1,\tau_2) = \begin{cases} \mathbf{K}_3 & (\text{ if } \tau_1=0 \text{ and } \tau_2=0 \;) \\ 0 & (\text{ otherwise }) \end{cases} \qquad (30)$$

MODEL CONSTRUCTION

In this section, how to superpose the outputs is indicated. First, we show that the following fact. From the symmetry (3), the following relation holds for the third order autocorrelation function for any stationary discrete-time stochastic process.

$$R_3(\tau_1,\tau_2) = \sum_{r=0}^{\infty} \sum_{s=0}^{r} R_3(r,s) \, D(r,s;\tau_1,\tau_2) \tag{31}$$

where

$$D(r,s;\tau_1,\tau_2) \triangleq \begin{cases} 1 & (\text{if } (\tau_1,\tau_2) \in S_4(r,s)) \\ 0 & (\text{otherwise}) \end{cases} \tag{32}$$

$$S_4(r,s) \triangleq \{(r,s), (s,r), (-s,r-s), (-r,s-r), (s-r,-r), (r-s,-s)\} \tag{33}$$

If the third order autocorrelation function exists only for finite time lags, the sum in (31) is limited as

$$\sum_{r=0}^{L} \sum_{s=0}^{r}$$

Comparing (28)-(30) with (32)-(33) shows that if $0 < s < r$,

$$4K_3 \, D(r,s;\tau_1,\tau_2) = R_3^{y(r,s)}(\tau_1,\tau_2) - 2 \, R_3^{z(r)}(\tau_1,\tau_2) - 2 \, R_3^{z(s)}(\tau_1,\tau_2)$$
$$- 2 \, R_3^{z(r+s)}(\tau_1,\tau_2) + 8 \, R_3^{w}(\tau_1,\tau_2) \quad . \tag{34}$$

Similarly, if $r > 0$ and $s = 0$,

$$4K_3 \, D(r,s;\tau_1,\tau_2) = 2 \, R_3^{z(r)}(\tau_1,\tau_2) - 4 \, R_3^{w}(\tau_1,\tau_2) \quad . \tag{35}$$

If $r = s > 0$,

$$4K_3 \, D(r,s;\tau_1,\tau_2) = 2 \, R_3^{z(-r)}(\tau_1,\tau_2) - 4 \, R_3^{w}(\tau_1,\tau_2) \quad . \tag{36}$$

If $r = s = 0$,

$$4K_3 \, D(r,s;\tau_1,\tau_2) = 4 \, R_3^{w}(\tau_1,\tau_2) \quad . \tag{37}$$

The relations (31)-(37) shows that an arbitrary third order autocorrelation function can be written as a sum of those of $\{y_t^{(r,s)}\}$'s (r,s: integers), $\{z_t^{(d)}\}$'s (d: integer) and $\{w_t\}$ defined in the previous section. The following method for model construction is based on the well known fact that the cumulant of a sum of independent stochastic variables is identical to the sum of the respective cumulants of the for a desired third order autocorrelation function $R_3^{\#}(\tau_1,\tau_2)$, we define a process $\{a_t\}$ as

$$a_t \triangleq \sum_{r=1}^{L} \sum_{s=1}^{r-1} J(r,s)^{1/3} y_t^{(r,s)} + \sum_{d=-L}^{2L} K(d)^{1/3} z_t^{(d)} + H^{1/3} w_t \tag{38}$$

$$\lambda \triangleq \frac{1}{4K_3} \tag{39}$$

$$J(r,s) \triangleq \lambda \, R_3^{\#}(r,s) \tag{40}$$

$$K(d) \triangleq \begin{cases} - \lambda \sum_{k=d-L}^{[\frac{d-1}{2}]} R_3^{\#}(d-k,k) & (\text{if } L < d \leq 2L) \\ - \lambda \left[\sum_{k=1}^{[\frac{d-1}{2}]} R_3^{\#}(d-k,k) + \sum_{k=1}^{d-1} R_3^{\#}(d,k) + \sum_{k=d+1}^{L} R_3^{\#}(d,k) - R_3^{\#}(d,0) \right] & (\text{if } 0 < d \leq L) \\ 0 & (\text{if } d = 0) \\ \lambda \, R_3^{\#}(-d,-d) & (\text{if } -L \leq d < 0) \end{cases} \tag{41}$$

$$H \triangleq \lambda \left[\sum_{m=1}^{L} \sum_{n=1}^{m-1} 2 \, R_3^{\#}(m,n) - \sum_{k=1}^{L} R_3^{\#}(k,0) - \sum_{k=1}^{L} R_3^{\#}(k,k) + R_3^{\#}(0,0) \right] \quad . \tag{42}$$

Then the third order autocorrelation function of $\{a_t\}$ is given by

$$R_3^{a}(\tau_1,\tau_2) = \begin{cases} R_3^{\#}(\tau_1,\tau_2) & (\text{if } (\tau_1,\tau_2) \text{ is contained in the hexagon defined in (4)}) \\ 0 & (\text{otherwise}) \end{cases} \tag{43}$$

This means that if the desired third order autocorrelation function has nonzero values only for a finite region of time lags, then the process $\{a_t\}$ has the just desired third order autocorrelation function. So we can obtain stochastic processes whose bispectra are arbitrarily chosen if their Fourier series expansions are truncated finitely. In general, with $L \to \infty$, its bispectrum is identical to the desired one.

The number of required input i.i.d. processes is counted out as follows.

For $\{y_t^{(r,s)}\}$'s .... $\frac{1}{2} * (L-1) * L * 4 = 2L^2 - 2L$

For $\{z_t^{(d)}\}$'s .... $3L * 2 = 6L$

For $\{w_t\}$ 1

_____

Total sum .... $2L^2 + 4L + 1$

(Note that $\{s_t^{(\cdot)}\}$ is not required because of (41).) Recently, the authors found out another composite linear model which requires only about $\frac{1}{2}L^2$ input processes, which is not mentioned here.

THE POWER SPECTRUM OF THE GENERATED PROCESS BY THE MODEL

The process $\{a_t\}$ has very special power spectrum which is the same as that of white noises. Now we show this fact. The processes $\{y_t^{(r,s)}\}$ (r,s:integers) and $\{z_t^{(d)}\}$ (d: integer) have the following power spectra.

$$f_{\underline{y}^{(r,s)}}(\omega) = \frac{\sigma^2}{2\pi} \left[\left|H^{(+,r)}(\omega) H^{(+,s)}(\omega)\right|^2 + \left|H^{(+,r)}(\omega) H^{(-,s)}(\omega)\right|^2 \right.$$
$$\left. \left|H^{(-,r)}(\omega) H^{(+,s)}(\omega)\right|^2 + \left|H^{(-,r)}(\omega) H^{(-,s)}(\omega)\right|^2 \right]$$

$$= \frac{\sigma^2}{2\pi} \left[(1+z^r)(1+z^s)(1+z^{-r})(1+z^{-s}) + (1+z^r)(1-z^s)(1+z^{-r})(1-z^{-s}) \right.$$
$$\left. + (1-z^r)(1+z^s)(1-z^{-r})(1+z^{-s}) + (1-z^r)(1-z^s)(1-z^{-r})(1-z^{-s}) \right]$$

$$= \frac{8\sigma^2}{\pi} \qquad\qquad\qquad (\text{constant ! }) \qquad\qquad\qquad (44)$$

$$f_{\underline{z}^{(d)}}(\omega) = \frac{\sigma^2}{2\pi} \left[\left|H^{(+,d)}(\omega)\right|^2 + \left|H^{(-,d)}(\omega)\right|^2 \right]$$

$$= \frac{\sigma^2}{2\pi} \left[(1+z^d)(1+z^{-d}) + (1-z^d)(1-z^{-d}) \right] = \frac{2\sigma^2}{\pi} \qquad (\text{constant ! }) \qquad \cdot \qquad (45)$$

(Note that most terms vanish .) Moreover the process $\{w_t\}$ also has a constant power spectrum. In (38), therefore, the independent processes whose power spectra are all constants are summed. This means that the process $\{a_t\}$ has a constant power spectrum. In other words, 'colorless' of the second order, but with desired color of the third order. This property may enable us to apply this model for simulations for residual series of the linear prediction. Another possible application may be for the cancellation of nonGaussianness.

RESULTS OF NUMERICAL EXPERIMENTS

Actually we tried to make numerically some processes with given third order autocorrelation functions by our model. We used pseudorandom series instead of samples from i.i.d. processes. The third order autocorrelation function of an example in Table 1 (where some part is omitted, which are known from the symmetry). In the table, every (i,j)-th previously desired value is put under respective unbiased estimate obtained from 25000 segments of length 16 of the generated process by the third order averaged periodogram method. This result shows that the prescribed third order autocorrelation function is just realized. It was also turned out that the power spectral estimate of the generated process is very flat. We tried for other given third order autocorrelation functions, and obtained reasonable results.

CONCLUDING REMARKS

A composite linear model is proposed, which generates a process with given third order autocorrelation function. Another specific feature of the model is that the generated process has the same power spectrum of white noise. These properties are confirmed by some numerical experiments. The model requires a lot of i.i.d. input processes independent of one another, and it may be difficult for direct application. However, an important fact is pointed out that from any desired bispectrum we can inversely find out a model which generates linearly a process having it.

REFERENCES

[1] D. R. Brillinger and M. Rosenblatt,"Asymptotic theory of estimates of k-th order spectra", in 'Spectral Analysis of Time Series', ed. by B. Harris, New York: Wiley, pp.153-188, (1967).

[2] D. R. Brillinger and M. Rosenblatt,"Computation and interpretation of k-th order spectra", ibid.

[3] D. R. Brillinger,'Time series; Data and analysis', New York: Holt, Rinehart and Winston, (1975).

[4] D. R. Brillinger,"The identification of a particular nonlinear time series system", Biometrika, Vol. 64, pp. 509-515, (1977).

[5] K. S. Lii and M. Rosenblatt,"Deconvolution and estimation of transfer function phase and coefficients for non-Gaussian linear process", Ann. statist., Vol. 10, pp.1195-1208, (1982).

[6] T. Subba Rao and M. M. Gabr,"A test for linearity of Stationary time series", J. Time Series Anal., Vol. 1, pp.145-158, (1980).

[7] M. J. Hinich,"Testing for Gaussianity and linearity of a stationary time series", J. Time Series Anal., Vol. 3, pp. 169-176, (1982).

[8] E. Masry and B. Picinbono,"Linear/nonlinear forms and the normal law: Characterization by higher order correlations", Ann. Institute of Statistical Mathematics, vol. 39 pp. 417-428, (1987).

[9] J. Anděl,"On linear processes with given moments", J. Time Series Anal., Vol. 8 , pp. 373-378, (1987).

[10] M. R. Raghuveer and C. L. Nikias,"Bispectrum estimation: A parametric Approach", IEEE Trans. Acoust. and Signal Processing, Vol. ASSP-33, pp. 1213-1230, (1985).

[11] F. Sakaguchi and H. Sakai,"A spectrum separation method for the sum of two non-Gaussian time series using higher order periodograms", IEEE J. Ocean. Eng., Vol. OE-12, pp.80-89, (1987).

[12] F. sakaguchi and H. sakai,"Bisection algorithm for impulse response estimation from bispectrum", Trans. Institute of Electronics, Information and Communication Eng., Vol.J70-A, pp.1412-1417, (1987). (in Japanese).

[13] W. K. Li and A. I. McLeod,"ARMA Modelling with non-Gaussian innovations", J. Time Series Anal., Vol. 9, pp. 155-168, (1988).

[14] T. Subba Rao,"The bispectral analysis of non-linear stationary time series with reference to bilinear model", in 'Handbook of Statistics', Vol. 3, ed. by P. R. Krishnaiah, Amsterdam: Elsevier Science, pp. 293-319, (1983).

[15] M. M. Gabr,"On the third order moment structure and bispectral analysis of some bilinear time series", J. Time Series Anal., vol. 9, pp.11-20, (1988).

[16] S. Mao and P. Lin,"A test of nonlinear autoregressive models", Proc. ICASSP 1988, pp.2276-2279,(1988).

[17] N. Toda and S. Usui,"Parametric estimation of bispectrum and a measure of non-Gaussianness", Trans. Institute of Electronics, Information and Communication Eng., Vol.J71-A,pp.171-178,(1988),(in Japanese)

[18] I. G. Žurbenko,'The spectral analyssi of time series', Amsterdam: North Holland, (1986).

	0	1	2	3	4	5	6	7 $\rightarrow \tau_1$
0	0.352	0.234	10.370	-0.157	0.074	1.217	-0.123	1.030
	0.	0.	10.	0.	0.	0.	0.	0.
1	0.234	-0.172	-15.423	-0.023	-0.019	-0.141	-0.518	0.559
	0.	0.	-15.	0.	0.	0.	0.	0.
2	10.370	-15.423	0.185	0.078	-0.299	0.711	-0.775	0.095
	10.	-15.	0.	0.	0.	0.	0.	0.
3	-0.157	-0.023	0.078	0.092	0.395	0.256	0.818	-0.077
	0.	0.	0.	0.	0.	0.	0.	0.
4	0.074	-0.019	-0.299	0.395	0.747	0.152	-0.775	-0.023
	0.	0.	0.	0.	0.	0.	0.	0.
τ_2	⋮	⋮	⋮	⋮	⋮	⋮	⋮	⋮

TABLE 1
The estimates (the upper in (i,j)-th entry) and the required value (the lower) of the third order auto-correlation function for an example.

ESTIMATION OF FREQUENCY RESPONSE AND INTERMODULATION DISTORTION FROM BISPECTRA

W.X. Zhang
Shanghai University of Technology
149 Yan Chang Road, Shanghai
Peop. Rep. of China

M.R. Raghuveer
Electrical Engineering Department
Rochester Institute of Technology
Rochester, N.Y. 14623

ABSTRACT

Intermodulation distortion measurements are an important aspect of the design and test of communication systems. This paper provides a method based on the Volterra representation of nonlinear systems to measure the intermodulation distortion due to second order nonlinearities. As we show, this approach enables us to compute the distortion at more frequency points in the frequency plane than does the conventional two-tone test. Two methods, one based on cross-correlation and cross-third moments, and another, based on cross-spectrum and cross-bispectrum, are developed.

1   INTRODUCTION

Practically every communication system involves subsystems which are nominally linear time-invariant (LTI). A popular approach to verify if LTI system designs have frequency responses close to the desired ones, is to provide a system input which consists of a sum of sine waves, and then find the cross-power spectrum between the input and output. The cross-power spectrum will enable us to find samples of the frequency response at frequencies present in the input signal [1]. The procedure is considerably simplified by choosing input frequencies which are integer multiples of one frequency and then using the DFT. In actual implementation, systems do not behave entirely as LTI systems and an element of nonlinearity is almost always there. Usually, the nonlinearity can be characterized as being of order two. This is especially true of systems where signals are translated between baseband and passband, and modulation and demodulation is done at one or more stages. Since, a key characteristic of a nonlinear system is that when provided with sinusoidal inputs, it provides outputs which contain frequency components not originally in the inputs, procedures have been devised to measure the contribution of nonlinearities, using sinusoidal signals. Total harmonic distortion (THD) measurements are very common and practically every introductory textbook on communication systems deals with THD. Yet another approach is the two-tone test for *intermodulation* (IM) *distortion* [2]. In a two-tone test, a signal consisting of the sum of two sine waves at different frequencies, is provided as an input to the system, and the ratio of the output power at new frequencies to the output power at the input frequencies is taken as the measure of nonlinearity. Standard procedures specify the frequencies (which depends on the actual application; for example, for a 3-kHz voice channel, they are 1500 Hz and 2500 Hz) for the pair of sine waves to be used in the test. In the case of second order nonlinearities, the IM products are at the second harmonics of the input frequencies and at the sum and difference frequencies; the DC component is not taken into account in measuring IM distortion. In this paper, a modeling approach based on the Volterra representation [3, 4] for nonlinear systems is developed. The motivation for this, is provided by the fact that for a quadratic nonlinearity with memory, *the IM distortion is a function of the frequencies used in the two-tone test*. A complete picture of the contribution of the nonlinearity is provided by looking at different points in the frequency plane. As we show in this paper, the Volterra representation provides a model which enables us to compute the IM distortion as a function of frequency pair. The measurement involves computation of cross-spectra (cross-correlation) and cross-bispectra (cross-cumulant). The correlation based method is termed "time-domain", since only operations in the time domain are involved. The method involving the DFT is termed "frequency-domain" for obvious reasons. That the identification of nonlinearities is made easier using polyspectra, is well documented [5]-[9]. What we provide, is an approach quite analogous to the popular frequency-response measurement using sine waves, except that in addition to the frequency response of the linear part, the contribution of the nonlinear part is measured as well. Our interest is in quadratic nonlinearity, and therefore we will deal with Volterra kernels of orders one and two only. Only discrete systems are dealt with. Most results are given without proofs; these are available with the authors.

2 MATHEMATICAL DEVELOPMENT

Consider a second order Volterra system with input $x(n)$ and output $y(n)$.

$$y(n) = \sum_{m=-\infty}^{\infty} h_1(m)x(n-m) +$$
$$\sum_{m_1=-\infty}^{\infty} \sum_{m_2=-\infty}^{\infty} h_2(m_1,m_2)x(n-m_1)x(n-m_2) \tag{1}$$

The nonlinear kernel is assumed to be symmetric i.e,

$$h_2(m,n) = h_2(n,m) \tag{2}$$

Let $y_1(n)$ and $y_2(n)$ be the outputs of the linear and nonlinear parts respectively. Then,

$$y(n) = y_1(n) + y_2(n) \tag{3}$$

Suppose we have

$$x(n) = \sum_{i=1}^{I} \cos(\lambda_i n + \phi_i) \tag{4}$$

where $\phi_i, i = 1,\ldots,I$ are independent and uniformly distributed over $[0,2\pi]$. Then,

$$y_1(n) = \frac{1}{2}\sum_{\substack{i=-I \\ i\neq 0}}^{I} H_1(\lambda_i)\exp[j(\lambda_i n + \phi_i)] \tag{5}$$

where

$$H_1(\omega) = \sum_{n=-\infty}^{\infty} h_1(n)\exp[-j\omega n] \tag{6}$$

and

$$y_2(n) = \frac{1}{4}\sum_{\substack{i_1=-I \\ i_1\neq 0}}^{I}\sum_{\substack{i_2=-I \\ i_2\neq 0}}^{I} H_2(\nu_{i_1},\nu_{i_2})\exp[j\{(\nu_{i_1}+\nu_{i_2})n + \theta_{i_1}+\theta_{i_2}\}] \tag{7}$$

where

$$H_2(\omega_1,\omega_2) = \sum_{m=-\infty}^{\infty}\sum_{n=-\infty}^{\infty} h_2(m,n)\exp[-j(\omega_1 n + \omega_2 n)] \tag{8}$$

$$\nu_i = \begin{cases} \lambda_i & (i > 0) \\ \lambda_{-i} & (i < 0) \end{cases} \tag{9}$$

$$\theta_i = \begin{cases} \phi_i & (i > 0) \\ \phi_{-i} & (i < 0) \end{cases} \tag{10}$$

Alternatively, we can write

$$y(n) = \sum_{i=1}^{I} |H_1(\lambda_i)|\cos[\lambda_i n + \phi_i + \angle H_1(\lambda_i)] +$$

$$(1/2)\sum_{i=1}^{I}\sum_{j=1}^{I} |H_2(\lambda_i,\lambda_j)|$$
$$\cos[(\lambda_i+\lambda_j)n + \phi_i + \phi_j + \angle H_2(\lambda_i,\lambda_j)] \tag{11}$$
$$+ (1/2)\sum_{i=1}^{I}\sum_{j=1}^{I} |H_2(\lambda_i,-\lambda_j)|$$
$$\cos[(\lambda_i-\lambda_j)n + \phi_i - \phi_j + \angle H_2(\lambda_i,-\lambda_j)]$$

If we provide $\cos(\lambda_1 n) + \cos(\lambda_2 n)$, $\lambda_1 \neq \lambda_2$, as the input to the system, the resulting IM distortion (denoted by $IMD(\lambda_1,\lambda_2)$) at the output is given by,

$$IMD(\lambda_1,\lambda_2) = \frac{\text{Num}(\lambda_1,\lambda_2)}{\text{Den}(\lambda_1,\lambda_2)} \tag{12}$$

where

$$\text{Num}(\lambda_1,\lambda_2) = \begin{cases} (1/2)[|H_2(\lambda_1,\lambda_2)|^2 + |H_2(\lambda_1,-\lambda_2)|^2] + \\ (1/8)[|H_2(\lambda_1,\lambda_1)|^2 + |H_2(\lambda_2,\lambda_2)|^2] \end{cases} \tag{13}$$

and

$$\text{Den}(\lambda_1,\lambda_2) = (1/2)[|H_1(\lambda_1)|^2 + |H_1(\lambda_2)|^2] \tag{14}$$

2.1 Time Domain Approach

It can be shown that for $x(n)$ in (4) the cross-correlation between the input and output, $r_{xy}(m) = E\{x(n)y(n+m)\}$ is given by

$$r_{xy}(m) = \frac{1}{2}\sum_{i=1}^{I} |H_1(\lambda_i)|\cos[\lambda_i m + \angle H_1(\lambda_i)] \tag{15}$$

Notice that only the linear component affects the cross-correlation. The above expression can be modified to,

$$r_{xy}(m) = (1/2)\sum_{i=1}^{I} \begin{array}{l} [\text{Real}[H_1(\lambda_i)]\cos(\lambda_i m) \\ -\text{Imag}[H_1(\lambda_i)]\sin(\lambda_i m)] \end{array} \tag{16}$$

With $2I$ samples of $r_{xy}(m)$, it is possible to solve a set of simultaneous linear equations to get the real and imaginary parts of the frequency response at the I frequencies, and hence we can get $H_1(\lambda_i)$, $i = 1,2,\ldots,I$. When we have a finite number of samples of the input and the output, cross-correlation estimates can be computed. By estimating the cross-correlation at more than $2I$ lags, an overdetermined system of equations can be formed and the frequency response can be estimated using the pseudo-inverse of the corresponding matrix. We will next look at the cross-cumulant sequence $c(k,\ell) = E\{x(n+k)x(n+\ell)y(n)\}$. We can show that

$$c(k,\ell) = \frac{1}{8}\sum_{(i_1,i_2)\in S}\sum H_2(\lambda_{i_1},\lambda_{i_2})\exp[j(\lambda_{i_1}k + \lambda_{i_2}\ell)] +$$
$$\frac{1}{16}\sum_{\substack{i=-I \\ i\neq 0}}^{I} H_2(\lambda_i,\lambda_i)\exp[j\lambda_i(k+\ell)] +$$
$$Dr_{xx}(k-\ell) \tag{17}$$

where $S = \{(n_1, n_2) : 0 \cdots \cdots \quad I, n \cdots n_2\}$, D
$(1/2)\sum_i H_i(\lambda_i, \lambda_i)$, and $r(k) = r_i = E\{r(n-k)s(n-k)\}$
$k\} = (1/2)\sum_i \cos(k-i)\lambda_i$.

Define

$$Q_R(\lambda_i, \lambda_j) \quad \begin{cases} (1/16)\, \mathrm{Real}[H_2(\lambda_i, \lambda_j)] & i = j \\ (1/4)\, \mathrm{Real}[H_2(\lambda_i, \lambda_j)] & i \neq j \end{cases} \quad (18)$$

$$Q_I(\lambda_i, \lambda_j) \quad \begin{cases} (1/16)\, \mathrm{Imag}[H_2(\lambda_i, \lambda_j)] & i = j \\ (1/4)\, \mathrm{Imag}[H_2(\lambda_i, \lambda_j)] & i \neq j \end{cases} \quad (19)$$

and

$$g_+(x, y, m, n) = \cos(mx + ny) + \cos(nx + my)$$
$$g_-(x, y, m, n) = \sin(mx + ny) + \sin(nx + my) \quad (20)$$

Then, from (17),

$$c(m_1, m_2) = \begin{cases} \sum_i \sum_j [Q_R(\lambda_i, \lambda_j) g_+(\lambda_i, \lambda_j, m_1, m_2) + \\ Q_I(\lambda_i, \lambda_j) g_-(\lambda_i, \lambda_j, m_1, m_2)] + \\ \sum_i \sum_j [Q_R(\lambda_i, -\lambda_j) g_+(\lambda_i, -\lambda_j, m_1, m_2) + \\ Q_I(\lambda_i, -\lambda_j) g_-(\lambda_i, -\lambda_j, m_1, m_2)] + \\ Dr_{i,j}(m_1 - m_2) \end{cases}$$

$$(21)$$

Equation (21) suggests that with $2I^2 + 1$ samples of $c(m_1, m_2)$, the quantities Q_R, Q_I and D can be determined by solving a set of linear equations. In practice, with actual samples of the input and output signals, we can substitute estimates of the cross-cumulant sequence in place of the true values. If we have more than $2I^2 + 1$ values of the cross-cumulant sequence or its estimate, then an overdetermined set of equations can be formed and a pseudo inverse solution can be obtained.

2.2 Frequency Domain Approach

Corresponding expressions can be obtained in the frequency domain as well. Suppose in (1) we have

$$r(n) = \sum_{i=0}^{\cdots} \cos\left(\frac{2\pi i}{N} n + \phi_i\right) \quad (22)$$

Let $X(k) = \mathrm{DFT}\{r(0), r(1), \ldots, r(N-1)\}$. Then

$$X(k) \quad \begin{cases} \frac{N}{2} \exp(j\phi_k) & 0 < k < N/2 \\ N \cos(\phi_k) & k = 0, N/2 \end{cases} \quad (23)$$

If $Y(k)$ is the corresponding output DFT, then the cross power spectrum $S(k)$ is given by,

$$S(k) = E\{X^*(k)Y(k)\} \quad \begin{cases} N^2 H_1(k) & k \neq 0, N/2 \\ N^2 H_1(k) & k = 0, N/2 \end{cases}$$

$$(24)$$

By $H_1(k)$ we mean $H_1(\omega)$ of (6) with $\omega = \frac{2\pi}{N}k$. Values of $H_1(k)$ can be found from the cross power spectrum, as the above equation shows. The cross bispectrum (which happens to be one of the possible cross bispectra) $B(k_1, k_2)$

is given by,

$$B(k_1, k_2) = E\{X(k_1)X(k_2)Y^*(k_1 + k_2)\} \quad (25)$$

It can be shown that

$$B(k_1, k_2) \begin{cases} (N^3/8)H_2(k_1, k_2) + \\ 2\sum_{i=0}^{N/2} H_2(i, N-i) & k_1 = k_2 = 0, N/2 \\ (N^3/2)H_2(k_1, k_2) & (k_1, k_2) = (N/2, 0) \\ (N^3/4)H_2(k_1, k_2) & k_1 = N/2, k_2 \neq 0, N/2 \\ & \text{and} \\ & k_2 = 0, k_1 \neq 0, N/2 \\ (N^3/16)H_2(k_1, k_2) & k_1 = k_2 \neq 0, N/2 \\ (N^3/8)H_2(k_1, k_2) & k_1 \neq k_2, k_1 + k_2 \neq N, \\ & k_1, k_2 \neq 0, N/2 \end{cases}$$

$$(26)$$

It follows from (26) that given samples of the cross-bispectrum or its estimates, it is possible to estimate $H_2(k_1, k_2)$.

3 SIMULATIONS

Example 1 A true second order nonlinear system with finite extent $h_1(n)$ and $h_2(n_1, n_2)$ was considered with $h_1(0) = 0.3$, $h_1(1) = -0.1$, $h_1(2) = 0.5$, and $h_1(n) = 0$ for all other n; $h_2(0, 0) = 0.1$, $h_2(0, 1) = h_2(1, 0) = 0.6$, $h_2(1, 1) = -0.3$ and $h_2(m, n) = 0$ for all other (m, n). Experiments were performed to test the performance of the time and frequency domain methods as a function of SNR and number of segments of data. Output samples were generated by using an input consisting of a sum of sine waves of five different frequencies. The values of the frequencies were different for the time and frequency domain methods. Figures 1 and 2 show plots of the relative mean squared errors in estimating $H_1(\lambda)$ and $H_2(\lambda_1, \lambda_2)$ at these frequencies. The errors were measured as fractions of the true mean squared values of $H_1(\lambda)$ and $H_2(\lambda_1, \lambda_2)$. In both cases, 100 independent records of the input were generated by adding independent phases generated afresh for each record. Observation noise in the form of an additive Gaussian random process was added. The SNR was varied from -20 dB to 10 dB. As we see, good estimates of $H_1(\lambda)$ and $H_2(\lambda_1, \lambda_2)$ are possible from both methods at SNR close to 10 dB.

Figure 3 and 4 show the MSEs as a function of number of data records. The number of records was varied from 20 to 200 for the time domain, and 50 to 1000 for the frequency domain. The SNR was kept at 0 db for the time-domain method and 20 dB for the frequency domain. As can be seen, the time-domain approach is much less sensitive even at a lower SNR to the number of records, than is the frequency domain method.

Example 2 To test the Volterra approach in terms of

measuring IMD, a simple memoryless nonlinear system

$$y(n) = ax(n) + Ax^2(n) \qquad (27)$$

was considered with $a = 1$. A was varied from 0.01 (weak nonlinearity) to 1.96 (strong nonlinearity). The true IMD at any frequency pair is $(2A^2/a^2)$. Estimates of a and A were obtained from the frequency domain method. Five frequencies were used. a was estimated as the mean of the estimated $H_1(k)$ over all frequencies and A was estimated as the mean of estimated $H_2(k_1, k_2)$ over all frequency pairs. 500 records were generated. Figure 5 shows true and estimated (A^2/a^2). Good match is found between true and estimated values for $A > a$.

4   CONCLUSION

The paper has provided an approach to estimate samples of the Fourier transforms of the linear and nonlinear convolution kernels of a second order Volterra system using a sum of sinusoidal signals as the input. By using the Volterra modeling approach and the estimation procedures of the paper, it is possible to measure intermodulation distortion due to second order nonlinearities. Further research is being done to characterize the performance of the approach with different systems.

Acknowledgement

References

[1] O Series Recommendations. CCITT.

[2] R.L. Freeman. *Telecommunication Transmission Handbook*. John Wiley & Sons, second edition, 1981

[3] M. Schetzen. *The Volterra and Wiener Series of Nonlinear Systems*. Wiley, New York, N.Y., 1980.

[4] W.J. Rugh. *Nonlinear System Theory*. The Johns Hopkins University Press, 1981.

[5] D.R. Brillinger. "The Identification of Polynomial Systems by means of Higher Order Spectra". *J. Sound Vibr.*, 12:pp.301-313, 1970.

[6] M.J. Hinich and D.M. Patterson. "Identification of the Coefficients in a Nonlinear Time Series of the Quadratic Type". *Journal of Econometrics*, 30:pp. 269-288, 1985.

[7] M.R. Raghuveer and C.L. Nikias. "Bispectrum Estimation: A Parametric Approach". *IEEE Transactions on Acoustics, Speech, and Signal Processing*, vol. ASSP-33(4):pp. 1213-1230, October 1985.

[8] C.L. Nikias and M.R. Raghuveer. "Bispectrum Estimation: A Digital Signal Processing Framework". *Proceedings of the IEEE*, vol. 75(7):pp. 869-891, July 1984.

[9] K.I. Kim and E.J. Powers. "A Digital Method of Modeling Quadratically Nonlinear Systems with a General Random Input". *IEEE Transactions on Acoustics, Speech, and Signal Processing*, vol. 36(11):pp. 1758-1760, November 1988.
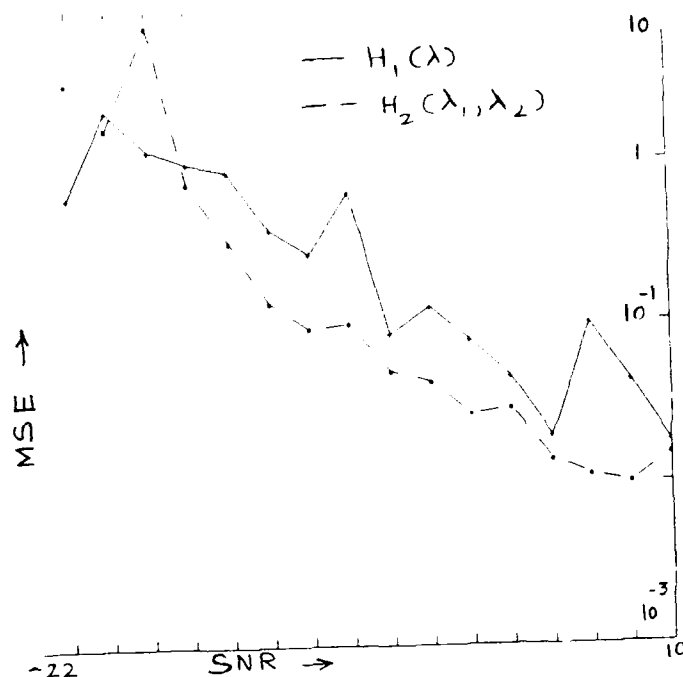

Fig. 1. Example 1. Time Domain method. SNR from -22 dB to 10 dB in 2 dB steps. MSE from 10^{-3} to 10 by factors of 10.
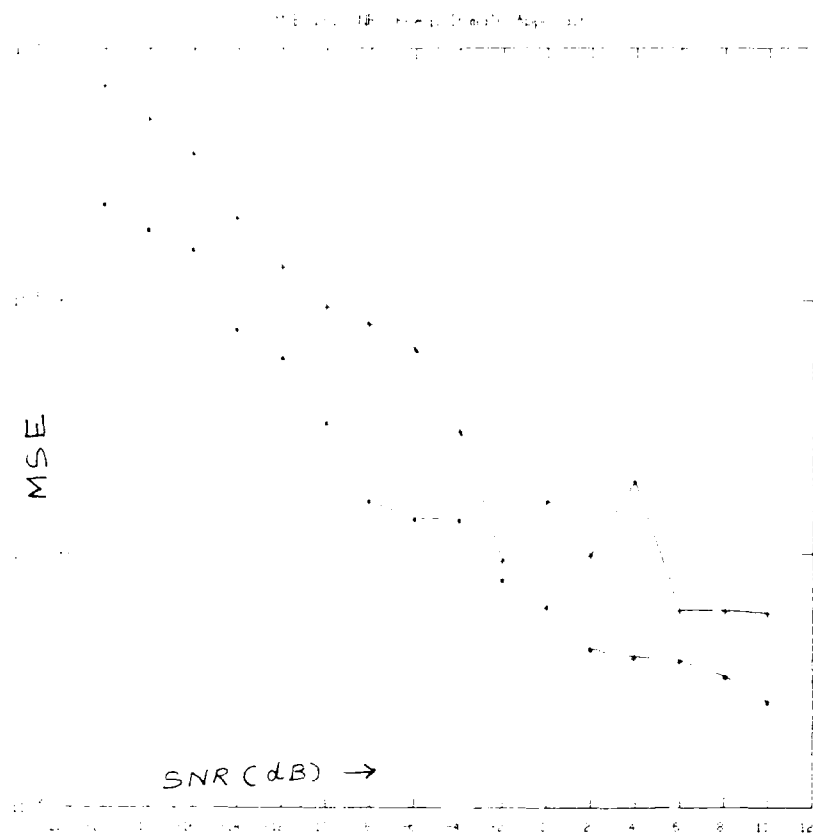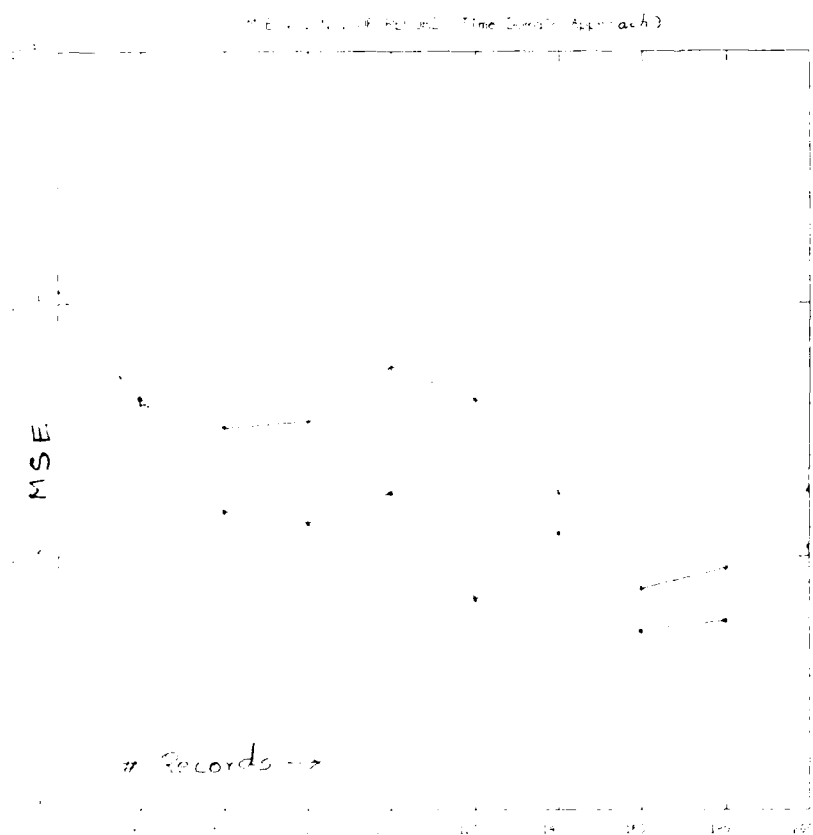
Fig. 2. Frequency Domain Method

— MSE for $H_1(\cdot)$
--- MSE for $H_2(\cdot, \cdot)$

MSE

SNR (dB) →

Fig. 3. MSE vs. No. of records. Time Domain method

— MSE for $H_1(\cdot)$
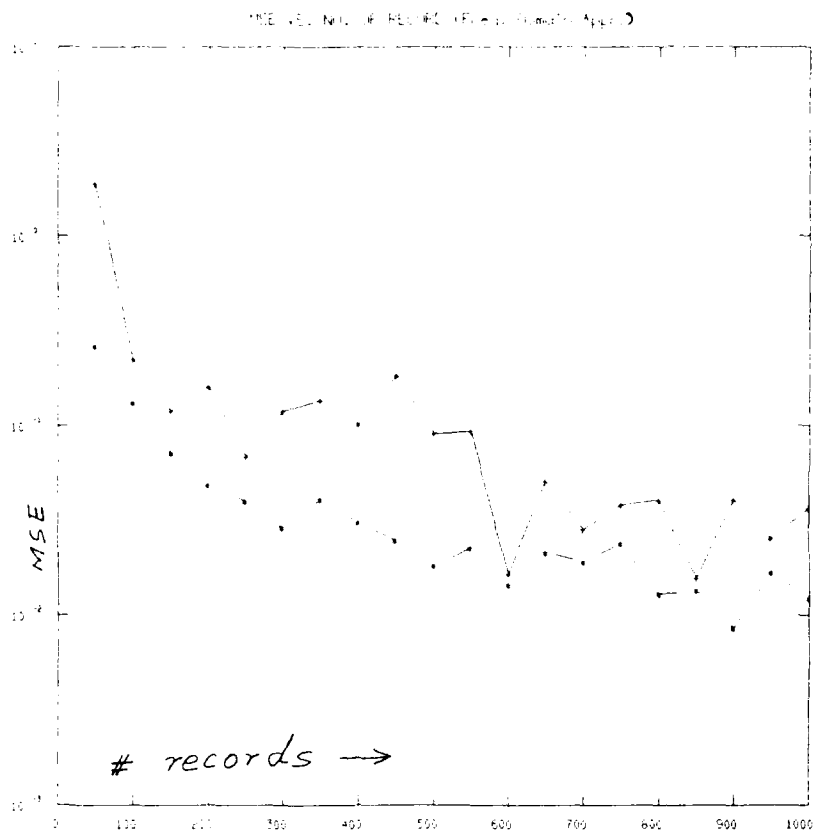-- MSE for $H_2(\cdot, \cdot)$

MSE

Records →

34

Fig. 4. MSE vs. No. of records. Frequency Domain method.

—— MSE for $H_1(\cdot)$
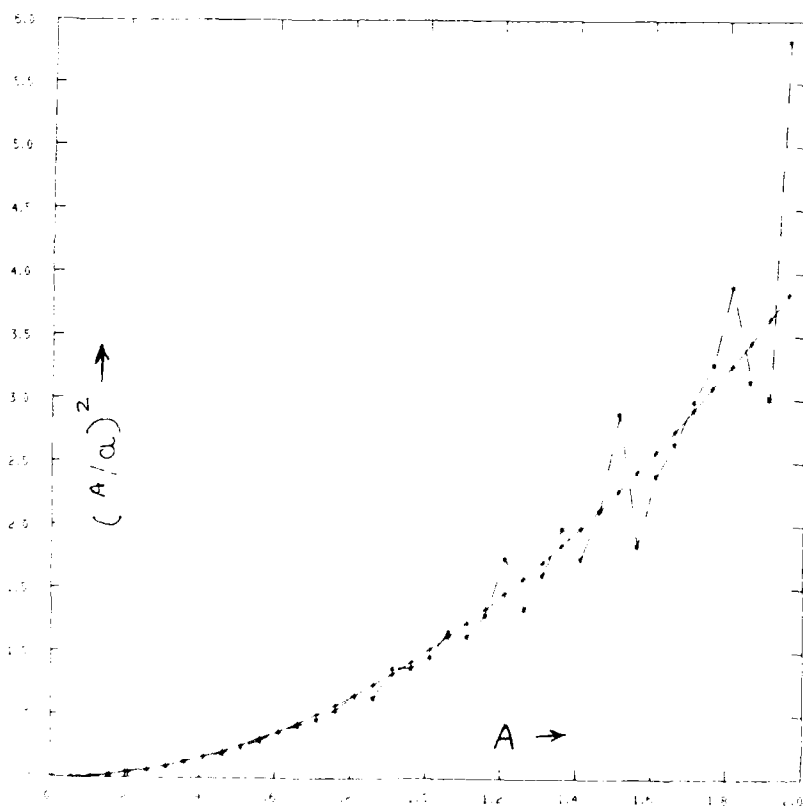
– – MSE for $H_2(\cdot,\cdot)$

Fig. 5. IMD vs. A for example 2

—— True

– – Estimated

THE RUNNING BISPECTRUM

John D. Thatcher

Boeing Helicopter Co.
P. O. Box 16838
Philadelphia, PA 19142

Moeness G. Amin

Dept. of ElectricalEngineering
Villanova University
Villanova, PA 19085

ABSTRACT

The recursive update of the bispectrum estimate which is based on the 2-D Fourier transform of the time-average estimates of the cumulants can be achieved using forward and reverse sequence running FT's of the data. The computationally block-invariance property of RFT may, therefore, be extended to yield a class of recursive Fourier-based bispectrum estimators in which the number of computations required to update the estimate is independent of the size of the employed 2-D lag window.

I. INTRODUCTION

This paper introduces a computationally efficient Fourier-based approach to real time bispectrum estimations. Forward and reverse sequence running Fourier transforms (RFT) are used to define a class of interactive bispectrum estimators in which the number of computations required to update the estimate every data sample is independent of both employed numbers of cumulants lags. Since the horizontal and vertical dimensions of the 2-D lag window define the bandwidth of the spectral window through which the bispectrum is observed, the proposed class of estimators offers resolution enhancement without additional computations.

Similar to the second order statistics, the conventional estimation of the bispectrum is Fourier-based and can be obtained by taking the two dimensional (2D) Fourier transform to the time-average estimates of the 3rd order cumulants. In time-varying environment, however, the bispectrum estimate becomes time-dependent, and the above estimation procedure can be depicted in Fig. 1. In this Figure, the 3-D window of the time and the two lag variables can be viewed as a multidimensional linear time-invariant filter of finite or infinite region of supports (ROS), applied to the cumulant samples terms of the data. Because of the symmetry properties of the cumulant in both lag variables [1], only $(L+1)(L+2)/2$ filters are required for $(L+1) \times (L+1)$ lag window.

In the proposed class of bispectrum estimators, the impulse responses $h(n,k,m)$ are related over the variables k and m such that the number of computations required to map the new data sample from the time domain to the bispectrum domain is independent of the extent of the filters K and M in the lag dimensions.

The paper details the conditions which lead to the computationally cumulant lag-invariance property of recursive bispectrum estimation. For illustration, two examples are presented which correspond to simple recursive and nonrecursive windows.

II. FORWARD AND REVERSED SEQUENCE RUNNING FOURIER TRANSFORMS

The FT of a data sequence can be recursively updated with a number of computations which is invariant with the data record length. Denote $F(n,\omega)$ as the FT of the set of the data samples $x(n)$, $x(n-1),\ldots,x(n-N+1)$, then [2,3]

then
$$F(n,\omega) = \sum_{m=0}^{N-1} x(n-m)e^{+j\omega m} \qquad (1)$$

$$= e^{j\omega} F(n-1,\omega) + x(n) - e^{j\omega N}x(n-N)$$

If the FT is taken to the reversed sequence, $x(n-N+1)$, $x(n-N+2),\ldots,x(n)$, then

$$G(n,\omega) = \sum_{m=0}^{N-1} x(n-N+1+m)e^{-j\omega m}$$

$$= e^{j\omega}G(n-1,\omega) - e^{j\omega}x(n-N) + e^{-j\omega(N-1)}x(n) \qquad (2)$$

The computational block-invariance of RFT is also maintained if the data sequence is windowed by w(n) prior to transformation. As discussed in [4], w(n) should, in general, be a summation of exponential functions. In Section III, the above two recursions (1) and (2) are used to establish the computational lag-invariance property in the recursive update of the bispectrum estimate.

III. COMPUTATIONALLY LAG-INVARIANT RECURSIVE BISPECTRUM ESTIMATORS

The time-average estimate of the cumulant $R(n,-k,-m)$ of the data $x(n)$ can be presented by the convolution

$$\hat{R}(n,k,m) = \sum_{\ell=-\infty}^{\infty} h(n-\ell,k,m) \; x(\ell)x(\ell+k)x(\ell+m) \qquad (3)$$

where h is a LTI filter impulse response, which may in general varies according to the cumulants lags (k,m). The filter transfer function is

$$H(z,k,m) = \left[\sum_{i=0}^{q-1} b(i,k,m)z^{-i}\right] \bigg/ \left[1+\sum_{i=1}^{p-1} a(i,k,m)z^{-i}\right] \qquad (4)$$

To avoid biased estimates $H(1,k,m) = 1$, which in part limits the flexibility of choosing the filter coefficients a's and b's. Equation (3) describes the system of Fig. 2 whose input is the cumulant sample $x(n)x(n+m)x(n+k)$ and output is the cumulant estimate $\hat{R}(n,k,m)$. The system output and input can be related by the difference equation

$$\hat{R}(n,k,m) = -\sum_{i=1}^{p-1} a(i,k,m)\hat{R}(n-i,k,m)$$

$$+ \sum_{i=0}^{q-1} b(i,k,m)x(n-i)x(n-i+k)x(n-i+m)$$

The time-dependent bispectrum estimate $\hat{B}$ is obtained by taking the 2-D FT of the above equation

$$\hat{B}(n,\omega_1,\omega_2) = -\sum_{i=1}^{P-1} C(i,\omega_1,\omega_2) \underset{\omega_1 \omega_2}{*\ *} \hat{B}(n-i,\omega_1,\omega_2) + A(i,\omega_1,\omega_2) \tag{5}$$

where

$$C(i,\omega_1,\omega_2) = \sum_{k=-K}^{K}\sum_{m=-M}^{K} a(i,k,m)W_1^k W_2^m \tag{6}$$

$$A(i,\omega_1,\omega_2) = \sum_{k=-K}^{K}\sum_{m=-M}^{M}\sum_{i=0}^{q-1} b(i,k,m)x(n-i)x(n-i+k)x(n-i+m)W_1^k W_2^m \tag{7}$$

where K and M are the maximum lags of interest of the cumulant function R and $W_1 = \exp(-j\omega_1)$, $W_2 = \exp(-j\omega_2)$. If the number of the filter zeros is lag-independent, then one can alter the sequence of summations in (7) to

$$A(i,\omega_1,\omega_2) = \sum_{i=0}^{q-1} x(n-i)\sum_{k=-K}^{K}\sum_{m=-M}^{M} b(i,k,m)x(n-i+k)x(n-i+m)W_1^k W_2^m$$

The 2-D FT in the above equation $A_1(i,\omega_1,\omega_2)$ can be expressed in terms of one sided Fourier transforms as

$$A_1(i,\omega_1,\omega_2) = \sum_{k=0}^{K}\sum_{m=0}^{M}\Big[b(i,k,m)x(n-i+k)x(n-i+m)W_1^k W_2^m$$

$$+ b(i,k,-m)x(n-i+k)x(n-i-m)W_1^k W_2^{-m}$$

$$+ b(i,-k,m)x(n-i-k)x(n-i+m)W_1^{-k} W_2^m$$

$$+ b(i,-k,-m)x(n-i-k)x(n-i-m)W_1^{-k}W_2^{-m}\Big]$$

$$-x(n-i)\sum_{k=0}^{K}\left[b(i,k,0)x(n-i+k)W_1^k + b(n,-k,0)x(n-i-k)W_1^{-k}\right] \tag{8}$$

$$-x(n-i)\sum_{m=0}^{M}\left[b(i,0,m)x(n-i+m)W_2^m + b(i,0,-m)x(n-i-m)W_2^{-m}\right]$$

$$+ b(i,0,0)x^2(n-i)$$

The computational lag-invariance property of recursive bispectrum estimation requires the number of computations of A_1 to be independent of both K and M. If the filter moving-average (MA) coefficients $b(i,k,m)$ are separable sequences, i.e.,

$$b(i,k,m) = b_1(i,k)b_2(i,m) \qquad \forall\, i \tag{9}$$

then A_1 can be expressed in terms of 1-D forward and reverse sequence running FT's

$$A_1(i,\omega_1,\omega_2) = G_1(n-i,\omega_1)G_2(n-i,\omega_2) + G_1(n-i,\omega_1)F_2(n-i,\omega_2)$$

$$+ F_1(n-i,\omega_1)G_2(n-i,\omega_2) + F_1(n-i,\omega_1)F_2(n-i,\omega_2)$$

$$- b_2(i,o)x(n-i)\left[G_1(n-i,\omega_1) + F_1(n-i,\omega_1)\right] \tag{10-a}$$

$$- b_1(i,0)x(n-i)\left[G_2(n-i,\omega_2) + F_2(n-i,\omega_2)\right]$$

$$+ b_1(i,0)b_2(i,0)x^2(n-i)$$

where

$$F_1(n,\omega_1) = e^{j\omega_1}F_1(n-1,\omega_1) + x(n) - e^{j\omega_1(K+1)}x(n-K-1) \tag{10b}$$

$$G_1(n,\omega) = e^{j\omega_1}G_1(n-1,\omega_1) + x(n+K)e^{-j\omega_1 K} - x(n-1)e^{j\omega_1}$$

$$F_2(n,\omega_2) = e^{j\omega_2}F_2(n-1,\omega_2) + x(n) - e^{j\omega_2(M+1)}x(n-M-1) \tag{10-c}$$

$$G_2(n,\omega_2) = e^{j\omega_2}G_2(n-1,\omega_2) + x(n+M)e^{-j\omega_2 M} - x(n-1)e^{j\omega_2}$$

The functions F and G are similar to those of equations (1) and (2) with minor differences which appear in the sign of the complex exponential in F and the time shift in G.

In the above equation both $b_1(i,k)$ and $b_2(i,m)$ assumed symmetry around the lag variables k and m. According to (10), four different running FT's are required to calculate A_1 at the ith coefficient. Therefore, for computational efficiency, fewer number of coefficients of the MA part of the employed filter should be used.

Since A_1 is formed from the functions F and G, the computational block-invariance property of RFT can be used to evaluate A_1 at each frequency sample (ω_1,ω_2) with a number of additions and multiplications independent of both lag K and M. The coefficients b_1 and b_2, however, must be selected consistent with the properties of the data window w(n) of Section II. To enforce the computational lag-invariance property over all terms in the bispectrum estimate in (5), the AR coefficients should be lag-independent so as to eliminate the need to perform the double convolution.

Recursive Windows

For the case of a single pole filter, $h(n,k,m) = (1-\gamma)\gamma^n$ $n \geq 0$ the parameters in the transfer function (4) simplifies to $q=1, p=2, b(0,m)=b(0,k)=(1-\gamma)$. In turn, equation (5) becomes

$$\hat{B}(n,\omega_1,\omega_2) = \gamma\hat{B}(n-1,\omega_1,\omega_2) + (1-\gamma)x(n)A_1(0,\omega_1,\omega_2) \quad (11\text{-}a)$$

$$A_1(0,\omega_1,\omega_2) = G(n,\omega_1)G(n,\omega_2) + G(n,\omega_1)F(n,\omega_2) \quad (11\text{-}b)$$

$$+ F(n,\omega_1)G(n,\omega_2) + F(n,\omega_1)F(n,\omega_2)$$

$$- x(n)\Big[G(n,\omega_1) + F(n,\omega_1) + G(n,\omega_2)$$

$$+ F(n,\omega_2)\Big] + x^2(n)$$

In the above equation, we chose M=K=L. Accordingly, $G_1 = G_2$ and $F_1 = F_2$, which reduces the required number of RFT's into half. The block diagram of recursion (11) is depicted in Fig. 3.

A simple comparison between the above bispectrum recursion and the single pole recursive structure of the power spectrum represented in [1] shows an additional running FT required in bispectrum estimation to account for the additional lag variable. The extension of the proposed approach for bispectrum computations to trispectrum may, therefore, require running three FT's of the data providing that the separability condition of the filter coefficients is maintained.

For VLSI implementation of the running spectrum, the computationally lag-invariance translates into a size-invariant array processor, in which the number of processing elements is independent of the maximum lags of interest. The systolic array implementation issue of the running Fourier transform is discussed in reference [5] and used to systolize recursive power spectrum estimators. Since RFT is the basic element in both recursive power spectrum and bispectrum estimation, devising the array structure for the underlying problem becomes a simple extension of the structure presented in [5].

If the bispectrum estimate is evaluated at a number of frequencies equals to the dimensions of the lag window, as is the case in the 2-D DFT, both F and G must be calculated at equally spaced frequencies $\omega_k = \frac{2\pi}{L}k$, and equation (11) can then be written in the matrix form

$$\hat{B}_n = \gamma\hat{B}_{n-1} + (1-\gamma)x(n)\ A_1$$

$$A_1 = G_n G_n^T + G_n F_n^T + F_n G_n^T + F_n F_n^T \quad (12)$$

$$- x(n)\Big[\hat{1}s^T + s\hat{1}^T\Big] + x^2(n)$$

where F and G are the DFT vectors of the forward and reverse sequences, $S = F + G$, $\hat{1}^T = [1\ 1\ 1\ ...1]$, and $\hat{B}_n$ is the matrix of the bispectrum estimate for $0 \leq \omega_1, \omega_2 \leq 2\pi$. The computations of the outer products in (12) depend on L and, therefore, violate the lag-independence property, which is always the case in DFT.

Nonrecursive Windows

The simplest FIR filter which satisfies the computationally lag-invariance property of the running bispectrum is the rectangular window, i.e., $h(n,k,m) = (1/N)\{u(n) - u(n-N)\}$, where $U(\cdot)$ denotes a unit step function. In this case, $b(o,k,m) = b(L,k,m) = -1$. The MA coefficients for $0 < i < L$ are all zeroes.

$$\hat{B}(n,\omega_1,\omega_2) = \hat{B}(n-1,\omega_1,\omega_2) + \frac{1}{N}\Big[x(n)A_1(0,\omega_1,\omega_2) - x(n-N)A_1(N,\omega_1,\omega_2)\Big]$$

where $A_1(N,\omega_1,\omega_2)$ is N - delayed version of $A_1(0,\omega_1,\omega_2)$. The block diagram of the running bispectrum using sliding rectangular window is shown in Figure 4.

CONCLUSIONS

It is shown that forward and reverse sequence one-dimensional running Fourier transforms of a data sequence can be used to construct a recursive algorithm for the bispectrum estimates. In this algorithm, the number of computations required to update the bispectrum estimate at each frequency sample (ω_1,ω_2) is independent of the cumulant maximum lags of interests (K,M). Since the size of the 2-D lag window defines resolutions in Fourier-based estimation, the proposed algorithm offers resolution enhancement without an increase in computational requirements. Two simple examples were presented in which recursive and non-recursive data windows are employed for time-averages.

REFERENCES

1. M. L. Raghuveer and C. L. Nikias, "Bispectrum Estimation: A Digital Signal Processing Framework", IEEE Proceedings, July 1987.

2. A. Papoulis, Signal Analysis, McGraw-Hill, Inc., New York, 1977.

3. L. Rabiner and B. Gold, Theory and Applications of Digital Signal Processing, Prentice-Hall, Inc., Englewood Cliffs, New Jersey, 1975.

4. M. G. Amin, "Computationally Lag-Invariant Recursive Spectrum Estimators", IEEE Transaction on Acoustics, Speech and Signal Processing, December 1987.

5. T. E. Stacy and M. G. Amin, "VLSI array processor implementation of a simple class of recursive spectrum estimators," Proceedings of the 32st Midwest Symposium on Circuits and Systems, Rolla, MO August 1988.

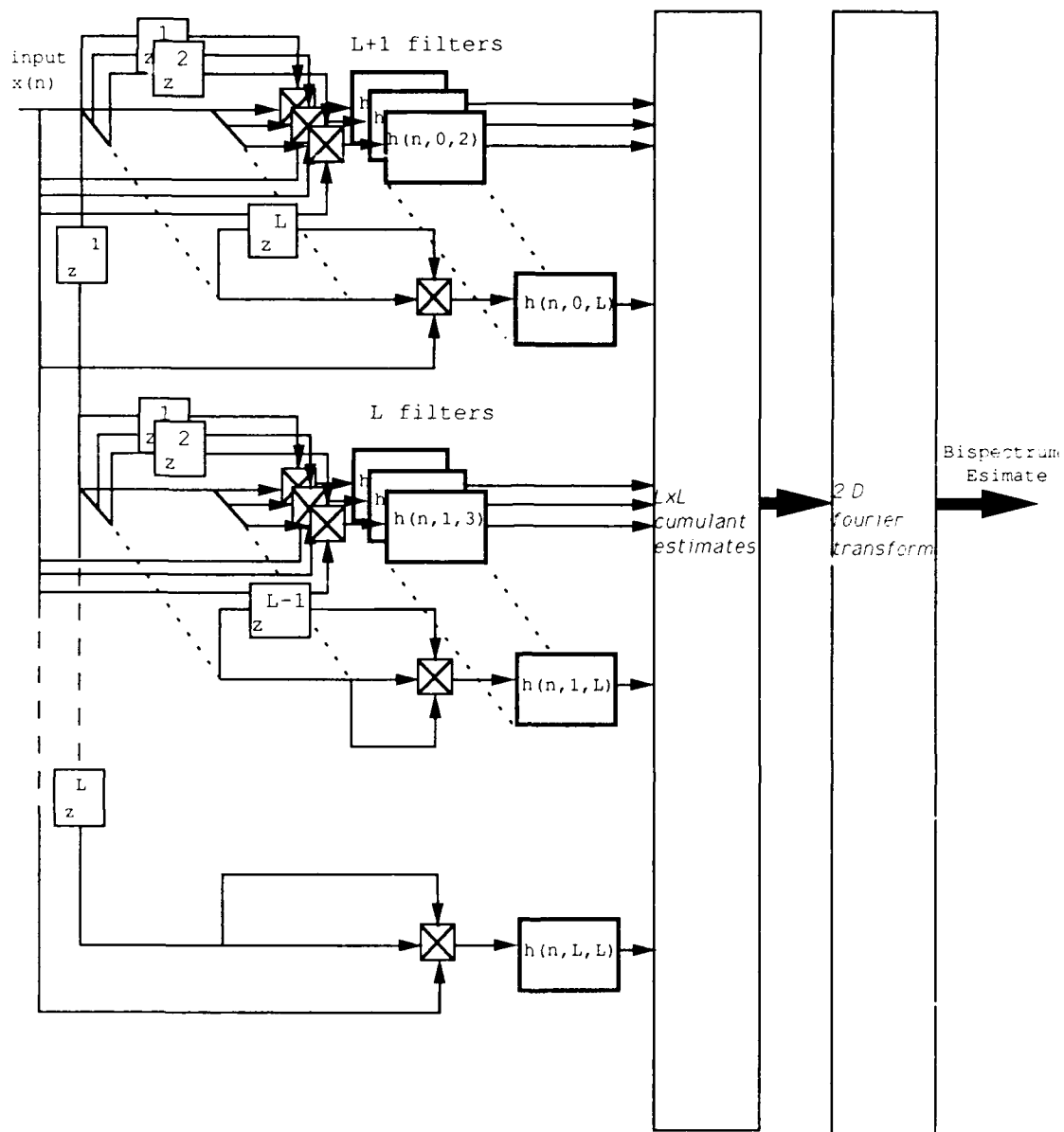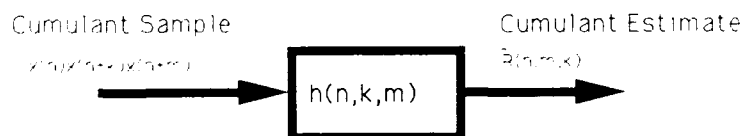Fig 1 System diagram of conventional
Bispectrum estimation

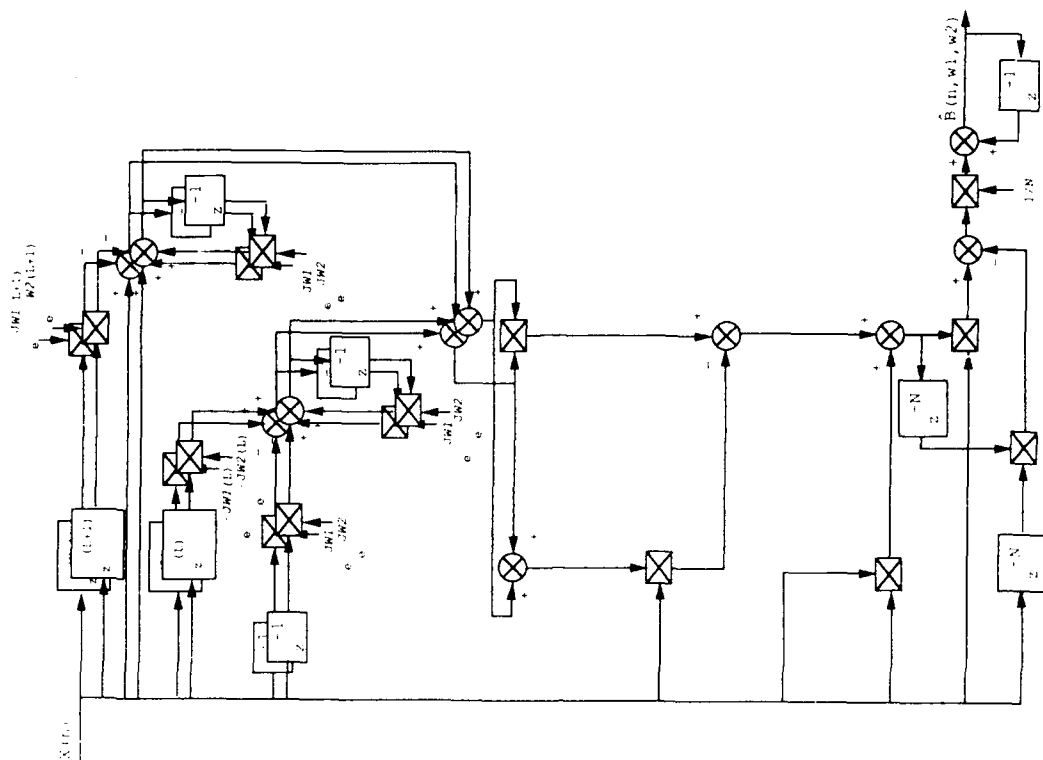Fig 2 System for cumulant estimation
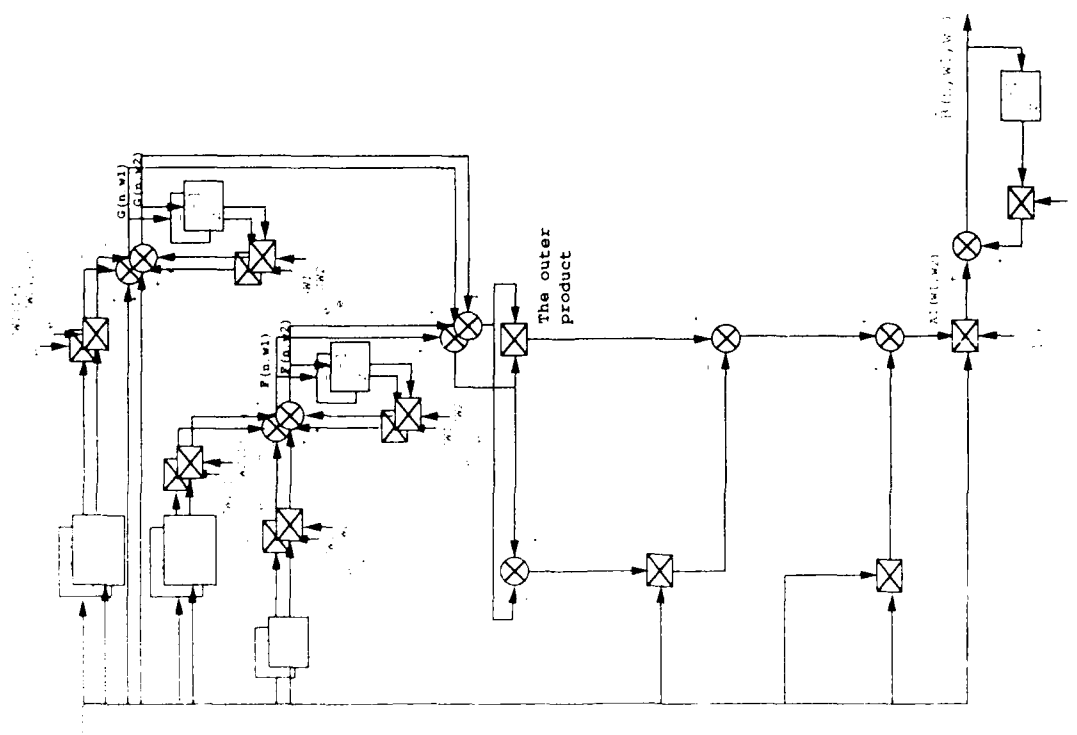
Fig. 4 Recursive update of FIR filter of length N.

Fig. 3 Recursive update of the bispectrum for a single pole filter.

SOME HISTORY OF THE STUDY OF HIGHER-ORDER MOMENTS AND SPECTRA

David R. Brillinger

Statistics Department, University of California, Berkeley, CA 94720

ABSTRACT

Some of the history of the development of random process higher-moments and spectra is set down for the period preceding 1980. Time-side and frequency-side properties are contrasted. Some uses of the concepts and associated techniques are mentioned as well as are some of the computational procedures that have been employed.

I. INTRODUCTION

It is not easy to set down the history of concepts used broadly throughout the sciences. The material is inevitably limited by an author's personal experience. Still it seems worth attempting even if for no other reason than to induce others to set down what they know. Since the work of the present paper is meant to be historical rather than review, consideration will be restricted to the pre-1980 period.

There are a variety of "sides" from which one can discuss the matter: theoretical-empirical, time-frequency, ordinary series - generalized process, discrete time - continuous time, computational-distributional, univariate-vector and so on. There is insufficient space and time to cover many of these aspects in any real detail, but a variety of aspects will be set down.

II. SECOND-ORDER MOMENTS AND SPECTRA

There will be minimal discussion of the second-order case for the principal concern is with the higher-order situation and because there exists an extensive commentary concerning the second-order case in Yaglom (1987). It is remarked that in Brillinger (1976) some specific history of the U. S. work is set down.

Time-side

Two early references to empirical work with the autocovariance function that will be mentioned are Hooker (1901) and Taylor (1921).

Frequency-side

A remarkable reference, turned up by A. M. Yaglom, is Einstein (1914). Commentaries on this paper are given in Masani (1986) and Yaglom (1987). An early reference to frequency-side analysis, pointed out in Rice (1945), is Kenrick (1929).

III. HIGHER-ORDER MOMENTS AND SPECTRA

The moments employed in the analysis of random processes and time series are direct extensions of those of ordinary statistics. The properties of these latter are laid out in Kendall and

Stuart (1969), for example. The moment approach in statistics is usually identified with the name of Karl Pearson. In anticipation of later development of time series techniques it is to be pointed out that Pearson's method of moments was largely replaced by R. A. Fisher's likelihood approach as the years have passed.

The joint product moment of the k-variate random variable $\mathbf{X} = (X_1,...,X_k)$ is

$$E\{X_1 \cdots X_k\}$$

The joint cumulant of the variate $\mathbf{X}$ is the combination of the joint product moments of subsets of the components of $\mathbf{X}$, that vanishes if any subset of the components is statistically independent of the remainder. It is also the coefficient of $\theta_1 \cdots \theta_k$ in the Taylor expansion of the log moment generating function. The joint cumulant will be written

$$cum\{X_1, \cdots, X_k\}$$

It has the additional property of vanishing for $k > 2$ in the case of jointly Gaussian variates.

In essence what has been done in the time series case is quite simple. The product moment function of order k of the process is defined by

$$m_k(t_1, \ldots, t_k) = E\{X(t_1) \cdots X(t_k)\} \qquad (1)$$

while the cumulant function is defined by

$$c_k(t_1, \ldots, t_k) = cum\{X(t_1), \ldots, X(t_k)\}$$

In the case that the process is stationary one has the simplifications

$$m_k(t+u_1, \ldots, t+u_{k-1}, t) = m_k(u_1, \ldots, u_{k-1})$$

and

$$c_k(t+u_1, \ldots, t+u_{k-1}, t) = c_k(u_1, \ldots, u_{k-1}) \qquad (2)$$

That is, one deals with functions of one fewer argument.

More insightfully however, in the stationary case the process has a spectral representation

$$X(t) = \int_{-\pi}^{\pi} e^{it\lambda} dZ(\lambda) \qquad (3)$$

involving the random function $Z(.)$. (Here time has been taken to be discrete, $t = 0, \pm 1, \pm 2, \ldots$, but this is no real restriction). This representation leads directly to the definition of higher-order spectra. The cumulant spectra, $f_k(.)$, are now given by

$$cum\{dZ(\lambda_1), \cdots, dZ(\lambda_k)\} =$$

$$\eta(\lambda_1 + \cdots + \lambda_k) f_k(\lambda_1, \cdots, \lambda_{k-1}) d\lambda_1 \cdots d\lambda_k \qquad (4)$$

with $\eta(.)$ the 2π-periodic extension of the Dirac delta function. (The concentration of the mass on the subspaces, $\lambda_1 + \cdots + \lambda_k = 0, \pm 2\pi, \pm 4\pi, \cdots$ results from the stationarity of the process.) The cumulant spectrum f_k may also be defined as the Fourier transform of the cumulant function of the right hand side of expression (2).

Consideration now turns to some historical aspects.

Time-side

A central idea in the time-side case is that of Kolmogorov's, (see Shiryaev (1960)), to base analyses on the cumulant functions rather than the product moment functions.

The use of the cumulant functions may be motivated in several ways. They remove the lower order information in a sense because they vanish if some proper subsets of the $X(t)'s$ is independent of the remainder. In many cases of interest they tend to 0 for large arguments and thus have convenient analytic properties. They also turn up in investigations of ergodicity. They provide a fashion by which to introduce mixing, leading to the later development of central limit results useful in suggesting statistical approaches. References developing these aspects include: Leonov (1960,1964), Shiryaev (1960,1963), Sinai (1960,1963) and Brillinger (1965). Shiryaev (1960) focuses on cumulant functions. Zhurbenko (1970) introduces an alternate form of mixing condition for example.

Frequency-side

Moments of order k of the dZ are considered in the seminal work of Blanc-Lapierre and Fortet (1953). It is interesting that in counterdistinction to the second-order case, the cumulant functions do not necessarily have a representation as the Fourier transform of a measure, see Kolmogorov (1960), Sinai (1960), that is f_k of (4) may have to be treated as a generalized function of some type. In many cases of interest however they are proper functions.

Brillinger and Rosenblatt (1967a,b) develop the result

$$cum\{d^T(\lambda_1), \cdots, d^T(\lambda_k)\} \approx$$
$$\Delta^T(\lambda_1 + \cdots + \lambda_k)f_k(\lambda_1, \cdots, \lambda_{k-1})$$

under a particular mixing condition, where

$$\Delta^T(\lambda) = \sum_{t=0}^{T-1} e^{-i\lambda t}$$

and

$$d^T(\lambda) = \sum_{t=0}^{T-1} e^{-i\lambda t} X(t)$$

This result suggests that even had cumulant spectra not been defined in their own right, researchers would have been led to them as they developed the statistical properties of empirical Fourier transforms.

Brillinger (1965) and Brillinger and Rosenblatt (1967a,b) set down estimates of cumulant spectra of general order and develop some properties of those estimates.

The case of $k = 3$ has been studied in some detail. In particular one may mention the works of: Tukey (1953), Tukey (1959), MacDonald (1963), Hasselman et al. (1963), Godfrey (1965), Rosenblatt and Van Ness (1965), VanNess (1966), Shaman (1966), Hinich and Clay (1968), Kleiner (1971), Subba Rao and Gabr (1980). A bibliography on the $k = 3$ case has been

prepared by Tryon (1981).

The point process case

In the case of a point process $N(t)$ the moment measures are defined via

$$E\{dN(t_1) \cdots dN(t_k)\} \quad \text{and} \quad cum\{dN(t_1), \cdots, dN(t_k)\}$$

respectively. The point process case is notable in that when the points are isolated, the first quantity here has an interpretation as

$$Prob\{point \text{ in } (t_1, t_1 + dt_1) \text{ and } \cdots \text{ and } point \text{ in}(t_k, t_k + dt_k)\}$$

The moments in the point process case are often densities

$$p_k(t_1, \ldots, t_k)dt_1 \cdots dt_k \tag{5}$$

assuming all the t's are distinct. The functions $p_k(.)$ have appeared in a variety of guises in the physics literature over a period of many years. In particular the references Ursell (1927), Yvon (1935), Bhaba (1950), Ramakrishnan (1950), Bogoliubov (1962) may be noted.

In the stationary case the process has a spectral representation analagous to (3) above, namely

$$N(t) = \int \frac{e^{it\lambda}-1}{i\lambda} dZ(\lambda) \tag{6}$$

The cumulant spectra are again given by (4).

Some comparative aspects of the time series and point process cases are brought out in Brillinger (1978).

IV. TERMINOLOGY

J. W. Tukey has introduced many of the terms of spectral analysis. In particular he called the spectra of a single series for $k = 3, 4$ the bi- and tri-spectra respectively. He introduced the general term - polyspectrum. This word being of mixed Latin and Greek origin, as Alan Stuart has emphasized to this writer, it might be better to switch to eg. multispectrum. The other terms commonly employed are cumulant spectrum and higher- or k- order spectrum. Tukey seems also to have introduced the terms bifrequency and bicoherence.

The moment functions (1) and (5) are often called correlation functions in the physical sciences literature even in the case of general k.

V. SOME USES

Single series

Brillinger (1965) points out several uses of higher-order cumulant spectra. For example that they may be used to examine a process for Gaussianity and that they may be used to examine a process for linearity. The later use is investigated in some detail for the $k = 3$ case in Subba Rao and Gabr (1980). Brillinger (1965) also indicates how higher-order spectra might be employed in looking back at the genesis of an observed series from more elementary series. Peaks in the second-order spectrum at frequencies in elementary relation are suggestive of the operation of a nonlinearity at some stage.

Van Ness (1966b) mentions how polynomial functional expansions may be employed for prediction.

Lii et al. (1976) and Rosenblatt (1978) show how bispectra occur in connection with energy transfer between distinct frequencies - a phenomenon not possible with linear systems.

Rosenblatt (1979) begins a study of how the bispectrum may be employed to estimate the phase function of nonGaussian linear systems.

As a final use, one can note that higher-order spectra appear in the variances of estimates of lower-order moment and cumulant functions and so must be estimated to have indications of the latter's uncertainty.

In the point process case, Davies (1977) makes use of the product densities to examine for Poissonness.

System identification

In his book, Wiener (1958) sets down a "polynomial" representation for a system with Gaussian white noise input and discusses the analysis and synthesis of the system.

Tick (1961) has considered the particular case of the identification of a quadratic system with Gaussian process input. Specifically he considers a system like

$$Y(t) = a_0 + \sum_u a_1(u)X(t-u) + \sum_u \sum_v a_2(u,v)X(t-u)X(t-v) + \varepsilon(t)$$

with $X(.)$ stationary Gaussian and with $\varepsilon(.)$ a noise series independent of X. Then the second- and third-order cross-spectra are given by

$$f_{YX}(\lambda) = A_1(\lambda)f_{XX}(\lambda) \tag{7}$$

and

$$f_{YXX}(\lambda,\mu) = 2A_2(-\lambda,-\mu)f_{XX}(\lambda)f_{XX}(\mu) \tag{8}$$

respectively, where A_1 and A_2 are the Fourier transforms of a_1 and a_2 respectively. (Here for example $f_{YXX}(\lambda,\mu)$ is defined via $cum\{dZ_Y(\lambda),dZ_X(\mu),dZ_X(v)\} = \eta(\lambda+\mu+v)f_{YXX}(\lambda,\mu)d\lambda d\mu dv$.) In theses Gasser (1972) and Feuerverger (1972) develop further aspects of the identification of quadratic systems. In particular Feuerverger determines some statistical properties of estimates of A_1, A_2 developed from (7) and (8).

Lee and Schetzen (1965) set down a way to estimate the kernels of Wiener's polynomial expansion by cross-correlating Gaussian white noise input with the output. The book by Marmarelis and Marmarelis (1978) presents details and many examples of the use of the Lee-Schetzen method.

VI. COMPUTATIONAL PROCEDURES

Higher-order spectra may be estimated in quite a variety of fashions and higher-order cumulant function estimates may be computed in at least two.

The product moments may be estimated directly by the method of moments. One way to then estimate the cumulant functions is to first estimate the product moments of all orders less than or equal to k and then to simply substitute into the formula giving cumulants from product moments. An indirect fashion is to back-Fourier transform the periodogram of order k avoiding the submanifolds in which proper subsets of frequencies sum to a multiple of 2π.

Brillinger (1965) suggested estimating higher-order spectra: by complex demodulation, or by narrow-band filtering or by computing windowed Fourier transforms of empirical cumulants. Brillinger and Rosenblatt (1967b) suggested estimating cumulant spectra by smoothing higher-order periodograms avoiding the submanifolds, on which the lower order spectra were concentrated. Lii et al. (1976) in the case of $k = 3$ suggested

estimating the bispectrum by averaging third-order periodograms based on separate time stretches of the series. This technique has the further advantage of allowing one to estimate the variability of the estimate directly.

It may be remarked that for the last form of estimate, tapering the data before computing the Fourier transform can be quite crucial.

VII. EXTENSIONS

There are near-immediate extensions of the concepts of higher-order moments and spectra to spatial, particle, generalized and stationary increment processes. Streater and Wightman (1964) define them in an abstract quantum mechanical situation. There are generalizations to hybrid processes of the type $X(\tau_j)$ where X is an ordinary process and τ_j a point process. Other types of nonlinear systems, eg. those containing an instantaneous nonlinearity or bilinear systems, may be studied by higher-order spectra. Novel forms of mixing may be introduced for complex processes. The second-order procedure that Whittle (1953) introduced for estimating finite-dimensional parameters may be extended to the higher-order case.

VIII. DISCUSSION

Key ideas that may be recognized on the time-side are: Kolmogorov's suggestion that cumulant functions be the basic entities employed (probably many had considered product moment functions) and Wiener-Lee-Schetzen's that polynomial systems may be identified via Gaussian white noise input and cross-correlation. Key ideas on the frequency-side are perhaps: Blanc-Lapierre and Fortet's idea of considering moments of the $dZ(.)$ variates and the use of higher-order periodograms avoiding submanifolds in estimation of cumulant spectra.

ACKNOWLEDGEMENT

References

[1] H. J. Bhabha, "On the stochastic theory of continuous parametric systems and its application to electron-photon cascades," PROC. R. SOC. LONDON Ser. A Vol. 202, pp. 301-332:1950.

[2] A. Blanc-Lapierre and R. Fortet, "Theorie des Fonctions Aleatoires," Paris, Masson: 1953.

[3] N. N. Bogoliubov, "Problems of a Dynamical Theory in Statistical Physics," Moscow, Gostekhizdat, 1962.

[4] D. R. Brillinger, "An introduction to polyspectra," ANN. MATH. STATIST. vol. 36, pp. 1351-1374:1965.

[5] D. R. Brillinger, "The frequency analysis of relations between stationary spatial series," pp. 39-81 in Proc. 12-th Biennial Seminar on Time Series, Stochastic Processes, Convexity, and Combinatorics, (ed. R. Pyke), Montreal, Canadian Math. Congress: 1970.

[6] D. R. Brillinger, "Some history of the data analysis of time series in the United States," pp. 267-280 in History of Statistics in the United States (ed. L. J. Owen), New York,

Dekker: 1976.

[7] D. R. Brillinger. "Comparative aspects of the study of ordinary time series and of point processes." pp. 33-133 in Developments in Statistics, vol. 1 (ed. P. R. Krishnaiah): 1978.

[8] D. R. Brillinger and M. Rosenblatt, "Asymptotic theory of estimates of k-th order spectra," pp. 153-188 in Spectral Analysis of Time Series (ed. B. Harris), New York, Wiley: 1967a.

[9] D. R. Brillinger and M. Rosenblatt, "Computation and interpretation of k-th order spectra," pp. 189-232 in Spectral Analysis of Time Series (ed. B. Harris), New York, Wiley: 1967b.

[10] R. B. Davies, "Testing the hypothesis that a point process is Poisson," ADV. APPL. PROB. Vol. 9, pp.724-:1977.

[11] A. Einstein, "Method pour la determination de valeurs statistiques d'observations concernant grandeurs soumises a des fluctuations irregulieres," ARCH. SCI. PHYS. ET NATUR. VOL. 37, pp. 254-256:1914. This paper is reproduced in Masani (1986).

[12] A. Feuerverger, "On the Cumulant Spectra Approach to Polynomial Regression of Stationary Time Series," Ph. D. Thesis, University of California, Berkeley: 1972.

[13] T. Gasser, "System Identification, Polyspectra and Related Functions," Ph.D. Thesis, Swiss Federal Institute of Technology, Zurich: 1972.

[14] M. D. Godfrey, "An exploratory study of the bi-spectrum of economic time series," APPLIED STATISTICS Vol. 14, pp. 48-69:1965.

[15] K. Hasselman, W. Munk and G. J. F. MacDonald, "Bispectra of ocean waves," pp. 125-139 in Time Series Analysis (ed. M. Rosenblatt). New York, Wiley: 1963.

[16] M. J. Hinich and C. S. Clay, "The application of the discrete Fourier transform in the estimation of power spectra, coherence and bispectra of geophysical data," REV. GEOPHYSICS Vol. 6, pp. 347-363:1968.

[17] R. H. Hooker, "Correlation of marriage-rate with trade," J.ROYAL STAT. SOC. Vol. 64, pp. 485-492:1901.

[18] M. C. Kendall and A. Stuart, "The Advanced Theory of Statistics," London, Griffin: 1969.

[19] G. W. Kenrick, "The analysis of irregular motions with applications to the energy frequency spectrum of static and of telegraph signals," PHIL. MAG. Ser.7 Vol. 7, pp. 176-196:1929.

[20] B. Kleiner, "Die Berechnun von Bispektren," Ph. D. Thesis, Swiss Federal Institute of Technology, Zurich: 1971.

[21] A. N. Kolmogorov, "On the $\Phi^{(n)}$ classes of Fortet and Blanc-Lapierre," THEORY PROB. APPL. Vol. 5, 337:1960.

[22] Y. W. Lee and M. Schetzen, "Measurement of the Wiener kernels of a nonlinear system by cross-correlation," INTERNAT J. CONTROL Vol. 2, pp. 237-254:1965.

[23] V. P. Leonov, "The use of the characteristic functional and semi-invariants in the ergodic theory of stationary processes," SOVIET MATH. Vol. 1, pp. 878-881:1960.

[24] V. P. Leonov, "Some applications of Higher-Order Semi-invariants to the Theory of Stationary Random Processes,"

Moscow, Izdatistvo Nauka:1964.

[25] K. S. Lii, M. Rosenblatt and C. Van Atta, "Bispectral methods in turbulence," J. FLUID MECH. Vol. 77, pp. 45-62:1976.

[26] G. J. F. MacDonald, "The bispectra of atmospheric pressure records," pp. 247-264 in Proceedings IBM Scientific Computing Sympo ium on Statistics. White Plains, IBM: 1963.

[27] T. Madden, " Spectral, cross-spectral and bispectral analysis of low frequency electromagnetic data," pp. 429-450 in Natural Electromagnetic Phenomena Below 30 kc/s, New York, Plenum: 1964.

[28] P. Z. Marmarelis and V. Z. Marmarelis, "Analysis of Physiological Systems," New York, Plenum: 1978.

[29] P. R. Masani, "Einstein's contribution to Generalized Harmonic Analysis and his intellectual kinship with Norbert Wiener," JAHRBUCH UBERBLICKE MATHEMATIK Vol. 109, pp. 190-209:1986.

[30] B. Mazelsky, "Extension of power spectral methods of generalized harmonic analysis to determine non-Gaussian probability functions of random input disturbances and output responses of linear systems," J. AERONAUTICAL SCIENCES Vol. 21, pp. 145-153:1954.

[31] A. Ramakrishnan, "A stochastic process relating to particles distributed in a continuous infinity of states," PROC. CAMBRIDGE PHIL. SOC. Vol. 46, pp. 596-602:1950.

[32] M. R. Rosenblatt, "Remarks on higher order spectra," pp. 383-389 in Multivariate Analysis (ed. P. R. Krishnaiah). New York, Academic: 1966.

[33] M. R. Rosenblatt, "Energy transfer for the Burgers' equation," PHYS. FLUIDS Vol. 21, pp. 1694-1697:1978.

[34] M. R. Rosenblatt, "Linearity and nonlinearity in time series: prediction," Proc. 42nd Session Inter. Statist. Inst., vol. 1, pp.423-434: 1979.

[35] M. Rosenblatt amd J. W. Van Ness, "Estimation of the bispectrum," ANN. MATH. STATIST. Vol. 36, pp. 1120-1136:1965.

[36] P. Shaman, "Large-Sample Approximations to the First- and Second-Order Moments of Bispectral Estimates". Technical Report, School of Engineering, New York University: 1966.

[37] A. N. Shiryaev, "Some problems of the spectral theory of higher-order moments, I," THEORY PROB. APPL. Vol. 5, pp. 265-284:1960.

[38] A. N. Shiryaev, "On conditions for ergodicity of stationary processes in terms of higher order moments," THEORY PROB. APPL. Vol. 8, pp. 436-439:1963.

[39] Ya. G. Sinai, "Properties of spectra of ergodic dynamical systems," SOVIET MATH. Vol. 4, pp. 875-877:1960.

[40] Ya. G. Sinai, "On higher order spectral measures of ergodic stationary processes," THEORY PROB. APPL. Vol. 8, pp. 429-436:1963.

[41] R. F. Streater and A. S. Wightman, "PCT, Spin & Statistics, and All That," New York, Benjamin: 1964.

[42] T. Subba Rao and M. M. Gabr, "An Introduction to Bispectral Analysis and Bilinear Time Series Models," Lecture Notes in Statistics, No. 24, New York, Springer: 1980.

[43] G. I. Taylor, "Diffusion by continuous movements," PROC.

LONDON MATH. SOC. Ser. 2 Vol. 20, pp. 196-212:1921.

[44] L. J. Tick, "The estimation of transfer functions of quadratic systems," TECHNOMETRICS Vol. 3, pp. 563-567:1961.

[45] P. V. Tryon, "The Bispectrum and Higher-Order Spectra: A Bibliography," Technical Note 1036, National Bureau of Standards: 1981.

[46] J. W. Tukey, "The spectral representation and transformation of higher moments of stationary time series,": 1953. Reprinted pp. 165-184 in The Collected Works of John W. Tukey, Vol. 1 (ed. D. R. Brillinger). Belmont, Wadsworth: 1984.

[47] J. W. Tukey, "An introduction to the measurement of spectra," pp. 300-350 in Probability and Statistics: The Harald Cramer Volume, (ed. U. Grenander). Stockholm, Alqvist and Wiksell: 1959.

[48] J. W. Van Ness, "Asymptotic normality of bispectral estimates," ANN. MATH. STATIST. Vol. 37, pp. 1257-1272:1966a.

[49] J. W. Van Ness, "Empirical nonlinear prediction and polyspectra," Tech. Report No. 18, Statistics Department, Stanford University: 1966b.

[50] P. Whittle, "The analysis of multiple stationary time series," J. ROYAL STATIST. SOC. B Vol. 15, pp. 125-139:1953.

[51] N. Wiener, "Nonlinear Problems in Random Theory," Cambridge, MIT Press: 1958.

[52] A. M. Yaglom, "Einstein's 1914 paper on the theory of irregularly fluctuating series of observations," IEEE ASSP MAG., pp. 7-11:1987.

[53] A. M. Yaglom, "Correlation Theory of Stationary and Related Random Functions," Two Volumes, New York, Springer :1987.

[54] J. Yvon, "La Theorie Statistique des Fluids et l'Equation d'Etat," Paris, Herman: 1935.

[55] I. G. Zhurbenko, "On bounds of mixed semi-invariants for a certain class of random processes," THEORY PROB. APPL. Vol. 15, pp. 541-554:1970.

EVALUATION OF BICORRELATIONS FOR TRANSIENT DETECTION

George E. Ioup, Juliette W. Ioup, and Kenneth H. Barnes

Department of Physics, University of New Orleans
New Orleans, LA 70148

Robert L. Field and James H. Leclere

Naval Ocean Research and Development Activity
Stennis Space Center, MS 39529-5004

Grayson H. Rayborn

Department of Physics and Astronomy, University of Southern Mississippi
Hattiesburg, MS 39406-5046

ABSTRACT

Correlations and bicorrelations of a model 20 Hz finback whale signal and two actual data sinusoidal transient signals are examined to investigate the suitability of correlation and bicorrelation processors for the detection of oscillatory transients. The connections to moments of the distribution of ordinate values of the signals and the signal bispectrum are also discussed. We show that the bicorrelation processor is not a particularly good detector compared to the correlation in the simplest detection scheme for the whale signal (and likely not for other signals of small third moment) and that the bispectrum of narrowband transients is generally small except for transients at very low frequency.

INTRODUCTION

The question addressed in this paper is that of the usefulness of higher order correlations for detection of certain underwater acoustic transients. Since the work of Hasselman et al. [4] and Tukey [10], much has been done on higher order correlations and their spectra. The excellent review of Nikias and Raghuveer [8] is a comprehensive guide to the literature up to 1987. More recent results are discussed by Toda and Usui [9] and Brockett et al. [1].

If three or more sensors (or sets of sensors) receive a signal from a single source, the signal may be detected using the cross correlation of the sensors two at a time or by using a correlation of three at one time. If a known transient is sought, it may be cross correlated with the signal at a single sensor (matched filtering) or it may be simultaneously correlated with the signal at two sensors. These approaches are the main concern of this paper. The research can be extended to correlations of four or more signals simultaneously, to localization in time or space, and to source identification.

In this work we consider only source detection and examine mainly the question of correlations three at a time versus those taken two at a time. We concentrate on some oscillatory signals which are of a type generated by vibratory sources. We do not include the complications of multipath arrivals and coherence loss.

Initially we discuss the problems of correlation processing for underwater acoustic transients and the role of the autocorrelation in the analysis. We give sample transients and their properties. Definitions are set forth for ordinary and higher order correlations, and their spectra are related to the spectra of the transients. The importance of moments of ordinate values of the transients is stressed and a histogram of ordinate values is analyzed. The principal domains of bispectra for narrow and medium band transients and low frequency transients are discussed. Initial performance analyses of correlation and bicorrelation detectors are given.

Preliminary results of this work have been given by J. Ioup et al. [6] and by G. Ioup et al. [5].

COMPLICATIONS FOR CORRELATION PROCESSING

Whether correlating for a known or unknown transient, the assumption one would like to make is that the transient arrives unchanged, except for a possible uniform attenuation, at the sensor. Aside from the pervasive problem of noise, there are other degradations which can make basic correlation processing difficult. The first of these is multipath arrivals due to surface and/or bottom bounces. Even if the separate multipath arrivals do not overlap, a travel path determination is needed to translate arrival times into source locations. When the multipath arrivals do overlap, the transient waveform changes and will no longer match the known transient. Since we expect different multipath interference at each sensor, the signals at two sensors will not match each other, either. The second degradation which prevents transients from matching is the loss of coherence due to passage through the ocean and/or the ocean bottom.

THE ROLE OF THE AUTOCORRELATION

If no complications are present, the output of a correlation processor is expected to be proportional to a translated autocorrelation of the transient. Therefore a study of the autocorrelation and a performance evaluation of the detection of the autocorrelation in the presence of noise will establish limits for correlation processing valid in the absence of other degradations.

We define the cross correlation for real data $x_1(t)$ and $x_2(t)$ as

$$c_{12}(\tau) = \int_{-\infty}^{\infty} x_1(t)x_2(t+\tau)dt \supset X_1^*(f)X_2(f) \qquad (1)$$

and the autocorrelation as

$$a(\tau) = \int_{-\infty}^{\infty} x(t) \ x(t+\tau) \ dt \supset |X(f)|^2 \quad , \qquad (2)$$

with corresponding summation definitions for discrete data. Since the transients are assumed to be of finite duration, the domain of integration is limited and not infinite, and we need not be concerned with truncation effects unless only part of a long transient is to be processed.

HIGHER ORDER CORRELATIONS

For the simultaneous correlation of three or four signals, the bicorrelation and the tricorrelation are defined. Nikias and Raghuveer [8] and Brockett et al. [1] and earlier authors discuss similar and related functions.

For three signals, bi-cross correlation is

$$c_{123}(\tau_1,\tau_2) = \int_{-\infty}^{\infty} x_1(t) \ x_2(t+\tau_1) \ x_3(t+\tau_2) \ dt$$

$$\supset X_2(f_1) \ X_3(f_2) \ X_1^*(f_1+f_2) \qquad (3)$$

and the bi-autocorrelation is

$$a(\tau_1,\tau_2) = \int_{-\infty}^{\infty} x(t) \ x(t+\tau_1) \ x(t+\tau_2) \ dt$$

$$\supset X(f_1) \ X(f_2) \ X^*(f_1+f_2) \quad . \qquad (4)$$

If the means of the functions are subtracted out, these become the bi-cross covariance and the bi-autocovariance. (See, for example, the summary discussion of covariance and correlation in Marple [7].)

These relations are generalized in straightforward fashion for four signals to give the tri-cross correlation

$$c_{1234}(\tau_1,\tau_2,\tau_3) = \int_{-\infty}^{\infty} x_1(t)x_2(t+\tau_1)x_3(t+\tau_2)x_4(t+\tau_3)dt$$

$$\supset X_2(f_1) \ X_3(f_2) \ X_4(f_3) \ X_1^*(f_1+f_2+f_3) \qquad (5)$$

and the tri-autocorrelation

$$a(\tau_1,\tau_2,\tau_3) = \int_{-\infty}^{\infty} x(t) \ x(t+\tau_1) \ x(t+\tau_2) \ x(t+\tau_3) \ dt$$

$$\supset X(f_1) \ X(f_2) \ X(f_3) \ X^*(f_1+f_2+f_3) \quad . \qquad (6)$$

FINBACK WHALE TRANSIENT

Our first example transient is that of the finback whale, whose 20 Hz amplitude and frequency modulated signal has been described verbally and graphically by Watkins et al. [11]. We have fitted the following equation to their description

$$p(t) = A(t) \cos[2\pi f(t)t], \quad 0 < t < T = 1 \text{ sec.} \quad (7)$$

The amplitude, $A(t)$, should have a linear increase for the first third of the interval, be constant for the second third, and have a linear decrease for the last third, so

$$A(t) = \begin{cases} (3/T) \ t & 0 < t < T/3 \\ 1.0 & T/3 < t < 2T/3 \\ 3 - (3/T)t & 2T/3 < t < T \end{cases} \qquad (8)$$

The frequency should decrease nonlinearly from 23 to 18 Hz, with the most rapid decrease occurring initially and a decreasing rate of decrease with time. We select an exponential,

$$f(t) = 23 \text{ Hz } \exp(-\alpha t)$$
$$\alpha = -\ln(18 \text{ Hz}/23 \text{ Hz}) \approx 0.25 \quad , \qquad (9)$$

to describe this effect. The result is shown in Fig. 1 and its spectrum is given in Fig. 2. The autocorrelation of this signal, displayed in Fig. 3, is more compact than the original signal due to the chirp character of the signal. Figure 4 is a plot of the bi-autocorrelation which shows considerable structure.
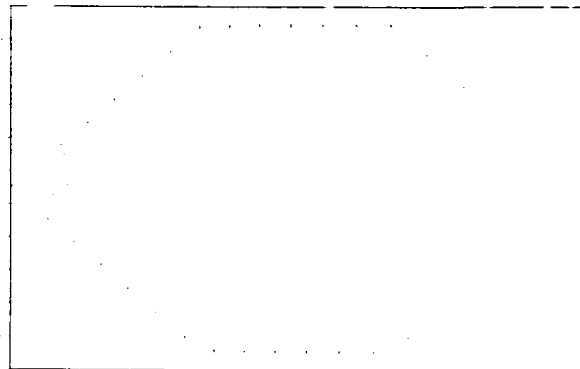

Fig. 1. Model of 20 Hz finback whale transient (an amplitude and frequency modulated signal) measured by Watkins et al. [11].

ACTUAL DATA SINUSOIDAL TRANSIENTS

We also had available two actual data sinusoidal transients, one identified as short and the other as long. Figure 5 shows the shorter of the two and Fig. 6 its Fourier transform.
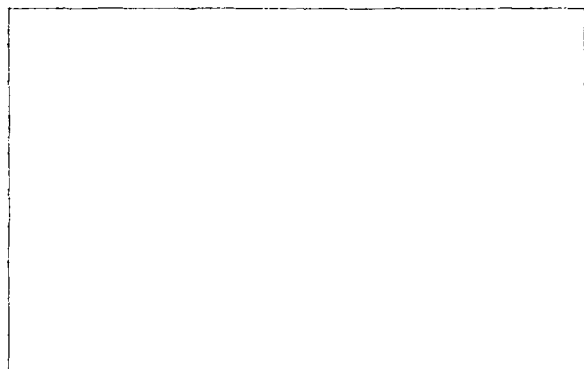
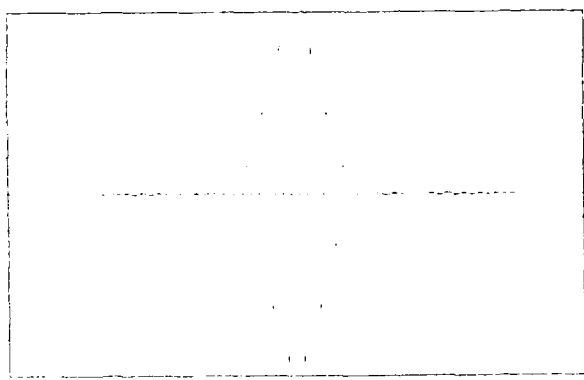Fig. 2. Fourier spectrum of 20 Hz finback whale transient.

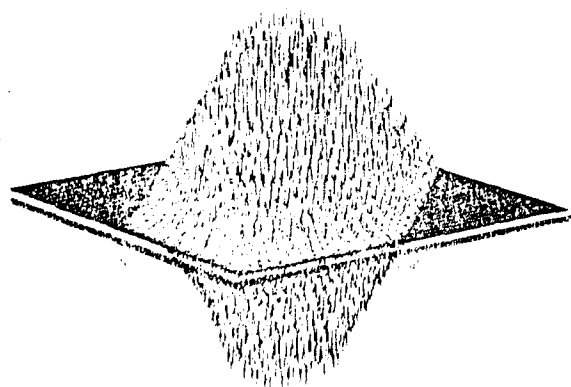Fig. 3. Autocorrelation of 20 Hz finback whale transient.

Fig. 5. Short actual data sinusoidal transient.

Fig. 6. Fourier spectrum of short actual data sinusoidal transient.

Fig. 4. Bi-autocorrelation of 20 Hz finback whale transient.

CENTRAL ORDINATE VALUES

The simplest correlation detector is one which detects on the peak of the correlation. Since the largest magnitude of the autocorrelation is its central value, this is a reasonable initial choice. The same is true of the tri-autocorrelation. For the bicorrelation, however, there is no guarantee that the maximum magnitude of the bi-autocorrela-
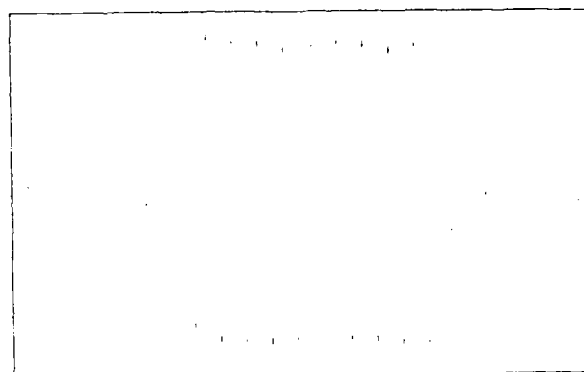
tion is its central value. Therefore caution must be used in designing a bicorrelation detector. Fortunately, for the previously discussed transients, the maximum magnitude of the bi-autocorrelation is at the origin for each signal and an ordinary detection scheme, comparable to the one used for the autocorrelation, was an appropriate first step. It should be noted that for the whale transient the maximum in the bi-autocorrelation is not necessarily at the origin if the signal is undersampled. The right half of a cut through the whale bi-autocorrelation, $a(\tau_1,0)$, adequately sampled, is shown in Fig. 7.

It is worthwhile to examine the peak values of the autocorrelations and bi-autocorrelations for the three transients mentioned. See Table 1. We note that the peak values of the bi-autocorrelations are small. This suggests that the simple bicorrelation processor may not be a good detector for these and similar signals. A performance analysis is needed for a definitive determination, however, and those results are given in a later section.

The central ordinate is related to the moment of the distribution of ordinate values and to the "area" under the power (energy) spectrum or the "volume" under the bispectrum of the signal. These relationships are discussed in subsequent sections.

It should be observed that more sophisticated detection schemes can be proposed, including those based on the near absence of a bicorrelation.
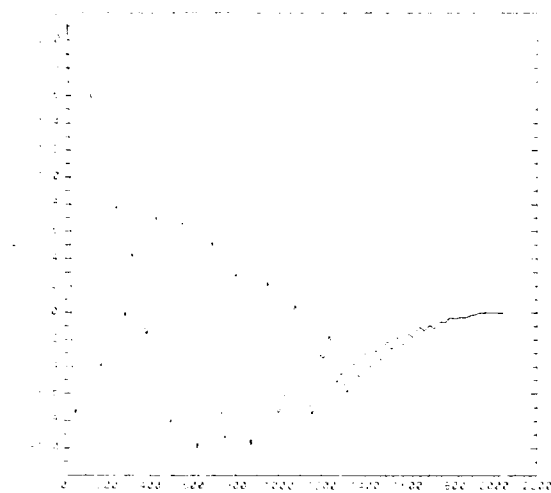
-69-

Fig. 7. Right half of a cut through the whale bi-autocorrelation surface, $a(\tau_1, 0)$.

Table 1

Central Ordinate

transient	autocorrelation (amplitude units)^{2}sec	bi-autocorrelation (amplitude units)^{3}sec
whale	0.278	1.07×10^{-3}
short sinusoid	1.46×10^{-3}	2.46×10^{-5}
long sinusoid	3.48×10^{-2}	8.83×10^{-5}

MOMENTS AND AUTOCORRELATIONS

The central values of the autocorrelations are related to the moments of the distribution of the ordinate values of the transient about the abscissa. (Elgar [3] discusses the third moment of x(t) about the ordinate.) For the autocorrelation the second moment is used,

$$\int_{-\infty}^{\infty} x^2(t)\, dt \quad , \tag{10}$$

and for the bi-autocorrelation the third moment,

$$\int_{-\infty}^{\infty} x^3(t)\, dt \quad . \tag{11}$$

For the autocovariance and bi-autocovariance the moments relative to the mean are needed,

$$\int \left(x(t) - \bar{x} \right)^2 dt \quad , \tag{12}$$

and

$$\int \left(x(t) - \bar{x} \right)^3 dt \quad . \tag{13}$$

For some applications it may be useful to normalize, such as by dividing by

$$\int_{-\infty}^{\infty} |x(t)|\, dt .$$

For discrete signals, the summations

$$\sum_{t=-\infty}^{\infty} x_t^2\, \Delta t \tag{14}$$

and

$$\sum_{t=-\infty}^{\infty} x_t^3\, \Delta t \tag{15}$$

are used. The transforms of $x^2(t)$ and $x^3(t)$ help determine adequate sampling for these calculations.

The small size of the central value of the bi-autocorrelation and the third moment for the oscillatory transients studied arises from their symmetry about zero or their mean ordinate. A histogram analysis of the whale signal, Fig. 8, illustrates the property. Even though the histogram is clearly non-Gaussian, as can be seen by its deviation from the best fit Gaussian shown in Fig. 8, it is almost symmetric. The figure suggests that the fourth moment will differ from the Gaussian and that the tricorrelation detector should be investigated.

PRINCIPAL DOMAINS OF BISPECTRA

A small central value of the bicorrelation corresponds to a small "volume" under the bispectrum surface. The small "volume" could be due to the oscillatory nature of the bispectrum (which implies that some other value(s) of the bicorrelation should be large) or it could mean simply that the bispectrum is small. For narrow band transients, especially those which do not include the lowest frequencies, we conclude that the latter is generally the case.

Although narrow and medium band transients are generally small, not zero, outside their passbands, for graphical clarity we assume they are zero. We label f_B the bottom frequency of the passband and f_T the top frequency. By shading the nonzero domain of $X(f_1)X(f_2)$ differently from the nonzero domain of $X^*(f_1+f_2)$, the nonzero domain of the bispectrum of the bi-autocorrelation, $X(f_1)X(f_2)X^*(f_1+f_2)$, which is the overlap of the two, is readily apparent. The whale signal is a narrow band transient and the "nonzero" domain of its bispectrum is shown in Fig. 9. The principal domains of $X(f_1)X(f_2)$ and $X^*(f_1+f_2)$ do not overlap and the bispectrum is small (but not zero because the whale transform is not zero outside its principal band). The nonzero domain for a transient with a wider passband (say 20 Hz to 60 Hz or 50 Hz to 150 Hz), which might be labeled medium band, is illustrated in Fig. 10. Only a small part of the nonzero domains of $X(f_1)X(f_2)$ and $X^*(f_1+f_2)$ overlap, and the bispectrum "volume" is limited. If the transient passband includes the lowest frequencies, the overlap is improved, as can be deduced from Fig. 11. Only the lower possible frequencies of the bispectrum (those closest to the origin) are nonzero, however, implying a relatively smooth bi-autocorrelation (low resolution).
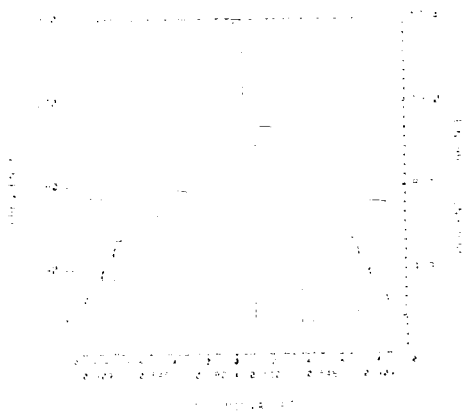
Fig. 8. Histogram analysis of the ordinate values of the whale signal and the best fit Gaussian.
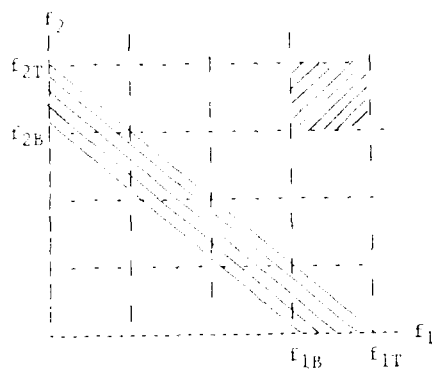

Fig. 9. Nonzero domains of bispectrum factors and bispectrum, narrow band transient.
///, nonzero domain for $X(f_1)X(f_2)$
\\\, nonzero domain for $X^*(f_1+f_2)$
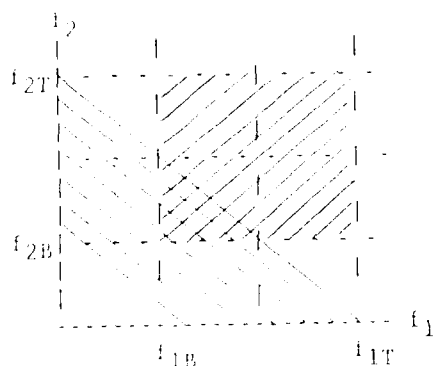crosshatch, nonzero domain for bispectrum, $X(f_1)X(f_2)X^*(f_1+f_2)$

Fig. 10. Nonzero domains of bispectrum factors and bispectrum, medium band transient.
///, nonzero domain for $X(f_1)X(f_2)$
\\\, nonzero domain for $X^*(f_1+f_2)$
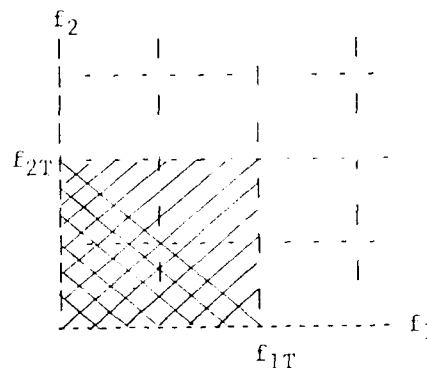crosshatch, nonzero domain for bispectrum, $X(f_1)X(f_2)X^*(f_1+f_2)$

Fig. 11. Nonzero domains of bispectrum factors and bispectrum, low frequency transient.
///, nonzero domain for $X(f_1)X(f_2)$
\\\, nonzero domain for $X^*(f_1+f_2)$
crosshatch, nonzero domain for bispectrum, $X(f_1)X(f_2)X^*(f_1+f_2)$

PERFORMANCE ANALYSIS

Performance analyses are being conducted for correlation processors as detectors, using the method of receiver operating characteristics (ROC) curves. (See, for example, Egan [2].) We have thus far completed initial tests for the cross correlation and bi-cross correlation detection of a known transient, the whale signal. We have used the cross correlation of the whale signal with a noisy whale signal and with noise alone to generate curves of probability of detection versus probability of false alarm for the cross correlation, and the bi-cross correlation of the whale signal with two independently noisy whale signals and with two independent noise sets to give the bi-cross correlation ROC curves.

We use Gaussian distributed time domain noise since this should be the most favorable type of noise for the bicorrelation detector. A histogram analysis of one 2048 sample noise set is given in Fig. 12. The deviations from the best fit Gaussian are small.
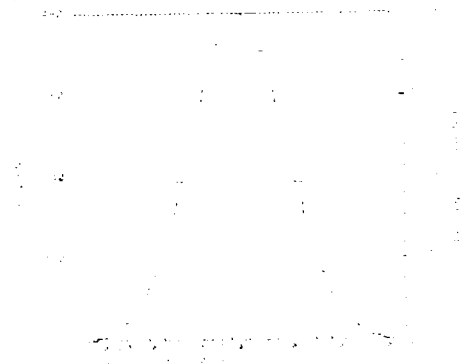

Fig. 12. Histogram analysis of a sample of 2048 point Gaussian distributed noise and the best fit Gaussian.

We define the signal-to-noise ratio (SNR) as the ratio of the standard deviation of the signal to the standard deviation of the noise. We have not converted to dB. The performance of the cross correlation detector is still very good at a SNR of 0.1, as shown in Fig. 13. The bi-cross correlation detector does not perform nearly as well for a 5.0 SNR (Fig. 14), and it fails at a 1.0 SNR (Fig. 15).
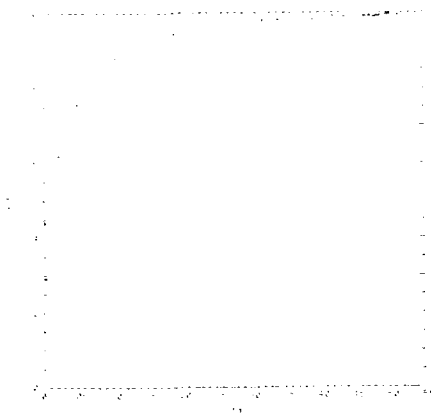
Fig. 13. Probability of detection versus probability of false alarm for a simple cross correlation detector for a known whale transient. Received signal has a SNR of 0.1.
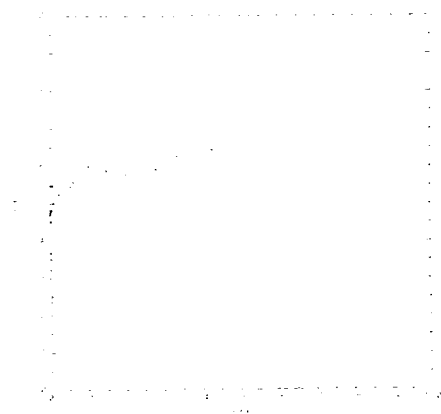
Fig. 14. Probability of detection versus probability of false alarm for a simple bi-cross correlation detector for a known whale transient. Received signals have SNR's of 5.0.

Fig. 15. Probability of detection versus probability of false alarm for a simple bi-cross correlation detector for a known whale transient. Received signals have SNR's of 1.0.

Our work is currently being extended to the case of the unknown transient (all signals noisy) and to tricorrelations and to other signals.

SUMMARY

Third moments and central ordinate values of the bi-autocorrelations of the oscillatory transients examined are small. For these transients the central ordinate happens to be the largest magnitude in the bi-autocorrelation. A performance analysis shows that the bi-cross correlation is not as good a detector for the whale signal as the ordinary cross correlation when each is used to detect on the peak value of the output (the simplest detector). The performance anaysis is being applied to other cases and other detectors.

For narrow-band transients, the principal domains of the factors of the bispectra often do not overlap. In these cases, the bispectra are small. The domain of overlap can be limited, even for medium bandwidth transients.

ACKNOWLEDGEMENTS

REFERENCES

[1] P. L. Brockett, M. Hinich, and G. R. Wilson, "Nonlinear and non-Gaussian ocean noise," J. Acoust. Soc. Am. Vol. 82, pp. 1386-1394: 1987.

[2] J. P. Egan, Signal Detection Theory and ROC Analysis, Academic Press: 1975.

[3] S. Elgar, "Relationships involving third moments and bispectra of a harmonic process," IEEE Trans. Acoust. Speech Signal Process. Vol. ASSP-35, pp. 1725-1726: 1987.

[4] K. Hasselmann, W. Munk, and G. MacDonald, "Bispectra of ocean waves," in Time Series Analysis, Murray Rosenblatt, editor, Wiley: 1963.

[5] George E. Ioup, Juliette W. Ioup, Robert L. Field, and James H. Leclere, "Higher Order Correlations for Transient Detection," Proc. of ONR ARI Transients Workshop: 15-16 Feb 1989.

[6] Juliette W. Ioup, George E. Ioup, Robert L. Field, and James H. Leclere, "Comparison of double and triple cross correlation for arrival time identification of amplitude- and frequency-modulated acoustic transient signals," J. Acoust. Soc. Am. Suppl. 1, Vol. 84, p. S17: 1988.

[7] S. Lawrence Marple, Jr., Digital Spectral Analysis with Applications, Prentice Hall: 1987.

[8] C. Nikias and M. R. Raghuveer, "Bispectrum estimation: A digital signal processing framework," Proc. IEEE Vol. 75, pp. 869-891: 1987.

[9] N. Toda and S. Usui, "Parametric estimation of bispectrum and a measure of non-Gaussianness," Trans. Inst. Electron. Inf. Commun. Eng. A (Japan) Vol. J71A, pp. 171-178: 1988.

[10] John W. Tukey, "An introduction to the calculations of numerical spectrum analysis," in Spectral Analysis of Time Series, Bernard Harris, editor, Wiley: 1967.

[11] William A. Watkins, Peter Tyack, Karen E. Moore, and James E. Bird, "The 20-Hz Signals of Finback Whales," J. Acoust. Soc. Am. Vol 82, pp. 1901-1912: 1987.

FOURTH-ORDER SPECTRA OF SONAR SIGNALS

Roger F. Dwyer

Naval Underwater Systems Center

New London, CT 06320

ABSTRACT

In active sonar, when a long pulse is transmitted
the return echo is usually amplitude modulated from
target dynamics, Doppler spreading, or medium effects.
Under these conditions, the spectrum can be severely
distorted making detection and classification impossi-
ble. Using an amplitude modulated coded pulse train,
it is shown in the paper that the fourth-order spectr. m
can extract range and Doppler information while for the
same conditions the spectrum cannot.

1. INTRODUCTION

The fourth-order spectrum represents a new way
of extracting information from sonar data. Used in
conjunction with the second-order spectrum (or power
spectrum) the fourth-order spectrum reveals otherwise
hidden relationships that are important for detection
and classification of sonar signals[1]. In addition, the
fourth-order spectrum can extract range and Doppler
information from an active sonar return under condi-
tions which render the conventional spectrum severely
degraded. Moreover, the Fourth-order spectrum sub-
tracts out additive Gaussian noise from its final result.

The paper will concentrate on the coded pulse ex-
ample. First, the envelope of an amplitude modulated
sonar return will be extracted. Then the autocorrelation
function and the fourth order cumulant function will
be derived. Finally, the spectrum and the fourth-order
spectrum will be obtained. The results will clearly show
the usefulness of the fourth order spectrum in extracting
range and Doppler information.

In general, the fourth order cumulant is a function
of three time delays[2,3,4,5,6,7,8]. However, for this
paper, a special case of the fourth-order cumulant will
be considered. It reduces to a function of one time
delay. But, nevertheless, this special case has interesting
properties that can be exploited in sonar and radar
applications. Being a function of only one time delay
it is also easily implemented.

Since, the envelope of the sonar return is not in gen-
eral a stationary process the second-order and fourth-
order spectra are obtained by a two-dimensional Fourier
transform of the autocorrelation and fourth-order cu-
mulant functions. For the amplitude modulated return,
it will be shown in the paper that the second-order
spectrum is interfered with by the modulating function
and, therefore, range and Doppler information cannot
be extracted. Whereas, the fourth-order spectrum can
extract range and Doppler information under the same
conditions.

2. Modulated Processes

Modulated processes arise in communications as
well as sonar and radar applications. Here the following
general modulated problem is treated. Let,

$$x(t) = a(t)z(t), \qquad (2.1)$$

be the modulated process. Where $a(t)$ and $z(t)$ are
both zero mean and mutually independent processes.
Equation (2.1) is in general a non-Gaussian Process
even if both $a(t)$ and $z(t)$ are Gaussian processes. It's
autocorrelation function,

$$R_x(\tau) = E[x(t)x(t+\tau)] = E[a(t)a(t+\tau)]E[z(t)z(t+\tau)]$$

$$R_x(\tau) = R_a(\tau)R_z(\tau). \qquad (2.2)$$

is a product of two autocorrelation functions. Therefore, it's spectrum will be a convolution of the two spectra. If $z(t)$ is the information bearing component then the modulating component $a(t)$ tends to interfere with the reception of $z(t)$.

Let $a(t)$ be a Gaussian process. Then the fourth-order cumulant of equation (2.1) reduces to

$$C'_{42}(\tau) = \text{Var}^2[a(t)]\left[E[z(t)^2 z(t+\tau)^2] - \text{Var}^2[z(t)]\right]$$

$$+ 2R_a(\tau)^2\left[E[z(t)^2 z(t+\tau)^2] - R_z(\tau)^2\right]. \quad (2.3)$$

Notice that (2.3) is not a simple product of autocorrelation functions. Therefore, it's spectrum will be different from the spectrum of (2.2).

Now let $z(t)$ be Gaussian also. Then (2.3) reduces to,

$$C'_{42}(\tau) = 2\text{Var}^2[a(t)]R_z(\tau)^2 + 2\text{Var}^2[z(t)]R_a(\tau)^2$$

$$+ 2R_a(\tau)^2 R_z(\tau)^2, \quad (2.4)$$

which can be seen to separate the two spectra into a sum and a product rather than just a product.

EXAMPLE 1.

Let,

$$x(t) = a(t)\cos(\omega_0 t + \phi),$$

where, φ is a random parameter uniformly distributed between 0 and 2π. Then,

$$R_x(\tau) = R_a(\tau)\frac{\cos(\omega_0 \tau)}{2}.$$

If,

$$R_a(\tau) = e^{-\alpha|\tau|},$$

then the spectrum of $R_x(\tau)$ is

$$S_x(\omega) = \frac{\alpha}{(\omega - \omega_0)^2 + \alpha^2} + \frac{\alpha}{(\omega + \omega_0)^2 + \alpha^2}. \quad (2.5)$$

If $\alpha \to \infty$, then $S_x(\omega) \to 0$. This means that the sinusoidal frequency ω_0 will not be observed in the spectrum of $R_x(\tau)$.

However, the fourth order cumulant,

$$C_{40}(\tau) = \frac{1}{4}R_a(\tau)^2 + \frac{\text{Var}^2[a(t)]}{8}\cos(2\omega_0 \tau),$$

has the following spectrum,

$$C_{42}(\omega) = \frac{\alpha}{\omega^2 + (2\alpha)^2}$$

$$+ \frac{2\pi\text{Var}^2[a(t)]}{8}\frac{\delta(\omega - 2\omega_0) + \delta(\omega + 2\omega_0)}{2}. \quad (2.6)$$

Now, the sinusoidal frequency $2\omega_0$ is seen in (2.6) even as $\alpha \to \infty$.

(Simulation: Amplitude Modulated Sinusoid)

The spectrum (in db) of a sinusoid amplitude modulated by white noise is shown in figure 1. The sinusoidal frequency is not discernable in this figure because of the interference of the modulation as predicted in (2.5). However, the fourth-order spectrum in figure 2 (plotted on a linear scale) reveals the underlying sinusoid but at twice its frequency. This result is predicted in (2.6).
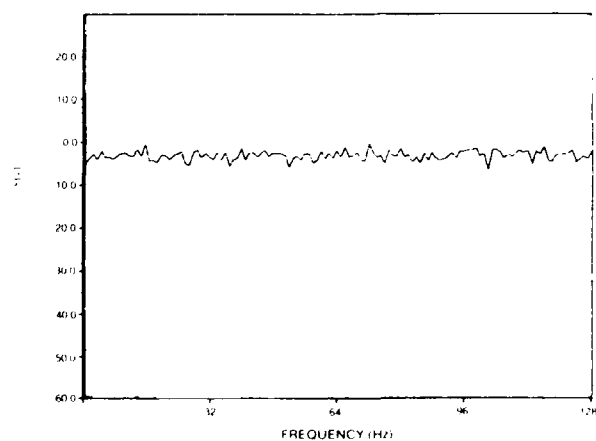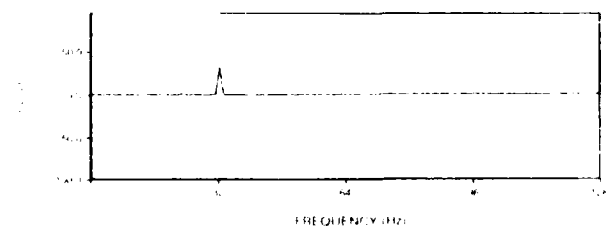

FIGURE 1. Modulated Spectrum.

FIGURE 2. Modulated Fourth-order Spectrum.

3. Sonar/Radar Application

Let,

$$y(t) = \sum_{n=-k}^{k} h(t - nT_p)e^{j(\omega_n t + \theta_n)},$$

$-\infty \leq t \leq \infty$, be the pulse coded transmitted signal of length, $2kT_p + T$. The pulses are defined as follows,

$$h(t - nT_p) = u(t - nT_p + \frac{T}{2}) - u(t - nT_p - \frac{T}{2}),$$

where u( ) is the unit step function. The parameters, T and T_p, for $T \leq T_p$, represent the pulse width and pulse repetition interval, respectively.

The received signal is assumed to be of the form

$$x'(t) =$$

$$a(t - \frac{T_R}{2}) \sum_{n=-k}^{k} h(t - nT_p - T_R)e^{j[(\omega_n + \omega_{nd})(t - T_R) + \theta_n + \phi]},$$

where, T_R is the range of the target, ω_{nd} is the Doppler radian frequency associated with each transmitted radian frequency ω_n, θ_n is the phase of the nth transmitted pulse, and ϕ is a random phase angle uniformly distributed between 0 and 2π. The real stochastic Gaussian modulating function a(t) represents a time fluctuating target[7]. This model usually applies for transmitted signals of long length.

Let,

$$y'(t) = \sum_{n=-k}^{k} h(t - nT_p - T_R')e^{j[\omega_n(t - T_R') + \theta_n]},$$

be the adjusted transmitted signal. Where T_R' is a parameter that is adjusted in order to search for the true range. For simplicity, it will be assumed that $T_R' = T_R$, ie, the range is known.

The envelope of the received signal is defined as follows,

$$x(t) = x'(t)y'^*(t),$$

where the asterisk is the complex conjugate.

Therefore, since the pulses are disjoint, ie,

$$h(t - n_1 T_p)h(t - n_2 T_p) = h(t - n_1 T_p), n_1 = n_2$$

$$h(t - n_1 T_p)h(t - n_2 T_p) = 0, n_1 \neq n_2$$

the envelope of the received signal is,

$$x(t) = a(t - \frac{T_R}{2}) \sum_{n=-k}^{k} h(t - nT_p - T_R)e^{j[\omega_{nd}(t - T_R) + \phi]}.$$

$$(3.7)$$

The objective of this example is to compare the autocorrelation function of (4.7) and its corresponding spectrum with the fourth-order cumulant function of (3.7) and its corresponding spectrum.

The autocorrelation function is given by the following expression,

$$E[x(t_1)x^*(t_2)] = R_a(t_2 - t_1) \sum_{n_1=-k}^{k} \sum_{n_2=-k}^{k}$$

$$h(t_1 - n_1 T_p - T_R)h(t_2 - n_2 T_p - T_R)e^{j(\omega_{n_1 d}t_1 - \omega_{n_2 d}t_2)},$$

$$(3.8)$$

where,

$$R_a(t_2 - t_1) = E[a(t_1 - \frac{T_R}{2})a(t_2 - \frac{T_R}{2})],$$

is a stationary autocorrelation function.

Therefore, since (3.7) is not in general a stationary process, the spectrum of (3.8) is defined as a two-dimensional Fourier transform of the autocorrelation function,

$$S(T_R, \omega_1, \omega_2) = \int_{-\infty}^{\infty} \int_{-\infty}^{\infty} E[x(t_1)x^*(t_2)]$$

$$e^{-j(\omega_1 t_1 + \omega_2 t_2)}dt_1 dt_2. \qquad (3.9)$$

To simplify the evaluation of (3.9) the modulating function will be assumed to be white noise,ie , $R_a(t_2 - t_1) = \delta(t_2 - t_1)$. Therefore, the spectrum of (4.8) reduces to

$$S(T_R, \omega_1, \omega_2) = Te^{-j(\omega_1 + \omega_2)T_R}$$

$$\left[\frac{\sin[(\omega_1 + \omega_2)\frac{T}{2}]}{[(\omega_1 + \omega_2)\frac{T}{2}]} \frac{\sin[(\omega_1 + \omega_2)(k + \frac{1}{2})T_p]}{\sin[(\omega_1 + \omega_2)\frac{T_p}{2}]} \right]. \qquad (3.10)$$

The spectrum (3.10) is concentrated along the line, $\omega_1 = -\omega_2$ with the same value , $T(2k+1)$, for all frequencies. Therefore, if $\omega_1 = -\omega_2$, then, $S(T_R, \omega) = T(2k + 1)$, $\forall\omega$. This clearly shows the interfering effect of the modulating white noise.

The fourth-order cumulant function reduces to the following result,

$$C_{42}(t_1, t_2) \quad \text{Var}^2[a] \sum_{n_1=-k}^{k} \sum_{n_2=-k}^{k} h(t_1 - n_1 T_p - T_R)$$

$$h(t_2 - n_2 T_p - T_R) e^{j2(\omega_{n_1 d} t_1 - \omega_{n_2 d} t_2)}. \qquad (3.11)$$

Where the Gaussian assumption for the modulating function was used to obtain (3.11).

Similarly, the fourth-order cumulant spectrum is defined as a two-dimensional Fourier transform,

$$C_{42}(T_R, \omega_1, \omega_2) - \int_{-\infty}^{\infty} \int_{-\infty}^{\infty}$$

$$C_{42}(t_1, t_2) e^{-j(\omega_1 t_1 + \omega_2 t_2)} dt_1 dt_2, \qquad (3.12)$$

which reduces to,

$$C_{42}(T_R, \omega_1, \omega_2) = \text{Var}^2[a] T^2 \sum_{n_1=-k}^{k} \sum_{n_2=-k}^{k}$$

$$e^{-j[\omega_1 + \omega_2 - 2(\omega_{n_1 d} - \omega_{n_2 d})][(n_1 + n_2)T_p + 2T_R]}$$

$$\left[\frac{\sin[(\omega_1 - 2\omega_{n_1 d}) \frac{T}{2}]}{(\omega_1 - 2\omega_{n_1 d}) \frac{T}{2}} \frac{\sin[(\omega_2 + 2\omega_{n_2 d}) \frac{T}{2}]}{(\omega_2 + \omega_{n_2 d}) \frac{T}{2}} \right]. \qquad (3.13)$$

Again, the spectrum is concentrated along the line, $\omega_1 = -\omega_2$, but now with peaks at twice the Doppler frequencies. To see this more clearly, let $\omega_1 = -\omega_2 = \omega$, and $\omega_{nd} = \omega_d, \forall n$, ie, all the Doppler frequencies are the same, then

$$C_{42}(T_R, \omega) - \text{Var}^2[a] T^2 (2k+1)^2 \left[\frac{\sin[(\omega - 2\omega_d) \frac{T}{2}]}{(\omega - 2\omega_d) \frac{T}{2}} \right]^2. \qquad (3.14)$$

It is clear that (3.13) and (3.14) are not interfered with by the modulating function, except for the constant representing its variance. Therefore, the fourth-order cumulant spectrum of the received signal will be discernable. Whereas, the spectrum of (3.8) may not be discernable depending on the modulating function $a(t)$ as shown in example 4.

4. Conclusions

For a special case of the fourth-order spectrum, it was shown in the paper that target information, from an active sonar return, could be extracted. Specifically, the fourth-order spectrum extracted Doppler shift frequencies from an amplitude modulated coded pulse train return, whereas, the spectrum was unable to do so.

5. References

1. R. Dwyer, "Higher-Order Spectra of Mixture Processes," IEEE ASSP Fourth Workshop on Spectrum Estimation and Modeling, Spring Hill Conference Center, Minneapolis, Minesota, 3-5 August 1988.

2. M. Hinich, "Testing for Gaussianity and Linearity of a Stationary Time Series," J. Time Series Anal., Vol. 3, No. 3, pp. 169-176, 1982.

3. K. Lii and M. Rosenblatt, "Deconvolution and Estimation of Transfer Function Phase and Coefficients for Non-Gaussian Linear Processes," Ann. Stat., Vol. 10, pp. 1195-1208, 1982.

4. D. Brillinger and M. Rosenblatt, "Asymptotic Theory of Kth- Order Spectra." In: **Spectral Analysis of Time Series** (B. Harris, ed.) 1967, pp. 153-188, Wiley, New York.

5. K. Lii and M. Rosenblatt, A Fourth-Order Deconvolution Technique for Non-Gaussian Linear Processes." In: **Multivariate Analysis** (P. Krishnaiah, ed) 1985, pp. 395-410, Elsevin Science Publishers.

6. C. Nikias and M. Raghuveer, "Bispectrum Estimation: A Digital Signal Processing Framework," Proceedings of the IEEE, Vol., 75, No. 7, pp. 869-891, July 1987.

7. M. Raghuveer and C. Nikias, "Bispectrum Estimation: A Parametric Approach," IEEE Trans. On ASSP, Vol. ASSP-33, No. 4, October 1985.

8. G. Giannakis and J. Mendel, "Identification of Nonminimum Phase Systems Using Higher Order Statistics," IEEE TRANS. On ASSP, Vol. 37, No. 3, March 1989.

9. H. Van Trees, **Detection, Estimation, and Modulation Theory: Part III, Radar-Sonar Signal Processing and Gaussian Signals in Noise**, John, Wiley & Sons, Inc. 1971, Chapter 11.

APPLICATION OF BISPECTRAL TECHNIQUES TO RADAR SIGNATURE ANALYSIS

Eric K. Walton and Ismail Jouny

The Ohio State University ElectroScience Laboratory
1320 Kinnear Road, Columbus, Ohio 43212

ABSTRACT

Spectral estimation techniques may be used in radar signature analysis to obtain a radar target impulse response. In general there is a one to one relationship between specific scattering mechanisms and the time such mechanisms appear in the impulse response. One of the difficulties that this type of analysis has is that complex targets often have multiple interactions. The result is that many of the terms in the impulse response are related to the interactions rather than due to the result of simple subcomponent scattering. Many of these multiple interaction mechanisms can be identified as such by the application of the bispectrum to the radar scattering data. Also, this study indicates that the individual target scattering mechanisms are more easily observed using the bispectrum under conditions of high noise or target dispersive effects.

I. INTRODUCTION

Radar scattering from an object is often measured as amplitude and phase at a set of evenly spaced frequencies. This permits a transformation to the time domain and thus the range domain by taking an inverse Fourier transform of the data [1]. The result is called the radar target impulse response. In general there is a one to one relationship between specific scattering mechanisms and the time such mechanisms appear in the impulse response. One of the difficulties that this type of analysis has is that complex targets often have multiple interactions. The result is that many of the terms in the impulse response are related to the interactions rather than due to the result of simple subcomponent scattering. Many of these multiple interaction mechanisms can be identified as such by the application of the bispectrum to the radar scattering data.

Also, this study indicates that the individual target scattering mechanisms are more easily observed using the bispectrum under conditions of high noise or target dispersive effects. It will be shown that these bispectral responses constitute robust features which may be used in radar target identification schemes.

II. BIRANGE PROFILE THEORY

The radar scattering from a complex target can be effectively modeled as a sequence of discrete scatterers. With this model each element of the set of complex radar scattering data is expressed as

$$\tilde{S}_p(f_j) = A_p \exp(-j2\pi R_p f_j / c), \tag{1}$$

where

$$
\begin{aligned}
\tilde{S}_p(f_j) &= p^{th}\text{scattering coefficient at} \\
& \quad j^{th} \text{ frequency} \\
A_p &= \text{amplitude of } p^{th} \text{ scattering} \\
& \quad \text{coefficient} \\
R_p &= \text{line of sight range between} \\
& \quad \text{scatterers and radar zero phase} \\
& \quad (\& \text{ time) reference plane.} \\
f_j &= j^{th} \text{ radar carrier frequency} \\
c &= \text{speed of light.}
\end{aligned}
$$

This can be usefully converted to scalar form by simply taking the real part of the scattering value.

$$\Re\left\{\tilde{S}_p(f_j)\right\} = A_p \cos(2\pi R_p f_j, c) \tag{2}$$

Note that when data are represented in this form for the scattering from a particular single point scatterer at a particular range from the radar phase zero reference point (which may be located near or on the target), a sinusoidal variation in the data as a function of frequency results. The amplitude of the sinusoid is proportional to the scattering coefficient of the scatterer, and the periodicity of the sinusoidal variation (as a function of radar carrier frequency) of the real part of the the scattered signal is proportional to the line of sight distance of the scatterer to the zero phase reference plane. If the scatterers do not interact, then the total received signal will have the form

$$\tilde{S}_t(f_j) \quad \sum_r A_p \cos(2\pi R_p f_j, c) . \tag{3}$$

Note that computation of the spectrum of $\tilde{S}_t$ will yield values of A_p for each R_p. Note on the other hand that if the scatterers interact (multiple interaction), then a signal scattered from the latter part of a particular target will be influenced (or modulated) by interaction with components of the target closer to the radar. This interaction with other parts of the radar target prior to scattering from a particular object on the radar target results in modulation-like effects in the range domain profile which can be uniquely identified when the bispectral estimation process is applied to $\tilde{S}_t$.

The definition of the bispectrum is the two-dimensional Fourier transform of the third moment sequence. In this study the bispectrum is a birange profile obtained by computing a two-dimensional Fourier transform of the third order autocorrelation function which is a function of frequencies f_1, f_2, in the two-dimensional frequency domain.

$$R_{S_t}(f_1, f_2) = E\left\{\tilde{S}_t(f_j)\tilde{S}_t(f_j + f_1)\tilde{S}_t(f_j + f_2)\right\} \quad (4)$$

$$B_{S_t}(R_1, R_2) = \sum_{f_1} \sum_{f_2} R_{S_t}(f_1, f_2)$$
$$\exp(-j2\pi/c[R_1 f_1 + R_2 f_2]) \quad (5)$$

The bispectral estimates in this study are computed using the indirect classical method which is based on computing an estimate of the third moment sequence. Windowing can also be applied to the estimates of the autocorrelation values. In this study the optimum window (minimum bispectrum bias supremum) [2] is used.

III. BLADE AND SPHERE EXAMPLE

Consider a blade of width $r_1 - r_0$ and a sphere at a distance $r_2 - r_1$ from the trailing edge of the blade. The zero reference is set at a distance r_0 from the leading edge of the blade (see Figure 1). It can be shown that if one considers four ray paths the backscattered signal is;

$$S_t(f_j) = A_1 + A_2 \exp\left(-j2\pi r_1 \frac{f_j}{c}\right)$$
$$+ A_3 \exp\left(-j2\pi r_2 \frac{f_j}{c}\right)$$
$$+ A_4 \exp\left(-j2\pi(r_1 + r_2 - r_0)\frac{f_j}{c}\right) \quad (6)$$

assuming that the amplitudes A_1, A_2, A_3, and A_4 are frequency independent. The impulse response of the blade and sphere target as computed using the inverse Fourier transform (with a Hanning window over a frequency band from 1.5 GHz to 12 GHz) is shown in Figure 2. Note the one to one relationship for the first three responses with the geometry of the target. The fourth response, however, is an interaction term and there is no target component which corresponds to it.

Figure 3 shows the bispectral response of the backscatter from the blade-sphere combination. In this figure, $r_0 = 0$ (zero reference at the leading edge of the blade). Note the response at $r_1 = 1.6$ meters and $r_2 = 2.4$ meters which is due to interaction between the trailing edge of the blade and the sphere and is represented by the term $\exp\left(-j2\pi(r_1 + r_2 - r_0)\frac{f_j}{c}\right)$. We can also notice the twelve symmetry regions of the bispectrum.

If the value of r_0 is increased to 1 meter, the bispectral response shown in Figure 4 results. Note that all of the response terms have moved along the associated diagonals, but the particular scattering and interaction terms are still observable.

IV. NOISE AND DISPERSION

If zero mean white Gaussian noise is added to the raw data, the resulting impulse response and bispectral response are shown in Figures 5 and 6. Note that although the detectability of the target scattering terms is greatly reduced in the impulse response, they can still be identified in the bispectral response.

The effect of dispersion in the data is shown in Figures 7 and 8. Dispersion is the result of scattering from a subcomponent of the radar target where the scatterer behavior varies as a function of frequency. In this case, the behavior is modeled as follows.

$$A_i(f_j) = A_i(1 + \alpha \exp(-k f_j)) \cos(\beta f_j) \quad (7)$$

where

$A_i(f_j)$ is the frequency dependent amplitude of the backscatter coefficient from the ith scatterer and α, k, and β are constants.

In this study, $\alpha = 0.6$, $k = 0.01$, and $\beta = 20\pi$.

Figures 7 and 8 show that the effect of dispersion is not critical to the bispectrum response.

V. BISPECTRUM OF EXPERIMENTAL RADAR DATA

The compact radar cross section measurement range at The Ohio State University ElectroScience Laboratory was used to make measurements of the radar scattering of a set of 5 scale models of commercial transport aircraft. The measurments were calibrated so that absolute values of amplitude (in square centimeters) and phase (in degrees from an absolute reference plane) were available over the band of frequencies from 1.5 to 12.0 GHz. This corresponds to frequencies in the HF band for full scale aircraft and means that the targets are in the resonance region of the radar (i.e., The wavelength is on the order of the target size) [3].

Using the techniques described above (including the use of the optimum window function), the bispectrum of each radar target signature was computed. The results are shown in Figures 9 to 12. Note that the different radar targets yield distinctly different bispectral responses. This implies that such responses are likely candidates for radar target identification.

Since each radar target is being measured in the resonance region (as mentioned above), it can be shown that the target signature is relatively insensitive to changes in aspect angle, (especially in the impulse response signature). The result of taking the bispectral response for the Boeing 707 as the aspect angle varies from 10 to 20 degrees is shown in Figures 13 and 14. It can be seen that the bispectral response is rather stable between each 10 degree angle change.

VI. CONCLUSIONS

In this paper the application of bispectrum estimation to radar signature analysis is investigated. It has been demonstrated that a bispectral response of radar backscatter signals has the advantage of identifying multiple interactions for complex radar targets. This leads to the conclusion that higher order interactions of radar backscatter may be identified using higher order spectral analysis. Therefore, the bispectrum and other high order spectral analysis methods may be considered as potential radar feature extraction techniques that may be effectively used jointly with the impulse response in radar target identification. Finally, it is shown that bispectral responses of radar backscatter signals are relatively robust under conditions of high noise and frequency dispersion.

References

[1] E.M. Kennaugh and R.L. Cosgriff, "The Use of Impulse Response in Electromagnetic Scattering Problems." *1958 IRE National Conv. Rec.*, pt. 1, pp. 72-77.

[2] L. Nikias, M.R. Raghuveer, "Bispectrum Estimation: A digital Signal Processing Framework," *Proc. IEEE*, Vol. 75, No. 7, pp. 869-891, July 1987.

[3] E.K. Walton, J.D. Young, "The Ohio State University Compact Radar Cross-section Measurement Range," *IEEE Trans. on Antennas and Propagation*, Vol. AP-32, No.11, pp. 1218-1223, November 1984.

$$\tilde{S}_1 = A_1 e^{-jk2r_c} \qquad A_1 = 10$$
$$\tilde{S}_2 = A_2 e^{-jk2r_1} \qquad A_2 = 23$$
$$\tilde{S}_3 = A_3 e^{-jk2r_2} \qquad A_3 = 45$$
$$\tilde{S}_4 = A_4 e^{-jk[2(r_2+(r_1-r_0))]} \qquad A_4 = 11$$
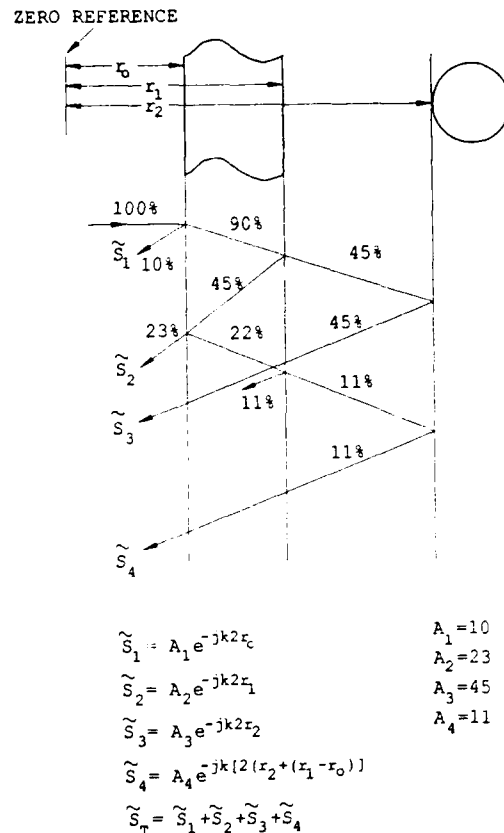$$\tilde{S}_T = \tilde{S}_1 + \tilde{S}_2 + \tilde{S}_3 + \tilde{S}_4$$

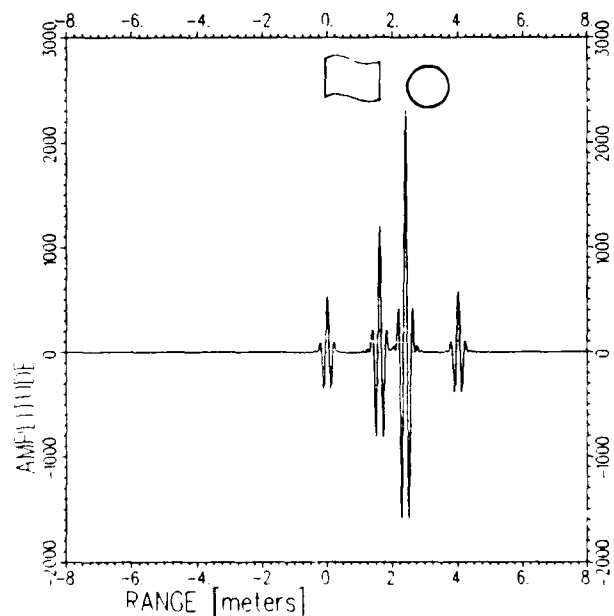Figure 1: Internal bounce diagram for blade-sphere interaction.

Figure 2: Impulse response for blade-sphere, $r_0 = 0$, $r_1 = 1.6$ m, $r_2 = 2.4$ m.
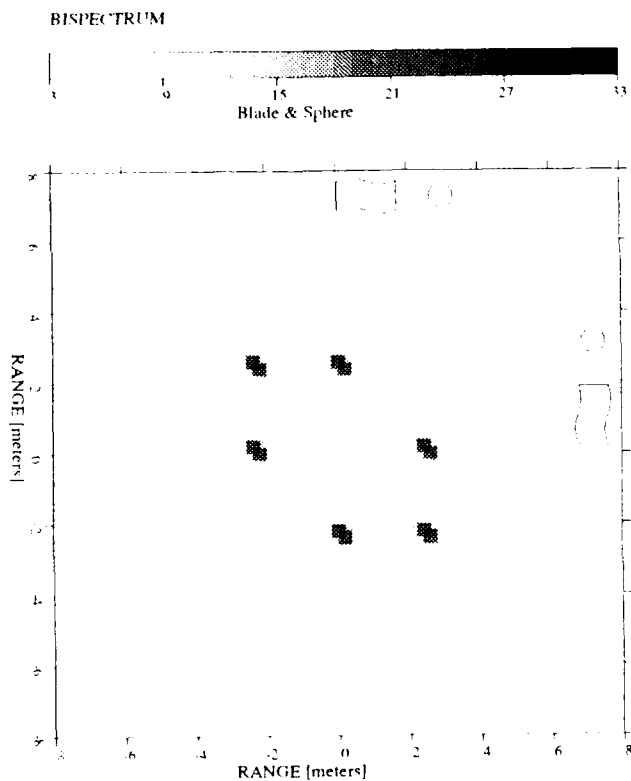
BISPECTRUM

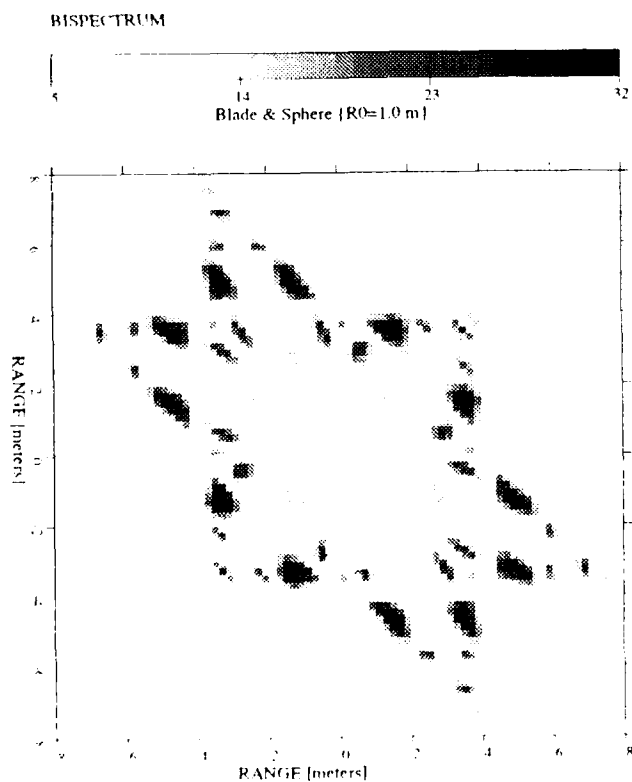Figure 3: Bispectrum for blade-sphere $r_1 = 1.6$ m, $r_2 = 2.4$ m.
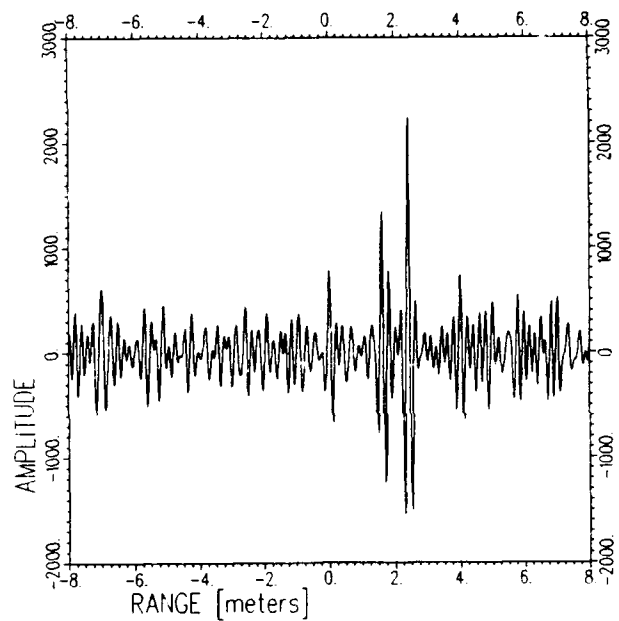

Figure 5: Impulse response for noisy backscatter from blade-sphere $\{SNR = -30dB\}$.

BISPECTRUM

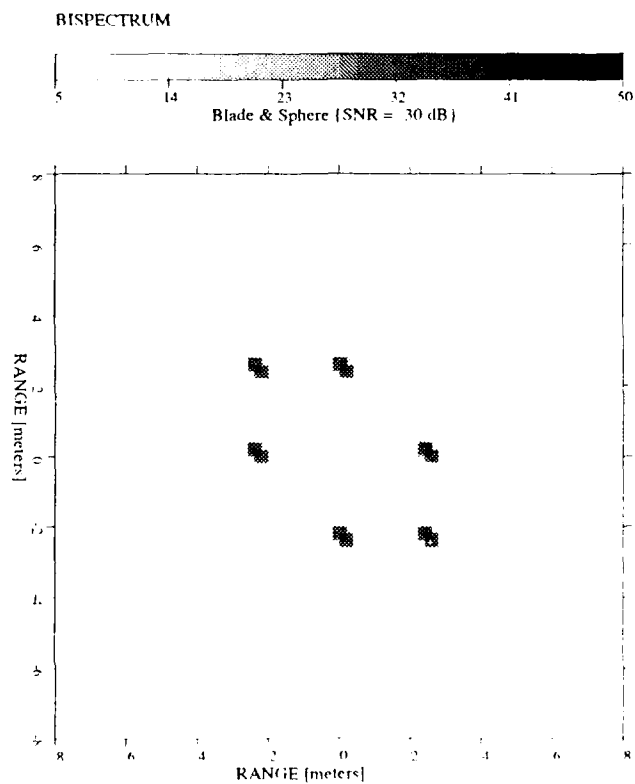Figure 4: Bispectrum for blade-sphere with $r_0 = 1$ m.

BISPECTRUM

Figure 6: Bispectrum for blade-sphere with noisy data $\{SNR = -30dB\}$.
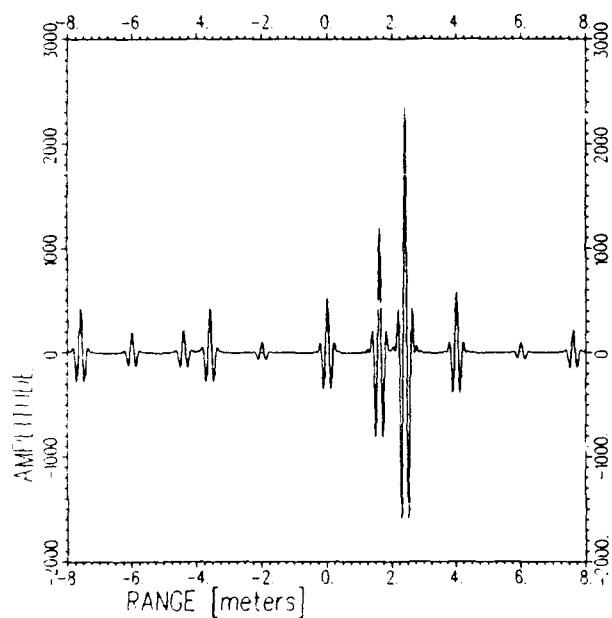
Figure 7: Impulse response of frequency dispersive backscatter for blade-sphere.
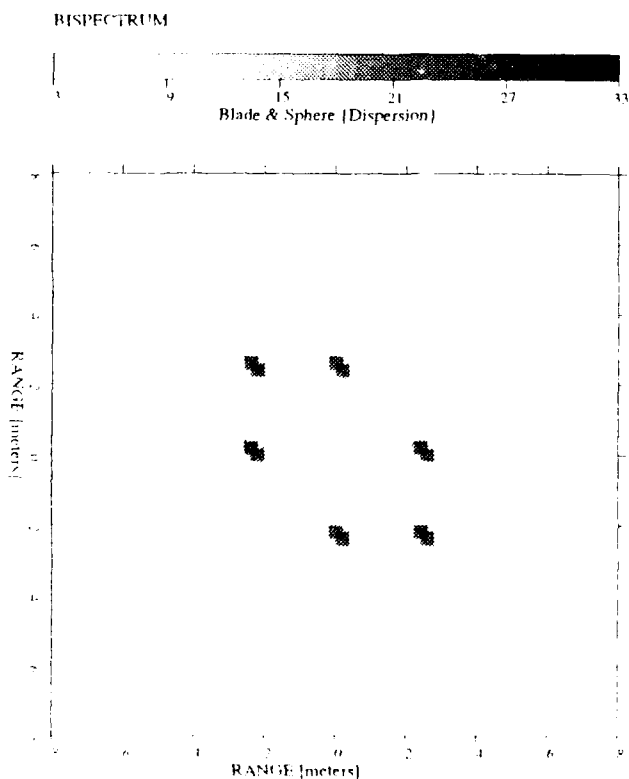

Figure 9: Bispectral response for 747 at 0 degrees azimuth, 0 degrees elevation.

Figure 8: Bispectrum of frequency dispersive backscatter for blade sphere.
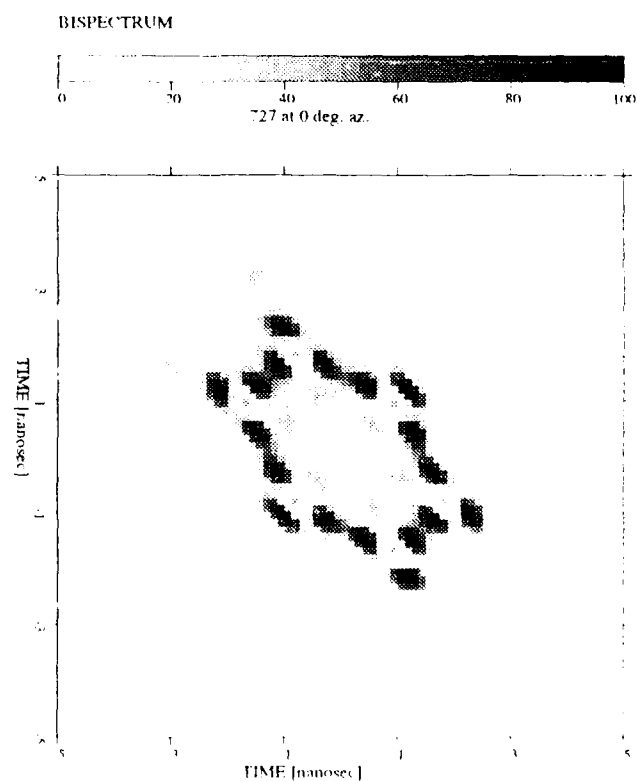
Figure 10: Bispectral response for 727 at 0 degrees azimuth, 0 degrees elevation.

BISPECTRUM
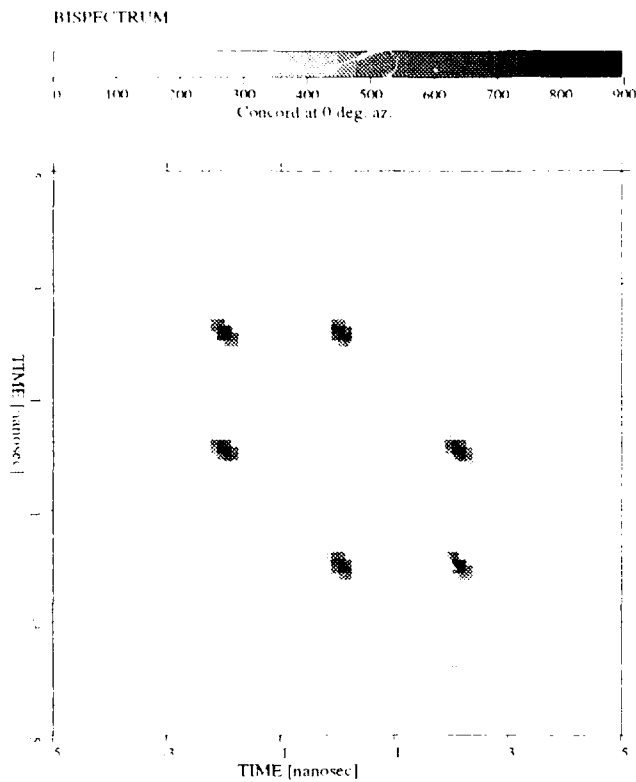
Concord at 0 deg. az.

Figure 11: Bispectral response for concord at 0 degrees azimuth, 0 degrees elevation.

BISPECTRUM

707 at 10 deg. az.

Figure 13: Bispectral response for 707 at 10 degrees azimuth, 0 degrees elevation.

BISPECTRUM

707 at 0 deg. az.

Figure 12: Bispectral response for 707 at 0 degrees azimuth, 0 degrees elevation.
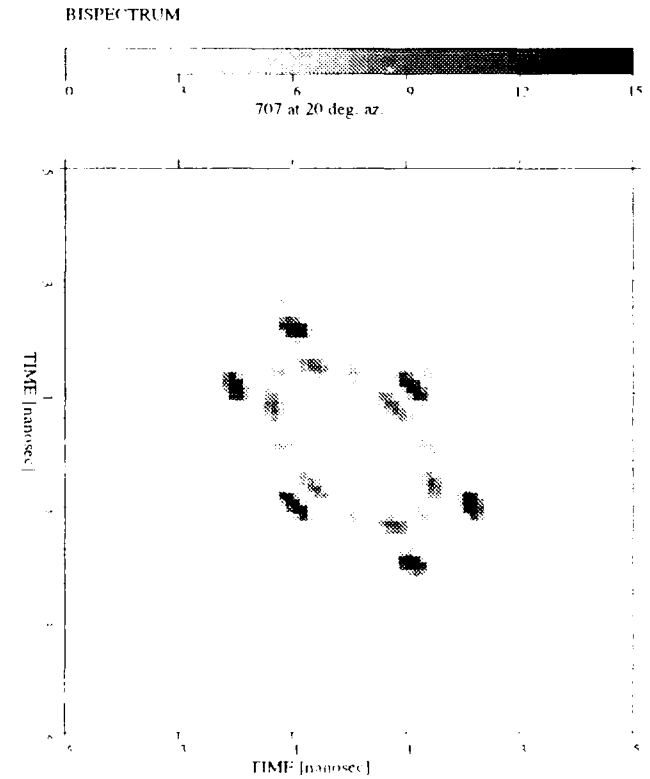
BISPECTRUM

707 at 20 deg. az.

Figure 14: Bispectral response for 707 at 20 degrees azimuth, 0 degrees elevation.

HIGHER-ORDER STATISTICAL SIGNAL PROCESSING WITH VOLTERRA FILTERS

B. Picinbono

Laboratoire des Signaux et Systèmes
ESE, Plateau du Moulon, 91192 Gif sur Yvette, France

Abstract. This paper presents a review of some applications of Volterra filters (VFs) in statistical signal processing. VFs are a particular class of nonlinear filters defined by an extension of the idea of impulse response to the nonlinear case. Linear and linear-quadratic filters are special examples of VFs limited to the first or second order respectively. The purpose of this paper is to extend to VFs the main ideas used in applications of linear filters for signal processing problems. To do this the first task is to simplify the notation of the input-output relationship of VFs which appears very tedious. Noting that this relation is nonlinear in terms of the input but linear in terms of the parameters defining the VF, it is possible to deduce that the output can be written as a scalar product quite similar to that used in the linear case. Using this form of scalar product, which is very easy to manipulate, and also the higher order statistics of the signals, we study some fundamental problems such as detection, estimation, array processing, etc. In doing this we avoid analytic calculations which are very complex with VFs and focus our attention on geometrical methods.

1. INTRODUCTION

The purpose of this paper is to present a review of some applications of Volterra filters (VFs) in statistical signal processing. It is well known that the use of linear filters as well as the assumption of Gaussian noise are sometimes quite inappropriate and give only approximate solutions in many signal processing problems. These approximations can be very good in some circumstances, but quite insufficient in others, and the need for new methods has been clear for a long time. The difficulty is that although the concept of a linear system is quite well defined, this is not the case for nonlinear systems. The same can been said for the Gaussian property : a non Gaussian process is not well defined and without other assumptions it is in general impossible to calculate an optimal signal processing system.

In this paper we intend to study a class of nonlinear systems which can be described by a Volterra expansion, and which are called simply VFs. On the other hand, the random signals appearing in the discussion will be described by their moments till a particular order, which corresponds exactly to the title of this workshop devoted to higher-order statistical analysis. With these tools we intend to review the basic problem of statistical signal processing such as detection, estimation, array processing etc.

The core of our analysis is that VFs can be written as linear filters in a proper linear space. In this space convenient scalar products can be introduced in such a way that most of the problems analyzed can be treated by methods deduced from the linear case. In this analysis the use of geometrical instead of analytical methods greatly simplifies the results, even though if the final calculation needs the use of analytical or numerical procedures. This kind of approach has not been widely explored in the literature. But those interested in a general description of VFs using analytical methods can find a good introduction with many results in [1].

2. FUNDAMENTALS OF VOLTERRA FILTERS

A VF of order v (v positive integer) is a nonlinear system the input-output relationship of which is described by a finite Volterra expansion. To simplify the presentation we will consider the discrete time case only, and we call $x[k]$ and $y[k]$ the input and output respectively. The output is expressed by

$$y[k] = h_0 + \sum_{m=1}^{v} \sum_{\{i_n^m\}} h_m[i_1^m, i_2^m, ..., i_m^m] x[k - i_1^m] x[k - i_2^m] ... $$

$$... x[k - i_m^m]. \qquad (2.1)$$

In this expression k and i_n^m are arbitrary integers and the symbol $\{i_n^m\}$ means that the sum is taken on all the i_n^ms. The term h_0 corresponding to $m = 0$ is a constant independent of the input and is sometimes omitted. In this latter case, and if $v = 1$, we obtain the classical convolution characterizing linear filters. By an obvious extension of the terminology used in the linear case, we will say that the VF has a finite impulse response if the integers i_n^m are taken in a finite interval, as for example $1 \le i_n^m \le N$. We make this assumption henceforth in order to avoid convergence problems. In this case the input at time k can be considered as a vector x with components $x[k - i]$, $1 \le i \le N$, written

for simplification $x[i]$, and the output at time k can be expressed as

$$y = h_0 + \sum_{m=1}^{v} \sum_{[i_m^m]} h_m[i_1^m, i_2^m, ..., i_m^m] \, x[i_1^m] \, x[i_2^m] ... x[i_m^m], \quad (2.2)$$

where the i_n^m's satisfy $1 < i_n^m \le N$.

For the discussion which follows it is necessary to simplify the notation of (2.2). For this we observe in (2.2) that the output y of the VF, considered as a function of the parameters h_m defining this filter, is linear in terms of these parameters. By introducing an appropriate space we intend to use this property to write y with a scalar product, or

$$y = h_0 + <h, v|X, v> , \quad (2.3)$$

where $|h, v>$ and $|X, v>$ are vectors of this space, and v is a reminder of the order of the VF.

To explain this method, let us begin with $v = 1$. In this case it is clear that if $h_0 = 0$, (2.2) becomes

$$y = h_1^{\mathsf{T}} x \quad (2.4)$$

and the vectors $|h, 1>$ and $|X, 1>$ are simply the vectors h_1 and x respectively.

Consider now the case where $v = 2$. Then (2.2) becomes

$$y = h_0 + h_1^{\mathsf{T}} x + x^{\mathsf{T}} H x , \quad (2.5)$$

where h_1 and H are a vector and a matrix respectively. The components of h_1 are $h_1[i]$ and the matrix elements of H are $h_2[i^2, i_2^2]$. As the matrix H can be considered as a vector of the space $\mathbb{R}^N \times \mathbb{R}^N = \mathbb{R}^{2N}$, a pair $[h, M]$ can be considered as a vector of the space $\mathbb{R}^N + \mathbb{R}^{2N}$ called $\mathbb{R}^N[2]$. This vector $|h, 2>$ is written as $|h, M>$ or also as $|h_1, h_2>$.

Similarly for $v = 3$ we can introduce the vector

$$|h, 3> = |h_1, h_2, h_3> \quad (2.6)$$

where h_1 is a vector, element of $\mathbb{R}^N$, h_2 a matrix, element of $\mathbb{R}^{2N}$ and h_3 a "matrix", element of $\mathbb{R}^{3N}$ with matrix elements $h_3[i, j, k]$. For this reason we say that $|h, 3>$ belongs to $\mathbb{R}^N[3]$. Now the extension to $|h, v>$ becomes obvious.

Finally, for arbitrary value of v we can introduce a vector $|h, v>$, also written $|h_1, h_2, ..., h_v>$, where h_m has the structure appearing in (2.2) and is the component of a vector of $\mathbb{R}^{mN}$. The vector $|h, v>$ then belongs to a linear space called $\mathbb{R}^N[v]$. This means that the vector $\lambda |h, v>$ is obtained by replacing all the hs by λh and the output of the VF is thus also multiplied by λ. On the other hand, the output of the sum of two VFs defined by $|h, v>$ and $|h', v>$ is a VF defined by the vector $|h, v>$ where the hs are replaced by $h + h'$. We have of course $\mathbb{R}^N[1] = \mathbb{R}^N$.

As in any linear vector space, we can introduce *linear operators* such as

$$A |h, v> = |h', v> \quad (2.7)$$

and all the concepts associated with these operators are valid in $\mathbb{R}^N[v]$.

More important is the concept of a *scalar product* of vectors of $\mathbb{R}^N[v]$. For this purpose it is interesting to simplify the notation even more and to write

$$h_m[i_1^m, i_2^m, ..., i_m^m] = h[i_m]. \quad (2.8)$$

where i_m stands for a vector of $\mathbb{R}^m$ with integer components $[i_1^m, i_2^m ...., i_m^m]$. With this notation the scalar product of two vectors $|h, v>$ and $|h', v>$ is defined by

$$<h, v|h', v> = \sum_{m=1}^{v} \sum_{i_m} h_m[i_m] \, h'_m[i_m], \quad (2.9)$$

which is a direct extension to $\mathbb{R}^N[v]$ of that used in $\mathbb{R}^N$. This allows the introduction of the transpose of an operator A defined by

$$<g, v| A |h, v> = <h, v |A^{\mathsf{T}} | g, v>. \quad (2.10)$$

Finally, an operator A is said to be symmetric if $A = A^{\mathsf{T}}$ and *definite non-negative* if for any $|h, v>$ we have

$$<h, v| A |h, v> \ge 0 . \quad (2.11)$$

Let us now define the input vector $|X, v>$ appearing in (2.3) to obtain y by (2.2). The input signal in (2.2) is a real N dimensional vector x with components $x[i]$. To this vector of $\mathbb{R}^N$ we associate the vector $|X, v>$ of $\mathbb{R}^N[v]$ defined by

$$|X, v> = |x_1, x_2, ... , x_v> , \quad (2.12)$$

where x_m is a vector of $\mathbb{R}^{mN}$ with components $x[i_1^m]x[i_2^m]... x[i_m^m]$. The vector $|X, v>$ is the v order input vector associated with the input x. With this notation Eq. (2.2) can be written in the form (2.3) which greatly simplifies the notation. Of course, the exact calculation of y requires the return to Eq. (2.2). It is also clear that if $v = 1$ or $v = 2$ we again find the linear and linear-quadratic filters. Finally, in order to simplify a little more, we will omit the letter v when no ambiguity is possible in the order of the filter. Thus in the following $|h>$ means $|h, v>$, whenever the order v of the filter is well specified.

In detection and estimation problems the input x is usually *random*. When this is the case, the vector $|X>$ also becomes random, as does the output y given by (2.3). The randomness of

the input introduces two points which must be briefly discussed. First, and most important, the output y can be undefined, in the sense that it is not a second order random variable. In order to avoid this situation we must assume that the input vector x has finite moments up to order 2ν. This ensures that y has a finite second order moment, or is a second order random variable. Secondly, y does not in general have a zero mean value. To define this value let us introduce

$$|m> \overset{\Delta}{=} E[|X>],$$ (2.13)

which is a vector of $\mathbb{R}^N[\nu]$ obtained by taking the expectation value of all the terms of (2.12). We then deduce from (2.3) that

$$E(y) = h_0 + <h|m>$$ (2.14)

and y has of course zero mean value if $h_0 = -<h\,|m>$. For any arbitrary $|h>$ it is then possible to use the constant term h_0 in the Volterra expansion (2.2) in such a way that y becomes zero mean. In the following we assume that this is realized. This was already the case in [2] when linear-quadratic systems were written

$$y = h^T x + x^T M x - \mathrm{Tr}(CM),$$ (2.15)

where x is zero mean and with covariance matrix C.

3. OPTIMAL VF FOR DETECTION

The most elementary and typical detection problem is an hypothesis testing problem between two simple hypotheses H_0 and H_1 specified by two probability distributions $p_0(x)$ and $p_1(x)$[3][4][5]. The optimal detection system, whatever the criterion, must calculate the likelihood ratio (LR) $L(x) = p_1(x)/p_0(x)$.

The decision between H_0 and H_1 is taken by comparing the LR with a threshold which can depend on the particular criterion of optimality used. This LR is in general a nonlinear function of the observation vector and sometimes di⁻ ult to implement. It is then interesting to approximate this L. y systems like (2.1) which are easier to realize. For this purpose we can use the property of invariance by a monotonic transformation [5], which sometimes allows us to simplify the structure. By this procedure the LR for detecting $N(0, \Gamma)$ against $N(s, \Gamma)$ can be transformed into a linear system which is the classical matched filter[5][6].

Another approach is to approximate the LR by using the *deflection criterion*. The deflection of a filter such as (2.1) is given by the ratio

$$D(x) \quad N/D$$ (3.1)

$$N \quad |E_1(x) \quad E_0(x)|^2$$ (3.2)

$$D = V_0(y),$$ (3.3)

where E_0 and E_1 mean expectation value under H_0 and H_1 respectively and V_0 means the variance under H_0.

The deflection criterion has long been used in detection theory and a more recent discussion of its history and its properties can be found in [2] and [5]. In particular, it is shown that the filter giving the maximum of the deflection is precisely the LR. Furthermore, using results of [5] it can be shown that the best approximation of the LR by a VF is precisely the VF giving the maximum value of the deflection. This indicates the interest of such a filter, which will now be determined from (3.1), (3.2) and (3.3).

In order to calculate the numerator N of (3.1) we introduce the notation

$$E_{1-0}(y) \overset{\Delta}{=} E_1(y) - E_0(y)$$ (3.4)

and we define the *signal vector* by an expression similar to (2.12) where the x_ms are replaced by their components

$$|s> \overset{\Delta}{=} E_{1-0} |X>$$
$$= |E_{1-0}(x[i_1^1]), E_{1-0}(x[i_1^2] x[i_2^2]), \dots , E_{1-0}(x[i_1^\nu].$$
$$x[i_2^\nu] \dots x[i_\nu^\nu])>.$$ (3.5)

It is clear that the first elements of (3.5) are deduced from the mean value and covariance of x under H_0 and H_1. The other terms have the same meaning for higher order moments. With this notation we get

$$N = <h|s>^2.$$ (3.6)

As y is zero mean under H_0, its variance is $E_0(y^2)$, or

$$V_0(y) = E_0|<h|X> <X|h>|,$$ (3.7)

which can be written

$$V_0(y) = <h|\,K\,|h>$$ (3.8)

with

$$K \overset{\Delta}{=} E_0|X> <X|.$$ (3.9)

This is a positive definite symmetric operator. As a result we can write N as $<h, \nu|\,KK^{-1}|s, \nu>$ and from the Schwarz inequality we deduce that the maximum value of the deflection obtained with a Volterra filter of order ν is

$$d_\nu^2 = <s, \nu|\,K^{-1}|s, \nu>.$$ (3.10)

It is obtained for $|h, \nu> = \alpha K^{-1}|s, \nu>$ and the corresponding optimal filter is

$$T_{0,v}(x) = \alpha <s, v| K^{-1} |X, v>. \tag{3.11}$$

We will assume henceforth that $\alpha = 1$. This result gives the classical matched filter [6] for $v = 1$, and the optimal linear-quadratic filter for $v = 2$ [2]. The exact calculation of this filter requires the calculation of $K^{-1} |s, v>$ or of $|\tilde{s}, v>$, solution of the equation

$$K |\tilde{s}> = |s>, \tag{3.12}$$

which can of course be a tedious job for high values of v. As a result, $T_{0,v}$ takes the form

$$T_{0,v}(x) = <\tilde{s}|X>. \tag{3.13}$$

Let us now consider the basic equation (3.12) defining the optimal VF for detection. The higher order statistics of the observation under H_0 and H_1 appears both in K and in $|s>$. The operator K is an expectation value under H_0, or under the hypothesis of noise only. But, looking at (2.12), we see that the exact calculation of K needs the knowledge of moments of x till the order $2v$. On the other hand, we see in (3.5) that the calculation of $|s>$ requires the knowledge of the moments of x till the order v, but under the two hypotheses H_0 and H_1 separately. A complete solution of (3.12) for $v = 2$ is discussed in [2].

4. OPTIMAL VF FOR MEAN SQUARE ESTIMATION

Consider a zero mean random vector $x(\omega)$ element of $\mathbb{R}^N$. When no ambiguity is possible, this vector is simply written x, and called the *observation vector*. From this observation we want to estimate a scalar random variable $y(\omega)$, also written simply y.

We will assume that the components x_i of x and y are second order zero mean random variables. As a result they can be considered as vectors of the Hilbert space L_2 for which the scalar product of two vectors u and v is $E(uv)$.

A *filter* similar to (2.1) is specified by its input-output relationship $z = g(x)$. As the input x is random, the output z is also random. Let us now introduce the subspace H_x of L_2 defined by

$$H_x = \{g(x) \mid g(x) \in L_2\}. \tag{4.1}$$

This space contains all the outputs of filters which are second order random variables. The space is indexed by x not only because the input is x, but also because it depends on the statistical properties of x. To explain this, consider the very common example $z = x^T x$, which is a quadratic filter used in many aspects of signal processing [7, 8]. The output of this filter belongs to L_2 only if x has finite fourth-order moments, which is not necessarily true even though the components x_i of x are second order. In MSE problems the input x is the result of an observa-

tion and the output z is an estimate of y, sometimes written as $\hat{y}(.)$. We will then use the term of *observation space* for H_x.

The optimum filter giving the best MSE $\hat{y}(x)$ of y is such that the distance between y and $\hat{y}(x)$ is minimum. As the observation space is a Hilbert subspace, we deduce immediately that $\hat{y}(x)$ is the *projection* of y onto the observation space H_x, or

$$\hat{y}(x) = \text{Proj}[y \mid H_x] \triangleq h(x). \tag{4.2}$$

This is the *geometrical* definition of the optimum filter. In order to calculate it explicitly we will use the orthogonality principle stating that $y - h(x)$ is orthogonal to H_x. This means that for any $g(x) \in H_x$ we have

$$E\{[y - h(x)] g(x)\} = 0. \tag{4.3}$$

It is well known [9] that the solution of this problem gives the conditional expectation value, sometimes called the *regression*, or

$$h(x) = E[y \mid x]. \tag{4.4}$$

After the introduction of these notations, we return to our problem of optimum MSE with Volterra filters. Clearly, the regression $h(x)$ defined by (4.4) is not in general a VF of any order. In order to find the best VF for the estimation of y, let us introduce the space $H_{v,x}$ defined by

$$H_{v,x} = \{g(x) \mid g(x) = <g, v |X, v> \text{ and } g(x) \in L_2\}. \tag{4.5}$$

It is clearly a subspace of H_x, because we restrict the possible filters to those having the structure of a VF of order v. With this restriction, the best optimal VF for estimation is still given by (4.2), where H_x is replaced by $H_{v,x}$.

The explicit solution is deduced from the orthogonality principle stating that for any $g(x) \in H_{v,x}$ we have

$$E\{[y - \hat{y}(x)] g(x)\} = 0. \tag{4.6}$$

Writing $g(x)$ as $<g|X>$ and the optimal estimate $\hat{y}(x)$ as $\hat{y}(x) = <h |X>$, we obtain

$$E\{[y - <h|X>] <X|g>\} = 0. \tag{4.7}$$

As this is valid for any $|g>$, we obtain $|h>$ by

$$K |h> = |c> , \tag{4.8}$$

where K is given by (3.9) and $|c>$ is defined by

$$|c> = E[y |X>]. \tag{4.9}$$

This vector specifies the correlation between the random variable y and all the components of $|X>$ appearing in (2.12).

The main conclusion of the calculation is that even though the structure of the Volterra filter is highly nonlinear, the optimum filter for estimation is obtained by a *linear equation* (4.8) which is exactly the same as for linear MSE.

Finally, note that the optimum Volterra filter for MSE is not an approximation of the regression $h(x)$ by a finite Taylor expansion. In fact, when the order v is increased, all the coefficients h_m of $|h, v>$ must be recalculated by (4.8), while they remain the same for a Taylor expansion.

5. RELATIONS BETWEEN DETECTION AND ESTIMATION

We will now extend to Volterra filters of order v a geometrical interpretation of optimal filtering for detection given for linear matched filters in [6] and for linear-quadratic filters in [2]. For this purpose let us note that from the projection theorem, any arbitrary vector $|a>$ of $\mathbb{R}^N[v]$ can be written as

$$|a> = a_s |s> + |a, s_\perp>, \tag{5.1}$$

where $|a, s_\perp>$ is the projection of $|a>$ onto the subspace of $\mathbb{R}^N[v]$ orthogonal to $|s>$. Furthermore the component a_s is given by

$$a_s = s^{-2} <s|a>; \quad s^2 \triangleq <s|s>. \tag{5.2}$$

This can be done for $|X>$ and $|\tilde{s}>$ used in (3.13), or

$$|\tilde{s}> = c_s |s> + |\tilde{s}, s_\perp> \tag{5.3}$$

$$|X> = x_s |s> + |X, s_\perp>. \tag{5.4}$$

Using (5.2) we obtain

$$c_s = s^{-2} <s|\tilde{s}> = s^{-2} <s| K^{-1} |s> = s^{-2} d_v^2, \tag{5.5}$$

where d_v^2 is defined by (3.10). Furthermore, as $|s>$ is orthogonal to any vector of the kind $|a, s_\perp>$, (3.13) can be written as

$$T_{o,v}(x) = d_v^2 x_s + <\tilde{s}, s_\perp|X, s_\perp> = d_v^2 [x_s - u(x)]. \tag{5.6}$$

Let us now demonstrate that the term $u(x)$ is the v-order mean square estimation of x_s in terms of $|X, s_\perp>$. For this purpose we must show that

1. $u(x)$ is obtained by a Volterra filter from $|X, s_\perp>$, or $u(x) = <g |X, s_\perp>$.

2. $x_s - u(x)$ is orthogonal, which means uncorrelated, to all the signals of the form $<a |X, s_\perp>$. This property is the orthogonality principle.

The first property is a direct consequence of (5.6) giving the value of $|g>$ equal to $|\tilde{s}, s_\perp>$. For the second property let us note from (5.1) and (5.4) that

$$a(x) \triangleq <a|X, s_\perp> = <a, s_\perp|X>. \tag{5.7}$$

As $x_s - u(x)$ is equal to $d_v^{-2} T_{o,v}(x)$, we deduce from (3.13) and (3.12) that

$$x_s - u(x) = d_v^{-2} <s| K^{-1} |X>. \tag{5.8}$$

Then

$$E[\{x_s - u(x)\} a(x)] = d_v^{-2} E[<s| K^{-1} |X> <X |a, s_\perp>]$$

$$= d_v^{-2} <s|a, s_\perp> = 0 \tag{5.9}$$

because of the definition of K by (3.9) and of $|a, s_\perp>$ by (5.1). This shows the orthogonality property.

As a result of the above we see that the optimal Volterra filter for detection can be written in the form

$$T_{o,v}(x) = d_v^2 [x_s - \hat{x}_s]. \tag{5.10}$$

In this expression x_s is the component of the observation vector $|X>$ in the signal direction $|s>$ defined by (3.5), while $\hat{x}_s$ is the v-order mean square estimation of x_s in terms of the observation orthogonal to the vector signal $|s>$. As $x_s - \hat{x}_s$ is the innovation $\tilde{x}_s$ in our estimation problem, the variance of $T_{o,v}(x)$ is directly connected to the error ε_v^2 of the estimation problem. More precisely, as the variance of $T_{o,v}(x)$ is d_v^2 defined by (3.11), we have

$$\varepsilon_v^2 = 1/d_v^2. \tag{5.11}$$

This shows a relation between singular estimation ($\varepsilon_v^2 = 0$) and singular detection ($d_v^2 \to \infty$).

Let us now give a more detailed interpretation of (5.10). As, from (3.11), the optimal receiver is invariant after a multiplication by a constant term, we can write (5.10) on the form

$$T_{o,v}(x) = x_s - \hat{x}_s \tag{5.12}$$

which is the simplest possible form of the optimal filter for detection. The term x_s is given by (5.2), or

$$x_s = s^{-2} <s|X> \tag{5.13}$$

and corresponds to (3.11) either when K is proportional to the unity operator or when $|s>$ is an eigenvector of K. For $v = 1$ the first situation corresponds to the case of second order white noise.

Let us discuss this last point a little more precisely by considering the cases of $v = 1$ and 2.

For $v = 1$, K defined by (3.9) becomes the correlation matrix of the vector x, because we have seen after (2.4) that $|X, 1> = x$. The assumption that K is diagonal means that the components of x are uncorrelated, which characterizes a *second order white noise*. Furthermore if s is an eigenvalue of K, the linear matched filter $s^T K^{-1} x$ is proportional to $s^T x$, exactly as for a white noise.

For $v = 2$ it is not necessarily possible to find a random vector x such that K defined by (3.9) is diagonal, and this is especially not the case for a Gaussian white noise, as we will now verify. For this we use some results presented in more detail in [2]. The linear problem $K|h, 2> = |g, 2>$ can be written as a set of two equations. For that we write $|h, 2> = |u, M>$, as after (2.5), and also $|g, 2> = |v, P>$, where u and v are two vectors while M and P are two matrices. The linear equation $K|u, M> = |v, P>$ then becomes

$$\sum_k C[i, k] \, u[k] + \sum_{k,l} B[i, k, l] \, M[k, l] = v[i] \quad (5.14)$$

$$\sum_k B[i, j, k] \, u[k] + \sum_{k,l} A[i, j, k, l] \, M[k, l] = P[i, j] \quad (5.15)$$

where

$$C[i, j] = E[x_i x_j] \quad (5.16)$$

$$B[i, j, k] = E[x_i x_j x_k] \quad (5.17)$$

$$A[i, j, k, l] = E[x_i x_j x_k x_l] - C[i, j]C[k, l] \quad (5.18)$$

If the random variables x_i are zero mean and IID with first moments m_2, m_3 and m_4, these expressions become

$$A[i, j, k, l] = m_2^2 \{ \delta[i, j]\delta[k, l] + \delta[i, l]\delta[j, k] \} + (m_4 - 3m_2^2).$$

$$\delta[i, j, k, l] \quad (5.21)$$

$$B[i, j, k] = m_3 \, \delta[i, j, k] \quad (5.22)$$

$$C[i, j] = m_2 \, \delta[i, j] . \quad (5.23)$$

If these relations are satisfied without any other knowledge on the higher order moments, we say that x_i is a *fourth order white noise*. Furthermore in the Gaussian case we have $m_3 = 0$ and $m_4 = 3m_2^2$. Suppose now, for simplification, that $m_3 = 0$. In this case it easy to verify that K is proportional to unity only if $m_2 = 1/2$, $m_4 = 1$. This last moment is greater than the Gaussian one. On the other hand, for a given value of m_2 and m_4 there are three eigenvalues $2m_2^2$, $(m_4 - 3m_2^2)$ and m_2 with the corresponding eigenvectors $|0, M_1>$, $|0, M_2>$ and $|h, 0>$ respectively. In these expressions M_1 is any symmetric matrix with null diagonal elements, M_2 is any diagonal matrix and h is any vector. This shows that the term x_i in (5.3) cannot in general be considered

simply as the output of the optimal filter for a white noise, as for $v = 1$.

6. EXTENSIONS

The same kind of method has been applied to parameter estimation [10] and also to spatial processing [11]. In this latter case it is necessary to extend all the previous results for complex random variables. This is very easy for second order moments, as is well known, but not for higher order moments. This is due to the choice of the complex conjugate in the structure of the higher order moments, which cannot be discussed in a few words.

REFERENCES

[1] M. Schetzen, *The Volterra and Wiener theories of nonlinear systems*, New-York: Wiley, 1980.

[2] B. Picinbono and P. Duvaut, "Optimal linear-quadratic systems for detection and estimation", *IEEE Trans. Inform. Theory*, vol. IT-34, pp.304-311, March 1988.

[3] H.L. Van Trees, *Detection, estimation, and modulation theory*, New-York: Wiley, 1968.

[4] C.W. Helstrom, *Statistical theory of signal detection*, Oxford, Pergamon Press.

[5] B. Picinbono and P. Duvaut, "Detection and contrast", in *Stochastic Processes in Underwater Acoustics*, C. Baker ed., New York, Springer-Verlag, 1986, pp.181-203.

[6] B. Picinbono, "A geometrical interpretation of signal detection and estimation", *IEEE Trans. Inform. Theory*, vol. IT-26, pp 493-497, July 1980.

[7] H. Clergeot, "Choix entre les différentes méthodes quadratiques d'estimation de spectre de puissance", *Annales des Télécommunications*, Vol.39, 1984, pp.113-128.

[8] H. El Ayadi and B. Picinbono, "NAR AGC adaptive detection of nonoverlapping signals in noise with fluctuating power", *IEEE Trans. Acoust. Speech, Signal Processing*, v 1. ASSP-29, pp.952-963, Oct. 1981.

[9] B. Picinbono, "Signaux deterministes et aléatoires: analyse et modélisation", in *Traitement du Signal*, J.L. Lacoume et al., eds., Les Houches, Session XLV, 1985, Elsevier, 1987.

[10] B. Picinbono, "Estimation non linéaire de l'amplitude d'un signal" 12° Colloque GRETSI, Juan-les Pins, 1989.

[11] P. Chevalier and B. Picinbono, "Optimal linear-quadratic array for detection", ICASSP Conference, Glasgow, 1989.

The Trispectrum

John W. Dalle Molle and Melvin J. Hinich

Applied Research Laboratories, The University of Texas at Austin
Post Office Box 8029, Austin, TX 78713-8029

Abstract : In this paper, we present the trispectrum as a tool for use in the analysis of nonlinear structural dependencies and deviations from multivariate normality of a random process. We develop the trispectrum based tests of linearity and Gaussianity. These tests are natural extensions of the corresponding tests which use the bispectrum. Together the bispectrum and trispectrum based tests form a stronger case for the rejection of the null hypotheses of linearity and Gaussianity than either one used alone.

This paper discusses the statistical properties of the trispectrum, and its application to the study of nonlinear or non-Gaussian structure in time series data. The trispectrum is the fourth order cumulant spectrum of a random process. In the analysis of random processes, the trispectrum complements the bispectrum[1], the third order cumulant spectrum as a tool for the study of nonlinear structural dependence. Also, both can be used to detect deviations from multivariate normality of a random process. Together they form a more powerful instrument for analyzing nonlinear time series models than either one used alone.

The trispectrum is the next polyspectral measure after the bispectrum. In the literature there are only a few papers that even hint at the computational aspects of the trispectrum ([15], [3], and [4]). Brillinger and Rosenblatt [4] actually reported trispectral values at various trifrequencies. The scheme developed in Lii and Rosenblatt [8] for estimating the coefficients of a linear model is extended for use with the trispectrum in Lii and Rosenblatt [9].

A procedure has been developed to compute the trispectral estimates over the complete principal domain. The diagnostic tests for linearity and Gaussianity, based on the bispectrum and developed by Subba Rao and Gabr [12] and Hinich [6] were extended for use with the trispectrum. The importance of and need for trispectral analysis comes fourfold:

1) a test with power of the hypotheses of Gaussianity

and linearity when the process has skewness measure of zero

2) an aid in determining the order of the major nonlinear term in times series data sequence

3) the identification of cubic nonlinearities arising as perturbations in linear models

4) a check on the validity of the use of the square of the power spectrum as an approximation for the large sample variance of the periodogram[2].

Assume that $\{X(t)\}$ is a discrete real valued strictly stationary process with $E(X(t)) = 0$, $E(X(t)^2) < \infty$, and a finite span of dependence. Define $C_{xxxx}(u_1, u_2, u_3)$ as the fourth order joint cumulant function[3] of the scalar time series of random variables $\{X(t)\}$ (Brillinger [2], section 2.6.1). Assuming the summability conditions of the fourth order cumulant as a function of the u_i's implies that

$$T(f_1, f_2, f_3) = \sum_{u_1 = \pm\infty} \sum_{u_2 = \pm\infty} \sum_{u_3 = \pm\infty} C_{xxxx}(u_1, u_2, u_3) *$$

$$\exp(-i2\pi(f_1 u_1 + f_2 u_2 + f_3 u_3)) \qquad (1)$$

where $T(f_1, f_2, f_3)$ is the trispectrum.and

$$C_{xxxx}(u_1, u_2, u_3) = E(X(t)X(t+u_1)X(t+u_2)X(t+u_3)) -$$
$$E(X(t)X(t+u_2))EX(t+u_1)X(t+u_3)) -$$
$$E(X(t)X(t+u_3))EX(t+u_1)X(t+u_2)) -$$
$$E(X(t)X(t+u_1))EX(t+u_2)X(t+u_3)) \qquad (2).$$

The Fourier transform of the fourth order moment $E(X(t)X(t+u_1)X(t+u_2)X(t+u_3))$ is the fourth order cumulant spectra plus three terms which are products of a pair of second order cumulant spectra. We need to eliminate the influence of

---

[1] Subba Rao and Gabr [14] and Niklas and Raghuveer [10] present overviews of the computational and statistical properties of the bispectrum. Some practical considerations for bispectral estimation are given by Subba Rao (13). Niklas and Raghuveer [10] is the most current extensive reference to the wide range of applications of the bispectrum.

[2] The fourth statement needs a little explanation. The complete expression for the variance of the periodogram is the sum of the power spectrum squared plus a trispectrum term which is divided by the sample size. The estimation of the trispectrum allows us to test the appropriateness in the use of the asymptotic estimate for the large sample variance of the periodogram.

[3] The joint cumulant functions are the coefficients of the power series expansion of the logarithm of the joint characteristic function.

the three lower order terms. To do this we stay on the principal manifold of the fourth order cumulant spectra, except for the region on this manifold that intersects the principal manifold of product of the second order cumulant spectra pairs. If we do this then the trispectrum is the fourth order cumulant spectra.

The trispectrum is in general a complex valued, bounded, and uniformly continuous function on the principal manifold $f_1 + f_2 + f_3 + f_4 = 0 \mod(2\pi)$ [2]. Where f_4 is related to the other frequencies by $f_4 = f_1 + f_2 + f_3$. The fourth order cumulant is the inverse Fourier transform of the fourth order spectrum or trispectrum. The fourth order cumulant can be written as

$$C_{xxxx}(u_1, u_2, u_3) = \int \int \int_{\Omega_4} T(f_1, f_2, f_3) \cdot$$

$$\exp(i2\pi(f_1 u_1 + f_2 u_2 + f_3 u_3)) df_1 df_2 df_3 \qquad (3),$$

where $\Omega_4 = \{-.5 \le f_i \le .5, i = 1,3\}$.

The condition, $f_1 + f_2 + f_3 + f_4 = 0 \mod(2\pi)$ is a frequency domain concept which corresponds to the time domain condition of strict stationarity. In other words, all the spectral mass of the fourth order cumulant is located on this hyperplane and if the frequency vector (f_1, f_2, f_3) does not lie on the principal manifold, the cumulant spectra will vanish. The strict stationarity and finite span of dependence assumptions are more restrictive than those made by Brillinger and Rosenblatt [3]. These additional assumptions are easier to understand and ensure that the asymptotic properties hold for the fourth-order spectral estimates that we will present.

The structure of the Gaussian probability distribution is completely determined by its spectral density. For the Gaussian case, there is no information in the higher order cumulant spectra. For a non-Gaussian process, the joint distribution depends on the higher order cumulants.

Higher order dependencies can be created by the action of a nonlinear filter with memory on a iid input signal. The dependencies induced by the nonlinear filter are confounded in the spectrum of the output. If we input a signal to a nonlinear filter that is non-Gaussian, then the output signal is not Gaussian. In general, if the filter is nonlinear then the output is a non-Gaussian dependent process. If we can characterize the structure of the joint distribution of a non-Gaussian time series that results from nonlinear filtering on an input signal, then we may be able to classify and identify the nonlinear mechanisms. The identification problem for nonlinear filters is an open question, even when the unobserved input is a Gaussian white noise process.

The relationships between the fourth order cumulant and the trispectrum is follows:

$$\mu_4 = \int \int \int_{\Omega_4} \text{Real}(T(f_1, f_2, f_3)) df_1 df_2 df_3 \qquad (4),$$

where the principal domain, $\Omega_4 = \{-.5 \le f_i \le .5, i = 1,3\}$.

Equation (4) can be depicted as the decomposition of the fourth order moment over the trifrequencies in the principal domain.

Taking the square of the trispectrum and normalizing it by the product of its power spectra at its three frequencies yields a standardized cumulant spectral function. The standardized cumulant spectral function was defined for the k-th order case by Brillinger [1] and is the square of the kurtosis function for the fourth order case:

$$\Psi_3^2 = |T(f_1, f_2, f_3)|^2 /$$

$$S_{xx}(f_1) S_{xx}(f_2) S_{xx}(f_3) S_{xx}(f_1 + f_2 + f_3) \qquad (5).$$

Equation (5) measures the degree to which the three frequencies interact or beat together. For a linear process, all orders of equation (5) are constant. If the process is Gaussian, then the constant is zero for all orders greater than two.

Before we describe the computational aspects of the estimation of the trispectrum, we need to survey the symmetries of the trispectrum. The trispectrum is defined over the cube $\{X, Y, Z: X \in (-.5, .5), Y \in (-.5, .5), Z \in (-.5, .5)\}$. There are symmetries introduced because some of the frequency components are related which reduces the region which we have to calculate the trispectral estimates over for a complete description of the trispectrum. The principal domain of the trispectrum $T(f_1, f_2, f_3)$ for a stationary continuous time process $\{X(t)\}$ is a triangular pointing cone in the positive octant $\{f_i, i = 1,3: 0 \le f_i\}$. The three sides of this cone are the planes are formed by the intersections of three of the trispectrum's symmetry planes.

The symmetry planes are easily derived from expressing the trispectrum using Stieljes integrals:

$$EdA(f_1) dA(f_2) dA(f_3) dA(f_4) = T(f_1, f_2, f_3) df_1 df_2 df_3 \qquad (6)$$

where $f_4 = -f_1 - f_2 - f_3$. The trispectrum is equal to zero in the four dimensional Euclidean space if $f_1 + f_2 + f_3 + f_4 \ne 0$ due to the stationarity of the process.

There are two types of symmetries we must concern ourselves with: 1) Permutations when one or two of the frequency pairs are equal and 2) Symmetries from the complex conjugation operation.

The first type of permutation symmetry we will discuss is when a pair of frequencies are equal. The symmetry planes determined by permuting the frequency indices are: 1) $f_1 = f_2$, 2) $f_1 = f_3$, 3) $f_1 = f_4$, i.e. $2f_1 = -(f_2 + f_3)$, 4) $f_2 = f_3$, 5) $f_2 = f_4$, i.e. $2f_2 = -(f_1 + f_3)$, and 6) $f_3 = f_4$, i.e. $2f_3 = -(f_1 + f_2)$. Where the frequency range is as follows, $\{f_i, i = 1,3: -\infty \le f_i \le \infty\}$ and $f_4 = -f_1 - f_2 - f_3$.

We have the second type of permutation symmetry where two frequency pairs are equal. The symmetries that correspond to this situation are: 1) $f_1 = f_2$ and $f_3 = f_4$, i.e. $f_1 = -f_3$,

2) $f_1 = f_3$ and $f_2 = f_4$, i.e. $f_1 = -f_2$, and 3) $f_1 = f_4$ and $f_2 = f_3$, i.e. $f_2 = -f_3$.

The last type of symmetry that comes into play is the symmetry that arises from the tricovariance function being only defined for real values. This is the symmetry from the complex conjugation operation, i.e. $T^*(f_1, f_2, f_3) = T(-f_1, -f_2, -f_3)$ where $*$ represents the conjugation operation. The conjugation symmetries form when one of the the four frequencies is set to zero. They are: 1) $f_1 = 0$, i.e. $f_2 + f_3 + f_4 = 0$, 2) $f_2 = 0$, i.e. $f_1 + f_3 + f_4 = 0$, 3) $f_3 = 0$, i.e. $f_1 + f_2 + f_4 = 0$, and 4) $f_4 = 0$, i.e. $f_1 + f_2 + f_3 = 0$.

From the forementioned symmetries, we can describe the continuous and discrete time principal domains of the trispectrum. The cone that forms the continuous time principal domain is a wedge-shaped hyperplane in the frequency triple (f_1, f_2, f_3). The continuous time principal domain is the wedge-shaped cone in the positive octant with coordinates $0 \le f_3 \le f_2 \le f_1 \le \infty$.

Now, if we band limit the process at the frequency f_0, there is no variance at any frequency greater than f_0. This will cause the continuous time principal domain to be cut off. This is because of the following constraints which are imposed by the band limiting of the process: 1) $f_i = \pm f_0$, i=1,3, 2) $f_1 + f_2 = \pm f_0$, 3) $f_1 + f_3 = \pm f_0$, 4) $f_2 + f_3 = \pm f_0$, and 5) $f_2 + f_3 + f_4 = \pm f_0$. For a band limited process, the continuous time support set is the pyramid-shape wedge with vertices $(0,0,0)$, $(1/2,0,0)$, & $(1/4, 1/4, 0)$, and apex $(1/6, 1/6, 1/6)$.

The principal domain of the trispectrum for the discrete time band limited process can be derived in a similar manner as was done for the principal domain of the bispectrum. If we sample at the Nyquist frequency $2f_0$, the principal domain of the trispectrum in discrete time is a pyramid with a triangular base that is larger than the support set for the continuous time band limited trispectrum. Sampling at the Nyquist frequency introduces a infinite number of parallel symmetry planes. These symmetry planes are formed when $f_1 + f_2 + f_3 + f_4 = nf_0$, n=0,1,2,3,...,∞. If we sample at the Nyquist frequency, we introduce the following planes of symmetry: 1) $2f_1 + f_2 + f_3 = nf_0$, 2) $f_i = 2f_0 - f_i = nf_0$, and 3) $f_1 + f_2 + 2f_3 = nf_0$ where n=0,1,...,∞.

The principal domain for the band limited discrete time domain is formed by the intersection of the planes $2f_1 + f_2 + f_3$, f_1 and $f_3 = 0$ under the constraint, $0 \le f_3 \le f_2 \le f_1 \le f_0$. The forementioned symmetries imply that for a complete description of the discrete time band limited trispectrum, we just need to compute the trispectral estimates over a principal domain which is a wedge shaped pyramid with a three-sided base. This pyramid has vertices $(0,0,0)$, $(1/2,0,0)$, & $(1/3,1/3,0)$, and apex

$(1/6,1/6,1/6)$. This wedge shaped region where the trispectrum is defined is one of 216 such equivalent principal domains that make up the cube $\{ X,Y,Z : X \in (-.5,.5), Y \in (-.5,.5), Z \in (-.5,.5) \}$.

The general procedure followed for the frequency domain estimation of a time series is described in Hinich and Clay [7] and Priestley [11]. A block averaging procedure is used to lower the variance of the periodogram estimates at the cost of having a coarser grid spacing for the spectral estimates. The block size must be chosen that will properly utilize this bias-variance trade off. Following the suggestion in Hinich [6] based on consistency, the suggested block length should be approximately the (n-1)-th root of the sample size if we are working with the n-th order spectrum. In the case of the trispectrum, the suggested block length is the cube root of the sample size.

First transform the data using a fast Fourier transform. At $f=0$, we set $X(f)=0$ which is equivalent to subtracting off the mean. We calculate the spectrum on each block and then calculate a block average spectrum. The trispectral estimates are the fourth order products normalized by the block size L_B:

$$T(f_1, f_2, f_3) = X(f_1) X(f_2) X(f_3) X(L_B - f_1 - f_2 - f_3) / L_B \quad (7).$$

where the $X(f)$'s are the Fourier transforms of the series $\{X(t)\}$ and are asymptotically complex Gaussian random variables. In the fourth order product of the transformed variables (equation (7)), if any subset of these four frequencies are equal, this product needs to be adjusted. This adjustment is for the different asymptotic estimates for the variance of equation (7) that arise for these cases. For the trispectrum, subsets of two and three frequencies can be equal. The appropriate scale factors for these two situations are two and six respectively.

Under the null hypotheses of linearity and Gaussianity, the estimated trispectrum should not be statistically different from zero. At a given frequency triple, the test statistic for the null hypothesis is

$$\chi^2_{f_1 f_2 f_3} = 2|T(f_1, f_2, f_3)|^2 / \sigma_A^2 \quad (8)$$

where $\chi^2_{f_1 f_2 f_3}$ is approximately a central chi-squared statistic with two degrees of freedom and σ_A^2 is the asymptotic variance of the trispectral estimates. The asymptotic variance is used to normalize the test statistic and is derived in Brillinger [2]. The asymptotic variance is given by the following:

$$\sigma_A^2 = (N_p / \Delta^2) S_{xx}(f_1) S_{xx}(f_2) S_{xx}(f_3) S_{xx}^*(f_1 + f_2 + f_3) \quad (9)$$

where Δ is the grid size $(1/L_B)$. From equation (8), we can get the following global statistic for testing the null hypothesis of Gaussianity,

$$\chi^2_{sum} = \sum_{f_1} \sum_{f_2} \sum_{f_3} \chi^2_{f_1 f_2 f_3} \quad (10)$$

Under the null hypothesis, χ^2_{sum} (equation (10)) is approximately chi-squared with $2N_t$ degrees of freedom, where N_t is the number of trifrequencies in the principal domain. When the sample size is large, we start to have difficulties in using the central chi-squared statistic. It is convenient to use a approximation for the sum of chi-squares χ^2_{sum}. We transform the chi-squared variates to Gaussian random variables which are easier to work with when you have large samples. We should be point out, that the rejection of Gaussianity in general does not imply that the process is non-linear.

The Hinich [6] and Subba Rao and Gabr [12] statistical tests serve as a criteria for testing whether to reject the null hypotheses of linearity and Gaussianity of a time series. Their tests are based on the sample bispectral estimates. Here we will extend the Hinich tests for linearity and Gaussianity for use with the sample trispectral estimates. The importance of these trispectral tests stem from the fact that a non-Gaussian process can have bispectral estimates $B(f_1,f_2)$ statistically equal to zero fo. ..ll frequency pairs (f_1,f_2) in the principal domain. Also, the test for the constancy of the square of the skewness function Ψ_2 does not always imply a linear model. This is because there are processes that are nonlinear, but have zero skewness measure.

The Hinich tests are nonparametric and robust in nature. The use of the large sample properties of the sample trispectrum will be the basis of the proposed trispectral tests. For the trispectrum, using the square of the average kurtosis function, we have the test for Gaussianity. Assume that a process $\{X(t)\}$ is a generated by a non-Gaussian linear process that is purely random. If $\{a(t)\}$ is a summable filter, i.e. $\sum |a(t)|<\infty$, the trispectrum can be written in terms of the transfer function $A(f)$ (Brillinger [2]):

$$T(f_1,f_2,f_3)=\mu_4 A(f_1)A(f_2)A(f_3)A^*(f_1+f_2+f_3) \qquad (11)$$

with $\mu_4 = E(X(t)^4)$, the asterisk denotes the complex conjugate and

$$A(f)=\sum_{t=0,\infty} a(t)e^{(-i2\pi ft)} \qquad (12).$$

Since the spectrum of X(t) is $S_{xx}(f)=\sigma_{xx}^2|A(f)|^2$, it follows for a linear process the square of the kurtosis function is the following constant:

$$\Psi_3^2=\mu_4^2/\sigma_{xx}^8 \qquad (13)$$

where Ψ_3^2 is defined as in equations (5), and σ_{xx}^2 is the estimate of the variance for the process $\{X(t)\}$. For a linear process equation (13) is constant. If the process is Gaussian, then the constant is zero for all orders greater than two.

As an extension of the bispectral tests developed in Hinich [6], we examine over the complete principal domain the collection of trispectral estimators of the form $2|\upsilon|^2$. υ is defined as follows:

$$\upsilon=(N/L_B^3)(T(f_1,f_2,f_3)/$$
$$(S_{xx}(f_1)S_{xx}(f_2)S_{xx}(f_3)S_{xx}^*(f_1+f_2+f_3))^{1/2}) \qquad (14).$$

These estimators are asymptotically independent non-central chi-squared variates, $\chi^2(2,2|\upsilon|^2)$ with non-centrality parameter $2|\upsilon|^2$.

If the series $\{X(t)\}$ is Gaussian, the trispectrum $T(f_1,f_2,f_3)$ is zero for all the trifrequencies in the principal domain. Under the null hypothesis of Gaussianity we have the statistic:

$$\zeta=2\sum_{f_1}\sum_{f_2f_3}(\upsilon_{f_1f_2f_3})^2 \qquad (15)$$

which is asymptotically distributed as a central chi-squared variate with 2ρ degrees of freedom. Where ρ is the number of frequency triples in the principle domain. See Hinich [6] for the asymptotic power of the test, and the proof of the consistency for the test.

The rejection of linearity using the bispectrum may not be adequate, especially if the non-linearities are of a cubic nature. This alone varrants the need for additional statistical tests of the null hypothesis for the linearity of a process. A test based on the sample trispectrum is the natural extension. Together, bispectral and trispectral based tests form a stronger case for the rejection of the null hypothesis of linearity.

Under the null hypothesis, having a sequence of observations $\{X(t)\}$ that is linear, although not necessarily Gaussian, Ψ_3^2 implies the non-centrality parameter is a constant over all the trifrequencies independent of the block size. This constant λ_0 can be estimated as the median of the ρ estimators of the form $2|\upsilon|^2$.

If we accept the null hypothesis, then the estimators of the form $2|\upsilon|^2$ are asymptotically independent samples from a $\chi^2(2\lambda_0)$ distribution. Under the null hypothesis, each of the statistics $2|\upsilon|^2$ is an independent sample from a $\chi^2(2,2|\upsilon|^2)$ distribution. With this in mind, a sample of size ρ of these statistics should have the sample dispersion of a $\chi^2(2,\lambda_0)$ distribution. The sample dispersion should converge to the actual dispersion coefficient as the number of trifrequencies approaches infinity. Accordingly, if the null hypothesis is rejected, then the non-centrality parameters are not all the same. This implies that each observed $2\upsilon^2$ is an independent sample from a non-central chi-squared distribution, each with a the

non-centrality parameter $2\upsilon^2$ that may not be the same for each realization. To reject linearity, the sample dispersion from each of these different non-central chi-squared distributions should be greater in value than the dispersion required under the null hypothesis.

The form of the sample statistic we will use for the null hypothesis of linearity is a variation of the one presented in Hinich [6]. The trispectral test for linearity is based on a comparison of the magnitude of the dispersion in the sample quantiles relative to the actual quantiles that are required under the null hypothesis. The sample quantile statistic is relatively robust to outliers. The sample quantiles are derived from the corresponding cumulative density function of the sample probability distribution of the ρ estimates of $2\upsilon^2$. The test statistic is

$$(\xi_s - \xi_a)/\sigma_q \qquad (16)$$

where ξ_a and ξ_s are actual and sample quantiles of the CDF of $\chi^2(2,\lambda_m)$, ρ is the sample size, and σ_q the standard deviation of the uniform order statistic (David [5]) and is defined as

$$\sigma_q = ((\xi_a*(1-\xi_a))/\rho)^{.5} \qquad (17).$$

This test statistic should be a standardized normal variate (i.e. $N(0,1)$) and take values within a $(1-\alpha)100\%$ symmetric confidence interval about the mean. The actual quantiles are those of the order statistics of the uniform distribution (David [5]).

The last step of the test is to compare the test statistic from equation (16) with the actual quantiles over a number of estimates from the cumulative distribution function over the interval $(0,1)$. If the non-centrality parameter is indeed a constant, then the values of the test statistic should fall within the $(1-\alpha)100\%$ symmetric confidence interval chosen. We reject the null hypothesis if the values of the test statistic are outliers of the standardized normal distribution. The consistency of the linearity test is proven in Hinich [6].

The real warrant to concern ourselves with the trispectrum comes from the fact that bispectral tests do not serve as complete tests for the rejection of Gaussianity and linearity hypotheses. Ideally, a complete test based on higher-order spectra would involve all possible polyspectra. There are non-Gaussian processes that have zero bispectral values and in turn a zero skewness measure over the complete principal domain. Since most non-Gaussian processes have non-zero high-order cumulants, it would seem unlikely that a process would have both its skewness and kurtosis functions identically equal to zero over the whole principal domain. Therefore, the bispectral and trispectral based tests together make a stronger case for the rejection of the null hypothesis of Gaussianity. In the same vein, the constancy of the skewness function does not always imply a linear model. With the trispectrum test in hand we have a more powerful tool for analyzing nonlinear and non-Gaussian times series.

[1] Brillinger, D. (1965), "An Introduction to Polyspectrum", Annals of Mathematical Statistics. (1975), Time Series, Data Analysis and Theory, New York: Holt, Rinehart, and Winston.

[2] Brillinger, D. (1975), Time Series, Data Analysis and Theory, New York: Holt, Rinehart, and Winston.

[3] Brillinger, D. and Rosenblatt, M. (1967), "Asymptotic Theory of kth Order Spectra", in Spectral Analysis of Time Series, edited by B. Harris, New York: John Wiley, 153-158.

[4] Brillinger, D. and Rosenblatt, M. (1967), "Computation and Interpretation of kth Order Spectra", in Spectral Analysis of Time Series, edited by B. Harris, New York: John Wiley, 189-23.

[5] David, H.A. (1970) Order Statistics, Wiley: New York.

[6] Hinich, M.J. (1982), "Testing for Gaussianity and Linearity of a Stationary Time Series", Journal of Time Series Analysis, 3 (3), 169-176.

[7] Hinich, M.J. and Clay, C. (1968), "The Application of the Discrete Fourier Transform in the Estimation of Power Spectra, Coherence, and Bispectra of Geophysical Data", Review of Geophysics, 6 (3), 347-363.

[8] Lii, K.S. and Rosenblattt, M. (1982),"Deconvolution and Estimation of Transfer Function Phase and Coefficients for Non-Gaussian Linear Processes", Annals of Mathematical Statistics, 10, 1195-1208.

[9] Lii, K.S. and Rosenblatt, M. (1985), "A Fourth Order Deconvolution Technique for Non-Gaussian Linear Processes", Multivariate Analysis VI, edited by P.R. Krishnaiah, Amsterdam: Elsevier, 395-410.

[10] Nikias, C.L. and Raghuveer, M.R. (1987), "Bispectrum Estimation: A Digital Signal Processing Framework", Proceeding of the IEEE, 5 (7), 869-891.

[11] Priestley, M. (1981), Spectral Analysis and Time Series, Vol. 2, New York: Academic Press.

[12] Subba Rao, T., and Gabr, M. (1980), "A Test for Linearity of Stationary Time Series," Journal of Time Series Analysis, 1, 145-158.

[13] Subba Rao, T. (1983), "The Bispectral Analysis of Nonlinear Stationary Time Series with Reference to Bilinear Time Series Models", in Handbook of Statistics, Vol. 3, edited by D. Brillinger and P. Krishnaiah, Amsterdam: North-Holland, Chapter 14.

[14] Subba Rao, T., and Gabr, M. (1984), An Introduction to Bispectral Analysis and Bilinear Time Series Models; Lecture Notes in Statistics No. 24, New York: Springer.

[15] Tukey, J.W. "Discussion Emphasizing the Connection Between Analysis of Variance and Spectrum Analysis", Technometrics, 3, 191-228.

APPLICATIONS OF DIGITAL POLYSPECTRAL ANALYSIS TO NONLINEAR SYSTEMS MODELING AND NONLINEAR WAVE PHENOMENA

E.J. Powers, Ch.P. Ritz[1], C.K. An, S.B. Kim, R.W. Miksad[2], and S.W. Nam

Department of Electrical and Computer Engineering
The University of Texas at Austin
Austin, Texas 78712-1084

ABSTRACT

The objective of this paper is to point out how innovative application of digital bispectral analysis techniques enables one to gain new physical insight into nonlinear three wave coupling processes associated with turbulence phenomena in fluids and plasmas. Both the approach and an experimental result are presented.

I. INTRODUCTION

This paper is concerned with the application of digital spectral analysis techniques to detect and quantify three-wave interaction phenomena associated with turbulence in continuous media such as fluids and plasmas. In such media, departures from thermodynamic equilibrium (as manifested, for example, by gradients in temperature, density, pressure, velocity) can act as a source of energy for various unstable modes or waves. Initially the unstable modes grow in a linear fashion, then, at sufficiently large amplitudes, begin to nonlinearly interact. As a result of this interaction energy is transferred from the most unstable modes to new sum and difference frequency waves or modes. For this reason, nonlinear wave interactions constitute an important mechanism whereby energy is redistributed from the most unstable waves to damped waves. This process is often referred to as energy cascading. The final result of the energy cascading process is turbulence which is manifested by fluctuations of various physical parameters in both space and time.

In analyzing and interpreting turbulence data, classical ... techniques are obviously of limited ... to detect and quantify the associated energy cascading phenomena. In this paper ... digital spectral analysis techniques are

utilized to: (1) detect the presence of nonlinear wave interactions, (2) quantify their strength in terms of a three-wave coupling coefficient, and (3) quantify the associated energy cascading.

Experimental knowledge of the three-wave coupling coefficient is important for the following reasons. All the nonlinear physics of the situation is imbedded in the coupling coefficient. Secondly, experimental knowledge of the coupling coefficient is necessary to compare with existing (and often competing) theories, and to compute the associated rate of energy cascading.

II. THREE-WAVE COUPLING EQUATION

Three wave coupling results from a quadratic nonlinearity appearing in the governing equations (such as the Navier Stokes equation for fluids) for the physical system under consideration. This quadratic nonlinearity manifests itself in the temporal spatial frequency domain as a convolution integral. In particular the so-called three wave coupling equation is often used to model such quadratic effects. It is given as follows:

$$\frac{\partial \Phi(f_n, x)}{\partial x} = \Lambda_1(f_n)\Phi(f_n, x) + \sum_{f_i}\sum_{f_j}\Lambda_2(f_i, f_j)\Phi(f_i, x)\Phi(f_j, x)$$

where $f_i + f_j = f_n$, and $\Phi(f_n, x)$ is the Fourier transform (i.e., complex amplitude) of the fluctuating wave monitored at a point x. The quantity Λ_1 is

$$\Lambda_1(f_n) = \gamma(f_n) + i\kappa(f_n)$$

where $\gamma(f_n)$ is the linear growth rate and κ is the dispersion relation. The quantity Λ_2

three-wave coupling coefficient and is the quantity we wish to estimate from time series records of the fluctuation field observed at two spatial points. Note that the convolution nature of the three-wave coupling equation becomes clear when we substitute $f_j = f_m - f_i$ in Eq.(1).

The three-wave coupling equation may be interpreted as follows: The left hand side indicates the spatial rate of change (at point x) of the complex amplitude of wave at frequency f_m as it propagates through space. The first term on the right hand side indicates the contribution to this rate of change due to linear effects. The second term models the quadratically nonlinear contributions. The double summation ensures that we consider all possible three-wave interactions that add or subtract to yield f_m. The contribution of a particular three-wave interaction to $\frac{\partial \Phi(f_m, x)}{\partial x}$ is given by the product of the complex amplitudes $\Phi(f_i, x)\Phi(f_j, x)$ times the three-wave coupling coefficient $\Lambda_2(f_i, f_j)$. Thus $\Lambda_2(f_i, f_j)$ denotes the strength of the interaction and is intrinsically a two-dimensional function of frequency. Thus it should come as no surprise that a two-dimensional spectral density function, namely, the bispectrum is required to measure this quantity.

Since the complex amplitude of wave at frequency f_m changes as it propagates through space, the power spectral density $P(f_m, x)$ also changes. It is fairly straight forward to show [1] that

$$\frac{\partial P(f_m, x)}{\partial x} = 2\gamma(f_m)P(f_m, x) + \sum_{f_i}\sum_{f_j} T(f_i, f_j). \quad (3)$$

where $f_i + f_j = f_m$, and $T(f_i, f_j)$ is the three-wave energy transfer function and is given by

$$T(f_i, f_j) = 2Re[\Lambda_2(f_i, f_j)B^*(f_i, f_j)]. \quad (4)$$

$B(f_i, f_j)$ is the auto-bispectrum of the fluctuation field measured at point x and is given by

$$B(f_i, f_j) = E[\Phi^*(f_i, x)\Phi^*(f_j, x)\Phi(f_m = f_i + f_j, x)] \quad (5)$$

where E denotes an expected value. An approach, based on Eq.(1), to measuring $B(f_i, f_j)$ is given in [2].

Clearly, the first term on the RHS of Eq.(3) models the increase or decrease of power of wave f_m due to linear growth or damping as it propagates through space. The second term is the energy cascading term, referred to in the introduction, in that it models the contribution to the power spectral density at frequency f_m due to all possible three-wave interactions satisfying the frequency selection rule, $f_i + f_j = f_m$. Note that the energy transfer function is sensitive to both the amplitudes and phase difference of the coupling coefficient and the auto-bispectrum.

Finally, we note that in order to quantify the energy cascading it is necessary to have knowledge of the coupling coefficient. An approach to measuring this quantity of fundamental importance is overviewed in the next section.

III. DETERMINATION OF COUPLING COEFFICIENTS

Our approach to experimentally measuring the three-wave coupling coefficient rests upon nonlinear system identification techniques. Specifically, the fluctuation field is monitored at two points that are closely spaced relative to a typical wavelength and coherence length of the fluctuations. One signal is regarded as a "input" and the other as an "output". The linear and quadratically nonlinear wave physics which occurs between the intervening points is modeled with the aid of a parallel combination of linear and quadratic transfer functions. The situation is depicted in Fig.1 where $X(f_m)$ and $Y(f_m)$ denote the Fourier transforms of the observed "input" and "output" signals, and $H_1(f_m)$ and $H_2(f_i, f_j)$ denote the linear and quadratic transfer functions respectively. The determination of $H_1(f_m)$ and $H_2(f_i, f_j)$ will be considered in the next section.

The approach is basically a frequency domain version of the well known Volterra model [3] where the input and output quantities are related by

$$Y(f_m) = H_1(f_m)X(f_m) + \sum_{f_i}\sum_{f_j} H_2(f_i, f_j)X(f_i)X(f_j)$$

$$\text{where} \quad f_i + f_j = f_m. \quad (6)$$

Thus, the linear contribution to the model output $\hat{Y}(f_m)$ is given by the input $X(f_m)$ times the linear transfer function $H_1(f_m)$. In addition, three-wave interaction contributions that sum (in an algebraic sense) to f_m are modeled by the second term on the RHS. The contribution of a particu-
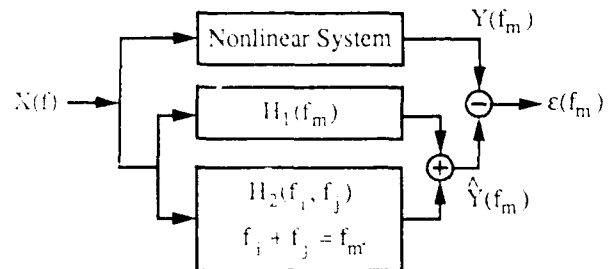

Fig. 1. Frequency domain Volterra model of a quadratically nonlinear system.

lar pair of frequencies f_i and f_j in the input is given by the product of their complex amplitudes $X(f_i)X(f_j)$ times the quadratic transfer function $H_2(f_i, f_j)$. In this sense $H_2(f_i, f_j)$ models the "strength" or the "efficiency" of the three-wave interaction.

Comparison of the three-wave coupling equation Eq.(1) and the Volterra second order model, Eq.(6), suggests that if one can measure $H_1(f_m)$ and $H_2(f_i, f_j)$ from the input-output data, then one can determine $\Lambda_1(f_m)$ and $\Lambda_2(f_i, f_j)$. Once one has $\Lambda_2(f_i, f_j)$, one can then determine the energy-cascading transfer function $T(f_i, f_j)$ given in Eq.(4).

For these reasons, the determination of the linear and quadratic transfer functions is of utmost importance. An important point in this determination is to utilize an approach that takes into account the fact that that "input" waveform will be nonGaussian due to its past nonlinear history. We have utilized two approaches to this problem [4, 5] and the latter will be summarized in the next section.

IV. SINGLE-INPUT/SINGLE-OUTPUT QUADRATIC SYSTEM

The Volterra system model of a single-input/single-output quadratically nonlinear system can be expressed in the discrete frequency domain as follows:

$$Y(m) = H_1(m)X(m) + \sum_i \sum_j H_2(i,j)X(i)X(j) \qquad (7)$$

where $i + j = m$, and $X(m)$ and $Y(m)$ represent the discrete Fourier transforms (DFT's) computed from a finite number M of observations of the input and output signals. The quantity $H_1(m)$ is the linear transfer function and $H_2(i,j)$ is the quadratic transfer function. The transfer functions are given at a discrete set of frequencies $\{m : m = -\frac{M-1}{4}, \ldots, -1, 0, 1, \ldots, \frac{M}{4}\}$.

The quadratic transfer functions are assumed to be symmetrical in the sense that changing order of the arguments does not change the value of the system output:

$$H_2(i, j) = H_2(j, i)$$
$$H_2(-i, -j) = H_2(i, j). \qquad (8)$$

If the input is assumed to be zero-mean Gaussian, we

$$H_1(m) = \frac{S_{yx}(m)}{S_{xx}(m)}$$

$$H_2(i, j) = \frac{S_{yxx}(i,j)}{2S_{xx}(i)S_{xx}(j)}$$

where $S_{yx}(m)$ is the cross-power spectrum, $S_{xx}(m)$ is the auto-power spectrum of the input, $S_{yxx}(i,j)$ is the cross-bispectrum $(i + j \neq 0)$ [6, 7].

If the input is not zero-mean Gaussian, the linear and quadratic terms are not orthogonal, and they can not be obtained separately. In this case, we need to solve matrix equations which include the linear and quadratic transfer function terms. Kim and Powers calculated the linear and quadratic transfer functions of the single-input/single-output quadratic system, subject to nonGaussian excitation, by solving a set of large matrix equations [5] and we follow their approach here.

We may rewrite Eq.(7) using vector notation as follows:

$$Y(m) = \mathbf{x}^t(m)\mathbf{h}(m) \qquad (9)$$

where t denotes transpose, and

$$\mathbf{x}(m) = \begin{bmatrix} X(m) \\ X(\frac{m-1}{2})X(\frac{m-1}{2}) \\ X(\frac{m-2}{2})X(\frac{m-2}{2}) \\ \vdots \\ X(\frac{M}{4})X(m - \frac{M}{4}) \end{bmatrix} \qquad (10)$$

and

$$\mathbf{h}(m) = \begin{bmatrix} H_1(m) \\ H_2(\frac{m-1}{2}, \frac{m-1}{2}) \\ H_2(\frac{m-2}{2}, \frac{m-2}{2}) \\ \vdots \\ H_2(\frac{M}{4}, m - \frac{M}{4}) \end{bmatrix} \qquad (11)$$

for odd m. For even m, we can obtain similar equations for $\mathbf{x}(m)$ and $\mathbf{h}(m)$.

In a simple yet more subtle approach used to determine the linear regression coefficients in the case of the quadratic transfer functions, to the least squares error M, we multiply Eq.(9) by $\mathbf{x}^*(m)$ and then taking the expected value on both sides, we obtain the normal equations in matrix form,

$$E[\mathbf{x}^*(m)Y(m)] = E[\mathbf{x}^*(m)\mathbf{x}^t(m)]\mathbf{h}(m) \qquad (12)$$

where $\mathbf{x}^*(m)$ is the complex conjugate vector of $\mathbf{x}(m)$. We can

calculate the transfer functions, which are the elements of the transfer function vector h(ω), from the linear matrix equation in Eq.(12).

V. EXPERIMENTAL RESULTS

Plasma density fluctuations associated with plasma turbulence were monitored with two Langmuir probes in the edge region of the TEXT tokamak [8]. First the linear and quadratic transfer functions were determined and the complex three-wave coupling coefficient was computed. The magnitude of this quantity is shown in Fig.2. Note, however, that Eq.(4) indicates that the actual amount of energy cascading associated with three-wave interactions depends not only on the amplitudes of the complex three-wave coupling coefficient and the interacting waves, but also on their relative phase as well. With this caveat in mind, we note that $\Lambda_2(f_1, f_2)$ is largest for difference frequencies. In fact, we find after a more detailed analysis of the three-wave energy transfer function $T(f_1, f_2)$ that the dominant direction of energy cascading is from the most unstable modes down to lower frequencies. For more complete information the reader is referred to [9].
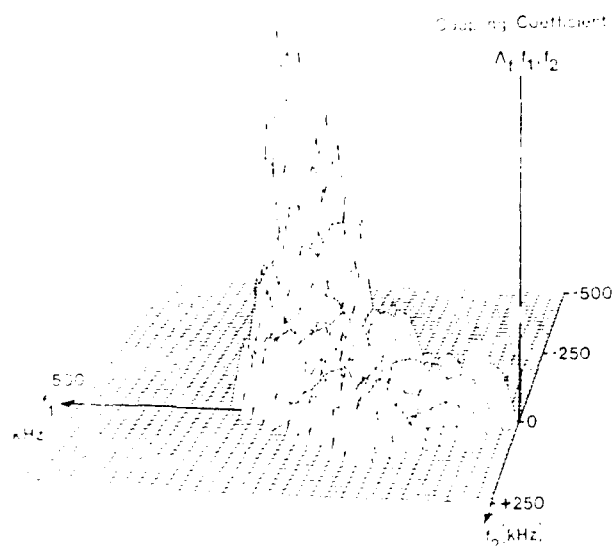

Fig. 2 Plot of the amplitude of the three-wave coupling coefficient determined using digital bispectral analysis.

VI. SUMMARY

Digital bispectral analysis has proven to be a powerful tool that is capable of providing heretofore unavailable physical insight into three-wave interaction phenomena associated with energy-cascading in turbulence. In particular, digital bispectral analysis makes it possible to measure three-wave coupling coefficients for the first time from "turbulent" data. Furthermore, digital bispectral analysis also makes it feasible to quantitatively investigate energy cascading both up and down in the frequency spectrum.

It should also be apparent to the reader that both the three-wave coupling equation Eq.(1) and the Volterra model of Eq.(6) could be extended to higher order. Specifically, a four-wave coupling term would be added to Eq.(1) and a cubic transfer function to Eq.(6). This would necessitate using the trispectrum to quantify these next higher-order effects, a subject we are currently investigating.

ACKNOWLEDGEMENT

REFERENCES

[1] Y.C. Kim, J.M. Beall, E.J. Powers and R.W. Miksad, "Bispectrum and Nonlinear Wave Coupling," Physics of Fluids, Vol. 23, No. 2, pp. 258-263, Feb. 1980.

[2] Y.C. Kim and E.J. Powers, "Digital Bispectral Analysis and its Applications to Nonlinear Wave Interactions," IEEE Trans. Plasma Science, Vol. PS-7, No. 2, pp. 120-131, June 1979.

[3] M. Schetzen, The Volterra & Wiener Theories of Nonlinear Systems, Wiley Interscience, New York, 1980.

[4] Ch. P. Ritz and E. J. Powers, "Estimation of Nonlinear Transfer Function for Fully Developed Turbulence," Physica D, 'Nonlinear Phenomena', Vol. 20D, No. 2/3, pp.320-334, June/July 1986.

[5] K. I. Kim and E. J. Powers, "A Digital Method of Modeling Quadratically Nonlinear Systems with a General Random Input," *IEEE Trans. on Acoustics, Speech, and Signal Processing*, Vol. 36, No. 11, pp. 1758-1769, Nov. 1988.

[6] L. J. Tick, "The Estimation of Transfer Functions of Quadratic Systems," *Technometrics*, Vol. 3, No. 4, pp. 563-567, Nov. 1961.

[7] J. Y. Hong, Y. C. Kim and E. J. Powers, "On Modeling the Nonlinear Relationship between Fluctuations with Nonlinear Transfer Functions," *Proc. IEEE*, Vol. 68, No. 8, pp. 1026-1027, Aug. 1980.

[8] K.W. Gentle, *Nucl. Technol. Fusion*, Vol. 1, pp.479, 1981.

[9] Ch. P. Ritz, E. J. Powers and R. D. Bengtson, "Experimental Measurement of Three-Wave Coupling and Energy Cascading," *Phys. Fluid. B*, vol. 1, No. 1, pp.153-163, Jan. 1989.

THE IDENTIFICATION OF CERTAIN NONLINEAR SYSTEMS BY ONLY OBSERVING THE OUTPUT

NOVELLONE ROZARIO
GE ASTRO SPACE DIVISION
PRINCETON, N.J

ATHANASIOS PAPOULIS
POLYTECHNIC UNIVERSITY
FARMINGDALE, N.Y

ABSTRACT

We propose a method for identifying a certain type of non-linear system from observations of the output only. The input to the system is assumed to be Gaussian, and the system itself is made up of two minimum-phase linear systems separated by a memoryless nonlinearity. Our method is based on the simple obeservation that the polyspectrum of a Gaussian process is real-valued.

I. INTRODUCTION

Given a stationary process, a familiar problem in signal analysis is the representation of this process as the output of a system driven by white-noise. An assumption commonly made is that the system is linear. In this paper we consider a nonlinear model, and we propose a method to identify the model.

When the model is linear, its identification can be accomplished in a variety of ways [1-8], and the methods that use higher-order spectra and moments have recently gained wide popularity. But it is in the study of nonlinear systems that one discovers the undisputed strength of higher-order spectra [9-12]. For example, the presence of intermodulation and harmonics that result from nonlinear interactions are easily revealed by an examination of the bispectrum [10,18]. And the question of whether a process can be considered linear or not can also be answered in a similar manner [9]. For processes whose underlying model is nonlinear, the problem of identifying the model usually requires knowledge of both the input and the output [11-14]. It has been shown [11-12] that higher-order cross-spectral methods are very effective in these situations.

In this paper we consider the system shown in figure 1. This system is composed of two linear systems separated by a nonlinear memoryless system. The input is gaussian white noise. The identification of such a system has also been considered in [12], and it is performed by calculating the cross-polyspectra between $x(t)$ and $y(t)$. This approach therefore requires knowledge of both the input and the output. However, we can show that the above system can be identified from knowledge of the output $y(t)$ only, provided we assume that (a) $H_1(\omega)$ and $H_2(\omega)$ are minimum-phase, and (b) $G(.)$ is monotonic.

Our method is based on the following observation: The polyspectrum of $y(t)$ is real-valued because it is a function of the power spectrum of the Gaussian process $u(t)$, and for a memoryless nonlinear system, this function maps the set of reals into the set of reals. Hence, the phase of the polyspectrum of $y(t)$ is entirely due to the phase of the linear system $H_2(\omega)$. Therefore, we can use the methods in [1,4,8] to estimate the phase of $H_2(\omega)$, and then use the minimum-phase assumption to obtain its magnitude. With $H_2(\omega)$ thus determined, we can obtain $v(t)$ with an inverse operation. Once $v(t)$ is known, its probability density function (pdf) can be found and compared with the gaussian pdf of $u(t)$ to yield the memoryless nonlinear transformation $G(.)$. From this we get the process $u(t)$. And finally, we estimate $H_1(\omega)$ by factorizing the power spectrum of $u(t)$.

Our motivation for studying this problem is due to its applications in communications [15]. In many satellite systems, the solid state power amplifier or TWTA must be operated in a highly nonlinear mode in order to conserve power. Although the baseband signal $x(t)$ is not necessarily gaussian, the effect of a band-limiting filter such as $H_1(\omega)$ on $x(t)$ is to render it more gaussian, and hence the methods presented here are applicable. Also, in some cases, there are several subcarriers simultaneously present, thereby giving rise to intermodulation effects. In this case the bispectrum is composed of lines but its phase is completely determined by $H_2(\omega)$, and using high resolution parametric estimation techniques [16], one can hope to identify $H_2(\omega)$. It must also be added, that although magnitude information is missing in the evaluation of $H_2(\omega)$, most of the distortion is due to the phase of $H_2(\omega)$.

In section II, a justification of the real-valuedness of $v(t)$ is presented. We also discuss the method for obtaining $G(.)$. In section III, we consider the effects of a slight nongaussian component in $u(t)$. Finally, in sectionIV, we present simulation results.

$$x(t) \longrightarrow \boxed{H_1(\omega)} \longrightarrow u(t) \longrightarrow \boxed{G(.)} \longrightarrow v(t) \longrightarrow \boxed{H_2(\omega)} \longrightarrow y(t)$$
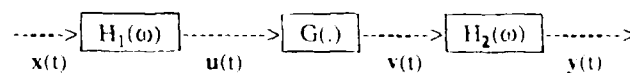
Figure 1. The model.

Notation:- $x(t)$, $u(t)$, $v(t)$ and $y(t)$ are the stationary processes shown in figure 1, and their Fourier integrals [20] will be denoted by $X(\omega)$, $U(\omega)$, $V(\omega)$, and $Y(\omega)$ respectively. Thus, for example,

$$x(t) = (1/2\pi)\int X(\omega)e^{j\omega t}d\omega \quad \text{and} \quad X(\omega) = \int x(t)e^{-j\omega t}dt .$$

When the limits of an integral are omitted, it will be understood that the integral is to be evaluated from $-\infty$ to $+\infty$. On the other hand, by writing $\int_{(-\pi,+\pi)}$ we shall mean that this integral is to be evaluated from $-\pi$ to $+\pi$. A similar remark applies in using Σ.
The nth order cumulant of the random variables $z_1, z_2, ... z_n$ will be denoted by $K\{z_1, z_2, ... z_n\}$. Similarly, the nth order moment of these random variables will be denoted by $E\{z_1, z_2, ... z_n\}$. The autocorrelation of $x(t)$ will be denoted by $R(\tau)$; ie $R(\tau) = R_{xx}(\tau) \equiv K\{x(t),x(t+\tau)\}$, the subscript being omitted only when the context is obvious. This notation will be also be used for the higher-order case. For example,

$$R(\tau_1,\tau_2) \equiv R_{xxx}(\tau_1,\tau_2) \equiv K\{x(t),x(t+\tau_1),x(t+\tau_2)\},$$

and, $$R_{xxy}(\tau_1,\tau_2) \equiv K\{x(t),x(t+\tau_1),y(t+\tau_2)\}.$$

The power spectrum of $x(t)$ will be denoted by $S(\omega) \equiv S_{xx}(\omega) \equiv$ Fourier Transform of $R_{xx}(\tau)$. Higher-order spectra will be denoted in a similar manner. For example,

$$S(\omega_1,\omega_2) \equiv S_{xxx}(\omega_1,\omega_2) \equiv \text{Fourier Tansform of } R_{xxx}(\tau_1,\tau_2),$$

and, $$S_{xxy}(\omega_1,\omega_2) \equiv \text{Fourier Tansform of } R_{xxy}(\tau_1,\tau_2).$$

II. NONLINEAR TRANSFORMATION OF A GAUSSIAN PROCESS

Consider the process $v(t)$ obtained from $u(t)$ by a memoryless nonlinear transformation,

$$v(t) = G(u(t)). \tag{1}$$

Now the polyspectrum of $v(t)$ is a function of the polyspectra of $u(t)$. Also, since $G(.)$ is a memoryless transformation, this function must be such that the set of reals is mapped into the set of reals. As for the polyspectra of $u(t)$, the only nonzero polyspectrum of $u(t)$ is its power spectrum, which is real valued. Hence all the polyspectra of $v(t)$ are real valued. These statements can be justified analytically b   ning that $G(u(t))$ may be written as a Taylor series

$$v(t) = \sum_n a_n u^n(t). \tag{2}$$

We may now use a theorem stated and proved in [19] to show that the polyspectrum of $v(t)$ can be written as a function of the polyspectra of $u(t)$. However, for the benefit of the reader, we will give a brief sketch of the proof. We may write (2) as

$$v(t) = \sum_n a_n u^n(t)$$

$$= \sum_n a_n [(1/2\pi)\int U(\omega)e^{j\omega t}d\omega]^n$$

$$= \sum_n a_n (1/2\pi)^n \iint..\int U(\omega_1)U(\omega_2)..U(\omega_n)e^{j\bar\omega t}d\omega_1 d\omega_2 ..d\omega_n$$

$$= \sum_n v_n(t), \tag{3}$$

where,

$$v_n(t) = a_n(1/2\pi)^n \iint..\int U(\omega_1)U(\omega_2)..U(\omega_n)e^{j\bar\omega t}d\omega_1 d\omega_2 ..d\omega_n \tag{4}$$

and $$\bar\omega = \omega_1 + \omega_2 + ..+ \omega_n . \tag{5}$$

Taking the transform $V_n(\omega)$ of $v_n(t)$, we get

$$V_n(\omega) = \int v_n(t)e^{-j\omega t}dt$$

$$= a_n(1/2\pi)^n \iint..\int U(\omega_1)U(\omega_2)..U(\omega_n).\delta(\omega-\bar\omega)d\omega_1 d\omega_2 ..d\omega_n \tag{6}$$

and, $$V(\omega) = \sum_n V_n(\omega) . \tag{7}$$

From (6),(7) and from the linearity property of cumulants, it can be seen that the cumulant $K\{V(\omega_1), V(\omega_2),..., V(\omega_k)\}$ is a function of cumulants of the form

$$K\{U(\omega_{11})U(\omega_{12})..U(\omega_{1n}),U(\omega_{21})U(\omega_{12})..U(\omega_{2n}),$$
$$...,U(\omega_{k1})U(\omega_{k2})..U(\omega_{kn})\} \tag{8}$$

and this function maps the set of reals into the set of reals. Using the product theorem in [13,19], (8) may be further reduced to a sum of cumulants of the form $K\{U(\lambda_1),U(\lambda_2),...,U(\lambda_m)\}$. And since $U(\omega)$ is Gaussian, only the second order cumulants will be nonzero. That is, the cumulant $K\{V(\omega_1),V(\omega_2),..., V(\omega_k)\}$ is a real valued function of the power spectrum of $u(t)$. The $k-1^{th}$ order polyspectrum of $v(t)$ is then given by

$$S\{\omega_1,\omega_2,...,\omega_{k-1}\} \ d\omega_1 d\omega_2 ..d\omega_{k-1}$$
$$= K\{dV(\omega_1),dV(\omega_2),....,dV(\omega_k)\}.$$

with $\omega_1 + \omega_2 + .. + \omega_k = 0$.

In order to estimate $G(.)$ from the pdf of $v(t)$ we must assume that $G(.)$ is monotone increasing. Otherwise the solution is not unique. For example, suppose the function $v=G(u)$ were monotone increasing. Then, in terms of probability distributions, we can obtain the relationship $v=G(u)$ by requiring that

$$P\{v(t)\leq v\} = P\{u(t)\leq +u\} \tag{9}$$
or, $$F_v(v) = F_u(u) .$$

Here, $F_v(v)$ and $F_u(u)$ are the probability distribution functions of $v(t)$ and $u(t)$ respectively, and P denotes probability. On the other hand, suppose the function $v=G(u)$ were not monotonic, say $v(t)=u^2(t)$. Then the distribution functions would be related by

$$P\{v(t)\leq v\} = P\{-u\leq u(t)\leq +u\}$$
or, $$F_v(v) = F_u(u) - F_u(-u).$$

Thus, we see that the solution to $v=G(u)$ is not unique, and the proper solution requires prior information.

III. DEVIATIONS FROM GAUSSIANITY

Consider the process
$$u(t)=n(t)+e(t) , \tag{10}$$

where, $n(t)$ is a Gaussian process

$e(t)$ is a non-Gaussian process, and $e(t)<<n(t)$.
Assume also that $e(t)$ is independent of $n(t)$.

Let $v(t) = G(u(t)) = G(n(t)) + e(t).G'(n(t))$
$$= a(t) + e(t).b(t). \tag{11}$$

We shall assume that $\mathbf{n}(t)$ and $\mathbf{e}(t)$ are zero-mean. Note that this, however, does not imply that $\mathbf{a}(t)$ and $\mathbf{b}(t)$ are zero-mean. Let us evaluate the third-order moments of $\mathbf{v}(t)$.

$$R_{vvv}(\tau_1,\tau_2)$$

$$= K\{\mathbf{v}(t),\mathbf{v}(t+\tau_1),\mathbf{v}(t+\tau_2)\}$$
$$= K\{\mathbf{a}(t)+\mathbf{e}(t)\mathbf{b}(t),\mathbf{a}(t+\tau_1)+\mathbf{e}(t+\tau_1)\mathbf{b}(t+\tau_1),\mathbf{a}(t+\tau_2)+\mathbf{e}(t+\tau_2)\mathbf{b}(t+\tau_2)\}$$
$$= K\{\mathbf{a}(t),\mathbf{a}(t+\tau_1),\mathbf{a}(t+\tau_2)\}$$
$$+ K\{\mathbf{e}(t)\mathbf{b}(t),\mathbf{a}(t+\tau_1),\mathbf{a}(t+\tau_2)\}$$
$$+ K\{\mathbf{a}(t),\mathbf{e}(t+\tau_1)\mathbf{b}(t+\tau_1),\mathbf{a}(t+\tau_2)\}$$
$$+ K\{\mathbf{a}(t),\mathbf{a}(t+\tau_1),\mathbf{e}(t+\tau_2)\mathbf{b}(t+\tau_2)\}$$
$$+ K\{\mathbf{e}(t)\mathbf{b}(t),\mathbf{e}(t+\tau_1)\mathbf{b}(t+\tau_1),\mathbf{a}(t+\tau_2)\}$$
$$+ K\{\mathbf{e}(t)\mathbf{b}(t),\mathbf{a}(t+\tau_1),\mathbf{e}(t+\tau_2)\mathbf{b}(t+\tau_2)\}$$
$$+ K\{\mathbf{a}(t),\mathbf{e}(t+\tau_1)\mathbf{b}(t+\tau_1),\mathbf{e}(t+\tau_2)\mathbf{b}(t+\tau_2)\}$$
$$+ K\{\mathbf{e}(t)\mathbf{b}(t),\mathbf{e}(t+\tau_1)\mathbf{b}(t+\tau_1),\mathbf{e}(t+\tau_2)\mathbf{b}(t+\tau_2)\} \qquad (12)$$

Now,

$$K\{\mathbf{e}(t)\mathbf{b}(t),\mathbf{a}(t+\tau_1),\mathbf{a}(t+\tau_2)\} = K\{\mathbf{e}(t),\mathbf{b}(t),\mathbf{a}(t+\tau_1),\mathbf{a}(t+\tau_2)\}$$
$$+ K\{\mathbf{e}(t)\}.K\{\mathbf{b}(t),\mathbf{a}(t+\tau_1),\mathbf{a}(t+\tau_2)\}$$
$$= 0 , \qquad (13)$$

because, $\mathbf{e}(t)$ is a zero-mean process independent of $\mathbf{a}(t)$ and $\mathbf{b}(t)$. Hence the 2nd, 3rd, and 4th term in ( ) are zero. Now lets look at the 5th term.

$$K\{\mathbf{e}(t)\mathbf{b}(t),\mathbf{e}(t+\tau_1)\mathbf{b}(t+\tau_1),\mathbf{a}(t+\tau_2)\}$$
$$= K\{\mathbf{e}(t),\mathbf{e}(t+\tau_1)\}.K\{\mathbf{b}(t),\mathbf{b}(t+\tau_1),\mathbf{a}(t+\tau_2)\}$$
$$+ K\{\mathbf{e}(t),\mathbf{e}(t+\tau_1)\}.K\{\mathbf{b}(t),\mathbf{a}(t+\tau_2)\}.K\{\mathbf{b}(t+\tau_1)\}$$
$$+ K\{\mathbf{e}(t),\mathbf{e}(t+\tau_1)\}.K\{\mathbf{b}(t+\tau_1),\mathbf{a}(t+\tau_2)\}.K\{\mathbf{b}(t)\}$$
$$= R_{ee}(\tau_1).[R_{bba}(\tau_1,\tau_2)+(R_{ba}(\tau_2)+R_{ba}(\tau_2-\tau_1))\mu_b] . \qquad (14)$$

Now $\mathbf{a}(t)$ and $\mathbf{b}(t)$ are obtained via memoryless nonlinear transformations of the same Gaussian process $\mathbf{n}(t)$. Hence $R_{bba}(\tau_1,\tau_2)$ will only be a function of the autocorrelations of $\mathbf{n}(t)$, namely, $R_n(\tau_1)$, $R_n(\tau_2)$ $R_n(\tau_1-\tau_2)$. Similar remarks apply to $R_{ba}(\tau_2)$ and $R_{ba}(\tau_2-\tau_1)$. From this it follows that substituting $-\tau_1$ for τ_1 and $-\tau_2$ for τ_2 leaves (14) the same. In other words, the Fourier transform of (14) is real-valued. The same conclusion holds for the Fourier transform of the 6th and 7th terms of (12). Finally, for the last term of (12), we have

$$K\{\mathbf{e}(t)\mathbf{b}(t),\mathbf{e}(t+\tau_1)\mathbf{b}(t+\tau_1),\mathbf{e}(t+\tau_2)\mathbf{b}(t+\tau_2)\}$$
$$= K\{\mathbf{e}(t),\mathbf{e}(t+\tau_1),\mathbf{e}(t+\tau_2)\}.E\{\mathbf{b}(t).\mathbf{b}(t+\tau_1).\mathbf{b}(t+\tau_2)\}$$
$$= R_{eee}(\tau_1,\tau_2)[R_{bbb}(\tau_1,\tau_2)+(R_{bb}(\tau_1)+R_{bb}(\tau_2)+R_{bb}(\tau_1-\tau_2))\mu_b+\mu_b^3] \qquad (15)$$

The Fourier transform of this term is, in general, not real valued. Substituting our results back in (12) we obtain

$$R_{vvv}(\tau_1,\tau_2)$$

$$= R_{aaa}(\tau_1,\tau_2)$$

$$+ R_{ee}(\tau_1).[R_{bba}(\tau_1,\tau_2)+(R_{ba}(\tau_2)+R_{ba}(\tau_2-\tau_1))\mu_b]$$

$$+ R_{ee}(\tau_2).[R_{bba}(\tau_2,\tau_1)+(R_{ba}(\tau_1)+R_{ba}(\tau_1-\tau_2))\mu_b]$$

$$+ R_{ee}(\tau_2-\tau_1).[R_{bba}(\tau_2-\tau_1,-\tau_1)+(R_{ba}(-\tau_1)+R_{ba}(-\tau_2))\mu_b]$$

$$+ R_{eee}(\tau_1,\tau_2)[R_{bbb}(\tau_1,\tau_2)+(R_{bb}(\tau_1)+R_{bb}(\tau_2)+R_{bb}(\tau_1-\tau_2))\mu_b+\mu_b^3] \qquad (16)$$

In deriving this result we have also shown that it is the last term of (16) that causes the phase of $S_{vvv}(\omega_1,\omega_2)$ to deviate from zero.

IV. THE EFFECT OF $H_1(\omega)$ ON THE STATISTICS OF THE PHASE (AN EXAMPLE)

We have seen that the phase of the bispectrum of $\mathbf{v}(t)$ is theoretically zero. Therefore, an estimation of this phase, when $H_1(\omega)$ and $G(u)$ are simple functions, should give some idea of the kind of errors to be expected. Let $H_1(\omega)$ be as shown in figure 2 a) and b). Thus, $H_1(\omega)$ is a lowpass filter with bandwidth $\sigma=\pi/2$ and let $\mathbf{v}(t) = G(\mathbf{u}(t)) = \mathbf{u}^2(t)$. Let $\mathbf{u}(t)$ and $\mathbf{v}(t)$, be *discrete* stochastic processes which we shall denote by $\mathbf{u}[n]$ and $\mathbf{v}[n]$ respectively. The autocorrelation of $\mathbf{v}[n]$ is then

$$R_v[m] = K\{\mathbf{v}[n], \mathbf{v}[n+m]\}$$
$$= K\{\mathbf{u}^2[n], \mathbf{u}^2[n+m]\}$$
$$= 2K\{\mathbf{u}[n], \mathbf{u}[n+m]\}^2$$
$$= 2(R_u[m])^2. \qquad (17)$$

And the power spectrum of $\mathbf{v}[n]$ is therefore

$$S_v(\mu) = \Sigma_n R_v[m] e^{-j\mu m}$$
$$= (2/2\pi)\int_{(-\pi,+\pi)} S_u(\omega)S_u(\mu-\omega)d\omega$$
$$= (2/2\pi) S_u(\mu) * S_u(\mu) . \qquad (18)$$

Next, let's evaluate the third-order moment $R_v[l,m]$:

$$R_v[l,m] = K\{\mathbf{v}[n], \mathbf{v}[n+m], \mathbf{v}[n+m] \}$$
$$= K\{\mathbf{u}^2[n], \mathbf{u}^2[n+m], \mathbf{u}^2[n+m] \}$$
$$= 8K\{\mathbf{u}[n], \mathbf{u}[n+l]\}K\{\mathbf{u}[n+l], \mathbf{u}[n+m]\}K\{\mathbf{u}[n], \mathbf{u}[n+m]\}$$
$$= 8R_u[l] R_u[l-m] R_u[m]. \qquad (19)$$

In going from the second to the third line of (19), we used the "indecomposable-partition product rule"[13,19], and the fact that $\mathbf{u}[n]$ is a stationary zero-mean gaussian process.

The bispectrum of $\mathbf{v}[n]$ is now given by

$$S_v(\lambda,\mu) = \Sigma_{l,m} R_v[l,m] e^{-j(\lambda l+\mu m)}$$
$$= 8 \Sigma_{l,m} R_u[l] R_u[l-m] R_u[m] e^{-j(\lambda l+\mu m)} \quad [\text{from (19)}]$$
$$= 8 \Sigma_l (R_u[l] e^{-j\lambda l} (\Sigma_m R_u[m-l] R_u[m] e^{-j\mu m}))$$
$$= 8 \Sigma_l \{R_u[l]e^{-j\lambda l} (1/2\pi)\int_{(-\pi,+\pi)} S_u(\omega)S_u(\mu-\omega)d\omega e^{-j\omega l}\}$$
$$= 8 (1/2\pi)\int_{(-\pi,+\pi)} S_u(\omega)S_u(\mu-\omega)\{\Sigma_l R_u[l]e^{-j(\lambda+\omega)l}\}d\omega$$
$$= 8 (1/2\pi)\int_{(-\pi,+\pi)} S_u(\omega)S_u(\mu-\omega)S_u[\lambda+\omega] d\omega$$
$$= 8 (1/2\pi) [S_u(\lambda) * S_u(\mu+\lambda)] S_u(\lambda) \qquad (20)$$

From (18) and (20), the *bicoherence* [18] of $\mathbf{v}[n]$ is given by

$$bic_v(\lambda,\mu) = S_v(\lambda,\mu) / \sqrt(S_v(\lambda) S_v(\mu) S_v(\lambda+\mu))$$

$$\frac{\sqrt(8/2\pi) [S_u(\lambda) * S_u(\mu+\lambda)] S_u(\lambda)}{\sqrt{[S_u(\mu) * S_u(\mu)].[S_u(\lambda) * S_u(\lambda)].[S_u(\mu+\lambda) * S_u(\mu+\lambda)]}} \qquad (21)$$

This expression may be evaluated for any function $S_u(\lambda)$ by means of FFT's.

It is important to examine the bicoherence function because its statistical properties are approximately independent of the power spectrum[17]. The bispectrum $S_v(\lambda,\mu)$, on the other hand, has a variance that is proportional to $S_v(\lambda) S_v(\mu) S_v(\lambda+\mu)$. In fig.3, we have plotted the bicoherence of $v[n]$ for the following three special cases:

(a) theory, with $H_1(\omega)$ and $G(u)$ as in fig 2.

(b) simulation, with $H_1(\omega)$ and $G(u)$ as in fig 2.

(c) simulation, with $H_1(\omega)=1$, and $G(u)$ as in fig 2.

The same artificial data was used for (b) and (c), and the parameters of the simulation such as sample size are indicated in figure 3. It must be mentioned that the method used for the estimation of the bispectrum was the same as the one developed by the authors [4]. For bandlimited data, it may be worthwhile to take advantage of the redundant data contained in the two-dimensional phase of the bispectrum[1], or else, to use parametric methods[16].

In figure 4 the phase estimation of the bispectrum of $v[n]$ (which should theoretically be zero) is shown, for cases (b) and (c).The errors are greatest when the bicoherence is low. This is to be expected, because the confidence set $(\psi -\delta\psi, \psi +\delta\psi)$ of the phase is approximately given by [18]

$$\Phi(-(r/\sigma).\sin(\delta\psi)) = \alpha/2,$$

where, $1-\alpha$ is the probability that the confidence set will contain the origin, r is the modulus of the bicoherence, σ is the standard deviation of the bicoherence estimate (and depends only on the sample size and the resolution imposed), and Φ is the standard normal probability distribution function.

Estimation of the phase of $H_2(\omega)$ (simulation):

To continue with the same example, we took $H_2(\omega)=H_1(\omega)$, with $H_1(\omega)$ and $G(u)$ the same as that in figure 2. The phase $\psi_{H_2}(\lambda,\mu)$ of the theoretical bispectrum (ie $H_2(\lambda)H_2(\mu)H_2(\lambda+\mu)$) of $H_2(\omega)$ is shown in fig 5 a), and using this along with the algorithm of Lii-Rosenblatt [8] we can calculate, approximately, the phase $\phi(\omega)$ of $H_2(\omega)$. Here, we took $\mu=\omega_o= 2\pi/16$, a constant.The same phase $\psi_v(\lambda, \omega_o)$ was obtained from the data $y[n]$ using the method in [4]. The results are shown in figures 6 and 7 for $\omega_o= 2\pi/16$ and $\omega_o = 2\pi/32$ respectively. Notice the close agreement between theory (fig 5) and simulation (fig 6). And we also see that by decreasing ω_o, the resolution improves (fig.7 vs fig.2).

V. CONCLUSION

We have shown that certain nonlinear systems can be identified from observations of the output only. However, in order to obtain a unique solution it is necessary to make strong assumptions regarding the nature of the nonlinear system and the input process. The effect of a nongaussian input was considered both analytically . The effect that the bandlimiting filter $H_1(\omega)$ (before the memoryless nonlinearity) has on the the statistics of the bispectrum was studied by means of simple examples.

REFERENCES

[1] Matsuoka T. & Ulrych T.J., Proc IEEE, Oct '88
   "Phase estimation using the bispectrum".
[2] Benveniste A. & Goursat M., IEEE Trans Comm, Aug'84
   "Blind Equalizers".
[3] Wiggins R.A. Geoexploration Apr '78
   "Minimum Entropy Deconvolution"
[4] Rozario N. & Papoulis A.,4th ASSP Workshop on
   Spectrum Estimation and Modelling, Aug 88, Minneapolis
   "Transfer function phase estimation using a low variance
   higher order spectrum".
[5] Giannakis G.B, Univ of S. California, Phd Thesis, '86
   "Signal processing via higher order statistics".
[6] Nikias C.L & Venetsanopoulis, Proc ICC, Toronto,'86
   "Identification of non-minimum phase communication
   channels via parametric modelling of 3rd order moments".
[7] Mendel J.M, Academic Press NY, '83
   "Optimum seismic deconvolution".
[8] Lii K.S. & Rosenblatt M, Ann. Statistics, 1195-1208,'82
   "Deconvolution and estimation of transfer function phase
   and coeffs. for non-gaussian linear processes".
[9] Subha Rao & Gabr J., of Time series pp145-148,1980
   "A test for linearity of time series".
[10]Hasselmann, Munk & Macdonald, Time Series Analysis
   (M. Rosenblatt Ed.) Wiley NY, '63
   "Bispectra of ocean waves".
[11]Brillinger D.R, J. of Sound and Vibration 301-313, '70
   "The identification of polynomial systems by means of
   higher order spectra".
[12]Brillinger D.R., Biometrika, v64, '77
   "The identification of a particular nonlinear time series".
[13]Brillinger D.R., Ann. of Mathematical Statistics,36,'65
   "An introduction to polyspectra".
[14]Bussgang J.J. Ehrman L. & Graham, Proc IEEE,Aug'84
   "Analysis of nonlinear systems with multiple inputs"
[15]Shimbo, Nguyen, & Albuquerque, Proc IEEE, Apr '86
   "Modulation transfer noise effects among FM and digital
   signals in memoryless nonlinear devices".
[16]Raghuveer M.R & Nikias IEEE Trans ASSP p1213-29,'85
   "Bispectrum Estimation: A parametric approach".
[17]Brillinger D.R & Rosenblatt M. Spectral Analysis of Time
   Series (B.Harris Ed), Wiley NY '67
   "Asymptotic theory of estimates of kth order spectra".
[18]Huber, Kliener, Gasser & Dummermuth IEEE AU-19,'71
   "Statistical methods for investigating phase relations in
   stationary stochastic processes".
[19]Shiryaev A.N. Theory of Probability and applications 5, '60
   "Some problems in the spectral th. of higher order moments
[20]Papoulis A. Pobability, Random Variables and Stochastic
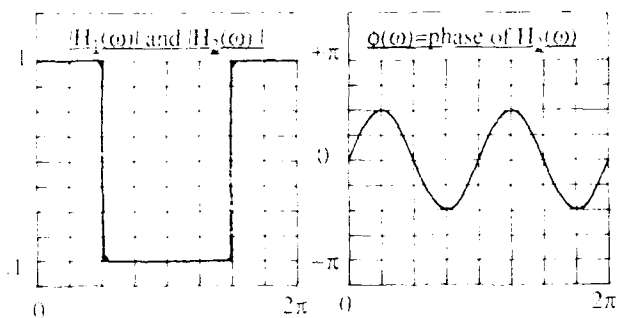   processes, McGraw Hill NY (2nd Edn, '84.

Theoretical (with $\omega_o = 2\pi/16$)

$H_1(\omega)$ and $H_2(\omega)$

$\varrho(\omega)$=phase of $H_2(\omega)$

$\Psi_{H2}(\omega, \omega_o)$

$\phi_{H2}(\omega)$=phase of $H_2(\omega)$

Figure 2a)   figure 2b)   Figure 5a)   figure 5b)
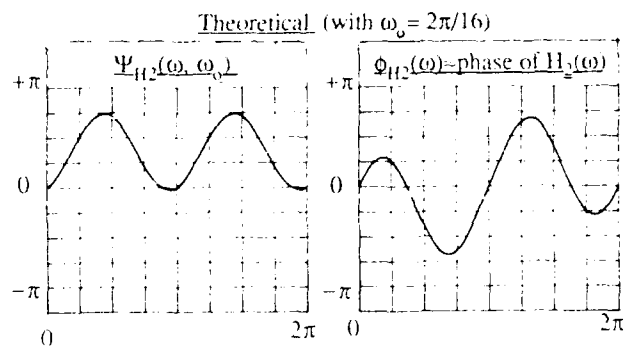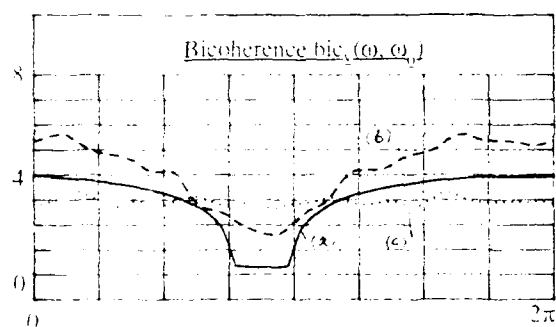
Bicoherence $bic_y(\omega, \omega_o)$

(b)

(a)   (c)

Figure 3

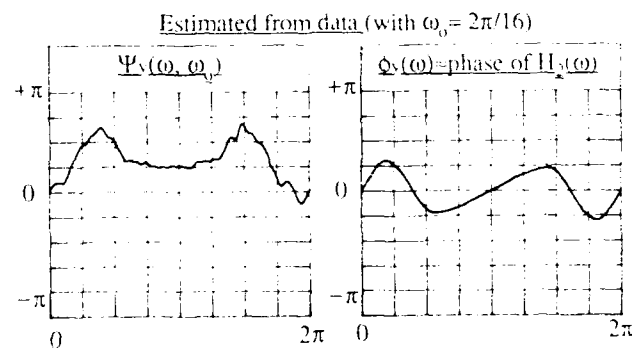Sample size: 1000, 50% overlap of data. Freq. resolution = $2\pi/256$, window bw = $2\pi/32$, $\omega_o = 2\pi/8$.

Estimated from data (with $\omega_o = 2\pi/16$)

$\Psi_y(\omega, \omega_o)$

$\phi_y(\omega)$=phase of $H_2(\omega)$

Figure 6a)   figure 6b)

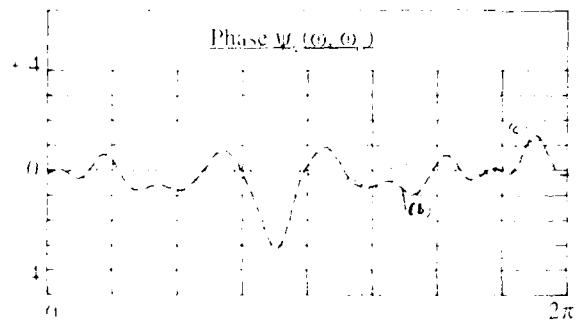(Sample size=1000, 50% overlap of data. Freq. resolution = $2\pi/256$, window bw= $2\pi/32$, $\omega_o = 2\pi/16$)
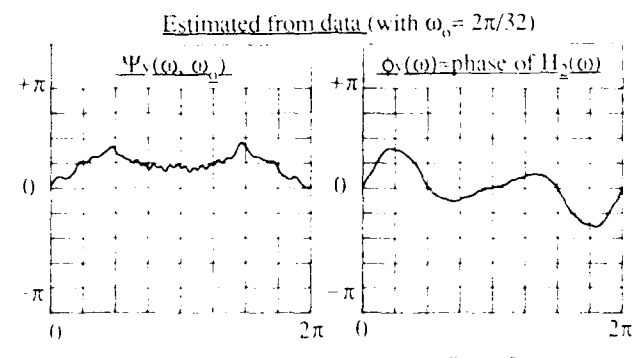
Phase $\Psi_y(\omega, \omega_o)$

(b)

Figure 4

Estimated from data (with $\omega_o = 2\pi/32$)

$\Psi_y(\omega, \omega_o)$

$\phi_y(\omega)$=phase of $H_2(\omega)$

Figure 7a)   figure 7b)

KEH-SHIN LII and TAI-HOUN TSOU

Department of Statistics
University of California, Riverside
Riverside, California

Abstract - We will discuss the problem of
ascertaining the number of sinusoids in nonGaussian
noise environment. Most tests of significance for
the existence of sinusoids are based on second order
statistics. Such testing procedures include
Fisher's test, Bartlett's test, Whittle's test among
others. We will use information contained in the
higher order (third and fourth) spectral function as
well as second order spectral function to form more
powerful tests. Some asymptotic results are
discussed. The question of signal to noise ratio
with respect to the sample size are considered.
Simulation example and sunspot data are used to
demonstrate the effectiveness of the methods.

I. INTRODUCTION

A typical signal plus noise model is of the
form

$$X_t = Y_t + Z_t \tag{1}$$

with Y_t is a periodic function given by

$$Y_t = \sum_{k=1}^{K} R_k \cos(\omega_k t + \phi_k) \tag{2}$$

where R_k, ω_k, and ϕ_k are the amplitude, frequency
and phase of the harmonic process Y_t. Z_t is an
additive noise process which is independent with Y_t.
When Z_t is a white Gaussian process, various authors
[6,7,12,13,15], discussed how to detect the harmonic
signal Y_t. In many applications of engineering,
meteorology and ecology problems, the background
noise may not be white, or it can be represented as
a linear process, such as

$$Z_t = \sum_u \alpha_u \epsilon_{t-u} \tag{3}$$

where ϵ_u's are independent, identically distributed
and α_u's are constants. Usually we assume that ϵ_t
has mean zero with variance σ^2. Testing and
estimation problems are dealt with in [2,9,10,16]
when the noise process is assumed to be colored.

The Fisher's test [6] is the case when the
noise process Z_t is assumed to be zero mean Gaussian
white noise with variance σ^2. The null hypothesis
can be stated as

H_0: the harmonic signal Y_t is zero in (1).
Under H_0, the periodogram of the process X_t,

$$I_N^X(\lambda_j) = (2/N) \left| \sum_{t=1}^{N} X_t \exp(-it\lambda_j) \right|^2 \text{ with } \lambda_j = 2\pi j/N$$

has a Chi-square distribution with 2 degrees of
freedom, if it is divided by σ^2. Furthermore,
$I_N^X(\lambda_j)$ and $I_N^X(\lambda_k)$ are independent if $j \neq k$ with
$\lambda_m = 2\pi m/N$ for $j,k = 1,2,\ldots,[N/2]$. This result also
holds for any fixed number of frequencies asymptoti-
cally when the noise process Z_t is independent,
identically distributed, but not necessarily
Gaussian ([4] p. 126). Based upon the previous
result, Fisher derived the exact distribution for
the test of the largest peak of the periodogram,
i.e.

$$G^{(f)} = \frac{\max\limits_{1 \le j \le [N/2]} I_N^X(\lambda_j)}{\sum\limits_{1 \le j \le [N/2]} I_N^X(\lambda_j)} \tag{4}$$

This test is uniformly most powerful when the
alternative is $K=1$ ([1] p. 124).

When the noise process is linear which has the
form given in (3) with the conditions that $E|\epsilon_t|^4 < \infty$
and $\sum |\alpha_u||u| < \infty$, then the power spectrum of Z_t is

$$f^Z(\lambda) = (\sigma^2/2\pi)|\sum \alpha_u \exp(-iu\lambda)|^2$$

and its periodogram has following relationship with
the periodogram of ϵ_t

$$I_N^Z(\lambda) = |\sum \alpha_u \exp(-iu\lambda)|^2 I_N^\epsilon(\lambda) + R_N(\lambda)$$

when $R_N(\lambda) = O(1/N)$ uniformly in λ ([1] p. 444).
From this, it is clear that asymptotically

$$\frac{I_N^Z(\lambda)}{|\sum \alpha_u \exp(-iu\lambda)|^2} = I_N^{\epsilon}(\lambda) \qquad (5)$$

if $|\sum \alpha_u \exp(-iu\lambda)| \neq 0$ for all λ. The asymptotic distribution of $I_N^{\epsilon}(\lambda)$ is known from the previous discussion. This observation motivated various methods which attempt to estimate the spectrum of the noise process Z_t which is proportional to $|\sum \alpha_u \exp(-iu\lambda)|^2$ under the null hypothesis that $Y_t = 0$. Conventional methods include Whittle's test, Bartlett's test and Priestley's $P(\lambda)$ test (see [1]).

All these methods are based on the second order moments of the time series. When the noise process is Gaussian then moments up to second order give all the information. If the noise process is non-Gaussian then cumulants of order greater than two might provide extra information in addition to those of less than or equal to second order moments. In the next section we will present a method which will take advantage of third and fourth order cumulants to improve the efficiency of detecting the existence of the periodic function Y_t under the assumption that the noise process is non-Gaussian. Computational details and other simulation results are given in [8].

II. TEST STATISTICS

For simplicity, we will study processes Y_t and Z_t separately. Assuming X_t is stationary up to order eight, and all cumulants are summable up to the eighth order. The bispectrum and the trispectrum is the Fourier transformation of third and fourth order cumulant function, i.e.

$$f^X(\lambda_1,\lambda_2) = (2\pi)^{-2} \sum_{u,v=-\infty}^{\infty} C^X(u,v)$$

$$\cdot \exp(-iu\lambda_1 - iv\lambda_2)$$

$$= f^Y(\lambda_1,\lambda_2) + f^Z(\lambda_1,\lambda_2)$$

[illegible]

Let $\delta_N(\theta) = \sin((N+(1/2))\theta)/2\pi\sin(\theta/2)$ be the Dirichlet kernel. Then, on the particular submanifolds $(\lambda,0)$ and $(\lambda,0,0)$, we have

$$I_N^Y(\lambda,0) = O(1)$$

$$I_N^Y(\lambda,0,0) = (-3R^4/16)[\delta_N(\omega-\lambda)+\delta_N(\omega+\lambda)]\delta_N^2(\omega) \qquad (7)$$

Now consider the noise process $\{Z_t\}$. When $\{Z_t\}$ is Non-Gaussian linear process with 3rd (4th) order cumulants γ_3 (γ_4) of ϵ_t finite and nonzero, then the bispectrum and the trispectrum can be represented as

$$f^Z(\lambda_1,\lambda_2) = (\gamma_3/(2\pi)^2)\Gamma(\lambda_1)\Gamma(\lambda_2)\Gamma^*(\lambda_1+\lambda_2)$$

$$f^Z(\lambda_1,\lambda_2,\lambda_3) = (\gamma_4/(2\pi)^3)\Gamma(\lambda_1)\Gamma(\lambda_2)\Gamma(\lambda_3)\Gamma^*(\lambda_1+\lambda_2+\lambda_3)$$

with $\Gamma(\lambda) = \sum \alpha_u \exp(-iu\lambda)$, and $*$ is the complex conjugate.

When the noise process Z_t is given in (3) such that the third order cumulant of ϵ_t is nonzero, the bispectrum of the process X_t, on the submanifold $(\lambda_1,\lambda_2) = (\lambda,0)$, can be represented as

$$f^X(\lambda,0) = f^Z(\lambda,0) = (2\pi)^{-2}\,\gamma_3\,\Gamma(0)|\Gamma(\lambda)|^2 .$$

Hence, when $\Gamma(0) \neq 0$,

$$|\Gamma(\lambda)|^2 = D_1 f^X(\lambda,0)$$

with $D_1 = (2\pi)^2/(\gamma_3\Gamma(0))$. From these discussions the following test statistics, from (5), is proposed

$$G^{(b)} = \frac{\max_{1\le j\le [N/2]} I_N^X(\lambda_j)/|\Gamma(\lambda_j)|^2}{\sum_{1\le j\le [N/2]} I_N^X(\lambda_j)/|\Gamma(\lambda_j)|^2}$$

$$= \frac{\max_{1\le j\le [N/2]} I_N^X(\lambda_j)/Rf_N^X(\lambda_j,0)}{\sum_{1\le j\le [N/2]} I_N^X(\lambda_j)/Rf_N^X(\lambda_j,0)}, \quad j=1,2,\ldots,[N/2] \qquad (8)$$

where $Rf_N^X(\lambda,0)$ is a consistent estimator of the real part of the bispectrum $f^X(\lambda_1,\lambda_2)$ at frequency $(\lambda,0)$, and the unknown constant D_1 is cancelled out.

When ϵ_t is symmetric distributed or [illegible] with a nonzero 4th order cumulant γ_4, [illegible]

[illegible]

... the harmonic components.

$$\max_{1 \le j \le N} I_N^X(\lambda_j) = R I_N^X(\lambda_j)$$

$$I_N^X(\lambda_j) = R I_N^X(\lambda_j)$$

$$j = 1, 2, \dots, N \qquad (7)$$

where $R I_N^X(\lambda_j)$ is the estimated real part of the ... of λ_j ...

We note that test statistics $G^{(b)}$ and $G^{(t)}$ given in (8) and (9) have the same distribution as that of Fisher's statistic $G^{(f)}$ given in ... asymptotically as sample size N increases under H_0. Note also that the peak of the periodogram of the harmonic process Y_t is proportional to NR^2. For any fixed sample size N, we are interested in the case that $NR^2 = \max I_N^X(\lambda_j)$, the maximum of the periodogram of the noise process Z_t. In this sense we have fixed signal to noise ratio for any sample size N.

III. NUMERICAL EXAMPLES

A simulated series which has mixed spectra and Wolfer's sunspot data set will be used to demonstrate the effectiveness of the $G^{(b)}$ and $G^{(t)}$ tests in equation (8) and (9). Consider the simulated series from equation (1) with $k=1$ for harmonic process Y_t and linear process Z_t defined as follow

$$Y_t = R\cos(\omega t)$$

$$Z_t = \phi_1 Z_{t-1} + \phi_2 Z_{t-2} = \epsilon_t$$

where the coefficient of AR(2) process Z_t are $\phi_1 = 0.3, \phi_2 = -0.8$, and ϵ_t are independent exponentially distributed random deviates with mean one generated from the GGEXN subroutine in the IMSL. The number of observations generated for each series is $N = ...$. We choose the amplitude $R = 0.4$ and the frequency $\omega/2\pi = ...$. The process of X_t and its periodogram are shown in Figure 1 and Figure 2.

To use the $G^{(b)}$ test, we first need to estimate the real part of the bispectrum $f_X(\lambda_j, 0)$ at the frequency $(\lambda_j, 0)$ by properly selecting the truncation lag and the two-dimensional smoothing window. Here we select the two-dimensional Bartlett window to be the smoothing function with $M = 15$. Some aspects of the computational details are discussed in ... Under H_0, $G^{(b)}$ has the same asymptotic distribution as the Fisher statistic. We get our critical points $z_{.10} = ..., z_{.05} = ..., z_{.01} = ...$ for the significance levels $\alpha = 0.1, 0.05$ and 0.01 respectively. Figure 3 shows the results of $I_N^X(\lambda_j) = R I_N^X(\lambda_j)$ vs. frequency. The results are summarized in Table 1, which show that $G^{(b)}$ test detected the harmonic processes at the right frequency.

Since the linear process $\{Z_t\}$ is generated from an exponential distribution, its fourth order cumulant certainly exists. We choose the 3-dimensional Bartlett window with lag $M = 10$. Figure 4 shows the plot of $I_N^X(\lambda_j) = R I_N^X(\lambda_j, 0, 0)$ vs. frequency. Table 1 presents the $G^{(t)}$ value for the suspected peak. The results show that the $G^{(t)}$ test also detected the harmonic component at the right frequency.

The sunspot numbers have been studied extensively in different literature [3, 14, 17]. The data consider is the Wolfer's sunspot in 11 from year 1700 to 1965. It is generally believed that there is 11 years (approximately) period in the data. In the rest of the paper we will focus on these data to find the existence of possible other periodicities by using the $G^{(b)}$ and $G^{(t)}$ statistics. Figure 5 and Figure 6 give the plots of the observation and its periodogram. The mixed spectra model (1) will be considered. The $G^{(b)}$ and $G^{(t)}$ tests will be used to detect the presence of harmonic terms. Here, we use the 2-dimensional and 3-dimensional Bartlett's window with smoothing lag 15 and 7 to estimate bispectrum and trispectrum. Figure 7 and Figure 8 show the plots of $I_N^X(\lambda_j) = R I_N^X(\lambda_j, 0)$ and $I_N^X(\lambda_j) = R I_N^X(\lambda_j, 0, 0)$ using bispectrum and trispectrum information for the first iteration. If a particular frequency is significant with $G^{(b)}$ and $G^{(t)}$ statistics, we removed it sequentially by least square method until no further harmonic component is detected. The final model obtained for the data has sinusoid components with additive AR(2) noise process with the form given by

$$X_t = \mu + \sum_{k=1}^{q} (A_k \cos(\omega_k t) + B_k \sin(\omega_k t)) + Z_t$$

with $Z_t = \phi_1 Z_{t-1} + \phi_2 Z_{t-2} + \epsilon_t$. Here we re-express R_k and ϕ_k in (2) in terms of A_k and B_k. Table 2 shows the estimated periodicities, coefficients, significant levels, and the residual variances of the fitted models. Note that for $G^{(b)}$ test we detected three significant periods at $\alpha = 0.1$ level while $G^{(t)}$ test detected four significant periods at $\alpha = 0.1$ level. Although we should remark that the fourth period in $G^{(b)}$ test has a p-value 0.115.

The residual variances for the final models using $G^{(b)}$ and $G^{(t)}$ are 458.85 and 456.8 which can be compared with the residual variance 500.1 of ARMA (3, 5) which was the best linear model fitting by ....

REFERENCES

1. Anderson, T. W. (1971), The Statistical Analysis of Time Series, Wiley, New York.

2. Bartlett, M. S. (1957), Discussion on Symposium on spectral approach to time series, J. R. Statist. Soc. B, 19, 1-63.

Bloomfield, P. (1976), Fourier Analysis of Time Series. John Wiley. New York.

Brillinger, D. R. (1975), Time Series Data Analysis and Theory. Holt, Rinehart and Winston, New York.

Hannan, E., Spjotvoll, E. (1983), Estimation of trigonometric components in time series. J. Amer. Statist. Assn., 71, 381-387.

Fisher, R. A. (1929), Tests of significance in harmonic analysis, Proc. Roy. A, 125, 54-59.

Grenander, U., Rosenblatt, M. (1957), Statistical Analysis of Stationary Time Series, Wiley, New York.

He, F. S., Tson, T. H. (1988), Computational aspects of harmonic signal detection. Proceedings of the 20th Symposium on the interface: Computationally intensive Methods in Statistics, Interface Foundation of North America Ed. J. Wegman, R. E. D. P. Gantz and J. T. Miller, 257-263.

Priestley, M. B. (1962a), The analysis of stationary processes with mixed spectra-I. J.R. Statist. Soc. B 24, 215-233.

Priestley, M. B. (1962b), The analysis of stationary processes with mixed spectra-II. J.R. Statist. Soc. B. 24, 511-529.

11 Priestley, M. B. (1981), Spectral Analysis and Time Series, Vols. I and II. Academic Press, New York.

12 Schuster, A. (1898), On the investigation of hidden periodicities with application to a supposed 26-day period of meteorological phenomena, Terr. Mag. Atmos. Elect., 3, 13-41.

13 Siegel, A. F. (1980), Testing the periodicity in a time series. J. Amer. Statist. Assn., 75, 345-348.

14 Subar Rao, T., Gabr M. M. (1984), An Introduction to Bispectral Analysis and Bilinear Time Series Models. Springer-Verlag, New York.

15 Whittle, P. (1952), The simultaneous estimation of a time series harmonic components and covariance structure, Trabajos. Estadist., 3, 43-57.

16 Whittle, P. (1954), The statistical analysis of a Seiche record, J. Marine Research, 13, 76-100.

17 Yule, G. U. (1927), On a method of investigating periodicities in disturbed series with special reference to Wolfer's sunspot numbers. Phils. Trans. Roy. Soc., London, A, 42, 267-298.
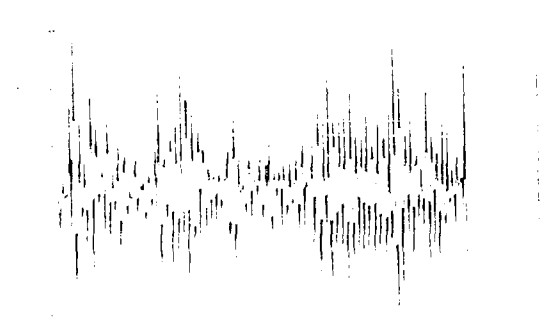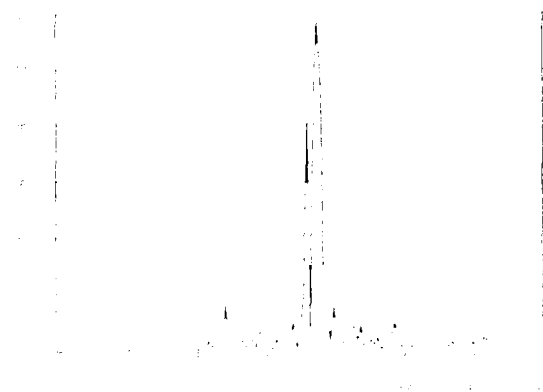
Figure 1(b). Periodogram of X_t

Figure 3. $I_N^X(\lambda_j)$, $(Rf_N^X(\lambda_j,0))$

Figure 4. $I_N^X(\lambda_j)$, $Rf_N^X(\lambda_j,0.00)$
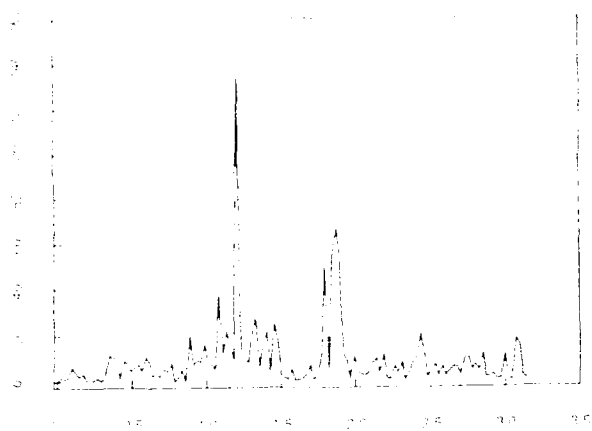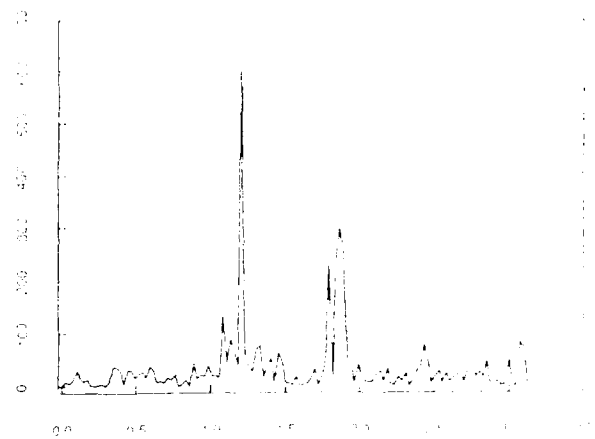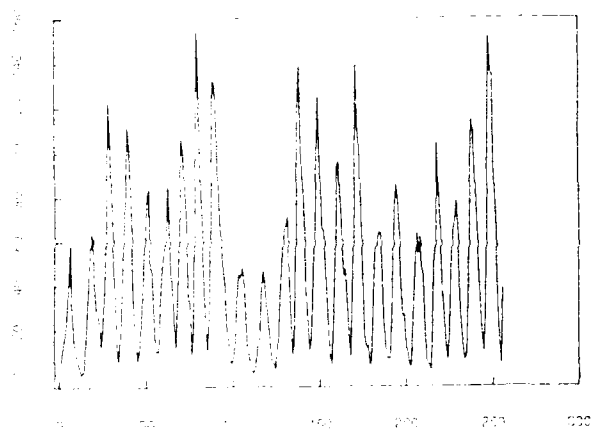
Figure 5. s_t, Wolfer's sunspot data 1700-1955
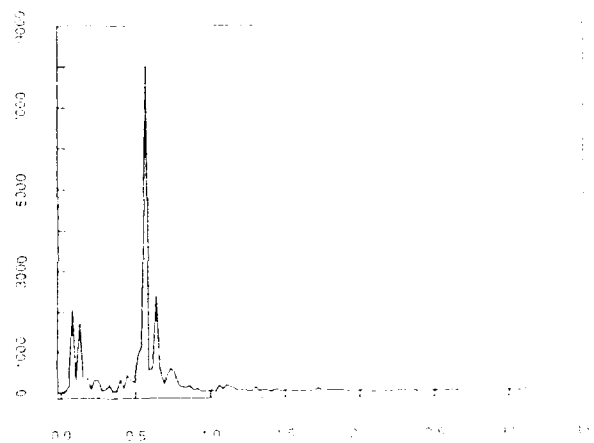
Figure 6. $I_N^S(\lambda_j)$, periodogram of Wolfer's sunspot data
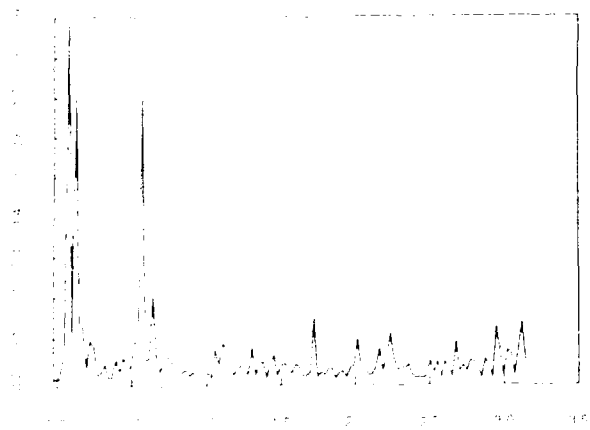
Figure 7. $I_N^S(\lambda_j)$, $Rf_N^S(\lambda_j,0)$

Figure 8. $I_N^S(\lambda_j)$, $Rf_N^S(\lambda_j,0.00)$
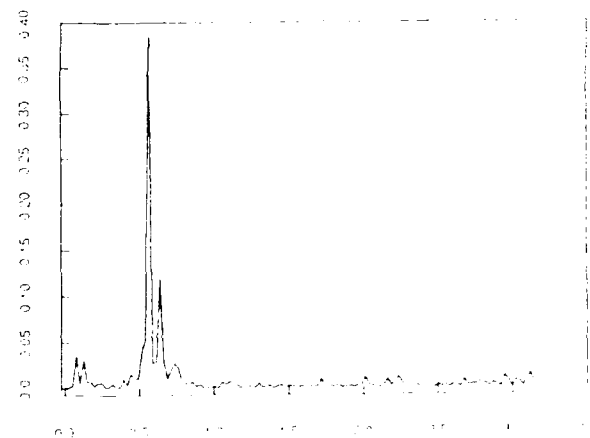
Tests	$\Sigma \dfrac{I^x(\lambda)}{h^x(\lambda)}$	ω	$\dfrac{I^x(\omega)}{h^x(\omega)}$	statistics
$q^{??}$	1196.01	1.2026	140.496	0.1185 ***
$q^{??}$	4475.91	1.2026	605.158	0.1358 ***

Table 1

$h^x(\lambda)$ represent the estimated noise spectrum of X. by real part of bispectrum and trispectrum. *, **, ***, den to that the test is significant at level (α = 0.1, 0.05 and 0.01.

$2\pi/\hat\omega$	statistics	$\hat A_k$	$\hat B_k$	SSR
93.40	0.182 ***	- 5.913	-13.790	289610
$G^{(b)}$ 11.12	0.149 *	-28.209	-	187674
54.78	0.060 **	-11.803	-	169648
$\hat\sigma_1$ = 1.195	$\hat\phi_2$ = -0.599			48584
11.12	0.321 ***	-28.091	-	218567
93.40	0.204 ***	- 5.972	-13.998	187639
$G^{(t)}$ 9.96	0.081 **	19.177	-	144062
55.14	0.05? *	-12.091	-	125078
$\hat\phi_1$ = 1.088	$\hat\phi_2$ = -0.501			44678

Table 2

*, **, and *** denote the test statistics are significant at level α =0.1, 0.05 and 0.01. SSR are sum of square residual for different estimated model.

TRANSIENT SIGNAL ESTIMATION WITH
HIGHER-ORDER-STATISTICS*

Christos K. Papadopoulos and Chrysostomos L. Nikias

Communications and Digital Signal Processing (CDSP) Center for Research and Graduate Studies
Northeastern University
Boston,MA 02115

ABSTRACT

Two methods for the estimation of the parameters of exponentially damped sinusoids are introduced based on third order statistics of the observation signal. These methods may be seen as extensions of the minimum norm principal eigenvectors method (Kumaresan-Tufts) to higher order statistics domains. The strong points and limitations of the new methods are discussed, as well as sufficient conditions for existence of their solutions. The utilization of these methods in the case of finite length signals in the presence of additive Gaussian noise (white or colored) is addressed. Monte-Carlo simulations demonstrate the effectiveness of the new methods when the additive noise is colored Gaussian with unknown autocorrelation sequence. The case of an ensemble of data records is studied when the exponentially damped sinusoids are assumed to have random phase.

I. INTRODUCTION

Assume that the observed signal $x(n)$ can be represented by a finite sum of complex exponentials of the form

$$x(n) = \sum_{m=1}^{L} h_m \cdot e^{b_m n}, \qquad n = 0,1,2,\dots \qquad (1)$$

where the complex constants are defined as

$$h_m = d_m e^{j\theta_m}$$

$$b_m = c_m + j w_m, \qquad c_m < 0.$$

Notice that the d_m and θ_m are the amplitude and initial phase of the mth signal, respectively; its damping factor is c_m ($c_m < 0$) and frequency w_m.

The problem of estimating the parameters of the above signal when it is observed in additive noise has been previously investigated [1-4]. There are two basic approaches: the exact maximum likelihood (ML) estimation of the parameters of the signal and Prony's method. The ML method turns out to be a nonlinear estimation problem. In the second approach, Prony has shown that e^{b_m}, $m = 1,\dots,L$ can be the roots of a complex polynomial where its coefficients can be found applying linear prediction on $x(n)$.

However, linear prediction fails to work in the presence of significant additive noise [5]. Kumaresan and Tufts in their pioneering work demonstrated performance close to maximum likelihood for the estimation of the signal parameters by using the principal eigenvectors of the data matrix to separate signal subspace from noise subspace in the form of singular value decomposition and the backward linear prediction equations of the noisy observations of $x(n)$ [1-4].

If the signals are steady-state sinusoids in additive colored Gaussian noise, previous work was based on making specific assumptions about the noise. In [6] the colored noise was represented as a first-order autoregressive (AR(1)) model. The AR(1) noise was also analyzed in [7] using the matrix inversion lemma. The purpose of this paper is to introduce new estimation procedures for the parameters of the signal described by (1) based on knowledge of its higher order statistics that also work in the presence of additive Gaussian noise (white or colored), without being necessary to make any model assumptions about the noise or even to know its autocorrelation sequence (i.e., spectrum characteristics).

The main motivation behind the use of higher-order statistics or cumulants [8-10] in this problem lies in their ability to suppress noise under certain conditions, without being necessary to know the exact probability density function (p.d.f.) governing the noise samples. For example, in the case where the additive noise has Gaussian p.d.f., then all its cumulants of order greater than two are identical to zero. Therefore, if the signal has non-zero bispectrum or trispectrum [8-13], then there might be a clear advantage to using third-order or fourth-order cumulants instead of autocorrelations.

The paper is organized as follows. In section II, the new methods are derived based on higher-order statistics for the estimation of the parameters of complex damped sinusoids and sufficient conditions of their unique solutions are clearly established. Section III shows application of these methods to the case of finite length and noisy data. Simulation examples are presented in section IV, for additive white and colored Gaussian noises. The extension of these methods to the case of complex damped sinusoids with random phase is shown in section V.

II. THE USE OF HIGHER-ORDER STATISTICS FOR TRANSIENT SIGNAL ESTIMATION

Consider the noise free signal $x(n)$ given by (1) for any time instant $n \geq 0$. For this signal there exists a unique

set of complex coefficients $\{a_i, \ i = 1, 2, \ldots, L\}$ such that

$$x(n) = \sum_{i=1}^{L} a_i \cdot x(n - i), \qquad n > 0. \qquad (2)$$

If we multiply the left and the right hand side of (2) by $x^*(n - l) \cdot x^*(n - l)$ and take a summation with respect to n ("$\cdot$" denotes complex conjugate), we obtain the following third order recursion equation

$$\sum_{i=0}^{l} a_i \cdot R_x(l - i, l - i) = 0 \qquad (a_0 = 1). \qquad (3.1)$$

for all l, where

$$R_x(l - i, l - i) = \sum_{n=0}^{\infty} x(n - i) \cdot x^*(n - l) \cdot x^*(n - l) \qquad (3.2)$$

is the true third order moment sequence of the energy signal $x(n)$.

Suppose that we now form the linear system of equations

$$\mathbf{R}_x \cdot \mathbf{a} = \mathbf{0} \qquad (4.1)$$

where

$$\mathbf{a} = (a_K \quad a_{K-1} \quad \ldots \quad a_0) \qquad (K + 1) \times 1. \qquad (4.2)$$

$K = 1/2 \cdot L(L + 1)$ and $\mathbf{R}_x$ is a Hankel matrix $(K + 1) \times (K + 1)$

$$\mathbf{R}_x = \begin{pmatrix} R_x(0,0) & \ldots & R_x(K,K) \\ R_x(1,1) & \ldots & R_x(K+1,K+1) \\ \vdots & \ddots & \vdots \\ R_x(K,K) & \ldots & R_x(2K,2K) \end{pmatrix}. \qquad (4.3)$$

Let us also define

$$A(m,v) = \sum_{l=1}^{L} h_l h_m^* h_v^* \cdot 1 \cdot (1 - e^{(b_l + b_m^* + b_v^*)}) \qquad (4.4)$$

$m = 1, 2, \ldots, L$. $v = 1, 2, \ldots, L$. $A(m,v) = A(v,m)$

Lemma 1: Assuming that we know the true third-order moments of the signal $x(n)$ in (1) and if $A(m,v) \neq 0$ $\forall m, v \in 1, L$ and $b_l + b_q \neq b_v + b_m$ $\forall l, q, v, m$, then for every vector $\mathbf{a}$ such that (4.1) and (4.3) holds and $K > 1/2 \cdot L(L + 1)$ the polynomial $A(z) = \sum_{i=0}^{K} a_{K-i} \cdot z^{-i}$ has $L = 1/2 \cdot L(L + 1)$ roots at $e^{(b_m^* + b_v^*)}$, $m, v \in 1, L$.

Proof: Substituting (1) into (3.2) for $l = K, K+1, \ldots, 2K$ and $i = 0, 1, \ldots, K$ in the form of (4.1), we obtain for each element of $\mathbf{R}_x$

$$R_x(z, \tau) = \sum_{n=0}^{\infty} \sum_{l, m, v=1}^{L} h_l e^{b_l n} \cdot h_m^* e^{b_m^*(n+\tau)} \cdot h_v^* e^{b_v^*(n+\tau)}$$

$$= \sum_{m=1}^{L} \sum_{v=1}^{L} A(m,v) e^{(b_m^* + b_v^*)\tau} \qquad (5.1)$$

where $A(m,v)$ is given by (4.4). Hence if we define $X(z)$ as

$$X(z) = \sum_{l=1}^{L} h_l \cdot (z - e^{b_l}). \qquad (5.2)$$

then from (4.4) and (5.2) we obtain

$$A(m,v) = h_m^* h_v^* e^{(b_m^* + b_v^*)} \cdot \sum_{l=1}^{L} h_l \cdot (e^{(b_m^* + b_v^*)} - e^{b_l})$$

$$= h_m^* h_v^* \cdot z \cdot X(z) \quad \text{for} \quad z = e^{(b_m^* + b_v^*)}. \qquad (5.3)$$

The third-order moment matrix $\mathbf{R}_x$ in (4.3) can be decomposed as

$$\mathbf{R}_x = \boldsymbol{\Phi} \cdot \mathbf{P} \qquad (6.1)$$

where

$$\boldsymbol{\Phi} = \begin{pmatrix} A_1 & \ldots & A_L \\ A_1 W_1 & \ldots & A_L W_L \\ \vdots & \ddots & \vdots \\ A_1 W_1^K & \ldots & A_L W_L^K \end{pmatrix} \qquad (6.2)$$

$$\mathbf{P} = \begin{pmatrix} 1 & W_1 & \ldots & W_1^K \\ 1 & W_2 & \ldots & W_2^K \\ \vdots & \vdots & \ddots & \vdots \\ 1 & W_L & \ldots & W_L^K \end{pmatrix} \qquad (6.3)$$

$$A_{m-v(v-1)/2} = A(m,v)(2 - \delta(m,v)).$$

$$W_{m-v(v-1)/2} = e^{b_v^* + b_m^*}, v \in 1, L ; m \in 1, v \qquad (6.4)$$

and $\delta(m,v)$ is the $2 - d$ Kronecker delta function.

Since $\mathbf{P}$ is a Vandermonde matrix and $b_l + b_q \neq b_v + b_m$ $\forall l, q, v, m$. it has full rank $\hat{L} = L(L+1)/2$ ($\leq K$). Matrix $\boldsymbol{\Phi}$ will have full rank $\hat{L}$ if all A_i, $i = 1, 2, \ldots, \hat{L}$ are nonzero; i.e., $A(m,v) \neq 0$ $\forall m, v \in 1, L$. Hence $\mathbf{R}_x$ has rank $\hat{L}$. Since vector $\mathbf{a}$ in (4.1) belongs to the null space of $\mathbf{R}_x$ $(K > \hat{L})$, then [1, 2]

$$a_K + a_{K-1} e^{b_m^* + b_v^*} + \ldots + a_0 e^{K(b_m^* + b_v^*)} = 0 \quad 1 < m, v < L. \qquad (7)$$

This means that $\hat{L} = 1/2 \cdot L(L+1)$ zeros of the Kth order polynomial $A(z)$ are located at $e^{(b_m^* + b_v^*)}$, $1 < m, v < L$, which are outside the unit circle. **Q.E.D.**

We now examine the conditions that the signal $x(n)$ in (1) should satisfy, so that $A(m,v)$ in (4.4) or (5.3) are nonzero for all $m, v \in 1, L$. The conditions are based on a theorem of complex polynomials that can be found in Marden [14, pp. 30-31].

Lemma 2: If the complex numbers h_l of $X(z)$ in (5.2) are such that

$$\mu < \arg h_l = \theta_m < \mu + \gamma < \mu + \pi \qquad l = 1, 2, \ldots, L \qquad (8)$$

and $\mathbf{C}$ is a circle of radius r which encloses all the poles e^{b_l}, $l = 1, 2, \ldots, L$ of $X(z)$, then $X(z) \neq 0$ at any point outside a circle of radius $\mathbf{R} = r \cdot \csc(\phi/2)$, where $\phi = \pi - \gamma$. The condition is only sufficient and its proof is given in [14]. The parameter γ corresponds to the spread of the initial phases of the complex damped sinusoids. If we apply Lemma 2 on $A(m,v)$ in (5.3), we see that the complex numbers $e^{(b_m^* + b_v^*)}$, $\forall m, v \in 1, L$ should be outside a circle of radius $\mathbf{R} = e^{c_i} \cdot \csc(\phi/2)$, where $c_i = \min\{c_1, c_2, \ldots, c_L\}$; i.e.,

$$\epsilon \cdots \csc \frac{(\pi \cdots \gamma)}{2} \cdots \epsilon^{2c_i} \tag{9.1}$$

or

$$\theta \cdots \gamma \cdots \pi \cdots 2 \cdot \sin^{-1}(\epsilon^{-3c_i}). \tag{9.2}$$

Hence, if (9.1) is satisfied then $A(m,r) \neq 0 \; \forall m, r \in 1..L$. We see that sufficient condition (9.2) depends upon the minimum value c_i of the damping coefficients $(c_i > 0)$ and the *spread* of initial phases γ. For example if $\theta_m \cdots \theta \; \forall m$. Then $\gamma \cdots 0$ and thus $A(m,r) \neq 0 \; \forall m, r \in 1..L$.

Lemma 3: If the signal $x(n)$ in (1) corresponds to the impulse response of a linear time-invariant autoregressive (AR) model described by

$$x(n) \cdots \sum_{i=1}^{L} a_i x(n \cdots i) \cdots \delta(n) \tag{10}$$

then $X(z) \neq 0$ for $0 < |z| < \infty$. Consequently, $A(m,r) \neq 0 \; \forall m, r \in 1..L$. The proof of this lemma is straightforward.

Instead of using in (4.1) the matrix $\mathbf{R}_x$ defined by (4.3), we use

$$\mathbf{R}_x \cdots \begin{pmatrix} R_x^*(0,0) & \cdots & R_x^*(-K, -K) \\ R_x^*(-1, -1) & \cdots & R_x^*(-K-1, -K-1) \\ \vdots & \ddots & \vdots \\ R_x^*(-K, -K) & \cdots & R_x^*(-2K, -2K) \end{pmatrix} \tag{11.1}$$

and define

$$A(l) \cdots \sum_{m=1}^{L} \cdots \sum_{r=1}^{L} h_l^* h_m h_r \cdot 1/(1 \cdots \epsilon^{(b_i^* + b_m + b_r)}) \quad l \in 1..L \tag{11.2}$$

Lemma 4: Assuming that we know the true third-order moments of the signal $x(n)$ in (1) and if $A(l) \neq 0 \; \forall l$. then for every vector $\mathbf{a}$ such that (4.1) and (11.1) hold and $K > L$, the polynomial $A(z) \cdots \sum_{i=0}^{K} a_{K-i} z^{-i}$ has $L - L$ roots at $\epsilon^{b_i^*}$, $l \cdots 1,2,\ldots,L$.

Proof: Substituting (1) into (3.2) for $l \cdots 0, 1, \ldots, -K$ and $\tau \cdots 0, 1, \ldots, K$. we obtain for each element of $\mathbf{R}_x$ in (11.1)

$$R_x^*(-\tau, -\tau) \cdots \sum_{n=-\tau}^{\infty} \cdots \sum_{l,m,r=1}^{L} h_l^* \epsilon^{b_i^* n} \cdot h_m \epsilon^{b_m(n-\tau)} \cdot h_r \epsilon^{b_r(n-\tau)}$$

$$\cdots \sum_{l=1}^{L} A(l) \epsilon^{b_i^* \tau} \tag{12.1}$$

where $A(l)$ is given by (11.2). If we define

$$Y(z) \cdots \sum_{m=1}^{L} \cdots \sum_{r=1}^{L} h_m h_r (z \cdots \epsilon^{b_m + b_r}). \tag{12.2}$$

then (11.2) becomes

$$A(l) \cdots h_l^* \cdot z \cdot Y(z) \quad \text{for} \quad z \cdots \epsilon^{b_i^*}. \tag{12.3}$$

The matrix $\mathbf{R}_x$ in (11.1) can be decomposed as (6.1)-(6.3) with the only difference now that

$$\Lambda_l \cdots A(l) \quad \text{and}$$
$$W_l \cdots \epsilon^{b_i^*}. \quad \text{for} \quad l \cdots 1,2,\ldots,L. \tag{12.4}$$

Thus, $\mathbf{P}$ has full rank $L \cdots L(\cdots K)$ and $\mathbf{\Phi}$ will be full rank L if $A_l \neq 0 \; \forall l$. Hence, the matrix $\mathbf{R}_x$ in (11.1) has rank L and the Kth order polynomial $A(z)$ will have L roots at locations $\epsilon^{-b_i^*}$, $l \cdots 1,2,\ldots,L$ which are outside the unit circle.   Q.E.D

If we apply Lemma 2 in (12.2) and (12.3) we obtain the following sufficient condition for $A(l) \neq 0 \; \forall l$

$$0 < \gamma' < \pi \cdots 2 \cdot \sin^{-1} \epsilon^{-3c_i} \tag{13.1}$$

where γ' is such that

$$\mu' < \arg h_m h_r \cdots \mu' \cdots \gamma' < \mu' \cdots \tau \tag{13.2}$$

i.e. γ' corresponds to the spread of initial phases $(\theta_m \cdots \theta_r)$ for $r \cdots 1,2,\ldots,L$ and $m \cdots 1,2,\ldots,r$

The Extraneous Zeros We deal here with the location of the remaining $K \cdots L$ zeros of the Kth order polynomial $A(z)$. Recall that $L \cdots 1/2 \cdot L(L-1)$ or $L \cdots L$. Also, we assume that the true third-order moments of the signal $x(n)$ are available.

Lemma 5 [1],[2]: The extraneous $K \cdots L$ zeros of $A(z)$ lie inside the unit circle if the following conditions are satisfied: (1) $\mathbf{a}$ is the minimum norm solution of the linear system of equations (4.1), (4.3) or (4.1),(11.1) and (2) $K > L$.

Equation (4.1) with the entries of $\mathbf{R}_x$ given by $R_x(\tau, \tau)$ or $R_x(-\tau, -\tau)$, $\tau \geq 0$ suggests that $\mathbf{a}$ is an eigenvector of the third-order moment matrix, corresponding to zero eigenvalue. However, this choice does not provide us with any means of identifying the signal zeros from the rest of the roots of the polynomial $A(z)$. We use instead the minimum norm solution (the proof of Lemma 5 can be found in [1],[2]) by choosing $\mathbf{a}$ such that:

1.) $a_K \cdots 1$. and

2.) $a_{K-1}^2 \cdots a_{K-2}^2 \cdots \ldots \cdots a_0^2$ is minimum

The extension of this analysis to the fourth-order cumulant domain is discussed in [15].

III. FINITE LENGTH AND NOISY DATA

Consider the signal $x(n)$ being observed in additive noise, so that

$$y(n) \cdots x(n) \cdots w(n), \quad n \cdots 0,1,\ldots,N-1 \tag{14}$$

where the noise $\{w(n)\}$ is assumed *zero-mean*, colored or white complex Gaussian process, with real and imaginary parts independent and identically distributed, independent of the signal. For the above noisy output $y(n)$ it is true that

$$R_y(\tau, \tau) \cdots R_x(\tau, \tau) \cdots R_w(\tau, \tau) \cdots r_{w \cdot w}(0) \cdot x$$
$$\cdots 2 r_w(\tau) \cdot x^* \cdots r_{x \cdot x}(0) \cdot w \cdots 2 r_x(\tau) \cdot w^* \tag{15.1}$$

where

$$R_x(\tau, \tau) \cdots \sum_n x(n) \cdot x^*(n \cdots \tau) \cdot x^*(n \cdots \tau) \tag{15.2}$$

is the third moment sequence of the signal.

$$r_x(\tau) = \sum_n x(n) \cdot x^*(n - \tau) \tag{15.3}$$

$$r_{x \cdot x}(0) = \sum_n x^*(n + \tau) \cdot x^*(n - \tau) \tag{15.4}$$

are the autocorrelation sequences of the signal, and

$$R_w(\tau, \tau) = E\{w(n) \cdot w^*(n + \tau) \cdot w^*(n + \tau)\} \tag{15.5}$$

$$r_w(\tau) = E\{w(n) \cdot w^*(n + \tau)\} \tag{15.6}$$

$$r_{w \cdot w}(0) = E\{w^*(n + \tau) \cdot w^*(n + \tau)\} \tag{15.7}$$

are respectively the third moment sequence and autocorrelation sequences of the noise $\{w(n)\}$. x, x^*, w, w^* are mean values of the signal and noise respectively.

Since $\{w(n)\}$ is Gaussian, $R_w(\tau, \tau) = 0$. Also since $y = x + w$ it follows that $y = x$. Thus, if we subtract the mean from the observation signal $y(n)$, the autocorrelation of the noise looses its impact on $R_y(\tau, \tau)$. Since the noise itself is zero mean, the autocorrelation of the signal does not contribute to the moments $R_y(\tau, \tau)$. Therefore under these assumptions

$$R_y(\tau, \tau) = R_x(\tau, \tau) \tag{16}$$

If we substitute (16) to the linear system of equations given by (4.1), we obtain

$$\mathbf{R}_y \, \mathbf{a} = 0 \tag{17}$$

where $\mathbf{R}_y$ is the Hankel matrix of (4.3).

Because of the statistical variance of the third order moments when only noisy data are available we use the singular value decomposition method (SVD) to solve (4.1). The algorithm proceeds as follows. Let $\{y(0), \ldots, y(N-1)\}$ be the given data set. Then we have the following:

1) Subtract the average value.
2) Estimate the third order moments.
3) Substitute $R_y^*(-\tau, \tau)$ in (4.1) to form the $(K + 1) \times (K + 1)$ matrix $\mathbf{R}_y$, and use a criterion to decide on the rank of the matrix.
4) Using the rank estimated from step 3, compute the least squares solution of (17).

IV. SIMULATION EXAMPLES

We demonstrate here the performance of higher order statistics for transient signal estimation via Monte Carlo simulations utilizing third order moments (TOM) and fourth order cumulants (FOC). For comparison purposes, we also show the performance of the Kumaresan Tufts (KT) method with the same examples. In the sequel, N is the number of data samples, K the order of the filter, c_i and w_i the damping factors and frequencies of the transient signals, respectively, and σ_w^2 the variance of the complex Gaussian noise (white or colored). The signal to noise ratio (SNR) is defined as $SNR = 10 \log_{10}(1/\sigma_w^2)$.

A. Additive White Gaussian Noise

The experiment is described by the following equation

$$y(n) = z^{b_1 \cdot n + j^{p_1}} + z^{b_2 \cdot n + j^{p_2}} + w(n) \tag{18}$$

where $b_1 = 0.2 - j2\pi(0.42)$, $b_2 = 0.1 - j2\pi(0.52)$, σ_w^2

$2\sigma^2$ and $\theta_1 = 0$, $\theta_2 = 0$. The noise is i.i.d complex Gaussian process and the variance of the real and imaginary parts of the process is σ^2. The noise process is generated by the GGNML subroutine of the IMSL library. Fig.1 shows the estimated signal zeros obtained with forty independent noise runs. In each run the transient signal was kept the same. Statistically independent noise realizations were added using different seeds. The filter length was chosen to be $K = 9$. From Fig.1 (a) and (b), it appears that the higher order statistics based method has comparative performance with the KT algorithm. Furthermore, the (TOM) version appears to perform worse than the (FOC) version of the higher order statistics based method.

We have also performed a statistical test over 500 independent runs for the computation of the bias and standard deviation of the estimated damping factors (c_i) and frequencies (w_i). Fig.2(a) – (d) shows the sample standard deviation of the estimated frequencies (0.52, 0.42) and damping factors (0.2, 0.1), respectively, as functions of the SNR ($K = 18$, $N = 25$ for KT and $K = 9$, $N = 64$ for TOM and FOC). Threshold points occurred when either the bias was too large (estimated mean var $> 70\%$ of the true value) or a break was observed in the standard deviation of the estimates. The frequencies and damping factors were estimated from the poles outside the unit circle in the Z plane.

B. Additive Colored Gaussian Noise

We consider additive colored noise that is generated by passing a complex white Gaussian process through an FIR filter with impulse response coefficients

$$.5, .6, .7, .8, .7, .6, .5, .0, .0, .5, .6, .7, .8, .7, .6, .5$$

In this signal plus noise example we use the same transient signal as that described by (18). The Monte Carlo results of this experiment are illustrated in Figures (3) – (4).

VI. COMPLEX DAMPED SINUSOIDS WITH RANDOM PHASE

Exactly Known Higher-Order Statistics Transient signals described by equation (1) can be either deterministic or stochastic. We assume in this section that $\{\theta_m\}$ are random variables independent and uniformly distributed over $[-\pi, \pi]$. The linear system of equations which has to be solved in this case becomes

$$\sum_{i=0}^{h} a_{K+i} \cdot R_x^*(l - i, l - i, l - i) = 0$$

$$K + \frac{1}{2} \cdot L(L+1) \qquad l = 0 \tag{19.1}$$

where

$$R_x^*(\tau, \tau, \tau) = E\{\sum_n x(n) \cdot x(n + \tau) \cdot (x^*(n + \tau))^2\} \quad \tau = 0 \tag{19.2}$$

Notice that the third order moments, $E\{x(n)(x(n + \tau))^2\}$, are identically zero except for the case where the signal in (1) contains quadratic phase coupled components, i.e., $\theta_m = (\theta_l + \theta_i)$. From (19.2), it is apparent that the summation over the time index n is included here because the transient signal is nonstationary. In this case the closed form expression for the fourth order moments becomes

$$R_x^*(\tau, \tau, \tau) = \sum_{j=1}^{l} A(j) e^{b_j \tau} \tag{20}$$

where

$$A(j) \quad d_j^2 \left(d_j^2 (1 \quad e^{-4c_j})\right) \cdot 2 \sum_{\substack{k=1 \\ j \neq k}}^{L} \left(d_k^2 (1 \quad e^{-2(c_j+c_k)})\right) \quad (20.1)$$

Notice that in this case $A(j) \neq 0 \; \forall j \neq 1, L$ and Lemma 4 can be applied unconditionally.

Finite Length and Noisy Data The treatment of this case is exactly the same as for the deterministic transients with the only difference that the fourth-order moment sequence is defined now by (19.2). The fourth-order cumulant sequence along the diagonal line $\tau > 0$ for zero mean signal and noise is given by [15]

$$Cum_y^4(-\tau, \tau, \tau) \quad 2R_x^2(\tau, \tau, \tau) \quad (21)$$

where $R_x^2(\tau, \tau, \tau)$ is given by (19.2)

REFERENCES

1 R. Kumaresan and D.W. Tufts. "Estimating the parameters of exponentially damped sinusoids and pole-zero modeling in noise", *IEEE Trans. Acoust. Speech, Signal Processing*. Vol. ASSP-30. pp. 833-840, December 1982.

2 R. Kumaresan, "On the zeros of the linear prediction-error filter for deterministic signals", *IEEE Trans. Ac Speech, Signal Processing*. Vol. ASSP-31. pp. 217-220. February 1983.

3 T.L Henderson. "Geometric methods for determining system poles from transient response", *IEEE Trans. Acoust. Speech, Signal Processing*, Vol. ASSP-29, pp. 982-988. October 1981.

4 S.L.Marple.Jr.. *Digital Spectral Analysis with Applications*. Englewood Cliffs, NJ: Prentice Hall 1987.

5 J. Makhoul, "Linear Prediction: A Tutorial Review", *Proc. IEEE*. Vol. 63. pp. 561-580. April 1975.

6 E.H Satorius and J. R. Zeidler. "Maximum entropy spectral analysis of multiple sinusoids in noise", *Geophysics*. Vol. 43. pp. 1111-1118. October 1978.

7 A. H Nehorai and M. Morf, "Enhancement of sinusoids in colored noise and the whitening performance of exact least squares predictors", *IEEE Trans. Acoust. Speech, Signal Processing*. Vol. ASSP-30. pp.353-362, June 1982.

8 M.Rosenblatt. "Cumulants and Cumulant Spectra." D. Brillinger and P. Krishnaiah (Eds.). in *Time Series in the Frequency Domain* pp. 369-382. Amsterdam, The Netherlands: North-Holland. 1983.

9 M.J. Hinich, " Testing for Gaussianity and linearity of a stationary time series". *Journal of Time Series Analysis* 3. pp. 169-176. 1982.

10 C.L. Nikias and M.R. Raghuveer, "Bispectrum estimation: A digital signal processing framework." *Proc. IEEE*. Vol. 75. pp. 869-891. July 1987.

11 M.R. Raghuveer and C.L. Nikias. "Bispectrum estimation: A parametric approach". *IEEE Trans. Acoust. Speech, Signal Processing*. Vol. ASSP-33. pp. 1213-1230. October 1985.

12 A. Swami and J.M Mendel. "Cumulant based approach to the harmonic retrieval problem". in *Proc. ICASSP'88*. New York. April 1988. pp. 2264-2267.

13 C.K. Papadopoulos and C.L Nikias. "Bispectrum estimation of transient signals", in *Proc. ICASSP'88*. New York, April 1988, pp. 2404-2407.

14 M. Marden, *Geometry of polynomials*. Providence, Rhode Island: American Mathematical Society. 1966.

15 C.K. Papadopoulos and C.L. Nikias. "Parameter estimation of exponentially damped sinusoids using higher order-statistics", *IEEE Trans. Acoust. Speech, Signal Processing* in review 1989.
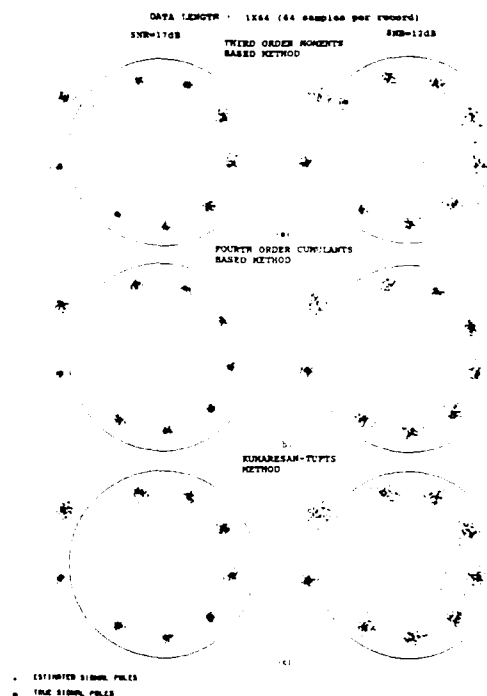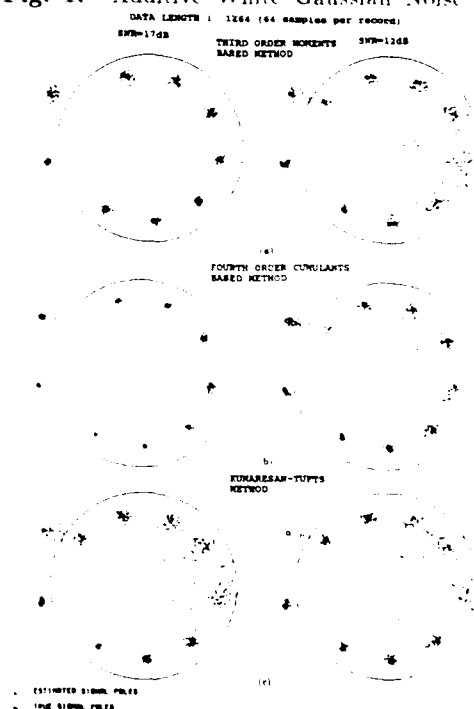
Fig. 1. Additive White Gaussian Noise

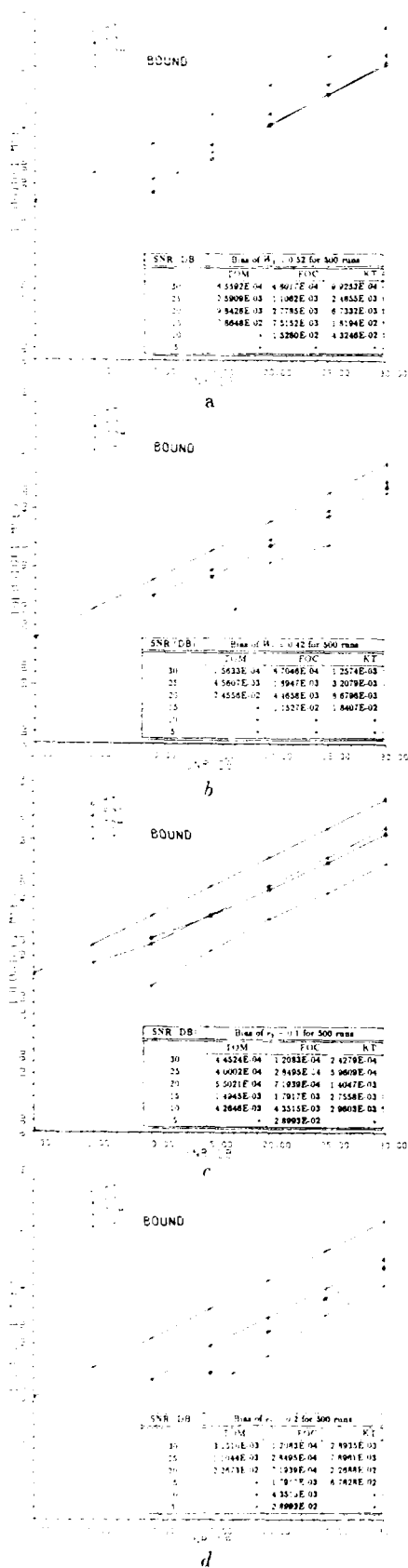**Fig. 3.** Additive Colored Gaussian Noise

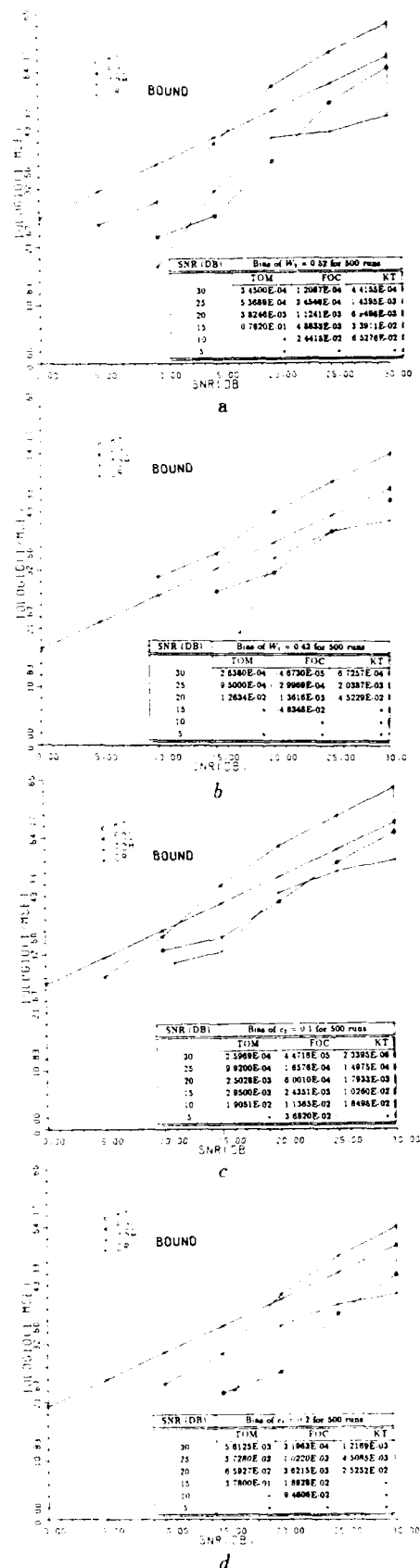**Fig. 2.** Additive White Gaussian Noise

Fig. 4. Additive Colored Gaussian Noise

DETECTION OF A NON-GAUSSIAN SIGNAL IN GAUSSIAN NOISE

USING HIGH-ORDER SPECTRAL ANALYSIS

by

DORON KLETTER and HAGIT MESSER

Faculty of Engineering, Department of Electronic Systems,

Tel-Aviv University, Tel-Aviv, Israel 69978

ABSTRACT

The most general solution to the classical problem of detecting a random signal in additive noise is known to be achieved by performing a likelihood ratio test (LRT) on the received data. When the signal and noise processes are both (stationary) Gaussian, the LRT processor is the simple, well-known, power spectrum based detector. With a non-Gaussian signal, however, the LRT processor becomes extremely complex and therefore is rarely considered to be a practical solution.

In this paper we propose the use of higher-order spectra (HOS) for improving (relative to the power spectrum detector) the detection performance in the general non-Gaussian case. The idea is to also detect the high order spectral content of the received signal (HOS domain detection). Under the assumption that the additive noise is Gaussian, the presence of such high HOS content would clearly indicate that a signal is present. The resulting processor consists of the HOS domain detector in parallel with the conventional power spectrum detector. The final decision whether the signal is present or not is based on all detectors outputs.

The new method is demonstrated using the third-order spectra (called bispectrum), although it can be extended to higher order analysis (e.g.- trispectrum, etc.). The performance of the above processor is analyzed, and it is shown that it always performs at least as well as the conventional power spectrum detector. Under certain conditions on the signal, it can also have a significantly better performance. The resulting performance improvement is most impressive in detecting non-Gaussian weak signals in a heavy noise environment. Such improvement is analytically demonstrated for a spectrally and bispectrally flat bandlimited signal.

I. INTRODUCTION AND PROBLEM FORMULATION

Let $\{x(t_i)\}$, $i=0,1,...,N-1$ be a sequence of N consecutive measurements from the (real valued) received process. Consider the following binary hypothesis problem, in which the signal $s(t)$ may, or may not, be present :

$$\begin{cases} H_1 : x(t_i) = s(t_i) + n(t_i) \\ H_0 : x(t_i) = n(t_i) \end{cases} \qquad i = 0,1,...,N-1 \qquad (1)$$

The noise process $n(t)$ is assumed to be a zero mean stationary Gaussian process, with spectral density function $S_N(\omega)$. The signal process is assumed to be of zero mean, band limited, and at least sixth-order weakly stationary, with spectral density function $S_S(\omega)$, and bispectrum $B_S(\omega_1,\omega_2)$. The bispectrum of a process $x(t)$ is defined as the (2-D) Fourier transform of the third order cumulant function $C_x(t_1,t_2)$:

$$B_x(\omega_1,\omega_2) = F\{ C_x(t_1,t_2) \} = F\{ E[x(t)x(t-t_1)x(t-t_2)] \} \quad (2)$$

The signal and noise processes are assumed to be statistically independent, with the result that in the power spectrum domain we have :

$$\begin{cases} H_1 : S_X(\omega) = S_S(\omega) + S_N(\omega) \\ H_0 : S_X(\omega) = S_N(\omega) \end{cases} \qquad (3)$$

where $S_X(\omega)$ is the spectral density function of the received signal. Examining eq. (3), it is clear that for low SNR (i.e. $S_S(\omega) \ll S_N(\omega)$) the received spectrum in nearly the same under both hypotheses. Hence, energy detection at low SNR's becomes extremely difficult for finite observation times. In the bispectrum domain, on the other hand, the Gaussianity of the noise immediately implies that $B_N(\omega_1,\omega_2) \equiv 0$ for every (ω_1,ω_2) pair, or :

$$\begin{cases} H_1 : B_X(\omega_1,\omega_2) = B_S(\omega_1,\omega_2) \\ H_0 : B_X(\omega_1,\omega_2) \equiv 0 \qquad \forall \omega_1,\omega_2 \end{cases} \qquad (4)$$

where $B_X(\omega_1,\omega_2)$ and $B_S(\omega_1,\omega_2)$ are the bispectral density functions of $x(t)$ and $s(t)$ respectively. Comparing (4) with (3), it is clear that the bispectrum domain detection might perform much better than the energy detection (especially in the interesting case of low SNR), provided that the signal contains a significant amount of (third-order) non-Gaussian information.

In reality, however, all the above spectral/bispectral density functions are generally unknown, and therefore must first be estimated from the data. The estimation errors, which always exist for finite SNR's and observation times, are greatly influenced by the amount of noise present.

II. DETECTOR STRUCTURE

The proposed detector is shown in figure 1. It consists of two parallel channels; The upper channel is the conventional power spectrum (energy based) detector, and the lower channel is the (third-order) HOS domain detector. In both cases the appropriate spectral density function (i.e. power spectrum or bispectrum) is first estimated from the data using conventional (high-order) spectral estimation techniques. The estimated spectrum is then used in an optimal generalized likelihood ratio test (GLRT), to independently detect the signal presence in the corresponding domain. Both channels outputs are then fed into a decision block, in which the final decision (weather the signal is present or not) is taken. The decision block logic is summarized in table 1. Usually the null hypothesis (i.e. signal absent) is accepted only when both channels agree that no signal is present, and it is sufficient that a signal is detected by one of the channels to eventually reject H_0. Table 1 also includes the meaning of each one of th' four possible cases. This additional information can be used for identifying the signal type. For example, if detection is only aimed at non-zero bispectrum signals (e.g. in an active system), then other

(disturbing) Gaussian sources can be prevented from causing unnecessary false-alarms. This is achieved by simply changing the final decision block logic as indicated by the note appearing for case 2 in the table.

The power spectrum detector is optimal for detecting Gaussian signals, and therefore it is commonly used and its behavior is well studyied by now, [e.g. 10]. The HOS domain detector is relatively new, and therefore must be further described. It is used, in conjunction with the power spectrum detector, for detecting non-Gaussian signals with non-zero bispectrum.

III. OPTIMAL DETECTION IN THE BISPECTRUM DOMAIN

The problem of estimating the bispectrum of a random process was already considered in great detail by many authors [e.g. 1-5,8,11]. An asymptotically (i.e. for large N) unbiased and consistent estimator of the bispectrum can be constructed using the direct method, [3]:

$$\hat{B}_x(\omega_m,\omega_n) = \frac{1}{NKL^2} \sum_{k=1}^{KL^2} X_k(\omega_m) X_k(\omega_n) X^*_k(\omega_m+\omega_n) \quad (5)$$

where K is the number of disjointed segments (records) to which the data is divided, and L^2 is the number of adjacent (2-D) frequency-pairs in which a uniform smoothing is done (assuming that the bispectrum is effectively constant in the averaged region). $X_k(\omega_m)$ is the DFT coefficient of the received signal in the k-th segment, and at frequency $\omega_m=2\pi m/N$, m=0,1,...,N-1. It is also desirable to set X(0)=0, [1]. The averaging operation does indeed reduce the variance, but it may also introduce bias, and therefore care should be taken when choosing the the proper values of K and L, [12]. For large N, the complex random variable $\hat{B}_x(\omega_m,\omega_n)$ is approximately complex Gaussian, with mean $B_x(\omega_m,\omega_n)$ and variance:

$$Var\left\{ Re\left[\hat{B}_x(\omega_m,\omega_n) \right] \right\} \simeq Var\left\{ Im\left[\hat{B}_x(\omega_m,\omega_n) \right] \right\} \simeq$$

$$\simeq \frac{N}{KL^2} S_x(\omega_m) S_x(\omega_n) S_x(\omega_m+\omega_n) \quad (6)$$

and the asymptotic covariance between the real and imaginary parts approaches zero, as is the covariance between the different frequencies, [5,chap.4 ; 2].

Suppose that there is a total of P bispectrum frequency-pairs inside the bispectrum principal domain. For equally spaced frequency points in the bispectrum domain, there are approximately $P = N^2/12L^2$ pair-points inside the principal domain, [13]. Each point is estimated using KL^2 observations. Collecting all the bispectrum estimates into a single vector, and changing indexing (m,n)→p :

$$\hat{B} = \left[\hat{B}_1 , ..., \hat{B}_P\right]^t \quad \text{where} \quad \hat{B}_p = \hat{B}_x(\omega_m,\omega_n) \quad (7)$$

Then, following the previous section, the vector $\hat{B}$ is complex-normal, with mean μ (the true bispectrum), and covariance matrix Σ (assumed Hermitian positive definite matrix).

It is obvious that if the null hypothesis is true (i.e. no signal) then $\mu \equiv 0$ for any frequency-pair. Under the alternative (H_1), on the other hand, we have assumed that there are some frequency-pairs (ω_m,ω_n) for which $\mu \neq 0$. Therefore the bispectrum domain detection is equivalent to a binary hypothesis testing problem, which

tests $H_0 : \mu \equiv 0$ against the alternative $H_1 : \mu^* \Sigma^{-1} \mu > 0$. The Generalized Maximum Likelihood (GML) ratio test for the above problem was analyzed in [6]. The test rejects the null hypothesis if:

$$T_c^2 \overset{\Delta}{=} \hat{\mu}^* \hat{\Sigma}^{-1} \hat{\mu} > T_0^2 \quad (8)$$

where T_c^2 is the extension of the Hotteling T^2 statistics to the complex case ,[7], and

$$\hat{\mu} \overset{\Delta}{=} \frac{1}{KL^2} \sum_{n=1}^{KL^2} \hat{B}_n \quad (9)$$

$$\hat{\Sigma} \overset{\Delta}{=} \frac{1}{KL^2} \sum_{n=1}^{KL^2} \left(\hat{B}_n - \hat{\mu}\right)\left(\hat{B}_n - \hat{\mu}\right)^* \quad (10)$$

are the ML estimates of the mean and covariance matrix, respectively. T_0 is the threshold with its value set according to the desired false alarm probability (significance level). Since the matrix Σ tends to be asymptotically diagonal, eq. (9) can be further simplified, although at the expense of a larger number of measurments, [15], to :

$$T_c^2 = \sum_{p=1}^{P} \frac{|\hat{\mu}_p|^2}{\hat{\sigma}_p^2} \underset{H_0}{\overset{H_1}{\underset{<}{>}}} T_0^2 \quad (11)$$

with $\hat{\mu}_p$ being the single element in $\hat{\mu}$, and $\hat{\sigma}_p^2$ being its corresponding diagonal element in $\hat{\Sigma}$.

IV. DETECTOR PERFORMANCE

The detection performance depends on the type of decision criterion selected. For the two criteria of most interest, the Bayes and the Neyman-Pearson, the optimum test is the likelihood ratio test. It can be shown that the proposed detector performs at least as well as the conventional power spectrum detector, which is optimal for detecting Gaussian signals, [15]. For non-Gaussian signals, a considerable performance improvement is possible, provided that the signal contains a sufficient amount of (third-order) HOS content to overcome the bispectrum estimation errors caused by the noise. The proposed detector is therefore modular, since it can always be used for any signal type (i.e. Gaussian or not). Each one of the two channels is asymptotically optimal in its domain, and it can also be shown that it is uniformly most powerful in a certain sense, [15].

The performance improvement is achieved by using the HOS domain. Under the simplified conditions of eq. (11), the detection probability in the bispectrum domain is found to be approximately:

$$P_D \simeq erf\left(\frac{T_0^2 - 2P-\lambda}{2\sqrt{P+\lambda}} \right) \quad (12)$$

where $erf(x) \overset{\Delta}{=} \int_x^\infty \frac{1}{\sqrt{2\pi}} e^{-x^2/2} dx$ is the error function, T_0^2 is the threshold (set by the desired false-alarm probability), and
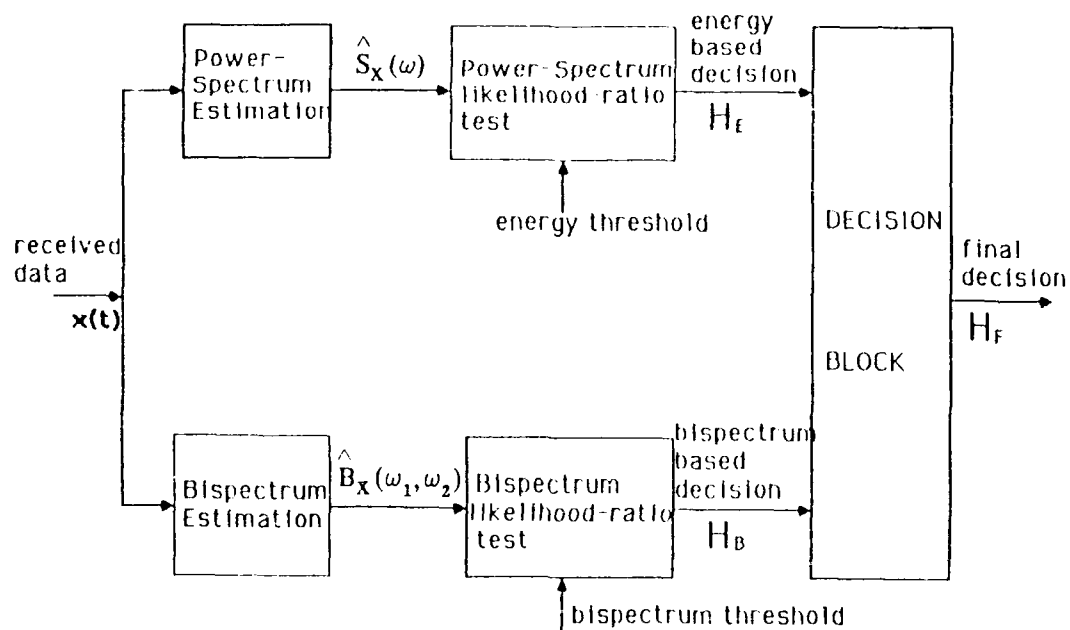
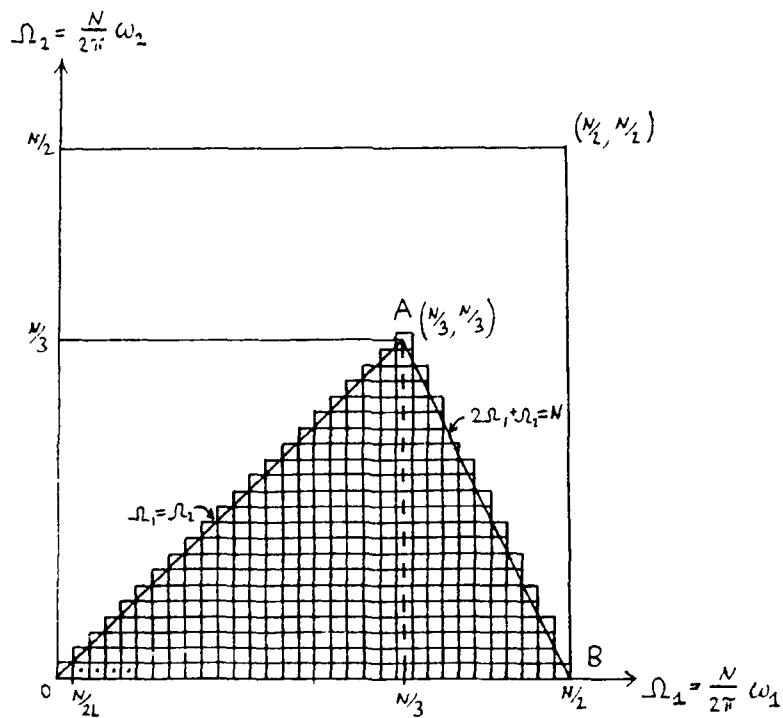**Figura 1:** Signal detection using combined spectral/bispectral analysis.

Figure 2: The bispectrum principal domain.

Table 1 : Decision block logic.

case	signal present in spectral detector	signal present in bispectral detector	meaning	final decision
1	false	false	both channels see no signal	signal absent
2	true	false	no bispectral content, decision is energy based	signal present *
3	false	true	low signal energy (low SNR) but high bispectral content	signal present
4	true	true	both channels agree - signal is present	signal present

*Unless detection is aimed at non-zero bispectrum signal only.
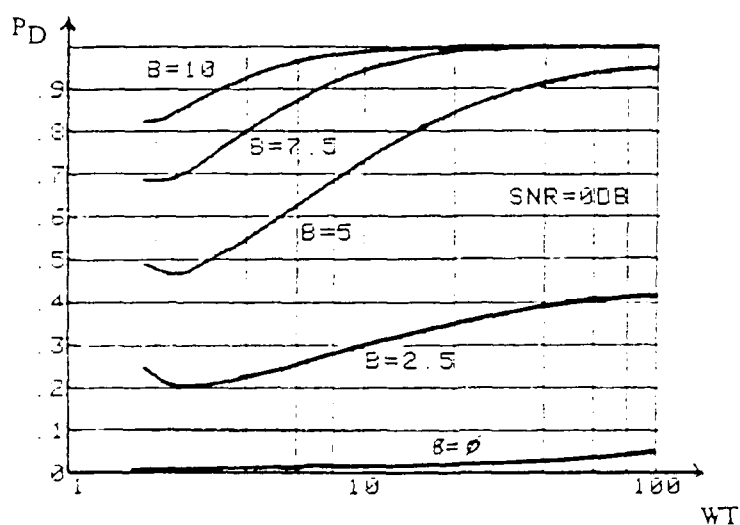If so - decide signal absent.

Figure 3: Detection probability vs. observation time (in samples), as a function of B.

$$\lambda \overset{\Delta}{=} \frac{2|B_x(\omega_m,\omega_n)|^2}{\frac{N}{KL^2}S_x(\omega_m)S_x(\omega_n)S_x(\omega_m+\omega_n)} \quad (13)$$

Therefore, in order to achieve high detection probability, it is required that

$$K_D \overset{\Delta}{=} \frac{2P + \lambda - T_0^2}{2\sqrt{P+\lambda}} \gg 1 \quad (14)$$

Note that the detection probability is a monotonically increasing function of the expression:

$$\rho \overset{\Delta}{=} \frac{2P+\lambda}{2\sqrt{P+\lambda}} \quad (15)$$

which can be considered as an equivalent SNR. The detection probability is therefore a function of the summation over all the true bicoherence magnitude-squared frequency pairs inside the bispectrum principal domain. The bicoherence function, or skewness function, is defined in [11] to be :

$$\beta_x(\omega_m,\omega_n) \overset{\Delta}{=} \frac{B_x(\omega_m,\omega_n)}{\left[\frac{N}{KL^2}S_x(\omega_m)S_x(\omega_n)S_x(\omega_m+\omega_n)\right]^{1/2}} \quad (16)$$

Note In the Neyman-Person test the value of the threshold is determined by the false-alarm probability, and it is given by [15]:

$$T_0 = \frac{1}{\sqrt{2}}\,\mathrm{erf}^{-1}(\,P_F\,) + \sqrt{2P-1/2} \quad (17)$$

V. A SPECTRALLY BISPECTRALLY 'WHITE' SIGNAL

Suppose that the signal sequence consists of independently, identically distributed random variables, with zero mean and:

$$\begin{cases} E\{S(t_i)S(t_i+\tau)\} = S_0\cdot\delta(\tau) \\ E\{S(t_i)S(t_i+\tau)S(t_i+\rho)\} = b_s\cdot\delta(\tau)\cdot\delta(\rho) \end{cases} \quad (18)$$

The noise process is zero mean white Gaussian, with spectral density $S_N(\omega)=N_0$, and bandlimited up to a frequency W (i.e. $\sigma_N^2=2WN_0$). For this example we find that the bispectrum domain test (eq.(11)) is given by :

$$T_c^2 = 2\sum_{\omega_m,\omega_n} |\,\hat\beta_x(\omega_m,\omega_n)\,|^2 \quad (19)$$

where $\hat\beta_x(\omega_m,\omega_n)$ is the estimated bicoherence function, obtained by replacing the true spectrum/bispectrum in (16) with their estimates. The condition $K_D \gg 1$ which assures high detection probability is found to be equivalent to, [15] :

$$|b_s| > \frac{12}{\sqrt{NK}}(S_0+N_0)^{3/2} \quad (20)$$

where NK is just the total number of available measurements in all the records. From (20) we conclude that the bispectrum detection technique can be used whenever there is enough bispectral content in the signal to overcome the bispectrum estimation errors caused by the energy variance.

In figure 3 we have plotted detection probability versus the time-bandwidth product, for different values of bispectral level. The SNR was held constant at 0 db. The lowest curve, marked B=0, is computed using the familiar Gaussian bound [10, vol III, p.110-111], and the three other curves indicate the bispectrum detection performance for increasing signal bispectral level. The improvement is clearly noticeable.

VII. CONCLUSIONS

The suggested method of detection is simple to implement, and requires no further assumptions on the underlying model driving the signal. It is especially useful for detecting non-Gaussian weak signals in a heavy noise environment. Although generally sub-optimal, the suggested method may yield significant performance improvement over the commonly used, energy based, detection method. The proposed method is not exhaustive, though, since many non-Gaussian signals may have a zero bispectrum (e.g., all symmetrically distributed signals). Nevertheless, there are many practical cases for which this detection scheme seems to be quite attractive.

REFERENCES

[1] Brillinger, D.R. (1965) "An Introduction to Polyspectra", Ann. Math. Statist. Vol. 36, p. 1351-1374.

[2] Brillinger, D.R. and Rosenblatt, M. (1967) "Asymptotic Theory of Estimates of k-th Order Spectra". In Spectral Analysis of Time Series, B. Harris ed. Wiley. p. 135-188.

[3] Van Ness, J.W. (1966) "Asymptotic Normality of Bispectral Estimates", Ann. Math. Statist., Vol. 37, p. 1257-1275.

[4] Rosenblatt, M. and Van Ness, J.W. (1965) "Estimation of the Bispectrum", Ann. Math. Statist., Vol. 36, p. 1120-1136.

[5] Brillinger, D.R. (1981) "Time Series, Data Analysis and Theory", Halt, Rinehart and Winston. Expanded ed.

[6] Giri, N. (1965) "On the Complex Analogues of T^2 and R Tests", Ann. Math. statist. 36, p. 664-670.

[7] Anderson, T.W. (1958) "An Introduction to Multivariate Statistical Analysis", Wiley.

[8] Lii, K.S. and Helland, K.N. (1981) "Cross-Bispectrum Computation and Variance Estimation" ACM Trans. on Math. Soft. ,Vol. 7, No. 3, Sept. 1981. p. 284-294.

[9] Kendall, M.G. and Stuart, A. (1958) "The Advanced Theory of Statistics", Vol. I, 3rd ed., Hafner NY.

[10] Van Trees, H.L. (1969),"Detection, Modulation and Estimation Theory", Vol. I and III, Wiley.

[11] Nikias, C.L. and Raghuveer, M.R. "Bispectrum Estimation: A Digital Signal Processing Framework" (1987), Proc. of the IEEE, Vol. 75, No. 7, July 1987, p. 869-9892, (plus references therein).

[12] Subba Rao, T. & M.M. Gaber (1980) "A Test for Linearity of Stationary Time Series", J. Time Series Anal. 1(1), p. 145-158.

[13] Hinich, M.J. (1982) "Testing for Gaussianity and Linearity of a Stationary Time Series", J. Time Series Anal 3(3) p. 169-176.

[14] Cramer, H (1951), "Mathematical Methods of Statistics", Princeton Univ. Press, chap. 20.

[15] Kletter, D. & Messer, H. (1988) "Sub-optimal Detection of a non-Gaussian Signal by the Higher-Order Spectral Analysis", Submitted for publication in the IEEE Trans. on Acoust., Speech, and Signal Processing.

TEXTURE DISCRIMINATION VIA HIGHER ORDER STATISTICS

G. Ramponi and G.L. Sicuranza

Dip. di Elettrotecnica Elettronica Informatica
University of Trieste
Via A. Valerio, 10   -   34127 TRIESTE   -   Italy

ABSTRACT

Fourth-order moments are proposed in this paper as tools for discerning different textures in an image. A linear combination of such statistics is shown to be estimated by convolving the input signal with a quadratic 2-D filter and measuring the output power. A method for designing suitable filters is proposed, and the performance of the structure is substantiated by putting it to work both in natural and synthetic images.

I - INTRODUCTION

The problem which is addressed in the present paper is texture recognition in natural or artificial scenes using high-order statistical properties. It is well known, after the work by Julesz [1], that textures having the same first- and second-order statistics cannot be easily separated, unless some human-recognizable clusters or lines are present in the image (connectivity detection). If the last condition is not satisfied, even the eye finds difficulties in discerning the textures, and classic discrimination algorithms fail.

The proposed approach to this case consists in using a set of quadratic 2-dimensional operators which are based on the truncated discrete Volterra series and are able, as it will be indicated in Sect.III, to estimate a subset of the fourth-order moment sequence of the input data. A bank of such filters is used, and the output power of each is evaluated as a feature able to distinguish different textures.

The filter bank method is often used in the literature to deal with texture recognition; a conventional approach consists in using linear filters able to identify structures such as lines, edges or spots and evaluating the power output from each operator. It can be easily seen that such an output is sensitive to second-order moments of the input data; thus it can fail in recognizing textures deprived of the above mentioned structures and which differ only in their higher-order statistical parameters. Our method, on the contrary, exploits the outputs of quadratic filters, and results to be sensitive to such higher-order moments.

In the next Section, some hints on the design of suitable quadratic filters are given. Sect.III establishes the bond between these filters and fourth-order moments; a possible description for such moments, which become quite involved to use in a 2-D environment if appropriate constraints are not used, is suggested too. Finally, some examples of the application of the method are given, together with an evaluation of the results.

II - FILTER DESIGN

If we consider the input-output relation of a quadratic 2-D Volterra operator, after having normalized the input data, we obtain an expression of the kind [3]

$$y_{n,m} = \sum_i \sum_j h(i,j) \, x_i \, x_j \qquad (1)$$

where the terms x_i and x_j are the values of the input pixels $x_{n,m}$'s belonging to the present support of the filter and the summations are extended to the same support. A general approach which simplifies the design of this family of filters is presented in [3]. Suffice it here to observe that some conditions can be established on the operator,

resulting in a strong reduction of the degrees of freedom: isotropy can first be imposed on the mask by applying suitable symmetry identities on some of the $a(i,j)$'s, to make the operator respond in the same way independently of the orientation of the features in the input signal. This corresponds to imposing a set of equality constraints on suitable subsets of the coefficients. Then, the bi-impulse response of the operator is defined. As it has been indicated in [3], a quadratic Volterra operator is described by its response to couples of unitary impulses located in well defined positions in the support; designing the filter corresponds to determining such a response. A bank of quadratic 1-D Volterra filters can be devised by considering all the independent configurations of couples of impulses and fixing a set of coefficients for each couple. We have chosen a 3*3 pixels wide support, with the elements ordered as follows:

$$\begin{array}{ccc} x_1 & x_2 & x_3 \\ x_4 & x_5 & x_6 \\ x_7 & x_8 & x_9 \end{array} \quad ;$$

in this case, it can be demonstrated that six input configurations are needed, and the bank is formed by six filters. The values of the coefficients of each filter still remain to be defined; unfortunately, no definite algorithms have been found up to now to solve this problem; as a first study solution, we have used for all the numbers the value 1, even though no claim is made on the optimality of such a choice for this particular application. With this choice, the six filters of the bank result as follows:

$$y_{11} = x_1^2 + x_2^2 + x_3^2 + x_4^2 + x_5^2 + x_6^2 + x_7^2 + x_8^2 + x_9^2 \quad ;$$

$$y_{12} = x_1 x_2 + x_2 x_3 + x_3 x_6 + x_6 x_9 + x_8 x_9 + x_7 x_8 + x_4 x_7 + x_1 x_4 + x_2 x_5 + x_4 x_5 + x_5 x_6 + x_5 x_8 \quad ;$$

$$y_{13} = x_1 x_3 + x_3 x_4 + x_1 x_7 + x_7 x_9 + x_3 x_8 + x_4 x_6 \quad ;$$

$$y_{14} = x_1 x_5 + x_1 x_6 + x_5 x_7 + x_5 x_9 + x_2 x_4 + x_2 x_5 + x_6 x_8 + x_4 x_8 \quad ;$$

$$y_{15} = x_1 x_5 + x_3 x_4 + x_1 x_5 + x_3 x_9 + x_2 x_7 + x_6 x_7 + x_4 x_9 + x_3 x_4 \quad ;$$

$$y_{16} = x_1 x_9 + x_3 x_7 \quad .$$

Indeed, using unitary coefficients leads to averaging the measures of different input moments of the input image; for certain applications, more powerful operators for discriminating textures can on the contrary be designed if their coefficients perform a sort of differentiation on the same moments. This has been the second solution studied; in this case the filter y_{11} can become, for example:

$$y_{21} = x_1^2 - x_2^2 + x_3^2 - x_4^2 - x_5^2 - x_6^2 + x_7^2 - x_8^2 + x_9^2 \quad ;$$

$$\vdots$$

$$y_{2n} = -x_1^2 - x_2^2 - x_3^2 - x_4^2 + 8x_5^2 - x_6^2 - x_7^2 - x_8^2 - x_9^2 \quad ;$$

The coefficients of the latter filters have been determined heuristically, basing on similar linear operators.

III - FOURTH-ORDER MOMENTS ESTIMATION

The bound between a quadratic Volterra operator and fourth-order statistics can be easily established by observing that, if the Volterra operator is described by $a(i,j)$, we can define some $b(i,j,k,l)$'s such that

$$E[y_{n,m}^2] = \sum_i \sum_j \sum_k \sum_l b(i,j,k,l) \, E[x_i x_j x_k x_l] \quad .$$

In other words, the power output of the Volterra filter can be considered as a sort of sum of a linear combination, with weights $b(i,j,k,l)$, of the fourth-order moments of the input.

As it would be very complicated to use the moments $E[x_i x_j x_k x_l]$ when the indices i,j,k,l are varied only on the 3*3 support of the filter, it is convenient to define a set of simplified 2-D 4th-order moments in a way similar to that used for lower-order statistics [4]. We must assume the input images to be samples of an order 4 wide-sense stationary process (order 4 stationarity), so that 4th-order moments depend only on the separations between the considered pixels. If the all-moments...

constraints are applied, such separations reduce, on a 3*3 support, to the following possible distances (naming codes in parentheses): zero (0), one (T) or two (U) step transversal, one (D) or two (E) step diagonal, oblique (F). By this notation, each 4th-order moment will be indicated by a triplet of distances between the first (reference) point and the others; e.g.:

$$E[x_3 x_6 x_8 x_9] = E[x_1 x_4 x_6 x_7] = m_4(TFU).$$

It is interesting to analyze the filters of the bank (2) from this point of view. Simple mathematical manipulations show that the output power of each operator can be expressed as follows:

$$E[y_{11}^2] = 9m_4(000)+24m_4(0TT)+12m_4(0UU)+16m_4(0DD)+4m_4(0EE)+16m_4(0FF)$$

$$E[y_{12}^2] = 20m_4(0TT)+20m_4(TTU)+44m_4(TTD)+18m_4(TUF)+26m_4(TDF)+12m_4(TEF)+4m_4(TFF)$$

$$E[y_{13}^2] = 8m_4(0UU)+14m_4(TUF)+10m_4(UUE)+2m_4(UDD)+\text{.}m_4(UFF)$$

$$E[y_{15}^2] = 12m_4(0DD)+12m_4(TTD)+16m_4(TDF)+16m_4(UDD)+4m_4(DDE)+4m_4(DFF)$$

$$E[y_{16}^2] = 14m_4(0FF)+14m_4(TUF)+4m_4(TDF)+12m_4(TEF)+12m_4(UFF)+8m_4(DFF)$$

$$E[y_{19}^2] = 2m_4(0EE)+2m_4(UUU)$$

(5)

The set (5) precisely relates, as anticipated above, the output power from a filter of the bank (2) with the estimate of some fourth-order momer... Similar relationships are of course valid for the operators (3).

A relevant problem which must now be considered is the stability of the measure of the $m_4(\cdots)$'s. In fact, many 4th-order cross moments suffer from the fact that an image signal can scarcely be considered as stationary, and their estimation is instable (i.e., when trying to measure them locally, very different values are obtained in different image zones). Trials on different images indicate that the most stable moments are the "slice" ones, and in particular $m_4(000)$ and the $m_4(0xx)$'s; this is why more attention has been paid to the first filter of the bank, the output power of which is a combination of these moments. To exploit them, the filters (3) have been devised, which performed well in texture discrimination.

IV - APPLICATIONS

The proposed approach has been applied to texture discrimination using both synthetic and natural images. The first example of its performance is given in Figs. 1 and 2. The former shows a concentric composition of two synthetic textures: both are formed by 4*4 pixel patterns with two light gray impulses on a dark gray background, but in one the impulses are adjacent, while in the other they are at distance two. The textures have been damaged by multiplicative noise having uniform distribution with variance 0.2 and mean 1, and possess the same global mean and variance. The latter contains the output from filter y_{16} of the bank (2), which gives the most significant results in this case, and it indicates that the difference between the two textures have been recognized; indeed, if we evaluate $E[y^2]$ for the two components of the output image we obtain clearly different outcomes.

Interesting results have been obtained also in processing real-world images. Fig.3 shows 16 texture images; each of its four parts (a), (b), (c) and (d) is formed by four samples of the same texture (respectively: THICKET, WALL, TILES, LEATHER). All the images had been preprocessed with histogram equalization (as described in [5]), so that they possess the same mean and variance. The other 2nd-order statistics of these images have been measured, too, and proved to be very similar (when stable); thus it make sense trying to extract information from higher-order moments. Of course, these textures possess some well-recognizable structures, which render their separation easy for the human eye; also an algorithm capable to evidentiate lines or edges could be helpful. Our method, however, will prove to be capable of discerning them without exploiting such structures but using only m_4 moments estimation.

The images have been passed through the filter bank (2) and their output power has been estimated. To evaluate the performance in discriminating the textures, a method presented in [6] has been followed: the 96-points (16*6) scatter plot of the output power, sketched in Fig.4, has been subdivided in six columns, each representing one filter of the bank. In each column, three thresholds have been chosen to separate in the best possible way the four classes of textures (which in the plots are grouped and

indicated by TH, WA, TI, LE). The number of correctly classified samples (over the maximum of 16) was taken as the score of the given mask. For the six filters (2) the scores resulted to be, respectively: 11,8,11,12,12,15. It should be observed that a large part of the failures come from the identification of the texture TILES, which has been inserted in the bench mark set as a hard test: it is highly organized (structural rather than statistical discrimination approaches would better fit) and, due to perspective, strongly changes from one sample to another (see Fig.2).

Filter (3a) offers more valid results: its scatter plot is presented in Fig.5 and its score is 14. It clearly appears that the textures are perfectly discerned (again with the exception of TILES); the results are strictly grouped cor espondingly to the original textures, with the output power ranging in a more than 4-to-1 ratio.

V - FUTURE WORK

The study presented in this paper supplies enough material to build up a texture discrimination procedure basing on estimates of higher-order statistical moments. Nevertheless, it is only a first hint on much work which can be developed in this field; at present, the key points which seem to deserve more research efforts are the following:
i) determining which are the most stable fourth-order moments for a possibly large class of textured images. To this purpose, the relative stationarity which is intrinsic in a texture should result helpful;
ii' establishing precise design relations for the quadratic filters which act as estimators of the m_4's; in particular, it would probably be convenient to choose coefficients able to put to evidence the differences among the moments for the given textures.

REFERENCES

[1] B.Julesz, "Visual Pattern Discrimination", IRE Trans. on Information Theory, vol.IT-8, pp.84-92, Feb.1962.
[2] G.Ramponi, "Bi-impulse Response Design of Isotropic Quadratic Filters", submitted to IEEE Proceedings, 1989.
[3] G.Ramponi, G.L.Sicuranza and W.Ukovich, "A Computational Method for the Design of 2-D Nonlinear Volterra Filters", IEEE Trans. on Circuits and Systems, vol.CAS-35, n.9, pp.1095-1102, Sept.1988.
[4] R.J.Clarke, "Transform Coding of Images", Academic Press, London, 1985.
[5] W.K.Pratt, "Digital Image Processing", J.Wiley, New York, 1978.
[6] M.Pietikäinen, A.Rosenfeld and L.S.Davis, "Experiments with Texture Classification Using Averages of Local Pattern Matches", IEEE Trans. on Systems, Man and Cybern., vol.SMC-13, n.3, pp.421-426, May/June 1983.
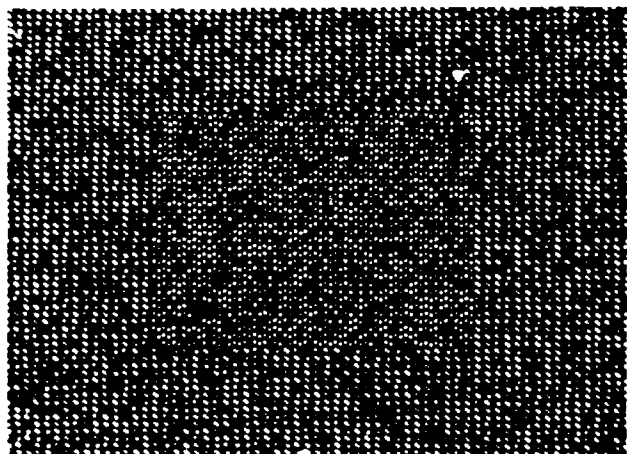
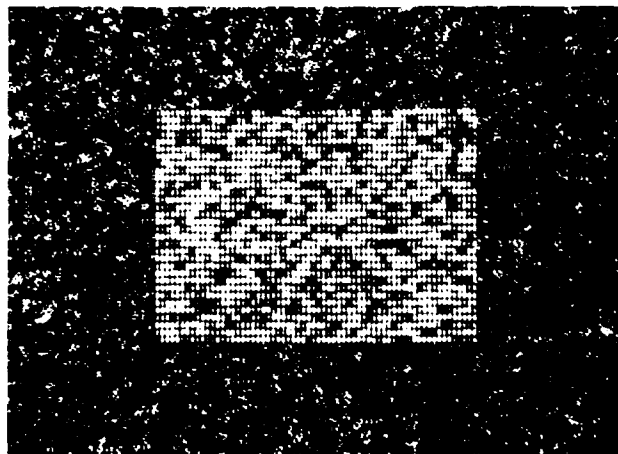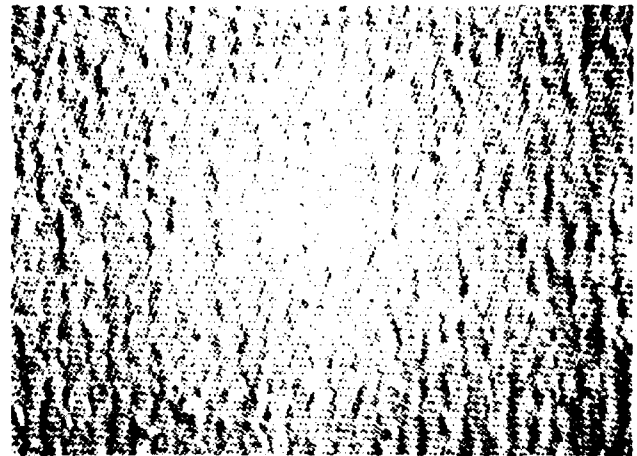Fig.1 - Synthetic image composed by two concentric noisy textures.

Fig.2 - Same as Fig.1 after processing with a filter of bank (2).

(a)

(b)

(c)

(d)

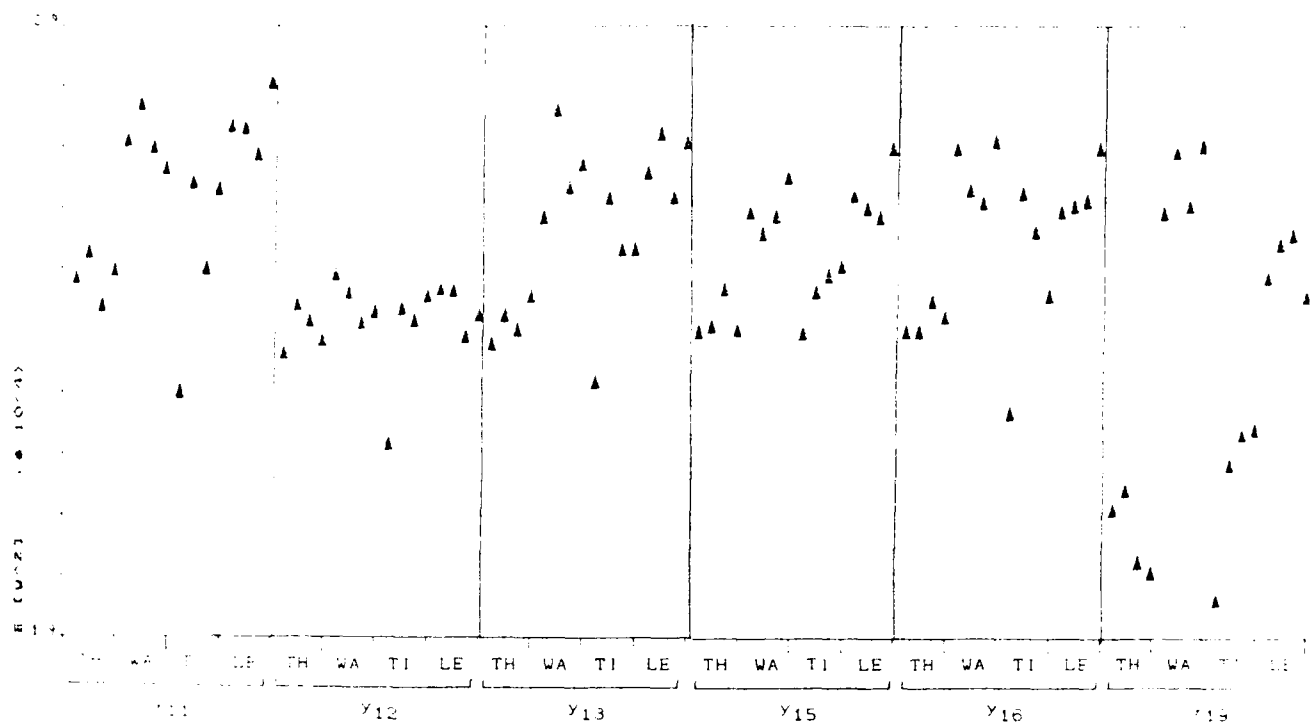Fig.3 - Real-world texture images: (a) THICKET, (b) WALL, (c) TILES, (d) LEATHER (four samples each).

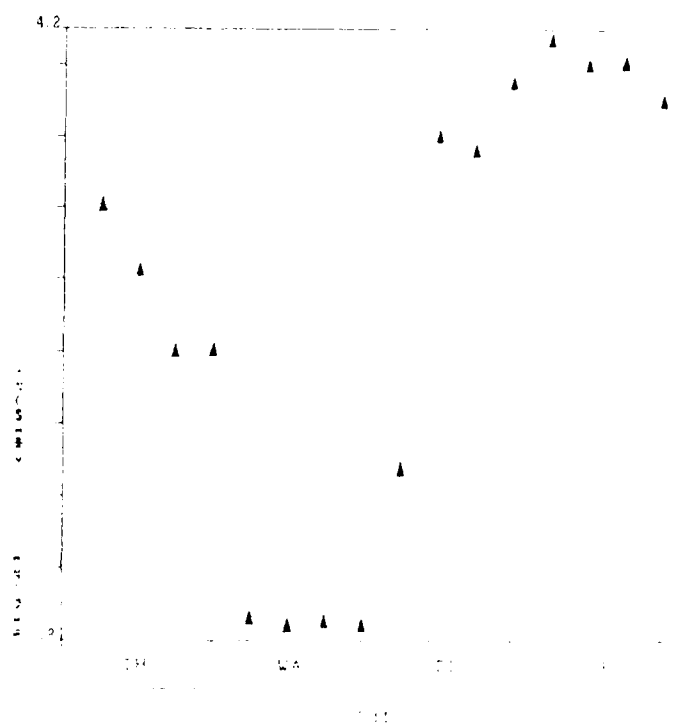Fig.4 - Scatter plots of the output power of bank (2) for real-world textures.

Fig.5 - Scatter plot of the output power of
filter (3a) for real-world textures.

Shift and Rotation Invariant Object Reconstruction
Using the Bispectrum

Brian M. Sadler
Dept. of Electrical Engineering
University of Virginia
Charlottesville, VA 22901

Abstract

Triple correlations and their Fourier transforms, called bispectra, have properties desirable for image sequence analysis. Specifically, the triple correlation of a 2-d sequence is shift-invariant, it vanishes for a zero-mean colored Gaussian random field, and can be used to uniquely recover the original sequence to within a linear phase shift. An FFT-based algorithm for reconstructing a 2-d sequence from its bispectrum is reviewed and tested. The bispectrum is also applied to estimate a randomly translating and rotating object from a sequence of noisy images. The technique does not require solution of the correspondence problem, and is insensitive to additive colored Gaussian noise of unknown spectral density. Some simulation results for the random translation case are presented.

1 Introduction

Consider the problem of reconstructing a randomly rotating and translating object from multiple noisy frames. Typically, the correspondence between frames would first be established so that averaging (or other filter function such as median filtering) can be applied to yield an improved estimate of the object. [1]. An alternative approach which does not require solution of the correspondence problem is to transform the image to a shift-invariant and high SNR domain, perform averaging or filtering in this domain, and then reconstruct an enhanced estimate of the object via an appropriate inverse transformation. Such a domain is that of higher than second-order correlations.

In this paper we employ *triple correlations* (or their corresponding Fourier transforms, called *bispectra*) for reconstructing an image of an object from noisy frames. Our motivation for using triple correlations comes from the following three facts.

- The triple correlation is shift-invariant.

- The triple correlation is invertible; i.e., we can uniquely reconstruct a two dimensional sequence from its triple correlation. The shift ambiguity is removed during reconstruction by specifying the centroid of the object to be at the origin.

- The triple correlation of a random zero-mean Gaussian field is identically zero; a fact which may be exploited to reduce additive noise effects.

It has been demonstrated in the 1-d case that significant processing gain may be achieved by utilizing the redundancy in the auto-triple correlation (or equivalently the bispectrum) when reconstructing the original signal [2]. The corresponding 2-d algorithm for reconstructing 2-d signals consists of calculating the auto-triple correlation of each frame (or equivalently the bispectrum of each frame), averaging the correlations (bispectra), and then reconstructing the object from the averaged correlation (bispectrum) [3,4].

Some investigators in optics, notably Lohmann [5,6], have used analysis of continuous deterministic signals without explicitly analyzing the noise effect. Here, discrete analysis is carried out for a deterministic signal in an additive random noise field. This approach yields discrete algorithms for implementation, and allows explicit treatment of the additive noise, [4]. A more general framework for ARMA modeling and phase reconstruction of multidimensional signals from higher-order correlations can be found in [7]. Use of higher-order statistics for signal detection and classification is treated in [8].

2 Background

The triple correlation of a zero-mean 2-d random field $f(\mathbf{m})$ is defined as

$$r_{3f}(\mathbf{n_1}, \mathbf{n_2}) = E[f(\mathbf{m})f(\mathbf{m} + \mathbf{n_1})f(\mathbf{m} + \mathbf{n_2})]. \quad (1)$$

where E represents the expectation operator. A natural estimator for the triple correlation of a zero-mean image $f(\mathbf{m})$ defined by (1) is given by

$$f_3(\mathbf{n_1}, \mathbf{n_2}) = \frac{1}{N^2} \sum_{\mathbf{m}} f(\mathbf{m}) f(\mathbf{m} + \mathbf{n_1}) f(\mathbf{m} + \mathbf{n_2}). \qquad (2)$$

Let $o(\mathbf{m})$ denote a deterministic object in a noisy $N \times N$ image as

$$f_i(\mathbf{m}) = o(\mathbf{m}) + v_i(\mathbf{m}), \qquad (3)$$

where $v(\mathbf{m})$ is a zero-mean additive noise process, and suppose there are L frames where i denotes the ith frame. Averaging estimates of the triple correlation for each frame yields

$$\frac{1}{L} \sum_{i=1}^{L} f_{3,i}(\mathbf{n_1}, \mathbf{n_2}) = o_3(\mathbf{n_1}, \mathbf{n_2}) + \frac{1}{L} \sum_{i=1}^{L} v_{3,i}(\mathbf{n_1}, \mathbf{n_2})$$

$$+ [\sum_{\mathbf{m}} o(\mathbf{m})] \frac{1}{L} \sum_{i=1}^{L} [v_i(\mathbf{m}) v_i(\mathbf{m} + \mathbf{n_1})$$

$$+ v_i(\mathbf{m}) v_i(\mathbf{m} + \mathbf{n_2}) + v_i(\mathbf{m} + \mathbf{n_1}) v_i(\mathbf{m} + \mathbf{n_2})]$$

$$+ \sum_{\mathbf{m}} [\frac{1}{L} \sum_{i=1}^{L} v_i(\mathbf{m})] [o(\mathbf{m}) o(\mathbf{m} + \mathbf{n_1})$$

$$+ o(\mathbf{m}) o(\mathbf{m} + \mathbf{n_2}) + o(\mathbf{m} + \mathbf{n_1}) o(\mathbf{m} + \mathbf{n_2})]. \qquad (4)$$

The fourth term in (4) vanishes due to the zero-mean of the noise. Similarly, the third term in (4) vanishes if the object is zero-mean. In practice the mean is subtracted before forming the estimate (2).

Thus, [2],

$$\frac{1}{L} \sum_{i=1}^{L} f_{3,i}(\mathbf{n_1}, \mathbf{n_2}) \xrightarrow{N, L \to \infty} o_3(\mathbf{n_1 n_2}) + r_{3v}(\mathbf{n_1}, \mathbf{n_2}). \qquad (5)$$

For $v(\mathbf{m})$ a zero-mean colored Gaussian random field, [9],

$$r_{3v}(\mathbf{n_1}, \mathbf{n_2}) = 0. \qquad (6)$$

Also, $v(\mathbf{m})$ can be non-Gaussian if it is i.i.d. and non-skewed (e.g., symmetrically distributed). Equation (5) states that the average triple correlation over multiple records of the deterministic zero-mean object plus random zero-mean noise is equal to the deterministic triple correlation of the object plus an estimate of the triple correlation of the noise. In the case of additive colored Gaussian noise the second term in (5) vanishes as the number of records L goes to infinity.

The discrete-time Fourier transform (DTFT) of an image $f(\mathbf{m})$ is defined as

$$F(e^{j\mathbf{u}}) = \sum_{\mathbf{m}} f(\mathbf{m}) e^{-j\mathbf{u} \cdot \mathbf{m}}. \qquad (7)$$

Denoting the four-dimensional DTFT of $f_3(\mathbf{n_1}, \mathbf{n_2})$, as $F_3(\mathbf{u_1}, \mathbf{u_2})$, it may be shown that

$$F_3(\mathbf{u_1}, \mathbf{u_2}) = F(\mathbf{u_1}) F(\mathbf{u_2}) F(-\mathbf{u_1} - \mathbf{u_2}). \qquad (8)$$

where $F(\mathbf{u})$ denotes the DTFT of the image $f(\mathbf{m})$.

Consider a translation of the object, $o(\mathbf{m} - \mathbf{m_0})$. The corresponding Fourier transform of the image is now, $e^{-j\mathbf{u} \cdot \mathbf{m_0}} F(\mathbf{u})$, where $(\mathbf{u} \cdot \mathbf{m_0})$ represents the vector dot product. Substitution of this transform into (8) reveals

that the bispectrum (and the triple correlation) are shift-invariant.

Therefore, we may form triple correlations of images of the object, where the object may be shifted but is otherwise unchanged, and average the correlations to reduce the additive noise effects. The resulting improved estimate of the triple correlation of the object may then be used to form an estimate of the object. This is possible since the triple correlation (or bispectrum) may be inverted to recover the original signal in amplitude and phase to within a shift ambiguity. Unlike the autocorrelation, higher-order correlations preserve phase information about the signal. A linear phase amibiguity arises in the triple correlation case due to the shift-invariance property. As will be seen in the following discussion of reconstruction from the bispectrum, the shift-invariance of the triple correlation allows us to place the centroid of the reconstructed object at the origin. Also, when dealing with a single frame, the original position of the object may be recovered by simply zero-padding the original image [2], so that after reconstruction any phase ambiguity will be apparent; i.e., the image will be circularly shifted within a field of zeros.

3 DFT Reconstruction

Several algorithms have been reported in [2] for reconstructing a 1-d signal from its higher-order correlations, or from the Fourier transforms of the higher-order correlations, called *polyspectra*. A 2-d FFT-based recursive algorithm for reconstructing the discrete Fourier transform (DFT) of an image from its bispectrum has been developed in [4], and is briefly reviewed here.

Consider a Cartestian sampled image given by $f(\mathbf{m})$. Denoting the 2-d DFT of the image as $F(\mathbf{k})$, the *discrete bispectrum* of the image is given by

$$F_3(\mathbf{k_1}, \mathbf{k_2}) = F(\mathbf{k_1}) F(\mathbf{k_2}) F^*(\mathbf{k_1} + \mathbf{k_2}). \qquad (9)$$

where $*$ denotes complex conjugation, and it is assumed that $f(\mathbf{m})$ is real valued.

Using the substitutions $\mathbf{k_2} = \mathbf{0}$ and $\mathbf{k_1} \mapsto \mathbf{k_1} - \mathbf{k_2}$ in (9) yields

$$F_3(\mathbf{k_1}, \mathbf{0}) = F(\mathbf{k_1}) F(\mathbf{0}) F^*(\mathbf{k_1}) \qquad (10)$$

and

$$F_3(\mathbf{k_1} - \mathbf{k_2}, \mathbf{k_2}) = F(\mathbf{k_1} - \mathbf{k_2}) F(\mathbf{k_2}) F^*(\mathbf{k_1}). \qquad (11)$$

Eliminating $F^*(\mathbf{k_1})$ and solving for $F(\mathbf{k_1})$ in (10) and (11) yields

$$F(\mathbf{k_1}) = \frac{F_3(\mathbf{k_1}, \mathbf{0})}{F_3(\mathbf{k_1} - \mathbf{k_2}, \mathbf{k_2}) F(\mathbf{0})} F(\mathbf{k_1} - \mathbf{k_2}) F(\mathbf{k_2}). \qquad (12)$$

Equation (12) may be used recursively to compute the 2-d DFT $F(\mathbf{k})$ from its bispectrum $F_3(\mathbf{k_1}, \mathbf{k_2})$.

An alternative to (12) is to rearrange (11) into

$$F^*(\mathbf{k_1}) = \frac{F_3(\mathbf{k_1} - \mathbf{k_2}, \mathbf{k_2})}{F(\mathbf{k_1} - \mathbf{k_2}) F(\mathbf{k_2})}. \qquad (13)$$

Note that this form does not rely on the mean value of the image being non-zero, i.e., does not rely on $F(\mathbf{0})$ being non-zero. This is important since noise reduction relies on the assumption of zero-mean. In practice the mean is subtracted before estimating the bispectrum.

The redundancy in the bispectrum implies that one or more values for $\mathbf{k_2}$ may be allowed for each choice of $\mathbf{k_1}$ in (12) or (13). Let $\mathbf{k_2} \in \mathbf{R_{k_1}}$ represent the set of allowable choices for $\mathbf{k_2}$ given $\mathbf{k_1}$. The allowable choices are $0 < \mathbf{k_2} < \mathbf{k_1}$. For $\mathbf{k_2} = (k_{21}, k_{22})$, there are $(k_{21} + 1)(k_{22} + 1) - 2$ elements in $\mathbf{R_{k_1}}$, since $\mathbf{k_2} = \mathbf{0}$ and $\mathbf{k_2} = \mathbf{k_1}$ are excluded. We can exploit this redundancy in (12) by averaging over $\mathbf{R_{k_1}}$ as

$$\hat{F}(\mathbf{k_1}) = \frac{1}{(k_{21} + 1)(k_{22} + 1) - 2} \times$$
$$\sum_{\mathbf{k_2} \in \mathbf{R_{k_1}}} \frac{F_3(\mathbf{k_1}, \mathbf{0})}{F_3(\mathbf{k_1} - \mathbf{k_2}, \mathbf{k_2}) \hat{F}(\mathbf{0})} \hat{F}(\mathbf{k_1} - \mathbf{k_2}) \hat{F}(\mathbf{k_2}) \quad (14)$$

yielding an improved estimate for $F(\mathbf{k_1})$. If a particular choice of $\mathbf{k_2}$ produces a zero denominator then that term is excluded from the average. A further reduction in computation of (14) is possible by considering only those values of the bispectrum in a single non-redundant region, e.g., using the bispectrum symmetry $F_3(\mathbf{k_1}, \mathbf{k_2}) = F_3(\mathbf{k_2}, \mathbf{k_1})$. As a result, half of the allowable values of $\mathbf{k_2} \in \mathbf{R_{k_1}}$ yield redundant computations in (14). Similar statements are true regarding use of (13). Note that the complex conjugate symmetry of the DFT may be exploited when estimating $\hat{F}(\mathbf{k})$, so that only $\frac{N^2}{2} + 2$ points of $\hat{F}(\mathbf{k})$ need be computed directly.

The shift-invariance of the bispectrum implies that reconstruction is unique to within a phase ambiguity. This ambiguity can be exploited during reconstruction to centroid the object at the origin. The kth derivative of the continuous Fourier transform, evaluated at the origin, is proportional to the kth moment of the image, [10]. A similar property is true for the discrete case. As a result specifying the phase of the points $\hat{F}(0,1)$ and $\hat{F}(1,0)$ to be zero will yield a reconstruction such that the object is centroided about the origin. The magnitude of $\hat{F}(0,1)$ and $\hat{F}(1,0)$ are found from (12) or (13) using an estimate of the mean for the value of $F(0)$. For computation of all other points of $\hat{F}(\mathbf{k})$ it is important that $F(\mathbf{0}) = 0$ to suppress the additive noise component. When multiple frames are available an estimate of the mean may be obtained by averaging the means of the frames.

Let $\phi(\mathbf{k})$ denote the phase of $\hat{F}(\mathbf{k})$. As a consequence of setting $\phi(1,0) = \phi(0,1) = 0$, it is necessary to apply a phase correction factor. A linear phase factor in the DFT corresponds to multiplying by $e^{-j\frac{2\pi}{N}m_0}$ in the frequency domain, or equivalently shifting in the time domain by m_0, where m_0 has purely integer components. In specifying $\phi(0,1) = \phi(1,0) = 0$, it is not clear that the implied

phase shift corresponds to a linear shift of the DFT. Alternatively, it is not true in general that the resulting estimates $\hat{F}(0, \frac{N}{2})$, $\hat{F}(\frac{N}{2}, 0)$ and $\hat{F}(\frac{N}{2}, \frac{N}{2})$ will be real valued, as required if the resulting reconstructed image is to be real valued. The phase correction will ensure that the phase of these points will be zero. After (12) or (13) are used to compute $\hat{F}(k, l)$ the phase corrected DFT is given by

$$\hat{F}_\phi(k, l) = \hat{F}(k, l) \exp[-j\frac{2k}{N}\hat{\phi}(\frac{N}{2}, 0) - j\frac{2l}{N}\hat{\phi}(0, \frac{N}{2})]. \quad (15)$$

Finally, $\hat{F}_\phi(\mathbf{0})$ may be set to the mean previously estimated.

Note also that just as high variance periodogram estimates require smoothing, estimates of the bispectrum also require smoothing [11]. The latter guarantees consistency of the sample estimates, and may be accomplished by window weighting the image, or by using a smoothing operation on the bispectrum such as local averaging.

4 Random Translation

The shift-invariance and invertibility of the bispectrum can be exploited when multiple noisy views of a randomly translated object are available. Let

$$f(\mathbf{m}) = o(\mathbf{m}) + v(\mathbf{m}) \quad (16)$$

be an image, where $o(\mathbf{m})$ is the object and $v(\mathbf{m})$ is an additive random Gaussian field independent of $o(\mathbf{m})$ and not necessarily white. Let

$$f_i(\mathbf{m}) = o(\mathbf{m} - \mathbf{m_i}) + v_i(\mathbf{m}) \quad (17)$$

be the ith frame, where the object is randomly translated by $\mathbf{m_i}$, and $v_i(\mathbf{m})$ represents an independent sample set of the noise field $v(\mathbf{m})$. Let $F_i(\mathbf{k})$ be the DFT of the ith frame, so that

$$F_{3,i}(\mathbf{k_1}, \mathbf{k_2}) = F_i(\mathbf{k_1})F_i(\mathbf{k_2})F_i^*(\mathbf{k_1} + \mathbf{k_2}) \quad (18)$$

is the discrete bispectrum if the ith frame. Due to the shift-invariance of the bispectrum

$$F_{3,i}(\mathbf{k_1}, \mathbf{k_2}) \simeq O_3(\mathbf{k_1}, \mathbf{k_2}) + V_{3,i}(\mathbf{k_1}, \mathbf{k_2}) \quad (19)$$

where $O_3(\mathbf{k_1}, \mathbf{k_2})$ is the bispectrum of the object and $V_{3,i}(\mathbf{k_1}, \mathbf{k_2})$ is the bispectrum of the ith sample set of the noise. Thus, given L available frames the bispectra are averaged to form the estimate

$$\hat{F}_3(\mathbf{k_1}, \mathbf{k_2}) = \frac{1}{L} \sum_{i=1}^{L} F_{3,i}(\mathbf{k_1}, \mathbf{k_2}). \quad (20)$$

$\hat{F}_3(\mathbf{k_1}, \mathbf{k_2})$ represents an improved estimate of the bispectrum of the object, due both to the averaging of the bispectra of the views of the object and the averaging of the bispectra of the noise sample sets. Under the Gaussian noise assumption

$$\frac{1}{L}\sum_{i=1}^{L} V_{3,i}(\mathbf{k_1}, \mathbf{k_2}) \xrightarrow{L \to \infty} 0. \tag{21}$$

Reconstruction of the object can now be performed by inverting the bispectrum.

The continuous version of this algorithm has been implemented optically on astronomical data to remove atmospheric turbulence effects [12,13]. It does not require knowledge of the object translation vector $\mathbf{m}_i$. Thus, the bispectrum technique offers the advantages of eliminating the correspondence problem, use of the FFT, and allowing averaging in the bispectrum-domain. Use of the Radon transform has also been suggested for estimating the bispectrum of a randomly translated object [14]. This approach reduces the dimensionality of the problem but requires reconstruction from projections.

5 Random Rotation

In this section it is again assumed that multiple noisy views of an object in an additive random Gaussian field are available. However, it is now assumed that the centroid of the object is always at the same fixed location (at the center of the frame, say), but that the object is randomly rotated about the centroid from frame to frame. It is desired to reconstruct the object given L noisy frames.

An algorithm for rotation-invariance has been suggested by Lohmann [15]. This algorithm relies on 1-d Fourier series formed by treating constant radius rings in the image as periodic sequences. In practice the Fourier series coefficients are found using the DFT, taken around each ring. These DFT's can be used to form discrete bispectra for each ring, and the bispectra can then be averaged over the image set. The dimensionality of the problem has been reduced, but the method leads to a phase correspondence problem between the rings after they are reconstructed which requires a solution from the DFT-domain.

A new algorithm for rotation-invariance is now developed which exploits the shift-invariance of the bispectrum. This algorithm relies on the following property of the discrete bispectrum given by (9), that *the discrete bispectrum is invariant under a circular shift of the image-domain sequence.* This is shown as follows. Let

$$y(n_1, n_2) = x(((n_1 - m_1))_N, ((n_2 - m_2))_N) \tag{22}$$

be a circularly shifted version of the $N \times N$ image $x(n_1, n_2)$, where $(\cdot)_N$ denotes a modulo-N operation. The respective DFT's of $y(n_1, n_2)$ and $x(n_1, n_2)$ are related by, [16],

$$Y(k_1, k_2) = e^{j\frac{2\pi}{N}(k_1 m_1 + k_2 m_2)} X(k_1, k_2). \tag{23}$$

Inserting $Y(k_1, k_2)$ into (9) reveals that the discrete bispectrum of $y(n_1, n_2)$ and $x(n_1, n_2)$ are identical.

Let

$$f_i(r, \phi) = o(r, \phi - \phi_i) + v_i(r, \phi) \tag{24}$$

represent regular polar samples of the ith image of an object, where $o(r, \phi - \phi_i)$ is the centroided object randomly rotated by ϕ_i, and $v_i(r, \phi)$ represents samples of an additive random Gaussian field. Let $F_i(\omega, \theta)$ represent regular polar samples of the DTFT of $f_i(r, \phi)$. It is known that $F_i(\omega, \theta)$ can be obtained with the use of Fourier and Hankel transforms; e.g., see [17]. However, it can readily be shown that the bispectrum formed by substituting $F_i(\omega, \theta)$ into (8) is *not* rotation-invariant. An alternative is to form for each frame

$$\check{F}(k, l) \triangleq \sum_r \sum_\phi f(r, \phi) e^{-jkr} e^{-jl\phi}. \tag{25}$$

Substitution of $\check{F}(k, l)$ into (8) reveals that the bispectrum formed with $\check{F}(k, l)$ *is* rotation-invariant. The definition of $\check{F}(k, l)$ may be thought of as mapping the polar coordinate system to a Cartesian coordinate system and then taking the DTFT in the new Cartesian system. Translation in ϕ in the new Cartesian system is equivalent to rotation in the original polar system. In practice (25) is computed using the DFT. Now, rotation corresponds to a circular shift in the new Cartesian system. However, as shown above, the discrete bispectrum is invariant to a circular shift. In order to avoid any circular shifting in r which may occur when inverting the bispectrum, it is only necessary to zero-pad $f(r, \phi)$ in the r variable. It is important to note that $\check{F}(k, l)$ does *not* represent samples of the DTFT of the original image, but merely exists to transform the rotation problem into an equivalent translation problem.

After forming $\check{F}_i(k, l)$ for each image, a bispectrum-based translation-invariant algorithm may be applied, as presented in section 4. The bispectra are computed for each frame from $\check{F}_i(k, l)$, an averaged bispectrum is formed, and then inverted, yielding an estimate of $\check{F}(k, l)$. Finally, (25) is inverted to yield an estimate $\hat{f}(r, \phi)$.

6 Translation and Rotation

In the preceding, algorithms have been described for reconstructing a translating object and reconstructing a rotating object with known centroid. An outcome of reconstructing a translated object is that the centroid of the reconstructed object is known, and in practice is easily placed at the origin. This suggests an algorithm [15] whereby the translation is first removed by forming the bispectrum and then reconstructing to remove translation; followed by a rotation-invariant algorithm to arrive at an estimate of the object. Thus, an algorithm for reconstructing a randomly rotated and translated object is as follows:

1. Form the bispectrum and reconstruct *for each frame.* This results in a series of frames in which the object has a common centroid but remains randomly rotated about the centroid.

2. A rotation-invariant bispectrum-based algorithm, as described in section 5, is applied to obtain an estimate of the object.

Note that the purpose of step one is only to remove the translation ambiguity, and averaging of bispectra occurs only in step two. This algorithm is computationally expensive in that the bispectrum is formed twice for each frame, once during step one, and once during step two. Also, a reconstruction algorithm must be applied to each of the bispectra found in step one.

7 Simulations

Simulations were performed to verify the reconstruction algorithm of section 3 and reconstruction of a randomly translating object presented in section 4. Figure 1 depicts the 64×64 pixel binary object "Calvin." Figure 2 depicts a reconstruction from the bispectrum of object "Calvin." The 2-d FFT of the object was found and the mean set to zero. Equation (9) was used to compute the bispectrum, so that the recursion of (13) could be applied. Averaging was performed when using (13). Finally, the mean was restored and the inverse FFT applied. No noise was added so that smoothing of the bispectrum estimates was not necessary for exact reconstruction. The reconstructed object is centroided about the origin which is at the upper left of the frame.

Next, Gaussian white noise was added to 10 frames of "Calvin" with random translations at a signal-to-noise ratio (SNR) of $-10dB$. SNR is defined as the sum of the squares of the signal over the sum of the squares of the noise. A single frame with SNR of $-10dB$ is shown in figure 3. The object is at the upper left in the frame. The reconstructed object is shown in figure 4. The algorithm of section 4 was used, so that the 10 bispectra were averaged before reconstruction. For ease of simulation, no local averaging of the bispectra was performed.

8 Conclusions

A recursive FFT-based algorithm for image reconstruction from the bispectrum has been reviewed and tested. The shift invariance and noise reduction properties of the triple correlation have been exploited to obtain estimates of a randomly translating and rotating object from multiple noisy frames. The bispectrum-based approach does not require solution of the correspondence problem, and is independent of object shape or connectedness. Simulation results are shown for a randomly translating object in additive Gaussian white noise. Successful reconstruction from 10 frames at $-10dB$ SNR per frame has been demonstrated.

Figure 1
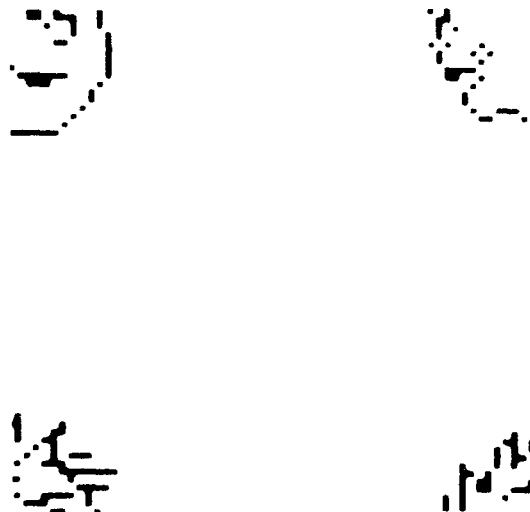Object "Calvin."

Figure 2
Reconstruction from bispectrum of figure 1.

Figure 3
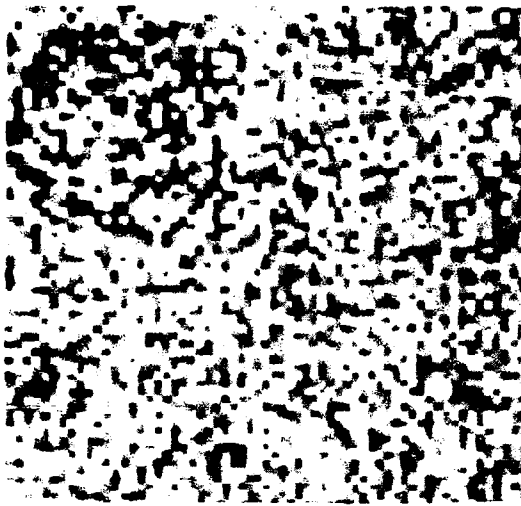
Object "Calvin" in white Gaussian noise.
$SNR = -10dB$.

Figure 4

Reconstruction from 10 frames with random translation.

References

[1] T. S. Huang ed., *Image Sequence Analysis*, Springer-Verlag, 1981.

[2] G. B. Giannakis, "Signal reconstruction from multiple correlations: frequency and time domain approaches," Jour. of the Optical Soc. of Amer., May 1989.

[3] H. Bartelt and B. Wirnitzer, "Shift-invariant imaging of photon-limited data using bispectral analysis," Optics Comm., 53, No. 1, 1 Feb. 1985.

[4] B. M. Sadler and G. B. Giannakis, "Image sequence analysis and reconstruction from the bispectrum," Proc. 1989 Conf. on Inf. Sci. and Syst., Baltimore, MD., March 1989.

[5] A. W. Lohmann and B. Wirnitzer, "Triple correlations," Proc. IEEE, Vol. 72, 1984.

[6] H. Bartelt, A. W. Lohmann, and B. Wirnitzer, "Phase and amplitude recovery from bispectra," Appl. Opt., 23, 3121(1984).

[7] A. Swami, G. B. Giannakis, and J. M. Mendel, "Modeling of multidimensional ARMA models using cumulants," submitted to Proc. IEEE, Jan. 1989.

[8] G. B. Giannakis, and M. K. Tsatsanis, "Signal detection and classification using matched filtering and higher-order statistics," University of Virginia Report No. UVA /192444B /EE89 /111, March 1989.

[9] D. R. Brillinger and M. Rosenblatt, "Computation and interpretation of kth-order spectra," in *Spectral Analysis of Time Series*, pp. 189-232, B. Harris, Ed., Wiley, 1967.

[10] J. D. Gaskill, *Linear Systems, Fourier Transforms, and Optics*, Wiley, 1978.

[11] T. Subba Rao and M. M. Gabr, *An Introduction to Bispectral Analysis and Bilinear Time Series Models*, New York: Springer-Verlag, 1984.

[12] A. W. Lohmann, G. P. Weigelt, and B. Wirnitzer, "Speckle masking in astronomy: triple correlation theory and applications," Appl. Opt. 22, 4028(1983).

[13] K. H. Hofmann and G. Weigelt, "Speckle masking observations of the central object in the giant H II region NGC 3603," Astron. Astrophys. 167, L15(1986).

[14] M. J. Northcott, G. R. Ayers, and J. C. Dainty, "Algorithms for image reconstruction from photon-limited data using the triple correlation," J. Opt. Soc. Am. A, Vol. 5, No. 7, July 1988.

[15] A. W. Lohmann, "Shift and rotation tolerant image recovery from triple correlations," OPTIK, 73, No. 3(1986), pp 127-131.

[16] D. E. Dudgeon and R. M. Mersereau, *Multidimensional Digital Signal Processing*, New Jersey: Prentice-Hall, 1984.

[17] R. M. Mersereau, A. V. Oppenheim, "Digital reconstruction of multidimensional signals from their projections," Proc. IEEE, Vol. 62, No. 10, Oct. 1974.

TWO-DIMENSIONAL NON-MINIMUM PHASE
SIGNAL RECONSTRUCTION

S.A. Dianat and M.R. Raghuveer

Electrical Engineering Department Rochester Institute of Technology
Rochester, NY 14623-0887

ABSTRACT

The existing techniques for reconstruction of one dimensional (1-D) signals from samples of its bispectrum are not efficient for reconstruction of (2-D) signals. In this paper we present a new technique for 2-D nonminimum phase signal reconstruction which uses a small segment of the 4-D bispectrum. The approach uses the facts that the phase of the Fourier transform of a 2-D discrete signal is periodic and odd while the magnitude is periodic and even. Thus, they can be expanded using Fourier series. The Fourier series coefficients of these expansions are then recovered from the Fourier series of bispectrum phase and magnitude. The implementation of the proposed technique is greatly simplified by using the FFT for computation of the Fourier series coefficients.

1 INTRODUCTION

The advantages of using the bispectrum for reconstruction of one dimensional, non-minimum phase signals has been well documented [1]-[3]. An issue that arises is whether multidimensional bispectrum estimation can be used for a similar purpose. We address this issue with respect to two-dimensional (2-D) signals. As pointed out in [4], a good way to sort signals on the basis of their phase properties to test bispectral signal reconstruction, is to use the classification provided by Ekstrom and Woods [5]. Their scheme classifies 2-D signals into four categories: min-min phase, min-max phase, max-min phase and max-max phase. A possible approach in devising schemes to recover a 2-D signal from its bispectrum, is to extend existing 1-D algorithms [1], ...[2] to two dimensions. If in principle, these extensions turn out to be straightforward, a consideration that would limit the usefulness of some of these is computational complexity. This arises mainly because of the greater amounts of data storage needed for 2-D signals. Recent results in parametric and non parametric bispectrum estimation can be found in [8], [1], [9]. In this paper, we provide a new approach which uses samples of the bispectrum taken from a sub-region of the fundamental region of support.

1.1 2-D Bispectrum: Definitions and Properties

Let $y(\underline{n})$, $\underline{n} = [n_1 \ n_2]^t$ be the output of a discrete, 2-D, linear space invariant (LSI) system driven by stationary non-Gaussian white noise (NGWN) $w(\underline{n})$. Let us assume that $E\{w(\underline{n})\} = 0$ and $E\{w^3(\underline{n})\} = 1$. Then, if the impulse response of the system is $h(\underline{n})$, the bispectrum of $y(\underline{n})$ is given by,

$$B(\underline{\omega}, \underline{\lambda}) = H(\underline{\omega})H(\underline{\lambda})H^*(\underline{\omega} + \underline{\lambda}) \qquad (1)$$

where $\underline{\omega} = [\omega_1 \ \omega_2]^t$, $\underline{\lambda} = [\lambda_1 \ \lambda_2]^t$ and

$$H(\underline{\omega}) = \sum_{\underline{n}} h(\underline{n}) \exp[-j(\omega^t \underline{n})] \qquad (2)$$

The vector notation for representing bispectra and third order cumulant sequences of multidimensional signals was introduced in [4], [9]. The bispectrum is periodic with period 2π in its four variables, and for a real signal satisfies the following,

$$B(\underline{\omega}, \underline{\lambda}) = B(\underline{\lambda}, \underline{\omega}) = \qquad (3)$$

$$B(\underline{\omega}, -\underline{\omega} - \underline{\lambda}) = B(-\underline{\omega} - \underline{\lambda}, \underline{\lambda}) \qquad (4)$$

$$= B^*(\underline{\omega}, -\underline{\lambda}) \qquad (5)$$

Equation (3) implies that it is enough to know the bispectrum over the region defined by,

$$S_1 = \{\omega_1 > \lambda_1\} \bigcup \{\omega_1 = \lambda_1, \omega_2 \geq \lambda_2\} \qquad (6)$$

From (4), along with the periodicity of the bispectrum, we see that it is enough to know the bispectrum in the region,

$$S_2 = \{|\omega_1 + \lambda_1| \leq \pi, |\omega_2 + \lambda_2| \leq \pi\} \qquad (7)$$

and finally, (5) implies that we require knowledge of the bispectrum only in the region,

$$S_3 = \{\omega_1 > 0\} \bigcup \{\omega_1 = 0, \omega_2 > 0\} \qquad (8)$$

Therefore the fundamental region of support of the bispectrum of a real signal is at most as large as $S_1 \cap S_2 \cap S_3$. Pictorially, this is shown in figure 1. For points with coordinates in the $\omega_1 - \lambda_1$ plane on the triangle ABC excluding the line AC, it includes coordinate values for ω_2 and λ_2 over the entire hexagon DEFGHI in the $\omega_2 - \lambda_2$ plane. For coordinate

values on the line AC excluding the origin in the $\omega_1 - \lambda_1$ plane, it includes all point in the $\omega_2 - \lambda_2$ plane covered by the pentagon DKJHL. For $\omega_1 - \lambda_1 = 0$, we need to look at just the triangular region, DKO in the $\omega_2 - \lambda_2$ plane. In this context, we must point out that the "non-redundant" region of support as given by [8] excludes regions that should actually be a part of the non-redundant region.

2 MATHEMATICAL DEVELOPMENT

2.1 2-D Fourier Series

Let $X(\omega_1,\omega_2)$ be a 2-D real, doubly periodic signal with period 2π in both its arguments. Assume that it satisfies the 2-D Dirichlet conditions. It can then be expressed in terms of its 2-D fourier series

$$X(\omega_1,\omega_2) = \sum_{m=-\infty}^{\infty} \sum_{n=-\infty}^{\infty} x(m,n)\exp[j(\omega_1 m + \omega_2 n)] \quad (9)$$

where

$$x(m,n) = \frac{1}{4\pi^2} \int_0^{2\pi} \int_0^{2\pi} X(\omega_1,\omega_2)\exp[-j(\omega_1 m + \omega_2 n)]d\omega_1 d\omega_2 \quad (10)$$

With $X(\omega_1,\omega_2)$ being real,

$$x(-m,-n) = x^*(m,n) \quad (11)$$

where * denotes complex conjugation. Let

$$a(m,n) = \frac{1}{2}\mathrm{Re}\{x(m,n)\}$$

$$b(m,n) = -\frac{1}{2}\mathrm{Im}\{x(m,n)\} \quad (12)$$

The trigonometric Fourier series representation of $X(\omega_1,\omega_2)$ follows from the above equations,

$$X(\omega_1,\omega_2) = \begin{cases} (1/2)a(0,0) + \\ \sum_{m=0}^{\infty}\sum_{n=0}^{\infty} a(m,n)\cos(\omega_1 m + \omega_2 n) + \\ \sum_{m=1}^{\infty}\sum_{n=1}^{\infty} a(m,-n)\cos(\omega_1 m - \omega_2 n) + \\ \sum_{m=0}^{\infty}\sum_{n=0}^{\infty} b(m,n)\sin(\omega_1 m + \omega_2 n) + \\ \sum_{m=1}^{\infty}\sum_{n=1}^{\infty} b(m,-n)\sin(\omega_1 m - \omega_2 n) \end{cases} \quad (13)$$

If $X(\omega_1,\omega_2)$ is even in its arguments, then the representation is purely in terms of cosines, and if it is odd, it is purely in terms of sines.

2.2 Algorithm Development

One's concern in this paper is the recovery of the phase and magnitude of $H(\omega)$ from the bispectrum $B(\omega_1,\omega_2)$. Let

$$B(\omega_1,\omega_2) = |B(\omega_1,\omega_2)|\exp[j\psi(\omega_1,\omega_2)] \quad (14)$$

and

$$H(\omega) = |H(\omega)|\exp[j\phi(\omega)] \quad (15)$$

From the above equations and (1),

$$2\phi(\omega) - \phi(2\omega) = \psi(\omega,\omega) \quad (16)$$

Since $\phi(\omega)$ can be assumed to be odd in its arguments, we can write it as

$$\phi(\omega) = \sum_{m=0}^{\infty}\sum_{n=0}^{\infty} b(m,n)\sin(\omega_1 m + \omega_2 n) + \sum_{m=1}^{\infty}\sum_{n=1}^{\infty} b(m,-n)\sin(\omega_1 m - \omega_2 n) \quad (17)$$

By the same token, we can expand $\psi(\omega,\omega)$ as

$$\psi(\omega,\omega) = \sum_{m=0}^{\infty}\sum_{n=0}^{\infty} \dot{b}(m,n)\sin(\omega_1 m + \omega_2 n) + \sum_{m=1}^{\infty}\sum_{n=1}^{\infty} \dot{b}(m,-n)\sin(\omega_1 m - \omega_2 n) \quad (18)$$

Taking into consideration the fact that $\{\sin(\omega_1 m + \omega_2 n), \sin(\omega_1 m - \omega_2 n) : 0 \le m,n \le \infty, (m,n) \ne (0,0)\}$ forms a complete orthogonal set over the region of interest, (16)-(18) yield the following algorithm to compute $b(m,n)$ from $\dot{b}(m,n)$

1. If either of m or n is odd, then

$$b(m,n) = \frac{1}{2}\dot{b}(m,n) \quad (19)$$

2. If either $(m/2)$ or $(n/2)$ is odd, then

$$b(m,n) = \frac{1}{2}\dot{b}(m,n) + \frac{1}{4}b(\frac{m}{2},\frac{n}{2}) \quad (20)$$

3. If both $(m/2)$ and $(n/2)$ are even, then

$$b(m,n) = \frac{1}{2}\dot{b}(m,n) + \frac{1}{2}b(\frac{m}{2},\frac{n}{2}) \quad (21)$$

In any implementation of the algorithm, steps 1 and 2 above should be first implemented over the range of interest and step 3 should be carried out afterwards to recursively compute $b(m,n)$ in terms of previously computed values. For example, if we are interested in finding $b(m,n)$ for $0 \le m,n \le 4$, steps 1 and 2 provide us with all necessary values except $b(4,0)$, $b(0,4)$ and $b(4,4)$, and these can be found from step 3 as

$$b(4,0) = \frac{1}{2}\dot{b}(4,0) + \frac{1}{2}b(2,0)$$

$$b(0,4) = \frac{1}{2}\dot{b}(0,4) + \frac{1}{2}b(0,2) \quad (22)$$

$$b(4,4) = \frac{1}{2}\dot{b}(4,4) + \frac{1}{2}b(2,2)$$

$$(23)$$

For larger grids, the recursion in step 3 will actually use values computed earlier in the same step. Let

$$H(\omega) = \ln[H(\omega)] \quad (24)$$

and

$$B(\omega) = \ln|B(\omega,\omega)| \qquad (25)$$

Then,

$$2H(\omega) - H(2\omega) = B(\omega) \qquad (26)$$

Since $H(\omega)$ and $B(\omega)$ can be assumed to be even in their arguments, they can be written as

$$H(\omega) = \begin{array}{l} \tfrac{1}{2}a(0,0) + \\ \sum_{m}\sum_{n} a(m,n)\cos(\omega_1 m + \omega_2 n) + \\ \sum_{m}\sum_{n} a(m,-n)\cos(\omega_1 m - \omega_2 n) \end{array} \qquad (27)$$

and

$$B(\omega) = \begin{array}{l} \tfrac{1}{2}\hat{a}(0,0) + \\ \sum_{m}\sum_{n} \hat{a}(m,n)\cos(\omega_1 m + \omega_2 n) + \\ \sum_{m}\sum_{n} \hat{a}(m,-n)\cos(\omega_1 m - \omega_2 n) \end{array} \qquad (28)$$

Similar to the phase reconstruction algorithm, we can formulate an algorithm for magnitude reconstruction as follows.

1.

$$a(0,0) = \frac{1}{3}\hat{a}(0,0) \qquad (29)$$

2. If either of m or n is odd, then

$$a(m,n) = \frac{1}{2}\hat{a}(m,n) \qquad (30)$$

3. If either $(m/2)$ or $(n/2)$ is odd, then

$$a(m,n) = \frac{1}{2}\hat{a}(m,n) + \frac{1}{4}\hat{a}\left(\frac{m}{2},\frac{n}{2}\right) \qquad (31)$$

4. If both $(m/2)$ and $(n/2)$ are even, then

$$a(m,n) = \frac{1}{2}\hat{a}(m,n) + \frac{1}{2}a\left(\frac{m}{2},\frac{n}{2}\right) \qquad (32)$$

It must be noted here that a necessary condition for the above algorithm to work is that $H(\omega)$ be non-zero. The discussion following the presentation of the algorithm for phase reconstruction, also applies to the magnitude reconstruction algorithm.

In a practical implementation, we can use FFT. Given $N \times N$ samples $B(\frac{2\pi}{N}n_1, \frac{2\pi}{N}n_2)$, $n_1, n_2 = 0, 1, \ldots, N-1$ of the bispectrum $B(\omega, \omega)$, then

$$b(k_1, k_2) = (1/2N)\mathrm{Imag}\{\mathrm{DFT}[\psi(n_1, n_2)]\} \qquad (33)$$

$$a(k_1, k_2) = (1/2N)\mathrm{Real}\{\mathrm{DFT}[B(n_1, n_2)]\}$$

where

$$\psi(\omega) = \psi(\omega,\omega)$$

The Fourier series coefficients of the reconstructed phase and magnitude can be obtained from the previously outlined algorithms. Only a finite number of coefficients are computed and the reconstruction is done with this truncated Fourier series. The phase reconstruction is performed as

$$\phi(\omega) = \sum_{(k_1,k_2)} b(k_1,k_2)\sin(\omega_1 k_1 + \omega_2 k_2) \qquad (34)$$

The magnitude reconstruction is performed as

$$|H(\omega)| = \exp\left[\sum_{(k_1,k_2)} a(k_1,k_2)\cos(\omega_1 k_1 + \omega_2 k_2)\right] \qquad (35)$$

3 SIMULATION RESULTS

Example 1 Consider the minimum phase signal

$$h(n_1,n_2) = \left\{ \begin{array}{l} \delta(n_1,n_2) + 0.333\delta(n_1-1,n_2) + \\ 0.25\delta(n_1,n_2-1) + 0.416\delta(n_1-1,n_2-1) + \\ 0.17\delta(n_1-2,n_2-1) + 0.125\delta(n_1-1,n_2-2) \\ +0.041\delta(n_1-2,n_2-2) \end{array} \right. \qquad (36)$$

The Fourier series coefficients of $\psi(\omega,\omega)$ and $\ln|B(\omega,\omega)|$ were obtained from (33) using 256×256 equally spaced samples of the true bispectrum over the grid $[0,2\pi] \times [0,2\pi]$. The estimated phase and magnitude of $h(n)$ are shown in figures 3 and 5 respectively. The true phase and magnitude response functions are shown in figures 2 and 4. As can be seen it is not possible to distinguish the true ones from their estimates. Both phase and magnitude were reconstructed using Fourier series coefficients over a small grid of size 8×8.

Example 2 In this example we try to reconstruct the phase and magnitude of a mixed-phase signal. Let

$$h(n_1,n_2) = \left\{ \begin{array}{l} \delta(n_1,n_2) + 0.333\delta(n_1-1,n_2) + \\ 0.25\delta(n_1,n_2-1) + 1.91\delta(n_1-1,n_2-1) + \\ 0.67\delta(n_1-2,n_2-1) + 0.5\delta(n_1-1,n_2-2) + \\ 0.166\delta(n_1-2,n_2-2) \end{array} \right. \qquad (37)$$

Similar to example 1 256×256 samples of the true bispectrum were used for reconstruction of both phase and magnitude. Figures 6 and 9 show the true phase and magnitude of the Fourier transform of $h(n)$. Figure 7 shows the estimated phase. The phase estimation error is shown in Figure 8. As it can be seen large errors occur only at frequencies where the phase response is not continuous. This problem can be eliminated by using phase unwrapped function $\psi(\omega,\omega)$. The true magnitude and its estimate are shown in figures 9 and 10 respectively. As can be seen the magnitude reconstruction error is almost zero. This is due to the fact that there is no discontinuity in magnitude of the Fourier transform of $h(n)$.

4   CONCLUSION

This paper has developed a new approach for 2-D non-minimum phase signal reconstruction using samples of its bispectrum along the hyperplane $\omega = \lambda$ in the bispectrum frequency domain. An advantage of the approach is that it uses a finite number of samples of the bispectrum function and provides estimates of the signal phase and magnitude at all frequencies. The approach is computationally cost effective since it can be implemented via the FFT algorithm.

References

[1] K.S. Lii and M. Rosenblatt. "Deconvolution and estimation of transfer function phase and coefficients for nongaussian linear processes". *Annals of Stat.*, vol. 10(4):pp. 1195-1208, 1982.

[2] C.L. Nikias and M.R. Raghuveer. "Bispectrum Estimation: A Digital Signal Processing Framework". *Proceedings of the IEEE*, vol. 75(7):pp. 869-891, July 1984.

[3] G.B. Giannakis and J.M. Mendel. "Identification of Non-Minimum Phase Systems using Higher-Order Statistics". *IEEE Transactions on Acoustics, Speech, and Signal Processing*, vol. ASSP-37(3):pp. 360-377, March 1989.

[4] S.A. Dianat M.R. Raghuveer and G. Sundaramoorthy. "Reconstruction of Non-Minimum Phase Multidimensional Signals using the Bispectrum". *SPIE Conference on Visual Communication and Image Processing III*, pp.666-671, November 1988.

[5] M.P. Ekstrom and J.W. Woods. "Two Dimensional Spectral Factorization with Applications in Recursive Digital Filtering". *IEEE Transactions on Acoustics, Speech, and Signal Processing*, vol. 24:pp. 115-128, April 1976.

[6] T. Matsuoka and T.J. Ulrych. "Phase Estimation Using the Bispectrum". *Proceedings of the IEEE*, vol. 72(10):pp. 1403-1411, October 1984.

[7] H. Bartelt, A.W. Lohmann, and B. Wirnitzer. "Phase and Amplitude Recovery from Bispectra". *Applied Optics*, vol. 23:pp. 3121-3129, September 1984.

[8] A. Swami and G.B. Giannakis. "ARMA Modelling and Phase Reconstruction of Multidimensional Non-Gaussian Processes using Cumulants". *IEEE Inter. Conf. on Acoust., Speech and Sig. Proc.*, pp.729-732, April 1988.

[9] M.R. Raghuveer and S.A. Dianat. "Detection of Non-linear Phase Coupling in Multidimensional Stochastic Processes". *International Conf. on Advances in Control and Communications*, pp.729-732, October 1988.
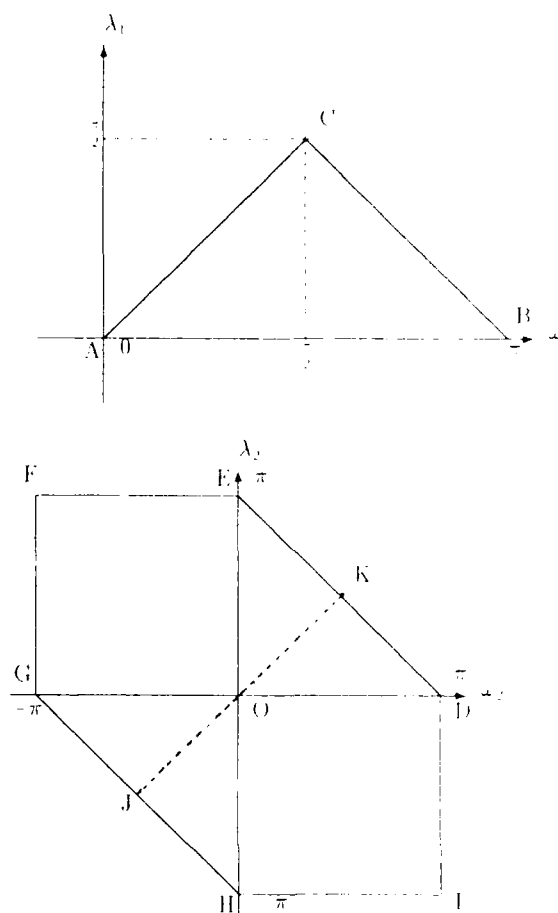
Figure 1: A sufficient region of support for the 2-D bispectrum of a real signal
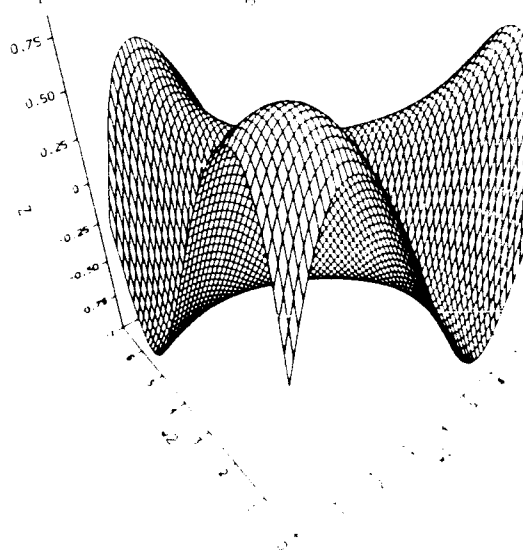

Figure 2 True phase for example 1
X-axis: Frequency in rads sample
Y-axis. Frequency in rads sample
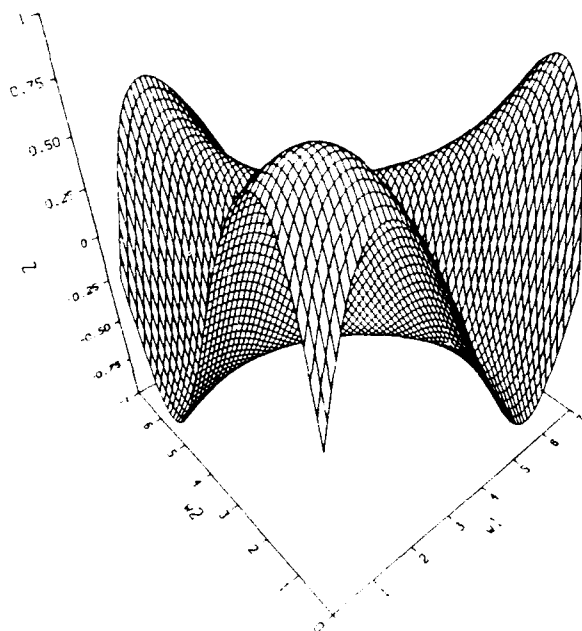Z axis. Phase in radians

Figure 3 Reconstructed phase for example 1.
X axis: Frequency in rads sample
Y axis: Frequency in rads/sample
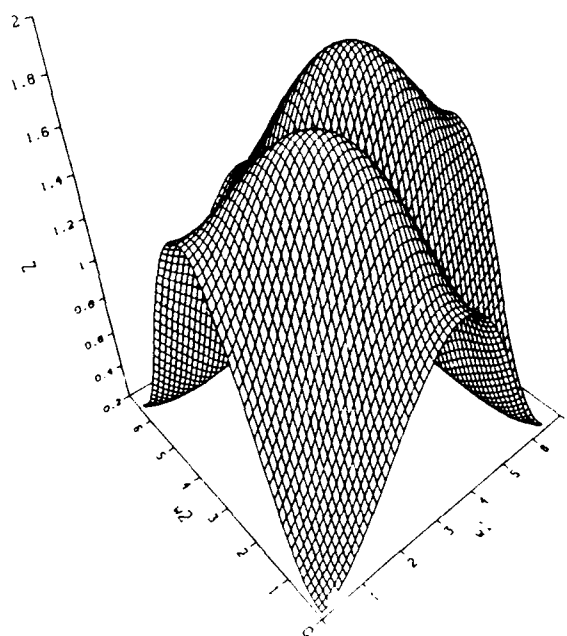Z axis: Phase in radians.

Figure 5 Reconstructed magnitude for example 1.
X-axis: Frequency in rads/sample
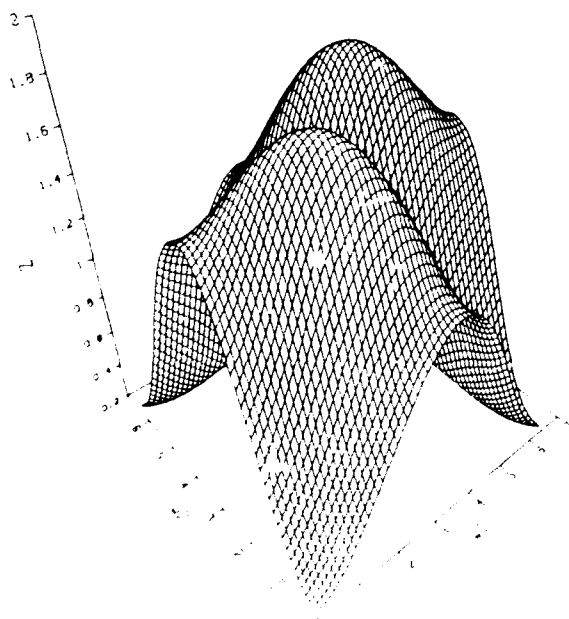Y-axis: Frequency in rads/sample

Figure 4 True magnitude for example 1
X axis: Frequency in rads sample
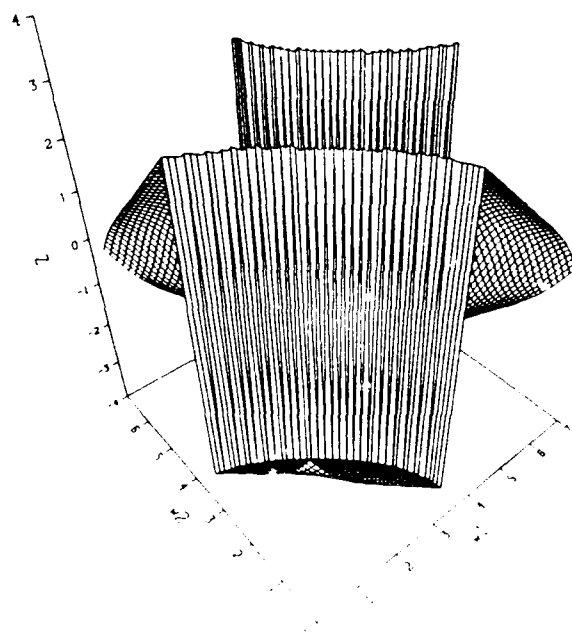Y axis: Frequency in rads sample

Figure 6 True phase for example 2.
X axis: Frequency in rads sample
Y axis: Frequency in rads sample
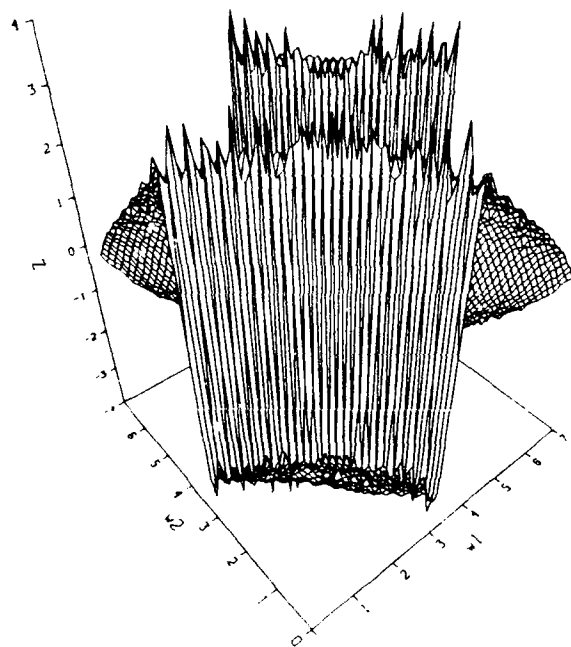Z axis: Phase in radians.

Figure 7 Reconstructed phase for example 2.
X-axis: Frequency in rads/sample
Y-axis: Frequency in rads/sample
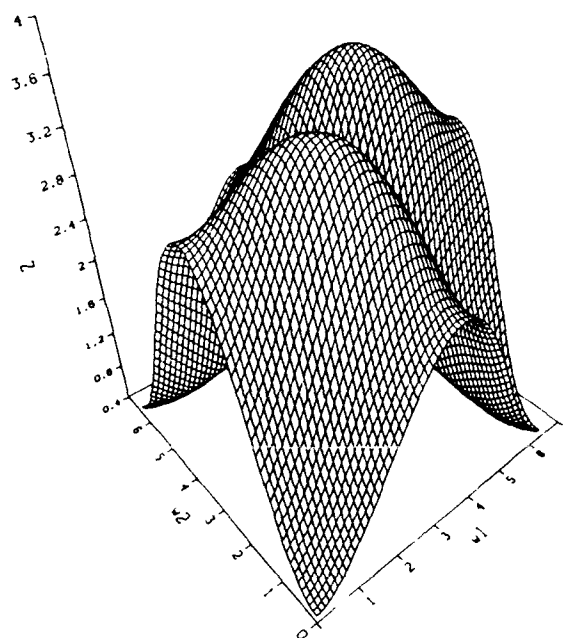Z axis: Phase in radians.

Figure 9 True magnitude for example 2.
X-axis: Frequency in rads/sample
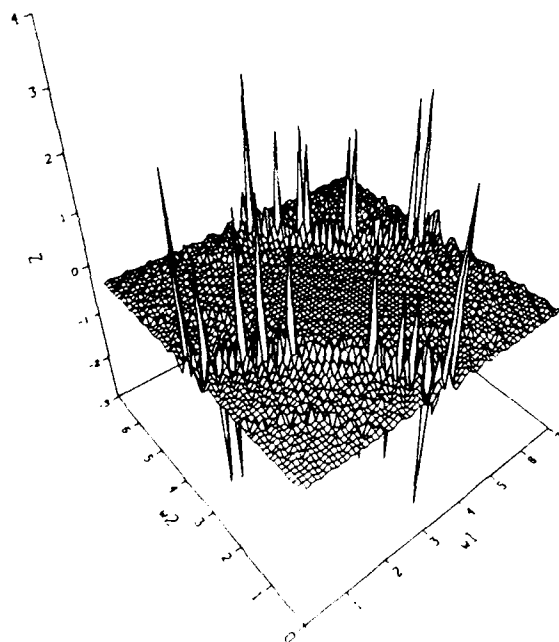Y-axis: Frequency in rads/sample

Figure 8 Reconstruction phase error for example 2.
X axis: Frequency in rads/sample
Y axis: Frequency in rads/sample
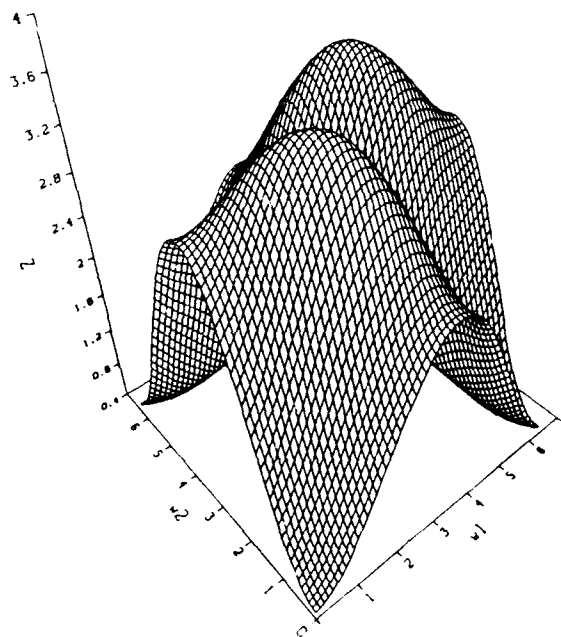Z axis: Phase in radians.

Figure 10 Reconstructed magnitude for example 2.
X-axis: Frequency in rads/sample
Y-axis: Frequency in rads/sample

3-D VELOCITY FIELD TOMOGRAPHY USING MULTIPLE PLANE DETECTORS
AND HIGH ORDER CORRELATION ANALYSIS

Kyung-Young JHANG and Takuso SATO

The Graduate School at Nagatsuta, Tokyo Institute of Technology,

Yokohama-shi, Japan

ABSTRACT

A new method for direct measurement of 3-D velocity field by using multiple plane detectors and corresponding high order cross-correlation analysis is proposed and the usefulness of this method is confirmed by preliminary experiments using 4.5 MHz ultrasonic wave system in a water tank.

INTRODUCTION

The conventional three basic means to measure the fluid flows are, i) Doppler velocimetry, which has been extensively used although it relies on the presence of some kinds of seeds in the flow, ii) the time-of-flight velocimetry which measures the average velocity between two detectors and, iii) the cross-correlation velocimetry which measures also the average velocity crossing the beams among the detectors by using random disturbances in the flow [1],[2],[3].

Recently, several devices have been developed for the measurement of 2-D velocity field which are based on the above techniques in connection with the tomographic reconstruction or scanning of the detectors [4],[5],[6]. As for 3-D velocity field measurement, however, only the scanning of these 2-D systems has been shown [7]. But, in practice, it becomes very complicated and takes quite a lot of time.

In this paper, a new method for direct measurement of 3-D velocity field by using multiple plane detector and corresponding high order cross-correlation analysis is proposed. In this method, the information about the velocity field is detected by multiple plane detectors, and its 3-D structure is reconstructed by applying corresponding high order cross-correlation analysis for them. Preliminary experiments using 4.5 MHz ultrasonic wave system in a water tank were carried out in order to confirm the usefulness of this method. In the following, the principles of the proposed method and obtained results are shown.

PRINCIPLES

First, let us consider stationary liquid streams through thin pipes as is shown in Fig.1a. In this case, parameters required to identify each stream are the velocity vector and position on a plane. We assume that the flow contains many small seeds such as bubbles as the source of the tagging signal. The required tagging signals, however, may also be generated by turbulent eddies and they will be sufficiently similar to be recognized by our correlation analysis to detect the delay time provided that the two stream detectors are arranged reasonably close.

Now we use six plane detectors (PD$_1$, PD$_2$,.., PD$_6$) which are arranged along $x=0$, $x=x_1$, $z=(x-x_2)\tan\beta$, $z=(x-x_3)\tan\gamma$, $y=(x-x_4)\tan\phi$, $y=(x-x_5)\tan\theta$, respectively, as is shown in Fig.1, where $0<x_1<x_2<x_3<x_4<x_5$ and $0<\beta<\pi/2$, $0<\phi<\pi/2$. They detect tagging signals generated over them as follows,

$$a_i(t) = \iint_{S_i} s_i(y_i, z_i, t)\, dS_i , \quad (i=1,2,....,6)$$

$$(1)$$

where $s_i(y_i, z_i, t)$ is the fluctuations (amplitude or phase) at (y_i, z_i) on the surface of i-th plane detector.

Then the six-th order moment function $m_6(\tau_1, \tau_2, ..., \tau_5)$ of the detected signals is derived,

$$m_6(\tau_1, \tau_2, ..., \tau_5) = \frac{1}{T} \int_0^T a_1(t) \cdot a_2(t+\tau_1) \cdot a_3(t+\tau_2) \cdots a_6(t+\tau_5)\, dt$$

$$(2)$$

where $\tau_1,...$ is the correlation time.

Now if the fluctuations along a stream has δ-function-like-moment functions up to sixth-order one, then it will give a corresponding peak in the sixth-order moment space of which coordinates are proportional to passing distances of the stream between the first detector and the others. Hence the stream can be reconstructed by finding its parameters from the coordinates of the peak observed in connection with the arrangement of the detectors. If, for instance, there are two streams of which velocities and directions are the same but their positions are different, then the relation among the delay times and the stream path lines becomes as is shown in Fig.1b and they will be distinguishable in the sixth-order moment space, because they have different distances between detectors due to the different inclinations of the detectors.

Actually, when a stream has the velocity vector w ($= v_x \mathbf{i} + v_y \mathbf{j} + v_z \mathbf{k}$) and position r ($= y_1 \mathbf{j} + z_1 \mathbf{k}$) on the plane $x=0$, the relations among the coordinates of the peak in the moment space (τ_1, τ_2,...,τ_5) and the parameters which define the stream are given as follows (the details of the derivation are omitted),

$$y_1 = x_1 \cdot (\tau_4 / \tau_1) \cdot (\tan \psi - \tan \theta_y) - x_4 \tan \psi \tag{3}$$

$$z_1 = x_1 \cdot (\tau_2 / \tau_1) \cdot (\tan \beta - \tan \theta_z) - x_2 \tan \beta \tag{4}$$

$$v_x = |W| \cos \theta_z' \cos \theta_y , \quad v_y = |W| \cos \theta_z' \sin \theta_y , \quad v_z = |W| \sin \theta_z' \tag{5}$$

where,

$$|W| = x_1 \sqrt{1 + \tan^2 \theta_y + \tan^2 \theta_z} \Big/ \tau_1 \tag{6}$$

$$\theta_y = \tan^{-1} \left\{ (\tau_5 \tan \phi - \tau_4 \tan \psi) / (\tau_5 - \tau_4) + I_2 / x_1 \cdot \tau_1 / (\tau_5 - \tau_4) \right\} \tag{7}$$

$$\theta_z = \tan^{-1} \left\{ (\tau_3 \tan \gamma - \tau_2 \tan \beta) / (\tau_3 - \tau_2) + I_1 / x_1 \cdot \tau_1 / (\tau_3 - \tau_2) \right\} \tag{8}$$

$$\theta_z' = \tan^{-1} (\tan \theta_z \cos \theta_y) \tag{9}$$

where,

$$I_1 = x_2 \tan \beta - x_3 \tan \gamma \tag{10}$$

$$I_2 = x_4 \tan \psi - x_5 \tan \phi \tag{11}$$
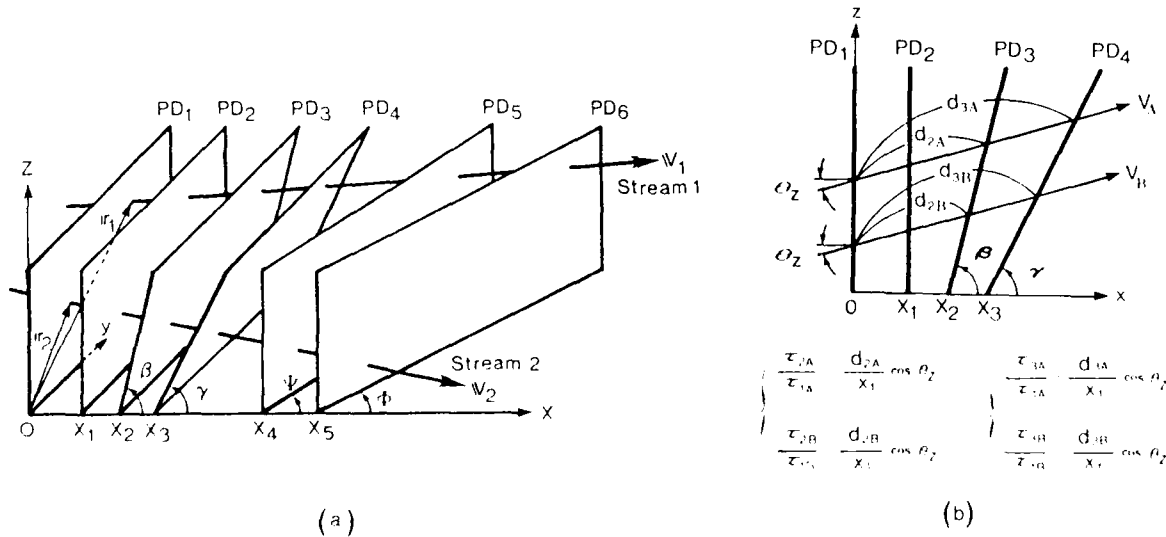

(a)

(b)

Fig. 1 The arrangement of plane detectors.

Now, when the flow field consists of many streams, each stream path lines can be reconstructed one by one from the corresponding peaks in the sixth-order moment space and the whole 3-D velocity field will be reconstructed.

In this method the information about the velocity field is detected as accumulated ones by the plane detectors just like the projections in the conventional X-ray tomography, and the 3-D structure is reconstructed by applying the high order cross-correlation analysis for the detected signals, hence, it may be said that it is a kind of tomographic reconstruction process combined with high order correlation analysis.

EXPERIMENTAL SETUPS AND RESULTS

System Construction and Signal Processings

Preliminary experiments using 4.5 MHz ultrasonic wave system in a water tank were carried out in order to confirm the usefulness of this method.

Fig.2 shows the constructed experimental system and the procedure of the signal processing. The specifications of the measuring system used in the experiment are : $x_1 = 30$, $x_2 = 60$, $x_3 = 100$, $x_4 = 140$, $x_5 = 160$, $w = 80$, $L = 100$ (mm), and $\beta = 69$, $\gamma = 57$, $\psi = 70$, $\phi = 60$ (deg). The thin plane detectors were constructed by combining proper acrylic cylindrical lenses as is shown in Fig.3. The region over L is used as the plane detector. Independent streams, for instance, were generated by passing water that was sparsely contaminated with air bubbles through thin acrylic tubes.

The detected signals were phase demodulated and passed through a low pass filter of cutoff frequency 10kHz. The sampling time of the A/D conversion was setted 1 msec. In the computer, high order correlation analysis was carried out. The estimation errors of the parameters due to the data sampling time are within ± 1.5 % as for the value of velocity up to 1.5 m/s and ± 5 % as for the positions. In the parameter estimation we neglected the time of flight of the ultrasonic wave along each path on the plane detector because fairly slow streams were used in the experiments compared with the sound speed.
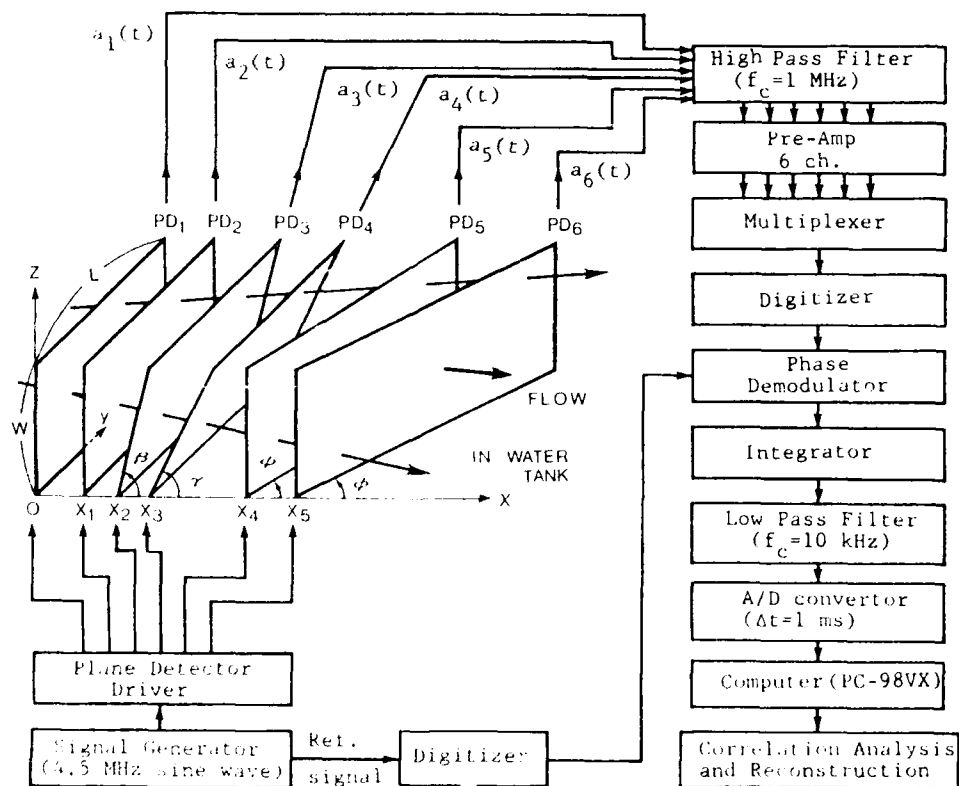

Fig.2 Schematic of the experimental set-up and the flow diagram of the signal processing.

An example of phase demodulated signals and its auto-correlation function of the plane detectors when a stream exists is shown in Fig.4. The signal has a lot of impulse-like variations and its auto-correlation has a sufficiently δ-function-like form. The sign of the variations, however, may be both positive and negative, hence their odd order moments may become to be zero. In order to avoid this, the absolute values of the variations were used so that δ-function-like moment function can be obtained for any order.

Then, the sixth-order correlation analysis was carried out and the peaks were found. Actually, the calculation time is reduced by adopting the following procedure; first, second-order moment functions for lag times τ_1, τ_2, τ_3, τ_4, τ_5 were calculated and peaks are obtained, then the sixth-order moment function was calculated for the combinations of those peaks and real peaks in the sixth-order moment space were picked up.
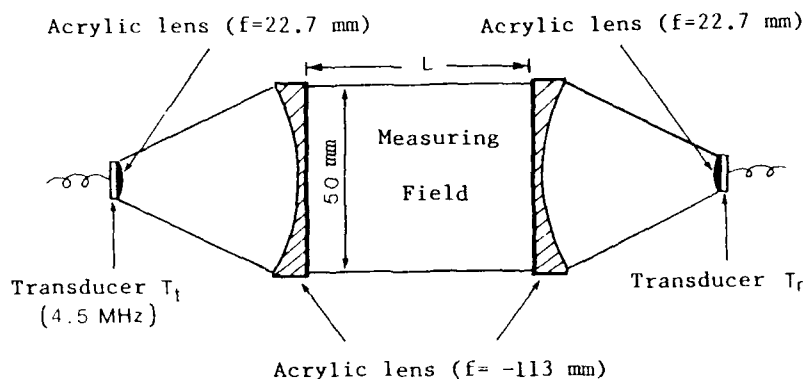

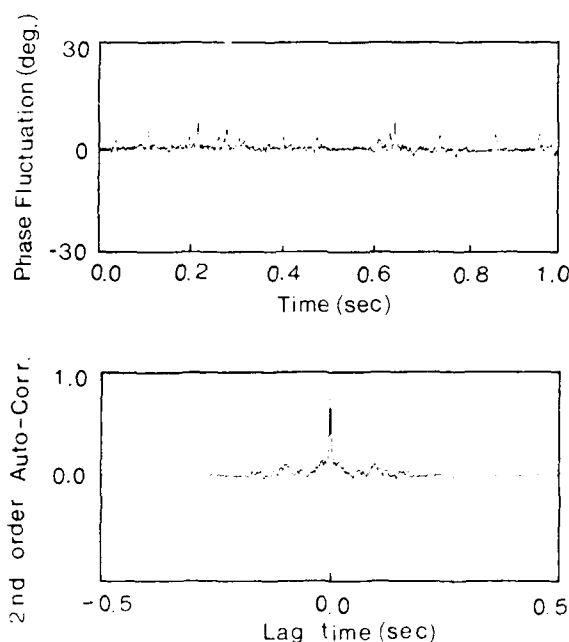Fig. 3 The concrete construction of the ultrasonic plane detector.

Fig. 4 An example of sampled time data of the phase fluctuation from one of the plane detectors when a stream exists and its auto-correlation.

First, as an example of velocity field which consists of two streams of opposite directions through a thin pipe of 6mm diameter is set as is shown in Fig.5a. From the correlation analysis of the observed signals two peaks could be found in the sixth-order moment space at P_1 (τ_1=21, τ_2= 49, τ_3=86, τ_4=133, τ_5=181 msec) and P_2 (τ_1=-21, τ_2=-49, τ_3=-79, τ_4= -133, τ_5=-180 msec). Fig.6 shows a section of the observed sixth-order moment function. From these peaks parameters of the velocity field were estimated according to the proposed process. The result is shown in Fig.5b and Table 1. They show quite good agreement with the given ones. As an another example, a laminar-like flow in a pipe is observed by increasing the diameter of the pipe to 30mm as is shown in Fig.7a. Where, the average velocity across the cross section of the pipe is 0.5 m/s. The result is shown in Fig.7b. It shows proper velocity result over the cross section of the pipe. We can observe higher velocity around the center of the pipe.
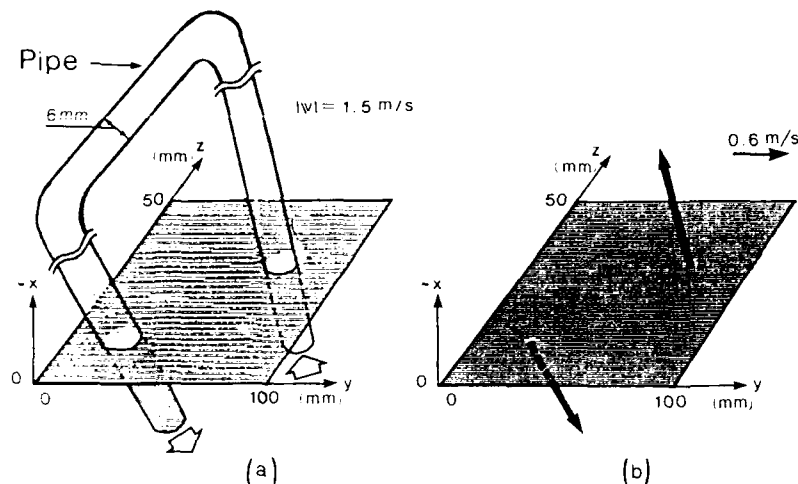

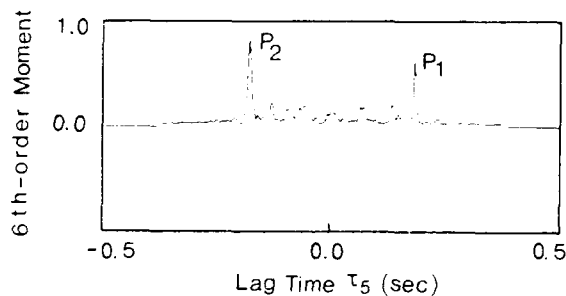Fig. 5 (a) Given stream lines and (b) reconstructed ones on the plane x=0.

Fig. 6 A sectional view of the observed sixth-order moment function.

Table 1. The given parameters of two streams (in the brackets) and the estimated ones.

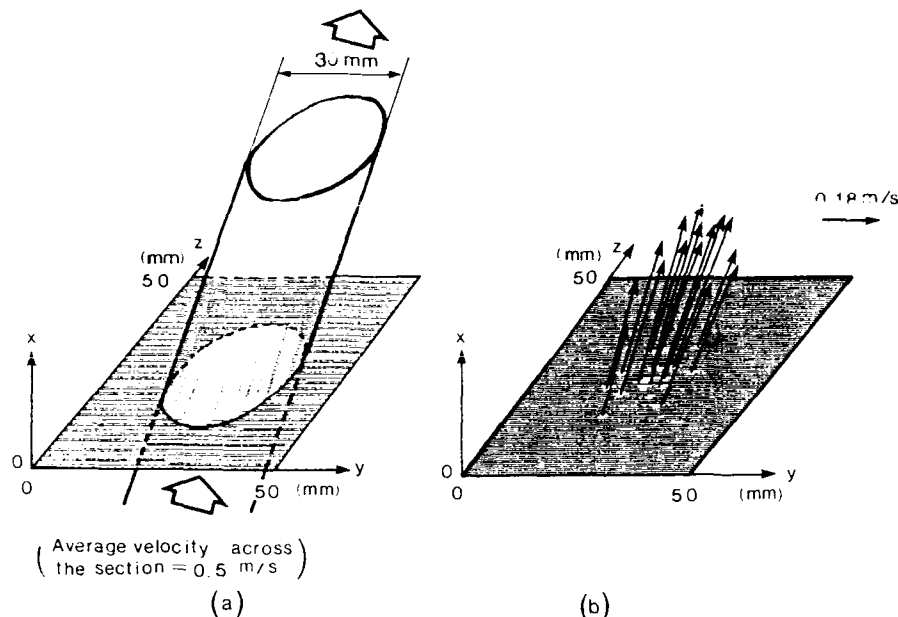| stream	1	2
velocity v (m/s)	1.43 $\mathbf{i}$ + 0.53 $\mathbf{j}$ + 0.25 $\mathbf{k}$ (1.39 $\mathbf{i}$ + 0.51 $\mathbf{j}$ + 0.25 $\mathbf{k}$)	-1.43 $\mathbf{i}$ - 0.07 $\mathbf{j}$ + 0.21 $\mathbf{k}$ (-1.48 $\mathbf{i}$ - 0.08 $\mathbf{j}$ + 0.21 $\mathbf{k}$)
position r (mm)	1.45 $\mathbf{j}$ + 1.39 $\mathbf{k}$ (1.50 $\mathbf{j}$ + 1.40 $\mathbf{k}$)	2.51 $\mathbf{j}$ + 3.63 $\mathbf{k}$ (2.50 $\mathbf{j}$ + 3.50 $\mathbf{k}$)

Fig. 7 (a) Given pipe flow and (b) reconstructed velocity field.

CONCLUSIONS

A new tomographic 3-dimensional velocity field reconstruction method which uses multiple ultrasonic plane detectors and high order correlation analysis was proposed. Concrete algorithms of the velocity field reconstruction was shown and their validity and usefulness were demonstrated by the preliminary experiments. The detailed analysis of the sensitivity of the system is under way.

REFERENCES

[1] T. S. Durrani, Laser Systems in Flow Measurement,pp.81-103 (Plenum Press, New York, 1977).
[2] W. P. Mason and R. N. Thurston, Physical Acoustics XIV,pp.407-516 (Academic Press, New York, 1979).
[3] M. S. Beck and A. Plaskowcki, Cross-Correlation Flowmeters-their Design and Application (Adam hilger, Bristol, 1987).
[4] W. H. Munk and C. Wunsch, " UP/DOWN Resolution in Ocean Acoustic Tomography," Deep-Sea Res. Vol.29(1)A,pp. 1415-1436:1982.
[5] T. Cato and M. Chiraki, " Tomographic Observation of Flow in a Water Tank," J.Acoust.Soc.Am. Vol.76, pp.1427-1432:1984.
[6] K. Y. Jhang and T. Cato, " Flow velocity Field Tomography Using Multiple Ultrasonic Beam Detectors and High order Correlation Analysis", Book of Abstracts in the 17th International Symposium on Acoustical Imaging, pp.106:1988.
[7] B. Snyder and L. Hesselink, " Measurement of Mixing Fluid Flows with Optical Tomography", Opt.Lett. 13, pp.87-89:1988.

Object Reconstruction Using
Third and Fourth Order Intensity Correlations

A. S. Marathay and Y. Hu

Optical Sciences Certer, University of Arizona, Tucson, AZ 95721

Paul S. Idell

Air Force Weapons Laboratory, Kirtland Air Force Base, NM 87117

1. INTRODUCTION

ABSTRACT

A phase retrieval method[1] using third and fourth order intensity correlations is employed to reconstruct the object. To study the effectiveness of the reconstruction technique with estimates of intensity correlations from measured data, we have developed a computer simulation of the light intensity measurement process, In this simulation, the speckle patterns of the object are generated and third and fourth order intensity correlation estimates are formed and used to recover complex spatial coherence function maps. Combining this simulation with the reconstruction procedure we have studied the behavior and efficiency of the end-to-end image reconstruction technique.

Two-point correlations of light intensity, as pioneered by Hanbury-Brown and Twiss[2], provide information about the modulus of the spatial coherence function of light received from a noncoherently radiating object. However the phase associated with the complex coherence function is lost, making unique recovery of the source map problematic. Third and fourth order correlations of intensity have recently been shown[1] to provide sufficient information to recostruct the real and imaginary parts of the spatial coherence function. With a complete mapping of the complex spatial coherence function produced in this way, a unique two-dimensional image of the original noncoherent object may be reconstructed by inverse Fourier transformation of the coherence function map.

This procedure deals with measurements in the pupil plane, in contrast with the focal plane measurement used by Weigelt et al[3]. Also our procedure attempts to reconstrust the phase explicitly as opposed to the interative procedure used by Fienup[4] and others.

After a brief review of the reconstruction procedure outlined in Reference 1, we describe computer simulation of an experiment set-up to generate the speckle patterns that is reflected from a coherently illuminated object. This experiment is described in detail in Reference 5. The third and fourth order correlation functions can be computed by ensamble averaging the speckle frames. To implement the reconstruction procedure we introduced a computer configuration to restore the complex spatial coherence function that is a 32x32 discrete two-dimensional map. In the configuration, we solved the real and imaginary parts of a unit cell, and then solved for the whole two-dimensional map from the nearest to the farther site, point by point.

2. THE PHASE RETRIEVAL ALGORITHM

If the wave amplitude of light sourse obeys Gaussian statistics, the third and fourth correlations of the intensity fluctuations ΔI from the mean are given by

$$A_{abh} = g_{abh} \cos(\phi_{ab} + \phi_{bh} + \phi_{ha}) \qquad (1)$$

$$\begin{aligned} B_{abch} = &g_{abch} \cos(\phi_{ab} + \phi_{bc} + \phi_{ch} + \phi_{ha}) \\ &+ g_{acbh} \cos(\phi_{ac} + \phi_{cb} + \phi_{bh} + \phi_{ha}) \\ &+ g_{abhc} \cos(\phi_{ab} + \phi_{bh} + \phi_{hc} + \phi_{ca}) \qquad (2) \end{aligned}$$

The symbols A_{abh} and B_{abch} are related to the third and fourth order correlations respectively. $g_{abh} \equiv |\gamma_{ab}||\gamma_{bh}||\gamma_{ha}|$ and the g_{abch}, etc., are defined in a similar way. The subscripts a, b, c, h stand for the 4 points of discrete spatial coherence function map, as in Fig. 1, and ϕ_{ab} is the phase of two points of the map. In these equations the $\cos\phi_{ah}$ and $\sin\phi_{ah}$ are unkown. The simultaneous equations resulting from the pair of Equations (1)-(2) are

$$\begin{bmatrix} A_{abh} \\ B'_{abch} \end{bmatrix} = \begin{bmatrix} M_{11} & M_{12} \\ M_{21} & M_{22} \end{bmatrix} \begin{bmatrix} \cos\phi_{ah} \\ \sin\phi_{ah} \end{bmatrix}. \qquad (3)$$

The symbols not used in the previous equations are defined by

$$\begin{aligned} B'_{abch} = &B_{abch} - g_{abhc} \\ &\cos(\phi_{ab} + \phi_{bh} + \phi_{hc} + \phi_{ca}) \qquad (4) \end{aligned}$$

$$M_{11} = g_{abh} \cos(\phi_{ab} + \phi_{bh}) \qquad (5)$$

$$M_{12} = g_{abh} \sin(\phi_{ab} + \phi_{bh}) \qquad (6)$$

$$\begin{aligned} M_{21} = &g_{abch} \cos(\phi_{ab} + \phi_{bc} + \phi_{ch}) \\ &+ g_{acbh} \sin(\phi_{ac} + \phi_{cb} + \phi_{bh}) \qquad (7) \end{aligned}$$

$$\begin{aligned} M_{22} = &g_{abch} \cos(\phi_{ab} + \phi_{bc} + \phi_{ch}) \\ &+ g_{acbh} \sin(\phi_{ac} + \phi_{cb} + \phi_{bh}) \qquad (8) \end{aligned}$$

These quantities are known either through measurement or because they relate to the unit cell. Hence the equations may be solved for the cosine and sine of ϕ_{ah}.
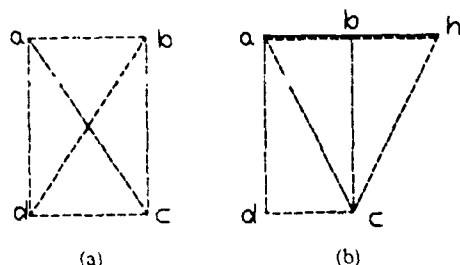

(a)   (b)

Fig. 1 (a) Unit cell. (b) The configuration used to solve for phase ϕ_{ah}

3. SIMULATION OF THE LIGHT INTENSITY MEASUREMENT

I.. order to test the object reconstruction procedure, we simulated a light intensity measurement process. In this experiment the object is attached to the mirror and illuminated by a laser. At the detector we obtain the speskle pattern of the object.

To get the data of this experiment we developed a computer simulation program to generate the speckle patterns of the object. Our amplitude object A_{ob} is a two valued pattern consisting of 32x32 discrete points as shown in Fig. 2. We add the random phase ϕ that is uniformiy distributed in $[-\pi, \pi]$ to the amplitude object points at discrete locations (x_i, y_j) of the rectangular grid. The object formed is given by

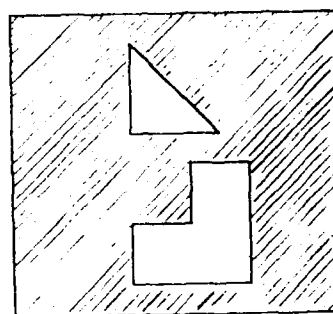$$A_{ob}{}^k(x_i, y_j) = A_{ob}(x_i, y_j)e^{i\phi(x_i, y_j)} \qquad (9)$$

Fig. 2 The object

The subscript k labels the random number seed used in generating the kth speckle patterns. Here k=1,2,....,N. That means we have generated n speckle frames. Fourier transforming the object,

$$s_k = F\{A_{ob}{}^k(x_i y_j)\} \qquad (10)$$

and taking the squared magnitude, we get the speckle frames

$$S_k = |s_k|^2, \quad k = 1,2,....,N \qquad (11)$$

The flowchart of the simulation program is shown in Fig. 3. The intensity of the speckle image generated in this way should obey the circular-complex Gaussian random distribution.

Once the bank of N speckle frames is available, we can derive the second, third and fourth order intensity correlations by averaging over the speckle frames. To compute the phase of a point relative to the origin, say from h to a, we only need 4 points a, b, c and h. So it is not necesary to

126

compute the whole set of the higher order intensity correlation functions. We only need to correlate 3 points, a, b and h, for the third, and 4 points, a, b, c and h, for the fourth order correlation functions as shown in Fig. 1. In this way we can save significant computing time and memory space, and have enough information to retrieve the phase in our problem.
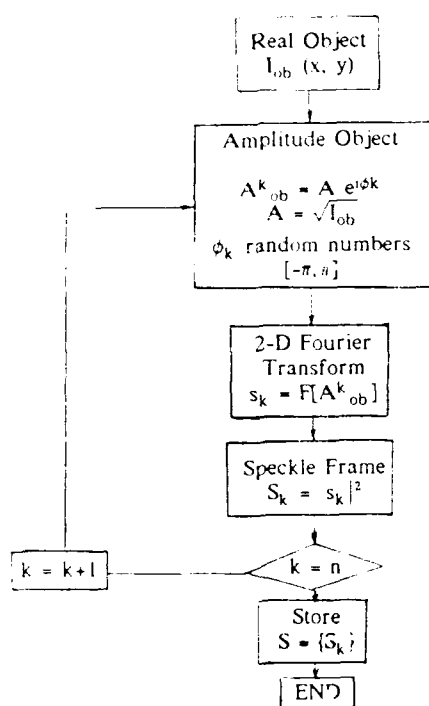

Figure 3. Flow Chart for simulation of speckle frames

4. PHASE RECONSTRUCTION PROCEDURE

Knowing the third and fourth order correlation functions we can use Eq. (1) and (2) to compute the phases of the intensity coherence functions. The configration we used is shown in Fig. 4. We start from the unit cell originated at zero points, and compute the phase from near points to farther points. So for each point we use only the points that were previosly computed.

Only the first quadrant of the map is shown in Fig. 4. The second quadrant can be calculated in the same way, and then the third and fourth quadrants can be obtained by the symmetry relations of the coherence function

$$\Gamma(x_{12}, y_{12}) = \Gamma^*(-x_{12}, -y_{12})$$
$$\Gamma(-x_{12}, y_{12}) = \Gamma^*(x_{12}, -y_{12}) \tag{12}$$

To reconstruct the object we only need complex intensity function. So, instead of solving for the set of phases, we solve for the real and imaginary parts of the coherence function. Thus Eq. (3) can be modified to

$$\begin{bmatrix} A_{abh} \\ B'_{abch} \end{bmatrix} = \begin{bmatrix} M'_{11} & M'_{12} \\ M'_{21} & M'_{22} \end{bmatrix} \begin{bmatrix} Re(\gamma_{ha}) \\ Im(\gamma_{ha}) \end{bmatrix} \tag{13}$$

where

$$M'_{11} = Re(\gamma_{ab})Re(\gamma_{bh}) - Im(\gamma_{ab})Im(\gamma_{bh})$$

$$M'_{12} = Re(\gamma_{ab})Im(\gamma_{bh}) - Re(\gamma_{bh})Im(\gamma_{ab}),$$

and M'_{21} and M'_{22} can be written in a similar way. The solutions reduces the number of steps in the computation and solve some problems in the calculation of the phases.
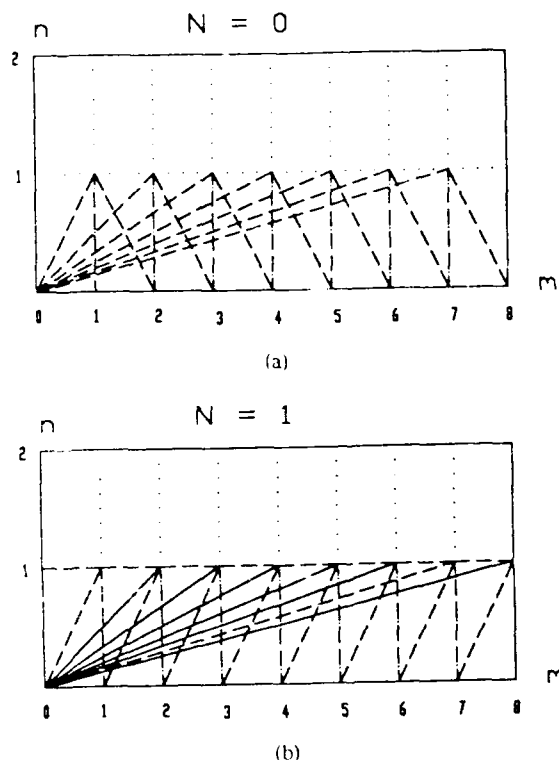
Fig. 4 The computing procedure for first quadrant of the intensity of coherence function. (a) The first line. (b) The second line

5. THE RECONSTRUCTED RESULTS

We reconstructed our object consisting a triangle and a coner embeded on a 32x32 zero paded array. Two thousand speckle frames are used to reconstruct the object. Fig. 5. is the reconstructed object compared with the true object. Fig. 6 shows the error maps recostructed coherence function. The error is defined by

$$E = |TV - CV| \qquad (14)$$

where TV is the true value and CV is the computed value at every sample point.

There are two main sources of error for this method. One is accumulated by the computer. For a point that is far away from the origin, it will take many computing steps to get there. When the errors are accumulated to a certain value, the simultaneous equations become ill-conditioned and we get wrong solutions of the phase. They are the peaks in the error maps as shown in Fig. 6. This kind of errors resembles noise with high frequencies. We have simply used a low-pass filter to suppress this noise.
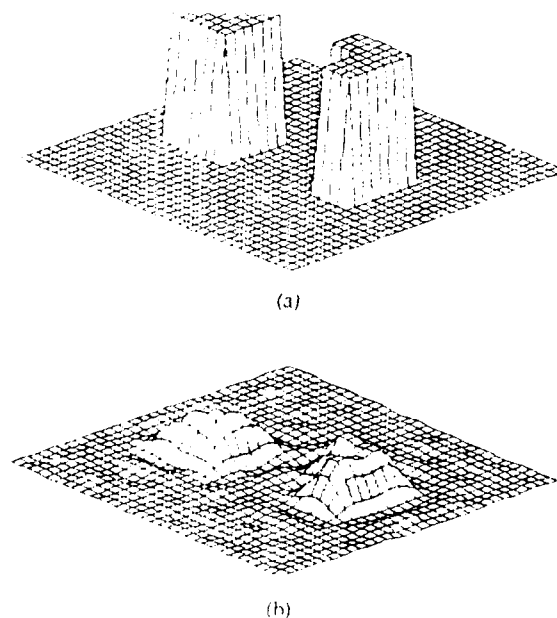

(a)

(b)

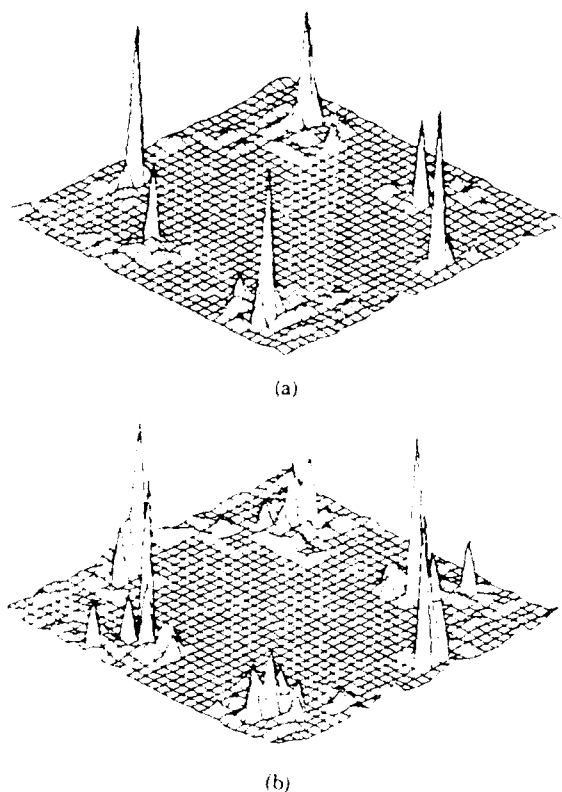Fig. 5 (a) True object. (b) Reconstructed object.

(a)

(b)

Fig. 6 Error maps of the reconstructed intensity coherence function. (a) Real part. (b) Imaginary part

Another kind of error depends on how accurate one can get the phases of the unit cell. The smaller the subdivided unit cell, the more accurate will be the phases of the unit cell. In this work we simply assume that the phases in the unit cell are known. How to get the phases of the unit cell is the objective of this method.

The statistical characteristics of the speckle pattern is another factor that affects the quality of the restored object. This can be avoided by using more speckle patterns

The next steps in this project are to improve the method and try to minimize the errors so that it is more efficient.

REFERENCES

1. A. S. Marathay, "Phase Function of Spatial Coherence from Multiple Intensity Correlations," in Advanced Technology Telescopes. Proc. Soc. Photo-Opt. Instrum. Volume 628 (1986).

2. R. Hanbury-Brown, The Intensity Interfrometer, Taylor and Francis, London (1974).

3. G. P. Weigelt and B. Wirnitzer, "Image Recostruction by the Speckle-Masking Method," Opt. Lett. 8, 389 (1983).

4. J. R. Fienup, "Phase Retrieval Algorithms: A Comparison," Applied Optics 15, 2758 (1982).

5. Paul S. Idell et al, "Image Synthesis from Nonimaged Laser-Speckle Patterns Experimental Verification," To be published in Optical Letters.

BISPECTRUM IMAGING THROUGH TURBULENCE

J C Dainty

Blackett Laboratory, Imperial College, London SW7 2BZ, UK

Abstract

This paper reviews some aspects of bispectral imaging through atmospheric turbulence. Particular attention is given to the effect of turbulence on the bispectrum, signal-to-noise ratio and algorithms for data that is photon-limited and two dimensional.

1 Background

Atmospheric turbulence limits the resolution of long exposure optical imaging in astronomy and other applications. For example, the diffraction-limited angular resolution of a 5m diameter telescope is approximately 0.025 arc seconds (in the visible), whereas in practice turbulence limits the resolution to ≈ 1.0 arc seconds (i.e. a 40 times loss in resolution). In effect, a large ground-based optical telescope has the same resolution as a 10cm diameter amateur telescope because of atmospheric turbulence.

In 1970, A Labeyrie invented the technique of *speckle interferometry*, in which short-exposure frames that "freeze" the turbulence (≈ 10ms exposure time) are recorded [1–3]. The short exposure frames have similarities to laboratory-generated laser speckle patterns; in particular, the average speckle size corresponds to that of the diffraction-limited Airy disc of the telescope. This gives the hope that an appropriate statistical analysis of the the short exposure data will give diffraction-limited information about the object.

Labeyrie proposed that the average energy spectrum of the image be calculated — if $i(\mathbf{x})$ denotes the instantaneous image intensity and $I(\mathbf{u})$ denotes its Fourier transform, with $o(\mathbf{x})$ and $O(\mathbf{u})$ denoting the object intensity and its Fourier transform, then the average energy spectrum of the image is related to that of the object by

$$<|I(\mathbf{u})|^2> \quad = \quad |O(\mathbf{u})|^2 \; <|T(\mathbf{u})|^2> \qquad (1)$$

or

$$<I^{(2)}(\mathbf{u})> \quad = \quad O^{(2)}(\mathbf{u}) \; <T^{(2)}(\mathbf{u})> \;.$$

where $<|T(\mathbf{u})|^2>$ is the speckle transfer function (note that this is a transfer function of energy spectra). It can be shown [2,3] that the speckle transfer function is non-zero up to the diffraction-limit of the optical system and therefore it is possible to obtain an estimate of the energy spectrum of the object, $|O(\mathbf{u})|^2$, by deconvolution. Although the general theory is written in terms of wave intensity, the results are valid for images consisting of detected photons and in practice photon correlation techniques are used to estimate, for example, the image energy spectrum. Under these circumstances, information about $|O(\mathbf{u})|^2$ can be extracted at photons rates as low as one detected photon per frame on average.

The problem with energy spectrum analysis, Eq (1), is that it is not possible, in general, to recover a function uniquely from its energy spectrum (or Fourier modulus) [4]. Various algorithms exist and

work with partial success, but one is never assured that the solution is unique and in any case the convergence properties of the algorithms in the presence of noise are uncertain. However, one *can* recover a function essentially uniquely from its bispectrum and this is the basis of bispectral imaging through turbulence.

2   Bispectral Imaging

2.1   Basic Method

Bispectrum imaging was first suggested by Weigelt under the name of "speckle masking" [5] and subsequently has been developed extensively by Weigelt and colleagues [6-10]. The instantaneous bispectrum is defined as

$$I^{(3)}(\mathbf{u}_1, \mathbf{u}_2) = I(\mathbf{u}_1) I(\mathbf{u}_2) I^*(\mathbf{u}_1 + \mathbf{u}_2) \qquad (2)$$

where $I(\mathbf{u})$ is the Fourier transform of the image intensity. In Eq.(2), $\mathbf{u}_1$ and $\mathbf{u}_2$ are two dimensional vectors and thus $I^{(3)}(\mathbf{u}_1, \mathbf{u}_2)$ is a four dimensional function. Since typical image sizes may be 512x512, it is clear that there are potential problems of computation time and storage when dealing with the bispectrum, even allowing for the inherent 12-fold redundancy of the bispectrum of a real function (such as the optical intensity). It is fairly straightforward to show that the average bispectrum of the image is related to that of the object by

$$<I^{(3)}(\mathbf{u}_1, \mathbf{u}_2)> = O^{(3)}(\mathbf{u}_1, \mathbf{u}_2) <T^{(3)}(\mathbf{u}_1, \mathbf{u}_2)> \qquad (3)$$

where $<T^{(3)}(\mathbf{u}_1, \mathbf{u}_2)>$ is the bispectrum transfer function of the imaging process.

The behaviour of $<T^{(3)}(\mathbf{u}_1, \mathbf{u}_2)>$ provides the key to bispectrum imaging. Figure 1 shows a schematic of the modulus of this function for one dimensional variables $\mathbf{u}_1$ and $\mathbf{u}_2$ — in fact, only a small band around the axes and a diagonal has a significant value and this has implications for the amount of computation and storage required. Theory also predicts that the phase of the bispectrum transfer function is approximately zero, implying that the
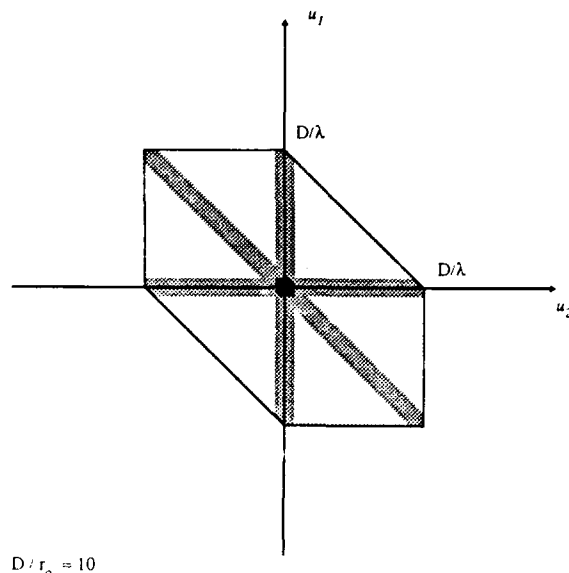

Figure 1

phase of the image bispectrum equals that of the object bispectrum. Figures 2(a) and (b) show the results of Monte Carlo calculations of the modulus and phase of the bispectrum transfer function, broadly confirming the theoretical prediction [11]. The significance of this is that the number of useful bispectrum values that need to be calculated is typically on the order of 4—8 per frequency point.

2.2   Signal-to-noise Ratio

Because the significant parts of the bispectrum lie close to the axes, i.e. $\mathbf{u}_1 \approx 0$ or $\mathbf{u}_2 \approx 0$ or $\mathbf{u}_1 \approx \mathbf{u}_2$, the modulus of the bispectrum is similar in value to the modulus of the energy spectrum and thus the signal to noise ratio of the bispectrum is similar to that of the energy spectrum. Detailed calculations of the signal-to-noise ratio of the energy spectrum and bispectrum have been made [10,12,13]. It is difficult to draw general conclusions, because the result is object-dependent. However, in broad terms, if the original data is sufficient to determine a reasonable estimate of the energy spectrum of the object, then it should be sufficient to provide a bispectrum of adequate quality to allow determination of an object map. Depending on object complexity, this implies photon levels anywhere between 1 and 10^3 per frame.
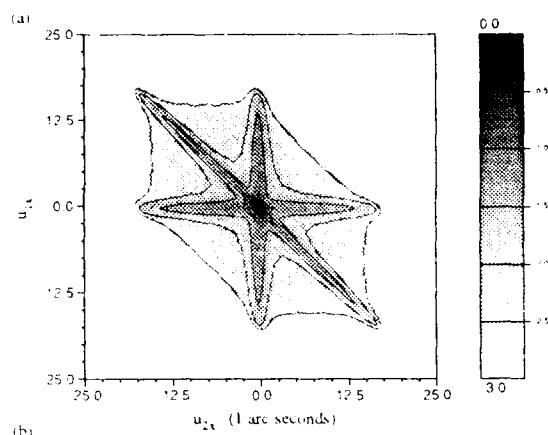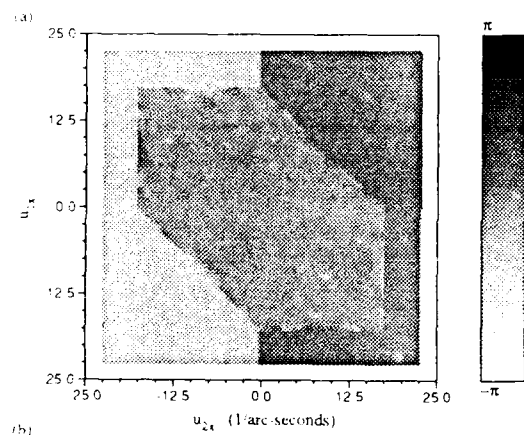
Figure 2(a)

Figure 2(b)

2.3 Algorithms

Algorithmic problems divide quite naturally into those concerned with the determination of the bispectrum from raw data and those concerned with the calculation of the object intensity from the object bispectrum.

Astronomical data is typically taken at low light level, so that an image, instead of being an array of pixels each consisting of a number of bits, consists of a list of photon (x,y) coordinates — in fact, since the whole process of turbulence is dynamic, the data set

as a whole is a list of (x,y) and time coordinates. A number of photon event detectors whose output are of this form are now available. This type of data is well-suited to photon-differencing algorithms, implemented either in the real or spectral domain [14]. In practical terms, photon differencing algorithms are most efficient on very sparse data, typically less than 100 detected photons per frame. An added feature of photon-differencing algorithms is that they allow the updating of the calculation for every photon that arrives. This has the effect of permitting a moving exposure window (rather than discrete frames of data) and yields an improvement of signal-to-noise ratio. The optimisation of the process of using time domain information is an important area of current research — this implies extending the (four-dimensional) spatial bispectrum to the time domain.

The amount of calculation necessary to compute an adequate number of bispectrum values is such that it is currently not possible to compute the bispectrum in real time. This represents a major bottleneck in the practical application of bispectrum imaging and further research, probably involving parallel algorithms is clearly necessary.

The object reconstruction problem is less onerous computationally, since it is only done once, after all the bispectra have been averaged. The method first by Weigelt is recursive: equating the phase of both sides of Eq(2) and using the fact that the phase of the bispectrum transfer function is approximately zero, we have

$$\theta(u_1,u_2) = \phi(u_1) + \phi(u_2) - \phi(u_1 + u_2) \qquad (4)$$

where $\theta(u_1,u_2)$ is the phase of the object bispectrum and $\phi(u)$ is the phase of the object spectrum. The recursive algorithm uses the values of the object phase at low frequencies, and selected values of the bispectrum phase, to calculate the phase of the object spectrum at higher frequencies. In a discrete matrix representation, the value of the phase of the object spectrum at the origin, $\phi(0)$, is zero and the value of $\phi(1)$ can also be set to zero (this means that the

reconstructed object is centred in its array). The signal-to-noise ratio of each point of the bispectrum is used as a weighting factor in this computation.

This procedure does not necessarily distribute the error in the best way in Fourier space and is not positive constrained (the object intensity is of course positive). Apart from ad hoc methods, it may be possible to enforce positivity by applying Bochner's theorem [15] and extensions of it [16,17].

Another factor which has to be taken into account is that the Fourier *modulus*, which is estimated from the energy spectrum Eq. (1), is often unreliable as it depends on accurate calibration by a point source. It may therefore be desirable to use only the Fourier phase in the reconstruction, applying a phase-only reconstruction algorithm [18].

A recently-proposed method for blind deconvolution [19] may also be applied to this problem.

3 Related Problems

The bispectrum is useful for imaging in astronomy because, unlike the average image, the average bispectrum is not degraded on atmospheric propagation. (The same is true of the energy spectrum but one cannot reliably reconstruct the object from its energy spectrum.) There are other situations in imaging where this is also the case, in particular the imaging a randomly moving objects [20–24].

Clearly. Eq (2) for the bispectrum is invariant on translation of the image i(x), since this simply adds a linear phase term to I(u). This means that the average bispectrum of a moving object is simply equal to that of the stationary object. In this case. the whole of the bispectrum is of value in estimating the object from the image bispectrum and the signal-to-noise ratio can be high. For example, for a one-dimensional object, we have demonstrated object reconstruction at photon rates of less than one detected photon per frame on average and $\approx 10^4$

frames [21]. For two dimensional objects, photons rates of a few tens per frame are more typical. Extensions to random rotation and scale are possible through coordinate transformations.

Recently, Lohmann has proposed the application of the bispectrum to pattern recognition [25,26].

Acknowledgements

References

1   A Labeyrie, Astron Astrophys, **6**, 85-87 (1970)

2   J C Dainty in *Laser Speckle and Related Phenomena*, Ed by J C Dainty, Springer-Verlag, 2nd Edition, 1984, pp255-320

3   F Roddier, Physics Reports, **170**, 97-166 (1988)

4   J C Dainty and J R Fienup in *Image Recovery: Theory and Practice*, Ed by H Stark, Academic Press, 1987, pp231-275

5   G Weigelt, Opt Commun, **21**, 55-59 (1977)

6   A W Lohmann, G Weigelt and B Wirnitzer, Appl Optics, **22**, 4028-4037 (1983)

7   G Weigelt and B Wirnitzer, Opt Lett, **8**, 389-391 (1983)

8   A W Lohmann and B Wirnitzer, Proc IEEE, **72**, 899-901 (1984)

9   H Bartelt, A W Lohmann and B Wirnitzer, Appl Optics, **23**, 3121-3129 (1984)

10 B Wirnitzer, J Opt Soc Am, **2**, 14-21 (1985)

11 G R Ayers, Thesis, University of London, 1988.

12 J C Dainty and A H Greenaway, J Opt Soc Am, **69**, 786-790 (1979)

13 G R Ayers, M J Northcott and J C Dainty, J Opt Soc Am A, **5**, 963-985 (1988)

14 M J Northcott, G R Ayers and J C Dainty, J Opt Soc Am A, **5**, 986-992 (1988)

15 S Bochner, *Lectures on Fourier Integrals*, Princeton University Press, 1959, pp 92-95

16 J Karle and H Hauptman, Acta Cryst, **3**, 181-187 (1950)

17 D J Granrath, Opt Commun, **67**, 107-111 (1988)

18 M H Hayes, in *Image Recovery: Theory and Practice*, Ed by H Stark, Academic Press, 1987, Ch 6.

19 G R Ayers and J C Dainty, Opt Lett, **13**, 547-549 (1988)

20 H Bartelt and B Wirnitzer, Opt Commun, **53**, 13-16 (1985)

21 J C Dainty and M J Northcott, Opt Commun, **58**, 11-14 (1986)

22 A W Lohmann, Optik, **73**, 127-131 (1986)

23 A W Lohmann, Optik, **73**, 174-180 (1986)

24 R H T Bates, Optik, **76**, 23-26 (1987)

25 A W Lohmann, Optik, **78**, 117-120 (1988)

26 A W Lohmann, Appl Optics, **28**, 200-201 (1989)

APPLICATION OF EIGENSTRUCTURE BASED BISPECTRUM ESTIMATION: EEG WAVE COUPLING IN COGNITIVE TASKS

David L. Sherman and Michael D. Zoltowski
School of Electrical Engineering, Purdue University

West Lafayette, IN 47907

Abstract: An orthogonal subspace-based approach for two dimensional sinusoids can be applied to the bispectrum and the estimation of the frequencies of quadratically phase coupled sinusoids. The method determines peaks in the bispectral domain by the direct partitioning of noise and signal subspaces without the need for transfer function parametrization. It can be used for determining dominant frequencies involved in EEG alpha wave coupling.

New high resolution methods for bispectral estimation have been developed in recent years. These model based procedures rely on the estimation of system parameters for the calculation of the bispectrum [2, 3]. In cases of quadratically phase coupled sine waves in noise with a non-zero third order moment, there is a set of autoregressive parameters which represent the the trio of sine waves. The sinusoid triple is a fundamental unit of analysis for bispectral estimation as the single (pure) sine wave is for conventional spectral analysis. Using a geometric approach, we have [1] developed a method for estimating the frequencies of discrete, phase locked sinusoids in noise of 3rd order whiteness. The method is an adaptation of the MUSIC (MUltiple SIgnal Classification) method used in conventional second order spectral analysis and direction-of-arrival estimation [14]. Employing eigendecomposition, the information in a matrix containing the third order cumulant information is used to compute the signal and "noise" (orthogonal) subspaces. Traditionally, the subsequent use of rank reduction and the orthogonality of subspaces eliminates much noise from the conventional spectral estimate. For higher order cumulants, our noise subspace is conveniently free of Gaussian noise and is comprised only of noise with a non-zero third order moment.

Rank reduction methods have already been utilized for system identification and single sine wave frequency estimation using the 4th order cumulant statistics by Giannakis [3] and Swami and Mendel [8], respectively A bispectral application can be developed by considering a fully two-dimensional region of support in the cumulant domain. We build an asymptotically Hermitian block-Toeplitz matrix composed of third order cumulants of our time series. Employing a "noise" subspace-based frequency estimator, we project a two dimensional frequency kernel on the orthogonal complement subspace. The reciprocal of this projection is our frequency estimator indicating the location of a triple of phase coupled sinusoids in the bispectral domain. Our method has proven successful in providing accurate, high resolution estimates of discrete bispectra. The use of a two dimensional cumulant cut provides a direct estimate of the bispectrum without transfer function parametrization that characterizes traditional periodogram methods of higher order spectrum estimation [4]. In general, transfer function parametrizaition is implicated in higher order spectral estimation when 1-D or diagonal slices are employed.

Our method is ideally suited for time series where detection of a small number of phase coupled sinusoids is critical for its characterization. Understanding the detailed specificity of the human electroencephalogram (EEG) and its behavioral correlates requires detailed knowledge of its statistics, especially Gaussianity and linearity. Elul [5] provides information on the changes in Gaussianity during the performance of mental tasks. He does not utilize the bispectrum, but relies instead on the chi-squared "goodness of fit" test. He alludes to the need for understanding Gaussianity in terms of synchronization of individual generators, i.e., phase coupling. He remarks that when the independent generators become de-synchronized we approach Gaussianity. Regaining synchrony suggests that the governing distribution tends away from a Gaussian character.

Dumermuth, et. al. [6] provide excellent evidence of the coupling between individual frequency bands in their application of the direct FFT-based bispectral analytic methods to EEG. They found evidence of synchronization of four major waveband interactions. They detected quadratic non-linearities with signal bands that do not have appreciable spectral representation. Even with FFT-based techniques, these authors remarked about the narrowness of the bands, especially the alpha band (8-13 Hz) involved in the couplings. The sidebands displayed little or no coupling. A high resol. tion technique such as the eigenstructure method can easily show sensitivity for narrow band discrimination.

The alpha band has long been associated with non-linear interactions [13]. It may be phase locked with subharmonics (theta: 4-8 Hz) or upraharmonics (beta I: 13-20 Hz) band. Lateral asymmetries in the alpha signal production reflect functional specialization and differential activity in each side of the brain. Sensory input causes a disruption in alpha synchrony. Beyond perceptual or purely exogenous activity, a loss of power in the alpha band is often an index of cognitive function. Alpha reception is decreased in the left half of the brain during tasks that require serial processing: language skills or mathematical operations. The right side of brain when active has been linked to holistic Ge talt, parallel, and spatial skill tasks. In a complimentary fashion, alpha desychronization occurs on the right hand

side of the brain when completing cognitive functions such as mental rotation of a geometric figure 7,9,10 . Most often researchers have devised specialized power measures to indicate alpha laterality. Phase coupling among dominant sinusoids may characterize localized cerebral functional specialization in addition to conventional measures.

Eigendecomposition of the Third Order Cumulant Matrix.

To develop eigendecomposition for bispectral analysis we first state that the bispectrum is the Fourier transform of the third order cumulant or autocorrelation sequence,

$$B(\omega_1, \omega_2) = \sum \sum c(m,n) \exp{-j(\omega_1 m + \omega_2 n)}$$

where

$$c(m,n) = E\{x(k)x(k+m)x(k+n)\}$$

is the third order autocorrelation of random process $\{x(k)\}$. There is an important symmetry relation among the cumulants, namely,

$$c(m,n) = c(n-m, -m) = c(-m, n-m) = c(-n, m-n) = c(-n, m-n) = c(n,m) \tag{1}$$

The bispectrum is then a function of two frequency indices as the third order cumulant is a function of two time indices. The bispectrum can detect quadratic non-linearity among a triple of sinusoids. Three sinusoids are said to be quadratically phase coupled if one sinusoids's frequency and phase are the sum or difference of the two other sinusoids' frequencies and phases. The *power spectrum* may only indicate the presence of sinusoidal components irregardless of phase relation. Only when the trio of sine waves are phase locked does a non-zero bispectral estimate result. In the bispectral domain a single peak occurs at coordinates (f, f) only if sinusoids with frequencies f, f and f (= f + f) exist and all these components are phase locked.

For N sets of phase coupled unit amplitude sinusoid triples in non-zero third moment white noise, the third order autocorrelation function is,

$$c(m,n) = \frac{1}{4} \sum_i [\cos 2\pi(\omega_{1i} m + \omega_{2i} n) + \cos 2\pi(\omega_{1i} m + \omega_{3i} n) + \cos 2\pi(\omega_{2i} m + \omega_{3i} n) + \cos 2\pi(\omega_{3i} m + \omega_{1i} n) \tag{2}$$

$$+ \cos 2\pi(\omega_{2i} m + \omega_{1i} n) + \cos 2\pi(\omega_{3i} m + \omega_{2i} n)] + \gamma(m,n)$$

where ω_j is the jth individual sinusoid of the ith set. γ is the magnitude of the third moment of the white noise process. $\delta(m,n)$ is the Kronecker delta.

We may then arrange the third order cumulant sequence in a $(p+1) \times (p+1)$ order block Toeplitz matrix, C, arranged thusly:

$$C = \begin{bmatrix} C(0) & C(1) & \cdots & C(p) \\ C(-1) & C(0) & \cdots & C(p-1) \\ \cdot & \cdot & \cdot & \cdot \\ \cdot & \cdot & \cdot & \cdot \\ \cdot & \cdot & \cdot & \cdot \\ C(-p) & C(-p+1) & \cdots & C(0) \end{bmatrix} \tag{3}$$

Each constituent block entry, C(i), is a $(p+1) \times (p+1)$ matrix which is also Toeplitz and is filled with third order cumulant entries,

$$C(i) = \begin{bmatrix} c(i,0) & c(i,1) & \cdots & c(i,p) \\ c(i,-1) & c(i,0) & \cdots & c(i,p-1) \\ \cdot & \cdot & \cdot & \cdot \\ \cdot & \cdot & \cdot & \cdot \\ \cdot & \cdot & \cdot & \cdot \\ c(i,-p) & c(i,-p+1) & \cdots & c(i,0) \end{bmatrix}$$

This doubly Toeplitz matrix is asymptotically hermitian for two reasons. First of all, we note that $c(m,n) = c(-m,-n)$ if we apply the symmetry to (1) above. Secondly, we can apply the symmetry properties in (1) to C. Eigenvectors of the signal subspace span the same subspace as the complex sinusoids which are quadratically phase locked. The signal autocorrelation matrix remains a positive definite matrix composed of the cumulants for each set of sinusoid triples. Signal subspace eigenvalues may be less than zero due to the fact that the third order moment of the noise may either

be positive or negative. The eigenvalues are skewed in the direction of the sign of the third order moment. For each of the sinusoid terms in the expected cumulant sequence we expect a pair of non-zero eigenvalues, hence the rank of the matrix is 12N. The corresponding spectral estimator is.

$$B(\ldots) = (e(\ldots) \sum v.)$$ (4)

where the p = 12N matrix *eigenvectors, v, used in the projection operator are those that span the* noise subspace. The kernel or complex sinusoid block vector, e(...) and its constituent, vector, e.(....), are subsequently.

$$
e(\ldots) = \begin{bmatrix} e(\ldots) \\ e(\ldots) \\ \vdots \\ e(\ldots) \end{bmatrix} \quad e(\ldots) \quad \exp(j\ldots kT) \begin{bmatrix} 1 \\ \exp(j\ldots T) \\ \vdots \\ \exp(j\ldots pT) \end{bmatrix}
$$ (5)

for k = 1, 2,...,p. Due to the orthogonality of signal and noise subspace. the projection of the frequency kernel onto the noise subspace will be small, whenever the this kernel assumes the values of constitutent phase locked frequencies. Therefore a peak will appear in the bispectrum.

Typically, the eigenvalues converge rapidly to real values for a large number of data points in the time series. For simulations run with sinusoids in white noise, the eigenvalues belonging to signal subspace eigenvectors are the 12 largest eigenvalues. Figures 1 and 2 show the bispectrum of three phase coupled sinusoids (f = 16Hz. and f = 10Hz.) immersed in white noise with positive and negative skewness, respectively. The signal-to-noise ratio was 3. In the case of negatively skewed noise, the smallest eigenvalue was less than zero.

Experimental Method and Preliminary Results

Three male subjects participated in a research study of cerebral specialization at Purdue University using EEG power spectral measurements [11]. Five sessions of EEG recording accompanied performance of several different cognitive tasks known to elicit differential alpha response on a lateral basis [12]. In each of four sessions, a single task was to be performed by the subject. Baseline (no experimenter specified task given) was recorded during the fifth session. Mental letter composition, geometric figure rotation, visual counting and mental arithmetic were the four tasks which subjects were instructed to perform. Each session consisted of five 10 second intervals the experimenter told the subject to engage in said task and during which EEG was recorded. Alpha was generated by having all subjects close their eyes during task performance. The recordings were made at sites: O1, O2, P3, P4, C3 and C4. The EEG amplifier was known to have linear phase over the entire frequency range of interest. The EEG was sampled at 250 Hz.

For each session the last forty seconds of EEG collected was assembled as a session data block. The EEG was low pass filtered with an FIR filter so that the sampling rate could be decimated by a factor of 2. The resulting time series was divided into 10 one-second sections and tested for stationarity in the third order moment by using the runs test. The FFT based periodogram bispectrum and bicoherence were calculated according to [6]. The bispectrum can normalize by individual power spectrum measurements P..., to form the bicoherence,

$$bic(\ldots) = \frac{B(\ldots)}{P(\ldots)[P(\ldots)][P(\ldots)]}$$

The bicoherence can be used as a laterality measure L, for each task such that

$$L = bic(\ldots) - bic(\ldots)$$

where ... and ... are the left and right bicoherences, respectively for a given frequency pair. A large positive measure is indicative that more coupling occurs on the left side of the brain than the right.

The third order cumulant sequence was calculated for each session's EEG and averaged over all 10 intervals. Eigenvector based bispectral estimates were made for matrix dimensions 25x25 and 36x36. Typically, the eigenvalues resulting from these cumulant matrices are complex. Partitioning eigenvectors to their respective subspaces was accomplished according to both real and complex eigenvalues. Real eigenvalues automatically had their eigenvectors assigned to the signal subspace. Complex eigenvalues were sorted according to the relative size of the imaginary part. Eigenvectors with large imaginary parts were contributed to modes belonging to the orthogonal subspace. Vectors until a total of 12 eigenvectors were assigned to the signal subspace according to the above criteria. Alpha eigenvalues were arranged in ascending order when ... Some estimate of theta theta and alpha beta 1 coupling was found in phase.

References

1. D.L. Sherman and M.D. Zoltowski, "Eigenstructure Based Bispectrum Estimation," *Proc. 26th Annual Allerton Conf.*, Champaign-Urbana, IL., Sept. 1988

2. M.R. Raghuveer and C.L. Nikias, "Bispectrum Estimation: A Parametric Approach," *IEEE Trans. Acoust, Speech & Signal Processing*, vol. ASSP-33, pp. 1213-1230, Oct. 1985

3. G.B. Giannakis, "Signal Processing via Higher-Order Statistics," Ph.D. dissertation, University of Southern California, Los Angeles, July 1986

4. D. Brillinger, *Time Series: Data Analysis and Theory*, San Francisco: Holden-Day, 1981

5. R. Elul, "Gaussian Behavior of the Electroencephalogram: Changes during Performance of Mental Tasks," *Science*, vol 169, pp.323-331, Apr. 1969

6. G. Dumermuth, P.J. Huber, B. Kleiner and T. Gasser, "Analysis of the Interrelations between Frequency Bands of the EEG by Means of the Bispectrum: A Preliminary Study," *Electroenceph. clin. Neurophysiol.*, vol. 31, 1971 p. 137-148

7. K. Osbourne and A. Gale, "Bilateral EEG differentiation of stimuli," *Biological Psychology*, vol. 4, 1976, p 185-196

8. A. Swami and J.M. Mendel, "Cumulant-Based Apporach to the Harmonic Retrieval Problem," *Proc. IEEE Int. Conf. ASSP*, p. 2264-2267, New York, NY, April 1988

9. D. Galin and R. Ornstein, "Hemispheric specialization and the duality of consciousness," In H. Widroe, (Ed.) *Human Behavior and Brain Functioning*, Springfield, IL.: Charles C. Thomas, 1973

10. R. Dumas and A. Morgan, "EEG Asymmetry as a Function of Occupation, Task and Task Difficulty," *Neuropsychologia*, vol. 13: 1975, p. 219-228

11. Z. Keirn, "Alternative Modes of Communication Between Man and Machine," MSEE Dissertation, Purdue University, West Lafayette, IN, Dec. 1988

12. A.S. Gevins, G.M. Zeitlin, C.D. Yingling, R. Schaffer, E. Callaway and C.L. Yeager, "Electroencephalogram Correlates of Higher Cortical Functions," *Science*, vol. 203, Feb. 1979

13. J.G. Okyere, P.Y. Ktonas, and J.S. Meyer, "Quantification of the Alphas EEG Modulation and Its Relation to Cerebral Blood Flow, *IEEE Trans. Biomed. Eng.* vol. BME-33, July 1986, pp. 690-696

14. R.O. Schmidt, "Multiple Emitter Location and Signal Parameter Estimation," *IEEE Trans. Antennas Propagat.*, vol. AP-34, pp. 276-280, March 1986
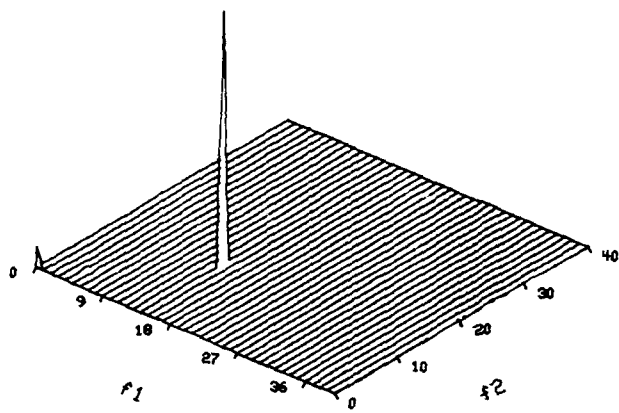
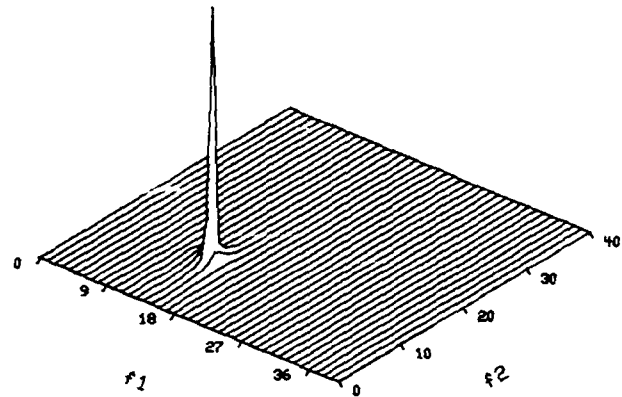Fig. 1: Coupled sinusoids in positively skewed white noise

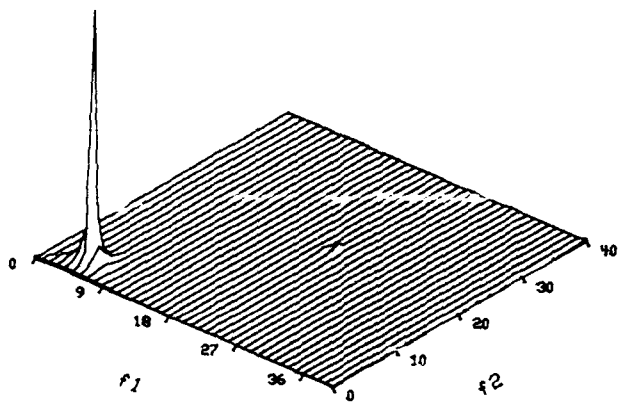Fig. 2: Coupled sinusoids in negatively skewed white noise
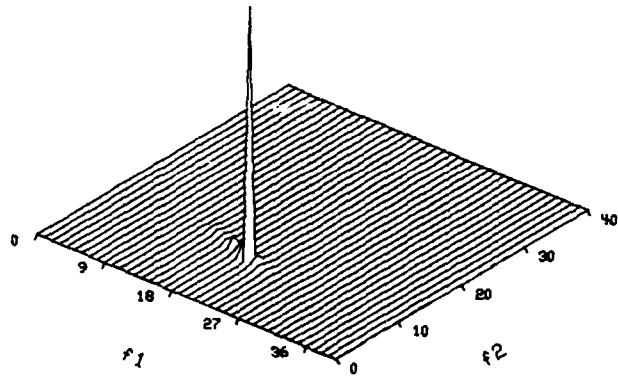
Fig. 3 Theta/Theta Coupling

Fig. 4 Alpha/Beta 1 Coupling

BISPECTRAL ANALYSIS OF FILTERED IMPULSE PROCESSES WITH APPLICATIONS TO THE ANALYSIS OF BIOELECTRIC PHENOMENA

Kazuo Yana, Member, IEEE,   Hiroshi Marushima[†]
Hiroyuki Mino[‡], Member, IEEE,   and   Noriko Takeuchi[‡]

Department of Electrical Engineering, College of Engineering, Hosei University
Koganei City, Tokyo 184 JAPAN
[†]Department of Electronic Engineering, Nippon Engineering College of Hachioji
Hachioji City, Tokyo 192 JAPAN
[‡]Department of Physiology, School of Medicine, Juntendo University
Hongo, Bunkyo-ku, Tokyo 113 JAPAN

ABSTRACT- This article presents two applications of bi-spectra for the analysis of bioelectric phenomena modeled as filtered impulse processes; the surface electromyogram and spontaneous synaptic potentials. Estimation of the elementary waveform and the frequency of its occurrence is important for the analysis of such phenomena when the frequency of elementary waveform occurrence is high enough to cause heavy waveform contamination. Explicit expressions of the elementary waveform and the frequency of its occurrence in terms of the power spectrum and bi-spectrum are first presented in the case that the waveform occurrence times form a stationary Poisson process. Then the computer simulation demonstrates the applicability of the method for the analysis of bioelectric phenomena under consideration. The estimation of the elementary waveform may be utilized as a means of making noninvasive diagnoses of neuromuscular disorder and estimation of the frequency of elementary waveform occurrence may be applied to the analysis of transmitter release at bio-synapses.

INTRODUCTION

A number of applications of higher-order spectra have been described in the literature (e.g. references in [1]). We would like to add two more examples to this list. One is the application to the analysis of surface Electromyogram(s-*EMG*), and another is that to the analysis of spontaneous synaptic potentials (*SSPs*). These are both bio-electric phenomena modeled as filtered impulse processes i.e. processes obtained by random linear superpositions of elementary waveforms. The filtered impulse processes are characterized by the elementary waveform and the statistical properites of elementary waveform occurrence. Hence, their estimations are important for the analysis of phenomena modeled as filtered impulse processes, especially in cases where frequent waveform occurrence cause heavy waveform contaminations making the observation of a single waveform impossible. First we will show that in such cases with heavy waveform contamination estimations of the elementary waveform and the mean frequency of elementary waveform occurrence are possible utilizing the bi-spectra and power spectra assuming that the waveform occurrence form a stationary Poisson process. Then we will present two applications to the analysis of bioelectric phenomena to demonstrate the practical significance of this method. In the analysis of s-*EMG*, it will be shown that the estimation of the elementary waveform in the s-*EMG* is possible and that the method is applicable to the diagnosis of myogenic disorders. It will also be shown that the estimation of frequency of occurrence of spontaneous potential releases at bio-synapses is possible and the method would be applied to the analysis of quantal transmitter release at bio-synapses. Preliminary results on these topics may be found elsewhere [2,3] and more detailed descriptions are now in preparation.

MOMENTS AND SPECTRA OF FILTERED IMPULSE PROCESSES

It will be shown below that both s-*EMG* and *SSPs* (the phenomena under consideration) may be described as filtered impulse processes i.e.

$$y(t) = \sum_i a_i f(t - \tau_i)$$ (1)

in which $h(t)$ represents the elementary waveform, a_i and θ_i respectively denote the ith waveform amplitude and time of occurrence. Here we assume that the a_is are *i.i.d.* random variables and that waveform amplitude is independent of occurrence time. Assuming that the θ_is form a non-stationary Poisson process with intensity $\lambda(t)$, the following joint characteristic function of the nth order is known for the process[4]:

$$M(\omega_1,\ldots,\omega_n) = \exp\left\{ \int \lambda(\theta) E\left[\exp\left\{ j\sum_{k=1}^{n} \omega_k h(t_k-\theta)\right\} - 1\right] d\theta\right\} \tag{2}$$

From Eq.(2), the arbitrary nth order auto correlation function is derived by evaluating

$$(-j)^n \frac{\partial^n}{\partial\omega_1\ldots\partial\omega_n} M(\omega_1,\ldots,\omega_n)\Big|_{\omega_1=\omega_2=\ldots=\omega_n=0} \tag{3}$$

In the doubly stochastic case where $\lambda(t)$ is also a stochastic process Eq.(3) gives the conditional nth order auto correlation function. Hence, taking its expectation over the intensity process gives the unconditional nth order auto correlation function of the process. Assuming that $\lambda(t)$ is a constant or stationary random process in the doubly stochastic case, taking the Fourier transforms of the correlation functions thus obtained yield the theoretical expressions of the power spectra and higher-order spectra. In the simplest case that $\lambda(t)$ and a_i are constants, power spectrum $\gamma(f)$ and bi-spectrum $\gamma_3(f_1,f_2)$ is expressed as follows (a_i is set to unity without any loss of generality).

$$\gamma(f) = \lambda|H(f)|^2 \tag{4}$$

$$\gamma_3(f_1,f_2) = \lambda H(f_1)H(f_2)H^*(f_1+f_2) \tag{5}$$

AN INVERSE SOLUTION FOR FILTERED IMPULSE PROCESSES

Filtered impulse processes are characterized by an elementary waveform $h(t)$, its amplitude distribution $f(a)$ and intensity $\lambda(t)$ (the statistical properties of $\lambda(t)$ in the doubly stochastic case). The forward problem of filtered impulse processes is defined as that of expressing statistics like amplitude distribution, power spectrum or bi-spectrum in terms of the triple $h(t)$, $f(a)$ and $\lambda(t)$. Similarly the inverse problem is that of finding specific expressions of $h(t)$, $f(a)$ and $\lambda(t)$ using a given set of statistics. In the previous section it was shown that the joint characteristic function of any order is described in terms of the triple $h(t)$, $f(a)$ and $\lambda(t)$. Thus, the essential forward problem expressing arbitrary order auto correlation function and spectrum in terms of the triple has the solution. Now in the simplest case where $\lambda(t)$ and a_i are assumed to be constant, simple manipulation of Eqs.(4)-(5) gives the inverse solution:

$$\lambda = \gamma^2(f)\gamma(2f)/|\gamma_3(f,f)|^2 \tag{6}$$

$$|H(f)| = \sqrt{\gamma(f)/\lambda} \tag{7}$$

$$arg H(f) = \sum_{k=1}^{\infty} \frac{1}{2^k} arg\gamma_3(2^{k-1}f, 2^{k-1}f) \tag{8}$$

In cases where the amplitude has random variations with the coefficient of variation expressed as σ_a, Eq.(6) remain holds, but Eqs.(7),(8) may be modified:

$$\lambda = \frac{(1+3\sigma_a^2)^2}{(1+\sigma_a^2)^3} \frac{\gamma^2(f)\gamma(2f)}{|\gamma_3(f,f)|^2} \tag{9}$$

$$|H(f)| = \sqrt{\gamma(f)/(1+\sigma_a^2)\lambda} \tag{10}$$

Eqs.(9),(10) enable us to estimate the amount of bias due to making the assumption that the waveform amplitude is constant. We will now demonstrate the application of the inverse solutions shown in eqs.(6)-(8) to the analysis of biological phenomena.

APPLICATION TO THE ANALYSIS OF s-EMG

Signal Model of s-EMG

A set of a motor-neuron and muscle fibers governed by the neuron is called the Neuro-Muscular Unit (NMU). Action potentials propagating along muscle fibers cause changes in potential at the skin surface. s-EMG, the temporal superposition of such potential changes, termed NMU waveforms, caused by a number of NMU activities observed at the skin surface above the active muscle. From statistical analysis of single NMU activities using needle electrodes, it has been thought that in moderate voluntary contractions NMU waveforms occur nearly periodically with a mean interval of approximately 60 to 100 ms and that NMU activities are statistically mutually independent[5]. According to a limit theorem, superposition of sparse point processes converge to a Poisson process as the number of superposed processes goes to infinity[6]. Hence, occurrence times of NMU waveforms in s-EMG may be regarded as a Poisson process within a time interval sufficiently less than the mean interval of NMU waveform occurrence in the single NMU activity. In this sense, s-EMG may be locally modeled as a filtered point process with a constant intensity.

NMU Waveform Estimation

NMU waveforms are known to be distorted when the subject is affected by neuromuscular disorders. Normally single NMU waveforms are not observable in s-EMG record due to high temporal waveform contamination. However, waveform distortion may be detected by the waveform reconstruction using Eqs.(7) and (8). Computer simulation was carried out to confirm the possibility of performing single NMU waveform estimation in the s-EMG. A biphasic single NMU waveform is assumed as $f(t) = t \cdot exp\{-|t|/\tau\}$. Here we set $\tau = 1$ (ms). Artificial EMG was generated as a superposed filtered impulse process. NMU waveform occurrence times of each filtered impulse process is assumed to form a renewal process with Gaussian interval distribution of mean 100 (ms); S.D. 20 (ms). NMU activities are assumed to be statistically independent of each other. Sample data thus generated is shown in Fig.1a. Eqs. (7) and (8) were applied to the data. Conventional non-parametric techniques (FFT methods) were applied to the estimation of power and bi-spectrum. The results are shown in Figs. 1b-1d. Solid curves in Fig.1b and 1c show respectively the amplitude and phase components of a single NMU waveform. Open circles in Fig.1b and 1c respectively show their estimated values, which show good agreement with the theoretical values. Fig. 1d shows the result of NMU waveform estimation (open circles) which shows good agreement with the actual waveform (solid curves).
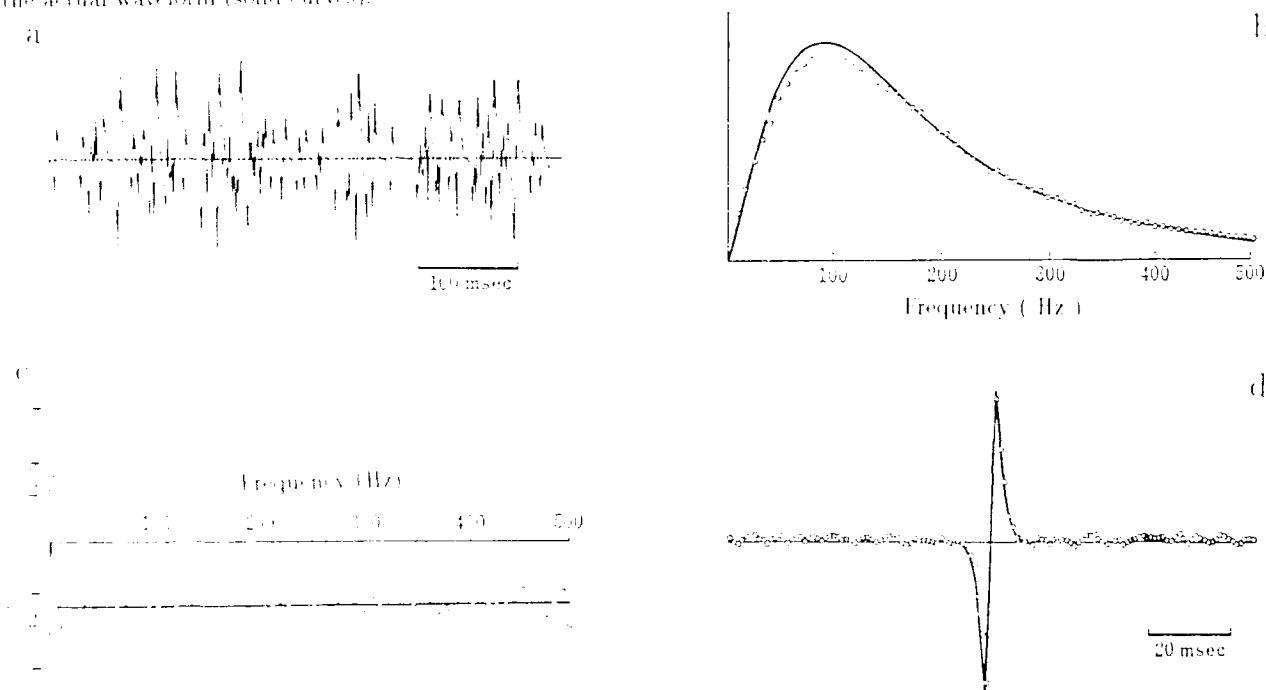

Fig. 1. NMU waveform estimation in s-EMG (computer simulation)
a: sample data b-d: estimated amplitude, phase and NMU waveform (open circles) and their true values (solid curves))

APPLICATION TO THE ANALYSIS OF *SSPs*

A Signal Model of SSPs

SSPs are spontaneous membrane potential changes observed at post-synaptic membranes. *SSPs* are caused by spontaneous quantal transmitter releases from pre-synaptic membranes. Their properties have been extensively examined to reveal the mechanism of transmitter releases[7][8]. *SSPs* may also be modeled as a filtered point processes with a constant intensity as a first approximation[9]. However, we must note that the assumption that the *SSP* occurrence times form a stationary Poisson process is still controversial[7]-[9].

Estimate of Frequency of SSP Occurrence

In some analyses of *SSPs*, the estimation of the rate of *SSP* occurrence is important. For example, it is important when examining the effects of extra-cellular ions or drugs on the release probability[10][11]. When the rate of *SSP* occurrence is high enough to cause waveform contamination, direct counting of the number of *SSPs* is difficult. In these cases equation (8) may be used to estimate the rate of *SSP* occurence. Computer simulation was carried out to confirm this possibility. The elementary waveform of an *SSP* is assumed to be a double exponential curve expressed as $h(t) = c_1 p\{-t/\tau_1\} + c_2\{-t/\tau_2\}$. Parameters were set as follows: $\tau_1 = 3$(ms), and $\tau_2 = 0.75$(ms). λ, the parameter to be estimated, was set at 200 or 500 occurrences/s. Figs.2a and 2b shows samples of the simulated data. Figs. 2c and 2d show the estimated power spectra. Figs. 2e and 2f show bi-spectra. Estimated λ using equations (7) and (8) are shown in Figs. 2g and 2h. In the middle frequency range fairly good estimates were given.
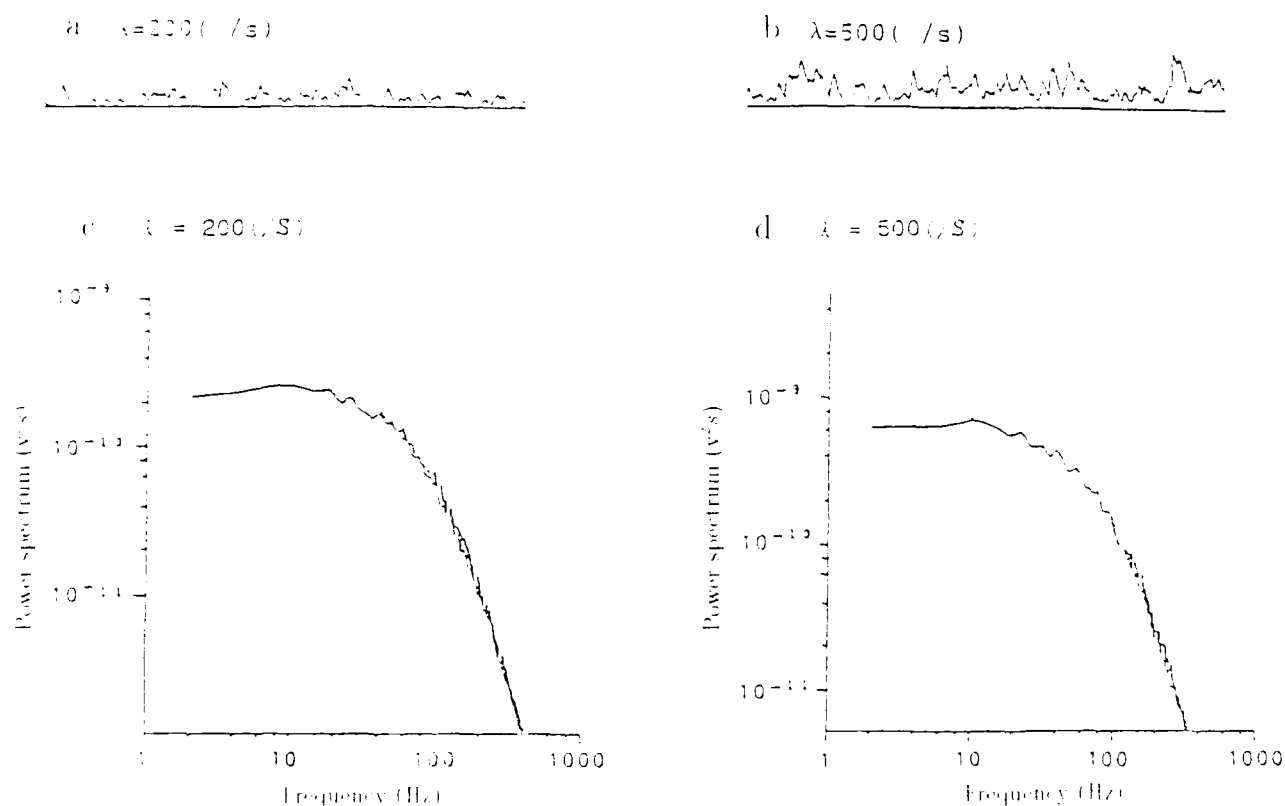

Fig. 2 Estimation of the rate of *SSP* occurrence (computer simulation)
a,b: sample data; c,d: estimated power spectra (next page); estimated bi-spectra; g,h(next page): estimated rate of *SSP* occurrence (Note that the estimates are obtained in each frequency.)
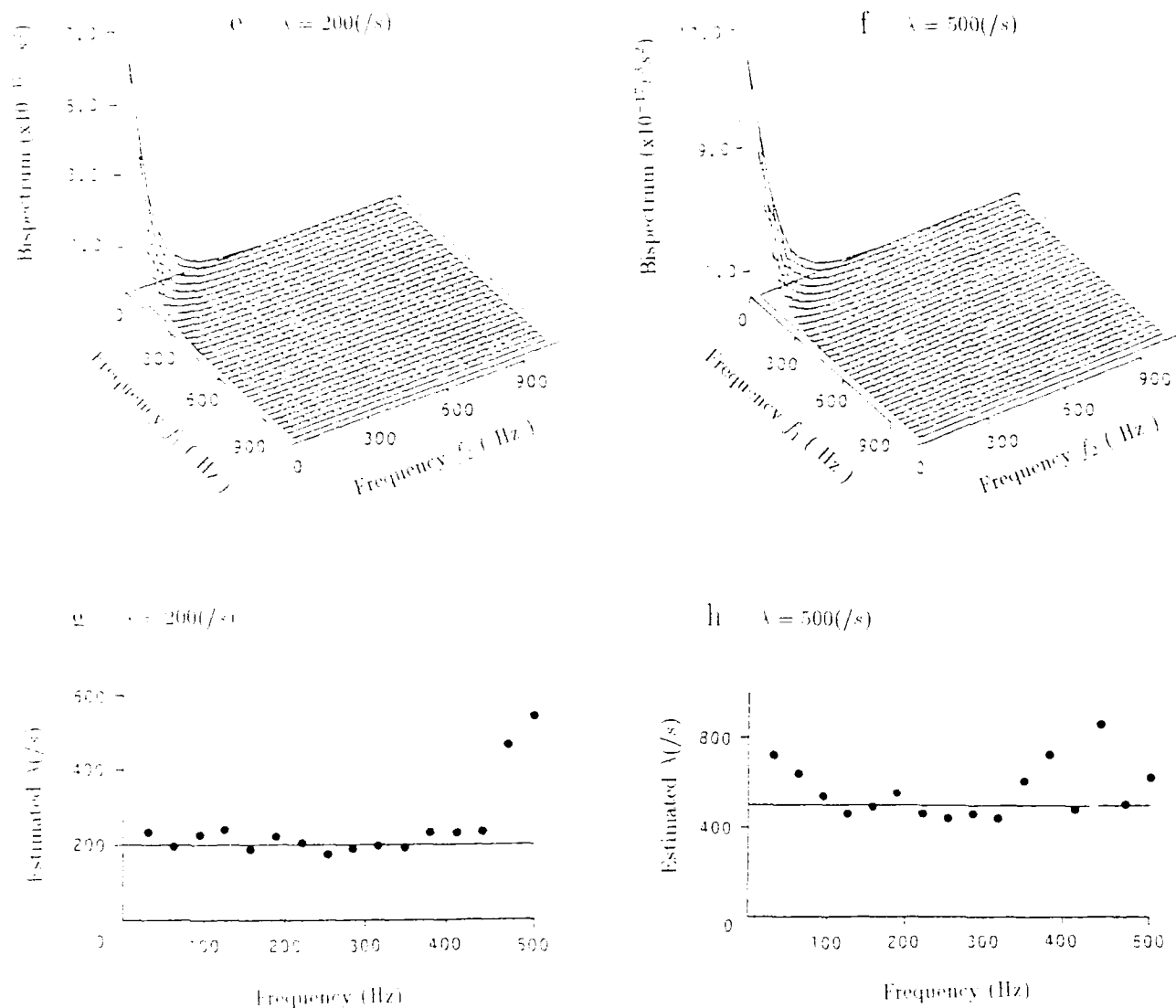
Fig. 2 (e)(f)(g)(h) Estimation of the rate λ of SSP occurrence(computer simulation)

CONCLUDING REMARKS

Two applications of higher order spectra to the analysis of bio-electric phenomena have been presented. Higher order spectra have not yet been commonly utilized for the analysis of bio-electric phenomena in spite of their potential usefulness. In the analysis of bio-electric phenomena, it is usually difficult to get a long stationary set of data due to the inherent non-stationary characteristics of biological systems. For this reason, conventional FFT methods sometimes fail to achieve reasonable estimation accuracy for higher order spectra with a given limited data length. Recent developments of new parametric methods [11,12,13] may make the higher order spectral analysis of bioelectric phenomena more practical by reducing the required data length for analysis.

REFERENCES

[1] C. L. Nikias and M. R. Raghuveer, "Bispectrum Estimation: A Digital Signal Processing Framework," *Proc. IEEE*, vol. 75, no. 7, pp. 869-891, 1987.

[2] K. Yana, I. Muramoto, Y. Arai and Y. Saito, "The High Order Moment Analysis of Bioelectric Noise: Theory and its Application for the Analysis of Surface EMG and Postsynaptic Membrane Noise," in *Recent Advances in EEG and EMG Data Processing*, N. Yamaguchi and K. Fujisawa editors, pp. 397-402, Elsevier, 1981.

[3] K. Yana, H. Marushima, H. Nojima and N. Takeuchi, "Frequency Estimation of Spontaneous Synaptic Potential or Current Releases," *Proc. the Eighth Ann. Conf. of the IEEE EMBS Soc.*, vol. 2, pp. 986-989, 1986.

[4] D. L. Snyder, *Random Point Processes*, Chap. 4, pp. 168-170, Wiley, New York, 1975.

[5] Y. Saito, "EMG as Stochastic Processes: Time Series Analysis of EMG Data," *Japanese Journal of Medical Electronics and Biological Engineering*, vol. 19, no. 6, pp. 1172-1220, 1975.

[6] E. Cinlar, "Superposition of Point Processes," in *Stochastic Point Processes: Statistical Analysis, Theory and Applications*, P. A. W. Lewis editor, pp. 549-606, Wiley, New York, 1972.

[7] J. I. Hubbard, "Mechanism of Transmitter Release," *Prog. Biophys. Mol. Biol.*, vol. 21, pp. 33-124, 1970.

[8] W. Van der Kloot, H. Kita and I. Cohen, "The Timing of the Appearence of Miniature End-Plate Potentials," *Prog. Neurobiol.*, vol. 4, pp. 271-326, 1975.

[9] K. Yana, N. Takeuchi, Y. Takikawa and M. Shimomura, "A Method for Testing an Extended Poisson Hypothesis of Spontaneous Quantal Transmitter Release at Neuromuscular Junctions," *Biophys. J.*

[10] J. L. Houser and R. Miledi, "Effect of Lanthanum Ions on Function and Structure of Frog Neuromuscular Junctions," *Proc. Roy. Soc. Lond. Ser. B.*, vol. 179, pp. 247-260, 1971.

[11] C. Martin and W. Finger, "Tonic Depolarization of Excitatorty Nerve Terminals in Crayfish at Low Concentrations of Extracellular Potassium," *Neuroscience Letters*, vol. 53, pp. 309-314, 1985.

[12] C. L. Nikias and H-H Chiang, "High-order Spectrum Estimation via Noncausal Autoregressive Modeling and Deconvolution," *IEEE Trans. Acoust., Speech, Signal Processing*, vol. ASSP-36, no. 12, pp. 1911-1913, 1988.

[13] G. B. Giannakis and J. M. Mendel, "Identification of Nonminimum Phase System Using Higher Order Statistics," *IEEE Trans. Acoust., Speech, Signal Processing*, vol. ASSP-37, no. 3, pp. 360-377, 1989.

EXTRACTION OF INDEPENDENT SOURCES
FROM CORRELATED INPUTS

A SOLUTION BASED ON CUMULANTS

P. Ruiz * and J.L. Lacoume **

* TECHNIPHONE SA, BP 22, 13610 Le Puy Ste Réparade, France
** CEPHAG, URA 346 CNRS, ENSIEG, BP 46, 38402 St Martin d'Hères, France

ABSTRACT

We propose here a way of extracting independent sources from correlated inputs.
The only hypothesis made is that the unknown relations between inputs and sources are linear, but that not more than one source is gaussian. We show the impossibility of extracting sources by only using spectral analysis, and make that extraction possible by using equations which relate inputs and sources, based on the cumulants and cross-cumulants of the inputs.

1. INTRODUCTION

The characterization of independent sources occurs when one studies the data obtained in an array of sensors. We generally assume that the relations between sensors and unknown sources are linear.

In order to identify the sources $s_i(t)$, at frequency f, we select sensors and try to extract some information concerning independent components. The common way consists in forming the spectral matrix of the sensors, from which we can extract the number of uncorrelated components q. Since the way of determining q has been largely discussed, through the use of different criteria [1], we now assume that in our situation, the information of the number of sources has been extracted.

However, a complete determination of the unknown sources requires more informations which concern the relations between sensors ans sources, or between each sensor. The former type of relation has been largely illustrated by Bendat and Piersol who use a particular decomposition of the spectral matrix [2] and obtain for measures a new basis of uncorrelated measures. However this linear decomposition cannot be successful if each sensor is a combination of several sources.

The latter approach, based on relations existing between sensors, is possible assuming for example the plane wave hypothesis .In our situation, we cannot hold such an hypothesis. From a larger point of vue, the introduction of supplementary hypothesis is necessary because the number of unknowns (the transfer functions between sensors and sources) is greater than the number of equations given by the spectral matrix.

We develop this aspect in part II.

Since the lack of equations is assumed, we introduce the cumulants and their properties in part III, and propose in part IV supplementary equations based on the cumulants of sensors, for completely identifying the model.

In part V, we develop the precautions to take to obtain a good accuracy of the algorithm which minimize one function of cumulants.

Part VI shows the results, with real signals, in the case of several independent sources.

II. MODEL

We consider from now on the model at frequency f.

$\underline{S}^T = (S_1(f), \ldots, S_q(f))$ is the vector which components are the unknown stochastic non-gaussian independent sources.

$\underline{X}^T = (X_1(f), \ldots, X_p(f))$ is the vector of sensors.
$\underline{\underline{H}}_i$ is the matrix of transfer functions between $\underline{X}_i$ and $\underline{S}$

$$\underline{X}_i = \underline{\underline{H}}_i \underline{S} \qquad (1)$$

The determination of unknown sources generally uses the properties of the spectral matrix of the measures.

We assume that the data are stationary and estimate spectral densities with averaged periodogram.

Since $p \geq q$, the interest of the spectral matrix is that the eigenvectors associated to non-null eigenvalues determine the signal space. However, that signal space can be successfully determined by using only q sensors [3] chosen between the previous p.

So the model (1) is equivalent to

$$\underline{X} = \underline{\underline{H}} \underline{S} \qquad (2) \qquad \text{where } \underline{X} \text{ is a vector of q sensors}$$

$\underline{\underline{H}}$ is a q x q matrix of transfer functions between $\underline{X}$ and $\underline{S}$.

We must be aware of the fact that with this modelisation, it is impossible to obtain exactly the signals S_i transmitted by the sources. A simple way to see that is to apply a linear transformation at one source S_i (say $S_i(f)$ gives $F(S_i(f)) = W_i(f)$) and to see that the problem is exactly the same if we replace S_i by W_i. This enables to consider the problem with real sources.

From the model (2) we can now exactly extract 2 submodels (3) and (3')

$$\text{Re } \underline{X} = \text{Re}(\underline{\underline{H}}) \underline{S} \quad (3)$$
$$\text{Im } \underline{X} = \text{Im}(\underline{\underline{H}}) \underline{S} \quad (3')$$

Considering now (3) and defining $G = \text{Re}(H)^{-1}$, since we cannot access the magnitude of S_i, we can also fix for exemple
$$G_{ii} = 1 \quad 1 \leq i \leq q.$$
The model to identify has now $q(q-1)$ unknowns.

The use of the spectral matrix brings some equations concerning the uncorrelation of the sources. From the sensors X_i we can extract a new uncorrelated basis of V_i related to X_i. The family of V_j verify

$$E [V_i(f) \, V_j(f)] = 0 \quad \forall_i , \ 1 \leq i \leq q-1 \quad \forall_j > i$$

The $(V_i)_{i=1...q}$ are now well known, but are not necessarly the true sources.

This is easily explained by the fact that the number of equations $E [V_i(f) \, V_j(f)] = 0$ is only $(q(q-1)/2)$, and the model to identify has $q(q-1)$ unknowns so the only use of the spectral matrix lets $\dfrac{q(q-1)}{2}$ parameters free.

The identification of the model (3) is complete if we can define $\dfrac{q(q-1)}{2}$ other q independent equations versus the G_{ij}.

Our purpose is to define equations translating the independancy of stochastic sources, by using fourth order cumulants.

III. THE CUMULANTS [4]

III.1 Definition

If $(Y_1, ..., Y_r)$ is a r variate random variable, the rth order joint cumulant $C [Y_1, ..., Y_r]$ of $(Y_1, ..., Y_r)$ is given by

$$C [Y_1, ..., Y_r] = \sum (-1)^{p-1} (p-1) ! \left(E \left\{ \prod_{j \in v_1} Y_j \right\} \right) ... \left(E \left\{ \prod_{j \in v_p} Y_j \right\} \right)$$

where the summation extends over all partitions $(v_1, ..., v_p)$, of $p = 1, ..., r$, of $(1, ..., r)$. For example, if X_1 and X_2 are two random variables, two partitions may occur :

one with $v_1 = \{1\}, v_2 = \{2\}$, one with $v_1 = \{1, 2\}$.

So $C[X_1, X_2] = E [X_1 X_2] - E[X_1] E[X_2]$ is the cross covariance function of X_1 and X_2.

III.2 Main properties of cumulants

• If any group fo the Y's are independent of the remaining Y's then

$C[Y_1, ..., Y_r] = 0$. Particularly, if two "sources" S_1 and S_2 are independent :

$$C[\underbrace{S_1, ..., S_1}_{p}, \underbrace{S_2, ..., S_2}_{n}] = C[S_1^p, S_2^n] = 0, \forall (p, n) \in N^2$$

• If S_1 is a zero mean Gaussian process,

$C[S_1^p] = 0$ with $p > 2$.

IV. SOURCES IDENTIFICATION : A SOLUTION BASED ON SECOND AND FOURTH ORDER CUMULANTS

IV.1 Definition of the system to identify

We consider again the model defined in (3):
$$\underline{S} = \underline{\underline{G}} \, \text{Re}\underline{X} \quad \text{with} \quad G_{ii} = 1$$
This model has $q(q-1)$ unknowns

If the model matrix builds an uncorrelated basis from the measures $X_i \ i=1,..., q$ this uncorrelation can be summarized by :
$$C_{2ij} = E(S_i \, S_j) = 0 \text{ for } i = 1, q-i \text{ and } j > i$$

Those equations are versus covariance, cross covariances of measures and the unknowns G_{ij}. Those $q(q-1)/2$ new equations are independent if the coherence between two any different measures is not 1. Assuming this hypothesis by an appropriate selection of sensors, there remain $q(q-1)/2$ parameters free.

Those $q(q-1)/2$ degrees of freedom can be cancelled by considering any equations using fourth order cross cumulants.

$$C_{4ij}(f) = \text{Cum} [S_i, S_i, S_j, S_j] = \text{Cum}\left[S_i^2 S_j^2 \right] = 0, \text{ for independent sources } S_i, S_j \text{ with } i = 1,..., q-1, j = i+1,..., q$$

Any C_{4ij} is a non-linear function of G_{ik}, G_{jl}, and fourth order cumulants and cross cumulants of X_k and X_l, for $\kappa = 1,..,q$, $l = 1,...,q$.

The new system to resolve has now $q(q-1)$ unknowns for $q(q-1)$ equations :

$$\left.\begin{array}{l} C_{2ij} = 0 \\ C_{4ij} = 0 \end{array}\right\} \text{ for } i = 1, ..., q-1 ; j = i+1, ..., q \quad (4)$$

Resolution of the model (4)

Because the model (4) is composed of non linear equations, we simplify it by defining $f_4 = \sum_{i=1}^{q-1} \sum_{j>i} C_{4ij}^2$

we contract the $q(q-1)/2$ equations $C_{4ij} = 0$ into a scalar function to resolve $f_4 = 0$ under $q(q-1)/2$ constraints C_{2ij}. This is a classical problem of minimization of non linear function under non linear constraints.

IV.2 Properties of the system of equations

IV.2.1. Existence of a solution
It is clear that the researched independent sources are solution of the model (4). However, one can notice that there can exist solutions of (4) which not correspond to independent sources ; this could be the case of sources identified such that

$$C_{2ij} = 0 , \quad C_{4ij} = 0 , C_{6ij} \neq 0 \quad \left(\text{Cum } [S_i S_i S_i S_j S_j S_j]\right)$$

Such an uncertainty can be raised, by testing the 6th order cross cumulants of estimated sources $\hat{S}_i$, $\hat{S}_j$.
Let's notice too, that the contraints $G_{ii} = 1$ are a way of avoiding non-null solution for the G_{ij} verifying (4).

IV.2.2. Uniqueness of the solution
From a model q sources - q sensors, we can extract q! solutions of sources statistically independent at order two and four. The reason why is :

if $(\hat{S}_1, \hat{S}_2, ..., \hat{S}_q)^T = \underline{\hat{S}}$ is solution of (4) , with

$$\underline{\hat{S}} = \underline{\underline{\hat{G}}} \text{ (Re } \underline{X})$$

where $\underline{\underline{\hat{G}}} = ((\hat{G}_{ij}))$ are the estimated matrix of transfer function between sensors and sources, then every

$$\underline{\hat{S}}_\sigma = (\hat{S}_{\sigma(1)} ... \hat{S}_{\sigma(q)})^T$$

will be solution of (4), where σ is a particular permutation on the $1,...,q$. So for a given solution the model makes q! solutions exist.

A complete identification is only possible if we have a priori knowledge between sensors and sources, for instance "sensor i is principally related to source i".

V. THE ALGORITHM

V.1 Normalization of the measures

The importance of that normalization deduces from :
1- the accuracy of the different steps of the algorithm of minimization under constraints.
2- the estimation of the cumulants (bias and variance)
The first point takes into account the fact that initially it is better to have magnitudes of the function, of the constraints around 1.

We now examine the second point of vue : the cumulants are estimated with fourth order moments

$$\hat{Cum}[X_i X_j X_k X_l] = \hat{E}[X_i X_j X_k X_l] - \hat{E}[X_i X_j] \hat{E}[X_k X_l] - \hat{E}[X_i X_k] \hat{E}[X_j X_l] - \hat{E}[X_i X_l] \hat{E}[X_j X_k]$$

$$(\hat{E}[X_i] = \hat{E}[X_j] = \hat{E}[X_k] = \hat{E}[X_l] = 0)$$

and the moments are estimated by averaged periodogram (n averages).
The estimator of cumulants is asymptotically unbiased, and for $n \gg 1$, $i = j = k = l$, and X_i gaussian

$$Var\left[\hat{Cum}[X_i^4]\right] = \frac{24 \sigma^8}{n}$$

Such a variance can be minimized by considering $\sigma < 1$
This is obtained by first normalizing the power of sensors p_i at frequency f

Re $\underline{X}$ is transformed into Re $\underline{X}_1 = \underline{\underline{\Lambda}}$ Re $\underline{X}$

with $\qquad \underline{\underline{\Lambda}} = \begin{pmatrix} \dfrac{1}{\sqrt{p_1}} & \\ & \dfrac{1}{\sqrt{p_q}} \end{pmatrix}$

we resolve (4) with the normalized sensors : we extract $\underline{\underline{\hat{G}}}$ such that

$$\underline{\hat{S}} = \underline{\underline{\hat{G}}}(\text{Re } \underline{X}_1) = (\underline{\underline{\hat{G}}}\ \underline{\underline{\Lambda}})\ (\text{Re } \underline{X}).$$

VI. RESULTS ON REAL SITUATIONS

VI.1 Identification of two independent sources from two correlated measures.

We consider the situation of 2 machines $s_1(n)$ and $s_2(n)$ vibrating at the same frequency f.
They are assumed stationary (this has been verified with a time-frequency representation)
We consider a data length of 8192 points, and make $s_1(n)$ growing during this time. Then we build from $s_1(n)$ and $s_2(n)$ two measures $x_1(n)$ and $x_2(n)$ such that

$$\begin{cases} x_1(n) = s_1(n) + s_2(n) \\ x_2(n) = s_2(n) + 0,3\ s_1(n) \end{cases} \qquad \text{(fig. (a))}$$

$x_1(n).$ $\qquad\qquad\qquad\qquad\qquad\qquad\qquad\qquad\qquad$ $x_2(n).$
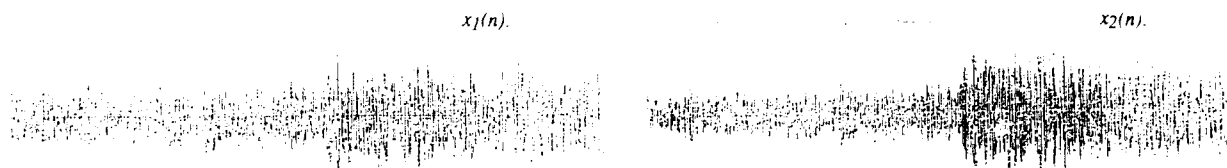

Fig. (a) : Correlated measures versus time : one source has been growing during data acquisition

Our purpose is to extract from correlated measures at frequency f two independent sources $\hat{\underline{S}}_1(f)$, and $\hat{\underline{S}}_2(f)$ to show that only using spectral analysis does not enable to extract independent components from x_1 and x_2.
Moments and cumulants are estimated at frequency f, with 32 averages on non overlapping slices of signal (length of a slice = 512 points). The minimization of the function of cumulants under constraints is obtained from a subroutine of " Harwell Subroutine Library". The algorithm estimates $\hat{\underline{S}}_1(f)$ and $\hat{\underline{S}}_2(f)$ versus $X_1(f)$ and $X_2(f)$:

$$\begin{cases} \hat{\underline{S}}_1(f) = X_1(f) - 0,97\ X_2(f) \\ \hat{\underline{S}}_2(f) = -0,29\ X_1(f) + X_2(f) \end{cases}$$

We find $\qquad \hat{\underline{S}}_1 = S_1 \text{ and } \hat{\underline{S}}_2 = S_2$

Figure (b) shows the power of the estimated sources versus time. We identify the varying source. The importance of using fourth order cumulants is shown in figure (c) and figure (d), where are shown the power of the uncorrelated bases at frequency f $(x_1(n), x_{2\perp 1}(n))$, $(x_2(n), x_{1\perp 2}(n))$, $(x_{2\perp 1}(n)$ is the part of $x_2(n)$ uncorrelated with $x_1(n), x_{1\perp 2}(n)$ is the part of $x_1(n)$ uncorrelated with $x_2(n))$.

power of $\hat{S}$ $\qquad\qquad\qquad\qquad\qquad\qquad\qquad\qquad\qquad$ power of $\hat{S}$

Fig. (b) : Power versus time of the estimated sources $\hat{S}_1$ et $\hat{S}_2$:
$\hat{S}_2$ is the varying source.

In figure (c), because $x_1(n)$ and $x_{2\perp 1}(n)$ still grow versus time, they can't be identify as the reasearched sources. The same conclusion occurs in figure (d) with $x_2(n)$ and $x_{1\perp 2}(n)$.
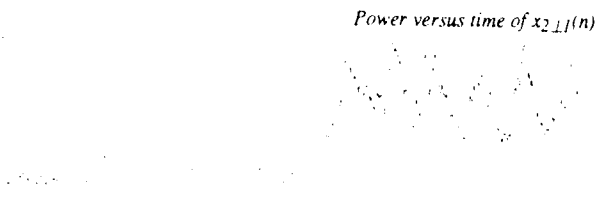
Power versus time of $x_{2\perp 1}(n)$

Power versus time of $x_{1\perp 2}(n)$

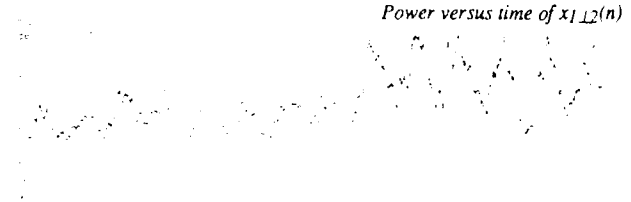*Fig. (c) : Power versus time of $x_{2\perp 1}(n)$ uncorrelated with $x_1(n)$.*

Fig. (d) : Power versus time of $x_{1\perp 2}(n)$ uncorrelated with $x_2(n)$.

VI.2 Extraction of 4 sources from 4 correlated sensors.

We build from $S_1(f)$, $S_2(f)$, $S_3(f)$, $S_4(f)$ independent sources at frequency f four correlated measures X_1, X_2, X_3, X_4 and make one source grow. We assume the hypothesis "source i is principally existing in measure i".
The measures are related to the sources with:

$$\begin{cases} X_1 = S_1 + 0,2\ S_2 + 0,3\ S_3 \\ X_2 = 0,3\ S_1 + S_2 + 0,5\ S_3 \\ X_3 = 0,1\ S_1 + S_3 \\ X_4 = S_1 + 0,2\ S_1 + 0,2\ S_2 + 0,2\ S_3 + S_4 \end{cases}$$

4 independent sources related to the measures are estimated with the algorithm of cumulants following the model

$$\hat{\underline{S}} = \hat{\underline{\underline{G}}}\ \underline{X} \quad \text{with} \quad \hat{\underline{\underline{G}}}^{-1} = \begin{pmatrix} 1,06 & 0,21 & 0,25 & -0,10 \\ 0,36 & 1,10 & 0,46 & 0 \\ 0,10 & 0,07 & 1,04 & -0,06 \\ 0,29 & 0,29 & 0,22 & 0,98 \end{pmatrix}$$

Figure (f) shows the power of the measures versus time, and the sources estimated with cumulants. We identify the faulty source and conclude that only S_3, principally related to measure X_3, has been growing.
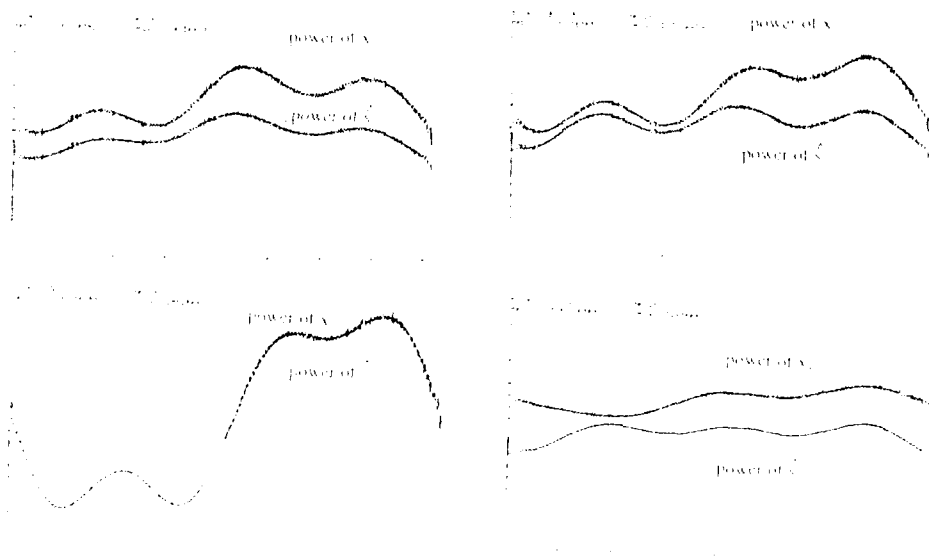
Fig. (f) : Power versus time of $x_1(n)$, $\hat{s}_1(n)$, $x_2(n)$, $\hat{s}_2(n)$, $x_3(n)$, $\hat{s}_3(n)$, $x_4(n)$, $\hat{s}_4(n)$.

VII CONCLUSION

We have shown in this paper
• the insufficiency of spectral analysis to extract independent sources from correlated measures.
• the identification of independent sources using fourth order cumulants.
Such an algorithm including second and fourth order cumulants opens a new field of research in multidimensional array processing and in other domains where we can only access correlated inputs, and not independent components.

ACKNOWLEDGMENTS

BIBLIOGRAPHY

[1]   I. Tas, C. Latombe, "Passive array treatment : detection of signals and estimation of the spectral matrix of the noise", Signal Processing III : EURASIP, 1986, pp. 1013-1016.
[2]   J.S. Bendat, A.G. Piersol, "Random Data, Analysis and Measurement Procedures", 2nd edition, Wiley Intersci., 1986.
[3]   J.L. Lacoume. P. Ruiz, "Quasi-solutions de problèmes mal posés", Colloque GRETSI, Juan-les-Pins. June 1989.
[4]   D.R. Brillinger, "Time Series Data Analysis and Theory", Holden Day, 1981.

A SECOND-ORDER EIGENSTRUCTURE ARRAY PROCESSOR*

R.R. Mohler

Oregon State University
Department of Electrical & Computer Engineering
Corvallis, OR   97331-3211

F.J. Bugnon

University of Western Australia
Centre for Water Research
Nedlands, Western Australia 6009, Australia

ABSTRACT

Higher-order eigenstructures are investigated to estimate the direction of arrival of a tonal wave impinging upon an array of receivers. In particular second-order sequences of received signals are generated by convolution to enhance detection and estimation by such classical methods as MUSIC. The method is most effective for such troublesome cases as low signal-to-noise, coherent sources, multiple sources in close proximity, and low number of receivers.

Simulations show that with the same signal-to-noise ratio the MUSIC algorithm for a linear array of thee receivers is unable to distinguish between two sources which are less than 4.5° apart while the second-order algorithm detects the two sources with less than 1.3° separation.

In general, Mth-order convolutions may be made of the received signals which are Fourier transformed and appropriately multiplied to form an Mth-order spectral density matrix. Similar to the traditional first-order (second moment) spectral density case, an orthogonality condition leads to the direction of arrival. While the theory suggests certain advantages for higher-order cases, simulations indicate the second-order method to be most feasible if used as an enhancement of a first-order method such as MUSIC.

INTRODUCTION

The direction-finding problem attempts to determine the angle of incidence of signals emitted by distant sources, from a sequence of measurements recorded on an array of receivers. Though the potential applications are broader, the problem historically evolved from the two-dimensional underwater acoustical case. The first solutions were based on beam forming techniques as early as 1942. In the last 15 years, the original work of Pisarenko [1] on harmonic retrieval triggered the start of a high resolution approach to the direction finding problem

estimation of the noise field [2]. This new method was based on the eigenstructure of the autocorrelation matrix. In this method, eigenvectors associated with the smallest, positive, eigenvalues that are generated by the independent, identically distributed (i.i.d.) noise field are orthogonal to the space spanned by the sources. Then a simple orthogonality test allows us to perform the multiple signal classification named the MUSIC method (i.e., the "first-order" method).

Further developments included the study of estimators for the location of sources [3,4] and the use of likelihood methods for the detection tests of the number of sources [5,6]. Fully correlated sources were dealt with by spatial smoothing [7] which was compared with the classical adaptive beam formers [8]. Other progresses, to name a few, addressed different noise structures [9] and improved resolution through the use of Toeplitz matrices [10].

The second-order eigenstructure method is a high-resolution method to solve the direction finding problem. This method generates, by convolution techniques, new data sequences, based on the original array measurements, with a higher signal-to-noise ratio. Then, an eigenstructure method is applied to these sequences, with a major modification in the orthogonality test. The new method can be used as an enhancement with any previously existing techniques with few modifications.

Mth-ORDER EIGENSTRUCTURES

Let $r_{i,1}$ represent a vector of random components measured at sensor i at different times t_k. Subscript 1 refers to the first-order sequence, that is, to the original measurements. On the other hand, the Mth-order sequences $r_{i,M}(t)$ are obtained by the recursive computation

$$r_{i,M} = r_{i,M-1} * r_{i,1} . \qquad (1)$$

where * is the convolution operation of the two sequences that are present. If N data points are recorded (i.e., $r_{i,1}$ is an N by 1 vector), then

sequences $r_{1,M}$ have length $M(N-1)+1$, and the second-order sequences $r_{1,2}$ have length $2N-1$.

In the frequency domain (upper case characters), a matrix of measurements of the array of size d is given by

$$R_M^T = \left[R_{1,M}, \ldots, R_{j,M}, \ldots, R_{d,M}\right] , \tag{2}$$

or, of good convergence is assumed,

$$R_M^T = \left[R_{1,1}^M, \ldots, R_{j,1}^M, \ldots, R_{d,1}^M\right] . \tag{3}$$

The frequency arguments have been dropped for brevity.

An Mth-order spectral density matrix can be defined as

$$D_{RM} = E\left[R_M \bar{R}_M\right] \tag{4}$$

where the overbar is the Hermitian transpose.

In (4), each element inside the expectation bracket is the same as the elements of D_{R1} but raised to power M. In order to better handle these matrices, let a new matrix operator Δ be defined as

$$A \Delta B = C , \text{ with } c_{ij} = a_{ij} \cdot b_{ij} , \tag{5}$$

Then,

$$D_{RM} = E\left[(R_1 \bar{R}_1)^{\Delta M}\right] \tag{6}$$

defines $(\cdot)^{\Delta M}$.

A Δ-exponential of a matrix A can similarly be defined as

$$e\Delta(A) = \sum_{M=0}^{\infty} A^{\Delta M}/M! . \tag{7}$$

Then, let the Mth-order, spectral density, generating function be given by

$$\phi_{\Delta R1}(t) = E\left[e\Delta (R_1 \bar{R}_1 t)\right] , \tag{8}$$

so that

$$\phi_{\Delta R1}(t) = \sum_{M=0}^{\infty} E\left[(R_1 \bar{R}_1)^{\Delta M}\right] t^M/M! \tag{9}$$

and

$$\phi_{\Delta R1}(t) = \sum_{M=0}^{\infty} D_{RM} t^M/M! . \tag{10}$$

The function $\phi_{\Delta R1}(t)$ generates the Mth order density matrices in a similar way that the moment generating function generates its moments.

Let r_1 represent a linear measurement of a signal vector $s_1 = [s_{1,1}, \ldots, s_{1,1}, \ldots, s_{1,N}]$ as

$$r_1 = A_1 s_1 + n_1 \tag{11}$$

where n_1 is a vector of i.i.d. noises, independent of the signal sequences $s_{1,1}$. Then, the first-order spectral density matrix D_{R1} is given by

$$D_{R1} = A_1 E\left[S_1 \bar{S}_1\right] \bar{A}_1 + E\left[N_1 \bar{N}_1\right] \tag{12}$$

or

$$D_{R1} = A_1 D_{S1} \bar{A}_1 + D_{N1} \tag{13}$$

where

$$D_{S1} = E\left[S_1 \bar{S}_1\right] \tag{14}$$

and

$$D_{N1} = E\left[N_1 \bar{N}_1\right] \tag{15}$$

are the densities of the source signals and noises according to definition (4).

For the second-order sequences, it can be shown that

$$D_{R2} = A_2 D_{S2} \bar{A}_2 + 2D_{N1}^{\Delta 2} - D_{N2} \tag{16}$$

where

$$A_2 = A_1^{\Delta 2} \tag{17}$$

is the second-order scalar direction matrix and, for independent source sequences

$$D_{S2} = D_{S1}^{\Delta 2} . \tag{18}$$

As a special case, for i.i.d. Gaussian noises of coefficient β^2,

$$D_{N2} = E\left[(N\bar{N})^{\Delta 2}\right] = 3\beta^4 I , \tag{19}$$

and

$$D_{R2} = A_2 D_{S2} \bar{A}_2 - \beta^4 I . \tag{20}$$

Reference [11] features formulae that compute the Mth-order eigenstructure for noises with odd moments that are zero, as well as a more detailed derivation of Eqs. (2) through (20).

APPLICATION TO DIRECTION FINDING

The first-order eigenstructure method is based on Eq. (13) where i.i.d. noises of density β^2; the generating function is

$$D_{R1} = A_1 D_{S1} \bar{B}_1 + \beta^2 I \ . \tag{21}$$

The elements of matrix A_1 are:

$$A_1(i,j) = e^{-j\Omega\mu_{ij}} \ . \tag{22}$$

where Ω is the frequency component and the delay is

$$\mu_{ij} = D_i \sin\phi_j/c \ . \tag{23}$$

Here D_i is the distance separating sensor i from the first sensor, c is the speed of propagation in the medium, and ϕ_j is the incident angle of source j on the array and is to be estimated.

Then, matrix D_{R1}, or, more conveniently, the autocorrelation matrix of the measurements, in the time domain, has as many non-minimum eigenvalues as incident sources. The eigenvectors associated with the multiple minimal eigenvalue β^2 are orthogonal to the columns of matrix A_1, thereby identifying the incident angles ϕ_j.

Likewise, the second-order eigenstructure method is based on Eq. (16) or, for i.i.d. Gaussian noises, on (20) which has the same structure and rank as (21). Thus, the same eigenstructure method can be applied to the spectral density (or autocorrelation matrix) based on the second-order sequences and to matrix A_2 with elements:

$$A_2(i,j) = \left[e^{-j\Omega\mu_{ij}} \right]^2 = e^{-j\Omega2\mu_{ij}} \tag{24}$$

where the delay becomes

$$2\mu_{ij} = (2D_i) \sin\psi_j/c \ . \tag{25}$$

When compared to (23), it becomes apparent that working with the second-order sequences is conceptually equivalent to working with an array of double size, with sensors spaced at distances $2D_i$ of the first sensor.

Therefore, for an array tuned at half the wave length, if the second order is performed, grating lobes appear due to a "conceptual spatial understanding.

Typical improvements in term of the detection of a unique source are shown in Figs. 1 and 2. The second order shows a more definite and thinner peak. The gains in terms of detection are difficult to quantify since it depends, to a large extent, on the criteria of detection and on the type of source signals used. Nevertheless, as seen by this simple example, gains are quite evident.

Throughout, unless otherwise specified, sim ulation is performed using a linear array of 3 sensors, separated by distances D from one another, recording 1024 snapshots of the signals
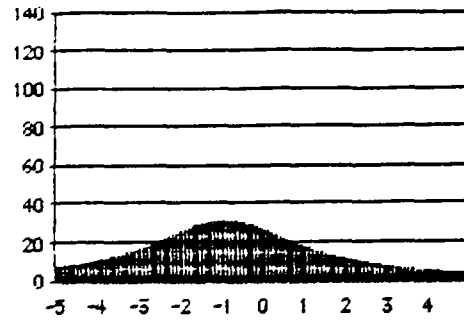

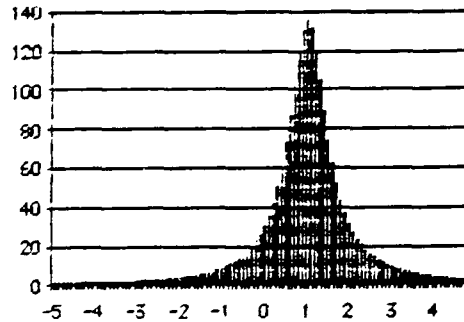Figure 1. ORDER 1: 1 Source at 0°

Figure 2. ORDER 2: 1 Source at 0°

corrupted by Gaussian independent noises. Each source signal consists of a sum of sine waves of different frequencies.

More impressive are the gains in terms of resolution, defined as the ability to distinguish two closely spaced sources. Figures 3, 4, 5, and 6 compare the resolution of the first- and second-order in the case of two sources separated by 4.8° and drawn closer to 1.3° apart. Signal-to-noise ratio conditions are, of course, identical. These two cases are a limit of the resolution for each method. The net improvement of the second-order method is seen as dividing the limit
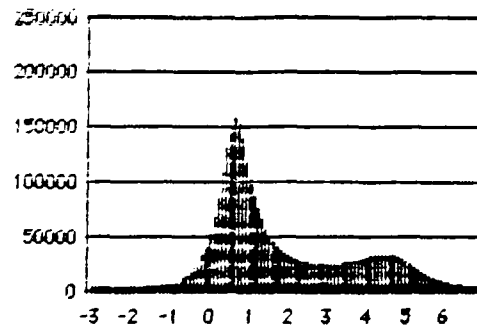

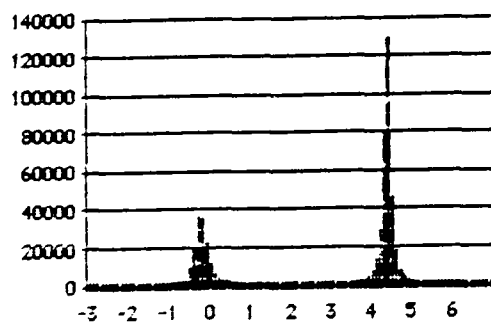Figure 3. ORDER 1: Sources at 0 and 4.8°
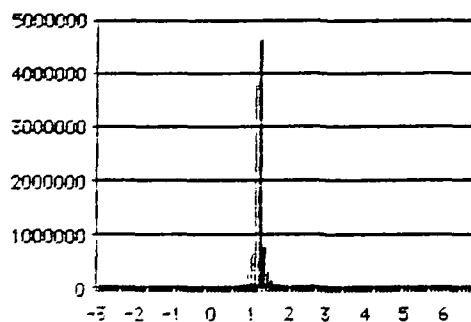
Figure 4. ORDER 2: Sources at 0 and 4.8°
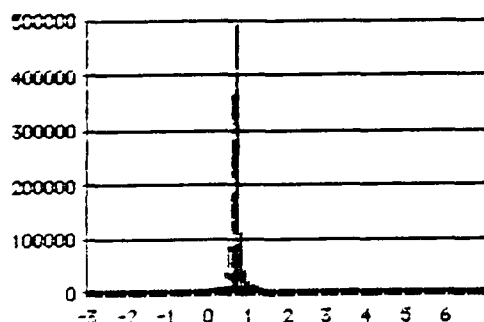

Figure 5. ORDER 1: D = 600, Sources at 0 and 1.3°

Figure 6. ORDER 2: D = 600, Sources at 0 and 1.3°
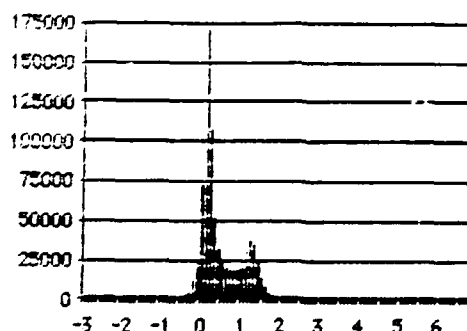

Figure 7. ORDER 1: D = 1200, Sources at 0 and 1.3°

Figure 8. ORDER 1: D = 2400, Sources at 0 and 1.3°
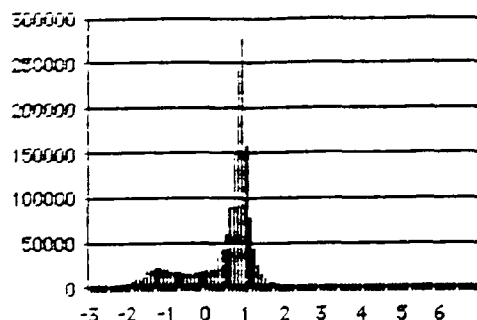

Figure 9. ORDER 1: 50% Correlation, Sources at 0 and 6°

resolution by a factor of 3.7. Note the high peak in Fig. 5, when the first order is unable to distinguish both sources. Bias is present but is always opposite for the second-order when it can be compared to the first-order basis. This might provide a criteria for further precision. Correspondingly, Figures 5, 6, and 7 show the results obtained under the same conditions by an array of twice the physical size. It does not compare to the "conceptual" double array case of the second order. Only in Fig. 8, with an array four times the original size, can the results be compared. Thus, the second-order method does perform better than an array of twice the original size.

Figures 9 and 10 show that the improvements offered by the second-order method are sustained, even in the case of a 50% correlation between source signals. The second-order method can be viewed as an effective tool to fight coherence by offering higher resolution.
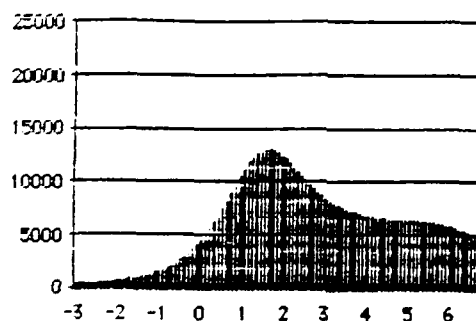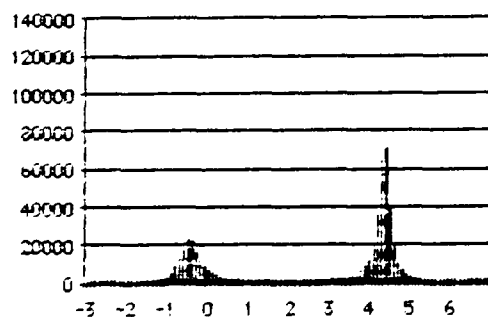
Figure 10. ORDER 2: 50% Correlation, Sources at
0 and 6°

CONCLUSION

The second-order eigenstructure method for
direction finding is a simple method to imple-
ment, through more complex to derive. The en-
hancement of the first-order method when a simple
MUSIC method is used are obvious. A main advan-
tage of the method is its relative independence
of the actual first-order method used. For
example, spacial smoothing techniques can readily
be implemented with the second-order method. On
the other hand, whether the second-order method
adds its improvements to another technique such
as a Toeplitz approach remains to be checked by
further study or simulation.

The added computational burden required by
the second-order method is increased by a factor
of, roughly, $\log_2 N/4$ for N point sequences on a
serial computer using the FFT. What would have
been a prohibitive factor 20 years ago is now
much more reasonable using, for example, parallel
processing. Besides, as shown, it can still
yield better results for fewer data points.

By conceptually doubling the array length,
however, it reduces the effective observing win-
dow angle for an array tuned at half the wave
length. This could force a maneuver of the array
to observe sources at certain angles using the
second-order method.

REFERENCES

[1] V.F. Pisarenko, "The Retrieval of Harmonics
from a Covariance Function," *Geophys. J.
Roy. Astron. Soc.*, Vol. 33, pp. 247–
226:1973.

[2] R.O. Schmidt, "Multiple Emitter Location
and Signal Parameter Estimation," *Proc.
RDAC Spectral Estimation Workshop*, pp. 243–
258:1979.

[3] G. Bienvenu and L. Kopp, "Optimality of
High Resolution Array Processing Using the
Eigensystem Approach," *IEEE Trans. Acous-
tics, Speech and Signal Processing*, Vol.
ASSP-31, pp. 1235–1247:1983.

[4] T.L. Henderson, "Rank Reduction for Broad-
band Waves Incident on a Linear Receiving
Aperture," *Proc. 19th Asilomar Conf. on
Circ., Syst., & Computer*, Pacific Grove,
CA, 1985.

[5] M. Wax and T. Kailath, "Detection of Sig-
nals by Information Theoretic Criteria,"
*IEEE Trans. Acoustics, Speech and Signal
Processing*, Vol. ASSP-33, pp. 387–392:1985.

[6] J. Rissanen, "A Universal Prior for the
Integers and Estimation by Minimum Descrip-
tion Length," *Ann. of Stat.*, Vol. 11, pp.
417–431:1983.

[7] T.J. Shan, M. Wax, and T. Kailath, "Spatial
Smoothing Approach for Location Estimation
of Coherent Sources," *Proc. 18th Asilomar
Conf. on Circ., Systs., & Computer*, Pacific
Grove, CA, 1984.

[8] V.U. Reddy, A. Paulraj, and T. Kailath.
"Performance Analysis of the Optimum Beam-
former in the Presence of Correlated
Sources and its Behavior Under Spatial
Smoothing," *IEEE Trans. Acoustics, Speech
and Signal Processing*, Vol. ASSP-35, No. 7,
pp. 927–936:July 1987.

[9] A. Paulraj and T. Kailath, "Eigenstructure
Methods for Direction of Arrival Estimation
in the Presence of Unknown Noise Fields,"
*IEEE Trans. Acoustics, Speech and Signal
Processing*, Vol. ASSP-34, pp. 13–20:1986.

[10] S.Y. Kung, C.K. Lo, and R. Foka, "A
Toeplitz Approximation Approach to Coherent
Source Direction Finding," *Proc. ICASSP*,
pp. 193–196, Tokyo, 1986.

[11] F. Bugnon and R.R. Mohler, "Nonlinear Proc-
essing With Mth-Order Signals" *Nonlinear
Time Series and Signal Processing*, R.
Mohler Ed., in Lecture Notes in Control and
Information Sciences, Vol. 106, pp. 119–
129, Springer-Verlag, New York, 1988.

BLIND IDENTIFICATION OF INDEPENDENT COMPONENTS
WITH HIGHER-ORDER STATISTICS

Jean-Francois Cardoso

Ecole Nat. Sup. des Telecommunications - Dept SIGNAL
46 rue Barrault, 75634 PARIS CEDEX 13, FRANCE.
and
CNRS-URA 820, GRECO-TDSI.

ABSTRACT

We consider a N-variate random process consisting in N (or less) independent components corrupted by additive noise. Identifying (or separating) these components without any a-priori information about their structure (blind identification) is theorically possible under the independence assumption. We propose a blind algorithm based on second- and fourth-order statistics. Its main feature is the use of tensor formalism allowing blind identification to be performed as a generalized eigen-decomposition of the "quadricovariance tensor". All non-Gaussian components (and possibly one Gaussian component) are separated even if they have identical probability distributions. Simulations in Array Processing context are included.

INTRODUCTION : SEPARATING COMPONENTS.

In this communication, we present an original method for blind identification and separation of independent components in a multivariate process. Finding components or "unmixing" a linear combination is a rather general problem, and various solutions are available, depending on the nature of data, on existence of a priori information, etc... The originality of our method lies in the processing of higher-order information which allows "blind" identification. By this we mean that no a-priori information is needed about component structure or, equivalently, that the method does not impose any special structure on the components to be found.

In order to illustrate this point and to introduce our work, we briefly review here two methods intended for different contexts: the first one is the Principal Components Analysis (PCA), a common tool in Data Analysis, the second one is MUSIC aiming at source localization in Passive Array Listening.

Principal Component Analysis.

Principal Component Analysis (PCA) considers a N-dimension random variable and operates on its covariance matrix. Projecting the variable on the N covariance eigen-vectors yields N components. These components are orthogonal in the geometric sense (since covariance eigen-vectors are always orthogonal) and are shown to be uncorrelated. PCA is of general use: it can be applied to any multivariate process, regardless of its structure, because it does not rely on an a-priori process model, but only on the covariance matrix. This versatility has a drawback: if a process actually is a superposition of non-orthogonal components, PCA is unable to identify them (and does not claim to do so!). So let us give some attention to a technique able to find actual (physically meaningfull) non necessarily orthogonal components.

High Resolution Array Processing.

In Passive Array listening, the N-dimension process under study is the output of a N sensors array. We consider the simple case where discrete sources are independently emitting narrow-band signals. Process covariance is then a simple sum of the contributions of each source. When propagation conditions and array geometry are known, each contribution has a known structure parameterized by source location. Essentially, high resolution is achieved by cleverly combining information gained from observations (summarized in data covariance matrix) and a priori information about component structure.

Blind separation.

Our approach to blind identification is intermediate between the two methods previously outlined. We consider a N-variate random process, hypothesized to be a superimposition of components, but we do not assume these components to have a known structure, justifying the "blind" qualificative: all information comes from data, and from data we want to determine the process constituting components. In order to separate **actual** components as in Array Processing, but without a priori information as in ACP, we make an essential additional hypothesis:

components statistical independence. Statistical independence is a strong property, much stronger than mere uncorrelation which is expressed by second-order statistics. It is the purpose of this communication to show that independence, expressed through second- and fourth-order "cumulant tensors", allows the blind identification problem to be solved in a direct manner.

Previous approaches.

The question of blind component separation by taking advantage of statistical independence has already been adressed in recent litterature. A non-linear adaptive procedure has been proposed in [2,3] while a direct solution using explicitely cumulants was given for the case of two sources and two sensors in [4]. We have proposed in [10] a simpler but less resolvent matrix-based method. It is derived (not explicitely) from the one to be exposed here by considering contracted cumulant tensors. Much work have been to exploit higher-order information in Spectral Analysis or non-minimum phase identification ([5,6,7], for instance) but the link with the present problem is not very direct: stationnary time processes are usually considered. Hence the "components" are complex exponentials (leading to the notion of poly-spectra) which are indeed of known structure. Some authors [8,9] use higher-order information for multivariate processes, but again this information is usually coupled with a-priori information (generally an harmonic structure) about the components.

BLIND SEPARATION OF INDEPENDENT COMPONENTS

Process model.

We consider a N-variate complex stochastic process, consisting in the superimposition of M independent components with $M < N$, and possibly corrupted by additive Gaussian noise.

$$(1) \qquad (M): \quad X = \sum_{p=1}^{M} \alpha_p X_p + B$$

The structure of each component is then determined by vector X_p which is deterministic while α_p is a scalar stochastic variable. Each α_p is statistically independent from the others and independent from the additive noise B. In addition, we assume that the noise process B is Gaussian and (in analogy to Array Processing) "spatially white" that is:

$$(2) \qquad R_B = E(B B^T) = \sigma^2 I.$$

where I denotes the identity matrix and σ^2 is called the noise variance. As fixed vectors X_p characterize influence of a given component, we shall call them "component signatures", while variables α_p, forming the stochastic part of the process, are sometimes refered to as "the signals".

Identification.

Starting only from process observation, the problem we address is: the number of components and noise variance being unknown, identify unknown signatures X_p and separate signals α_p. Before going further, it should be noted that exchange of a scalar factor between X_p and α_p leaves the process essentially unchanged. Hence, in the following, what is called "complete signature determination" has to be understood as "determination up to a scalar factor", because this is definitely the best that can be done. In addition, this "best" is not bad, as an unknown scalar factor in each signature still allows signal separation.

Reduced model. In order to expose our results as simply as possible, we shall derive them using a reduced model denoted (M'), simpler than (M). In this simplified model we assume that no noise is present and that process dimensionnality is equal to the number of sensors $(M = N)$:

$$(3) \qquad M': \quad X = \sum_{p=1}^{N} \alpha_p X_p$$

In a next section we show how the solution for reduced model is easily extended to the complete model.

HIGHER ORDER STRUCTURE.

This section briefly introduces tensor notations, define second- and fourth-order cumulant tensors and exhibits their particular structure when process follows model (M').

Tensor notations.

Cumulants may be defined as coefficients in the Taylor series expansion of the second characteristic function [1]. As a consequence, for multivariate processes, first- and second-order cumulants are vectors and matrices respectively and higher-order cumulants have to be represented as tensors. In the following, we use a simplified tensor notation: a column vector X is represented by the indexed quantity x_i, $i=1,N$ which is just its i-th coordinate in some orthonormal basis. Notation does not differentiate column vectors from line vectors, so that complex conjugate vector X^T is represented by x_i^*, $i=1,N$ where the star denotes complex conjugate. If a matrix A is represented by the doubly indexed quantity a_{ij}, then its transpose conjugate is a_{ji}^*, and so on. To make equations more readable we also use classical Einstein's summation convention: an implicit summation is to be understood over any index appearing twice in a given term. For instance: $a_{ij}x_j$ stands for $\sum_j a_{ij}x_j$ and trace of matrix A is just a_{ii}.

Cumulant tensors.

In this work, we only consider second- and fourth-order statistics. We define two "cumulant tensors": the covariance tensor (which is nothing but the covariance matrix) and the quadricovariance tensor, according to

(4)
$$r_{ij} = Cum(x_i, x_j^*)$$
$$q_{ijkl} = Cum(x_i, x_j^*, x_k^*, x_l)$$

By construction, covariance enjoys hermitian symmetry:

(5)
$$r_{ij} = r_{ji}^*$$

which is an essential property since it allows orthogonal eigendecomposition, as well as factorization. quadricovariance symmetry properties are more complex but for later use we only retain a symmetry analog to (5):

(6)
$$q_{ijkl} = q_{klij}^*$$

Let us explicit the effect of a linear transformation on the data. We denote x_i' the process obtained by linearily transforming original process x_i through matrix a_{ij} according to $x_i' = a_{ij}x_j$. Thanks to linear properties of cumulants, the link between cumulant tensors of the two processes is just:

(7)
$$r_{ij}' = r_{mn} a_{mi} a_{nj}^*$$
$$q_{ijkl}' = q_{mnop} a_{mi} a_{nj}^* a_{ok}^* a_{pl}$$

Cumulant tensors structure.

We now derive cumulant tensor structure in terms of model parameters. To keep notations simple, a concise notation for signature vectors is adopted: the i-th component of signature X_p is denoted p_i. With this notation, reduced model equation (3) reads:

(8)
$$x_i = \sum_p \alpha_p p_i$$

For each component, the scalar random variable α_p is described by its 2-4-order statistics: variance σ_p^2 and kurtosis μ_p defined by

(9)
$$\sigma_p^2 = Cum(\alpha_p, \alpha_p^*)$$
$$\mu_p \sigma_p^4 = Cum(\alpha_p, \alpha_p^*, \alpha_p^*, \alpha_p)$$

If we simply substitute eq (8) in definitions (4), it comes by linearity of cumulants and using the fact that joint cumulants of independent variables are zero:

(10)
$$a \qquad r_{ij} = \sum_p \sigma_p^2 p_i p_j^*$$

$$b \qquad q_{ijkl} = \sum_p \sigma_p^4 \mu_p p_i p_j^* p_k^* p_l$$

These equations relate observable 2-4-order data statistics to the p_i's i.e. the signatures we want to estimate. All we need is a procedure allowing signature extraction from equations (10). Next section proposes such a procedure, once we will show that 2-4-order equations uniquely determine the signatures.

SOLVING COUPLED 2-4-ORDER TENSOR EQUATIONS.

The proposed method for inversion of 2-4-order equations (10) operates in two steps. The first step is an orthogonalization procedure and, in some sense, "exhausts" the second-order information content. The second step is a kind of eigen-decomposition where "eigen-matrices" are extracted from quadricovariance tensor. These eigen-matrices are then shown to be the separating devices we are looking for.

Orthonormalization.

Covariance matrix, as any hermitian matrix, can be factorized (non-uniquely) into a product acccording to $R = C\,C^{f}$ where C is a (non necessarily hermitian) matrix. In tensor notations, this reads:

$$(11) \qquad r_{ij} = c_{im}\,c_{jm}^{*}$$

In model (M'), if signatures are assumed linearily independent, covariance is full rank so that C is invertible. Let us denote H its inverse ($h_{im}\,c_{mj} = \delta_{ij}$) and show its orthonormalizing effect by applying $h_{ki}\,h_{lj}^{*}$ to both sides of 10.a. The left-hand side yields:

$$r_{ij}\,h_{ki}\,h_{lj}^{*} = h_{ki}\,c_{im}\,h_{lj}^{*}c_{jm}^{*} = \delta_{km}\,\delta_{lm}^{*} = \delta_{kl}$$

and the right-hand side yields:

$$h_{ki}\,h_{lj}^{*}\,\sum_{p}\sigma_{p}^{2}\,p_{i}\,p_{j}^{*} = \sum_{p}\sigma_{p}^{2}\,h_{ki}\,p_{i}\,h_{lj}^{*}p_{j}^{*} = \sum_{p}p'_{k}\,p'_{l}^{*}$$

where we define:

$$(12) \qquad p'_{i} = \sigma_{p}\,h_{ij}\,p_{j}$$

Hence effect of h_{ij} on signatures is to produce a new set of "orthonormalized signatures" since they verify:

$$(13) \qquad \sum_{p}p'_{k}\,p'_{l}^{*} = \delta_{kl}$$

Let us apply a similar transformation to quadricovariance tensor. We define the orthonormalized quadricovariance q'_{ijkl} according to:

$$(14) \qquad q'_{ijkl} = q_{mnop}\,h_{im}\,h_{jn}^{*}\,h_{ko}^{*}\,h_{lp}$$

and the structure equation (10.b) gives:

$$(15) \qquad q'_{ijkl} = \sum_{p}\mu_{p}\,p'_{i}\,p'_{j}^{*}\,p'_{k}^{*}\,p'_{l}$$

Orthonormalized quadricovariance has a special structure: it is a sum of N components (eq. 15), each of them being constructed from a single orthonormalized signature.

Eigen-matrices.

Eigen-matrix of a 4-order tensor is the direct generalisation of a matrix eigen-vector. We know from eigen-theory that, if matrix a_{ij} is hermitian i.e. verifies for any i and j : $a_{ij} = a_{ji}^{*}$, then it admits a set of N real eigenvalues λ_{u}, $u = 1,N$ and N orthonormal eigenvectors u_{i} and can be decomposed according to:

$$(16) \qquad a_{ij} = \sum_{u}^{N}\lambda_{u}\,u_{i}\,u_{j}^{*}$$

If eigen-values are distinct, eigen-vectors are uniquely determined up to a unit-norm complex factor. We now consider quadricovariance q_{ijkl} as a linear operator on the N^{2}-dimension complex linear space of matrices. As quadricovariance tensor verifies an hermitian symmetry (eq. 6) it admits an eigen-decomposition according to:

$$(17) \qquad q_{ijkl} = \sum_{m}^{N^{2}}\lambda_{m}\,m_{ij}\,m_{kl}^{*}$$

where the λ_{m}'s are N^{2} real numbers and where the m_{ij}'s are N^{2} complex matrices with dimension $N \times N$. We naturally refer to quantities m_{ij} as "eigen-matrices" of the tensor. We also deduce from eigen-theory that if eigen-values are distinct, then eigen-matrices are uniquely determined up to unit-norm complex factor.

Solution.

Now the problem of extracting signatures from quadricovariance is solved by identifying the quadricovariance structure expression (15) and symmetric tensor eigen-decomposition (17). Using the facts that signatures have been orthogonalized and that, if an eigen-value is distinct from the others the corresponding eig n-matrix is unique (up to a unit-norm factor), we can identify **term to term** the two expressions (15) and (17). In the general case, component kurtosis are all different, so that tensor eigen-decomposition procedure will yield, for N among N^2 values of m, N non-zero eigen-values λ_m and N "significant" eigen-matrices m_{ij}, each one uniquely associated to a single component p:

(18)
$$\begin{cases} \lambda_m = \mu_p \\ m_{ij} = z_m \, p'_i \, p'^*_j \end{cases}$$

(z_m is an arbitrary irrelevant unit-norm complex number). In addition, there are $N^2 - N$ remaining null eigen values, associated to non significant eigen-matrices. Incidentally, this is where Gaussian components show (as expected) to be unseparable: they have zero kurtosis, hence their eigen-matrices can not be distinguished from the $N^2 - N$ non significant ones. (As a matter of fact, this is not absolutely true because Gaussian components are orthogonalized all the same, so that if only **one** Gaussian component is present, its signature can be determined as being orthogonal to the $N - 1$ other ones).

Algorithm summary. In summary, blind identification of independent components is possible, in the general case, through the following algorithm.

- From data, estimate second- and fourth-order cumulant tensors (4).

- Use covariance to orthonormalize quadricovariance (15)

- Feed an usual eigen-decomposition routine with orthonormalized quadricovariance considered as a $N^2 \times N^2$ matrix.

- Find the N non-zero eigen-values and retain the associated N^2-vectors.

- Consider each N^2-vector as a $N \times N$-eigen-matrix. These matrices being rank-one determine single vectors.

- Un-orthonormalize these vectors: they are component signatures. Signals can be separated.

Full solution.

Due to lack of place, we indicate only briefly how the method should operate when some of the assumptions we have made are not verified.

Identical kurtosis. When kurtosis are identical, non-zero quadricovariance eigen-values also become identical, and eigen-matrices no longer contain a single term in $p'_i p'^*_j$ but are mixes of such terms. Hence orthogonalized signatures remain identifiable because they still are the significant eigen-values of quadricovariance significant eigen-matrices.

Number of components inferior to dimensionnality: $M < N$. Covariance matrix is then no longer invertible but its pseudo-inverse can be used in place. This is equivalent to operating the method in the covariance image space (the linear subspace spanned by signatures which is also identical to the space spanned by covariance significant eigen-vectors).

Taking noise into account. With $M < N$ and a noise model as in (2), noise variance is estimated from the $N - M$ lowest covariance eigen-values which are equal to σ^2 rather zero. A noise-free covariance is estimated by substracting $\sigma^2 I$ from the measured covariance, allowing correct signature orhonormalization. If noise can be assumed Gaussian, it has no effect on fourth-order statistics and the algorithm runs along the same line.

Many Gaussian components. The presence of N' Gaussian components gives N' additionnal eigen-matrices does not impede identification of the remaining non-Gaussian components

SIMULATIONS.

We present a preliminary simulation in Array Processing context. We consider a linear array of 4 equispaced sensors located half a wavelength apart. There are two sources with equal powers located in the far field. First source has a 0 degree bearing and a binary density probability. Second source is at 20 degrees and is uniformely distributed. Independent Gaussian noise is added at sensor ouput. The separation is evaluated in terms of crosstalk rejection. After signatures are estimated, we construct a vector F in the plane generated by the two signatures and orthogonal to the second one. This is intended to isolate the first source signal by forming $F^T X$. Because of estimation error, this can not be exactly achieved and we define the performance index as the ratio in $F^T X$ between first source power and remaining second source power. First plot shows performance index versus signal-to-noise ratio (both in dB). The three curves correspond to cumulant tensors estimated with 20, 200 ,2000 data samples respectively. In the second plot, we show a more difficult separation: signatures are closer, the second source is now located at only 5 degrees. Space is lacking fore detailed comments but separation ability is perfectly clear in both plots.

Sources 20 degrees apart   Sources 5 degrees apart
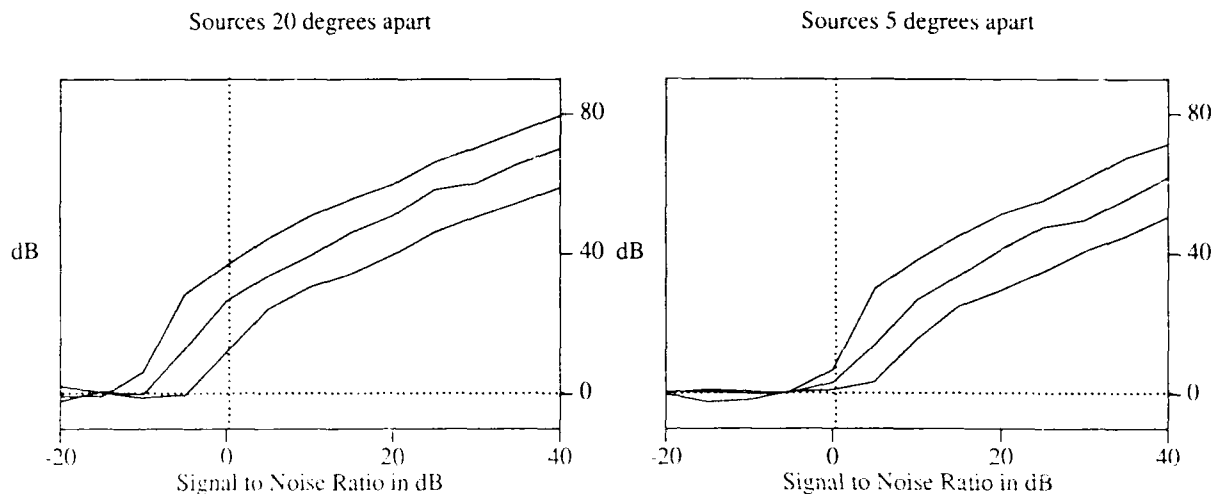
CONCLUSION.

We have shown that knowledge of second- and fourth-order statistics expressed through "cumulant tensors" is sufficient for blind identification of independent components of a N-variate process. We gave a constructive proof by proposing a direct identification algorithm operating in two steps: covariance based orthonormalization followed by quadricovariance tensor eigen-decomposition . This decomposition exploits a particular hermitian tensorial symmetry, but we feel that identification could be improved if all tensor symmetries were used. Although the method is quite general, we think that promising applications are in the field of Array Processing where high resolution methods are very sensitive to model inadequacies, a problem not affecting blind identification.

REFERENCES.
[1] D.R. Brillinger, "Time Series Data Analysis and Theory", Holden Day, 1981.
[2] C. Jutten and J. Herault, "Independent Components Analysis Versus Principal Components Analysis", Signal Processing IV: Theo. and Appl. Elsevier publishers, pp. 643-646, 1988.
[3] J. Herault, C. Jutten and B. Hans, "Detection de Grandeurs Primitives dans un Message Composite", 10th GRETSI Nice, pp. 1017-1022, 1985.
[4] J.L. Lacoume, P.Ruiz, "Source Identification: A Solution Based on the Cumulants", Proc. of the 4-th ASSP Workshop on Spectral Estimation and Modeling,pp. 199-203, Aug. 1988.
[5] A. Swami and J.M. Mendel, "Cumulant-Based Approach to the Harmonic Retrieval Problem", Proc. ICASSP-88,pp. 2264-2267, 1988.
[6] J.K. Tugnait, "Identification of Linear Stochastic Systems via Second- and Fourth-Order Cumulant Matching", IEEE Trans. on I.T., Vol. IT-33, No. 3, pp.393-407, May 1987.
[7] A. Benveniste, M. Goursat, G.Ruget, "Robust Identification of a Nonminimum Phase System: Blind Adjustement of a Linear Equalizer", IEEE Trans. on A.C., Vol. AC-25, No. 3, pp.385-399, June 1980.
[8] R. Pan and C.L. Nikias, "Harmonic Decomposition Methods in Cumulant Domains", Proc. ICASSP-88,pp. 2356-2359, 1988.
[9] M. Amengual, F. Vallverdu and G. Vazquez, "On the Use of Higher Order Information in SVD Based Methods", Signal Processing IV Theo. and Appl. Elsevier publishers,pp. 431-434, 1988.
[10] J. F. Cardoso, "Blind Identification of Independent Components with Higher-Order Statistics", to be published in Proc. ICASSP 89.

THE ESPRIT ALGORITHM WITH HIGHER-ORDER STATISTICS

Hsing-Hsing Chiang and Chrysostomos L. Nikias
Communications and Digital Signal Processing (CDSP)
Center for Research and C.aduate Studies
Northeastern University
Boston, MA 02115

ABSTRACT

We address in this paper the bearing estimation problem of sources from array measurements for signal environments where the signal is non-Gaussian and the additive noise sources are colored (spatially correlated) Gaussian with unknown second-order statistics. The ESPRIT bearing estimation problem is reformulated using fourth-order cumulant matrices instead of autocorrelation matrices. By doing so, the fourth-order cumulant matrices of the additive colored Gaussian noises can be suppressed and therefore knowledge of the noise cross-correlation matrix becomes unnecessary. Simulation results are presented and performance comparisons are made between the fourth-order cumulant-based ESPRIT and its equivalent second-order statistics-based version when the additive noise sources are colored Gaussian with unknown spatial correlation matrix.

I. INTRODUCTION

Array processing algorithms have been found very useful in many applications over the years including those to sonar, radar, geophysics and biomedicine [1], [2]. The objective in an array processing scenario is to estimate the number of sources and their bearings relative to the array configuration. Included in the class of array processing methods are the conventional beamforming, the signal subspace (Autoregressive, Maximum Norm and Maximum Likelihood of Capon with their modifications) as well as the noise subspace (Pisarenko, MUSIC, Root-Music, eigenvector) methods [1]-[3]. Several papers have been published in the literature over the past decade dealing with the estimation performance and computational complexity of the aforementioned array processing methods.

One of the most popular high resolution array processing techniques has been the MUSIC algorithm due to Schmidt which has been shown to yield asymptotically unbiased and efficient estimates [4]-[6]. An important new approach to the bearing estimation problem from array data has recently been proposed based on the idea of Estimating Signal Parameters via Rotational Invariance Techniques (ESPRIT). Although the ESPRIT is similar to MUSIC in that it provides estimates that are asymptotically unbiased and efficient, it exhibits several advantages over MUSIC [8], [9]. These are: (i) ESPRIT exhibits better performance than MUSIC for certain signal scenarios, (ii) it does not require knowledge of the array geometry, and (iii) it requires less computations than MUSIC. It has been reported in [6], [10] that ESPRIT is equivalent to the Toeplitz Approximation Method (TAM) introduced in [11] for the solution of harmonic retrieval problems.

The array processing methods have been developed using second-order statistics (autocorrelations) of the array data and assuming that the additive noise is spatially white; i.e., diagonal spatial correlation matrix. The sensitivity of these methods to spatially colored noise has yet to be quantified, especially in those scenarios where the spatial autocorrelation matrix of the additive noise is unknown or cannot be estimated accurately. Array processing (or harmonic retrieval) problems in the presence of spatially correlated colored noise have been studied assuming either known noise autocorrelation or estimated one from secondary inputs [12], [14].

The bearing estimation problem from array data in the presence of spatially correlated Gaussian noise sources has been addressed in [15] by employing fourth-order cumulants of the array snapshots instead of autocorrelations. In particular, it was shown that the signal and noise subspace array processing methods can be easily reformulated using fourth-order cumulant matrices. Simulation results were presented and comparisons were made that demonstrated the improved performance of the fourth-order cumulant-based methods over their equivalent autocorrelation-based versions when the additive noise sources were colored Gaussian with unknown autocorrelation matrix.

The main motivation behind the use of higher-order statistics or cumulants in array processing problems lies in their ability to suppress noise under certain conditions, without being necessary to know the exact probability density function (pdf) governing the noise samples [16], [17]. In particular, if the additive noise has Gaussian pdf, then all its cumulants of order greater than two are identically zero [16]-[18]. The purpose of this paper is to show an extension of the ESPRIT bearing estimation problem using fourth-order statistics and demonstrate its performance with simulation examples. Comparisons will also be made between the fourth- and second-order statistics-based ESPRIT algorithms.

The organization of the paper is as follows. Section II summarizes the problem formulation and assumptions. In Section III, the ESPRIT algorithm based on fourth-order statistics is given and its properties outlined. Simulation results and performance comparisons are discussed in Section IV. Finally, Section V is devoted to concluding remarks.

II. PRELIMINARIES AND PROBLEM FORMULATION

Let us assume that a sensor array consists of M equispaced sensors and that the signals from N ($N < M$) narrowband non-Gaussian stationary sources, statistically independent from each other, have bearings $\theta_1, \theta_2, \ldots, \theta_N$ relative to the array configuration. The signal received at the nth sensor is given by

$$x_i(t) = \sum_{k=1}^{N} s_k(t) \exp\{-j w_k(i-1)\} + W_i(t) \qquad (1)$$
$$i = 1, 2, \ldots, M$$

where $s_k(t)$ is the signal emitted by the kth source and received at the first sensor (e.g. reference sensor) of the array and $W_i(t)$ is the zero-mean Gaussian noise of the ith sensor. The noise sources $\{W_i(t)\}$ may be spatially correlated with each other but are assumed independent from the source signals. The spatial frequency w_k is defined by

$$w_k = (2\pi f_o\, d \sin\theta_k)/c \qquad (2)$$
$$k = 1, 2, \ldots, N$$

where f_o is the center frequency of all source signals, d is the spacing between sensors, θ_k is the direction of arrival (or bearing) of the kth source and c is the speed of plane wave propagation.

Combining the sensor signals $x_i(t)$ in two subarrays, X and Y, of the form [7]-[9]

$$X(t) = [x_1(t), x_2(t), \ldots, x_{M-1}(t)]^T \qquad (M-1) \times 1$$
$$Y(t) = [x_2(t), x_3(t), \ldots, x_M(t)]^T \qquad (M-1) \times 1 \qquad (3)$$

the received data can be written as

$$X(t) = AS(t) + W_x(t)$$
$$Y(t) = A\Phi S(t) + W_y(t) \qquad (4)$$

where

$$S(t) = [s_1(t), \ldots, s_N(t)]^T \qquad N \times 1$$
$$W_x(t) = [W_1(t), \ldots, W_{M-1}(t)]^T \qquad (M-1) \times 1$$
$$W_y(t) = [W_2(t), \ldots, W_M(t)] \qquad (M-1) \times 1$$

$$A = \begin{pmatrix} 1 & 1 & \cdots & 1 \\ e^{jw_1} & e^{jw_2} & \cdots & e^{jw_N} \\ \vdots & \vdots & \vdots & \vdots \\ e^{jw_1(M-2)} & e^{jw_2(M-2)} & \cdots & e^{jw_N(M-2)} \end{pmatrix} \quad (M-1) \times N$$

is the direction matrix and

$$\Phi = \begin{pmatrix} e^{jw_1} & 0 & \cdots & 0 \\ 0 & e^{jw_2} & \cdots & 0 \\ \vdots & \vdots & \vdots & \vdots \\ 0 & 0 & \cdots & e^{jw_N} \end{pmatrix} \qquad N \times N$$

The problem in array processing is how to estimate the number of sources, N, and their bearing $\theta_1, \theta_2, \ldots, \theta_N$ from the given measurements $\{x_i(t)\}$, $i = 1, 2, \ldots, M$.

III. THE ESPRIT ALGORITHMS

A. SECOND-ORDER STATISTICS CASE

The autocorrelation matrix of the array snapshot data is given by

$$R_{xx} = E\{X(t)X^H(t)\} = A \Sigma A^H + R_{xx}^w \qquad (M-1) \times (M-1) \quad (5)$$

where "H" denotes Hermitian conjugate operation, $\Sigma = \mathrm{diag}\{\sigma_1^2, \ldots, \sigma_N^2\}$ where σ_k^2 is the variance of $\{s_k(t)\}$ and R_{xx}^w is the autocorrelation matrix of the noise sources which is assumed here to be a **non-diagonal** matrix. On the other hand, the cross-correlation between subarray data X and Y is given by

$$R_{xy} = E\{X(t)Y^H(t)\} = A \Sigma \Phi^H A^H + R_{xy}^w, \quad (M-1) \times (M-1) \quad (6)$$

Notice that if the noise sources, $\{W_i(t)\}$, are spatially uncorrelated, then

$$R_{xx}^w = \sigma^2 I$$

and

$$R_{xy}^w = \begin{pmatrix} 0 & \cdots & 0 \\ \sigma^2 I & & \vdots \\ & & 0 \end{pmatrix} \qquad (7)$$

where I is the identity matrix. It is for the special case of spatially uncorrelated noise sources that the ESPRIT algorithm has been formulated using R_{xx} and R_{xy} matrices. Its key steps are the following [8], [9]:

(i) Compute the eigenvalues and eigenvectors of R_{xx}. From (5) and (7), it follows that the noise subspace eigenvalues are equal to σ^2.

(ii) Form matrices $\hat{R}_{xy} = R_{xy} - R_{xy}^w$, where R_{xy}^w is given by (7).

(iii) The matrix pair $(R_{xx}, \hat{R}_{xy})$ has N general eigenvalues at $\{\exp j\, w_k\}$, $k = 1, 2, \ldots, N$.

As pointed out in [8], it is preferable to operate directly on the data using singular value decomposition (SVD) instead of autocorrelation matrices.

One of the main limitations of the ESPRIT algorithm based on second-order statistics is that it will fail to work well in the presence of spatially correlated noise sources; i.e., when R_{xx}^w is non-diagonal and R_{xy}^w has non-zero elements beyond its first subdiagonal. If the additive noise sources are Gaussian, the aforementioned limitation could be overcome by the use of fourth-order statistics.

B. FOURTH-ORDER STATISTICS CASE

We can define the fourth-order cumulant matrix of the array snapshots as

$$C_{xx} \equiv \mathrm{Cum}\left\{ \begin{pmatrix} x_1(t) & x_1^*(t) & x_1(t) \\ x_2(t) & x_2^*(t) & x_2(t) \\ \vdots & \vdots & \vdots \\ x_{M-1}(t) & x_{M-1}^*(t) & x_{M-1}(t) \end{pmatrix} \cdot \right.$$
$$\left. [x_1(t), x_2^*(t), \ldots, x_{M-1}(t)] \right\}$$

where "$*$" denotes conjugate and "Cum" is the abbreviation of cumulant. Notice that the definition of cumulants of complex array data is non-unique. However, it is the one described by [8] which will be useful to our problem. If a non-Gaussian stationary random process, $x(k)$, has zero mean, its fourth-order cumulants are given by [16]-[18]

$$\mathrm{Cum}\left\{ x(k), x^*(k + \tau_1), x(k + \tau_2), x^*(k + \tau_3) \right\}$$

$$\approx c_4(\tau_1, \tau_2, \tau_3)$$

$$= E\left\{x(k)x^*(k+\tau_1)x(k+\tau_2)x^*(k+\tau_3)\right\}$$

$$- E\left\{x(k)x^*(k+\tau_1)\right\} \cdot E\left\{x(k+\tau_2)x^*(k+\tau_3)\right\}$$

$$- E\left\{x(k)x(k+\tau_2)\right\} \cdot E\left\{x^*(k+\tau_1)x^*(k+\tau_3)\right\}$$

$$- E\left\{x(k)x^*(k+\tau_3)\right\} \cdot E\left\{x^*(k+\tau_1)x(k+\tau_2)\right\}. \quad (9)$$

Thus, the fourth-order cumulants are functions of moments from first to fourth-order. Similarly, the cross fourth-order cumulant matrix of the array data is given by

$$C_{xy} \equiv \mathrm{Cum}\left\{ \begin{pmatrix} x_1(t) & x_1^*(t) & x_1(t) \\ x_2(t) & x_2^*(t) & x_2(t) \\ \vdots & \vdots & \vdots \\ x_{M-1}(t) & x_{M-1}^*(t) & x_{M-1}(t) \end{pmatrix}, \right.$$

$$\left. \left[x_2^*(t), x_3^*(t), \ldots, x_M^*(t) \right] \right\} \quad (10)$$

Substituting (4) into (8) and (10), we obtain

$$C_{xx} = A \Gamma A^H \qquad (M-1) \times (M-1) \quad (11)$$

$$C_{xy} = A \Gamma \Phi^H A^H \qquad (M-1) \times (M-1) \quad (12)$$

even when the additive noise sources are Gaussian and spatially correlated with unknown correlation function.

Matrix $\Gamma = \mathrm{diag}\left\{\gamma_1, \ldots, \gamma_N\right\}$, where γ_k is the fourth-order cumulant (kurtosis) of the kth source signal defined by

$$\gamma_k \triangleq \mathrm{Cum}\left\{s_k(t), s_k^*(t), s_k(t), s_k^*(t)\right\}. \quad (13)$$

It follows from (11) and (12) that the matrix pair (C_{xx}, C_{xy}) has N general eigenvalues at $\{exp(j\omega_k)\}$, $k = 1, 2, \ldots, N$. In practice, however, due to errors in estimating C_{xx} and C_{xy} from finite data, expression (11) and (12) do not valid exactly. Hence, the procedure (i)-(iii) previously described with autocorrelation matrices can also be adopted with C_{xx} and C_{xy}.

IV. SIMULATION RESULTS

In this section simulation results are presented and comparisons are made to demonstrate the performance of the ESPRIT algorithms that are based on second- and fourth-order statistics when the additive noise sources are Gaussian spatially uncorrelated, as well as spatially correlated with unknown autocorrelation matrix.

The array we consider in the simulations is uniform and linear with $M = 8$ sensors. We assume $N = 2$ sources in the far field, and non-Gaussian stationary source signals with $f_1 = 0.1$ Hz and $\omega_1 = 0.8[3]$ and $\omega_2 = 1.3277$. Fig. 1 illustrates the spectral eigenvalues (GE) estimates via second- and fourth-order statistics-based ESPRIT algorithms for the **noise free** case, as we are concerned with 32 samples per segment (16 × 32) for the estimation of R_{xx}, R_{xy}, C_{xx} and C_{xy} matrices. Clearly, both methods demonstrate good performance (as expected).

Fig. 2 illustrates the results of the ESPRIT algorithms when the additive noise sources are white and spatially uncorrelated with SNR = 20dB. Results are shown for 16 × 32 and 64 × 32 data lengths. From this figure, it is apparent that the overall performance of the ESPRIT algorithm with second-order statistics (ESPRIT (2)) is better than that of the fourth-order statistics version (ESPRIT (4)) in the sense that the noise subspace GEs of ESPRIT (2) are scattered closer to the origin. However, both algorithms resolve the two closely spaced sources successfully.

The same source signals are used in the third example but with additive white Gaussian noise sources that are spatially correlated. Fig. 3 shows the performance of ESPRIT (2) and ESPRIT (4) algorithms for 16 × 32 and 64 × 32 data lengths and SNR = 20dB. From Fig. 3, it appears that although the ESPRIT (2) algorithm resolves the two sources, it does not suppress the spatially correlated noise which shows as another one peak at $\theta = 0^o$ (e.g. high concentration of GE's at the cross-section between x-axis and unit circle.) On the other hand, ESPRIT (4) resolves the two sources with significantly less concentration of GE's near the point ($|r| = 1, \theta = 0^o$).

Finally, Fig. 4 illustrates the results of an example where the noise sources are Gaussian, color and spatially correlated. The source signals are the same as before and SNR = 20dB. Clearly, the ESPRIT (4) method exhibits better performance than the ESPRIT (2) algorithm in resolving the two sources and suppressing the noise at the same time.

V. CONCLUSIONS

The purpose of this paper was to introduce a reformulation of the original ESPRIT algorithm with higher-order statistics and specifically with fourth-order cumulants. The extension was simple and somewhat straightforward. The main motivation behind the use of the ESPRIT algorithm with fourth-order cumulants was to suppress additive Gaussian spatially correlated noise sources without knowing their spatial correlation matrix. Simulation results demonstrated the effectiveness of the new ESPRIT method.

REFERENCES

[1] D.H. Johnson, *The Application of Spectral Estimation Methods to Bearing Estimation Problems*, **Proc. IEEE**, Vol. 70, pp. 1017-1028, September 1982.

[2] S. Haykin (Ed.), **Array Processing**, Prentice-Hall, Inc., Englewood Cliffs, NJ, 1985.

[3] S.L. Marple, Jr., **Digital Spectral Analysis with Applications**, Ch. 13, Prentice-Hall, Inc., Englewood Cliffs, NJ, 1987.

[4] R.O. Schmidt, *Multiple Emitter Location and Signal Parameter Estimation*, **Proc. RADC Spectral Estimation Workshop**, Griffiths AFB, pp. 243-258, 1979.

[5] P. Stoica and A. Nehorai, *MUSIC, Maximum Likelihood and Cramer-Rao Bound*, **Proc. ICASSP'88**, pp. 2296-2299, New York, NY, April 1988.

[6] B.D. Rao and K.V.S. Hari, *Performance Analysis of Subspace-Based Methods*, **Proc. 4th ASSP Workshop on Spectrum Estimation**, pp. 92-97, Minneapolis, MN, August 1988.

[7] A. Paulraj, R. Roy, and T. Kailath, *Estimation of Signal Parameters via Rotational Invariance Techniques - ESPRIT*, **Proc. 19th Asilomar Conf. Circuits, Syst. Comput.**, Asilomar, CA, November 1985.

[8] R. Roy, A. Paulraj, and T. Kailath, *Direction-of-Arrival Estimation by Subspace Rotation Methods - ESPRIT*, **Proc. ICASSP'86**, pp. 2495-2498, Tokyo, Japan, April 1986.

[9] R. Roy, A. Paulraj, and T. Kailath, *ESPRIT - A Subspace Rotation Approach to Estimation of Parameters of Cisoids in Noise*, **IEEE Trans. Acoust., Speeech, and Signal Processing**, Vol. ASSP-34(5), pp. 1340-1342, October 1986.

[10] S. Mayrargue, *ESPRIT and TAM are Theoretically Equivalent*, **Proc. ICASSP'88**, pp. 2456-2459, New York, NY, April 1988.

[11] S.Y. Kung, K.S. Arun, and D.V. Bhaskar Rao, *State-Space and Singular Value Decomposition-Based Approximation Methods for the Harmonic Retrieval Problem*, **Proc. 2nd ASSP Workshop on Spectral Estimation**, Tampa, FL, November 1983.

[12] V.U. Reddy, A. Paulraj, and T. Kailath, *Performance Analysis of the Optimum Beamformer in the Presence of Correlated Sources and Its Behavior under Spatial Smoothing*, **IEEE Trans. Acoust., Speech, and Signal Processing**, Vol. ASSP-35, pp. 927-936, July 1987.

[13] E.J. Kelly, *An Adaptive Detection Algorithm*, **IEEE Trans. Aerospace and Electronic Systems**, Vol. AES-22(1), pp. 115-127, March 1986.

[14] H. Sakai, *Estimation of Frequencies of Sinusoids in Colored Noise*, **Proc. ICASSP'86**, pp. 177-180, Tokyo, Japan, April 1986.

[15] R. Pan and C. L. Nikias, *Harmonic Decomposition Methods in Cumulant Domains*, **Proc. ICASSP'88**, pp. 2356-2359, New York, NY, April 1988.

[16] C.L. Nikias and M.R. Raghuveer, *Bispectrum Estimation: A Digital Signal Processing Framework*, **Proc. IEEE**, Vol. 75(7), pp. 869-891, July 1987.

[17] C.L. Nikias, *Higher-Order Spectral Analysis*, in **Advances in Spectrum Estimation**, S. Haykin (ed.), Prentice-Hall, Inc., 1990.

[18] M. Rosenblatt, *Stationary Sequences and Random Fields*, Birkhauser, Boston, MA, 1985.

FIG. 1

ESPRIT(2)   ESPRIT(4)
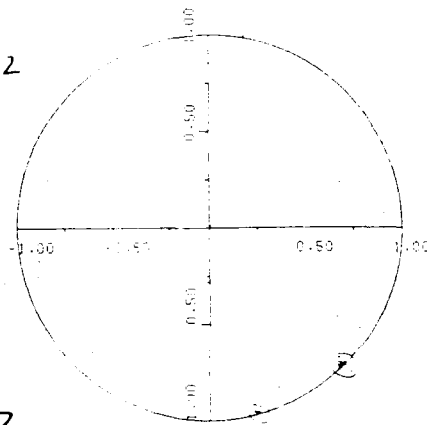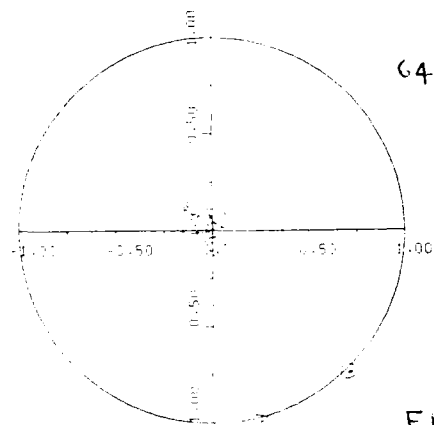
16 x 32

-1.00   -0.50   0.50   1.00

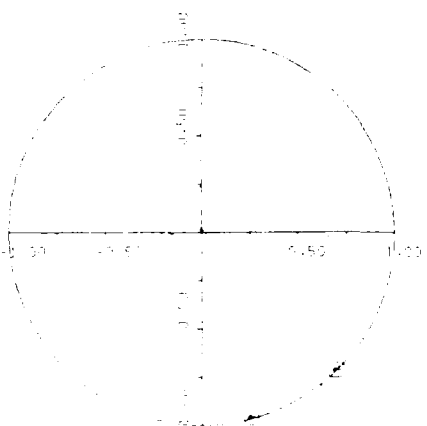64 x 32

-1.00   -0.50   0.50   1.00
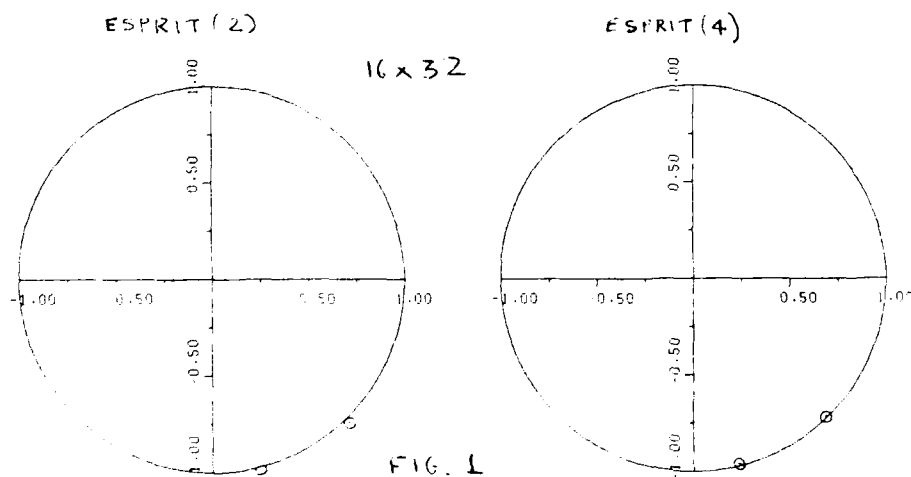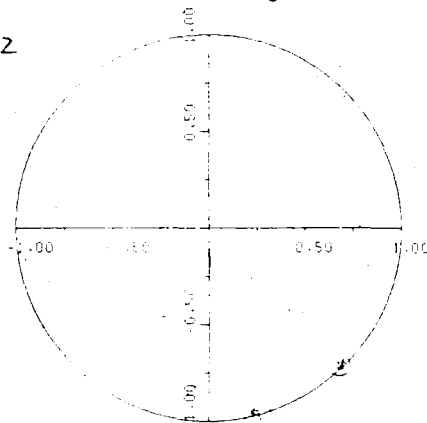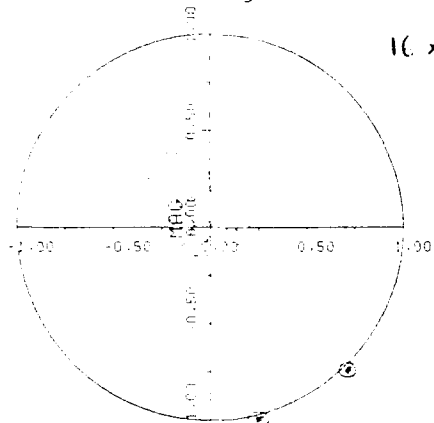
FIG 2

ESPRIT(2)   ESPRIT(4)

16 x 32

-1.00   -0.50   0.50   1.00

FIG 3

64 x 52
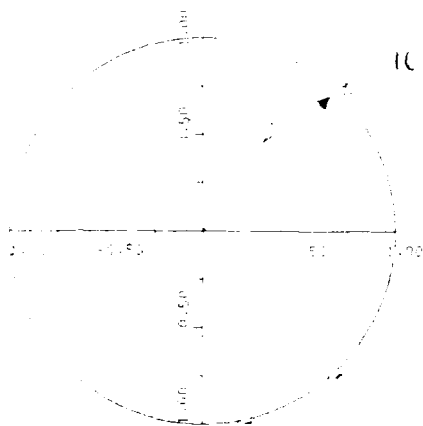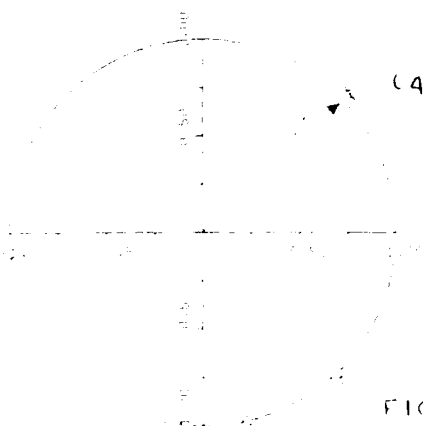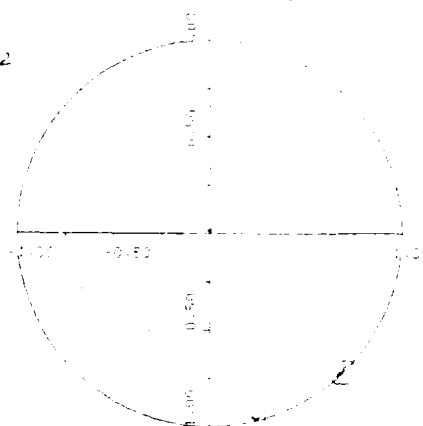
FIG 3

FOINT(2)
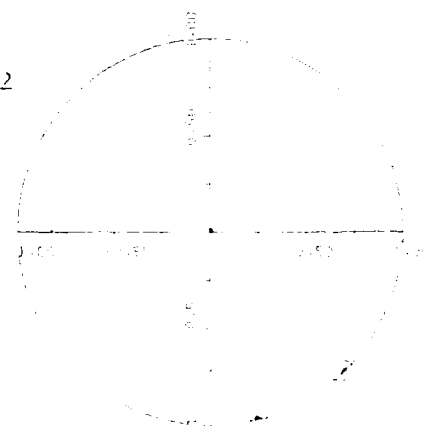
FOINT(4)
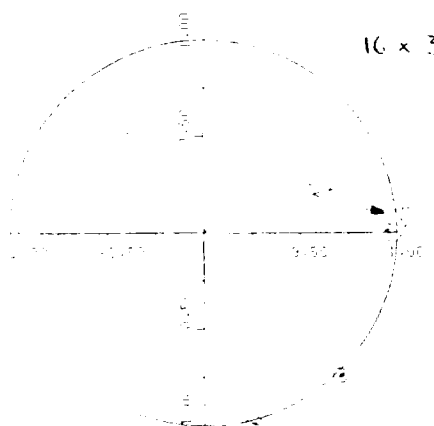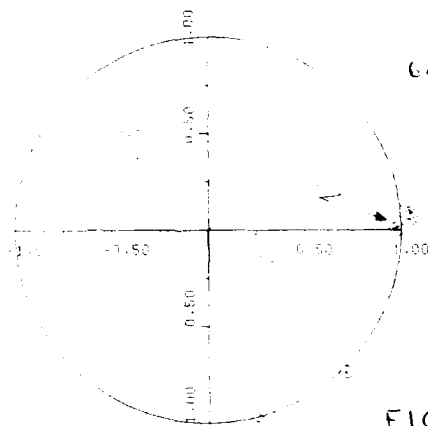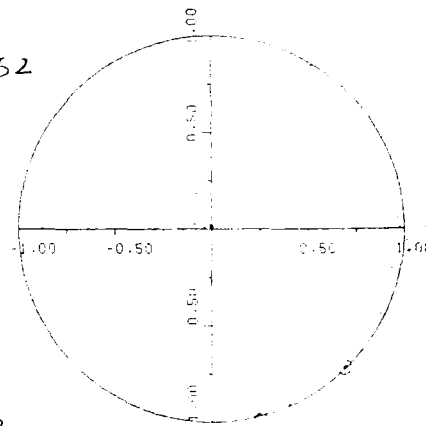
16 x 32

64 x 32

FIG 4

PERFORMANCE OF BISPECTRAL ANGLE ESTIMATION IN THE PRESENCE OF NON-GAUSSIAN NOISE

Charles L. Weigel

Honeywell Inc. Underseas Systems Division

Hopkins, Minnesota

Bispectral angle estimation techniques are receiving some attention because they would ignore any Gaussian noise. If the noise on the phase beams is indeed Gaussian and the information part of the phase beam is sufficiently non-Gaussian, then bispectral techniques should be very effective. Some research has been done which indicates that noise in many systems is close to Gaussian and information is non-Gaussian [1], but under what conditions are bispectral angle estimation techniques effective? The purpose of this work is to analyze the performance of bispectral target angle estimators and compare that performance with power spectral techniques.

This analysis compares the probability distributions of the angle estimates from the different techniques. Since a closed form error analysis has not been worked out for the phase of a bispectral estimate, this analysis determines the performance of the angle estimators by computing a large number of estimates and then calculating their first two moments. Essentially, this work is an empirical error analysis of bispectral and power spectral angle estimation techniques. The analysis controls the different noise levels and the spatial correlation of the noise on the phase beams and calculates the mean and the variance of the angle estimates.

Complex Properties

All of this analysis has been performed with complex baseband representations of signals so that it has been necessary to define a complex bispectrum. The properties of the complex bispectrum have been stated here to make them clear. Refer to [2] for a development of the real case. The definition of the bispectrum of a complex signal is similar to that of a real signal as follows:

$$B_{xxx}(\omega_1,\omega_2) = E\ dX(\omega_1)dX(\omega_2)dX(-\omega_1-\omega_2) \qquad \text{where} \qquad x(t) = \int_{-\infty}^{\infty} e^{+j\omega t}dX(\omega)$$

(E denotes statistical expectation.) Similarly the definition of the xyx cross-bispectrum of complex signals x(t) and y(t) is as follows:

$$B_{xyx}(\omega_1,\omega_2) = E\ dX(\omega_1)dY(\omega_2)dX(-\omega_1-\omega_2) \qquad \text{where} \qquad y(t) = \int_{\infty}^{\infty} e^{+j\omega t}dY(\omega)$$

The following equalities completely describe the six fold symmetry of the auto-bispectrum [2]:

$$B_{xxx}(\omega_1,\omega_2) = B_{xxx}(\omega_2,\omega_1) = B_{xxx}(\omega_1,-\omega_1-\omega_2) = B_{xxx}(\omega_2,-\omega_1-\omega_2) = B_{xxx}(-\omega_1-\omega_2,\omega_1) = B_{xxx}(-\omega_1-\omega_2,\omega_2)$$

In addition if the signal is a sampled signal then the bispectrum also has two dimensional square periodicity with period 2π.

$$B_{xxx}(\omega_1,\omega_2) = B_{xxx}((\omega_1+2\pi),\omega_2) = B_{xxx}(\omega_1,(\omega_2+2\pi)) = B_{xxx}((\omega_1+2\pi),(\omega_2+2\pi))$$

The following equality completely describes the symmetries of the cross-bispectrum [2]:

$$B_{xyx}(\omega_1,\omega_2) = B_{xyx}(-\omega_1-\omega_2,\omega_2)$$

In addition the cross-bispectrum has the same two-dimensional square periodicity as the auto-bispectrum.

Bispectral Angle Estimation Techniques

For the purposes of time delay estimation the following form of signals will be considered:

$$x(t) = s(t) + n_x(t) \qquad\qquad y(t) = s(t-\tau) + n_y(t)$$

The signals $x(t)$ and $y(t)$ are real valued, bandlimited and therefore can be represented in complex baseband form. The baseband representations of the signals will be defined as follows:

$$x(t) = Re\{x_c(t)\cdot e^{j\omega_o t}\} \qquad\qquad y(t) = Re\{y_c(t)\cdot e^{j\omega_o t}\}$$

In this representation ω_o is the center frequency of the band. By calculating the auto-bispectrum and the cross bispectrum of the signals, the time delay can be estimated. The following shows the development of the estimation technique:

$$x_c(t) = s_c(t) + n_{xc}(t) \qquad\qquad y_c(t) = s_c(t-\tau)\cdot e^{-j\omega_o \tau} + n_{yc}(t)$$

where $s_c(t)$ is the complex baseband representation of $s(t)$ and $n_{xc}(t)$ and $n_{yc}(t)$ are complex random noise processes. Calculating the bispectra, and comparing the phase of the auto-bispectrum to that of the the cross-bispectrum:

$$B_{xxx}(\omega_1,\omega_2) = F\{ E\, s_c(t+\tau_1)s_c(t+\tau_2)s_c(t) + E\, n_{xc}(t+\tau_1)n_{xc}(t+\tau_2)n_{xc}(t) \}$$

$$B_{xxx}(\omega_1,\omega_2) = B_s(\omega_1,\omega_2) + N_{xxx}(\omega_1,\omega_2)$$

$$B_{xyx}(\omega_1,\omega_2) = F\{ e^{-j\omega_o \tau}\cdot E\, s_c(t+\tau_1)s_c((t-\tau)+\tau_2)s_c(t) + E\, n_{xc}(t+\tau_1)n_{xc}(t+\tau_2)n_{xc}(t) \}$$

$$B_{xyx}(\omega_1,\omega_2) = B_s(\omega_1,\omega_2)\cdot e^{-j(\omega_o-\omega_2)\tau} + N_{xyx}(\omega_1,\omega_2)$$

$$B_{xyx}(\omega_1,\omega_2) \approx B_{xxx}(\omega_1,\omega_2)\cdot e^{-j(\omega_o-\omega_2)\tau}$$

If the noise is Gaussian, then the approximation of the phase relationship between the bispectra of the two phase beams is a true equality. Estimating the time delay in the signals simply becomes measuring the phase difference between the two spectra and averaging over the range of frequencies.

$$\frac{B_{xxx}(\omega_1,\omega_2)}{B_{xyx}(\omega_1,\omega_2)} = e^{j(\omega_o-\omega_2)\tau}$$

solving for τ and averaging over the range of frequencies:

$$\tau = (\omega_o - \omega_2)^{-1}\, arg\!\left(\frac{B_{xxx}(\omega_1,\omega_2)}{B_{xyx}(\omega_1,\omega_2)}\right) \qquad\qquad \hat{\tau} = \left(\frac{1}{2\pi}\right)^2 \int_{-\pi}^{\pi}\!\!\int \tau\cdot d\omega_1 d\omega_2$$

One need not average over all frequencies. With the symmetry properties the $[-\pi,\pi]$ square has redundant information, but averaging over this region is very simple. The time delay estimate $\hat{\tau}$ and the geometry of the phase beams are used to calculate the bearing angle:

$$\theta = Sin^{-1}\!\left(\frac{v\cdot\hat{\tau}}{d}\right)$$

where v is the speed of the signal and d is the distance between the phase centers. Refer to bispectral holography for a related development with real signals [3].

This method is not the only means to calculate the phase angle between the two signals. Several combinations of cross-bispectra and auto-bispectra can be used to measure the phase angle between the two

signals.

Signal Models.

For application into a real system, the noises on the phase beams will be neither perfectly Gaussian nor perfectly uncorrelated. In order to determine the effectiveness of bispectral techniques, one must assess the performance with different levels of power, skewness, and correlation. The complex baseband representations of the phase beams have the following form:

$$x(t) = s(t) + n_x(t) \qquad\qquad y(t) = s(t-\tau)\cdot e^{-j\omega_o \tau} + n_y(t)$$

The information component of the phase beams is an independent identically distributed, i.i.d., complex exponential series. In general the time delay is less than the sampling period of the baseband time series. The delay has been modeled by generating one phase signal, giving it the appropriate phase shift in the frequency domain, and transforming the new phase signal back into the time domain. The additive noise for each of the phase beams has both an i.i.d. Gaussian component and an i.i.d. exponential component.

$$n_x(t) = g_x(t) + e_x(t) \qquad\qquad n_y(t) = g_y(t) + e_y(t)$$

These are the complex baseband representations of the noise. Both the real and imaginary parts are statistically independent and both have the same distribution. Gaussian and exponential signals are generated numerically using a uniform random number generator [4].

If the noise has only a Gaussian component, then bispectral target angle estimation techniques would ignore the noise. Power spectral techniques must contend with the Gaussian component of the noise, and their performance degrades with the power level of the noise. If the noise has a non-Gaussian component, bispectral target angle estimation techniques suffer similar degradation and lose their advantages at a certain level. Two signal to noise ratios become important when using bispectral estimation techniques: (1) Power Ratio, the ratio of the power in the signal to the power in the noise; (2) Skewness Ratio, the ratio of the skewness of the signal to the skewness of the noise. These noise ratios have been defined as follows in dB form:

$$\text{power ratio} = \cdots = 10\cdot\log_{10}\left(\frac{E\, s\cdot s^{*}}{E\, n\cdot n^{*}}\right) \qquad\qquad \text{skewness ratio} = SR = 10\cdot\log_{10}\left(\frac{|E\, s^{3}|}{|E\, n^{3}|}\right)$$

where E denotes statistical expectation. Both phase beams have the same signal to noise ratio.

If the noise on both of the phase beams is spatially correlated, then the performance of the estimation techniques will worsen. In order to test the effect of spatial correlation, the noise on each of the phase beams are generated and then summed with the appropriate correlation as follows:

$$n = A\cdot\begin{bmatrix} n_x \\ n_y \end{bmatrix} \qquad \text{with that} \quad E\, n\cdot n^{*} = E\,(n_x\cdot n_x^{*})\cdot R = E\,(n_y\cdot n_y^{*})\cdot R \qquad \text{and} \qquad R = A\cdot A^{*}$$

where R has the form

$$R = \begin{bmatrix} 1 & \alpha \\ \alpha & 1 \end{bmatrix} \qquad \alpha \in [0,1)$$

This technique preserves power in both phase beams with the desired correlation between the two beams, but changes the skewness. The noise component is not correlated with the information part of the phase beams, but the non-Gaussian noise components on each of the phase beams are correlated. This correlation shows in the bispectrum, unlike purely Gaussian noise.

Numerical Algorithms

The algorithms for estimating the power spectra and bispectra use the Fast Fourier Transform of a windowed estimate of the time correlations. This estimation technique is standard and follows the model in [ ] Koopmans and M. M. son's analysis [5], and the indirect class of estimators in the survey paper by Nikias and Raghuveer [ ]. The time correlations are the average of non-overlapping records with 64 samples per record. The angle estimates are made from the average of 256 records. The time correlations for each of the records are averaged, then the average spectrum is calculated and used to estimate the bispectrum. The window function is a Daniell window with a width of M = 6.0 as defined in [5].

The bispectral angle estimates are calculated using the technique described earlier in this paper. The power spectral angle estimates are calculated using an analogous technique. Refer to [7] for a development of the power spectral technique. With the estimates from these techniques the first four moments are approximated and used to analyze the performance of the estimation techniques.

Simulation Results

Signals were generated according to the models provided and the angle estimates were calculated using the numerical algorithms described in the previous section. The results of the simulation are the estimates of the first two moments of the angle estimates. The analysis included these moments from several combinations of power ratios, skewness ratios, and spatial correlations.

Without any spatial correlation of the noise the power spectral technique performs better than the bispectral estimator. The mean of the angle estimates are closer to the true angle and the variances are smaller. Figure 1 shows the standard deviations of the estimates as a function of power ratio. The standard deviations of the power spectral estimates are better than that of bispectral estimates for all cases of power ratios and skewness ratios. This figure also shows that the skewness ratio does not have a great effect on the performance of the techniques. The bispectral technique is very dependent on the power ratio and independent of the skewness ratio. Even with a skewness ratio as high as 100. The mean of the estimates are always within one standard deviation of the actual angle.

When considering spatially correlated noise the bispectral angle technique performs better than the power spectral technique. The variances for each case changes very little with correlated noise, but the mean of the power spectral estimates move toward zero with increasing correlation faster than the bispectral estimates. Figures 2 and 3 show the mean of the estimates as a function of the correlation coefficient. The actual angle is 30 degrees. The graphs show several curves for three power ratios, and each figure is a fixed skewness ratio. As without spatial correlation, the skewness ratio has little effect on performance.

Acknowledgements

Figures

(Figure 1)

Estimate Mean with Skewness Ratio: 10
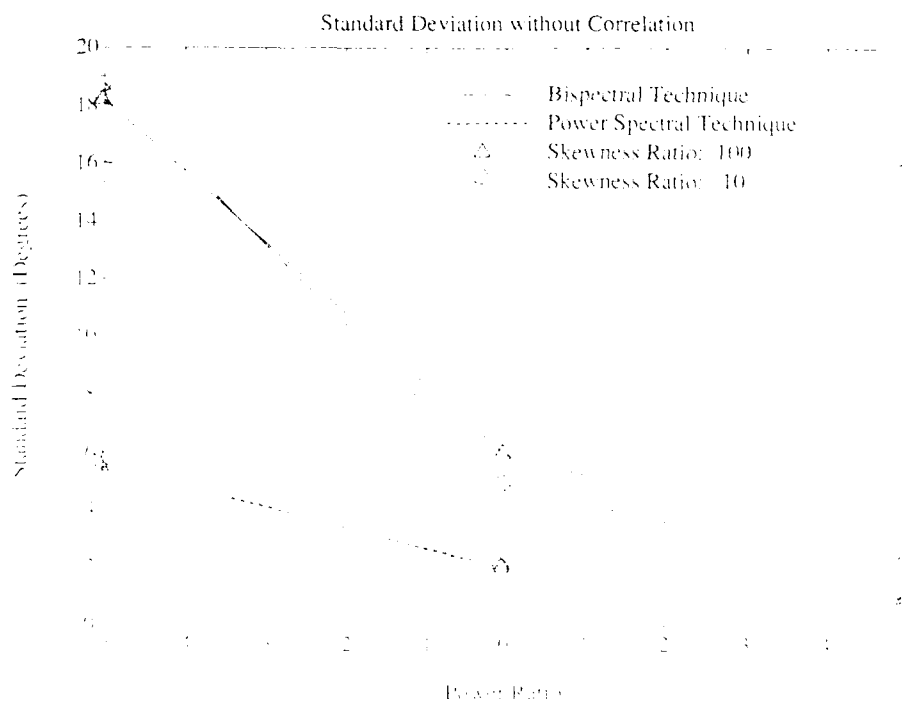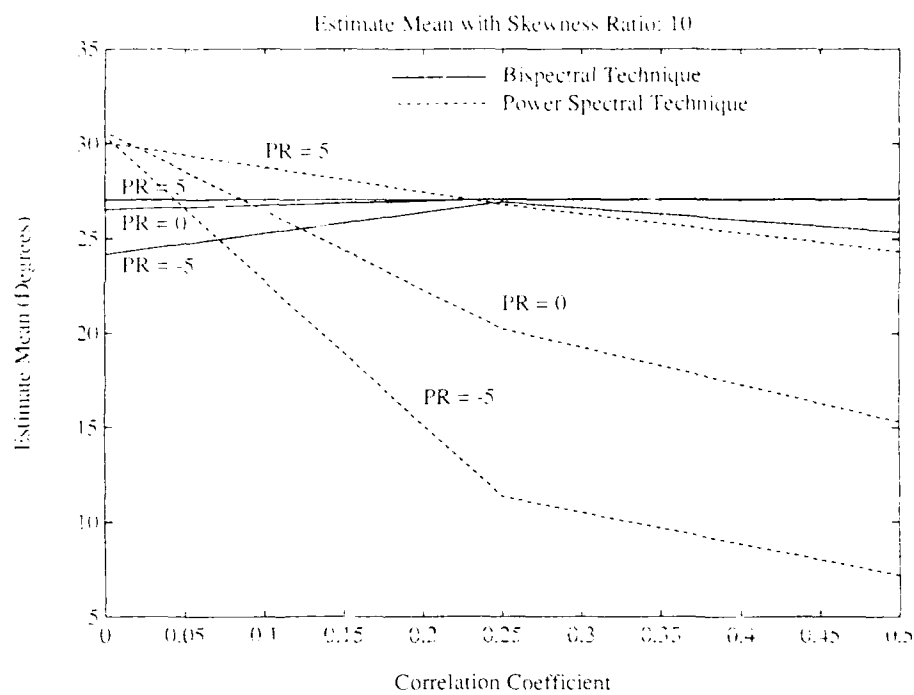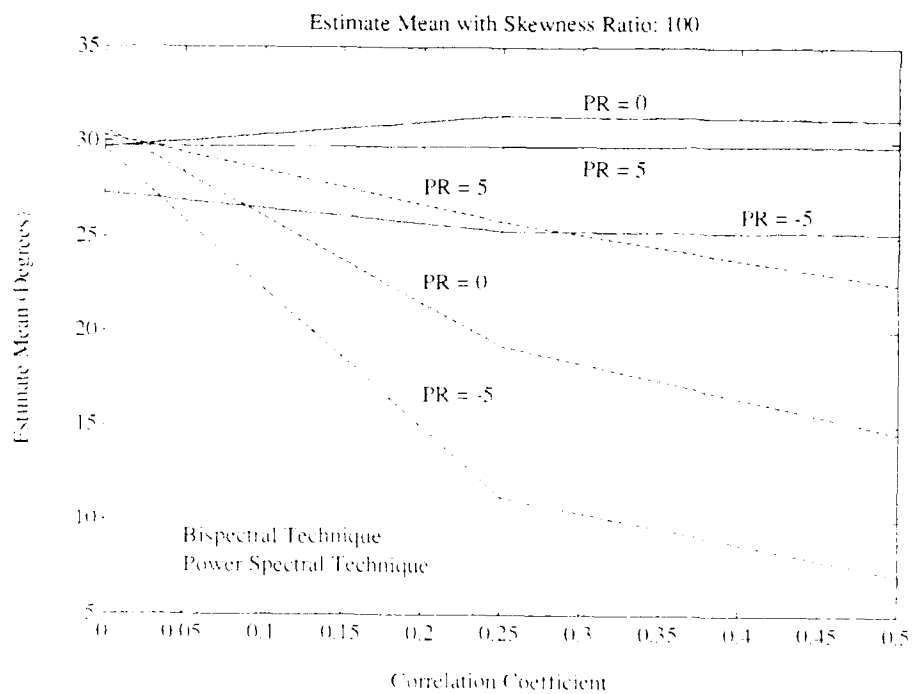

(figure 2)

Estimate Mean with Skewness Ratio: 100

(figure 3)

SEPARATION OF STOCHASTIC PROCESSES

Pierre COMON

THOMSON SINTRA, BP53, F - 06801 France.

ABSTRACT

Assume we observe an unknown linear combination of p
stochastic processes. The problem we are addressing here is to
recover original source processes by applying an inverse
transform, F, based solely upon their statistical independence.
The conditions under which this problem is solvable are first
pointed out. Then, by imposing the cancellation of output cross-
cumulants, we obtain a polynomial system of equations that the
entries of the linear transform F must cancel. In the ring of
polynomials with real or complex coefficients, obtaining a
greatest common divisor is not easy; for instance Euclid's
algorithm is unstable. Our approach is rather based on a detailed
analysis of properties of input cumulants, and provides when
p=2 a direct solution, which can be also implemented in an
adaptive fashion. The extension to p>2 sources raises several
specific problems; the solution we propose in this more general
case becomes iterative.

1. INTRODUCTION

This work was motivated by a solution proposed by
Jutten and Herault [1] using a single-layer of linear neurons,
whose adaptation rule for the connection weights was
heuristically determined. This was the first algorithm able to
recover stochastic processes from a linear mixture. Since no
reliable theoretical justification had been given up to now, our
first goal was to explain the behavior of their algorithm and
determine the conditions under which it would converge in an
acceptable time [2]. In fact, it has been proved that the former
network could slowly diverge, or might be extremely slow to
converge in various standard situations [2], even when p=2.
Our second goal is now to design a new algorithm avoiding
these drawbacks.

Several other ways exist that cope with the problem we
are going to study, and one philosophy is to exhibit a subset of
relations that the unknowns must satisfy [3] [5]. Another
approach could be designed via Volterra filters which utilize not
only the data samples, but also some of their powers [6]. This
kind of technique is definitely suboptimal, and we rarely know
how far from optimal it is. Another example of this class of
approaches is the minimization of a nonlinear function, which
actually includes in its expansion an infinite linear combination
of higher order cumulants (see [1] for instance, and references
cited therein). This can be implemented rather easily with neural
networks. Unfortunately, a more detailed analysis of the
adaptation rule often reveals that the convergence is very subject
to initial conditions, as with any stochastic iterative algorithm
aiming at minimizing a nonlinear function.

In our approach, since the nonlinearity is polynomial, the
problem is rather stated as a direct solving of the nonlinear
system. We point out that the main obstacles are due to the
presence of polynomials of several variables, when more than
two sources are to be recovered. Some particular results give
more insights to the intrinsic properties of the polynomial
system, and justify the derivation of a simple solution.

There are currently many applications to signal separation,
which have been identified by Herault and Jutten for a few
years. Let us mention, among others, the application to noise
reduction with *unknown* signal and noise statistics, to direction
finding when the propagation medium features are uncertain,
and to image enhancement as a preprocessing instead of the
principal component analysis.

2. BASIC I/O RELATIONS BETWEEN CUMULANTS

2.1. Notations and problem statement

The observation $e(t)$ is a deterministic linear transform of a p-valued stochastic process, $x(t)$. This unknown linear transform is assumed constant for the sake of simplicity though the principle may be extended to a convolution transform. So denote A the constant square matrix characterizing completely the transform. This may be written in a compact form as:

$$e(t) = A x(t);$$
$$x(t) = [x_1(t), ..., x_p(t)]^T \qquad (1)$$
$$e(t) = [e_1(t), ..., e_p(t)]^T.$$

The problem consists of finding an inverse transform, F, which is necessarily a constant regular matrix, such that the outputs

$$s(t) = F e(t)$$

are statistically independent. The unknowns we are searching are then the entries of the pxp matrix, F.

2.2. Input-output relations between cumulants

The output cumulants of order n, denoted abstractly $\text{cum}^{(n)}(s)$, are linear functions of input cumulants $\text{cum}^{(n)}(e)$, and homogeneous polynomials of degree n in the unknowns (the entries of F). In order for the outputs $s_i(t)$ to be independent, it is necessary and sufficient that the joint characteristic function $\Phi(s)$ separate into the product of marginal characteristic functions, $\Phi(s_i)$. In other words, all the cross cumulants of any order must be zero:

$$\text{cum}^{\sigma(1)\cdots\sigma(p)}(s_1^{\sigma(1)}, ..., s_p^{\sigma(p)}) = 0. \qquad (2)$$

If we restrict our attention to a finite order n, then the system obtained (2) is formed of $N(n,p) = C_{n+p-1}^{p-1} - p$ polynomial equations of degree n.
So for fixed n and as p increases, the number of unknowns grows as p^2 whereas the number of equations of degree n grows as p^n. The system (2) alone is overdetermined for $n>2$ and $p\geq 2$. The conclusion we can derive from this is that it is not realistic to solve such a system for large values of p, even for moderate n. If n=4 for example, we have N=3 polynomials of one variable for p=2, but already $N=65$ polynomials each of 10 variables for p=5. In practice, we are forced to utilize a limited number of equations of low order, and this will be sufficient provided they are well-conditioned.

2.3. Standard methods for solving polynomial systems

Solving a polynomial system of equations is obviously equivalent to finding the greatest common divisor (GCD) to all polynomials. Unfortunately, due to measurement and coding errors, the GCD of two polynomials with real (or complex) coefficients turns out to be always one in practice, if computed in a standard way. Thus, it is necessary to look for an approximate GCD.
It is possible to define a *quasi-GCD*, $D(X)$, of two polynomials of a single variable, $A(X)$ and $B(X)$, by minimizing a norm $\|U(X)A(X)+V(X)B(X)-D(X)\|$ instead of defining an exact GCD $C(X)$ as satisfying $C(X)=U(X)A(X)+V(X)B(X)$ [7]. So, the backbone of the GCD computation is still the Bezout identity. Of course, this principle can be extended to any finite number of polynomials. Unfortunately, neither the Bezout identity nor the standard Euclidean division are valid anymore in $K[X,Y]$, even if the GCD can still be defined as in any factorial ring [4]. Consequently, the computation of a quasi-GCD raises serious problems for polynomials of several variables, and to our knowledge there exist no numerically stable algorithm carrying out this task.

3. ESTIMATION OF THE INVERSE TRANSFORM

3.1. A two-steps processing

In the light of the considerations enumerated in the previous sections, the main difficulty to overcome is to get rid of polynomials of several variables, that appear as soon as p>2. *This difficulty does not appear in the two-sources case.* This is done (i) by splitting the transform F into a triangular matrix L^{-1} and a rotation Q^T on one hand, and (ii) by expressing Q^T as a product of Givens rotations on the other hand. So the set of unknowns (the entries of F) is split into the subset of $p(p+1)/2$ entries of L, and the subset of $p(p-1)/2$ free parameters in Q. The justification of our final procedure (9) is based on the preliminary results below.

Lemma (3)
Let Q be a rotation matrix and Λ a diagonal signs matrix (i.e., formed of ± 1's). Then there exist a rotation matrix $\tilde{Q}$ such

$$\Lambda Q = \tilde{Q} \Lambda. \; \Diamond$$

P. $\tilde{Q} = \Lambda Q \Lambda$ is a rotation matrix since it has the same eigenvalues as Q, namely its spectrum is formed of ones and of complex

conjugated pairs $\{e^{j\theta}, e^{-j\theta}\}$, this is obvious. ◊

Lemma (4)

Any matrix G may be factorized in the following form

$$G = L \, Q \, \Delta \tag{3}$$

where L is lower triangular with positive or zero diagonal entries

    Q is a product of Givens rotations

    Δ is a diagonal signs matrix. ◊

P. This factorization is a direct consequence of the QR factorization and of lemma 3. ◊

Corollary (5)

Let $|\lambda_i|$ a given sequence of strictly positive real numbers. Then any regular matrix A admits a unique factorization of the form

$$A = L \, Q \, \Lambda, \Lambda = \text{diag}\{\pm |\lambda_i|\}. ◊ \tag{5}$$

Theorem (6)

Let the unknown transform A be factorized as in (5), with $|\lambda_i| = 1/\text{std}(x_i)$, the inverses of the standard deviations of the sources. It is possible to recover matrix L with the help of the second order moments of e, and matrix Q up to a permutation matrix P by resorting to higher order cumulants. ◊

This allows us to search the matrix F under the form $\bar{F} = Q^T L^{-1}$. Note that in the LQΛ factorization of A, the sign matrix Δ is merged into Λ and is therefore ignored.

Corollary (7)

Let a random variable s be defined as s = Mx. If the components of both x and s are mutually independent, then, matrix M is necessarily of the form M=PΛ, where Λ is diagonal and P is a permutation. ◊

The above theorems show that one cannot expect better than estimating the inverse transform, F, up to the undetermination:

$$F A = P\Lambda. \tag{8}$$

The presence of the matrix P means that it is not possible to recover the original ordering of the components of x, and that sources may have been flipped; on the other hand the presence of a diagonal matrix, Λ, involves that the outputs may have different amplitudes and signs from the original sources. These undeterminations are inherent in the problem, and do not affect mutual independence of the outputs.

Weaker independence criterion

In the following, instead of imposing the mutual independence of the outputs, we shall try to impose only pairwise independence. Pairwise independence is known to be a weaker condition, though both are equivalent in the case of p=2 sources, or in the case of rotational invariant probability densities. We insist that pairwise processing be a *limitation only for more than two sources*. Both notions might be equivalent in our problem, but we have been unable to prove it. This limitation lead us to cope successively with polynomial systems *of a single variable* provided the inputs have been whitened by the transform L^{-1}, as shows the procedure below. Proceeding pairwise may be viewed as a relaxation scheme upon the p(p-1)/2 orthogonal planes. For p>2, the procedure is in principle iterative and nothing is opposed to run several sweeps. However, no convergence proof has been yet derived in this case, and one sweep has always been sufficient in our simulations.

Procedure (9)

step 1: Transformation to uncorrelated outputs.

- Compute the Cholesky factor, L, of the covariance matrix of the input, $E\{ee^T\}$. One may prefer to compute the LQΛ factorization of e, which is better regarding rounding errors.

- Preprocess the input e into a random variable $\bar{e} = L^{-1}e$. As a result, the components of $\bar{e}$ are uncorrelated. ◊

    Preprocessing of $\bar{e}$ and computing L may be carried out in a single step as shown in section 3.3.

step 2: Estimation of Q: description of one sweep.

    Denote $\bar{s}(0)=\bar{e}$, $s=\bar{s}(J)$ and $\bar{s}(j) = Q(j)\bar{s}(j-1)$. For $0<j\leq J = p(p-1)/2$, determine the plane rotation Q(j) to apply to $\bar{s}(j-1)$ in order to cancel the cross-cumulants between the $k(j)^{th}$ and $\ell(j)^{th}$ components of $\bar{s}(j)$. ◊

In a sweep, the rotations Q(j) are defined in a plane containing the $k(j)^{th}$ and $\ell(j)^{th}$ coordinates, where $1\leq k<p$ and $k<\ell<p$ describe the J possible couples. For the sake of precision, let us insist that

$$j = (k-1)(p-k/2) + \ell, \text{ and } 1 \leq \ell \leq p - k.$$

This corresponds to a cyclic by column ordering of indices. For convergence issues, ordering has likely the same importance as in parallel algorithms for eigenvalues and eigenvectors computation. Now Q(j) is designed in such a way to cancel the pairwise cumulants of component k and component ℓ of $\bar{s}(j)$, the other components being unchanged. For each j, this could be done by computing the quasi-GCD of the three cross-cumulants of order four for instance (or of higher order if they are not well

conditioned). This is possible since they are polynomials of a single variable (the tangent of the angle). However, a direct computation may be derived as pointed out in the next section. The overall matrix Q resulting of the product of the J plane rotations, is expected to approximate the transposed rotation factor in the LQA factorization of A, up to a permutation-and-sign matrix. If we denote $F=\prod Q(j)L^{-1}$, then it may be checked that the product FA is effectively of the form PA.

3.2. Basic relation between input cumulants

There is a better way to proceed than computing the quasi-GCD of the three cross-cumulants of order four at each stage j, $1 \leq j \leq J$. Assume we want to determine the plane rotation Q(j) to apply to a pair at stage j, and drop index j for convenience. So we can assume in this section that we have p=2 inputs and outputs without loss of generality since Q(j) is entirely defined by two inputs $\{e_1, e_2\}$.

Theorem (10)

Denote γ_{ij} the cumulants $cum^{(i+j)}(e_1^i, e_2^j)$ of the two-variate random variable e=Ax, where A is a plane rotation. Then one can exhibit the relation:

$$\rho^2 - \sigma + 2 = 0$$
where (10)
$$\sigma = (\gamma_{04}+\gamma_{40})/\gamma_{22} \text{ and } \rho = (\gamma_{13}-\gamma_{31})/\gamma_{22}. \Diamond$$

P. Based on the fact that the components x_i are mutually independent, relation (10) can be proved by simply replacing the cumulants γ_{ij} by their expressions in function of source cumulants, κ_{ij}:

$$\gamma_{40}/c^4 = \kappa_{04}\theta^4 + \kappa_{40}.$$
$$\gamma_{31}/c^4 = \kappa_{04}\theta^3 - \kappa_{40}\theta.$$
$$\gamma_{22}/c^4 = (\kappa_{40} + \kappa_{04})\theta^2.$$
$$\gamma_{13}/c^4 = \kappa_{40}\theta^3 + \kappa_{04}\theta.$$
$$\gamma_{04}/c^4 = \kappa_{40}\theta^4 + \kappa_{04}$$

Here θ denotes the tangent of the rotation angle and c its cosine. [...] a particular case of a more general result (11) that we [...] below. [...]

Theorem (11)

[...]

which has p^2 degrees of freedom. Output cumulants $cum^{(n)}(e)$ define a point in a space of dimension C_{n+p-1}^{p-1}. When A describes all the possible transforms, this point moves on a manifold of dimension p^2; (11) follows from the fact that $C_{n+p-1}^{p-1} > p^2$. $\Diamond$

If p=2 and n=4, theorem (11) predicts that there exist one relation. Relation (10) is very satisfactory since only cross-cumulants are involved. This is not true in general from theorem (11). Now, a Givens rotation in the plane (e_1, e_2) is completely defined by an angle, α, or similarly by its tangent, θ, up to an angle undetermination of π. Since adding π to the angle only changes the sign of the rotation matrix, Q, it may be incorporated in the undetermination pointed out in section 3.1. Moreover, changing θ into $-1/\theta$ transforms Q into ΔPQ, where

$$\Delta = \begin{pmatrix} -1 & 0 \\ 0 & 1 \end{pmatrix} \text{ et } P = \begin{pmatrix} 0 & 1 \\ 1 & 0 \end{pmatrix}.$$

Thus, since the solutions Q, -Q, ΔPQ and $-\Delta PQ$ are all described by the single solution, Q, up to the undetermination described in section 3.1, we impose the angle to lie within the interval $]-\pi/4, \pi/4]$ without loss of generality, i.e. its tangent must lie in $]-1,1]$.

Denote c the cosine of angle α. Then Q may be written as

$$Q(\theta) = c \begin{pmatrix} 1 & \theta \\ -\theta & 1 \end{pmatrix}.$$

Let $\bar{s} = Qe$, $\Gamma_{ki} = cum^{(k+i)}(\bar{s}_1^i, \bar{s}_2^i)$ and $\gamma_{ki} = cum^{(k+i)}(e_1^i, e_2^i)$. With these notations, relation (2) is at order n=4 and for p=2:

$$\Gamma_{31}/c^4 = -\gamma_{13}\theta^4 + (\gamma_{04} - 3\gamma_{22})\theta^3 + 3(\gamma_{13} - \gamma_{31})\theta^2 - (\gamma_{40} - 3\gamma_{22})\theta + \gamma_{31}. \quad (12-1)$$
$$\Gamma_{13}/c^4 = -\gamma_{31}\theta^4 - (\gamma_{40} - 3\gamma_{22})\theta^3 + 3(\gamma_{31} - \gamma_{13})\theta^2 + (\gamma_{04} - 3\gamma_{22})\theta + \gamma_{13}. \quad (12-2)$$
$$\Gamma_{22}/c^4 = \gamma_{22}\theta^4 + 2(\gamma_{31} - \gamma_{13})\theta^3 + (\gamma_{40} - 4\gamma_{22} + \gamma_{04})\theta^2 + 2(\gamma_{13} - \gamma_{31})\theta + \gamma_{22}. \quad (12-3)$$

First, it may be checked that the cancellation of (12-1) and (12-2) provides *equivalent* rotations since $\Gamma_{13}(\theta) = -\theta^4\Gamma_{31}(-1/\theta)$. Second, theorem (10) proves that the cancellation of (12-3) leads to solve a polynomial of degree 4 that is tangent to the θ axis. In other words:

Lemma (13)

$\Gamma_{22}(\theta)$ is the square of a polynomial of degree two. It has only one root in the interval $]-1,1]$ which is

$$\theta = \rho/2 - sign(\rho)\sqrt{\dots} \quad (13)$$

P. The polynomial $\Gamma_{22}(\theta)$ satisfies $\Gamma_{22}(\theta) = \theta^4 \Gamma_{22}(-1/\theta)$. Thus it is necessarily of the form

$$P(\theta) = \theta^4 - a\theta^3 + b\theta^2 + a\theta + 1,$$

up to the multiplicative factor $1/\gamma_{22}$. Let $X = \theta - 1/\theta$. Then $P(\theta)/\theta^2$ is a polynomial in X of degree two:

$$R(X) = X^2 - aX + b + 2.$$

So its roots are $X = a/2 \pm \sqrt{a^2/4 - (b+2)}$.

Now the use of theorem (10) proves that this root is double, and that the single root is $X = \rho$. Result (13) follows by solving $\theta^2 - X\theta - 1 = 0$. ◊

Lemma (14)

$\Gamma_{31}(\theta)$ and $\Gamma_{13}(\theta)$ have only the root (13) in common with $\Gamma_{22}(\theta)$. ◊ (14)

P. Construct the polynomial $\Gamma(\theta) = \Gamma_{13}(-1/\theta) - \Gamma_{31}(\theta)$. A necessary condition for $\Gamma_{31}(\theta)$ and $\Gamma_{13}(\theta)$ to have two common roots at θ and $-1/\theta$ is that $\Gamma(\theta)$ vanishes at θ and $-1/\theta$. As for $\Gamma_{22}(\theta)$, $\Gamma(\theta)$ satisfies $\Gamma(\theta) = \theta^4 \Gamma(-1/\theta)$. Thus it can be shown in a similar manner that it has two roots $X=\rho$ and $X=-4/\rho$. The first root $X=\rho$ provides the two solutions θ_0 and $-1/\theta_0$; the spurious root $X=-4/\rho$ is not compatible with (12-3). ◊

Sensitivity

Results (13) and (14) are true in the noiseless case. Indeed, for observations of limited duration, deviations of the estimated cumulants γ_{ij} from their true values involve discrepancies in (10). One consequence is that $\Gamma_{22}(\theta)$ may have no real roots, or conversely four real roots, whereas only two (equivalent) solutions exist theoretically. Equation (13) gives in this case a solution closer to the minimum of $\Gamma_{22}(\theta)/\gamma_{22}c^4$ in $]-1,1[$ rather than to its roots. Our point is that (13) is almost as good as solving the system (12) in an approximate manner.
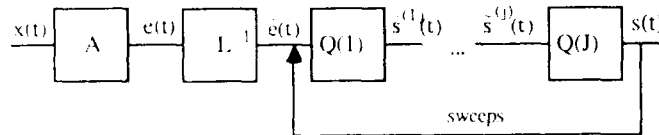
3.3. Adaptive algorithm

Based on procedure (9) and result (13), we are in a position to design an adaptive algorithm able to estimate the original

sources, and track them in a slightly nonstationary environment. With this purpose, the moments of a random variable, e(t), are estimated by an averaging of the form

$$m_{ij}(t) = \alpha(t)^2 e(t) e(t)^T + \beta(t)^2 m_{ij}(t-1), \qquad (15)$$

where $\alpha(t)$ and $\beta(t)$ are real and of modulus smaller than one satisfying $\alpha(t)^2 + \beta(t)^2 = 1$. The choice of the shape of $\alpha(t)$ is argued in section 4.

For each time step t, the adaptive implementation of our two-steps algorithm runs a single sweep of procedure (9). It may be summarized as follows.

Step 1: "Uncorrelator" (16)

1) Form the p+1 by p+1 matrix

$$M(t) = \begin{pmatrix} \beta(t) L(t-1) & \alpha(t) e(t) \\ 0 & 1/\alpha(t) \end{pmatrix}.$$

2) Find the sequence of p Givens rotations that cancel out the p first entries in the last column of M(t) by post-multiplication, such that the matrix obtained can be written as

$$M(t) \Pi = \begin{pmatrix} L(t) & 0 \\ \tilde{e}^{T} & \tilde{n} \end{pmatrix}.$$

It may be checked that the row vector $\tilde{e}^T$ obtained satisfies

$$L(t)\,\tilde{e}(t) = e(t),$$

i.e., the components of $\tilde{e}(t)$ are uncorrelated, as expected.

Step 2: Adaptive rotation: "AROT" (17)

Initialize $\tilde{s} = \tilde{e}$.

For $1 \le k < p$ and $k < \ell \le p$:

1) Isolate the pair $\tilde{s}(k), \tilde{s}(\ell)$.

2) Compute the three second order moments m_{20}, m_{11}, and m_{02} according to:

$$m_{qr}(t) = \beta(t)^2 m_{qr}(t) + \alpha(t)^2 \tilde{s}(k)^q \tilde{s}(\ell)^r, \ \{q, r\} \in \{0, 1, 2\}, \ q+r = 2.$$

3) Compute the three cross-moments of order four, m_{31}, m_{22}, and m_{13}:

$$m_{qr}(t) = \beta(t)^2 m_{qr}(t) + \alpha(t)^2 \tilde{s}(k)^q \tilde{s}(\ell)^r,$$
$$\{q, r\} \in \{0, 1, 2, 3, 4\}, \ q+r = 4.$$

4) Deduce the three input cross-cumulants of order four as:

$$\gamma_{31} = m_{31} - 3\ m_{20}\ m_{11}$$
$$\gamma_{22} = m_{22} - m_{20}\ m_{02} - 2\ m_{11}^2$$
$$\gamma_{13} = m_{13} - 3\ m_{02}\ m_{11}.$$

5) Compute $\rho = (\gamma_{13} - \gamma_{31})/\gamma_{22}$, and θ_0 in accordance with (13).

6) Apply the rotation $Q(\theta_0)$ to all components of s.

4. SIMULATION RESULTS

Simulation results are presented with p=3 sources. The direct

algorithm (9), which is a direct version of (17), has been utilized with a single sweep. Estimates of moments and cumulants have been performed with a square window of length N samples.

In our example, the sources $\{x_1(t),x_2(t),x_3(t)\}$ are respectively a uniform white noise, a ramp, and a pure sine. Of course, no a priori information upon source shapes or spectra is used, since they are assumed totally unknown. These simple signals have been chosen in order to be more "visual". Moreover, their histograms are very far from Gaussian, which allows an easy separation. The transform A was in this example

$$A = \begin{pmatrix} 0.2 & 0.6 & -0.6 \\ -2 & -1 & 1.5 \\ 1 & 1 & -0.7 \end{pmatrix}$$

and transform F obtained with the help of N=500 samples approaches (8) with Λ=I since source variances were all equal to one, and with

$$P = \begin{pmatrix} 0 & 1 & 0 \\ -1 & 0 & 0 \\ 0 & 0 & 1 \end{pmatrix}$$

For a smaller observation of N=200 samples, we have a larger discrepancy:

$$FA = \begin{pmatrix} -0.04 & 0.99 & 0.06 \\ -1.01 & -0.20 & 0.07 \\ -0.01 & -0.07 & 1.00 \end{pmatrix}$$

The distortion is visible of the last graphs.

REFERENCES

[1] C.JUTTEN and J.HERAULT, "Independent Components Analysis versus Principal Components Analysis", *European Conference on Signal Processing EUSIPCO*, Grenoble France, 1988, North Holland/Elsevier, 643-646.

[2] P.COMON, "Statistical Approach to the Jutten-Herault Algorithm", *NATO ARW on Neuro-Computing*, Les Arcs, feb 27-march 3, 1989, to be published by Springer Verlag.

[3] J.F.CARDOSO, "Source Separation Using Higher Order Moments", *Proceedings of ICASSP*, Glasgow, may 23-26, 1989.

[4] D.E.KNUTH, *The Art of Computer Programming*,vol.2, Addison Wesley, 1981.

[5] R.PAN and C.L.NIKIAS, "The Complex Cepstrum of Higher Order Cumulants and Nonminimum Phase System Identification", *IEEE Trans. ASSP*. vol.36, n°2, feb 1988, 186-205.

[6] B.PICINBONO, "Linear Quadratic Array Processing for Coherent Sources", *Proceedings of ICASSP*, New York, april 11-14, 1988, 2781-2784.

[7] A.SCHONAGE, "Quasi-GCD Computations", *Journal of Complexity*, vol.1, 1985, 118-137.
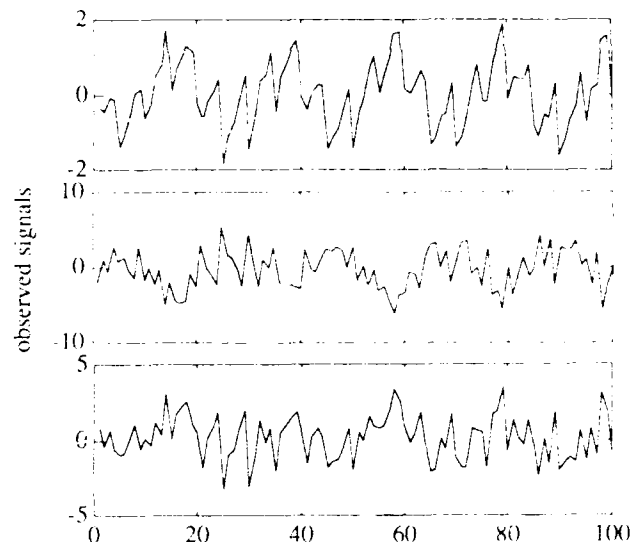
observed signals

Outputs after 1 sweep
Direct estimate with N = 500

Outputs after 1 sweep
Direct estimate with N = 200
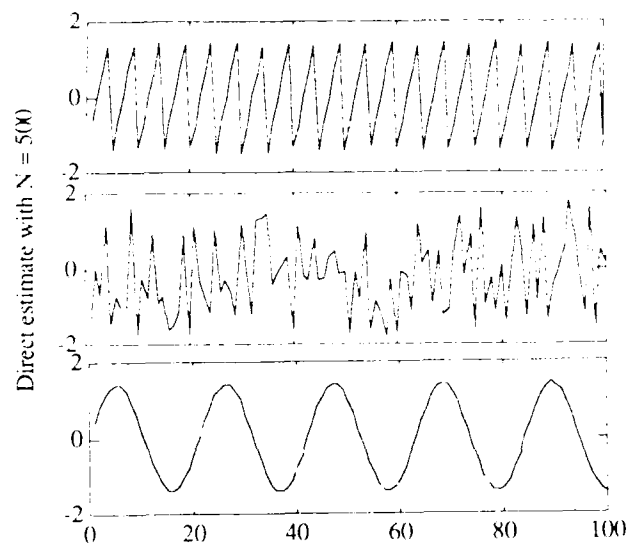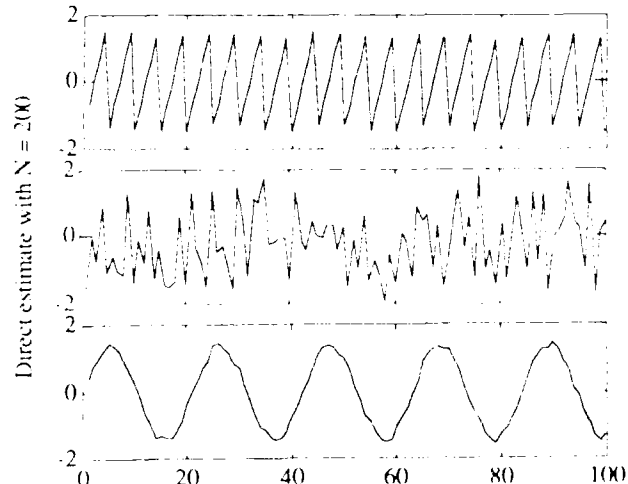
CUMULANT BASED PARAMETER ESTIMATION OF LINEAR SYSTEMS OF NONMINIMUM PHASE

Y. Inouye and T. Matsui
Dept. of Control Engineering, Faculty of Engineering Science
Osaka University, Toyonaka, Osaka 560, Japan

ABSTRACT

One of the basic problems in multivariate time series model fitting, is that of estimating ARMA models from the outputs using their statistics. Nonminimum phase ARMA models are not identifiable by using multichannel parameter estimation approaches based on second-order statistics, because these are limited to Gaussian processes. It is widely known that, if time series are non-Gaussian, then nonminimum phase parametric models are identifiable from the time series using their higher-order cumulants.

This paper propose a procedure for estimating the coefficient matrices of multichannel nonminimum phase ARMA models, and give a recursive algorithm for calculating the AR coefficient matrices. A simulation example is given to illustrate the results of the proposed procedure.

I. INTRODUCTION

In order to extract important statistical characteristics of an observed (univariate or multivariate) time series, it is common practice to assume that the time series is the output of a linear time-invariant system driven by an independent and identically distributed (i.i.d.) input sequence, and then to determine the unknown coefficients of the linear system. This is the problem of estimating a parametric ARMA model by using the noisy observations, which is important in applications such as linear prediction, spectral estimation, multivariable control, econometrics, and geophysical data processing.

A vast majority of existing methods of system parameter identification utilize only the second order statistics of observation processes under the assumption that the observation processes are Gaussian. Therefore, the best that one can do in this case is to identify spectrally equivalent minimum phase systems. In other words, a linear system is not identifiable from the noisy output using its second-order statistics if the system is nonminimum phase. It is, however, widely known that a nonminimum phase system is identifiable from the noisy output using its higher-order statistics called *cumulants* if the input process is non-Gaussian [1-5]. In the univariate case, cumulants have received a revived interest for ARMA parameter estimation and other signal processing tasks [4-7]. In the multivariable case, 3rd-order cumulants are employed for estimating multichannel AR models of known orders by Raghuveer [8], and for estimating multichannel MA models by Inouye et al. [9],[10].

In this paper, using the previous results in [9],[10], we propose a procedure for estimating the coefficient matrices of multichannel nonminimum phase ARMA models, and give a recursive algorithm for calculating the AR coefficient matrices. A simulation example is given to illustrate the results of the proposed procedure.

II. PARAMETER ESTIMATION OF LINEAR MODELS

Let $y(n)$ be a stationary r-variate, non-Gaussian, autoregressive moving-average ARMA (p,q) vector process with a noise vector process, which is described by

$$\sum A(k)y(n-k) = \sum H(l)u(n-l) + v(n), \qquad A(0) = I, \qquad (1)$$

where $u(n)$ is a zero-mean, stationary, s-variate, and non-Gaussian vector process with components $u_i(n)$ satisfying the 3rd-order temporal and spatial independence constraint defined by

$$E\{u_i(i)u_j(j)u_k(k)\} = \begin{cases} 1, & i=j=k, \ l=m=n \\ 0, & \text{otherwise,} \end{cases} \qquad (2)$$

and $v(n)$ is a stationary, r-variate, Gaussian, perhaps colored, zero-mean noise vector process independent of process $u(n)$. The coefficient matrices like $H(l)$ are of dimensions $r \times r$, $r \times s$ respectively.

To determine the AR coefficient matrices $\{A(k)\}$ and the MA coefficient matrices $\{H(l)\}$, we use 3rd-order cumulants for process $y(n)$, which are defined as the $r \times r$ matrices

$$C(m,n) = E\{y(n) \otimes y(n+m) \otimes y(n+n)\} \qquad (3)$$

For notational simplicity we assume ourselves to 3rd-order cumulants, although the results are extended to higher order cumulants. There are of course a number of different ways of estimating the cumulants for process $y(n)$ from an actual time series $y(n)$. In the sequel this matter is assumed to be known, i.e., the 3rd order cumulants for process $y(n)$.

The problem considered in this paper is to determine the coefficient matrices $\{A(k)\}$ and $\{H(l)\}$ together with the indices (orders) of the AR part and the MA part from the 3rd-order cumulants for process $y(n)$. We assume that the orders of the AR part and the MA part are known.

A. Estimation of MA models

Setting $p = 0$ in (1), we obtain an MA(p) process $y(n)$ as follows:

$$y(n) = \sum H(l)u(n - l) + v(n). \tag{4}$$

Substituting (4) into (3) and using the assumptions stated below (1), we obtain

$$C_i(m_1, m_2) = \sum H(l + m_1)diag[h_{i1}(l + m_1)\cdots h_{is}(l + m_2)]H^T(l), \quad 0 \le m_1, m_2 \le q. \tag{5}$$

where $h_{ij}(k)$ is the (m, j) element of matrix $H(k)$, and $diag[a_1 \cdots a_s]$ stands for a $s \times s$ diagonal matrix with diagonal elements $\{a_i\}$.

Considering (5) with $m_1 = k, m_2 = q$, $n_1 = 0, m_2 = q$, and $m_1 = q, m_2 = 0$, we obtain

$$C_i(k, q) = H(k)diag[h_{i1}(q)\cdots h_{is}(q)]H^T(0). \tag{6a}$$

$$C_i(0, q) = H(0)diag[h_{i1}(q)\cdots h_{is}(q)]H^T(0). \tag{6b}$$

$$C_i(q, 0) = H(q)diag[h_{i1}(0)\cdots h_{is}(0)]H^T(0). \tag{6c}$$

In the sequel, we assume that

$$H(0) \text{ and } H(q) \text{ are of full column rank } s, \quad (s \le r). \tag{7}$$

Under the above assumption, matrix $H^T(0)H(0)$ has its inverse. Premultiplying (6b) by $[H^T(0)H(0)]^{-1}H^T(0)$, and substituting the result into (6a), we have

$$C_i(k, q) = H(k)[H^T(0)H(0)]^{-1}H^T(0)C_i(0, q), \quad m = 1, \ldots, r. \tag{8}$$

Define the two $r \times r$ matrices $L(k, q)$ and $L(0, q)$ as

$$L(k, q) = [C_1(k, q), \cdots, C_r(k, q)], \quad L(0, q) = [C_1(0, q), \cdots, C_r(0, q)]. \tag{9}$$

Then we use (8) and (9) to obtain

$$L(k, q) = H(k)[H^T(0)H(0)]^{-1}H^T(0)L(0, q). \tag{10}$$

We substitute (6b) into the second of (9) and rewrite $L(0, q)$ as

$$L(0, q) = H(0)M(q)diag[H^T(0)]. \tag{11}$$

where $M(q) = [diag[h_{11}(q)\cdots h_{1s}(q)]\cdots diag[h_{r1}(q)\cdots h_{rs}(q)]]$, and $diag[H^T(0)]$ is a block diagonal $rs \times s$ matrix with the same diagonal block elements $H^T(0)$. It is easily shown from the assumption (7) that $M(q)$ has full row rank s. This means that $M(q)diag[H^T(0)]$ is of full row rank, because $diag[H^T(0)]$ is of full row rank. Therefore, (11) implies from the assumption (7) that $L(0, q)$ is of rank s. Thus, $L(0, q)L^T(0, q)$ becomes nonsingular in case of $s = r$. In this case, solving (10) for $H(k)$, we obtain

$$H(k) = L(k, q)L^T(0, q)[L(0, q)L^T(0, q)]^{-1}H(0). \tag{12}$$

Notice that if $C_m(0, q)$ is nonsingular for some $m = 1, 2, \cdots, r$, then (12) holds true even if $L(k, q)$ and $L(0, q)$ are replaced by $C_m(k, q)$ and $C_m(0, q)$, respectively. In case of $s < r$, we can solve (10) for $H(k)$, and obtain, instead of (12)

$$H(k) = L(k, q)L^T(0, q)[L(0, q)L^T(0, q)]^+H(0). \tag{13}$$

where A^+ denotes the pseudo-inverse (i.e., the generalized inverse defined by Penrose) of matrix A. Eq.(12) or (13) is a simple closed form expression which relates the output cumulants with the MA coefficients. To utilize (12) or (13), we should have the first value, $H(0)$ of the (impulse response) sequence $\{H(k)\}$.

To determine $H(0)$, we consider (13) for $k = q$ and substitute $H(q)$ into (6c) to obtain

$$H(0)diag[h_{i1}(0)\cdots h_{is}(0)]H^T(0) = B_q, \quad m = 1, \ldots, r. \tag{14a}$$

where

$$B_q = L(0, q)L^T(0, q)[L(q, q)L^T(0, q)]^+C_i(q, 0). \tag{14b}$$

Note that (14a) is in general not guaranteed to have a solution when B_q takes a value different from the value given by the right hand side of (14b). However, (14a) has always a solution whenever B_q is determined by (14b). Without any further assumption for $H(0)$, a unique solution of (14b) is impossible. However it is shown in [10], that a solution of (14a) is determined uniquely up to right multiplication by a permutation matrix, that is, if $H(0)$ and $\bar{H}(0)$ both satisfy (14a), then there exists a permutation matrix P such that $\bar{H}(0) = H(0)P$. This provides the following identifiability Theorem [9], [10].

Theorem 1 : If $\{H(k)\}$ satisfies (5), then $\{\tilde{H}(k) = H(k)P\}$ also satisfies (5), where P is a permutation matrix. Conversely, if $\{H(k)\}$ and $\{\tilde{H}(k)\}$ both satisfy (5), then there exists a permutation matrix P such that $\tilde{H}(k) = H(k)P$ for $k = 0, \cdots, q$.

The above discussion leaves yet the problem of finding a solution $H(0)$ of (14), which is considered in the sequel.

B. Solutions of (14)

As mentioned above, $H(0)$ is in general not uniquely determined from (14a) without any further assumption. However, (14a) has a unique solution under the assumption that the solution becomes an upper or lower triangular matrix. The unique solution is indeed obtainable in this case as follows. Let us consider the lower triangular case, and write (14a) elementwise as

$$b(i,j) = \sum h(0)h(0)h(0) = \sum h(0)h(0)h(0), \qquad m = 1, 2, \cdots, r, \qquad (15)$$

where we used the assumption that $H(0)$ is lower triangular to establish the second equality in (15).

Setting $m = 1$ in (15) yields

$$b(1,1) = (h(0)), \quad b(1,2) = (h(0))h(0), \quad \cdots, \quad b(1,r) = (h(0))h(0)$$

Because $h(0)$ must be non-zero, the entries of the first column of $H(0)$ can be found to become

$$h(0) = b(1,1), \quad h(0) = b(1,2)h^{-1}(1,1), \quad \cdots, \quad h(0) = b(1,r)h^{-1}(1,1).$$

The second column of $H(0)$ can be calculated if we set $m = 2$ in (15) to obtain

$$b(2,2) = h(0) + h(0), \quad b(2,3) = h(0)h(0) + h(0)h(0), \quad \cdots, \quad b(2,r) = h(0)h(0) + h(0)h(0).$$

Similarly, the n-th $(n = s)$ column of $H(0)$ can be computed if we use $m = n$ in (15), and observe that the equation corresponding to $b(n,l)$ can be used to be solved for $h(0)$ where $l = n, n+1, \cdots, r$. Note that the rest of the quantities involved in the equation corresponding to $b(n,l)$ are already available from the equations corresponding to $b(i,j)$ with $i < r$ and $j < l$. Thus, $H(0)$ can be found recursively from (15) in the lower triangular case. An analogous procedure can be followed to find a unique solution of (15) under the assumption that the solution $H(0)$ becomes upper triangular. In the case when $r = s = 2$, that is, when $H(0)$ becomes 2×2, $H(0)$ can be found comparatively simply as follows. Since B and B in (14b) must be symmetric, let us put

$$H(0) = \begin{bmatrix} a & b \\ c & d \end{bmatrix}, \qquad B = \begin{bmatrix} \alpha & \beta \\ \beta & \gamma \end{bmatrix}, \qquad B = \begin{bmatrix} \alpha & \beta \\ \beta & \gamma \end{bmatrix}, \qquad (15)$$

and write (14a) elementwise as

$$H(0)\begin{bmatrix} a & 0 \\ 0 & b \end{bmatrix}H^T(0) = \begin{bmatrix} a^2+b^2 & ac+bd \\ ac+bd & c^2+d^2 \end{bmatrix} = \begin{bmatrix} \alpha & \beta \\ \beta & \gamma \end{bmatrix}, \qquad (17a)$$

$$H(0)\begin{bmatrix} c & 0 \\ 0 & d \end{bmatrix}H^T(0) = \begin{bmatrix} ac+bd & ac+bd \\ ac+bd & c^2+d^2 \end{bmatrix} = \begin{bmatrix} \alpha & \beta \\ \beta & \gamma \end{bmatrix}, \qquad (17b)$$

which yields the following four equations.

$$a^2+b^2 = \alpha, \quad ac+bd = \beta, \quad ac+bd = \beta, \quad c^2+d^2 = \gamma, \qquad (18)$$

Putting $\alpha = \alpha$, $d = \beta$, $\alpha = \gamma$, $\gamma = \beta$, and $\delta = \gamma$ in (18), the above equations become

$$a^2+b^2 = \alpha, \quad ac+bd = \beta, \quad ac+bd = \gamma, \quad c^2+d^2 = \delta. \qquad (19)$$

Here (19) can be assumed to be solvable for a, b, c, and d, because (14a) has always a solution whenever B and B are determined by (14b). We note that (19) has two solutions by Theorem 1, because there are only two permutation matrices in this case. Using (19), we obtain the two identifies

$$\gamma = \delta\beta = cd(ad+bc), \quad \beta = \alpha\gamma = ab(ad+bc). \qquad (20)$$

We note $ad+bc \neq 0$, because $H(0)$ must be nonsingular. Thus, the first identify implies that $\gamma = \delta\beta$ if and only if $c = 0$ or $d = 0$. This is equivalent to the case when $H(0)$ becomes lower triangular. The second identify implies that $\beta = \alpha\gamma$ if and only if $a = 0$ or $b = 0$. This is equivalent to the case when $H(0)$ is upper triangular. These cases were already treated above, and therefore we assume below that none of a, b, c and d are non-zero. Putting

$$k = \frac{\gamma}{\beta} = \frac{\delta\beta}{\alpha\gamma} = \frac{cd}{ab} (\neq 0), \quad t = \frac{c}{a}, \qquad (21)$$

we obtain

$$c = at, \quad d = bk/t. \qquad (22)$$

where we used (20) for establishing the second equality in (21). Substituting (22) into (19) yields

$$a' + t' \alpha, \ ta' + (\frac{t}{k})b' \ \beta, \ t^2 a' + (\frac{t}{k})^2 b' \ \gamma, \ t^3 a' + (\frac{t}{k})^3 b' \ \delta \tag{23}$$

Because the above equations are linear in two unknowns a' and b', they are solvable for a' and b' if and only if rank $D(t) = 2$, where

$$D(t) = \begin{bmatrix} 1 & 1 & \alpha \\ t & \frac{t}{k} & \beta \\ t^2 & (\frac{t}{k})^2 & \gamma \\ t^3 & (\frac{t}{k})^3 & \delta \end{bmatrix} \tag{24}$$

Here we used the fact that rank $D(t) \geq 2$ because $t \neq t/k$ and $b \neq 0$. Therefore, if we can find a value t such that rank $D(t) = 2$, then the two unknowns a' and b' are calculated by solving the linear equation

$$\begin{bmatrix} 1 & 1 \\ t & \frac{t}{k} \end{bmatrix} \begin{bmatrix} a' \\ b' \end{bmatrix} = \begin{bmatrix} \alpha \\ \beta \end{bmatrix}, \tag{25}$$

and the unknowns c and d can be obtained by using (22).

To find t such that rank $D(t) = 2$, consider the determinant of the matrix composed of the first three rows of $D(t)$ and equate it to zero. Then, we get

$$\alpha(\frac{k}{t} - kt) + \beta(\frac{k}{t} - t') + \gamma(\frac{k}{t} - t) = 0, \tag{26}$$

which becomes

$$\alpha k + \gamma + \beta(\frac{k}{t} + t) = 0, \tag{27}$$

because $k \neq t, t \neq 0$. It becomes an algebraic equation of second-order in t in case of $\beta \neq 0$, and is solvable for t. In case of $\beta = 0$, consider the determinant of the matrix composed of the first two and the last rows of $D(t)$ with $\beta = 0$, and equate it to zero. Then, we obtain

$$\alpha k(\frac{k^2}{t} - t^2) + \delta(\frac{k}{t} - t) = 0, \tag{28}$$

which becomes

$$\alpha k(\frac{k}{t} + t) + \delta = 0, \tag{29}$$

because $k \neq t, t \neq 0$. It becomes also an algebraic equation of second-order in t when $\alpha k \neq 0$, and is solvable for t. Note that $\alpha k \neq 0$ for $\beta = 0$ by means of the first of (21).

Summarizing the above procedure, we first calculate k from the first of (21), and then solve (27) for $\beta \neq 0$, or (29) for $\beta = 0$, we next solve (25) to obtain a and b, and finally use (22) to obtain c and d.

C. Estimation of ARMA models

Postmultiplying both sides of (1) by $\mathbf{y}^I(n - i)y(n - i)$ and taking expectations, it is easy to see that

$$\sum_j A(k)C(i-k,0) = E\{\sum_l H(l)\mathbf{u}(n-l)\mathbf{y}^I(n-i)y(n-i)\} + E\{\mathbf{v}(n)\mathbf{y}^I(n-i)y(n-i)\} \tag{30}$$

$$= 0, \ \text{for} \ i > q,$$

where for the last equality we have used the facts that $\mathbf{y}^I(n-i)y(n-i)$ depends at most on $\mathbf{u}(n-i)$ and $\mathbf{v}(n-i)$, and that $\mathbf{v}(n)$ satisfies (2). Putting $C_i = C(k,0)$ and concatenating the above equations for $i = q+1, q+2, \ldots, q+p$, we obtain

$$AM = C \tag{31}$$

where

$$A = [A(1), A(2), \ldots, A(p)],$$

$$C = [C, C, \ldots, C], \ M = \begin{bmatrix} C & C & \cdots & C \\ C & C & \cdots & C \\ \vdots & \vdots & \ddots & \vdots \\ C & C & \cdots & C \end{bmatrix}$$

Eq.(31) is known as the higher-order *Yule-Walker* equation. The **AR** coefficients, $A(k)$'s are determined by solving (31). Because the coefficient matrix $M_{p,q}$ becomes a block-Toeplitz matrix, a fast algorithm for solving (31) is obtainable. This is shown in subsection D. In order to get the **MA** coefficients, $H(k)$'s, we adopt the so-called *residual time series procedure* in which the output $y(n)$ is applied to the p-th order FIR filter whose transfer function has coefficients equal to the **AR** coefficients obtained as described above. The residual time series can be expressed as

$$\bar{y}(n) = y(n) + \sum_{l=1} \hat{A}(l)y(n-l). \tag{32}$$

Substituting (32) into (1), we observe that the residual series is an **MA** process if $\hat{A}(k) = A(k)$, and hence, the **ARMA** case reduces to the **MA** case once the $A(k)'s$ have been computed.

D. A recursive algorithm

In the following, let A denote the solution, A of (31) for order (p.q). The recursive algorithm for solving (31) is composed of two sets of recursions, because (31) depends on the two orders p and q. The first one is for updating the order from p to $p+1$, and the second one is for updating the order form q to $q+1$.

Algorithm : The data $\{C, C, \cdots, C_N\}$ are given with N being a large integer. At order (p.q) the quantities A, B, D, have been calculated. To update the order from (p.q) to (p+1,q), calculate the following recursions given by

$$B = (I - F G)^{-1}(B,0 - F,0,D), \qquad D_{+} = (I - G_{p,q}F)^{-1}(0,D - G B,0)$$

$$A = A,0 - (H + C)D_{p+}$$

where

$$F = B \begin{bmatrix} C \\ \vdots \\ C_{j+} \end{bmatrix}, G_{-} = D_{j} \begin{bmatrix} C_{j} \\ \vdots \\ C_{j-} \end{bmatrix}, H_{j,q} = A_{-q} \begin{bmatrix} C_{j+}^{m} \\ \vdots \\ C_{j+} \end{bmatrix}$$

In the above calculations, if matrix $I - F_{j,q}G_{j,q}$ becomes singular, stop here. To update the order from (p.q) to (p.q+1), calculate the following recursions given by

$$B = [B(1), \cdots, B(p-1)] - B(p)A(p)^{-1}[I, A(1) \cdots A(p-1)], \qquad D_{j+} = F B$$

$$A = A - (C + H)D_{p+q+1}$$

where, $[B(1), \cdots, B(p)] = B$, $[A(1), \cdots, A(p)] = A_{p,q}$, and $F_{j,q}, G_{j,q}, H_{j,q}$ are respectively the same as above. In the above calculations, if F or $A(p)$ becomes singular, stop here.

As initial values for $p=1$, set

$$A = C(C)^{-1}, \quad B = D_{j,q} = (C^{m})^{-1} \qquad \text{for some } q = 0, \cdots, N-1.$$

The above algorithm is valid under the condition that the coefficient matrices, $M_{p,q}$'s are nonsingular (see the proposition below) and must be stopped if $p + q = N$. The proof of its validity is lengthy and omitted. As for the nonsingularity of the three matrices $I - F_{j,q}G_{j,q}$, $F_{j,q}$ and $A_{j,q}(p)$ needed to execute the algorithm, it holds the following proposition.

Proposition : Let M be the matrix defined below (31), and $F_{j,q}, G_{p,q}$ and $A_{j,q}(p)$ be respectively the matrices defined in the above algorithm.

a) Under the condition that M and $M_{p,q}$ both are nonsingular, $I - F_{p,q}G_{j,q}$ (or, equivalently $I - G F$) is nonsingular if and only if $M_{p,q}$ is nonsingular.

b) Under the condition that M is nonsingular, $F_{p,q}$ is nonsingular if and only if $M_{p,q+}$ is nonsingular.

c) $A(p)$ is nonsingular if M is nonsingular.

IV. A SIMULATION EXAMPLE

In order to see the effects of the proposed procedure, it has been implemented in a FORTRAN program. The computations are carried out for several 2-channels ARMA models by the ACOS-2000 computer. We employed for the input sequences independent exponentially distributed random deviates generated form the subroutine in the Statistical Library of the ACOS-2000 computer. To find the estimates $\hat{C}$ needed for the procedure, we used 8000 output samples after 100 transient output samples with the ARMA models. We took the following ARMA models, which is a 2-input, 2-output nonminimum phase system described by

$$y(n) + A(1)y(n-1) + A(2)y(n-2) = H(0)u(n) + H(1)u(n-1),$$

where $A(i)$'s and $H(i)$'s are presented in Table I. The values of the $A(i)$'s are selected so that the system is stable. Table II presents their estimated values. Table III presents the positions of the poles and zeros of the original model and the estimated one. The frequency responses of original model and the estimated one are shown in Fig. 1. In the Fig. 1, solid line (———) represents the true values; dotted line (-----), the estimated values. Fig. 1 shows respectively the gains and the phases of the (1,1)-th elements of the original model and the estimated one. The graphs for other elements are omitted. The above Tables and Figure imply that the estimated model is fitted well to the original one.

V. CONCLUSIONS

We have presented the procedure for estimating the coefficient matrices of multichannel nonminimum phase ARMA models, and given the recursive algorithm for calculating the AR coefficients matrices. A simulation example has been shown to illustrate the results of the procedure.
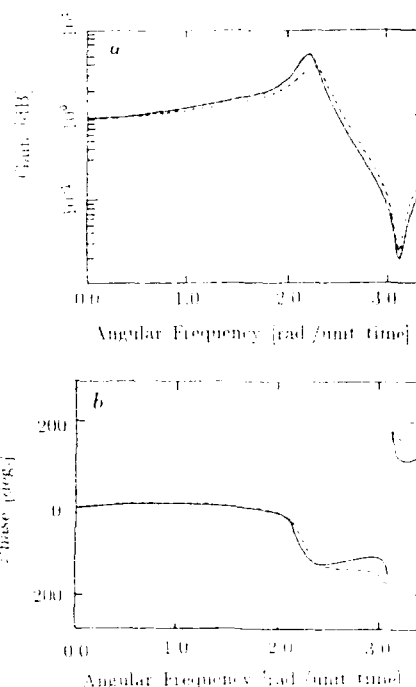

Fig. 1 (a) Gains of the (1,1) element of the original model and the estimated one. (b) Phases of the (1,1) element of the original model and estimated one.

TABLE I. COEFFICIENT MATRICES $A(k)$ AND $H(l)$ FOR THE ORIGINAL MODEL.

i	$A(i)$		l	$H(l)$	
1	0.650	-0.360	0	1.000	0.000
	0.270	0.460		1.000	1.000
2	0.280	0.270	1	0.770	0.000
	-0.220	0.350		0.650	1.100

TABLE II. COEFFICIENT MATRICES $\hat{A}(k)$ AND $\hat{H}(l)$ FOR THE ESTIMATED MODEL.

i	$\hat{A}(i)$		i	$\hat{H}(l)$	
1	0.684	0.376	0	0.963	0.000
	0.268	0.527		1.010	1.000
2	0.263	0.249	1	0.792	0.007
	0.139	0.245		0.706	1.180

TABLE III. POLES AND ZEROS FOR THE ORIGINAL MODEL AND THE ESTIMATED ONE.

	Original model	Estimated model
Poles	$0.557 + j0.731$	$0.580 + j0.668$
	$0.201 + j0.437$	$0.026 + j0.355$
Zeros	$0.770 + j0.000$	$0.822 + j0.000$
	$1.100 + j0.000$	$1.180 + j0.000$

REFERENCES

1. D. R. Brillinger, "An introduction to polyspectra", *Ann. Math. Statist.*, vol. 36, pp. 1351-1374, 1965.
2. M. Rosenblatt, "Linear processes and bispectra," *J. Appl. Probab.*, vol. 17, pp. 265-270, 1980.
3. K. S. Lii and M. Rosenblatt, "Deconvolution and estimation of transfer function phase and coefficients for non-Gaussian linear processes," *Ann. Statist.*, vol. 10, pp. 1195-1208, 1982.
4. C. L. Nikias and M. R. Raghuveer, "Bispectrum estimation: A digital signal processing framework." *Proc. of IEEE*, vol.75, pp. 869-891, July 1987.
5. J. K. Tugnait, "Identification of nonminimum phase linear stochastic system," *Automatica*, vol. 22, pp. 457-464, 1986.
6. G. B. Giannakis, "Signal processing via hight-order statistics," Ph.D. dissertation, University of Southern California, Los Angeles, CA, July 1986.
7. G. B. Giannakis. "Cumulants: A powerful tool in signal processing," *Proc. of IEEE*, vol. 75, pp. 1333-1334, Sep. 1987.
8. M. R. Raghuveer, "Multichannel bispectrum estimation," *Proc. of 3rd ASSP Workshop on Spectrum Estimation and Modelling*, pp. 21-24, 1986.
9. Y. Inouye, G. B. Giannakis and J. M. Mendel. "Cumulant based parameter estimation of multichannel moving-average processes," *Proc. of Int. Conf. on ASSP. (ICASSP'88)*, pp. 1252-1255, April 1988.
10. G. B. Giannakis, Y. Inouye and J. M. Mendel, "Cumulant based identification of multichannel moving-average models," to be published in *IEEE Trans. on AC*, 1989.
11. Y. Inouye and Y. Kimura, "A recursive algorithm of ARMA spectrum estimation," in *Proc. 12th SICE Symposium on Control, (Japan)*, pp. 141-144, May 1983 (in Japanese).

TWO-DIMENSIONAL HIGHER-ORDER SPECTRUM FACTORIZATION
WITH APPLICATION IN NONGAUSSIAN IMAGE MODELING *

A. MURAT TEKALP and A. TANJU ERDEM

Electrical Engineering Department
University of Rochester
Rochester, New York 14627

Abstract - We address the problem of modeling a given 2-D higher-order spectrum as that of the output of a 2-D linear time-invariant system driven by a higher-order white random signal. This is posed as a higher-order spectrum factorization problem. We first discuss the existence and uniqueness of such a factorization. A fast algorithm for efficient implementation of the higher-order spectrum factorization is then proposed. When an exact factorization does not exist, this algorithm computes the transfer function of a linear time-invariant system that approximately models the given higher-order spectrum function. We present nonGaussian image modeling as an application.

I. INTRODUCTION

Signal modeling is of primary importance in many signal processing applications. Signal modeling, in the general sense, aims at constructing a white-noise driven linear time/space invariant system such that the nth-order spectrum of its output matches the nth-order spectrum of the given signal, both in magnitude and in phase. Classical linear signal models have been developed to match the power spectrum of a given signal. Since the power spectrum does not carry phase information, signal models that are based on the power spectrum have arbitrary phase.

Signal modeling based on higher order spectra is especially desirable in the following cases: (i) If the process is linear nonGaussian, a linear model with unique phase (up to a linear phase factor) can be obtained based on the higher-order spectra (HOS) that matches the magnitude and phase characteristics of the given higher-order spectrum. (ii) If the signal model is desired to be driven by an nth-order white noise.

In general, a nonlinear signal model is necessary to exactly match the HOS of an arbitrary nonGaussian process [1]. However, in this paper, we are interested in linear modeling of a 2-D nonGaussian process based on its HOS. We pose this as a higher-order spectrum factorization problem, i.e., if an exact linear model, $H(w, z)$, exists, then $H(w, z)$ is the solution of

$$S(w_1, z_1; \ldots; w_n, z_n) = H(\prod_{i=1}^{n} w_i^{-1}, \prod_{i=1}^{n} z_i^{-1}) \prod_{i=1}^{n} H(w_i, z_i),$$
(1)

where $S(w_1, z_1; \ldots; w_n, z_n)$, $n \geq 2$, is the given higher-order spectrum of the 2-D signal.

It is the purpose of this paper to study the necessary and sufficient conditions for the existence of a solution to (1). These are stated in Theorem 1. An efficient algorithm is then presented for the factorization of the HOS based on cepstrum operations, when such a factorization exists. The cepstral projection method developed in this paper can also be used, under certain conditions, for nonminimum phase system identification and phase reconstruction in the HOS domain [2]. Finally, we apply the HOS factorization algorithm to obtain a nonminimum phase AR model for a real image.

II. PRELIMINARIES

In this section, we present some preliminary definitions and lemmas, before formally stating Theorem 1 in the next section. We use the terms 'higher-order' and 'n^{th}-order' interchangeably to indicate that the order is greater than or equal to two, where second-order spectrum corresponds to the bispectrum. We refer the reader to [3] for the definition of the nth-order moment and the nth-order cumulant of a 1-D random signal. The definition of higher-order cumulants can be extended to two-dimensional signals straightforwardly by considering each lag index, m_i, as an ordered pair (k_i, l_i) [4]. We denote the nth-order cumulant of an nth-order wide-sense stationary random signal, $\{x(o, p)\}$, by $r_x(k_1, l_1; \ldots; k_n, l_n)$.

Definition: *The nth-order spectrum of an nth-order wide-sense stationary random signal, $\{x(o, p)\}$, is defined as:*

$$S_x(w_1, z_1; \ldots; w_n, z_n) = \mathcal{Z}\{r_x(k_1, l_1; \ldots; k_n, l_n)\}$$
(2)

if the region of convergence (ROC) of $S_x(w_1, z_1; \ldots; w_n, z_n)$ includes the unit $2n$-circle in C^{2n}, i.e., $\{(w_1, z_1; \ldots; w_n, z_n) : |w_1| = |z_1| = \cdots = |w_n| = |z_n| = 1\}$.

Definition: [5] *A random signal, $\{w(k, l)\}$, is called n^{th}-order white if its nth-order spectrum is a constant, i.e.,*

$$S_{w(w_1, z_1; \ldots; w_n, z_n)} = \beta, = constant. \qquad (3)$$

Lemma 1: [5] *The output $\{y(o, p)\}$ of a 2-D stable LTI system with the transfer function $H(w, z)$ driven by an nth-order wide-sense stationary random signal $\{x(o, p)\}$ is n^{th}-order wide-sense stationary with the nth-order spectrum, $S_{y(w_1, z_1; \ldots; w_n, z_n)}$, given by*

$$S_{y(w_1, z_1; \ldots; w_n, z_n)} = S_x(w_1, z_1; \ldots; w_n, z_n)$$

$$H\left(\prod_{i=1}^n w_i^{-1} \cdot \prod_{i=1}^n z_i^{-1}\right) \prod_{i=1}^n H(w_i, z_i) \qquad (4)$$

where $S_{x(w_1, z_1; \ldots; w_n, z_n)}$ is the nth-order spectrum of the input random signal.

Definition: *The nth-order complex cepstrum of an nth-order wide-sense stationary random signal $\{x(o, p)\}$ is defined as*

$$c_x(k_1, l_1; \ldots; k_n, l_n) = \mathcal{Z}^{-1}\{\log[S_x(w_1, z_1; \ldots; w_n, z_n)]\}. \quad (5)$$

where $\mathcal{Z}^{-1}\{\cdot\}$ denotes the inverse z-transform operation, $\log(\cdot)$ denotes complex logarithm, and the inverse z-transform is taken on the unit $2n$-circle.

Lemma 2: [2] *The nth-order complex cepstrum $c_y(k_1, l_1; \ldots; k_n, l_n)$ of the output $\{y(o, p)\}$ of a stable LTI system with the transfer function $H(w, z)$ driven by an nth-order wide-sense stationary random signal $\{x(o, p)\}$ exists if the nth-order cepstrum of $\{x(o, p)\}$ exists and $H(w, z)$ has no zeros on the unit bi-circle, i.e., $\{(w, z) : |w| = |z| = 1\}$, and is given by*

$$c_y(k_1, l_1; \ldots; k_n, l_n)$$

$$= c_x(k_1, l_1; \ldots; k_n, l_n) + g(-k_i, -l_i) \prod_{\substack{j=1 \\ j \neq i}}^n \delta(k_j - k_i, l_j - l_i)$$

$$+ \sum_{i=1}^n g(k_i, l_i) \prod_{\substack{m=1 \\ m \neq i}}^n \delta(k_m, l_m), \text{ for any } i = 1, \ldots, n \qquad (6)$$

where

$$g(k, l) = \mathcal{Z}^{-1}\{\log[H(w, z)]\}. \qquad (7)$$

where the inverse z-transform is taken on the unit bi-circle, and $c_x(k_1, l_1; \ldots; k_n, l_n)$ is the nth-order cepstrum of $\{x(o, p)\}$, and $\delta(\cdot, \cdot)$ denotes the 2-D Kronecker delta function.

The support of the complex cepstrum sequence $c_y(k_1, l_1; \ldots; k_n, l_n)$ is in general the entire $2n$ dimensional space. However, if we define the difference cepstrum sequence $c_d(k_1, l_1; \ldots; k_n, l_n)$ as

$$c_d(k_1, l_1; \ldots; k_n, l_n) = c_y(k_1, l_1; \ldots; k_n, l_n)$$

$$c_x(k_1, l_1; \ldots; k_n, l_n), \qquad (8)$$

then the support of the sequence $c_d(k_1, l_1; \ldots; k_n, l_n)$ falls only on specific planes in the $2n$-dimensional space. A 3-D cross-section of the support of the complex cepstrum sequence $c_y(k_1, l_1; \ldots; k_n, l_n)$, for the case $n = 2$, is illustrated in Fig. 1.

Lemma 3: *The system transfer function $H(w, z)$ in Lemma 1 can be recovered uniquely (up to a linear phase factor) for $n \geq 2$, given the complex cepstrum sequences $c_y(k_1, l_1; \ldots; k_n, l_n)$ and $c_x(k_1, l_1; \ldots; k_n, l_n)$.*

Proof: We will prove the lemma by constructing an $H(w, z)$ given $c_y(k_1, l_1; \ldots; k_n, l_n)$ and $c_x(k_1, l_1; \ldots; k_n, l_n)$.

From (6) and (8),

$$c_d(k_1, l_1; \ldots; k_n, l_n)$$

$$= g(-k_i, -l_i) \prod_{\substack{j=1 \\ j \neq i}}^n \delta(k_j - k_i, l_j - l_i)$$

$$+ \sum_{i=1}^n g(k_j, l_j) \prod_{\substack{m=1 \\ m \neq j}}^n \delta(k_m, l_m), \text{ for any } i = 1, \ldots, n. (9)$$

The following regions

$$R_i = \{(k_1, l_1; \ldots; k_n, l_n) : k_j = l_j = 0$$
$$\text{for } j = 1, \ldots, n \text{ and } j \neq i\}, i = 1, \ldots, n,$$

$$R_{n+1} = \{(k_1, l_1; \ldots; k_n, l_n) : k_1 = \cdots = k_n, l_1 = \cdots = l_n\}.$$
$$(10)$$

are planes in the $2n$-dimensional Cartesian space intersecting only at the origin, and correspond to the supports of the multiplicative factors in (1). Therefore, $H(w, z)$ can be recovered by projecting $c_d(k_1, l_1; \ldots; k_n, l_n)$ onto any R_i, $i = 1, \ldots, n + 1$. Since the contribution to the complex cepstrum of each of these factors are the same at the origin of the $2n$-dimensional space, we divide up the complex cepstrum value at the origin equally among the $n + 1$ factors.

The projection operators, $\mathcal{P}^{(i)}$, in

$$\hat{c}_d^{(i)}(k, l) = \mathcal{P}^{(i)}\{c_d(k_1, l_1; \ldots; k_n, l_n)\}, \text{ for } i = 1, \ldots, n + 1. \qquad (11)$$

that project from the $2n$-dimensional complex cepstrum space onto R_i, $i = 1, \ldots, n$, are implicitly given as follows

$$\hat{c}_d^{(i)}(k, l) = \begin{cases} \dfrac{1}{n+1} c_d(0, 0; \ldots; 0, 0) & \text{if } k = l = 0 \\ c_d(k_1, l_1; \ldots; k_n, l_n)\Big|_{\substack{k_i = k, l_i = l, \\ k_j = l_j = 0, j = 1, \ldots, n, j \neq i}} & \text{otherwise} \end{cases} \qquad (12)$$

whereas the projection onto R_{n+1} is given as follows

$$\hat{c}_d^{(n+1)}(k, l) = \begin{cases} \dfrac{1}{n+1} c_d(0, 0; \ldots; 0, 0) & \text{if } k = l = 0 \\ c_d(k_1, l_1; \ldots; k_n, l_n)\Big|_{k_i = l_i = \ldots = l} & \text{otherwise} \end{cases} \qquad (13)$$

The sequences obtained by projecting $c_d(k_1, l_1; \ldots; k_n, l_n)$ onto any R_i, $i = 1, \ldots, n + 1$, are identical, except that the

one projected onto R_{n+1} is reverse-ordered. Hence, we define

$$c_q(k,\ell) = \hat{c}_i^{(n)}(k,\ell) = \cdots = \hat{c}_i^{(n)}(k,\ell) = \hat{c}_d^{(n+1)}(-k,-\ell).$$
(14)

Finally, $H(w,z)$ can be calculated via a 2-D z-transform

$$H(w,z) = \exp[\mathcal{Z}\{c_q(k,\ell)\}]$$
(15)

where $\exp(\cdot)$ denotes complex exponentiation. Note that the ROC includes the unit bi-circle. The function that is constructed as described above, is unique up to a linear phase factor, since $H(w,z)$ and $H(w,z)w^{\alpha}z^{\gamma}$, where α and γ are constants, yield identical n^{th}-order spectra. □

III. HIGHER-ORDER SPECTRUM FACTORIZATION IN TWO-DIMENSIONS

In this section we provide a theorem that establishes the necessary and sufficient conditions for the existence of a stable 2-D LTI system such that its output will have the given two-dimensional n^{th}-order spectrum when its input is an nth-order white random signal. An efficient algorithm to implement this factorization, is also provided. When a factorization does not exist, the algorithm provides the transfer function of an LTI system that approximately models the given higher-order spectrum function.

A. THEOREM

Theorem 1: *Given a higher-order spectrum function $S(w_1,z_1;\ldots;w_n,z_n)$ with no zeroes on the unit $2n$-circle.*

(a) There exists a unique (up to a time shift and a scaling factor) stable LTI system, with the transfer function $H(w,z)$, such that

$$S_y(w_1,z_1;\ldots;w_n,z_n) = A_0 H(\prod_{i=1}^n w_i^{-1}, \prod_{i=1}^n z_i^{-1}) \prod_{i=1}^n H(w_i,z_i),$$
(16)

where A_0 is a non-zero arbitrary constant, if and only if the complex cepstrum function

$$c(k_1,\ell_1;\ldots;k_n,\ell_n) = \mathcal{Z}^{-1}\{\log[S(w_1,z_1;\ldots;w_n,z_n)]\},$$
(17)

where the inverse z-transform is taken on the unit $2n$-circle, exists, and has the following property:

$$c(k_1,\ell_1;\ldots;k_n,\ell_n) = 0 \quad \text{for all} \quad (k_1,\ell_1;\ldots;k_n,\ell_n) \notin \bigcup_{i=1}^{n+1} R_i,$$
(18)

where $R_i, i = 1,\ldots,n+1$, are as defined in Lemma 3.

(b) There does not always exist a stable LTI system, with the transfer function $H(z,w)$, such that (16) is satisfied with A_0 being an arbitrary constant.

Proof: See [2].

Corollary: *If there is a stable LTI system that satisfies (16) for a given $S(w_1,z_1;\ldots;w_n,z_n)$, $n_0 \geq 2$, then any n^{th}-order spectrum as well as the power spectrum of the output of the system when its input is an nth-order white random signal can be computed (up to a scaling factor) from the knowledge of $S(w_1,z_1;\ldots;w_n,z_n)$ only.*

Proof: By Theorem 1, we can find an $H(w,z)$ given $S(w_1,z_1;\ldots;w_n,z_n)$. Then, all the other higher order spectra and the power spectrum can be determined using the knowledge of $H(w,z)$ up to a scaling factor. □

Definition: *We define the linearity measure, ρ_n, of a 2-D process based on its nth-order cepstrum as*

$$\rho_n = \frac{\sum\limits_{(k_1,\ell_1;\ldots;k_n,\ell_n) \in \cup_{i=1}^{n+1} R_i} |c(k_1,\ell_1;\ldots;k_n,\ell_n)|^2}{\sum\limits_{(k_1,\ell_1;\ldots;k_n,\ell_n)} |c(k_1,\ell_1;\ldots;k_n,\ell_n)|^2}$$
(19)

where $c(k_1,\ell_1;\ldots;k_n,\ell_n)$ is the nth-order cepstrum given by (17).

Remarks: (i) For an nth-order spectrum, the union of the regions, $R_i, i = 1,\ldots,n+1$, does not cover the entire $2n$-dimensional space, furthermore, the regions coincide only at the origin. However, for the case $n = 1$, corresponding to the power spectrum, which was excluded by Theorem 1, the regions R_1 and R_2,

$$R_1 = R_2 = \{(k,\ell) : -\infty < k < \infty, -\infty < \ell < \infty\}. \quad (20)$$

coincide everywhere; moreover they cover the entire 2-D space. It follows from this fact that, for $n = 1$, there are infinitely many possible factorizations, and, hence, the true system phase in general cannot be recovered from the power spectrum.

(ii) The factorization of a 2-D power spectrum function that can be represented as a finite-degree polynomial, in general, results in factors of *infinite* degree. On the other hand, although a factorization of a finite-degree 2-D higher-order spectrum function is, in general, not possible; when exact factorization is possible, it will produce *finite*-degree factors.

B. AN ALGORITHM

In this subsection, we present an efficient algorithm for the factorization of a given HOS, without using any FFT operations. This algorithm can also be used for nonminimum phase image modeling as shown in Section IV.

The algorithm can be summarized as follows:

(1) *Estimation of the higher-order spectrum*

(i) Given a time series, choose the order of the spectrum, $n \geq 2$, to be factorized.

(ii) Subtract the average of the data if it is not *a priori* known that the time series is a realization of a zero-mean process. Then, segment the data into K records of length M. Estimate the samples of the nth-order spectrum, $S(w_1,v_1;\ldots;w_n,v_n)$, $w_1,v_1;\ldots;w_n,v_n = 0,\ldots,N-1$, where

$$S(w_1,v_1;\ldots;w_n,v_n) = S(w_1,z_1;\ldots;w_n,z_n)\Big|_{w_i=e^{j\frac{2\pi}{N}w_i}, z_i=e^{j\frac{2\pi}{N}v_i}},$$

$$w_i,v_i = 0,\ldots,N-1, \quad i = 1,\ldots,n. \quad (21)$$

using one of the techniques given in [6].

(iii) If $S(u_1, v_1; \ldots; u_n, v_n) = 0$ for any $(u_1, v_1; \ldots; u_n, v_n)$, then go to (i) and choose a different value for n. Otherwise continue.

(2) *Projection of the complex cepstrum*

(i) Compute $\{C'(u, v)\}_{u,v=0}^{N-1}$ given by

$$C'(u_1, v_1) = \frac{1}{N^2} \sum_{u_2, v_2=0}^{N-1} \cdots \frac{1}{N^2} \sum_{u_n, v_n=0}^{N-1} \log[S(u_1, v_1; u_2, v_2; \ldots, u_n, v_n)],$$
$$u_1, v_1 = 0, \ldots, N-1. \qquad (22)$$

(ii) Calculate c_0 given by

$$c_0 = \frac{n}{n+1} \frac{1}{N} \sum_{u,v=0}^{N-1} C'(u, v). \qquad (23)$$

(iii) Subtract the bias term c_0 from $\{C'(u, v)\}_{u,v=0}^{N-1}$ (to scale the value of $c(0, 0; \ldots; 0, 0)$ by $1/(n+1)$) to obtain $\{G(u, v)\}_{u,v=0}^{N-1}$:

$$G(u, v) = C'(u, v) - c_0, \qquad u, v = 0, \ldots, N-1. \qquad (24)$$

(3) *Computation of the system frequency response*

Finally, compute the system frequency response $\{H(u, v)\}_{u,v=0}^{N-1}$:

$$H(u, v) = \exp[G(u, v)], \qquad u, v = 0, \ldots, N-1. \qquad (25)$$

Remarks: (i) In general, we can reconstruct an aliased version of the impulse response corresponding to the system transfer function, $H(w, z)$ in (16), due to sampling of the nth-order spectrum. This is because $H(w, z)$ can in general be an infinite impulse response system. Therefore, in practice the number of samples, N, should be chosen large enough.

(ii) In certain cases the calculation of $G(u, v)$ may require phase unwrapping. This can be traded with more severe aliasing by using the differential cepstrum of the signal [7], instead of directly computing the complex logarithm of its higher order spectrum.

IV. RESULTS

In what follows, we use a real image as an example of a nonGaussian signal, $s(o, p)$. We use the method developed in Sections II-III to construct a linear model for the signal, based on its bispectrum.

The linearity measure of the signal based on its bispectrum is calculated to be 0.93. This is an indication that the linear model may be quite satisfactory.

To obtain an AR model,

$$s(o, p) = \sum_{(i,j)} c_{ij} s(o - i, p - j) + w(o, p), \qquad (26)$$

we factorize the inverse of the bispectrum. We then truncate the factor to achieve a finite order AR model. The normalized $\{c_{ij}\}$ AR parameters are tabulated in Table I.

We, then, compute the bispectrum based on the identified AR model. Fig. 2 compares (the 2-D cross sections of) the two bispectra. The average-squared error between the phase sequences of the estimated and the reconstructed bispectra is calculated to be 3.5. The success of the model is limited by the linearity measure of the image bispectrum and should be judged by the second-order whiteness of the error sequence which could be generated using this model.

The results show that bispectrum factorization can successfully be used to model the HOS of a nonminimum phase signal.

V. DISCUSSION

There are a few points to be cautious about in using the proposed method. (i) The factorization method yields the exact system model transfer function for a linear process when the higher-order correlations are of finite-extent. Otherwise, we can only obtain an aliased version of the model transfer function because of the sampling process. (ii) The proposed algorithm may require phase unwrapping in certain cases. It is possible to express the results of this paper in terms of differential cepstrum [7], rather than complex cepstrum, to avoid phase unwrapping. However, this would correspond to trading phase wrapping with more severe aliasing.

REFERENCES

1. M.J. Hinich and D.M. Patterson, 'Identification of the Coefficients in a Non-Linear Time Series of the Quadratic Type,' *Journal of Econometrics*, Vol. 30, pp. 269-288, 1985.

2. A.M. Tekalp and A.T. Erdem, 'Higher-Order Spectrum Factorization in One and Two Dimensions with Applications in Signal Modeling and Nonminimum Phase System Identification', to appear in *IEEE Trans. Acoust., Speech and Sign. Proc.*, October, 1988.

3. D.R. Brillenger, 'An Introduction to Polyspectra,' *Annals of Math. Statis.*, Vol. 36, pp. 1351-1374, 1965.

4. A. Swami and G.B. Giannakis, 'ARMA Modeling and Phase Reconstruction of Multidimensional NonGaussian Processes Using Cumulants', *Proc. ICASSP-88*, pp. 729-732, New York, NY, 1988.

5. G.B. Giannakis and J.M. Mendel, 'Stochastic Realization of Nonminimum Phase Systems,' *Proc. Amer. Cont. Conf.*, pp. 1254-1259, 1986.

6. C.L. Nikias and M.R. Raghuveer, 'Bispectrum Estimation: A Digital Signal Processing Framework,' *Proceedings IEEE*, Vol. 75, No. 7, pp. 869-891, July 1987.

7. R. Pan and C.L. Nikias, 'The Complex Cepstrum of Higher Order Cumulants and Nonminimum Phase System Identification,' *IEEE Trans. Acoust., Speech and Sign. Proc.*, Vol. ASSP-36, No. 2, pp. 186-205, Feb. 1988.

$$\alpha_{0,0} = 3g_{0,0}$$

Figure 1. A 3-D cross-section ($t_2 = 0$) of the support of the complex cepstrum sequence $c_l(k_1, t_1, \ldots, k_n, t_n)$, for $n = 2$.

$i \uparrow \quad j \rightarrow$	-1	0	1
1	-.060680	0.110262	-.038716
0	0.332518	x	0.345242
-1	-.177404	0.447343	-.025165

Table 1. Identified nonminimum phase (normalized) AR parameters, $c_{i,j}$, using bispectrum factorization on the Cameraman image.

Figure 2. (a) A 2-D cross-section ($u_1 = v_1 = 0$) of the estimated bispectrum of the Cameraman image.

Figure 2. (Continued) (b) A 2-D cross-section ($u_1 = v_1 = 0$) of the bispectrum corresponding to the linear model.

FOURTH ORDER STATISTICS FOR SEISMIC DECONVOLUTION

T.J. Deeming

Digicon, Inc.
Houston, Texas 77098

ABSTRACT

Two approaches to using fourth-order statistics for seismic deconvolution applications are described. The first, oldest, and least successful, involves an AR wavelet model together with a maximum kurtosis assumption about the reflectivity spectrum. The second approach is based on a linear system continuous time model for the seismic wavelet, producing an ARMA model in discrete time. The properties of this model lead fairly naturally to an estimation method which uses a fourth order statistic of the data to estimate both the AR order and the AR component of the wavelet. The method is exact for noise-free synthetic ARMA wavelets. In real seismic data, the estimated AR order is surprisingly small.

1. Introduction

The convolutional model of a seismic trace describes the recorded signal, x, as the convolution of a wavelet, w, with a reflectivity sequence, r, together with additive noise:

$$x_t = \sum_k w_k \cdot r_{t-k} + \varepsilon_t \qquad (1)$$

The seismic trace is a record of earth motion, either velocity (for land exploration) or pressure (for marine exploration). It is sampled at a finite sample interval which is usually 2ms or 4ms, and contains frequencies roughly from 5Hz to 100Hz. Seismic data are significantly band-limited, which causes difficulty when algorithms expecting a fully broad-band spectrum are used.

The system identification problem is to estimate the reflectivity sequence. The standard model of the reflectivity is that it is spectrally white, so that the autocovariance of the seismic trace is equal in expectation to the autocovariance of the wavelet. This autocovariance is then used as the basis for wavelet estimation and/or deconvolution operator design, using well-known Toeplitz recursion algorithms.

The distinction between AR, MA and ARMA model wavelets is often not carefully made in the seismic literature. Most traditional deconvolution methods design a finite length causal deconvolution operator to apply to the trace [1], so that the wavelet model is implicitly AR.

These methods involve second order statistics of the seismic data, and corresponding second order statistical assumptions about the reflectivity. When second order methods fail, the natural next step for seismic deconvolution is to go to fourth order methods, since reflection coefficients have nearly a symmetric distribution about a zero mean so that no information about third moments of the waveform is obtainable from the data.

The introduction of higher order methods has been motivated partly by the desire to relax the minimum phase assumption about the wavelet, but also by the observation that real reflectivity sequences, as obtained from well data, have a distinctly non-Gaussian distribution. One aspect of this is that they exhibit a tendency to sparseness, characterized by a kurtosis larger than that for a Gaussian distribution. A few fairly large reflection coefficients corresponding to lithologic boundaries in the earth are separated by regions of low or nearly zero reflectivity. The first fourth-order method described below is an attempt, largely unsuccessful, to exploit this non-Gaussian sparse character of the reflectivity.

The second method grew out of a desire
to understand the physics of mininimum
phase, particularly as applied to
sources for seismic exploration: what
physical properties of such sources
determine that their output will be
minimum phase? This work has been
presented in detail elsewhere [2].

2. Maximum kurtosis deconvolution

Introduced by Wiggins [3] in 1977, under
the name "Minimum Entropy
Deconvolution", and subsequently
modified by various authors (see Walden
[4] for an excellent review), this
technique designs a deconvolution
operator so as to maximize the sample
kurtosis of the processed trace. In its
original formulation, an un-normalized
kurtosis was used, called the Varimax
norm:

$$V = \sum y_i^4 / (\sum y_i^2)^2 \qquad (2)$$

y is the result of applying an operator,
f, to the seismic trace:

$$y_i = \sum_k f_k \cdot x_{i-k} \qquad (3)$$

The coefficients of f are chosen so as
to maximize V for the output trace. If f
is constrained to be causal of length m
points, then the wavelet model is
implicitly AR(m). In practice, the
constraint to causality is not usually
made, since V is completely insensitive
to time shifts of the data or the
operator.

The practical implementation of the
optimization typically involves an
iterative procedure starting with an
initial guess at f, and there is often
difficulty in getting the iteration to
converge, as well as sensitivity to the
starting form of f [4].

There are many local maxima relative to
variation of f. Worse, the more degrees
of freedom are allowed (by increasing
the number of components of f), the more
the reflectivity will converge to an
unconstrained local maximum kurtosis
state having the samples either zero or
a constant value [5], which is
geophysically unreasonable. Only by
severely limiting the number of degrees
of freedom can this condition be
avoided. A recent variant of the
procedure determines a single phase
rotation to maximize the kurtosis of the
result. The idea is to generate an
effective wavelet on the processed trace
which is zero phase and as "sharp" as

possible. Unfortunately, the zero phase
form of a wavelet is not necessarily its
maximum kurtosis form, and this
technique further requires highly
non-Gaussian reflectivity statistics for
its success [6,7].

While the idea of maximum kurtosis
processing is not quite dead in the
seismic industry, it has never become a
part of standard seismic data processing
practice.

3. Linear system model

In justifying the use of minimum phase
wavelet models for seismic
deconvolution, the claim is typically
made that seismic sources are close to
minimum phase. It was in the attempt to
understand what physics of the sources
themselves might justify (or disprove)
this claim that the present
investigation was begun. Details are
given in [2].

A (marine) seismic source generates an
outgoing pressure pulse, typically
measured as the received pressure in
bars at a standard distance of 1 meter.
This is the source strength, s(t). The
mathematical ingredients of an
appropriate physical model of s(t) can
be expected to be: (1) A differential
equation obeyed by s(t), the equation
containing coefficients which are
related to the structure and design of
the source; (2) A specification of the
firing mechanism of the source. In
mathematical terms, this will involve
initial values for s(t) and its
derivatives; (3) Specification of the
sample interval, Δt, at which the output
will be recorded.

The simplest model with the above
ingredients is one in which the
differential equation is linear with
constant coefficients. If such an
equation is of degree m, then it can be
shown [2] that the sampled output is
ARMA(m,n) with n≤m. In z-transform
notation

$$S(z) = B(z)/A(z) \qquad (4)$$

where B is the MA(n) component and A is
the AR(m) component.

The minimum phase character of A(z) is
guaranteed, for any sample interval, by
the physical stability of the linear
system, while the minimum phase
character of B(z) depends on the initial
conditions, and can also be changed from
minimum phase to non-minimum phase (or

vice-versa) by changing the sample interval. This is potentially quite a serious problem for seismic deconvolution processing.

In seismic data, the source waveform is not usually available for analysis, but a reasonable estimate of its autocovariance can be obtained. It is fairly easy to show that if s is ARMA(m,n), then its one-sided autocovariance, c, is ARMA(m,n'), with

$$n' = max(n,m-1) \qquad (5)$$

In particular, if $n \leq m$, then $n' \leq m$. Furthermore, $C(z)$ has the same AR component as $S(z)$, but a different MA component:

$$C(z) = B'(z)/A(z) \qquad (6)$$

It follows that if an algorithm can determine the AR component of an ARMA waveform without being perturbed by the presence of the MA component, then we can find $A(z)$ by using the observed one-sided autocovariance as the input waveform to such an algorithm.

We use a fairly straightforward least-squares approach in the domain of c. The application of the AR(m) operator of length m to an ARMA(m,n') waveform leaves a residual pulse of length n', after which all samples will be zero. Since we know that $n' \leq m$, we define a measure of the result of applying an AR operator to c as

$$E = \sum_{\iota = m}^{N} [\sum_{k=0}^{m} a_k \cdot c_{\iota - k}]^2 \qquad (7)$$

where N is the upper limit of the index of c to be used. (N is potentially infinite, since a process with an AR component is of infinite duration.) The values of a are then chosen to minimize E, subject to the constraint $a_o = 1$. This leads to the equation

$$\sum_{k=1}^{m} a_k \cdot D_{k j} = D_{o} \qquad (8)$$

where D is the matrix

$$D_{k j} = \sum_{\iota = m}^{N} c_{\iota - k} \cdot c_{\iota - j} \qquad (9)$$

Taking the lower limit of the sum as m avoids interference from the MA component, which we know to be of length $n' \leq m$. This treatment of the end conditions makes the approach essentially the same as the covariance method of system estimation [8], but

applied to the system autocovariance, rather than the system output itself. In fact, as long as the lower limit of the sum in (9) is greater than or equal to m, we are free of interference from the MA component.

To compute D, we use the autocovariance of the seismic trace as an estimate of c. Since the algorithm is essentially determining the predictability of c, the zero lag value of c need not be used. The zero lag value is most subject to the effects of random noise, so that the method is therefore relatively robust against random noise.

We solve equation (9) via an LU decomposition of D. We do not know the order, m, we should use. However, the LU decomposition of a leading principal submatrix of D is obtained by truncating the L and U matrices of the decomposition of the full matrix. Therefore, provided we compute D and its LU decomposition for an order equal to the largest value of m we want to consider, then the solutions for all lower values of m may be obtained very easily. Furthermore, the decision as to the appropriate value of m can be made by examining the diagonal elements of U, and stopping at the value of m for which the diagonal of U first goes to zero (subject to some numerical tolerance). Thus the algorithm both determines the coefficients of the AR component and also estimates its order.

4. Fourth order statistics and the convolutional model

The algorithm can be viewed as second order, with the essential data statistic being the trace autocovariance, and with the statistical condition on the reflectivity being that it is second-order white so that an accurate estimate of the wavelet autocovariance is obtained. This autocovariance estimate is then subject to further (non-linear) processing to determine the coefficients of the AR component of the model. (There is nothing unusual about non-linear processing of an autocovariance estimate. That is exactly what any Toeplitz recursion algorithm does.) From this point of view, the algorithm is merely a modified approach to estimating the AR component of an ARMA waveform, given the autocovariance of that waveform.

The algorithm can also be viewed as fourth order, with the essential data statistic being the covariance matrix of

the autocovariance of the data. From this point of view, success of the method requires that D as computed from a seismic trace be equal in expectation to D computed from the wavelet.

To analyze the method from a fourth-order point of view, we investigate what happens if the fourth moment of the reflectivity has the form of the fourth moment of a zero mean iid process. In this case, the the fourth moment of x may be shown to be

$$X_{abcd} = \langle x_{t-a} x_{t-b} x_{t-c} x_{t-d} \rangle$$

$$= \langle r^2 \rangle^2 . [c_{ab} c_{cd} + c_{ac} c_{bd} + c_{ad} c_{bc} +$$
$$(K_r - 3) . K_{abcd}] \qquad (10)$$

where

$$c_{ab} = \sum_k w_{k-a} w_{k-b} \qquad (11)$$

is the wavelet autocovariance,

$$K_{abcd} = \sum_k w_{k-a} w_{k-b} w_{k-c} w_{k-d} \qquad (12)$$

is the fourth order moment of the wavelet, and K_r is the kurtosis of the distribution of r.

In computing D from a seismic trace we use the sample trace autocovariance in place of the wavelet autocovariance. This means that we estimate D (except for normalizing constants) as:

$$\hat{D}_{kj} = \sum_t \hat{X}_{tk} . \hat{X}_{tj} \qquad (13)$$

with

$$\hat{X}_{tk} = \sum_t x_{t-t} . x_{t-k} \qquad (14)$$

(using a hat (^) notation to indicate sample values). The expectation of $\hat{D}$ is therefore

$$\langle \hat{D}_{kj} \rangle = \sum_t \sum_t \sum_s \langle x_{t-t} x_{t-k} x_{s-t} x_{s-j} \rangle \qquad (15)$$

Writing s = t-u, this can be brought into a form which explicitly involves the fourth order moment of x:

$$\langle \hat{D}_{kj} \rangle = \sum_t \sum_t \sum_u \langle x_{t-t} x_{t-k} x_{t-u-t} x_{t-u-j} \rangle$$

$$\Rightarrow \sum_t \sum_u X_{tk(u+t)(u+j)} \qquad (16)$$

where we have dropped the summation over t since it yields only a multiplicative constant. Using (10) in this expression, we find that, while there is a leading term proportional to D, there are other terms present which do not generally vanish, even for a Gaussian reflectivity sequence. Therefore the sample estimate of D is biassed. This result could be anticipated from the well-known fact that covariances at different lags estimated from a single sample data set are correlated with each other.

5. MA component estimation

The fact that the MA component of the ARMA wavelet arising from a linear system model may or may not be minimum phase, depending on "accidental" parameters such as the sample rate, implies that any method for estimating the MA component must involve statistics other than second order. The estimation of non-minimum phase wavelets from third and higher order statistics has recently been discussed by Giannakis and Mendel [9]. The symmetry of the reflectivity distribution implies that we should look at the fourth order statistics of the data as the next alternative.

If the reflectivity is Gaussian, then $K_r = 3$ and, from (10), the fourth order data moment contains no information concerning the fourth order wavelet moment, and hence no information concerning the wavelet phase. If the reflectivity is non-Gaussian, then some phase information concerning the wavelet may be present in the fourth order data moment. This information is potentially of use in extracting a non-minimum phase MA wavelet component.

Practically, a one-dimensional fourth order statistic will be the easiest to handle. In terms of the general fourth order auto-moment defined in (12), the only possibilities for a one-dimensional wavelet fourth-order moment are:

$$K_{000\tau}, \quad K_{00\tau\tau}, \quad K_{0\tau\tau\tau}$$

The first and last are essentially equivalent, being time-reverses of each other, while the second is the autocovariance of the square of the wavelet samples. Since such a function could not distinguish between a waveform and its time reverse, it is not a promising candidate for extracting phase information. The only one-dimensional possibility is therefore:

$$K_{000\tau} = \sum_t w_t^3 \cdot w_{t-\tau} \qquad (17)$$

To estimate $K_{000\tau}$ we determine the sample one-dimensional auto-cumulant of the seismic data, derived from (10):

$$Q_\tau \equiv \hat{X}_{000\tau} - 3 \cdot \hat{X}_{00} \cdot \hat{X}_{0\tau} \qquad (18)$$

using sample values in place of expectations. We have computed this quantity for synthetic seismic traces and can report that, while it does discriminate between minimum, maximum, and mixed phase wavelets, the discrimination is not strong, and requires lengthy, stationary, highly non-Gaussian reflectivity statistics for its success. In this respect, the method suffers from many of the same problems as the maximum kurtosis method described previously. Details of this work will be reported elsewhere.

6. Data examples

Unlike the maximum kurtosis method for which it is easy to generate examples which fail, the algorithm described in paragraph 3 performs exactly on noise-free synthetic wavelets. It selects both the correct order and the correct AR coefficients and is quite stable.

Figure 1 shows a synthetic pulse of character similar to a real seismic pulse. It is a sampled version of the signal

$$s(t) = e^{-\delta \cdot t} \cdot \sin(2\pi \cdot f \cdot t) \qquad (19)$$

giving an ARMA(2,1) sampled pulse [2] with

$$A(z) = 1 - [2 \cdot e^{-\delta \cdot \Delta t} \cdot \cos(2\pi \cdot f \cdot \Delta t)] \cdot z$$
$$+ [e^{-2 \cdot \delta \cdot \Delta t}] \cdot z^2$$
$$\qquad (20)$$
$$B(z) = [e^{-\delta \cdot \Delta t} \cdot \sin(2\pi \cdot f \cdot \Delta t)] \cdot z$$

For the example in Figure 1, $\delta = 35$ sec^{-1}, $f = 25$ Hz, $\Delta t = 4$ ms, yielding

$$A(z) = 1.0 - 1.406651\, z + 0.755784\, z^2$$
$$\qquad (21)$$
$$B(z) = 0.510996\, z$$

Figure 2 shows the autocorrelation of this pulse. When this was input to our algorithm, the estimated AR parameters were

$$A(z) = 1.0 - 1.406651\, z + 0.755784\, z^2$$
$$\qquad (22)$$

This merely verifies the correctness of the algorithm for noise-free data.

Figure 3 shows the autocorrelation of a synthetic seismic trace made by convolving the original pulse with a 1000 point simulated reflectivity series generated as a non-Gaussian distribution with kurtosis K=4.5. The autocorrelation shows slight deviations from that of the pulse alone. When input to our algorithm, the estimated AR parameters were

$$A(z) = 1.0 - 1.4432\, z + 0.7935\, z^2 \qquad (23)$$

The discrepancy between this and the true value gives some measure of the effect of bias in determining the fourth order matrix, D, from real data.

Figure 4 shows the autocorrelation of a portion of real seismic data, taken from a single shot record in a marine survey. This autocorrelation was input to our algorithm, yielding the surprisingly small estimate of m=4 for the order, with the following AR parameter estimates

$$A(z) = 1.0 - 3.59\, z + 5.10\, z^2 - 3.38\, z^3$$
$$+ 0.89\, z^4 \qquad (24)$$

According to the theory outlined earlier, if a linear system model is applicable to such a system, the effect of applying the AR(m) operator to the autocorrelation should yield a residual pulse of length $n' \le m$. When the estimated AR(4) operator is applied to the autocorrelation of Figure 4, the residual autocorrelation shown in Figure 5 results. Note that the autocorrelation is effectively reduced to zero after a small number of samples which is, however, $n'=4$ rather than $n'=3$.

The surprise in the size of m comes from at least two directions. First, standard deconvolution practice typically uses much higher orders - operators of 50, 70 or 100 points are not uncommon. Second, a real-world marine seismic source is a complicated system, consisting of some tens of airguns of varyious sizes arranged in a spatial array for the purpose of suppressing horizontally traveling energy. The oscillation of the air-bubble from an airgun is known to be a highly non-linear affair; furthermore there are non-linear interactions between the guns in such an array. It

therefore seems *a priori* unlikely that a low order linear system would describe such a system adequately.

REFERENCES

[1] E.Robinson and S.Treitel, "Geophysical Signal Analysis", Prentice-Hall, NJ, 1980.

[2] T.J.Deeming, "The physics of minimum phase", presented at the 51'st meeting of the European Association of Exploration Geophysicists, Berlin, 1989

[3] R. Wiggins, "Minimum entropy deconvolution", Proceedings of IEEE symposium on computer-aided seismic analysis and discrimination, Falmouth, MA, 1977

[4] A.T.Walden, "Non-Gaussian reflectivity, entropy and deconvolution", Geophysics, v50, pp2862-2888, 1985

[5] T.J.Deeming, "Why minimum entropy deconvolution doesn't work", S.E.G. Research workshop on deconvolution, Vail, CO, 1984.

[6] J.Longbottom, A.T.Walden and R.E.White, "Principles and application of maximum kurtosis phase estimation", Geophysical Prospecting, v36, pp115-128, 1988

[7] T.J.Deeming, "Phase estimation by minimum entropy", presented at the 50'th meeting of the European Association of Exploration Geophysicists, The Hague, 1988.

[8] S.J.Orfanidis, "Optimum signal processing", Macmillan, New York, 1988

[9] G.B.Giannakis and J.M.Mendel, "Identification of non-minimum phase systems using higher order statistics", IEEE Transactions on Acoustics, Speech and Signal Processing, v37, pp360-377, 1989
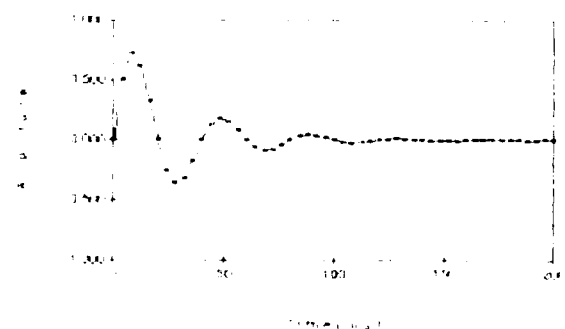
Figure 1: Synthetic AR(2,1) pulse
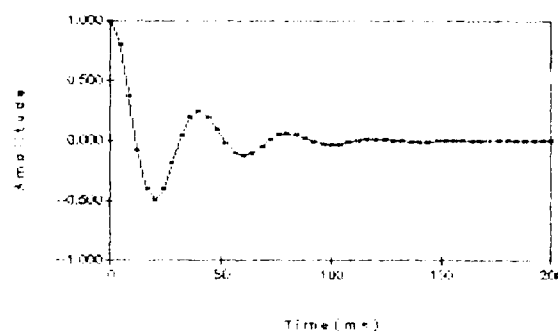
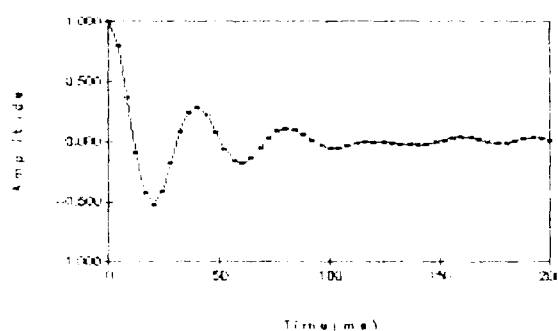Figure 2: Autocorrelation of synthetic pulse

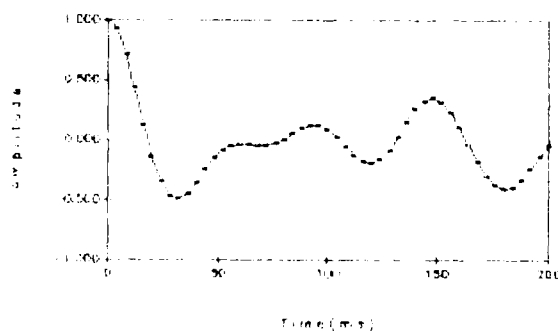Figure 3: Autocorrelation of synthetic seismic trace
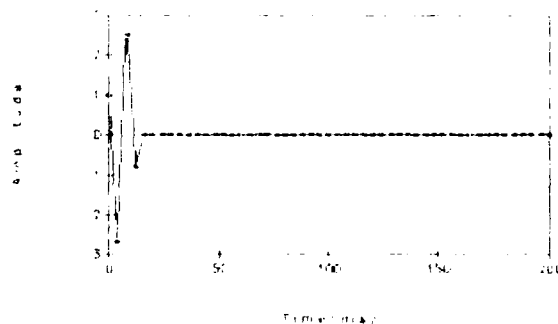

Figure 4: Autocorrelation of real seismic trace

Figure 5: Residual MA component of seismic trace autocorrelation

A NOTE ON PARAMATERS ESTIMATED BY CUMULANTS

XU LIU, JOHN J. SORAGHAN, TARIQ S. DURRANI

Dept. of Electrical and Electronic Engineering
University of Strathclyde, U.K.

Abstract

This paper presents the recursive solution to the Yule-Walker equation which is described by a non-symmetric Toeplitz matrix. It is shown that the correlation and the degree of non-stationary of the input random process can result in greater performance degradation in higher-order moment based algorithms than in autocorrelation based algorithms. The deconvolution algorithms are developed for an input series that exibits a slight degree of correlation. Simulation results are presented that make use of NAG generated random distributions.

1 Introduction

Cumulants are a very useful tool in signal processing. Since cumulants can provide the phase information, they can be used to identify systems which is particularly attractive in a non minimum phase (NMP) situation[1].

Statistical provides us with some methods to identify a time series using cumulants. In this present paper the performance of algorithms [,] used to estimate time series parameters using cumulants are further discussed, and some factors which may influence the estimated performance are noted.

In section 2 the parameters estimation algorithms are developed for a general ARMA system. In section 3 the performance degradation due to a correlated non-white input series is analised. The correlated input series is assumed non-white and modeled as an AR(1) or MA(1) process. By the recursive algorithms are obtained. Section 4 presents the simulated results which use Matlab NAG and other libraries.

$$c(-m) - \sum_{i=1}^{p} a(i)c(-m+i) = 0 \qquad \text{for } m \geq q \qquad (2)$$

For non-symmetric Toeplitz matrix, the third-order recursive solutions of the Yule-Walker equations are

$$\bar{a}_p^{p+1} = \bar{a}_p^p - J_p \bar{b}_p^p a_{p+1}^{p+1} \qquad (3)$$

$$a_{p+1}^{p+1} = \frac{c(-p-q-1) - \sum_{j=1}^{p} c(-j-q)a_{p+1-j}^p}{c(-q) - \sum_{j=1}^{p} c(-j-q)b_j^p} \qquad (4)$$

$$b_p^{p+1} = \bar{b}_p^p - J_p \bar{a}_p^p b_{p+1}^{p+1} \qquad (5)$$

$$b_{p+1}^{p+1} = \frac{c(p-q+1) - \sum_{j=1}^{p} c(j-q)b_{p+1-j}^p}{c(-q) - \sum_{j=1}^{p} c(j-q)a_j^p} \qquad (6)$$

where $\bar{a}_p^p = (a_1^p , a_2^p , ..., a_p^p)^T$ is the pth forward recursive estimating vector, $\bar{b}_p^p = (b_1^p , b_2^p , ..., b_p^p)^T$ is the pth backward recursive estimating vector. J_p is the exchange matrix, and

$$\bar{a}_p^{p+1} = (a_1^{p+1} , a_2^{p+1} , ... , a_p^{p+1})^T$$

$$\bar{b}_p^{p+1} = (b_1^{p+1} , b_2^{p+1} , ... , b_p^{p+1})^T$$

Similarly for second-order moment based algorithm, formulae (4),(6) can be used to determine the order of AR model.

Having obtained the AR parameters a(i), we can construct a residual time series s(n)

$$s(n) = x(n) - \sum_{i=1}^{p} a(i)x(n-i) \qquad (7)$$

Obviously s(n) is an MA process. According to [2], the MA parameters are

$$h(i) = \frac{c(q,i)}{c(-q,-q)} \qquad (i=1,2,\ldots,q) \qquad (8)$$

Formula (8) reveals the equivalent relation between the higher-order moments and the MA coefficients i.e. the Wold decomposition coefficients only differ from cumulants by a scalar factor. The application of cumulants to the MA parameter estimate problem yields a linear solution, and the solution can be obtained uniquely. Therefore cumulants are very useful in the identification of NMP systems. Furthermore, for minimum phase system, the estimated paramater h is only depends on c(q,i) as indicated by equation (8), but it depends on more than one statistic in second-order moment based algorithms for i=q. Therefore we can expect to get better performance by using higher-order moments than the second-order moments based algorithms.

3. Algorithm Performance

In theory, the above formulae are very good and easy to implement. However in practice, we must be careful, and pay more attention to whether or not the real time series satisfy the third-order stationary white assumption given in equation 1.

Using cumulants to identify a system requires the input random process to be third-order or higher-order i.e. white. When we use a APMA p,q model to fit a stationary time series, we are using a theoretical model to fit a practical process, of course the MA part of the model consists of white series. However, if we do deconvolution i.e. we want to estimate the parameter h k, k 1,2,.....,q from the model

$$x(t) = \sum_{k=0} h(k) v(t-k) \qquad (9)$$

we must pay particular attention to {v(k)} to check whether or not it is kth-order white when the kth-cumulants are used. For example, if {v(k)} is the reflection signal, corresponding to the impulse response of the earth in a Seismic survey, v(k) must be kth-order white in order to use cumulants.

When doing deconvolution, if {v(k)} is not third-order white, then errors are produced. Consider a simple example:

$$x(t) = v(t) + h v(t-1) \qquad (10)$$

$$R_x(1) = h c_v(1) + (1+h^2) c_v(1) + 2h c_v(-1)$$

$$+ h c_v(2) + 2h^2 c_v(1,2) \qquad (11)$$

In theory $c_x(1) = h^2 c_v(0)$, however if {v(k)} is not third-order white then many extra terms are added to $h^2 c_v(0)$ as seen in equation (11). If the order of MA increases, there will be many more terms in (11). But the second-order moment of x(t) is

$$R_x(1) = h R_v(0) + (1+h^2) R_v(2) \qquad (12)$$

Comparing (11) with (12), it is clear that the error caused by third-order correlation in third-order based algorithms is larger than the error caused by second-order correlation in second-order moment based algorithms.

If h(q) is very small, the performance of the estimation algorithm will degrade seriously, this is due to the error in c(-q,-q) which effects all h(k)
(k=1,2,......,q) as indicated by equation (8).

4. The Deconvolution of Correlated Multiple Interferences

In the above section, we have seen that, if we treat a correlated noise as a white noise then errors result. The deconvolution algorithms for correlated input signals are now developed.

CASE (a): AR Multiple Interference:

Assume that {v(t)} in (9) is a stationary AR(1) series i.e.

$$v(t) = w(t) + c v(t-1) \qquad (13)$$

where w(t) is kth-order white noise and c is a very small constant. Therefore

$$x(t) = \sum_{k=0}^{q+1} h'(k) w(t-k) + O(c^2) \qquad (14)$$

If we consider first-order approximation of c only then

$$x(t) = \sum_{k=0}^{q+1} h'(k) w(t-k) \qquad (15)$$

where   h'(0)=1

      h'(1) = c + h(1)

      h'(j) = c h'(j-1) + h(j)   j=1,...,q

      h'(q+1) = c h'(q)

Therefore c = h'(q+1)/h'(q)   (16)

      h(0) = h'(0) = 1

      h(j) = h'(j) - c h'(j-1)   j=1,...,q.

We can use (8) to estimate the h'(k), then obtain h(k) and c from (16).

CASE (b): MA Multiple Interference:

Assume that {v(t)} in (5) is an MA(1) process i.e.

$$v(t)=w(t)+dw(t-1) \qquad (17)$$

Therefore

$$x(t) = \sum_{k=0}^{q+1} h'(k)w(t-k)$$

where $h'(0)=1$

$h'(j)=b(j)+dh(j-1)$ $j=1...,q$.

$h'(q+1)=dh(q)$

If the MA paramater d is known then

$h(0)=1$

$h(j)=h'(j)-dh(j-1)$ $j=1...,q$.

If the paramater d is not known a priori, we need to solve the above non-linear equations for d and $h(i)$, $i=1,2,....,q$. When d is very small, the MA(1) model can be transformed into an AR(1) model and solved by using equation (16).

5 Simulation

Previously we have analysed the estimating error caused by the third-order correlation. Some simulation results are now presented.

Having done simulations to estimate the ARMA parameters, we have found that the performance is dependent on the input sequence {w(i)}. The samples were generated from the G05DBF(exponentially distribution) and G05DEF(LOG-Normal distribution) subroutines in the NAG Library respectively.

The results indicate that in general the performance, with G05DEF as the input random process {w(i)}, is better than that with G05DBF (see Table(1)). When the MA parameters are excessively large, as in NMP systems, the performance degrades seriously. The reasons are (1) The random numbers adopted are not third-order uncorrelated perfectly, so that we can't ignore the influence caused by $E\{w(i)w(j)\}$, $i \neq j$, as the magnitude of MA parameters reach a certain size. (2) The random numbers generated from G05DEF are more third-order uncorrelated than the numbers generated from G05DBF, see Table(2).

Table 1 indicates that the estimating performance degrade when MA parameters increase due to the random number is not third-order uncorrelated perfectly. Of course it is no problem that we use formula (8) to get the world deconvolved the coefficients of a nonstatic process. But we must concern about whether it is not satisfy third-order un-

correlation when (8) is used in deconvolution.

When using third-order statistics for DSP, the stability of random numbers is more important than when second-order moment based algorithms are used. Sometimes, one or two extremly large samples destroy the performance, although we may have used thousands of samples. Simulation results indicate that the results are not as stable as the second-order moment based algorithm, this is because the random numbers are not third-order stationary, see Table 3.

h(1)	h(2)	G05DBF		G05DEF	
		$\hat{h}(1)$	$\hat{h}(2)$	$\hat{h}(1)$	$\hat{h}(2)$
-0.500	0.677	-0.4921	0.6865	-0.5023	0.6664
-1.000	0.667	-0.9890	0.6989	-1.0042	0.6673
-1.500	0.667	-1.5513	0.7211	-1.4924	0.6697
-2.000	0.667	-2.5101	0.8174	-1.9754	0.6748
-2.333	0.667	-2.8812	0.5493	-2.3933	0.6887
-2.500	0.667	-3.5941	0.5230	-2.6645	0.7062
-3.000	0.667	-17.0756	-4.0188	-2.0607	0.8527

Table 1. MA parameters from 50 Monte Carlo runs of the MA identification algorithm.

	c(1)/c(0)	c(2)/c(0)	c(3)/c(0)	c(4)/c(0)	c(5)/c(0)
G05DBF	13	15	16	13	14
G05DEF	26	21	24	22	26

Table 2. The figures represent the number of the normal cumulants < 1.01 in 50 random number groups each has 2048 samples.

		Mean	Standard deviation
G05DBF	R(0)	4.008	0.2378
	C(0)	15.800	2.6068
G05DEF	R(0)	573.72	398.72
	C(0)	284225	618959

Table 3. The Mean and Standard deviation of C(0), R(0) in 50 random groups with each having 2048 samples.

We see that the G05DEF is extremely unstationary and it may cause some trouble when we use it. We can limit the extreme samples by robust methods to improve the performance.

Finally, it is proposed to construct a new random number generator, which is perfectly third-order stationary and uncorrelated, to use as a base for simulation of third-order statistics.

References

[1] G.B. Giannakis, "Signal Processing via Higher-order Statistics," Ph.D. Thesis, University of Southern California, 1986.

[2] G.B. Giannakis, "Cumulants: A Powerful Tool in Signal Processing," Proc. of IEEE, Vol.75, pp1333-1334, 1987.

[3] K.S.Lii and Rosenblatt, "Deconvolution and Estimation of Transfer Function Phase and coefficients for Nongaussian Linear Processes," Annals of Statistics, Vol.10, pp.1195-1208, 1982.

NONLINEAR SPECTRAL DECOMPOSITION OF THE DRIFT RESPONSE OF TETHERED OFFSHORE STRUCTURES SUBJECT TO NONGAUSSIAN IRREGULAR SEAS

S. B. Kim, E. J. Powers, R. W. Miksad, F. J. Fischer[1], and J. Y. Hong[2]

College of Engineering
The University of Texas at Austin
Austin, Texas 78712

ABSTRACT

By utilizing the concepts of bispectra and quadratic transfer functions and nonlinear coherence, we are able to spectrally decompose and quantify the surge response of a tension leg platform (TLP) into its linear and quadratically nonlinear components and identify experimentally the low-frequency wave drift force in a simulated irregular nonGaussian sea state. The approach is demonstrated with the aid of experimental data of TLP surge motion obtained from a scaled (1:54) model of a prototype TLP anchored in 1500 feet of water.

1. Introduction

In relatively recent analytical investigations of wave added resistance and lateral drifting forces and moments of vessels[1], "quadratic frequency response functions" (QFRF) were calculated to describe such quadratically nonlinear phenomena. The QFRF is intrinsically a two dimensional function of frequency and effectively models the "efficiency" with which pairs of frequencies present in a random sea wave excitation interact to yield sum and difference frequencies in the response. Knowledge of such QFRF's is desirable in order to "predict" the quadratic nonlinear force, moments, and resistance of vessels and tethered offshore structures associated with random seas.

We have developed a digital software technique[2,3,4] which may be used to compute, from experimental data, quadratic frequency response functions, which we refer to as quadratic transfer functions (QTF), and nonlinear coherence functions. The ability to compute such QTF's and nonlinear coherence functions from experimental data, make it possible to bring the experiment and theory closer together and, thus enhance the probability of developing the tools necessary to predict the nonlinear response of ships and tethered and moored offshore structures to irregular seas.

The approach rests upon Volterra nonlinear system modelling[5] and innovative utilization of polyspectra[6], particularly digital bispectral analysis. Compared to much of the earlier work on nonlinear system modeling where the input was assumed to be Gaussian, we have recently developed[4] a new approach which is valid for excitation with arbitrary amplitude statistics and arbitrary spectral density. This is an important practical advance since sea wave excitation is not necessarily Gaussian, due to prior nonlinear wave interactions, for example.

The practicality of the approach has been studied by utilizing it to model and "predict" the nonlinear low-frequency drift oscillation of a TLP (Tension Leg Platform) subject to nonGaussian irregular seas. The experiments were carried out in scaled model wave basin. The time traces of the input wave height and the output surge motion of the TLP are shown in Fig. 1 and their auto-power spectra are shown in Fig. 2. Notice that the power spectrum of the TLP surge motion (Fig. 2-b) indicates significant response in two principal frequency bands. The upper band at around 0.4 Hz corresponds to the same frequencies present in the irregular
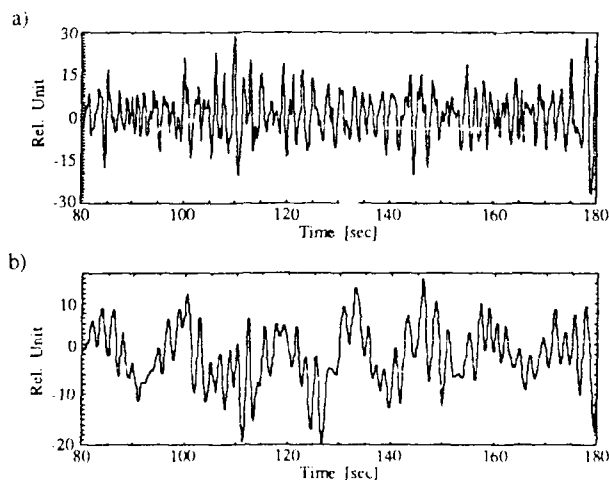
[1] Shell Development Company, Houston, Texas 77001
[2] Intelligent Signal Processing, Austin, Texas 78731

Fig. 1. Measured time series of an input/output of a TLP system. a) Input (sea wave), b) Output (surge motion).

wave spectrum (Fig. 2 a), thus suggesting a linear response. In addition, the TLP has a significant surge response at a low frequency of 0.07 Hz (approximately 0.01 Hz prototype, which corresponds to the surge natural frequency of the TLP) that is not present in the wave excitations, which suggests a nonlinear response.
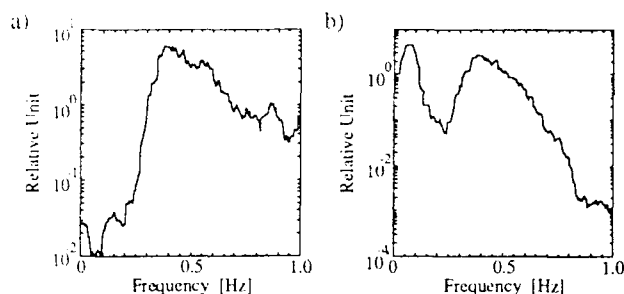

Fig. 2. Auto-power spectrum of an input/output of a TLP system. a) Input(sea wave), b) Output(surge motion).

From a physical point of view, the systems are nonlinear since there is a weak second-order force (the so-called wave drift force), which is proportional to the square of the wave height, exerted on the moored structures. As a result of this quadratic-type nonlinearity, pairs of frequencies present in the sea wave excitation mix to form sum and difference frequency second-order force components. Although the second-order force components may be relatively weak, those low frequency difference components which lie within the resonant bandwidth of the TLP result in large responses, since they are forcing the system at its resonant frequencies.

2. Quadratic Volterra System Analysis of the TLP Surge Response Subject to Irregular Waves

Though the hydrodynamic equation of motion of a TLP is very complicated because of nonlinear effects such as viscous drag, restoring force, frequency dependent added mass and radiation damping, and coupling between different motions[?], one can simplify the problem by linearizing the equation of motion with a nonlinear driving force related to the irregular sea waves. In this way, the TLP motion can be modeled as a second-order Volterra system which keeps [illegible] in the equation of the TLP [illegible] the TLP motion subject [illegible] functions (linear [illegible] origin of the resonant be [illegible] the order mechanism.

[illegible] $\gamma(t)$ can be writ-

[illegible]

[illegible] is the damping coefficient.

[illegible] the surge displace-

ment of the TLP. The quantity $f_1(t)$ is the linear wave excitation force and $f_2(t)$ is the second-order wave drift force[8]. Considering the time delay between wave measurement and actual wave action on the displaced TLP, $f_1(t)$ and $f_2(t)$ can be written using the linear and quadratic Volterra functionals as follows

$$f_1(t) = \int \alpha(t - \tau)x(\tau)d\tau \qquad (2)$$

$$f_2(t) = \int\int \beta(t - \tau_1, t - \tau_2)x(\tau_1)x(\tau_2)d\tau_1\,d\tau_2 \qquad (3)$$

where $x(t)$ denotes the time series of the irregular wave amplitude, and $\alpha(t)$ and $\beta(t_1,t_2)$ are the linear and quadratic Volterra kernels, respectively.

If one takes the Fourier transform of the equation of the motion after substituting Eqs. (2) and (3) into (1), we get

$$Y(\omega) = L(\omega)\,[\,T_1(\omega)X(\omega) + \int\int T_2(\omega_1,\omega_2)$$
$$\cdot X(\omega_1)X(\omega_2)\,\delta(\omega - \omega_1 - \omega_2)\,d\omega_1 d\omega_2\,] \qquad (4)$$

where $Y(\omega)$, $X(\omega)$, $T_1(\omega)$, and $T_2(\omega_1,\omega_2)$ are the Fourier transforms $y(t)$, $x(t)$, $\alpha(t)$, and $\beta(t_1,t_2)$, respectively. $L(\omega)$ is $[-M\omega^2 + i\omega D + R]^{-1}$ and $\delta(\omega)$ is the Dirac delta function.

This process is indicated schematically in Fig. 3. The TLP is acted upon by wave forces produced by linear as well as quadratically nonlinear mechanisms. The TLP is assumed to respond in a linear manner to the imposed force field.

$$y(t) = \int \gamma(\tau)f(t - \tau)d\tau. \qquad (5)$$

where $f(t) = f_1(t) + f_2(t)$. and $\gamma(t)$ is the inverse Fourier transform of $L(\omega)$.
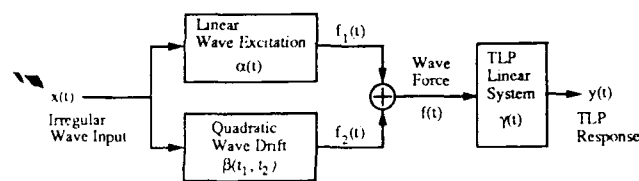

Fig. 3. Schematic diagram of a second-order Volterra model of TLP surge response with respect to irregular sea wave excitation.

In general, one can re-write the Eq. (4) using the discrete form $\omega_j = j\Delta\omega$ as

$$Y(n) = H_1(n)X(n) + \sum H_2(j,k)X(j)X(k) + \epsilon(n) \qquad (6)$$

where $\epsilon(n)$ is the difference between the measured output $Y(n)$ and the model output $Y(n)$ (the first two terms of the RHS of Equation at frequency ω_n. $H_1(n)$ and $H_2(j,k)$ are the linear and quadratic system transfer functions, respectively, and are given as

$$H_1(n) = L(n)T_1(n)$$
$$H_2(j,k) = L(n)T_2(j,k), \quad j+k = n$$

where $T_1(n)$, $T_2(j,k)$ and $L(n)$ are the discrete Fourier transforms of $\alpha(t)$, $\beta(t_1,t_2)$, and $\gamma(t)$, respectively.

The model output $\tilde{Y}(n)$ can be rewritten using vector notation as follows

$$\tilde{Y}(n) = \mathbf{H}(n)\mathbf{X}(n) \tag{7}$$

where the bold symbol denotes a vector quantity, and $\mathbf{H}(n)$ and $\mathbf{X}(n)$ are given as

$$\mathbf{H}(n) = [H_1(n), \mathbf{H}_2(n)] \tag{8}$$
$$\mathbf{X}^t(n) = [X_1(n), \mathbf{X}_2^t(n)] \tag{9}$$

where the superscript 't' denotes the transpose of a matrix and the subscript '1' and '2' denote linear and quadratic, respectively. The jth elements of $\mathbf{H}_2(n)$ and $\mathbf{X}_2^t(n)$ are

$$H_{2,j}(n) = \mu H_2(m+j, n-m-j) \tag{10}$$
$$X_{2,j}^t(n) = X(m+j)X(n-m-j) \tag{11}$$

where $0 \le j \le (N-n)/2$, $m = (n + mod[n,2])/2$, and $\mu = 2$, except when n is even and $j = 0$ where $\mu = 1$.

The optimum solution of $\mathbf{H}(n)$ in Eq.(6) is well known, and is given as

$$\mathbf{H}^t(n) = \langle \mathbf{X}^*(n)\mathbf{X}^t(n)\rangle^{-1}\langle \mathbf{X}^*(n)Y(n)\rangle$$
$$= \begin{bmatrix} S_{xx}(n) & \mathbf{B}_{xxx}^\Lambda(n) \\ \mathbf{B}_{xxx}(n) & \mathbf{C}_{xxxx}(n) \end{bmatrix}^{-1} \begin{bmatrix} S_{yx}(n) \\ \mathbf{B}_{yxx}(n) \end{bmatrix} \tag{12}$$

where Λ denotes Hermitian operator. $S_{xx}(n)$, $\mathbf{B}_{xxx}(n)$, and $\mathbf{C}_{xxxx}(n)$ are the auto-power spectrum, the column vector of the auto-bispectrum, and the 4th order cumulant spectral matrix of the input, respectively. $S_{yx}(n)$ is the cross-power spectrum, and $\mathbf{B}_{yxx}(n)$ is the column vector of the cross-bispectrum between the sea wave input $x(t)$ and the sway response output $y(t)$.

When the input statistics are Gaussian, the input auto-bispectrum $\mathbf{B}_{xxx}$ and the off-diagonal elements of $\mathbf{C}_{xxxx}$ (for $j \ne k$) are zero so that the matrix $\langle \mathbf{X}^*(n)\mathbf{X}^t(n)\rangle$ becomes diagonal. Thus, the linear and quadratic transfer functions can be estimated independently and Eq. (12) is reduced to the well known expressions of the linear and quadratic transfer functions for Gaussian input[3].

Now we return to the general (nonGaussian) case and estimate the model output power of the quadratic Volterra system using the transfer functions we obtained in Eq. (12). Using Eqs. (7) ~ (9), the model output power, $S_{\tilde{y}\tilde{y}}(n)$, is given as

$$S_{\tilde{y}\tilde{y}}(n) = \langle|\tilde{Y}(n)|^2\rangle$$
$$= \langle|H_1(n)X_1(n) + \mathbf{H}_2(n)\mathbf{X}_2(n)|^2\rangle$$

$$\equiv S_l + S_{lq} + S_q \tag{13}$$

where,

$$S_l(n) = |H_1(n)|^2 S_{xx}(n)$$
$$S_{lq}(n) = 2Re\left[\sum_{j=m}^{(N-n)/2} H_1(n)H_2^*(j, n-j)B_{xxx}^j(n)\right]$$
$$S_q(n) = \sum_{j=m}^{(N-n)/2}\sum_{k=m}^{(N-n)/2} H_{2,j}^*(n)H_{2,k}(n)C_{xxxx}^{j,k}(n)$$

Here, $S_l(n)$ is the mean square value (that is, the "power") of the TLP sway response at the frequency ω_n due to the linear wave excitation force of the irregular sea, $S_q(n)$ is the contribution to the mean square value due to the quadratic wave drift force of the irregular sea, and $S_{lq}(n)$ is the contribution due to the coupling of those two forces. This coupling exists when the irregular sea is nonGaussian. (Note that in the Gaussian case it will be zero, since $B_{xxx}^j(n)$ will be zero for Gaussian irregular seas.) Furthermore, $S_{lq}(n)$ can be either positive or negative depending on the phase relationship between those two forces.

3. Quadratic System Coherence Analysis

In a single-input linear system, it is well known that the coherence function $\gamma^2(\omega)$ is defined as

$$\gamma^2(\omega) \equiv \frac{|S_{yx}(\omega)|^2}{S_{xx}(\omega)S_{yy}(\omega)} = \frac{S_{\tilde{y}\tilde{y}}(\omega)}{S_{yy}(\omega)} \tag{14}$$

The ordinary concept of the coherence function is valid only for a linear system. The term $\gamma^2(\omega)$ defined in Eq. (14) represents only the linear relationship between the input $X(\omega)$ at frequency ω and the output $Y(\omega)$ at the same given frequency. Thus, when more than one frequency component of the input couple and interact in a nonlinear system to produce new frequencies in the output (harmonic generation, or frequency coupling), or when a single frequency component of the input is split and appears in the output at more than one frequency (subharmonic generation or chaos), or when more than one frequency component of input interacts and generates output at more than one frequency (scattering, chaos), the coherence function defined in Eq. (14) does not represent the proper relationship between the input and the output.

In general, there appears to be no unique way to define a coherence function which represents all possible nonlinear relationships between input and output, since it depends on the system model that one uses. However, for weakly nonlinear systems, one can often represent the system using Volterra functional series. In this case it is possible to extend the concept of the coherence function to higher order nonlinear systems. This is done by also extending the concepts of ordinary spectra, transfer functions, coherence, and correlation within the framework of a Fourier representation

of a signal.

A useful interpretation of the ordinary coherence function, which serves as a basis to generalize the concept, is that of the ratio of the model output power (in the sense of mean squared value per unit time) to the true output power. The coherence function can be generalized using the above definition, for the second-order Volterra system of Eq. (6) in the frequency domain[4]. From Eq. (13), we have

$$\gamma^2(n) = \frac{S_{\hat{y}\hat{y}}(n)}{S_{yy}(n)} = \gamma_l^2(n) + \gamma_{l_q}^2(n) + \gamma_q^2(n)$$

where,

$$\gamma_l^2(n) = \frac{S_{ll}(n)}{S_{yy}(n)}, \quad \gamma_{l_q}^2(n) = \frac{S_{l_q}(n)}{S_{yy}(n)}, \quad \gamma_q^2(n) = \frac{S_q(n)}{S_{yy}(n)}.$$

The terms $\gamma_l^2(n)$, $\gamma_{l_q}^2(n)$, and $\gamma_q^2(n)$ are the linear coherence function, hybrid coherence function, and quadratic coherence function of the second-order Volterra system, respectively. Notice that the terms $\gamma_l^2(n)$ and $\gamma_q^2(n)$ are positive, but not bounded by unity since $\gamma_{l_q}^2(n)$ can be positive or negative depending on the phase relationship between the linear response and quadratic response. However, the total coherence $\gamma^2(n)$ at each n is bounded by zero and unity.

4. Nonlinear spectral analysis of the TLP Surge Response

Using the model test data obtained from a scaled (1:54) model of a prototype TLP anchored in 1500 feet of water, we calculate and interpret the resulting quadratic transfer functions and coherence functions, and compare with the results of the linear spectral analysis.

The cross-power spectrum and linear coherence spectrum of the wave input and the surge output are plotted in Fig. 4 and 5, respectively. Comparing with the frequency band around 0.4 Hz where the linear coherence is close to one, notice that the cross-power spectrum at the surge natural frequency of 0.07 Hz is negligible and its linear coherence is almost zero, which suggests that the TLP surge resonance motion is due to a nonlinear interaction with the irregular wave input.
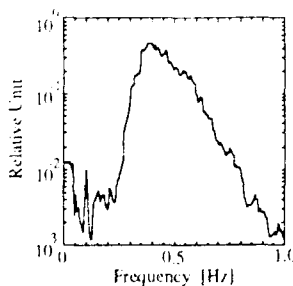
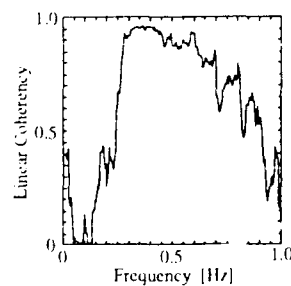Fig. 4. Cross power spectrum of sea wave/TLP surge motion.

Fig. 5. Coherence spectrum of sea wave/TLP surge motion.

In Fig. 6, we plot the cross-bispectrum of the system. Now, we can see the large peaks along the line $f_1 - f_2 = f_o$ in the difference interaction zone, where f_o is the surge natural frequency. This indicates that the resonance phenomena of the TLP is quadratically related to the irregular wave amplitude. The quadratic transfer function is plotted in Fig. 7, and large peaks are positioned along the line $f_1 - f_2 = f_o$ as in the cross-bispectrum. However, the largest peak appears at low frequency in the difference interaction zone. This suggests that, if the wave spectrum moves to lower frequency band and if the system remains same as we identified, the quadratic nonlinear force may cause considerable effect on the TLP.
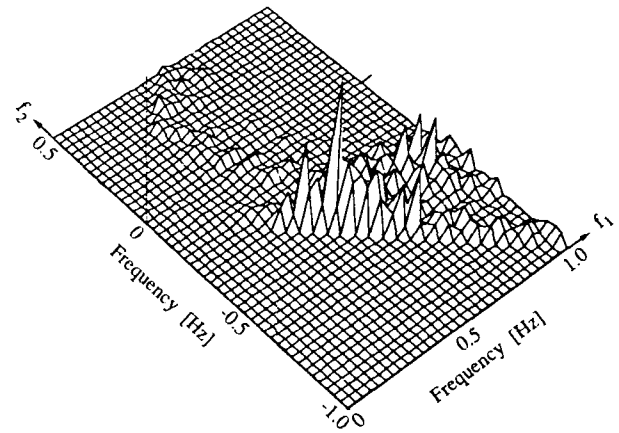
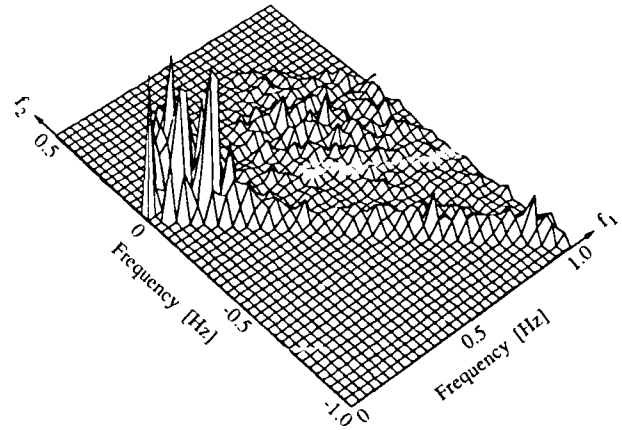Fig. 6. Cross-bispectrum of TLP surge motion for an irregular sea.

Fig. 7. Quadratic transfer function of a second-order Volterra model of a TLP surge motion for an irregular sea.

One can quantify the nonlinear effect with respect to the linear effect using the concept of bicoherence as we discussed in Section 3. We compute $\gamma_l^2(n)$, $\gamma_{l_q}^2(n)$, and $\gamma_q^2(n)$, and plot them in Fig. 8. Notice that the quadratic coherence spectrum $\gamma_q^2(n)$ at 0.07 Hz and at ~ 0.4 Hz is close to one and zero, respectively, while the linear coherence spec-

203

trum $\gamma_l^2(n)$ has opposite values and is consistent with the coherence spectrum from linear model as shown in Fig. 5. The coupled coherence spectrum $\gamma_{lq}^2(n)$ at these frequencies is approximately zero. Thus, we conclude that the surge motion of the TLP is quadratically correlated with the irregular seas at 0.07 Hz, and linearly correlated at ~ 0.4 Hz. The total coherence spectrum $\gamma^2(n)$ shown in Fig. 8-b, which is the sum of $\gamma_l^2(n)$, $\gamma_{lq}^2(n)$, and $\gamma_q^2(n)$, is close to unity up to 0.7 Hz suggesting that the linear and quadratic surge motion in irregular seas is adequately modeled as a second-order Volterra system. Note that although $\gamma_l^2(n)$ and $\gamma_q^2(n)$ are greater than unity in some frequency bands, $\gamma_{lq}^2(n)$ is negative, thus the overall model coherence is less than or at most equal to one.
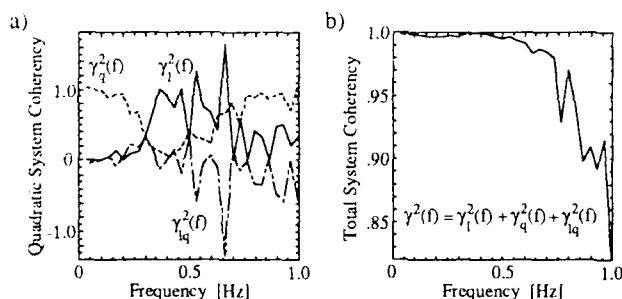

Fig. 8. Nonlinear coherence spectrum of a second-order Volterra TLP system for an irregular sea. a) Linear coherency ($\gamma_l^2(f)$, ———), Quadratic coherency ($\gamma_q^2(f)$, — —), and Hybrid coherency ($\gamma_{lq}^2(f)$,- - - -). b) Total coherency $\gamma^2(f)$ (= $\gamma_l^2(f)$ + $\gamma_q^2(f)$ + $\gamma_{lq}^2(f)$).

The surge "power" quantities $S_l(n)$ and $S_q(n)$, and the absolute value of $S_{lq}(n)$ as "predicted" by the Volterra model are plotted in Fig. 9-a. Notice that the model surge power at 0.07 Hz is predominantly due to quadratic nonlinearity (i.e., $S_q(n)$) and the power at ~ 0.4 Hz is mainly due to linear response ($S_l(n)$). Fig. 9-b shows "true" power spec-
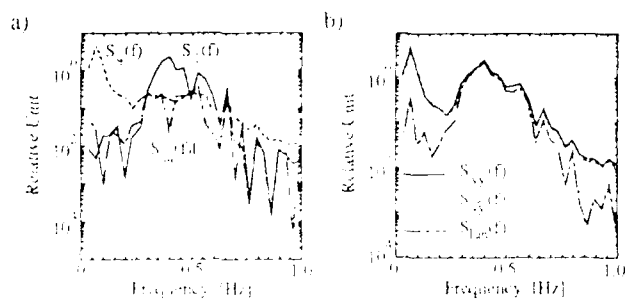

Fig. 9 Second order Volterra model (SVM) TLP surge power spectrum. a) Linear power spectrum ($S_l(f)$, ———), Quadratic power spectrum ($S_q(f)$, - - - -), and Hybrid spectrum ($S_{lq}(f)$, —— —). b) Measured surge power spectrum ($S_{yy}(f)$, ———), Total SVM spectrum ($S_{\bar{y}\bar{y}}(f)$, - - - -), and Linear model power spectrum ($S_{Lin}(f)$, —— —).

trum of the observed surge motion $S_{yy}(n)$ (solid line), the total model power spectrum using the second-order Volterra model $S_{\bar{y}\bar{y}}(n)$ of Eq. 13 (fine dotted line), and the "predicted" output power spectrum using purely a linear model $S_{Lin}(n)$ (coarse dotted line, $S_{\bar{y}\bar{y}}(n\Delta\omega)$ of Eq. 14). Notice that the linear model cannot account for the spectral peak at 0.07 Hz, though it is quite a good model for frequency band centered at ~ 0.4 Hz. However, the second-order Volterra model predicts the true power spectrum of the surge response over the entire frequency band. One can hardly notice the difference between the true surge power spectrum $S_{yy}(n)$ and Volterra model power spectrum $S_{yy}(n)$. Thus, one can safely conclude that the spectral peak of surge motion at the surge natural frequency of the TLP is due mainly to quadratic nonlinear difference interaction of irregular waves, namely wave drift force, while the broad band peak at ~ 0.4 Hz is a linear response.

4. Conclusion

Experimentally we are able to estimate the linear and quadratic transfer functions of TLP response which one can compare with theory, and identify the quadratic nonlinear resonance response of a TLP surge motion subject to irregular nonGaussian seas using bispectral analysis. We demonstrate the validity of the results by inputting the irregular sea time series data into the parallel combination of two filters characterized the linear and quadratic transfer functions. Thus, we are able to decompose the power spectrum of a TLP surge motion into linear and quadratic response to the irregular waves and quantify which quadratic interactions of the sea waves contribute most significantly to the TLP resonance response. Specifically, the notion of quadratic coherence is utilized to verify that the low-frequency response at the surge natural frequency is truly a quadratically nonlinear response, which is identified as "low-frequency wave drift force". Such studies substantiate the ability of the quadratic transfer function to correctly model the nonlinear mechanisms whereby the energy associated with the "high-frequency" irregular seas is converted to a "low-frequency" resonant surge response.

REFERENCES

[1] C. H. Kim and J. F. Dalzell. "*An Analysis of the Quadratic Frequency Response for Lateral Drifting Force and Moment*," J. Ship Res., Vol. 25, pp. 117-129, 1981.

[2] Y. C. Kim and E. J. Powers, "*Digital Bispectral Analysis and Its Applications to Nonlinear Wave Interactions,*" IEEE Trans. Plasma Sci., Vol. PS-7, pp. 120-131, 1979.

[3] D. W. Choi, R. W. Miksad, E. J. Powers, and F. J. Fischer, "*Application of Digital Cross-Bispectral Analysis Techniques to Model the Nonlinear Response of a Moored-Vessel System in Random Seas,*" J. Sound Vibration, Vol. 99. No. 3, pp. 309-326 1985.

[4] K. I. Kim, and E. J. Powers, "*A Digital Method of Modelling Quadratically Nonlinear Systems with a General Random Input,*" IEEE Transactions on Acoustics, Speech, and Signal Processing, Vol. 36, pp. 1758-1769, Nov. 1988.

[5] S. A. Billings. "*Identification of Nonlinear Systems - A Survey,*" Proc. IEE, Vol. 127, pt. D, No. 6, pp. 272-285, 1980.

[6] D. R. Brillinger and M. Rosenblatt,"*Asymptotic Theory of Estimates of K-th Order Spectra,* Spectral Analysis of Time Series, (B. Harris, Ed.), Wiley, New York, pp. 153-188, 1967.

[7] H. G. Albrecht, D. Koenig, and K. Kokkinowrachos, "*Nonlinear Dynamic Analysis of Tension-Leg Platforms for Medium and Greater Depths,*" OTC 3044, 1978.

[8] J. P. Hooft. "*Advanced Dynamics of Marine Structures,*" John Wiley & Sons, 1982.

BISPECTRA OF SHOALING OCEAN SURFACE GRAVITY WAVES

Steve Elgar
Electrical and Computer Engineering
Washington State University
Pullman, WA 99164-2752

ABSTRACT

Aspects of the nonlinear dynamics of waves shoaling between 9 and 1 m water depths are elucidated via the bispectrum. Bispectral signal levels are generally high, indicating significant nonlinear coupling. In 9 m depth, the biphases of interactions involving frequencies at, and higher than, the peak of the energy spectra are suggestive of Stokes-like nonlinearities. Further shoaling gradually modifies these biphases to values consistent with a wave profile that is pitched shoreward, relative to a vertical axis. Bicoherence and biphase observations of waves with a double peaked (swell and wind wave) power spectrum provide evidence for excitation of modes at intermediate frequencies via difference interactions, as well as the sum interactions responsible for harmonic growth. Shoreward propagating low frequency (surf beat) energy is shown to have statistically significant coupling to higher frequency modes within the power spectral peak. In 18 m depth, the biphase of these interactions is close to 180°, a value consistent with the classical concept of bound long waves. In shallower water, however, substantial biphase evolution occurs, and there is no longer a unique phase relationship between surf beat and the envelope of high frequency waves. The observed bispectral evolution is predicted accurately by a model based on the nonlinear Boussinesq equations.

1. INTRODUCTION

Since its introduction more than twenty years ago [Hasselman et al. 1963], bispectral analysis has been utilized by many investigators to study nonlinear phenomena. Hasselman et al. (1963) obtained good agreement between observations of bispectra of ocean surface gravity waves in intermediate water depth (11 m) and predictions based on Stokes-like, non-resonant, nonlinear interactions. Nonlinearities in a wide range of other phenomena have been studied with bispectral techniques since Hasselman et al.'s (1963) seminal paper. See Nikias and Raghuveer (1987) for a recent review. The present study returns to the question of ocean gravity waves, but considers waves in water depths between 9 m and 1 m. Waves in this shoaling region are particularly well suited to analysis with bispectral techniques for several reasons, the most important being that bispectral signal levels are relatively high. In addition, waves in the shoaling region are of a short enough time scale

that many degrees of freedom can be obtained without losing stationarity. This combination of many degrees of freedom and high bispectral signal levels leads to statistical stability of the bispectral estimates.

The field experiment is described in §2. Observations of bispectra for several different shoaling wave power spectra are discussed in detail in §3. Data with broad band power spectra show some surprising similarities to narrow band data in certain aspects of bispectral evolution (§3.1), in particular, the biphase. Similarities are also evident in the evolution of sea surface elevation skewness and asymmetry (skewness about a vertical axis). Evidence of excitation of modes via difference interactions as well as sum interactions is observed in a data set with a double peaked power spectrum. Low frequency motions (surf beat) are shown to be nonlinearly coupled to energy at frequencies closely spaced within the power spectral peak (§3.2), as suggested by the classical notion of surf beat [Munk, 1949]. However, biphase analysis shows that the surf beat modes in the shoaling region are not 180° degrees out of phase with the envelope of higher frequency waves. Nonlinear model predictions of bispectra of shoaling waves compare favorably to field measurements (§3.3).

2. EXPERIMENT AND DATA REDUCTION

Most of the field data discussed were obtained at Santa Barbara, California during the Nearshore Sediment Transport Study experiment conducted in January and February 1980 (Gable, 1981) and at Torrey Pines, California during September, 1980 (Freilich and Guza 1984). The observations used in the present study were obtained primarily from near bottom mounted pressure sensors, located along a line perpendicular to the beach, from approximately 10 m depth to less than 1 m depth (300 m horizontal distance).

Complete data processing details can be found in Elgar and Guza (1985b). Statistical stability of bispectral estimates was obtained by frequency merging over squares in (f_1, f_2)-space, where f is the frequency in Hz, and ensemble averaging over many records (each of 512 s length). The resulting number of degrees of freedom ranged from 160 to 310 for the data presented here.

3. OBSERVATIONS OF BISPECTRA

This section describes the bispectra of shoaling waves observed in the field. The three data sets that will be discussed in detail have approximately the same total variance, but very different power spectra. First, interactions involving the swell and wind wave band (0.04 < f < 0.4 Hz) will be discussed, and then interactions involving the infragravity wave, or low

frequency band (f < 0.04 Hz) will be examined. The ability of a nonlinear wave propagation model (Freilich & Guza 1984) to predict accurately the observed bispectral evolution is also briefly discussed.

3.1 Swell and wind wave frequencies (f >.04 Hz)

The 2 Feb wave field is dominated by swell (f = 0.06 Hz) from a distant storm. The significant wave height (defined here as 4 times the sea surface standard deviation) in 4 m depth is 65 cm, and there is a very small peak at the first harmonic (f = 0.12 Hz, Figure 1a). As the waves shoal, the power in the first and higher harmonic (f = 0.18, 0.24, 0.30 Hz) peaks increases (Figure 1b-1f, upper panels). The growth of these harmonics is not predicted by any linear theory, but is well modelled by the nonlinear Boussinesq type equations described in Freilich and Guza (1984). The bicoherence spectrum at the deepest sensor (Figure 1a) indicates nonlinear coupling between modes within the power spectral peak and modes at twice the peak's frequency. For example, b(.06.06) = .30, indictating a self-self wave interaction at f = 0.06 Hz coupled to energy at f = 0.12 Hz. As the waves shoal, the excitation of phase coupled harmonics is reflected in the bicoherence, Figure 1. In 4 m depth (Figure 1c), the bicoherence indicates stronger (than in deeper water) coupling within the peak [b(.06, .06) = .49], and also coupling be ween the peak and its first two harmonics [b(.06, .12) = .28; b(.06, .18) = .14]. In shallower water, nonlinear coupling spreads not only to encompass interactions between the power spectral peak and its higher harmonics, but also to interactions between the harmonics themselves. For example, in 2 m depth (Figure 1e) b(.06, .24) = .16; b(.12, .12) = .43; b(.12, .18) = .41; b(.18, .18) = .33. Although these bispectral calculations indicate only that nonlinear coupling is occurring, and not the direction of energy flow (i.e. which modes are receiving energy), the sequence of energy spectra in Figure 1 show that energy is being received by high frequencies.

Along with the increase in bicoherence shown in Figure 1, there is substantial biphase evolution as the waves shoal (Figure 2). The evolution of biphases for a few selected frequency pairs (those pairs with the highest observed values of bicoherence, combinations of the power spectral peak and its harmonics) are displayed in Figure 2.

Features of the self-self interaction at the spectral peak in the 9 m depth data are consistent with Stokes-type nonlinearities. As shown in Figure 2 in 9 m depth, the two lowest order interactions [(f , f), (f , 2f)], where f is the frequency of the power spectral peak, have biphase of about -15°, and two of the other interactions are also within 25° of the Stokes biphase (β = 0°). Since only the lowest order interactions have significant bicoherence and substantial biphase stability, the 9 m data are interpreted as qualitatively consistent with Stokes-like nonlinearities. A similar conclusion, based on an analysis which included directional effects in 11 m depth, was reached by Hasselman et al. (1963).

As the waves shoal, the biphases of harmonic interactions tend towards β = -π/2 (Figure 2). The complete biphase spectrum not shown shows that many frequencies, not just the harmonics (Figure 2) are nonlinearly coupled, and have biphase values that approach β = -π/2. In 4 m depth many frequency triads have similar values of biphase (β = -50°, Figure 2). As the water depth decreases, the region of approximately constant biphase increases to encompass more and more frequency pairs. The value of almost all biphases steadily approaches β = -π/2.
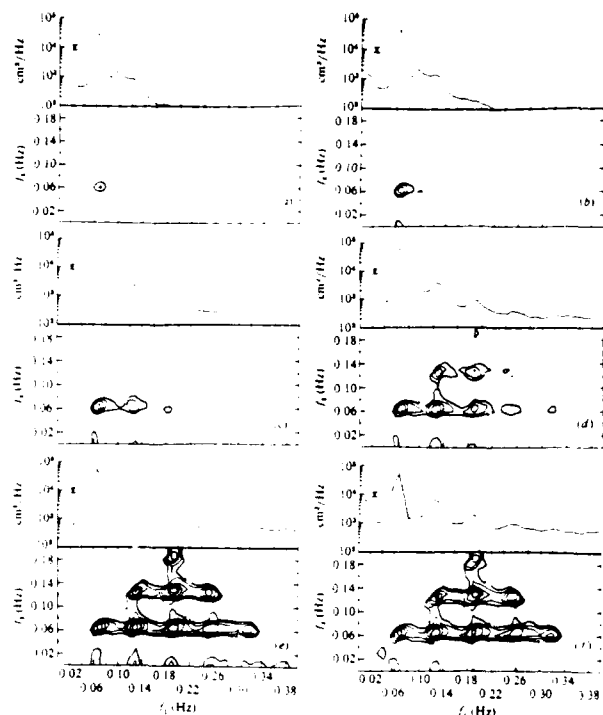

Figure 1. Power spectra and contours of bicoherence for the 2 Feb data at various depths. The power spectra (bars indicate 95% confidence levels) are immediately above the corresponding bicoherence plots. The minimum bicoherence contour level is b = 0.1 with additional contours every 0.05. There are 310 degrees of freedom (dof) and the 95% significance level for zero bicoherence is b = 0.14. Depths are a) h = 9.0 m, b) h = 6.4 m, c) h = 3.9, d) h = 2.7 m, e) h = 2.0 m, f) h = 1.3 m.

Since the biphase depends on the ratio of imaginary to real parts of the bispectrum, which are related to skewness and asymmetry, respectively, it is not surprising that the biphase is related to the wave's shape (Masuda and Kuo 1981, Elgar and Guza 1985b). Masuda and Kuo (1981) showed that a primary and its first harmonic with zero biphase is associated with a wave with sharp peaks and broad, flat troughs, but with symmetry about a vertical axis, as in a Stokes wave. On the other hand, a biphase of -π/2 is associated with a wave pitched forward (skewed with respect to a vertical axis, or vertical asymmetry), but symmetrical with respect to a horizontal axis (zero skewness). The observed evolution of biphase is consistent with the visual observation that as waves shoal they evolve from a nearly sinusoidal shape in deep water to a shape characterized by a steep forward face and a relatively gently sloping rear face. In very shallow water the data are suggestive of a sawtooth shape. It is readily shown that the sawtooth biphase is β(i,j) = -π/2.

In contrast to the 2 Feb data, the 15 Feb data (Figure 3) have quite broad band energy spectra. The significant wave height in 4 m depth for the 15 Feb data is 65 cm, the same as the 2 Feb data. The 15 Feb energy spectra show very little evolution as the wave field shoals (Figure 3, upper panels). The increase in high frequency energy (f > 0.2 Hz) at 4 m depth (Figure
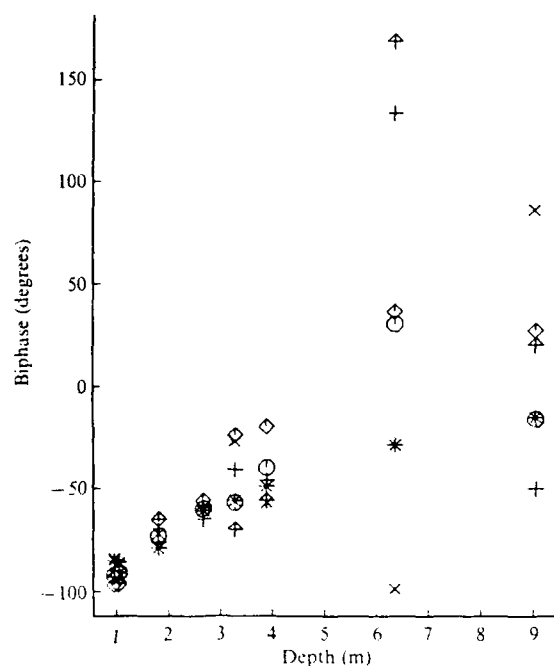
Figure 2. Biphase versus depth for selected frequency pairs for the 2 Feb data set. Asterisk, (f, f); octagon, $(f, 2f,)$; plus, $(f, 3f)$; cross, $(f, 4f)$; triangle on a stick, $(2f, 2f)$; diamond, $(2f, 3f)$, where $f = .06$ Hz corresponds to the power spectral peak frequency.

Figure 3. Power spectra and contours of bicoherence for the 15 Feb data set, with the same format as Figure 2. DOF = 160, and the 95% significance level for zero bicoherence is b = 0.19. Depths are a) h = 8.0 m, b) h = 6.0 m, c) h = 3.5 m, d) h = 2.2 m, e) h = 1.6 m, f) h = 0.9 m.

3c) is an artifact of not correcting the two deeper measurements (Figures 3a, b) for depth attenuation. The bicoherences (Figure 3) also show little structural evolution, although the average level of bicoherence does steadily increase from near zero in 9 m depth (Figure 3a) to about b = .15 in 0.9 m depth (Figure 3f). In contrast to the sharp peaks and steep valleys of the bicoherence spectra for the narrow band 2 Feb data (Figure 2), the 15 Feb data evolve from near zero bicoherence values to low (but non-zero) values broadly spread over most of the wind wave frequency band pairs (Figure 3).

Despite the radically different evolution of power spectra and bicoherence for the 2 Feb (Figure 1) and 15 Feb (Figure 3) data sets, the evolution of biphase is remarkably similar. The 15 Feb data have no equivalent of the Stokes-like interaction within the narrow spectral peak of the 2 Feb data in 9 m depth, but by the shallower sensors no features distinguish the biphase spectra of the broad band data from the narrow band data (s = - $\pi/2$ in both cases). The similar biphases are not surprising considering that the shapes of waves in very shallow water are qualitatively similar for broad and narrow power spectra, i.e., steep front faces and flat rear slopes. Although the bicoherence spectra for the 2 Feb and 15 Feb data sets are quite different in structure, various integrals of the bispectrum of each data set are similar. In particular, the skewness (the sum of the real parts of the bispectrum) and asymmetry (the sum of the imaginary parts) of each data set, band pass filtered between f = 0.04 and f = .4 Hz, have similar evolution and values, as shown in Figure 4. Similar structure of skewness and asymmetry evolution was observed in several other data sets, with various power spectral shapes, and with a wide range of wave heights. The slight increase in asymmetry (Figure 4) in
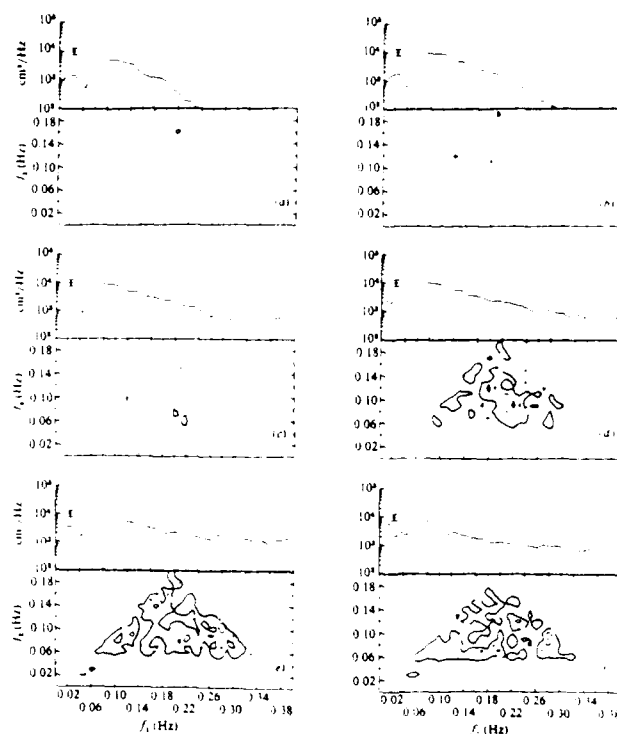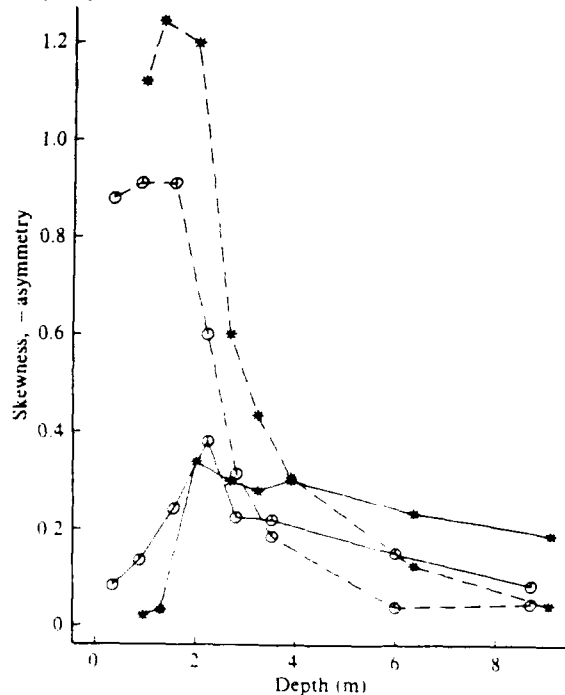

Figure 4. Skewness and asymmetry evolution with depth. Asterisk, 2 Feb; octagon, 15 Feb (solid line is skewness; dashed line is -asymmetry). The data are band pass filtered between 0.04 and .4 Hz.

very shallow water occurs at depths where substantial dissipation (i.e. wave breaking) begins to occur (depth = 1.0 m and 1.5 m for 2 Feb and 15 Feb, respectively).

The bispectral calculations for the narrow band 2 Feb data are consistent with the nonlinear transfer of energy from the power spectral peak frequency to higher frequencies via (quadratic) sum interactions. On the other hand, the 12 Feb data (Figure 5, significant wave height in 4 m depth is 56 cm) have double peaked power spectra with a narrow swell peak located at f = 0.07 Hz and a broad sea peak above f = 0.24 Hz, and suggest that excitation of modes through difference interactions can also be important. The bicoherence spectra for 12 Feb (Figure 5) are consistent with nonlinear coupling within the lower frequency swell peak [b(.07, .07) = .24 at 2 m depth] transferring energy through sum interactions to modes in the spectral valley (f = 0.14 Hz). Simultaneously, there is coupling between the low frequency swell peak and the high frequency sea peak [e.g., b(.05, .19) = .13 at 2 m depth], consistent with a difference interaction between f = 0.24 and f = 0.05 Hz transferring energy into the spectral valley at f = 0.19 Hz. By 1.3 m depth (Figure 5) the spectral valley and the high frequency peak are almost equal in energy, and the sea-swell interactions are weaker than in deeper water [b(.05, .19) = .04 at 1.3 m depth]. The large increase in energy in the spectral valley, and decrease in energy in the sea peak are not predicted by linear theory (Elgar and Guza 1985a). The biphase spectra of the 12 Feb data (Figure 5) are quite different than those of the 2 Feb (Figure 2) and 15 Feb (not shown) data. As shown in Figure 5, in the regions of non-zero bicoherence there are three distinct regimes of biphase. The frequency pairs within the low frequency swell peak (f = .07 Hz) undergoing sum interactions have biphases similar to the previously described data sets, with, for example, B(.07, .07) evolving from near zero to approximately $-\pi/2$ as the waves progress from 9 m to 1 m depth. Sum interactions between sea and swell show similar biphases (B₃ in Figure 5). On the other hand, as shown in Figure 5, the frequency pairs corresponding to difference interactions between sea and swell peaks [(.05, .19), for example] have biphase values that evolve from close to 180° in deeper water to about 140° just prior to breaking. The biphase values measured in 5 m depth are consistent with the biphase of π for a bound wave produced by a Stokes-like difference interaction. However, similar to the sum interactions, the biphase evolves away from the Stokes value.

By the shallowest sensor (Figure 5), in the zone of wave breaking, the biphases of those frequency pairs previously associated with sea-swell difference interactions have changed substantially, and resemble the biphases of the frequency pairs within the low frequency swell peak.

3.2 Infragravity frequencies (f < 0.04 Hz)

The discussion above concentrated on interactions within the swell and wind wave frequency band of the energy spectrum. However, there is considerable interest in the infragravity wave band (f < 0.04 Hz), evident in the low power level energy spectra of all the data sets displayed at shore (1, 3, 5). A detailed study of the spatial structure and energy levels of the waves in this frequency band observed in this experiment are presented by Guza and Thornton (1985). They have shown that energy at infragravity wave frequencies is highly correlated with the wind wave energy at the beach. Additionally, it was shown by Guza and Thornton (1985), that the height of the lower frequency, infragravity waves at the beach is highly correlated with that of the higher frequency, swell and sea waves.

The biphase of the wave triad with frequencies ω_n, ω_m, and $\omega_{n-m} = \omega_n - \omega_m$ is $B(\omega_{n-m}, \omega_m) = \pi$.

In a field experiment with limited (16) degrees of freedom, Suhayda, (1972, 1974) did not observe significant bicoherence values for very shallow water interactions involving surf beat. There are two primary differences between Suhayda's work and the present results which do show statistically significant nonlinear coupling. First, there are an order of magnitude more degrees of freedom in the present work, thereby considerably reducing the bicoherence significance levels. The second, and equally important refinement, is the separation of the surf beat signal into shoreward and seaward propagating components. Observations on a wide variety of beaches suggest that surf beat is a standing wave in the cross shore direction [Suhayda, 1972, 1974; Guza and Thornton, 1985 and references therein]. When averaged over a finite width frequency band, the low frequency reflected waves will have phase relationships relative to their incoming counterparts that tend to decrease bispectral levels. Consequently, removing the reflected waves from the time series should enhance the bicoherence of frequency pairs involving low frequency modes. Colocated pressure-gauge-current-meter pairs were used to crudely decompose the records into incoming and outgoing waves for f < 0.04 Hz (Guza et al., 1986).

Bispectral calculations were performed on records with only incoming energy below f = 0.04 Hz, but no changes above f = 0.04 Hz. Comparisons of bicoherence for frequency pairs (f_1, f_2), where f_1 is a low frequency $(f_1 = .01, .02$ Hz) mode and f_2 is the frequency of the power spectral peak, were made between records with and without reflected surf beat energy. As expected, removing the long wave reflections increased the bicoherence levels of almost all the pertinent frequency pairs (Elgar and Guza 1985b). Statistically significant nonlinear coupling occurs between neighboring frequencies within the power bispectral peak, and their difference frequency.

According to Longuet-Higgins and Stewart (1962, 1964), the biphase of these surf beat type interactions should be $\beta = \pi$. At the deepest sensor locations where reflections could be removed, the observed biphase is somewhat different than 180°. It is important to note that $\beta = 180°$ is a deep water result, and the deepest stations used here are in only 4 m depth. Similar calculations for data obtained in 18 m depth in a different experiment produced biphases of about $\beta = 170°$ (for frequency pairs comparable to those discussed here). In most of the cases investigated, the surf-beat biphase evolves toward lower values as the wave field shoals. This evolution of surf-beat biphase observed in the field data is not predicted by the bound long wave model of Longuet-Higgins and Stewart (1962, 1964).

3.3 Nonlinear model predictions of bispectra

A nonlinear model (Freilich and Guza 1984) based on the Boussinesq equations for waves traveling over a shallow, sloping bottom (Peregrine 1967) has been shown to predict accurately many aspects of the observed evolution of shoaling waves (Freilich and Guza 1984, Elgar and Guza 1985a, Elgar and Guza 1986). Bispectral analysis allows comparison of model predictions and data on a triad-by-triad basis. The nonlinear interactions between waves with frequencies corresponding to the power spectral peak and its first harmonic for the case of narrow band swell are accurately predicted by the model, as shown in Figure 7. Model predictions of the strength of the interaction (bicoherence, Figure 7a) and the resulting change in wave shape (biphase, Figure 7b) are essentially identical to observed values. Since these data are dominated by the narrow spectral peak, it is not surprising that the evolution of skewness and asymmetry are also predicted accurately (Figure 8). Moreover, the model has similar skill in predicting bispectra, and correspondingly the third moments, of a wide variety of wave fields (narrow band, broad band, and multi-peaked spectra).
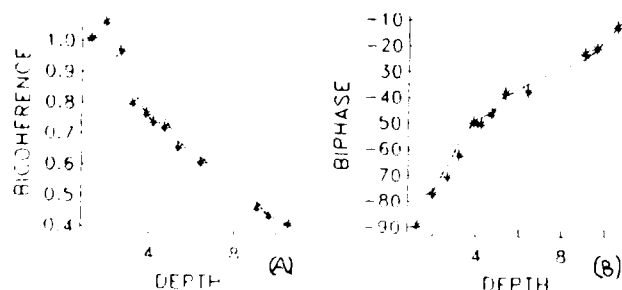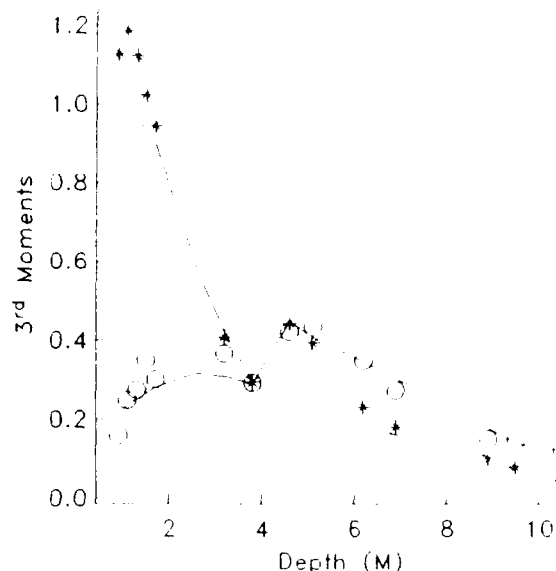

Figure 7. Predicted and observed third moments versus depth for the narrow band data. Solid lines are Boussinesq model predictions of skewness, dashed lines are Boussinesq model predictions of asymmetry, circles are observed values of skewness, asterisks are observed values of asymmetry.

6. CONCLUSIONS

The nonlinear evolution of shoaling ocean surface gravity waves is particularly well suited for bispectral analysis. The development of harmonics as a wave field with a narrow band energy spectrum shoals is clearly due to quadratic interactions between the power spectral peak and its harmonics. The same type of nonlinear interaction occurs among a wide range of frequencies when the shoaling wave field has a broad band power spectrum. Other similarities in the nonlinear evolution of narrow band and broad band power spectra are seen in the bispectrum. For example, the biphases of both types of data evolve from mostly random values in 9 m water depths to a value which is constant over most frequency pairs in the wind wave band (0.04 < f <.4 Hz), approaching $\beta = -\pi/2$ as the waves shoal. The biphase values are consistent with Stokes-like nonlinearities (at least for narrow band data) in 9 m depth. However, as the water depth decreases, the waves evolve through a slightly skewed, somewhat asymmetrical (with respect to a vertical axis) shape, toward a highly asymmetrical, unskewed, sawtooth-like shape.

Bicoherence and biphase calculations provide evidence for excitation of Fourier modes via difference interactions as well as sum interactions for a data set with a double peaked power spectrum. Low frequency motions (surf beat) are coupled to high frequency energy located within the power spectral peak. These infragravity modes do not appear to be bound with a fixed phase relationship to the high frequency wave groups since their biphases evolve as the wave field shoals.

The nonlinear shoaling wave model of Freilich and Guza (1984) predicts accurately the observed bispectra of shoaling waves seaward of the zone of wave breaking.

Figure 8. Bicoherence and biphase of of the triad consisting of the power spectral peak frequency and its first harmonic $(f_1 = 0.06, f_2 = 0.06, f_3 = 0.12$ Hz) for narrow band data versus depth. The solid line is Boussinesq model predictions and the asterisks represent field observations.

REFERENCES

Elgar, Steve and R.T. Guza, 1985a, "Shoaling gravity waves; comparisons between field observations, linear theory and a nonlinear model," J. Fluid Mechanics V. 158, p. 47-70.

Elgar, Steve, and R. T. Guza, 1985b, "Observations of bispectra of shoaling surface gravity waves," J. Fluid Mech., v. 161, p. 425-448.

Elgar, Steve and R.T. Guza, 1986 "Nonlinear model predictions of bispectra of shoaling surface gravity waves," J. Fluid Mechanics V. 167, p. 1-13.

Freilich, M. H., and R. T. Guza, 1984, "Nonlinear effects on shoaling surface gravity waves," Phil. Trans. Roy. Soc. London A311., p. 1-41.

Gable, C. G. (ed), 1981, "Report on data from the Nearshore Sediment Transport Study experiment at Leadbetter Beach, Santa Barbara, California, January-February, 1980," IMR Ref. 80-5., Univ. of Calif., Inst. of Marine Resources, La Jolla, CA.

Guza, R. T., and E. B. Thornton, 1985, "Observations of surf beat," J. Geophys. Res., v. 90, p. 3161-3172.

Guza, R. T., E. B. Thornton, and R. A. Holman, 1985, "Swash on steep and shallow beaches," Proc. 19th Coastal Engineering Conf.

Hasselman, K., W. Munk, and G. MacDonald, 1963, "Bispectra of ocean waves," in M. Rosenblatt (ed) Time Series Analysis, Wiley, New York p. 125-139

Longuet-Higgins, M. S., and R. W. Stewart, 1962, "Radiation stress and mass transport in gravity waves, with application to 'surf beats'," J. Fluid Mech., v.13, p.481-504.

Longuet-Higgins, M. S., and R. W. Stewart, 1964, "Radiation stresses in water waves; a physical discussion with applications," Deep Sea Research, v.11, p. 529-562.

Masuda, A. and Y. Y. Kuo, 1981, "A note on the imaginary part of bispectra," Deep-Sea Research, v. 28, p. 213-222.

Munk, W. H. 1949, "Surf beats," Trans. Amer. Geophys. Union, v. 30, p. 849-854.

Nikias, C.L. & M. R. Raghuveer, 1987 "Bispectrum estimation, a digital signal processing framework," Proc. IEEE V. 75, p. 869-891.

Peregrine, D.H. 1967 "Long waves on a beach," J. of Fluid Mechanics, V. 27, p. 815-827.

Suhayda, J. N., 1972, "Experimental study of the shoaling transformation of waves on a sloping bottom," Ph.D. dissertation, Scripps Institution of Oceanography, Univ. of Calif. La Jolla, CA.

Suhayda, J. N., 1974, "Standing waves on beaches," J. Geophys. Res., v. 72, p. 3065-3071.

A Triple Cross-Correlation Approach for Enhancing Noisy Signals

Amod V. Dandawate and Georgios B. Giannakis

Dept. of Electrical Engineering

University of Virginia

Charlottesville, VA 22901

Abstract

Noise cancelers are traditionally designed based on second-order statistics of the available observation. The design assumes availability of a reference signal in the secondary input, which is highly correlated with the noise, while being independent of the zero-mean information signal in the primary input. In this paper triple correlation based cancelers are derived for enhancing noisy signals. It is shown that cancelers based on second- and higher-order statistics are equivalent when the additive noise and the reference signal are related by a linear time-invariant transformation. The triple correlation based noise canceler outperforms the classical design when the reference signal is corrupted by additive Gaussian noise of unknown covariance. Simulations illustrate the performance of the proposed design.

I. Introduction

Noise cancelers have been used in several applications, [1]. In speech processing, the performance of linear prediction (LP) filters degrades in the presence of wide-band noise, [2], making it necessary to process the corrupted signal by a noise canceler before applying the LP filtering.

The noise canceler described in [1], uses a reference signal in the secondary input to cancel the noise in the corrupted signal, which forms the primary input to the noise canceler. The reference signal, assumed to be independent of the noise-free information signal and highly correlated with the noise, is processed by a filter, possibly adaptively, and then subtracted from the primary input, as an estimate of the noise, to obtain the enhanced signal (see Fig 1. in Section II). The filter impulse response is obtained by solving a set of linear equations involving second-order statistics of the available data.

It is shown in Section III that the filter thus derived attempts at canceling the noise by essentially matching the cross-correlation between the reference signal and the unknown noise and that between the reference signal and the estimate of the noise. As an extension of this property a filter is derived in Section III that matches the triple cross-correlation between the reference signal and the unknown noise with the triple cross-correlation between the reference signal and the estimate of the noise. The impulse response of this filter is obtained by solving a set of linear equations involving third-order statistics of the observations. Designs using third-order statistics in other signal processing tasks, such as signal reconstruction and modeling are known to yield high SNR estimates, [3], [4]. Higher-than-second-order statistics and their potential for speech processing applications are also discussed in [5] and [6].

In Section III, it is shown that if the noise and the reference signal are related by a linear time-invariant transformation then the cancelers based on the true, second- and higher-order statistics are equivalent and cancel the noise exactly. In other cases the second-order canceler cancels the noise in the mean-square sense. Although the higher-order canceler can be obtained by finding inflection points of a weighted mean-square function, it does not necessarily serve a minimization criterion. This is because, in cases other than the linear time-invariant transformation, the Hessian of the weighted mean-square function cannot be shown to be positive-definite in general. The triple correlation-based canceler outperforms the second-order canceler when the reference signal is corrupted by zero-mean additive Gaussian noise of unknown covariance.

Simulation results illustrating the performance of the second- and higher-order canceler implemented in batch form are presented in Section IV. Noise cancelers can also be implemented adaptively, along the lines of [7].
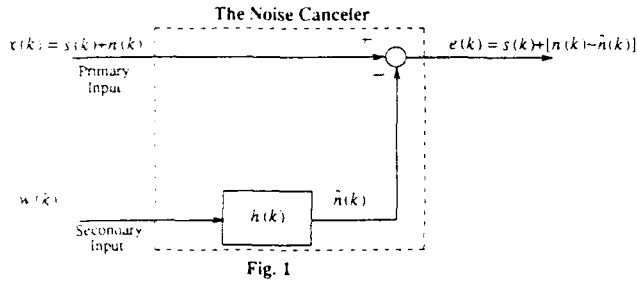
II. Noise Canceler

The primary input $x(k)$ to the noise canceler (see Fig.1) is,

$$x(k) = s(k) + n(k), \tag{1}$$

where $s(k)$ is the noise-free information signal and $n(k)$ is the additive noise component. The signal $w(k)$, derived for example from $x(k)$ in the absence of the signal (silent periods in speech) forms the secondary input to the noise canceler. The

reference signal $w(k)$ is processed by a filter with impulse response $h(k)$ producing an output $\hat{n}(k)$ which is subtracted from $x(k)$ to give $e(k)$. The output of the noise canceler $e(k)$ is thus,

$$e(k) = x(k) - \hat{n}(k) = s(k) + [n(k) - \hat{n}(k)]. \quad (2)$$

The Noise Canceler

Fig. 1

The noise in the output of the canceler is $[n(k)-\hat{n}(k)]$. Therefore, if $\hat{n}(k)$ is appropriately produced to cancel $n(k)$ in some sense, then there will be reduction in the effect of the noise on the information signal in $e(k)$. Hence, the design of the noise canceler consists of finding $h(k)$ that processes the reference signal $w(k)$ and produces an output $\hat{n}(k)$ that matches the noise $n(k)$ as closely as possible.

In [1] Widrow et al., design the filter $h(k)$ to minimize $E\{|n(k)-\hat{n}(k)|^2\}$ resulting in the mean-square-sense cancellation of the noise. The same effect can be obtained, under certain assumptions by designing $h(k)$ to minimize $E\{e^2(k)\}$. These assumptions are:

(AS1)   All signals are zero mean and stationary.

(AS2)   The information signal $s(k)$ is independent of both $n(k)$ and $w(k)$.

(AS3) $n(k)$ and $w(k)$ are highly correlated with each other.

The equivalence of the two design approaches can be shown to be true under the given circumstances by first considering the minimization of the objective function.

$$J = E\{e^2(k)\}, \quad (3a)$$

with respect to $h(k)$ and then using (AS1)-(AS3) to simplify and show that this is equivalent to the minimization of $E\{|\hat{n}(k)-n(k)|^2\}$, with respect to $h(k)$. [1].

Substituting (2) into (3a) and expressing $\hat{n}(k)$ in terms of $w(k)$ and $h(k)$ we obtain,

$$J = E\{[x(k)-\sum_i h(i)w(k-i)]^2\}. \quad (3b)$$

By minimizing (3b) with respect to $h(k)$ we obtain the following set of linear equations

$$r_{xw}(l) = \sum_i h(i)r_{ww}(i+l), \quad (4)$$

where $r_{xw}(l) \equiv E\{x(k)w(k+l)\}$ is the cross-correlation of $x(k)$

and $w(k)$ and $r_{ww}(l) \equiv E\{w(k)w(k+l)\}$ is the autocorrelation of $w(k)$.

Taking Z-transforms on both sides of (4) we obtain the transfer function $H(z)$ of the filter $h(k)$ as,

$$H(z) = S_{xw}(z^{-1}) / S_{ww}(z^{-1}), \quad (5)$$

where $H(z) \equiv Z\{h(k)\}$, $S_{xw}(z) \equiv Z\{r_{xw}(k)\}$ and $S_{ww}(z) \equiv Z\{r_{ww}(k)\}$.

II. Triple correlation-based noise canceler

Substituting for $\hat{n}(k)$ in the cross-correlation $r_{\hat{n}w}(l) \equiv E\{\hat{n}(k)w(k+l)\}$ we obtain,

$$r_{\hat{n}w}(l) = E\{\sum_i h(i)w(k-i)w(k+l)\} = \sum_i h(i)r_{ww}(i+l). \quad (6a)$$

It then follows from (4) and (6a) that

$$r_{\hat{n}w}(k) = r_{xw}(k) = r_{nw}(k), \quad (6b)$$

where the right-most equality follows by noting that $s(k)$, present in $x(k)$, and $w(k)$ are independent and zero-mean [cf. (AS1) and (AS2)]. Thus the filter $h(i)$ obtained from (4) attempts at canceling the noise by essentially matching $r_{nw}(k)$ and $r_{\hat{n}w}(k)$ [cf. (6b)].

If $n(k)$ and $w(k)$ are related by a linear-time-invariant (LTI) transformation, i.e.,

$$n(k) = \sum_i h_1(i)w(k-i), \quad (7a)$$

then multiplying both sides of (7a) by $w(k+l)$ and taking expectations we obtain,

$$r_{nw}(k) = r_{xw}(k) = \sum_i h_1(i)r_{ww}(k+l). \quad (7b)$$

We recognize from (7b) and (4) that under (7a) the designed $h(i)$ would exactly be equivalent to $h_1(i)$ leading to complete cancellation of $n(k)$ by $\hat{n}(k)$.

As a first step towards extension of property (6b) to higher-than-second-order statistics of the available data, while preserving equivalence of $h(i)$ and $h_1(i)$, under (7a), we investigate into the usage of triple cross-correlations. The triple correlation-based counterpart, $\bar{h}(k)$ of $h(k)$ is designed to match the triple cross-correlation $r_{nww}(m,l) \equiv E\{n(k)w(k+m)w(k+l)\}$, with the triple cross-correlation $r_{\hat{n}ww}(m,l) \equiv E\{\hat{n}(k)w(k+m)w(k+l)\}$.

Analogous to the design of $h(i)$, the triple cross-correlation based noise canceler is designed by solving the following set of linear equations for $\bar{h}(k)$,

$$\sum_i \bar{h}(i)r_{www}(m+i,l+i) = r_{xww}(m,l). \quad (8a)$$

Notice that $\bar{h}(i)$ can be obtained from (8a) in more than one ways by choosing different sets of values for $\{m,l\}$. Also $\bar{h}(i)$ may be estimated adaptively along the lines of [7].

Substituting for $\hat{n}(k)$ in $r_{\hat{n}ww}(m,l)$ we obtain,

$$r_{\hat{n}ww}(m,l) = \sum_i \overline{h}(i) r_{www}(m+i,l+i) \equiv r_{xww}(m,l), \qquad (8b)$$

showing that if $\overline{h}(i)$ is designed using (8a) then it indeed matches, $r_{nww}(k)$ and $r_{\hat{n}ww}(k)$ exactly.

Taking Z-transforms on both sides of (8a) we have,

$$\overline{H}(z_1 z_2) = S_{xww}(z_1^{-1}.z_2^{-1}) / S_{www}(z_1^{-1}.z_2^{-1}), \qquad (9)$$

where $\overline{H}(z) = Z\{\overline{h}(k)\}$, $S_{xww}(z_1,z_2) = Z\{r_{xww}(m,l)\}$ and $S_{www}(z_1,z_2) \equiv Z\{r_{www}(m,l)\}$.

Multiplying (7a) on both sides by $w(k+m)$ and $w(k+l)$ we obtain

$$r_{nww}(m,l) = r_{xww}(m,l) = \sum_i h_1(i) r_{www}(m+i,l+i). \quad (10a)$$

From (8a) and (10a) we observe that, under (7a), the designed $h(i)$ will be exactly same as $h_1(i)$ leading to a complete cancellation of $n(k)$ by $\hat{n}(k)$. Further, it can be shown that under (7a), $H_1(z) \equiv Z\{h_1(k)\}$ can be obtained from $\overline{H}(z)$ in more than one ways; e.g.,

$$H_1(z) = \overline{H}(z_1 z_2)|_{z_1=z,z_2=1}. \qquad (10b)$$

It can be shown that any inflection point $[\partial J_o/\partial \overline{h}(l)=0]$ of the objective function,

$$J_o = E\{e^2(k)w(k+m)\} = E\{[\sum_i \overline{h}(i)w(k-i)]^2 w(k+m)\}, (11)$$

satisfies (8a). This inflection point cannot in general be shown to be a minimum of J_o, and hence does not necessarily serve a minimization criterion. Perhaps, $J_o|_{m=0}$ becomes meaningful as a weighted-mean-square function when $w(k)>0 \ \forall \ k$.

Remarks:

(i) Filters $h(k)$ and $\overline{h}(k)$ are in general non-causal but exponentially stable and hence can be truncated.

(ii) Both the second- and third-order canceler yield the same $H_1(z)$, when true statistics are available. The difference is that the third-order canceler contains redundancy in its estimation [see (8a) and (10b)].

(iii) The second-order noise canceler is built to minimize the noise power in the output, and hence to maximize the output SNR, unlike its third-order counterpart.

(iv) The third-order noise canceler is insensitive to corruption of $w(k)$ by additive zero-mean Gaussian noise of unknown covariance, while its second-order counterpart is not. This follows from the fact that $r_{www}(m,l)$ in (8a) being a triple correlation is insensitive to signal-independent, additive Gaussian noise, [8], while the autocorrelation $r_{ww}(l)$ in (4) is affected by the presence of colored Gaussian noise. In both the cases, $r_{xww}(m,l)$ and $r_{xw}(k)$ are unaffected by the presence of the Gaussian noise since it is zero-mean and independent of $x(k)$ and $w(k)$.

(v) The results of this section extend to higher-order statistics of the observations e.g., $r_{xww}(m,l)$ and $r_{www}(m,l)$ may be

replaced by $r_{xwww}(m,l)$ and $r_{wwww}(m,l)$ to obtain the fourth-order correlation canceler. But the higher-than-third-order correlation based designs are not insensitive to additive zero-mean colored Gaussian noise, since fourth- and higher-order correlations, unlike third-order correlations, are not equal to the corresponding cumulants and hence are sensitive to Gaussian noise.

Due to availability of finite length data in practice the ensemble averages needed in (8a) are replaced by sample averages to yield,

$$\sum_{i=0}^{q} \hat{h}(i) \frac{1}{N} \sum_{k=0}^{N} w(k)w(k+m+i)w(k+l+i)$$

$$= \frac{1}{N} \sum_{k=0}^{N} x(k)w(k+m)w(k+l), \qquad (12)$$

where $\hat{h}(i)$ is the order q FIR estimate of $\overline{h}(i)$, and N is the length of the available data.

As an alternative to the linear equation based solution of (8a) the triple correlation canceler can be designed in the frequency domain using (9). After discretizing the frequency range $[0,2\pi)$, the DFT counterpart of (9), in practice becomes,

$$\hat{\overline{H}}(k+l) = \hat{S}_{xww}(-k,-l) / \hat{S}_{www}(-k,-l), \qquad (13)$$

where $\hat{\overline{H}}(k+l)$ is the estimate of $\overline{H}(z_1 z_2)|_{z_{1,2}=e^{j\frac{2\pi}{N}k}.e^{j\frac{2\pi}{N}l}}$,

$$\hat{S}_{xww}(-k,-l) = \frac{1}{N} \sum_{k,r=-(N-1)}^{N-1} \{\sum_{i=0}^{N} x(i)w(i-m)w(i-r)\}e^{j\frac{2\pi}{N}mk}e^{j\frac{2\pi}{N}rl}$$

and

$$\hat{S}_{www}(-k,-l) = \frac{1}{N} \sum_{k,r=-(N-1)}^{N-1} \{\sum_{i=0}^{N} w(i)w(i-m)w(i-r)\}e^{j\frac{2\pi}{N}mk}e^{j\frac{2\pi}{N}rl}.$$

Although the frequency-domain based design is faster, when implemented using FFT's, the time-domain solution appears more reliable since periodogram type estimates of, $\hat{S}_{xww}(-k,-l)$ and $\hat{S}_{www}(-k,-l)$ exhibit variance which can be reduced using windowing.

IV. Simulations

The information signal $s(k)$ was generated as an AR(1) process. The reference signal $w(k)$ was generated as a zero-mean, i.i.d., exponentially distributed noise with $\gamma_{3w}=2$. The noise $n(k)$ was generated by passing $w(k)$ through an AR(2) filter $h_1(k)$, with poles at $0.35\pm j0.45$. The primary input $x(k)$ was obtained by adding $s(k)$ and $n(k)$. Two test cases were examined, each at input SNR=10db (see Figs. 2a,3a and Tables 1,3a), and 0db (see Figs. 2b, 3b and Tables 2,3b). The input SNR was defined as $E\{s^2(k)\} / E\{n^2(k)\}$.

In test case #1, Figs. 2a,2b depict the true and estimated impulse responses obtained after approximating $h_1(k)$ by an FIR filter of order 5 and solving eqs. (4) [2nd-order approach] and (8a) [3rd-order approach]. Tables 1 and 2 show means and

standard deviations of the first five impulse response (IR) coefficients averaged over 50 Monte-Carlo runs. Although the mean of the estimated coefficients is almost the same for both cancelers, the parameter variance of the 3rd-order canceler is slightly higher than that of its 2nd-order counterpart. As expected, the (average) output SNR of the 2nd-order canceler is (by design) higher than that of the 3rd-order canceler (see last two rows of Tables 1 and 2). The output SNR was defined as $E\{s^2(k)\} / E\{[e(k)-s(k)]^2\}$.

In test case #2, $w(k)$ was corrupted by zero-mean Gaussian noise of the same variance as $w(k)$ while being independent of $x(k)$ and $w(k)$. Corresponding quantities to test case #1, appear in Figs. 3a,3b and Tables 3a,3b. At least in this case the 3rd-order noise canceler outperformed the classical approach both in terms of the IR coefficient estimates as well as the (average) output SNR.

V. Conclusions and Discussions

The second- and third-order noise cancelers are equivalent when the noise is linearly related to the reference signal. The third-order noise canceler outperforms the classical design when the reference signal is corrupted by zero-mean colored Gaussian noise of unknown covariance.

The noise canceler discussed in this paper attempts at approximating the relationship between the noise and the reference signal by an LTI filter. Currently under investigation are nonlinear cancelers, whose parameters can be estimated using higher-order statistics. Such nonlinear filters have been considered in [9], and have been shown to yield smaller mean-square-error than the linear filter approximation case.

REFERENCES

[1] B. Widrow et al., "Adaptive noise canceling : principles and applications," Proc. of IEEE , pp. 1695-1716, 1975.

[2] M. R. Sambur and N. S. Jayant, "LPC analysis/synthesis from speech inputs containing quantizing noise or additive white noise," IEEE trans. on ASSP , pp. 419-423, 1978.

[3] G. B. Giannakis, "Signal reconstruction from multiple correlations: Frequency and time-domain approaches," Journal of the Optical Society of America, May, 1989.

[4] C. L. Nikias and M. R. Raghuveer, "Bispectrum estimation : A digital signal processing framework," Proc. of IEEE , pp. 869-891, 1987.

[5] B. Wells, "Voiced/unvoiced decision based on the Bispectrum," Proc. of Intl. conf. on Acoust. Speech and Signal Proc., ICASSP-85 , pp. 1589-1592, March 1985.

[6] S. Seetharaman and M. E. Jernigan, "Speech signal reconstruction based on higher-order spectra," Proc. of Intl. Conf. on Acout. Speech and Signal Proc., ICASSP-88 , pp. 703-706, April 1988.

[7] A. Swami, and J.M. Mendel, "Adaptive cumulant based estimation of ARMA parameters," Proc. Amer. Control Conf., pp. 2096-2101, Atlanta, GA, June 1988.

[8] D.R. Brillinger and M. Rosenblatt, "Computation and interpretation of kth-order spectra," in Spectral Analysis of Time Series, pp. 189-232, B. Harris, Ed., New York, Wiley, 1967.

[9] G. B. Giannakis, "New results on multiple correlations," Proc. 22nd Asilomar Conf. on Signals, Systems, and Computers, pp. xx-xx, Pacific Grove, CA, November 1988.
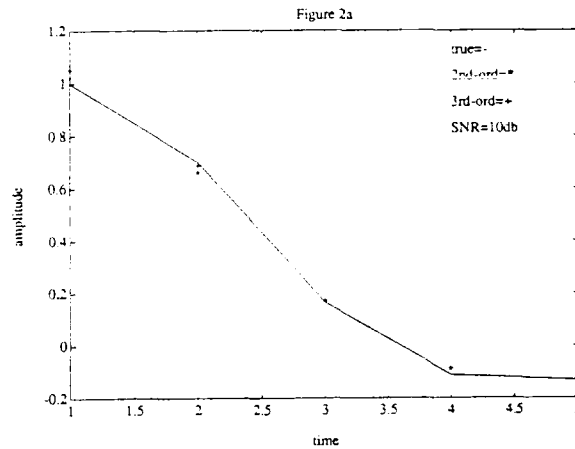
Figure 2a

Table 1

50 runs, N=2048 (8x256), SNR=10db					
IR	$h_1(0)$	$h_1(1)$	$h_1(2)$	$h_1(3)$	$h_1(4)$
True values	1.000	0.700	0.165	−0.112	−0.132
Proposed method	1.050 ±0.110	0.685 ±0.111	0.170 ±0.110	−0.087 ±0.099	−0.116 ±0.095
Classical method	1.027 ±0.083	0.663 ±0.098	0.172 ±0.098	−0.087 ±0.074	−0.144 ±0.083
Output SNR	Classical	30 db			
	Proposed	28 db			

Figure 2b

Table 3a

50 runs, N=2048 (8x256), SNR=10db, Colored AGN					
IR	$h_1(0)$	$h_1(1)$	$h_1(2)$	$h_1(3)$	$h_1(4)$
True values	1.000	0.700	0.165	−0.112	−0.132
Proposed method	1.036 ±0.134	0.705 ±0.111	0.176 ±0.144	−0.148 ±0.123	−0.097 ±0.106
Classical method	0.606 ±0.061	0.448 ±0.066	−0.075 ±0.072	−0.239 ±0.064	−0.224 ±0.060
Output SNR	Classical	15 db			
	Proposed	25 db			
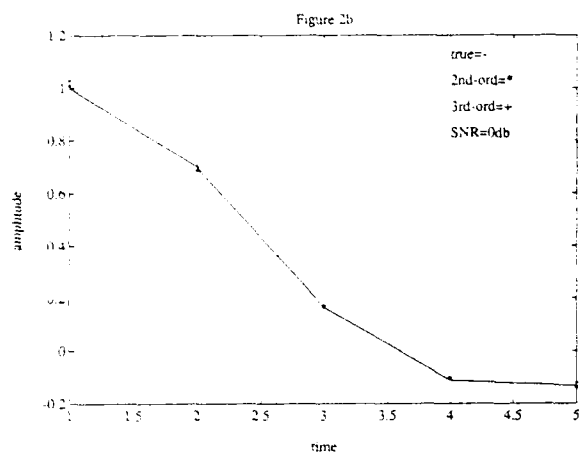
Table 2

50 runs, N=2048 (8x256), SNR=0db					
IR	$h_1(0)$	$h_1(1)$	$h_1(2)$	$h_1(3)$	$h_1(4)$
True values	1.000	0.700	0.165	−0.112	−0.132
Proposed method	1.027 ±0.036	0.703 ±0.037	0.172 ±0.035	−0.102 ±0.032	−0.123 ±0.033
Classical method	1.009 ±0.027	0.688 ±0.033	0.167 ±0.033	−0.104 ±0.024	−0.137 ±0.027
Output SNR	Classical	24 db			
	Proposed	23 db			

Figure 3b

Figure 3a
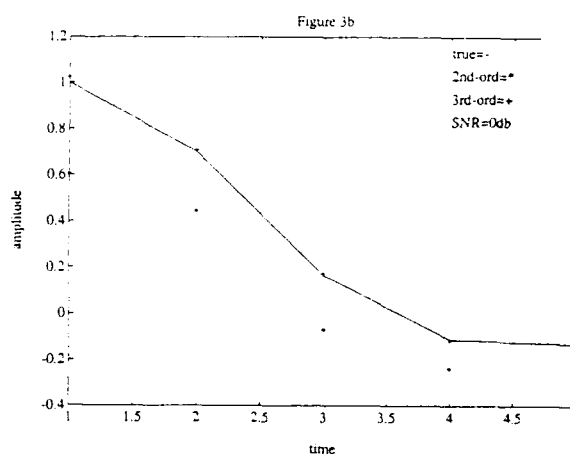
Table 3b

50 runs, N=2048 (8x256), SNR=0db, Colored AGN					
IR	$h_1(0)$	$h_1(1)$	$h_1(2)$	$h_1(3)$	$h_1(4)$
True values	1.000	0.700	0.165	−0.112	−0.132
Proposed method	1.023 ±0.054	0.705 ±0.057	0.171 ±0.055	−0.119 ±0.053	−0.114 ±0.044
Classical method	0.605 ±0.023	0.445 ±0.025	−0.064 ±0.025	−0.237 ±0.026	−0.231 ±0.023
Output SNR	Classical	7 db			
	Proposed	20 db			

TWO ADVANCED IMAGE PROCESSINGS IN POLYSPECTRAL PASSIVE ACOUSTICAL IMAGING SYSTEM FOR NOISY MECHANICAL SYSTEM DIAGNOSIS

Kimio Sasaki

University of Tsukuba, Institute of Engineering Mechanics

Tsukuba, Ibaraki, Japan

ABSTRACT

Two advanced image processings in PSPAI (polyspectral passive acoustical imaging) system are proposed to make the more detailed estimation of noise source distributions possible. One is the highly stable superresolution imaging by using the hemispherical detection and the least squared extrapolation of hologram detected in a limited spatial frequency, with the aid of the a priori knowledge about the source distribution, and the other is the straightforward imaging of spatial distribution of the dependency among frequency components through multiplication of primary images reconstructed by 2nd and n-th order spectral analyses. Principles of the proposed processings and the effectiveness as the more detailed information extraction means for passively estimating the function of acoustic or vibration noise sources are shown, with fundamental results of experiments, including numerical ones.

INTRODUCTION

Several passive acoustical imaging systems [1]-[3] have been developed as a promising means not only for extracting the precise information about radiation noise sources, but also of exploiting the sounded ones from mechanical systems and/or diagnosing the system malfunctions, because of the special features such that they are able to visualizing the various radiation states of acoustic or vibration sources without any affection on their stationary working conditions. Each of them uses the power spectra of the detected signals for imaging, so that it may visualize sufficient information about the object only when object emitting signals are Gaussian. However, for non-Gaussian signals such as the noises from mechanical systems, other imaging methods were required.

To this end, we proposed a PSPAI(polyspectral passive acoustical imaging) system [4]-[6], by developing the conventional synthetic aperture method of imagery, in a unified manner so as to image not only the radiation amplitude distribution of individual frequency components but also of the degree of dependency among them, and made clear through fundamental experiments that it has the following main special features:

(SF1) It can be applied to any acoustic sources which radiate stationary random signal, and

(SF2) visualize the various radiation structures of the source simply by choosing the order of spectral analysis at the stage of extracting image information, i.e., hologram signal. Moreover,

(SF3) the image by the higher order spectral analysis is not affected from any Gaussian noises theoretically, as well as

(SF4) considered to be useful for detection of the subtle abnormality of the mechanical system.

Apart from such superior characters, the PSPAI system uses the holographic scheme of image reconstruction, so its azimuth resolution is limited at most to a half of the wavelength used for imaging [7]. This is a big drawback for actual use, especially in an area of long wavelength. For this purpose, some methods of superresolution imaging [8],[9] were proposed, but a contradictory relation between the improvement of the resolution and the enhancement of SNR is resulted, in every method.

In this article, we propose two methods of image processing that can be carried out straightforwardly as advanced processing in a computer-aided PSPAI system. That is, (I) a superresolution imaging with the most suppressed degradation of expected SNR of reconstructed images by the hemispherical detection and the least squared extrapolation of hologram of limited spatial frequency, with the aid of a priori information about the object source size, and (II) the multiplicative processing of several primary images, reconstructed with individual frequency contents as well as through the dependency among them, to make a more refined estimation of the status of the object source possible.

Basic ideas for these processings on a common standpoint of effective utilization of the wholly spatial and temporal information of multiple random signals, associated with the source.

After a brief review of the PSPAI system, the principles of the proposed processings, and the effectiveness as the more detailed information extraction means for passively estimating the function of acoustic or vibration noise sources as well as their limitations are shown with some numerical and experimental results in the following.

PRINCIPLE

A) Brief Review of the PSPAI System

Fundamental construction of the system is shown schematically in Fig. 1. Random waves radiated from an object are detected by a rotating array of microphones in the hemispherical plane. The detected signals are subjected to auto- and cross-polyspectral analyses, so that the hologram signal at the desired frequency is derived. Reconstructed images are displayed after a certain process of image reconstructions, such as the holographic, algebraic, and LMS(least mean squared) methods, and so on.

Precedingly, let us state the main assumptions required for the following mathematical developments:

(A1) Position and Area X_0 of object distribution are known, and its finite size is negligibly small, compared to the radius D of detection plane.

(A2) Sound waves propagate spherically through the homogeneous and uniform medium.

Let the complex amplitude of object emitting wave field of frequency f at an object point x be $a(x,f)$, then the object radiation signal is generally expressed as follows [5]:

$$s(x,t) = \int_{-\infty}^{\infty} a(x,f)e^{j2\pi ft}dz(f), \qquad (1)$$

where $dz(f)$ denotes a random function, representing the temporal random nature of the signal. From the assumptions (A1)-(A3), the detected signal $u(\xi,t)$ at a point $\xi=(D,\alpha,\beta)$ can be written as in Eq. (2), by using the complex amplitude of the wave field to be detected at the point ξ, defined by Eq. (3).

$$u(\xi,t) = \int_{-\infty}^{\infty} e^{j2\pi ft}K(\xi,f)dz(f) \qquad (2), \qquad K(\xi,t) = \int_{x_0} a(x,f)[e^{-jkd(x,\xi)}/d(x,\xi)]dx, \qquad (3)$$

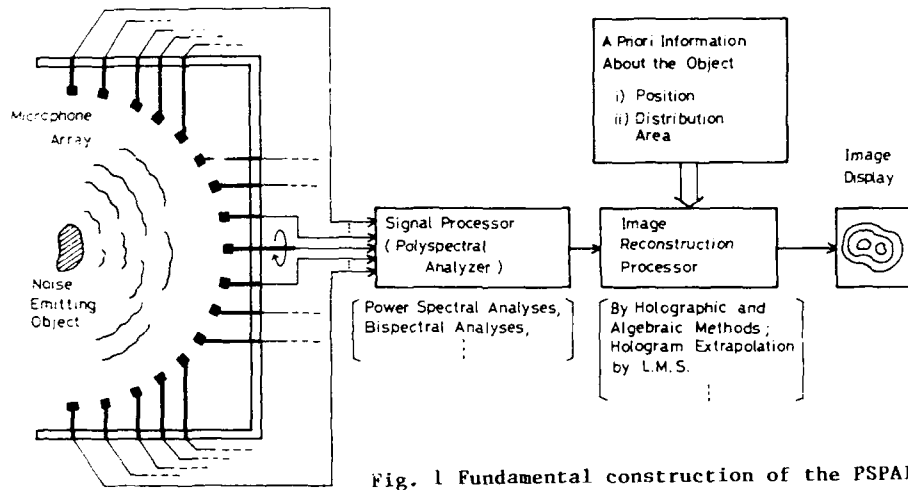where $d(x,\xi)$; distance between points x and ξ, and $k=2\pi f/c$; wave number (c; wave velocity).

Fig. 1 Fundamental construction of the PSPAI system

Thus, by regarding the detected signals, $u_1(\xi_0,t)$ at a spatially fixed point, $\xi_0=(D,0,0)$ and $u_2(\xi_1,t)$ at any scanning point ξ_1, as the the input and output of a linear space invariant system, respectively, its spatial transfer function, that is, the required hologram signal at ξ_1, can be derived from the cross-spectral analysis of $u_1(\xi_0,t)$ and $u_2(\xi_1,t)$ as follows [5]:

$$H(\xi_1,f_1) = S_{n;21...1}(f_1,...,f_{n-1})/S_{n;11...1}(f_1,...,f_{n-1}) = K(\xi_1,f_1)/K(\xi_0,f_1) = const\, K(\xi_1,f_1). \qquad (4)$$

Once the same kind of hologram signals as in the conventional acoustical holography are obtained, image can also be reconstructed, in the same manner, i.e., by calculation of the wave back-propagation. However, physical meanings of the resultant images are quite different for cases of n=2 and n≥3. The image for n=2 represents the radiation distribution of individual spectral components, while the result for n≥3 is the image through the degree of dependency among n frequency components. As the result, the latter has the special features (SF1)-(SF4) as mentioned previously.

Under the assumption (A1), the distance approximation as shown in Eq. (5) permits the FT(Fourier transform) approximation given by Eq. (6) (see Fig. 2) [6],

$$d(x,\xi) = \{D^2+x^2+y^2+z^2-2D(xsin\alpha cos\beta+ysin\alpha sin\beta+zcos\alpha)\}^{1/2}$$

$$\approx D-(xsin\alpha cos\beta+ysin\alpha sin\beta+zcos\alpha), \qquad (5)$$

$$H(\xi_1,f) = const \int_{x_0} a(x,f)e^{j2\pi(ux+vy+wz)}dx. \qquad (6)$$

where $\kappa=(u,v,w)$ is the spatial frequency vector of rectangular elements, $u=sin\alpha cos\beta/\lambda$, $v=sin\alpha sin\beta/\lambda$, and $w=cos\alpha/\lambda$ (λ; wavelength). Thus the detection plane forms a 3D FT plane of the source field, so that the azimuth and range resolutions are shown to be at most $\lambda/2$ and λ, respectively, from the

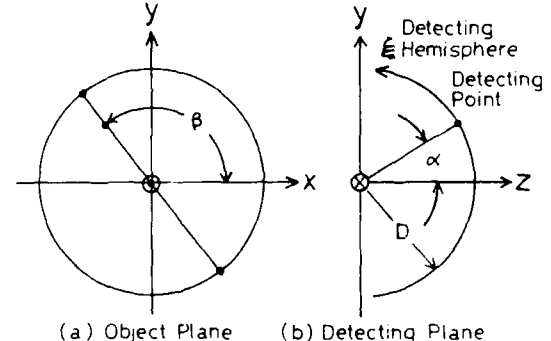(a) Object Plane   (b) Detecting Plane

Fig. 2 Geometry of hologram detection

Hi theory. This is one of the special features resulted from the use of hemisperical detection.

B) Principles of the Proposed Image Processings

1) Principle of the Superresolution imaging: For brevity, consider a planar source, the known distribution area X_0 : which is limited within $[-X_0,X_0]\times[-Y_0,Y_0]$, in the followings. In this case, the sampling theory asserts the next interpolation formula,

$$H(\alpha_k,\beta_l) = \sum_{i=-m}^{m}\sum_{j=-n}^{n} A(i_{u_0},j_{v_0})s(k,l;i,j), \qquad (7) \qquad u_0 = 1/2X_0; \quad v_0 = 1/2Y_0,$$

$$s(k,l;i,j) = \mathrm{sinc}(\sin\alpha_k\cos\beta_l/\lambda u_0-i)\mathrm{sinc}(\sin\alpha_k\sin\beta_l/\lambda v_0-j); \quad \mathrm{sinc}(x) = \sin\pi x/\pi x,$$

where $A(i_{u_0},j_{v_0})$s are the sampled values to be estimated and $H(\alpha_k,\beta_l)$s are the detected hologram signals.

Thus, when the object spatial frequency distribution $A(u,v)$ is negligible for $|u| > m u_0$, and $|v| > n v_0$, the infinite summation in Eq. (7) is replaced by the finite one of $L=(2m+1)(2n+1)$, so L dimensional spatial frequency vector **A**, consisting of $A(i_{u_0},j_{v_0})$s, is estimated from the detected hologram vector of $H(\alpha_k,\beta_l)$s with K elements, for example, by the LMS method as follows:

$$\mathbf{A} = (\mathbf{S}^T\mathbf{S})^{-1}\mathbf{S}^T\mathbf{H} = \mathbf{R}\mathbf{H}, \qquad (8) \qquad \text{S; KxL matrix of } s(k,l;i,j)\text{s, reordered to match with } \mathbf{A} \text{ and } \mathbf{H}.$$

The resolution of the system is given by $\Delta x=2X_0/(2m+1)$ and $\Delta y=2Y_0/(2n+1)$ in x- and y-directions respectively. Moreover, when no noise exists, the exact spatial frequency contents and hence the very radiation field of the source can be reconstructed completely, at least in a mathematical sense, so far as the source field is band limited and number of hologram detecting points is greater than that of spatial frequency samples to be estimated, i.e., K L. In actual circumstances, however, the hologram extrapolation error, induced from detection noises or spectral estimation and processing errors, limits the available rate of resolution enhancement, that is, the concrete application of the proposed method.

The RMS(root mean squared) sensitivity E of the method to the additive noises is easily evaluated, after variance analysis of detected hologram, as follows:

$$E = \|R\| /\sqrt{L}, \qquad (9) \qquad \|R\|; \text{ Frobenius' norm of reconstruction matrix } \mathbf{R}.$$

From Parseval's theorem, the RMS sensitivity of the hologram detection is that of reconstructed images, too, so that the result in Eq. (9) provides quite an important information about the use of the proposed superresolution imaging, with the most suppressed SNR degradation.

2) Principle of Multiplicative Image Processing: As is stated previously, the PSPAI system provides the image of the source radiation distribution related to a specific frequency component separately, even when higher order spectral analysis is used, and each image thus reconstructed may physically represent such a marginal distribution through dependency among frequency components, that depends on those of the other related frequencies. Thus, if we multiply the marginal distribution with those of the related individual frequencies, the whole spatial distribution, taking into account the temporal dependency, must be resulted. This kind of direct imaging of the dependency among frequency components may serve a more
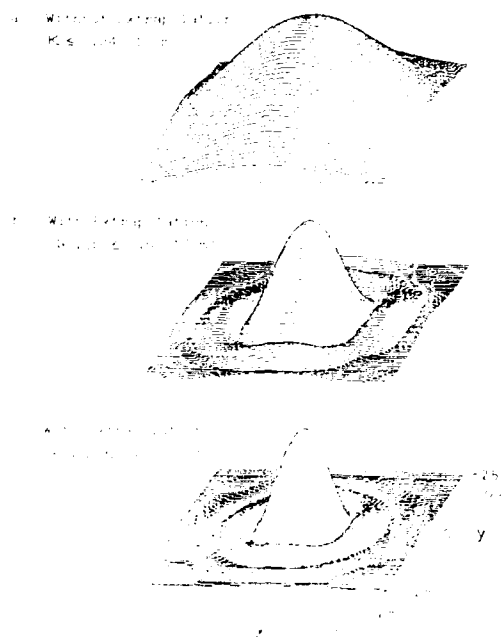

Fig. 3 Numerical examples of point spread
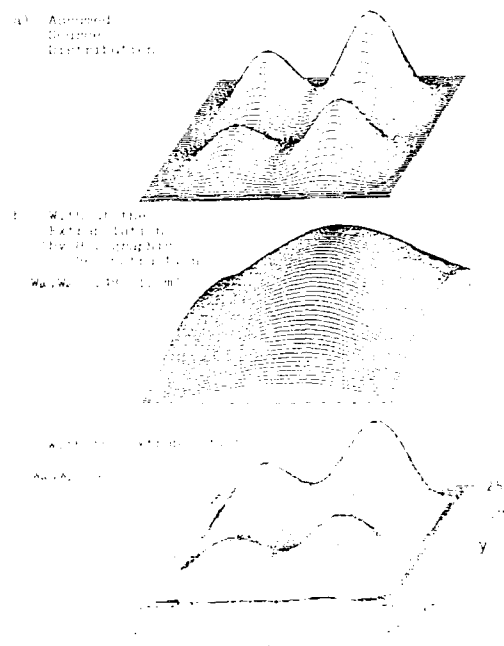function of the system

Fig. 4 Reconstructed images of a Gaussian
noise source with 4 peaks

detailed estimation of the source status, resulting in an effective means of sophisticated information extraction for noisy mechanical system diagnosis.

NUMERICAL AND EXPERIMENTAL RESULTS

A) Results for the Superresolution Imaging

Some numerical experiments were carried out, by assuming planar objects under the conditions,
(a) Radius of microphone array : $D=100$ (cm), (b) Maximum angle of array aperture : $c_{max}=53$ (deg)
(c) Number of detecting points : $K=289$, (d) Reconstruction frequency : $f=10$ (kHz).
In this setting, the maximum spatial frequency available is about $=\{a^{-2}+ \cdot\}^{1/2}$ 0.24 (1/cm), so the conventional holographic method can not discriminate two point objects within the distance of 4 (cm).

Fig. 3 shows the numerical examples of the PSF (point spread function) of the system with and without hologram extrapolation. As the frequency contents are extrapolated from the original in the figure (a) to those in (b) and (c), the obtained PSF of the system becomes more and more sharp in accordance with the extrapolation bandwidth. As a more complex object, a planar gaussian noise source with 4 peaks within the area of 5 (cm)x 5 (cm) is assumed. Fig. 4 shows shows typical examples of the reconstructed images of the source. The image by the conventional method in the figure 4(b) simply exhibits a smoothly spread hill, while the result by the proposed method with enhanced resolution rate of about 2 in the figure 4(c), not only discriminates the 4 peaks clearly, but also quite resembles the original distribution in the figure 4(a). These two basic results clearly shows the appropriateness of the fundamental principle of the proposed method of superresolution imaging.

The sensitivity of the proposed method to detection noises was examined through 50 trials of image reconstruction of the Gaussian source shown in the figure 4(a), by corrupting the hologram signals at all the detecting points with independent additive noises of several RMS(root mean squared) level. Fig. 5 shows numerical results of the relation between the RMS error of reconstructed images and the RMS noise level when the extrapolation bandwidth changed parametrically. Solid lines represent the theoretically expected values calculated from relation (9) and dots denote the experimental values. Quite a good coincidence is seen between the experimental and theoretically expected values. Hence, this result shows the properness of the precision analysis given previously, moreover implies such an important feature for implementation of the proposed method that when SNR at the information detection is given, then an available rate of resolution enhancement to suppress image variation within a tolerance is automatically determined from this figure.

Finally, to see the effectiveness of the proposed superresolution method, imaging of a pseudo-planar acoustic source was carried out. It was generated by driving two small apertures of diameter 1.4 (cm) and central distance 3.0
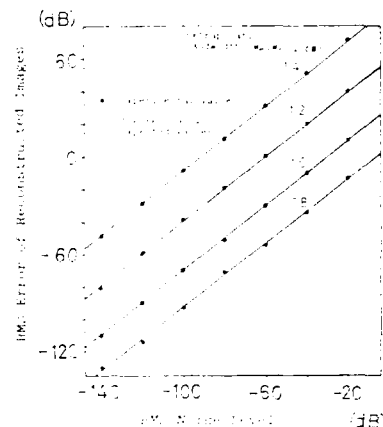

Fig. 5 RMS sensitivity of reconstructed image to additive detection noises
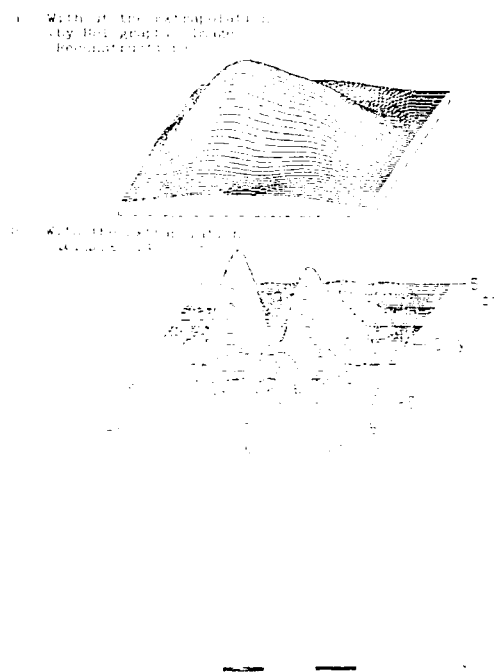

Fig. 6 Experimental results of super resolution imaging of two point like sound sources

B) Results for the Multiplicative Image Processing

To examine the fundamental characters of the proposed multiplicative processing, imaging of acoustic noise fields from a widely used sweeping machine of axial flow type was carried out.

Firstly, temporal characteristics of the machine emitting noises were analyzed from viewpoint of the power spectral and bispectral characteristics. Fig. 7 shows these amplitude characteristics of the noise detected in front of the inlet side of the machine when it is slightly loaded. In the power spectrum $P(f)$ in the figure 6(a), several sharp peaks are seen over a slowly varying back ground hill. Their central frequencies are distributed almost at multiples of about 430 (Hz), and well correspond to the harmonics of the blade passing frequency determined by the machine structure and its operating conditions, such as number of blades of a rotor, inlet and outlet structure of air flow and revolution rate of the rotor.

Correspondingly, a few peaks of high amplitude are also observed in the bispectral and bicoherence characteristics in the figure 6(b) and 6(c), particularly at the neighborhood of (3017 Hz, 3017 Hz), (429 Hz, 3447 Hz) and (215 Hz, 215 Hz) in the (f_1, f_2)-plane. These spectral characteristics mean the high dependency among the harmonically related spectral components, and matches well with the machine noise model, already proposed in Ref. [10].

To see more closely the radiation status of the sweeping machine noises a few experiments of image reconstruction were conducted by using the proposed method of multiplicative processing as well as the conventional one. Typical examples of the reconstructed images are shown in figures 8 and 9, where a broken line represents an outer form of the machine inlet side, for reference. From these figures, the following features about the radiation field of the noise are clearly shown:

(i) Although the reconstructed images of individual frequencies exhibit a fairly different aspect, each of them takes the maximum value near the inlet, but distribute widely even outside of the machine (see the figures 8(a) and 9(a)).

(2) Direction of the reconstructed images by bispectral analysis, shown in the column (b) of these figures, are inverted globally, compared to those by the power spectral analysis, shown in the first column (a). This direction-inverted nature is interpreted as the result of interference with the shadowed phase conjugate wave of negative frequency.

(3) Moreover, in the image of figure 9(b), a considerable fine structure is observed, resulting in the exhibition of the more strong interference between the wave fields of frequencies 6.034 (kHz) and -3.017 (kHz).

(4) This interference phenomenon stated above appears more strongly in the reconstructed image by the proposed multiplicative processing in the figure 9(c), while the result in 8(c) does not show this effect, but only spreads more widely than the image in the figure 8(a).

As the result, it may be said from these observations that

(a) Power Spectrum
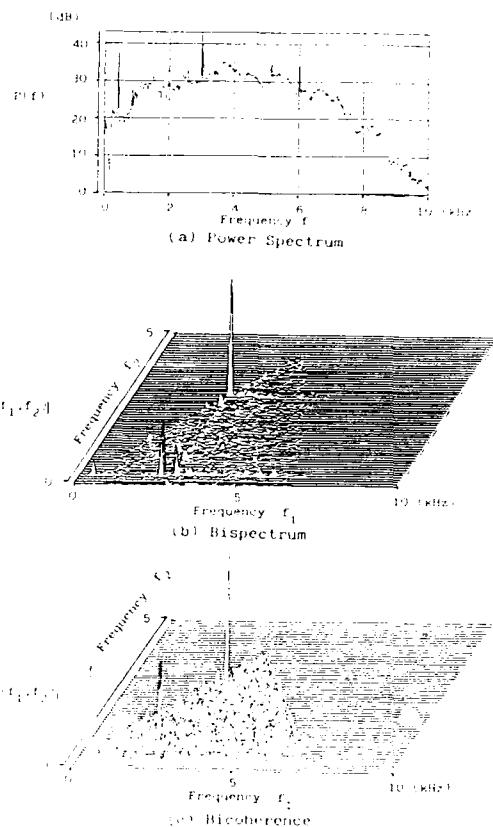

(b) Bispectrum

(c) Bicoherence

Fig. 7 Measured 2nd and 3rd order spectral characteristica of an axial flow type sweeping machine noise under slightly loaded condition

$(f_1 = 3.017$ kHz, $f_2 = 3.017$ kHz$)$

Fig. 8 Experimental results for multiplicative wave processing of reconstructed images of the sweeping machine noise, where reconstruction frequency f_1 is 3.017 (kHz).

the spectral and spatial distributions of frequencies 3.017 (kHz) and 6.034 (kHz) are strongly dependent each other, and moreover, the former is influenced more heavily by the latter, compared to the contrary case, as far as the bispectral characteristics are concerned. These special features can not be obtained only from the conventional methods of imaging, but together with the newly proposed method of multiplicative processing in this article, which suggests the possibility of a new information retrieval means for noisy mechanical system diagnosis.

a. by Power Spectral Analysis

(b) by Bispectral Analysis

(c) by Compound Analyses

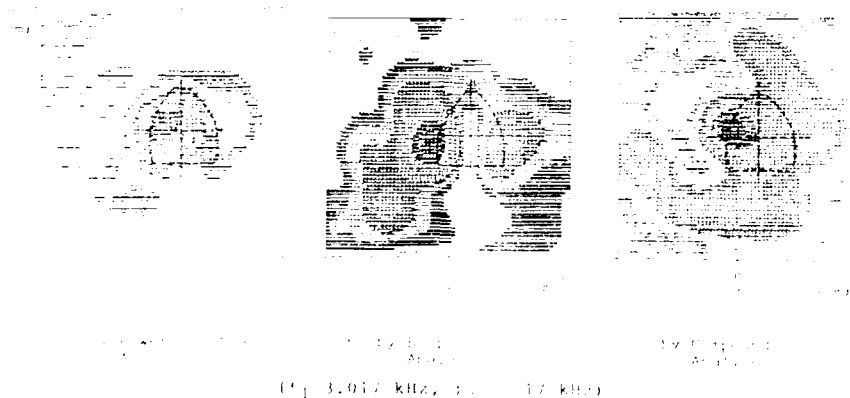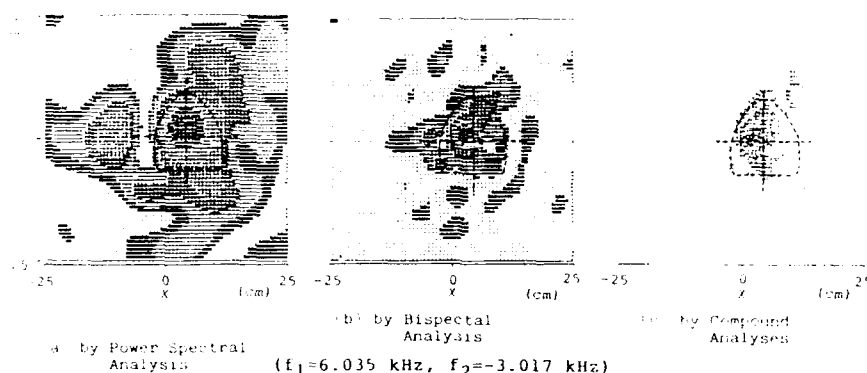$(f_1 = 6.035$ kHz, $f_2 = -3.017$ kHz$)$

Fig. 9 Experimental results for multiplicative image processing of reconstructed images of the sweeping machine noise, where reconstruction frequency f_1 is 6.034 (kHz).

CONCLUSIONS

To develop a passive acoustical imaging system that can really afford to industrial use, two basic problems were considered, in this paper, that is, (I) how to obtain stably superresolved images even in an area of long wavelength, and (II) how to find image information, useful to the individual purposes.

To this end, two image processings were proposed as an advanced processing in the PSPAI system that utilize both the spatial and temporal information about the noise source, and the principles of the proposed processings were presented with some numerical or experimental results, which illustrated their effectiveness for the detailed analysis of the acoustic noise source status.

The proposed methods of imaging may be expected to be a promissing means in a passive measurement not only for the precise imaging of subtle faults of mechanical systems or the more precise diagnosis, but also for many applications to the other fields, based on the analysis of random waves such as seismic waves, sonic and ultrasonic waves under the sea, heart sounds and noises, and so on.

REFERENCES

[1] S.Ichi, M.Fujinami, K.Umezawa and I.Tsujiuchi,"Mapping of Noiselike Sound Sources with Acoustical Holography,"Appl.Opt.,Vol.14,pp.1478-1479,1975.

[2] K.Finns,"Binaural Source Location,"I.Sound Vib.,Vol.44,pp.275-289,1976.

[3] E.Williams, J.D.Maynard and E.Skudrzk,"Sound Source Reconstruction Using a Microphone Array," I.Acoust.Soc.Am.,Vol.68,pp.340-344,1980.

[4] K.Sasaki, I.Sato and Y.Nakamura,"Holographic Passive Sonar,"IEEE Trans.Series Ultrason.,Vol.SU-24, pp.193-200,1977.

[5] I.Sato, K.Sasaki and M.Nonaka,"Prototype of Bispectral Passive Imaging Systems Aiming Machine-System Diagnosis,"J.Acoust.Soc.Am.,Vol.63,pp.1611-1616,1978.

[6] I.Sato, Y.Nakamura, K.Sasaki and K.Temura,"Three Dimensional Passive Acoustical Imaging System Using Hemispherical Array Detectors,"Acoustical Imaging Vol.8,Plenum Press,pp.187-200,1980.

[7] B.P.Hildebrand and B.B.Brenden,"An Introduction to Acoustical Holography,"Plenum Press,pp.67-144,1972.

[8] I.Sato, K.Sasaki and K.Temura,"Super-resolution Imaging Using a Sequential Estimation of a Hologram in an Extended Area from Data Obtained in a Limited Area,"J.Acoust.Soc.Am.,Vol.65,pp.976-984,1979.

[9] I.Sato, K.Temura and K.Sasaki,"Super-resolution Acoustical Passive Imaging System Using Algebraic Reconstruction,"J.Acoust.Soc.Am.,Vol.67,pp.1802-1808,1980.

[10] K.Sasaki, I.Sato and M.Fins,"A Synthesizer of Random Signals with Bispectral Characteristics - A Machine Noise Simulator,"J.Acoust.Soc.Am.,Vol.69,pp.286-292,1981.

STATISTICS OF BICOHERENCE AND BIPHASE

Gloria Sebert and Steve Elgar

Electrical and Computer Engineering Department
Washington State University
Pullman, Washington 99164-2752

ABSTRACT

Statistics of estimates of bicoherence and biphase were obtained from numerical simulations of nonlinear random (harmonic) processes with known true bicoherence and biphase. Expressions for the bias, variance, and probability distributions of estimates of bicoherence and biphase as functions of the true bicoherence and number of degrees of freedom (dof) used in the estimates are presented. The pdfs are consistent with theoretical distributions derived for the limit of infinite dof and are used to construct confidence limits on estimates of bicoherence and biphase. Maximum likelihood estimates of true values of bicoherence and biphase given observed values are also presented.

I. INTRODUCTION

Bispectral analysis has been used to study nonlinear interactions in a variety of ocean processes, including surface gravity waves in intermediate water depths (Hasselman et al. 1963), perturbations from the mean profiles of temperature, salinity, and sound velocity (Roden et al. 1973), internal waves (Neshyba and Sobey 1975, McComas and Briscoe 1980), shoaling surface gravity waves (Elgar and Guza 1985, 1986; Doering and Bowen 1987), and temperature fluctuations (Müller 1987). A wide range of phenomena in other physical systems has also been investigated with the bispectrum (see Nikias and Raghuveer 1987 for a recent review). In most of these studies, the bispectrum was used to determine whether or not the process under investigation was consistent with linear dynamics. Specifically, nonlinear interactions are associated with nonzero values of the bicoherence, defined here as (Haubrich 1965, Kim and Powers 1979)

$$b^2(\omega_1, \omega_2) = \frac{|B(\omega_1, \omega_2)|^2}{E[|A(\omega_1)A(\omega_2)|^2]E[|A(\omega_1 + \omega_2)|^2]} \quad (1)$$

where B is the bispectrum,

$$B(\omega_1, \omega_2) = E[A(\omega_1)A(\omega_2)A^*(\omega_1 + \omega_2)] \quad (2)$$

$A(\omega)$ is the complex Fourier coefficient of the time series at radian frequency ω and $E[\ ]$ is the expected, or average, value. For a finite-length time series, even a truly linear (e.g. Gaussian) process will have nonzero bicoherence. Haubrich (1965) shows that for a Gaussian process, the bicoherence (whose true value equals zero) is approximately Chi-square (χ^2) distributed in the limit of large degrees of freedom (dof), and, thus, significance levels for zero bicoherence as a function of dof can be calculated. Elgar and Guza (1988) demonstrated that estimates of bicoherence from a Gaussian process are also approximately χ^2 distributed for low values of dof (dof=32) and are not sensitive to smoothing procedures used to increase dof.

Although the significance levels for zero bicoherence can be used to statistically detect the presence or absence of nonlinear interactions, the statistics of estimates of bicoherence and biphase, $\beta(\omega_1, \omega_2)$ - the phase of $B(\omega_1, \omega_2)$ - for the case of nonzero true bicoherence have not previously been reported. The purpose of this study is to present such statistics. Brillinger (1965), Rosenblatt and Van Ness (1965), Brillinger and Rosenblatt (1966a,b), and others (see Nikias and Raghuveer 1987) give some of the statistical properties of higher-order spectra, including asymptotic distributions of the real and imaginary parts of the bispectrum. Haubrich (1965), Hinich and Clay (1968), Kim and Powers (1979), Hinich (1982), and Ashley et al. (1986) discuss the estimation of bicoherence.

For the present study, harmonic random processes with true values of bicoherence (b^2) between 0.1 and 1.0 were numerically simulated (Section 2), and the statistics of estimates of bicoherence ($\hat{b}^2$) and biphase ($\hat{\beta}$) obtained from the simulated time series were calculated (Section 3). The probability distributions of $\hat{b}^2$ and $\hat{\beta}$, including the bias of $\hat{b}^2$ and the variances and confidence limits of $\hat{b}^2$ and $\hat{\beta}$, were determined as functions of b^2 and dof (Sections 3.1-3.2). These values are useful for experimental design. On the other hand, once an experiment has been conducted, maximum likelihood techniques may be used to estimate true values of b^2 and β based on the observed values. Maximum likelihood estimates of bicoherence are presented in Section 3.3. These results are then briefly applied to estimates of the bicoherence and biphase of narrow band surface gravity waves observed in 9 meter water depth (Section 3.4). Conclusions follow in Section 4.

2. SIMULATION PROCEDURE

Time series consisting of triads of sinusoids (with frequencies ω_1, ω_2, and ω_{1+2}) were numerically simulated on the CRAY XMP at the San Diego Supercomputer Center. By adjusting the amplitudes of the component sinusoids, some of whose phases were chosen from a uniform random distribution $(0-2\pi)$, the true bicoherence value of the triad could be varied. For example, consider the case of a single triad:

$$x(t) = \cos(\omega_1 t + \phi_1) + \cos(\omega_2 t + \phi_2) + a \cos(\omega_3 t + \phi_3)$$
$$+ \cos(\omega_3 t + \phi_1 + \phi_2)$$
$$(3)$$

where $\omega_3 = \omega_1 + \omega_2$, ϕ_1, ϕ_2 and ϕ_3 are random phases, and a is an adjustable parameter. As a increases from 0 to ∞, $b^2(\omega_1, \omega_2)$ decreases from 1.0 to 0.0. For the example given in equation (3), if $a = 0$, then $\beta(\omega_1, \omega_2) = 0$. Time series consisting of the following triads were simulated: a single triad, $(\omega_1, \omega_2, \omega_3)$; two triads with the same sum frequency, $(\omega_4, \omega_5, \omega_6)$ and $(\omega_3, \omega_3, \omega_6)$; and two triads with a common frequency other than the sum frequency, $(\omega_1, \omega_3, \omega_4)$ and $(\omega_3, \omega_5, \omega_8)$. True values of $\beta = 0$ and $\beta = \frac{\pi}{4}$ were used. For each case, the true bicoherence of each triad could be adjusted. The statistics of estimates of bicoherence and biphase reported here were found to depend only on true values of b^2 and dof; they did not depend on the number of triads, nor on how the triads were interrelated, nor on β. Additional time series were simulated with Gaussian distributed Fourier coefficients rather than uniformly distributed random phases (Elgar et al. 1985 and references therein). The resulting statistics of b^2 and β were essentially identical to those of the random phase simulations.

Each simulation consisted of generating many realizations of 65,536 point time series, each of which was subdivided into short sections of 256 points. By ensemble averaging the bispectrum over all 256 of the short records, estimates of bicoherence and biphase with 512 dof were produced from each 65,536-point time series. Each 65,536 point record was also subdivided into 16 groups of 16 short records, each group producing estimates with 32 dof. Estimates with dof between 32 and 512 were obtained in a similar manner. One thousand of the 65,536 point time series were generated, and, thus, 1000 (dof=512) to 16000 (dof=32) bicoherence and biphase estimates were produced for each true value of bicoherence. Results from simulations using 100 realizations were indistinguishable from those where averages of 1000 realizations were used.

3. SIMULATION RESULTS

3.1 Bicoherence

As shown below, b^2 is approximately chi square distributed and, thus, will have a positive bias, similar to the ordinary coherence between two time series (Jenkins and Watts 1968, Beningus 1969). Following Beningus (1969),

the bias was empirically found to be approximately given by

$$\text{BIAS}[\hat{b}^2] = \left(\frac{2}{\text{dof}}\right)(1 - b^2)^2 \qquad (4)$$

Equation (4) is similar to the corresponding expression for coherence (Beningus 1969) and is compared to the observed bias in figure 1. Guided by expressions based on somewhat heuristic theoretical arguments (Hinich and Clay 1968, Kim and Powers 1979), the variance of $\hat{b}^2$ was empirically found to be approximately

$$\text{VAR}[\hat{b}^2] = \left(\frac{4b^2}{\text{dof}}\right)(1 - b^2)^3 \qquad (5)$$

Equation (5) is similar to the analogous approximate theoretical equation for coherence (Jenkins and Watts, 1968), and the agreement between (5) and the simulated data is excellent, as shown in figure 2.

Haubrich (1965) suggests that for a process with $b^2 = 0.0$, $\hat{b}^2$ will asymptotically (large dof) approach a chi square distribution with parameter $\nu = 2$. Hinich (1982) shows that bicoherence is approximately asymptotically distributed as a non-central chi-squared random variable. The non-central chi-square distribution can be approximated by an $\alpha \chi^2$ distribution (Abramowitz and Stegun), given by

$$f_{\chi^2}\left(\frac{b^2}{\alpha}\right) = \frac{(b^2)^{\frac{\nu}{2}-1} e^{-b^2/2}}{2^{(\nu/2)} \Gamma(\frac{\nu}{2})} \qquad (6)$$

where $\Gamma(\ )$ is the gamma function. The mean and variance of an $\alpha\chi^2$ distributed random variable are $\alpha\nu$ and $2\alpha^2\nu$, respectively. Thus, the parameters α and ν can be determined from the bicoherence as

$$\alpha = \frac{E[b^2]}{\nu} \quad , \quad \nu = \frac{2E^2[b^2]}{\text{VAR}[b^2]} \qquad (7)$$

Combining (5) and (7), and using the biased value of bicoherence,

$$\nu = \frac{(\text{dof})b^2}{2(1 - b^2)^3} \qquad (8)$$

As $b^2 \to 1$ and/or dof increases, the parameter ν increases and $f_{\chi^2}(b^2/\alpha)$ approaches a Gaussian distribution. Probability distributions of the simulated data are compared to $\alpha\chi^2$ distributions, with α and ν obtained from (7) and (8), respectively, in figure 3. According to a χ^2 goodness-of-fit test, the theoretical and observed distributions with 32 dof and $b^2 \leq 0.1$ do not differ significantly at the 95% confidence level. There is even better agreement as $b^2 \to 1$ and/or dof $\to \infty$.

Assuming b^2 is $\alpha\chi^2$ distributed with α and ν given by (7) and (8), respectively, confidence limits for b^2 can be constructed as functions of b^2 and dof. The 90% confidence limits are compared to the corresponding values observed in the simulations in figure 4.

3.2 Biphase

Similar to the phase of the cross spectrum (Jenkins and Watts 1968), the biphase is approximately Gaussian dis-

tributed, unbiased, and has variance (in units of radians)

$$\text{VAR}[\beta] = \left(\frac{1}{\text{dof}}\right)\left(\frac{1}{b^2} - 1\right) \tag{9}$$

The theoretical variance and confidence limits (calculated from a Gaussian distribution with variance given by (9)) for β are compared to simulated values in figures 5 and 6, respectively.

3.3 Maximum Likelihood Estimation

The results of the previous sections describe the statistics of bicoherence given the true value, b^2, thus enabling the design of experiments to measure bicoherence. On the other hand, it is often the case that b^2 must be estimated from a limited set of data. In this section maximum likelihood estimates (Jenkins and Watts 1968) of the true value of bicoherence given an observed value, $\hat{b}^2$, with finite dof are presented. Freilich and Pawka (1987) present a similar analysis for estimates of the cross spectrum, with results analogous to those reported here. Maximum likelihood estimation consists of determining parameters of the underlying pdf from samples of the distribution. The pdf is recast as a function of the parameters to be determined, and those values of the parameters that maximize this likelihood function are considered the maximum likely estimates (mle) of the true parameters of the underlying distribution given the particular samples at hand. For the case of bicoherence, the likelihood function, $L(b^2)$, is given by the $\alpha\chi^2$ distribution (equation (6)) and is shown as a function of dof and $\hat{b}^2$ in figure 7. For large values of $\hat{b}^2$ and/or dof, $L(b^2)$ is symmetrical about its maximum. However, for small $\hat{b}^2$ and/or dof, $L(b^2)$ has long tails extending toward high values of b^2 (figure 7). In order to better account for the asymmetrical shape of the likelihood function, Jenkins and Watts (1968) suggest using the mean of the likelihood function (mele) as an estimate of the true parameter. Both mle and mele estimates of bicoherence are listed in Table 1. As $L(b^2)$ becomes more symmetrical, $b^2_{mele} \to b^2_{mle} \to \hat{b}^2$ (Table 1 and figure 8); although the likelihood estimates of b^2 are always greater than the corresponding measured values (figure 8). This can be understood by considering the χ^2 pdfs shown in figure 9. It is more likely that an observed value comes from the center of the distribution with high ν (i.e., high b^2) than from the upper tail of a distribution with lower ν. Table 1 and figure 8 both show that except for small $\hat{b}^2$ and/or dof, b^2_{mele} does not differ substantially from $\hat{b}^2$.

$L(b^2)$ can also be used to calculate confidence intervals for the estimated true values of bicoherence. The likelihood functions presented here (figure 7) are approximately Gaussian, and, thus, the mele and the variance of $L(b^2)$ determine the entire likelihood function (see also Jenkins and Watts 1968). The standard deviations of $L(b^2)$ and the b^2 values whose likelihoods are down by a factor of 7.5 from the mle (95% confidence limits on b^2 if $L(b^2)$ is Gaussian) are presented in Table 1. From the table it can be seen that the standard deviation of $L(b^2)$ is nearly independent of b^2, and

depends primarily on dof.

Since the distribution of biphase is approximately Gaussian, $\beta_{mele} \approx \beta_{mle} \approx \beta$.

3.4 Application to Shallow Water Surface Gravity Waves

Using bispectral analysis, Elgar and Guza (1985) concluded that narrow-band swell (peak period about 16 seconds) observed in 9 m water depth was "... qualitatively consistent with Stokes-like nonlinearities." Their conclusion was based on observed values of biphase for triads consisting of the power spectral primary peak frequency (f_p) and its first few harmonics. Based on the results presented above, bispectral estimates from these data can now be interpreted quantitatively. For dof=256, the observed values of bicoherence and biphase for the two lowest order triads were $b^4(f_p, f_p) = 0.161$, $\hat{\beta}(f_p, f_p) = -7°$ and $b^2(f_p, f_{2p}) = 0.067$, $\hat{\beta}(f_p, f_{2p}) = -35°$. (Bicoherences at other triads were not significantly greater than zero.) Accounting for the bias, equation (1), $b^2_{mele}(f_p, f_p) = 0.160$ and $b^2_{mele}(f_p, f_{2p}) = 0.070$.

For dof=256 and b^2_{mele} as given above, 90% confidence limits for biphase can be constructed. For the self-self interaction (f_p, f_p, f_{2p}), the 90% limits are ±13.5°. Thus, the observed value $(-7°)$ is within the 90% limits of the Stokes biphase, $\beta = 0°$, and the data are consistent with Stokes-like nonlinearities. On the other hand, 90% confidence limits for the biphase of the triad (f_p, f_{2p}, f_{3p}) are ±21.6°, and do not include the observed value $(-35°)$. Consequently, with a 10% possibility of being incorrect, it is concluded that the biphase of this triad is not consistent with Stokes-like nonlinearities and that shallow water resonance effects (Freilich and Guza 1984) are important.

4. CONCLUSIONS

Numerical simulations of random processes with nonzero bicoherence were used to investigate the statistics of estimates of bicoherence and biphase. Bicoherence is biased (figure 1) and is approximately $\alpha\chi^2$ distributed (figure 3), with parameter ν a function of the true bicoherence and the degrees of freedom associated with the estimate (equation (8)). Confidence limits for estimates of bicoherence can be constructed from the $\alpha\chi^2$ distribution (i.e. from b^2 and dof) and agree with the corresponding values observed in the simulations (figure 4). The statistics of biphase are similar to those of the phase of the cross spectrum (equation (9) and figure 5), and confidence limits for biphase estimates based on b^2 and dof also agree with corresponding values observed in the simulations (figure 6). Maximum likelihood estimates of the true value of bicoherence given an observed value were obtained from the $\alpha\chi^2$ distribution (Table 1 and figure 7). The ratio of maximum likelihood estimates of bicoherence to observed values approaches 1 as b^2 and/or dof increases, with less than 10 percent differences if $b^2 > 0.25$ (for dof > 32) and/or dof > 150 (for $b^2 \geq 0.1$) (figure 8).

REFERENCES

Abramowitz, M. and I. Stegun, *Handbook of Mathematical Functions*, Dover, N.Y., 1046, 1972.

Ashley, R.A., D.M. Patterson, and M.J. Hinich, A diagnostic test for nonlinear serial dependence in time series fitting errors, *J. Time Series Analysis*, 7, 165-178, 1986

Benignus, V.A., Estimation of the Coherence Spectrum and Its Confidence Interval Using the Fast Fourier Transform, *IEEE Trans. on Audio and Electroacoustics*, 17, 145-150, 1969.

Brillinger, D.R., An introduction to polyspectra, *Ann. Math Statist.*, 36, 1351-1374, 1965.

Brillinger, D.R., and M. Rosenblatt, Asymptotic theory of estimates of k-th order spectra, *Advanced Seminar on Spectral Analysis of Time Series* (ed. B. Harris), 153-188, Wiley, 1967.

Brillinger, D.R., and M. Rosenblatt, Computation and interpretation of k-th order spectra, *Advanced Seminar on Spectral Analysis of Time Series* (ed. B. Harris), 189-232, Wiley, 1967.

Doering, J.C., and A.J. Bowen, Skewness in the nearshore zone: A comparison of estimates from Marsh-McBirney current meters and collocated pressure sensors, *J. Geophys. Res.*, 92, 13173-13183, 1987.

Elgar, Steve, and R.T. Guza, Observations of bispectra of shoaling surface gravity waves, *J. Fluid Mech.*, 161, 425-448, 1985.

Elgar, Steve, and R.T. Guza, Nonlinear model predictions of bispectra of shoaling surface gravity waves, *J. Fluid Mech.*, 167, 1-18, 1986.

Elgar, Steve, and R.T. Guza, Statistics of Bicoherence, *IEEE ASSP*, 36, 1667-1668, 1988.

Elgar, Steve, R.T. Guza and R.J. Seymour, Wave group statistics from numerical simulations of a random sea, *Applied Ocean Res.*, 7, 93-96, 1985.

Freilich, M.H., and R.T. Guza, Nonlinear effects on shoaling surface gravity waves, *Phil. Trans. Royal Soc. London*, A311, 1-41, 1984.

Freilich, M.H., and S.S. Pawka, Statistics of S_{xy} Estimates, *J. Phys. Oceanography*, 17, 1786-1797, 1987.

Hasselman, K., W. Munk, and G. MacDonald, Bispectra of ocean waves, *Time Series Analysis* (ed. M. Rosenblatt), 125-139, Wiley, 1963.

Haubrich, R.A., Earth noises, 5 to 500 millicycles per second, 1, *J. Geophys. Res.*, 70, 1415-1427, 1965.

Hinich, M.J., Testing for Gaussianity and linearity of a stationary time series, *J. Time Series Analysis*, 3, 66-74, 1982.

Hinich, M.J., and C.S. Clay, The application of the discrete Fourier transform in the estimation of power spectra, coherence, and bispectra of geophysical data, *Rev. Geophys.*, 6, 347-363, 1968.

Jenkins, G.M., and D.G. Watts, *Spectral Analysis and its Applications*, Holden-Day, 1968.

Kim, Y.C., and E.J. Powers, Digital bispectral analysis and its application to nonlinear wave interactions, *IEEE Trans. Plasma Science*, 1, 120-131, 1979.

McComas, C.H., and M.G. Briscoe, Bispectra of internal waves, *J. Fluid Mech.*, 97, 205-213, 1980.

Müller, D., Bispectra of sea-surface temperature anomalies, *J. Phys. Oceanography*, 17, 26-36, 1987.

Neshyba, S., and E.J.C. Sobey, Vertical cross coherence and cross bispectra between internal waves measured in a multiple layered ocean, *J. Geophys. Res.*, 80, 1152-1162, 1975.

Nikias, C.L., and M.R. Raghuveer, Bispectrum estimation: A digital signal processing framework, *Proceedings of the IEEE*, 75, 867-891, 1987.

Roden, G.I., and D.J. Bendiner, Bispectra and Cross Bispectra of Temperature, Salinity, Sound Velocity, and Density Fluctuations with Depth off Northeastern Japan, *J. Physical Oceanography*, 3, 308-317, 1973.

Rosenblatt, M., and J.W. Van Ness, Estimation of the bispectrum, *Ann. Math. Statist.*, 36, 1120-1136, 1965.

b^2	dof	b^2_{mle}	b^2_{mode}	sdv	(7.5:1)
.1	32	.129	.116	.017	(.018,.237)
.1	64	.116	.125	.011	(.026,.201)
.1	128	.108	.113	.032	(.039,.172)
.1	256	.104	.107	.021	(.051,.151)
.2	32	.217	.223	.051	(.078,.314)
.2	64	.209	.212	.012	(.109,.281)
.2	128	.201	.206	.031	(.135,.261)
.3	32	.309	.310	.017	(.191,.387)
.3	64	.301	.305	.037	(.224,.361)
.4	32	.403	.404	.045	(.323,.462)

Table 1. Parameters for the likelihood functions. b^2 is the unbiased observed bicoherence, dof is the degrees of freedom associated with the measurement, b^2_{mle} is the maximum of the likelihood function (L), b^2_{mode} is the mean of L, sdv is the standard deviation of L, and (7.5:1) indicates values of b^2 corresponding to likelihood values down by a factor of 7.5 from the maximum of L (if L is Gaussian, these values correspond to 95% confidence limits).
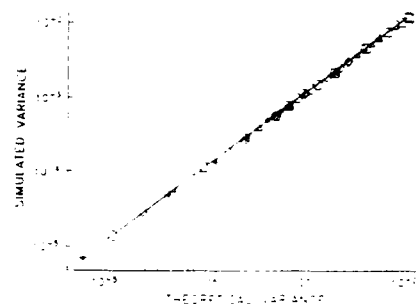

Figure 2. Variance of bicoherence observed in simulated data versus the theoretical variance (equation (5)). Each symbol represents different dof, as described in the caption to figure 1.
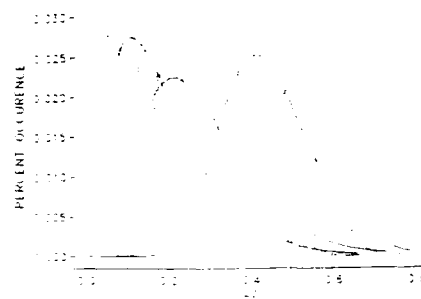

Figure 3. Probability distribution of $\hat{b}^2$ observed in the simulated data for dof=32 (dashed line) and theoretical $\alpha\chi^2$ distribution (solid line). From left to right, $b^2 = 0.1$, 0.2, and 0.4. The bin width is $\Delta(b^2) = 0.0067$.

Figure 1. Bias of bicoherence observed in simulated data versus the theoretical bias (equation (4)). Squares, dof=32; triangles, dof=64; diamonds, dof=128; circles, dof=256; asterisks, dof=512. $b^2 = 0.1$, 0.2, ...0.9 for each dof.

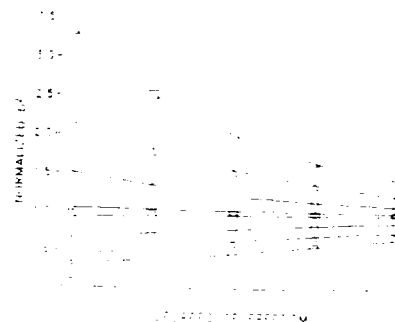Figure 4. 90% confidence limits for bicoherence. The values shown have been normalized by the corresponding true value of bicoherence. Thus, 90% of the time, b^2 will be in the range given by the appropriate ordinate values times b^2. Solid lines are theoretical values and symbols are values observed in the simulated data. Squares, $b^2=0.1$; triangles, $b^2=0.2$; diamonds, $b^2=0.4$; circles, $b^2=0.8$.
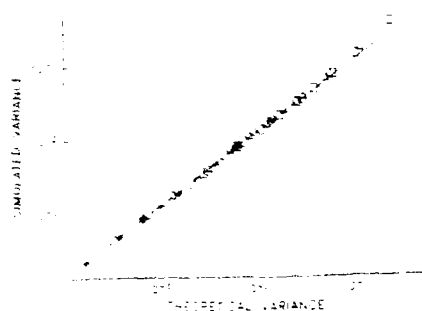
Figure 5. Variance of biphase observed in simulated data versus the theoretical variance (equation (9)). The units are radians^2. Each symbol represents different dof, as described in the caption to figure 1.

Figure 8. Ratio of b^2_{mle} to $\hat{b}^2$ versus $\hat{b}^2$. Each curve is for different dof, increasing by factors of 2 from dof=32 (upper curve) to dof=256 (lowest curve).
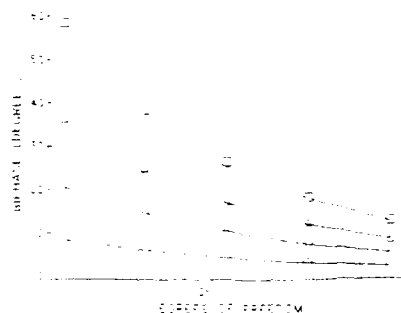

Figure 6. 90% confidence limits for biphase. Solid lines are theoretical values and symbols are values observed in the simulated data. Each symbol represents different b^2 as described in the caption to figure 4.

Figure 9. χ^2 probability distribution functions. From outermost to innermost curves, $\nu = 4, 12, 20,$ and 28, respectively. The abscissa has been normalized by ν so that the mean of each distribution is 1, and the scale of the ordinate is arbitrary.
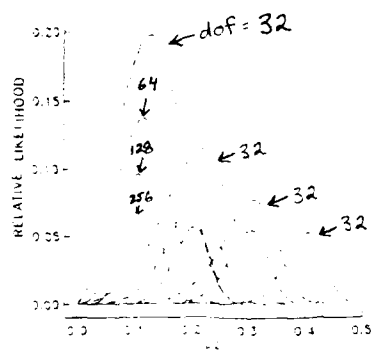
Figure 7. Likelihood functions $I(b^2)$ for various measured bicoherence and dof values. Solid lines unbiased $b^2 = 0.1$; longest dashes, $b^2 = 0.2$; medium dashes, $b^2 = 0.3$; shortest dashes, $b^2 = 0.4$. For each b^2 the outermost curve has 32 dof and the dof increase by factors of 2 for each succeeding inner curve. The number of such curves decreases for increasing b^2. Unbiased values are obtained by subtracting the bias (equation (11)) from the observed value, where the observed value of bicoherence is used on the right hand side of (1). Replacing b^2 with b^2_{mle} in (1) results in negligible differences in the bias.

EFFICIENT MAXIMUM LIKELIHOOD USING HIGHER RANK SPECTRAL ESTIMATION.

Ira J. Clarke

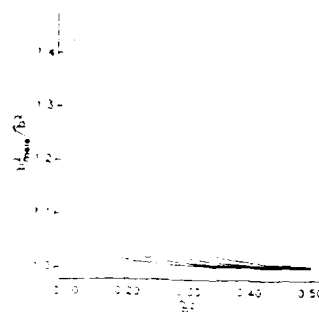Royal Signals and Radar Establishment, Malvern,
Worcestershire WR13 3PS, England.

Abstract

In practical data processing applications, an engineer is required to develop a processing system which selects one 'best' option from a span of possible interpretations of the data. A fully optimal approach requires a search through a full range of predefined complex high rank solutions. The solutions on offer must have a sufficient number of degrees of freedom to cater for complex scenarios. It is shown that a well supervised search is significantly more efficient.

1. Introduction

The primary objectives of Digital Signal Processing (DSP) are inference, deduction and/or estimation based on limited observations through sensor systems. Modern high discrimination DSP algorithms have been shown to have the potential, in ideal conditions, to greatly enhance signal acquisition and tracking performance in radar, sonar and other sensors. Although it is generally accepted that it is not possible for any signal processing technique to violate basic information theoretic limitations, it is easily demonstrated by simulation that, in reasonable conditions, the resolving power of modern algorithms, such as MUSIC, exceeds that of the long established Rayleigh resolution criterion by an order of magnitude or more. High discrimination algorithms can also resolve signals with magnitudes far below the sidelobe leakage levels of large signals and interference. However current adaptive methods are not robust, they require relatively high signal to noise and are susceptible to small errors in the collateral knowledge needed to solve generic underdetermined problems of the type associated with resolution limited sensor systems.

This paper attempts to draw together insights from a number of disciplines and puts forward several basic ideas and concepts appropriate to tackling the generic limitations of existing signal analysis and control techniques. The aim is to develop a methodology which fully stretches the flexibility of modern parallel computing technology. By way of illustration, the principle features are introduced of a novel multi-stage matrix decomposition algorithm based on concepts which facilitate the exploitation of 'a priori' knowledge. Many of the questions posed in the paper are however, as yet, only partially answered.

2 The task

2.1 Description.

Three separate stages can be identified in the design of a proposed high performance signal analysis system:

a) the learning stage — represent knowledge as relationships between cause and effect as observed through sensors. It is also necessary to predefine output actions since otherwise there is no point in performing DSP on subsequent data.

b) the processing stage — *infer, deduce and/or estimate the most probable input conditions* given limited samples of sensor data (the inverse problem — observe the effect, find the cause). Initiate output. The basic functions are of interpretation and decision taking, based on limited evidence.

c) the hardware implementation — develop cost effective computing hardware able to satisfy the computational demands of a suitable high performance algorithm.

Clearly *accurate* representation of 'a priori' knowledge during the learning phase is a prerequisite for the optimum interpretation of sensor data. Errors are likely to lead to false decisions. Without due regard to the possible consequences, it is tempting to simplify important relationships between cause and effect. The use of standard assumptions and convenient, but restrictive, mathematical models is common but, as a result, engineers acquiesce to performance loss and/or tighter (more costly) sensor specifications. It is surprisingly difficult to separately quantify algorithmic shortcomings and modelling deficiencies since information theoretic performance limits are often ill defined in absolute terms. Robust algorithms are intended to withstand possible deficiencies in the representation of knowledge resulting from the use of imperfect model criteria. In principle, since we can never eliminate uncertainty, we see that the optimum solution requires a) that we extend the models to include estimates of uncertainties and b) we develop algorithms able to utilise this data. Currently relatively crude control of response characteristics is sometimes attempted by the addition of artificial 'white' noise.

Clearly the above principle is valid only if the problem is over-determined. In general, we see that, in addition to sensor data, 'a priori' knowledge is essential. However this knowledge may itself have some degree of associated uncertainty and should, by the TLS principle, be given a weighting factor via a suitable algorithmic procedure.

We begin to realise that the learning stage must include estimating the structure and statistics of anticipated stocastic observation uncertainties together with errors in all 'a priori' models. Clearly this information is best obtained by direct measurement rather than by inference based on qualitive features or from simple 'guesstimates'. The use of artificial 'white' noise as a simple indirect way of controlling algorithm response must be regarded as sub-optimal in most respects.

Theoretical performance predictions should also be based on the total uncertainty in the available evidence.

2.2 The computational hardware.

It is well known that parallel computing systems require careful design. Architectures can be specifically developed to minimise memory access and communication requirements between individual processors in a given application. Remarkable improvements in efficiency and power consumption can be achieved but at the expense of specialised development effort. Economy of scale comes from multi-function software and mass produced hardware which, in the DSP case, can perhaps only be achieved through a sound design methodology.

The mapping of an algorithm onto an architecture can, in principle, be a two way compromise. It may, for example, be possible to realise significant computational advantages by utilising available hardware devices and by modifying minor features of an algorithm.

In general there are key algorithmic functions which constitute the majority of the computational load. These include, for example, eigen decomposition, matrix inverse and spectral estimation. If any of these stages can be eliminated then, potentially, there are substantial savings. We must therefore consider all aspects when developing an algorithm for a given application.

3. Basic concepts in high performance data analysis algorithms.

3.1 Array manifold.

As already stated, the primary aim of the learning phase is to index, cause to effect and also to designate the output action. The first conceptual step is therefore to tentatively set up a system comprising suitable sensors, processing hardware and output devices. The next requirement is to define the operations to be performed by the processor. We must therefore present a *known* test input scenario to the sensor and demand that the output devices give the appropriate response. We need first to record the sensor output state as a template or fingerprint for future reference. If the similar *identifying features* subsequently appear at the sensor output then we shall infer that the corresponding input condition has been re-applied. Clearly it is preferable that the template as observed through the sensor should be unique at least in some small way.

3.1.1 Basic concept – Single emitter case.
Successive frames or snapshots of sensor output data, $\underline{d}_1, \underline{d}_2 ...$, should be capable of description in terms of the product of a single steering vector and a series of real or complex weights, $f_1, f_2 ...$ plus additive measurement error:

$$[\hat{\underline{d}}_1, \hat{\underline{d}}_2 ...] = \underline{a}(\theta).[f_1^h, f_2^h ...] + \text{observation errors} \quad (1)$$

We denote the reference vector or template as a complex (or real) valued column vector $\underline{a}(\theta)$ comprising 'n_s' elements. Each template is scaled in magnitude to correspond to an emitter of unit power at a suitable reference point. The pointer, θ, represents a discrete or continuous variable, or set of variable parameters, which indexes a given sensor output description to the corresponding input condition. In general, θ may relate to azimuth, elevation, range, polarisation, carrier or doppler frequency in any selected combination and may therefore have a large number of elements. The span, denoted θ, defines, for example, the

field of view of an antenna array. If θ is sampled discretely on a grid then we obtain a set of discrete reference vectors, the full set is commonly termed the *array manifold*. In parametric modelling problems, we are required to record at least one template per classical resolution cell in order to satisfy the well established Nyquist criterion. Frequently it is necessary to provide an oversampling factor of two or even three to minimise loss of peak signal between sample points. In general, we shall need to interpolate either to generate intermediate templates or to generate spectral or likelihood estimates between selected grid points.

We can also define a set of rank one 'matched filters', $\underline{a}^\dagger(\theta)$, such that:

$$a^\dagger(\underline{\theta}).a(\underline{\theta}) = 1 \text{ for each } \theta \quad (2)$$

where † denotes the Moore Penrose psuedo inverse. For the narrowband rank one case, it follows that the row vector $\underline{a}^\dagger(\theta)$ is given by:

$$\underline{a}^\dagger(\underline{\theta}) = [a^h(\underline{\theta}).a(\underline{\theta})]^{-1}.\underline{a}^h(\underline{\theta}) \quad (3)$$

where ^{h} denotes the conjugate transpose of a vector or matrix. The conjugation reverses phase shifts introduced between emitter and the individual sensor outputs or sample points. The magnitudes of the individual elements in $\underline{a}(\theta)$ determine the relevance factors discussed in the previous section. The vector inner product term within the brackets has a single value at a given pointer position θ; to aid the reader more easily identify such cases, underlining is omitted.

Clearly the calibration process must, in principle, be repeated separately for a representative number of values of θ, at for example, various emitter test sites, to give a set of matched filters and reference vectors. It is, however, common practice to employ various mathematical data compression techniques and analytic models to simplify the description of the templates. Such models reduce storage requirements. Also, if the underlying problem is continuous, interpolation within the discrete grid of sampled points and, to a limited extent, extrapolation outside the sampled range my be eased. However the use of a convenient mathematical model often puts costly restrictions on the system design.

3.1.2. Expanded array manifold – Multiple emitter case.
In a complex multiple emitter environment, a single rank one template or reference vector is no longer sufficient to model the sensor state. If the emitters are not coherent, then any attempt to collect real data at every possible combination of emitter position, $\theta_1, \theta_2 ... \theta_m$, suffers the obvious difficulty of a *combinatorial explosion* in the number of separate templates we require. Further still we must include also a represent the range of different relative power levels and phases.

We note that, for a linear system, the resulting sensor data vectors are linear combinations of the templates, $\underline{a}(\theta_1)$, $\underline{a}(\theta_2), ... \underline{a}(\theta_m)$, corresponding to individual emitters. Such linear combinations define a subspace which can also be defined by a set of orthonormal vectors. Therefore given the basic array manifold for single emitters, we can, in principle, *synthesise* the appropriate candidate subspace for every allowed combination of emitter parameters. We can economise on storage at the expense of computational load, by deferring the synthesis task until the search or processing phase where we can compare the incoming data directly against a set of computed candidate subspaces. The span of the basis single emitter array manifold has therefore been expanded to include higher rank templates. *The search process is, in effect, a higher rank spectral estimation*

In practice, however, there is a daunting problem: the sheer size of the computational task caused by the combinatorial explosion in the number of templates. In the majority of applications, a *full* multi-parameter 'Maximum Likelihood' search of this type is well beyond technological feasibility in, for example, radar applications.

The only clear option which retains the prospect of near optimality in the multi-parameter case, involves resorting to a limited but well directed search of the most likely set of synthesised candidates. Clearly if 'a priori' evidence can be identified which predicts a partial solution, an approximate solution or a small range of alternatives, then a large proportion of higher rank solutions can be eliminated immediately from the initial search. The full higher rank (Maximum Likelihood) spectral estimate need not then be computed.

The directed search approach provides the basis for novel, computationally efficient, multi-stage algorithms discussed in Section 4.

3.2 Reduced rank modelling of data matrices.

3.2.1 Rank one modelling using templates.

We see that $\underline{a}^\dagger(\theta)$ operating on a series of frames of data $\underline{d}_1, \underline{d}_2, \dots$ re-generates estimated values, $\underline{f}(\theta)$, for the series of complex emitter weights (referred to the input reference point):

$$\underline{\hat{f}}^h(\theta) = \underline{a}^\dagger(\theta).[\underline{\hat{d}}_1, \underline{\hat{d}}_2 \dots] \qquad (4)$$

$$= \underline{a}^\dagger(\theta).\underline{\hat{D}}$$

where, for notational simplicity, successive frames of data, $\underline{d}_1, \underline{d}_2, \dots$ are held as a column vectors in an 'n_s by n_f' matrix $\underline{\hat{D}}$. We must regard the regenerated weights, $\underline{\hat{f}}(\theta)$, at any candidate value of θ, as estimated values due to inevitable uncertainty both in the $\underline{a}^\dagger(\theta)$ vectors themselves and due to the observation noise added to the data vectors. System attenuation relative to the chosen reference point, which in practice generally varies with θ, is directly accounted for by the scaling factor included in the $\underline{a}(\theta)$ templates and therefore also in the inverse operators $\underline{a}^\dagger(\theta)$.

Given computed estimates $\underline{\hat{f}}(\theta)$, it follows from the original definition (Equation 1) that we can also synthesise a rank one model of the data vectors (at any value of θ):

$$\underline{\hat{D}}_1 = \underline{a}(\theta).\underline{\hat{f}}^h(\theta) = [\underline{a}(\theta).\underline{a}^\dagger(\theta)].\underline{\hat{D}} \qquad (5)$$

The resulting estimate, $\underline{\hat{D}}_1$, represents a rank one model of the measured data and can be compared directly with that data. The difference:

$$\underline{\hat{R}}_1 = \underline{\hat{D}} - \underline{a}(\theta).\underline{a}^\dagger(\theta).\underline{\hat{D}} = [\underline{I}_s - \underline{a}(\theta).\underline{a}^\dagger(\theta)].\underline{\hat{D}} \qquad (6)$$

$$= \underline{C}_1.\underline{\hat{D}}$$

defines a modelling residue, $\underline{\hat{R}}_1$, as a function of θ. $\underline{I}_s$ denotes an identity matrix of rank 'n_s'. We shall frequently need to refer to projection through the matrix $\underline{C}_1$ defined above. We can regard $\underline{C}_1$ as a *signal blocking matrix* orthogonal to $\underline{a}(\theta)$ and $\underline{a}^\dagger(\theta)$. The rank of the '$n_s$ by n_s' matrix $\underline{C}_1$ is '$n_s - 1$'. The rank of $\underline{\hat{R}}_1$ is less than or equal to '$n_s - 1$'. A rank one LMS solution, as a function of θ, can be found by minimising the trace of the matrix $\underline{\hat{R}}_1.\underline{\hat{R}}_1^h$ or of $\underline{\hat{R}}_1^h.\underline{\hat{R}}_1$. We see that the trace of $\underline{\hat{D}}_1.\underline{\hat{D}}_1^h$, or of $\underline{\hat{D}}_1^h.\underline{\hat{D}}_1$, plotted as a function of θ, is equivalent to rank one spectral estimation.

3.2.2 Higher rank modelling using templates.

The principle given above extends to higher rank modelling

with little difficulty (Clarke[3]):

$$\underline{\hat{D}}_m = \underline{A}_m.\underline{A}_m^\dagger.\underline{\hat{D}} \qquad (7)$$

$$= \underline{A}_m.[\underline{A}_m^h.\underline{A}_m]^{-1}.\underline{A}_m^h.\underline{\hat{D}}$$

where $\underline{A}_m$ defines a column matrix holding the candidate vectors, $\underline{a}(\theta_1), \underline{a}(\theta_2), \dots \underline{a}(\theta_m)$. $\underline{A}_m^\dagger$ denotes the Moore Penrose psuedo inverse of $\underline{A}_m$. The corresponding estimate, $\underline{\hat{D}}_m$ defines a rank 'm' model of the measured data and, as in the rank one case:

$$\underline{\hat{R}}_m = \underline{\hat{D}} - \underline{A}_m.[\underline{A}_m^h.\underline{A}_m]^{-1}.\underline{A}_m^h.\underline{\hat{D}} \qquad (8)$$

$$= [\underline{I}_s - \underline{A}_m.[\underline{A}_m^h.\underline{A}_m]^{-1}.\underline{A}_m^h].\underline{\hat{D}}$$

$$= \underline{C}_m.\underline{\hat{D}}$$

where $\underline{\hat{R}}_m$ denotes a residue at model order m and $\underline{C}_m$ is the corresponding signal blocking transform. For gaussian statistics, minimising the trace of the covariance matrix $\underline{\hat{R}}_m.\underline{\hat{R}}_m^h$ or maximising the trace of $\underline{\hat{D}}_m.\underline{\hat{D}}_m^h$ (the higher rank spectrum) against the parameters $\theta_1, \theta_2, \dots \theta_m$ leads to Maximum Likelihood parameter estimates $\theta_1, \dots \theta_m$ at model order 'm'.

We see that a rank 'm' LMS version of the data matrix can also be regenerated from the decomposition components $\underline{a}(\hat{\theta}_1) \dots \underline{a}(\hat{\theta}m)$ and $\underline{\hat{f}}(\hat{\theta}_1) \dots \underline{\hat{f}}(\hat{\theta}_m)$. We are free to use the components and/or parameter estimates for whatever purpose is intended of the system.

3.3 Background interference and observation uncertainty.

A typical requirement of radar or sonar is to 'acquire' and 'track' an unknown (variable) number of possible emitters or reflecting targets. If the number of targets is not estimated correctly then severe tracking errors usually ensue. Frequently the signals of most interest are by far the weakest and are easily masked by sidelobe leakage. In order not to over or under-estimate the number of targets, contributions from strong signals must modelled accurately since otherwise modelling residues may either appear as additional targets or may prevent the identification of weaker components. It is also clear that an algorithm must have access to sufficient discriminatory information to enable background noise and interference to be differentiated from the 'real' signals. Such information is best provided explicitly as data in the form of quantitive statistical estimates of the various background components. Much effort is devoted to explicitly modelling the properties of interference and to developing corresponding algorithms able to efficiently exploit these models.

We see that DSP algorithms are required to decompose sensor data into recognised basis templates plus deterministic (predictable) background components. An acceptable candidate decomposition, when reconstituted as a model of the data matrix, should match the input data to within bounds set by the stochastic bounds corresponding to that model. It is therefore the total observation uncertainty which should determine whether a model of given rank is adequate or whether a model of higher rank is required or whether a simpler model is adequate.

We now proceed to examine the fundamentals of spectral estimation which is needed as part of a basic toolkit for developing algorithms.

3.4 Rank one spectral estimation

3.4.1 Basic version.

It has already been indicated that the majority of DSP algorithms are based on spectral or likelihood estimation in

some form when attempting to determine which of a number of candidate solutions is most likely. We have seen that prior knowledge of a basic array manifold or library of templates is required from which higher rank models can be synthesised and we have seen that a reduced rank model of the data can be generated by a projection through a candidate subspace. We define the classical power spectral density estimation function, for rank one templates, as:

$$s_d(\underline{\rho}) = \text{Trace}\{\underline{a}(\underline{\rho}).\underline{a}^\dagger(\underline{\rho}).\hat{\underline{D}}\} \tag{9}$$

$$= \frac{a^h(\underline{\rho}).\hat{\underline{D}}.\hat{\underline{D}}^h.a(\underline{\rho})}{a^h(\underline{\rho}).a(\underline{\rho})}$$

where the real valued normalising terms, $a^h(\underline{\rho}).a(\underline{\rho})$, may vary with θ due to system losses and, in principle, may be far from isotropic. The matrix $\hat{\underline{D}}.\hat{\underline{D}}^h$ defines an estimate of covariance for the data. We assume that all covariance estimates are normalised correctly according to the number of frames and any weighting coefficients employed in the frame to frame integration.

The value, $\hat{\theta}_{max}$, of θ at the maximum point of $s_d(\underline{\rho})$ identifies which rank one model best models the data. The summation of error components is based on a power or mean squares metric. The error is minimised since the total power or energy in the data is constant – partitioned by projection through a subspace between the model and the errors:

$$\mathcal{R}_d(\underline{\rho}) = \text{Trace}\{[\underline{I}_s - \underline{a}(\underline{\rho}).\underline{a}^\dagger(\underline{\rho})].\hat{\underline{D}}\}$$

$$= \text{Trace}\{\underline{\Omega}.\hat{\underline{D}}\} \tag{10}$$

If the templates, $\underline{a}(\underline{\rho})$, refer to discrete samples from a *continuous function of* $\underline{\rho}$ then it is generally necessary, from an accuracy viewpoint, to interpolate $s_d(\underline{\rho})$ to find the maximum, $s_d(\hat{\theta}_{max})$. A three point curve fitting procedure is generally more efficient and more stable, in a DSP environment, than a (two point) gradient ascent (or descent) method. Given any interpolated $\hat{\theta}_{max}$, it is relatively easy to find the corresponding template, $\underline{a}(\hat{\theta}_{max})$, if needed.

3.4.2 Modified spectral estimation.
If we algorithmically modify the output of the sensor by a weighting transform or filter, $\underline{W}$, then, to be consistent, the array manifold templates $\hat{\underline{R}}.\hat{\underline{R}}^h$ and $\underline{M}.\underline{M}^h$ should also be similarly modified. We note that:

a) the sensor system inclusive of transform $\underline{W}$ can be regarded as a modified sensor,
b) the effect of the transform need not be isotropic with $\underline{\rho}$,
c) the Mean Squares metric is also modified, we now have Weighted Mean Squares and
d) we may concatenate several such weighting transforms.

The classical rank one spectrum in the domain of the modified sensor becomes:

$$s_{wd}(\underline{\rho}) = \frac{a^h(\underline{\rho}).\underline{W}.[\underline{W}^h.\hat{\underline{D}}.\hat{\underline{D}}^h.\underline{W}].\underline{W}^h.a(\underline{\rho})}{a^h(\underline{\rho}).\underline{W}.\underline{W}^h.a(\underline{\rho})} \tag{11}$$

The normalising term, $a^h(\underline{\rho}).\underline{W}.\underline{W}^h.a(\underline{\rho})$, again compensates for system losses as a function of $\underline{\rho}$ irrespective of the choice of weighting transform. Numerical difficulties may however occur if the denominator approaches zero.

We observe that the spectrum is isotropic if $\underline{W}^h.\hat{\underline{D}}.\hat{\underline{D}}^h.\underline{W}$ is

an identity matrix. The major application for the transform $\underline{W}$ is as a pre-whitening transform chosen such that the spectrum of $\underline{M}.\underline{M}^h$ is isotropic. It can then shown that if the matrix $\underline{W}^h.\hat{\underline{M}}.\underline{M}^h.\underline{W}$ is forced to be an identity matrix then, for Gaussian statistics, the resulting spectrum is related monotonically to a spectrum of likelihood ratios for the corresponding rank one candidate solutions.

We can explore the effect of a weighting transform by replacing the data matrix $\hat{\underline{D}}$ by any selected reference template. The resulting spectrum defines a 'point spread function' from which we can estimate the 'leakage' from that template into filters 'matched' to each of the remaining templates in turn. The width of the mainlobe and level of sidelobes is of direct concern if we wish to identify more than one signal component.

We note that we can also include a projection transform in place of or in addition to $\underline{W}$. A most useful concept is that of exploiting 'a priori' knowledge via a signal blocking transform, $\underline{\Omega}$.

3.5 Higher rank spectral estimation.

3.5.1 Basic version.
If we are presented with data from an unknown scenario in which there may be multiple emitters and we do not have prior estimates of 'm' or of $\theta_1, \theta_2, ..\theta_m$, then we need to find a solution with sufficient degrees of freedom to model the data. We must therefore be prepared to synthesise and compare candidate solutions at different values of model order 'm'. Based on standard scientific principle, we normally prefer to select the simplest solution which is consistent with observed data. Clearly it seems sensible for reasons of computational economy, to compute candidate solutions in small groups, according to 'a priori' estimates of relative likelihood, curtailing the search process when a satisfactory solution first appears. We can, for example, generate likelihood spectra for candidate models in strict order of increasing rank. We therefore generate a separate higher rank spectral estimate at each value of 'm'.

At each value of 'm', we must select candidate basis templates, $\underline{a}(\theta_1)$, $\underline{a}(\theta_2)$, $...\underline{a}(\theta_m)$ which we can represent as a column matrix denoted $\underline{A}_m$. A corresponding 'matched' filter, $A_m^\dagger$, can be defined by:

$$A_m^\dagger.A_m = I_m \tag{12}$$

where $\underline{I}_m$ is a rank 'm' identity matrix. If observation noise and interference has zero mean then the rows of $\underline{A}_m^\dagger$ can be regarded as matched filters for the columns of $\underline{A}_m$. We therefore need to remove mean background components from the data covariance estimate: $\hat{\underline{D}}.\hat{\underline{D}}^h - \hat{\underline{R}}.\hat{\underline{R}}^h$.

If the 'm' basis vectors are linearly independent then the inverse operator, $A_m^\dagger$, can be computed using the Moore Penrose psuedo inverse, $[A_m^h.A_m]^{-1}.A_m^h$, by SVD or by utilising the Woodbury matrix inversion lemma. The corresponding signal blocking matrix is:

$$\underline{\Omega}_m = \underline{I}_s - \underline{A}_m.\underline{A}_m^\dagger \tag{13}$$

A rank 'm' power density spectral estimate can be defined as follows:

$$S_{md}(\underline{\rho}_1, \theta_2, ..\theta_m) = \text{Trace}\{\underline{A}_m.\underline{A}_m^\dagger.[\hat{\underline{D}}.\hat{\underline{D}}^h - \hat{\underline{R}}.\hat{\underline{R}}^h].\underline{A}_m.\underline{A}_m^\dagger\} \tag{14}$$

Similarly, a spectrum of the modelling residue is given by:

$$R_m(\underline{\mu}_1, \underline{\mu}_2, \dots \underline{\mu}_m) = \mathrm{Trace}\{\underline{C}_m \cdot [\underline{D}.\underline{D}^h - \underline{\hat{R}}.\underline{\hat{R}}^h].\underline{C}_m\} \quad (15)$$

Maximising S_m or minimising R_m as a function of all parameters is equivalent to choosing the best rank 'm' model in a LMS sense and is therefore potentially a good approximation to a Maximum Likelihood solution at that rank.

An example of a rank two spectral estimate is given in Figure 1 where the vertical scale corresponds to S_{md} and is linear in the weighted squares metric. The arrowed values of μ define emitter parameters used in generating simulated data (10 frames) from a linear antenna array. The μ_1 and μ_2 ordinates are in the horizontal plane and may, of course, be interchanged. We therefore observe symmetry about the diagonal line $\mu_1 = \mu_2$ where we might expect to find the rank one spectrum. However the foreground symmetric half of selected plots is cut away to reveal that the rank one spectrum (solid line) is markedly different from the corresponding rank two section. The effect can be explored mathematically by evaluating the limit as $\mu_1 - \mu_2 \to 0$ via Equation 14, further consequences on algorithm performance require careful evaluation.

3.5.2 Computation of higher rank spectra.

We note that:

$$\underline{A}_m^\dagger \cdot \underline{A}_m^\dagger \cdot [\underline{D}.\underline{D}^h - \underline{\hat{R}}.\underline{\hat{R}}^h].\underline{A}_m \cdot \underline{A}_m^\dagger \quad (16)$$
$$= \underline{A}_m \cdot [\underline{A}_m^h \cdot \underline{A}_m]^{-1} \cdot \underline{A}_m^h \cdot [\underline{D}.\underline{D}^h - \underline{\hat{R}}.\underline{\hat{R}}^h].\underline{A}_m \cdot [\underline{A}_m^h \cdot \underline{A}_m]^{-1} \cdot \underline{A}_m^h$$

and that:

$$\underline{A}_m^h \cdot [\underline{D}.\underline{D}^h - \underline{\hat{R}}.\underline{\hat{R}}^h].\underline{A}_m$$

is essentially a set of points from the basic rank one spectrum. We also observe that $[\underline{A}_m^h \cdot \underline{A}_m]^{-1}$ comprises cross correlation coeficients which can be precomputed. The required matrix inverse is computationally simple if 'm' is small.

We conclude that clear distinctions should be drawn between shortcomings in data analysis procedures due to i) knowledge representation, ii) algorithmic deficiencies iii) lack of available evidence in data from sensors iv) lack of 'a priori' information and v) observation uncertainies.

4   Incremental multi-stage parameter estimation.

4.1 Discussion

In this section we discuss how the guidelines suggested by the discussion of previous sections might be put into practice. The aim is to demonstrate exploitation of a) the expanded array manifold concept and b) higher rank spectral estimation based on a directed search. The basic illustrative example chosen relates to overcoming some of the inherent limitations associated with currently available high resolution algorithms such as MUSIC. The problem refers to estimating model order or minimum number of manifold components needed to model a data matrix. The decomposition procedure is based on multiple stages of spectral estimation to identify components progressively and robustly in the face of inevitable array calibration errors.

We can define a signal blocking matrix, $\underline{C}_m$, orthogonal to the 'm' set as stored in the low rank model, $\underline{A}_m$, derived by our algorithm and corresponding to a model of the stronger signals. We can then examine the modelling residue using a modified spectral estimate to find weaker signal components indicated by $\underline{C}_m$. The process could be repeated.

Clearly, we need identify the principal maximum alone at any stage including the first. This approach is potentially advantageous since this maximum should not be due to a sidelobe. It is also becomes feasible to avoid preliminary eigen decomposition by computing the spectra directly from the whitened *difference* matrix $\underline{W}_0^h.[\underline{D}.\underline{D}^h - \underline{R}.\underline{R}^h].\underline{W}_0$. This approach forms the basis of the Incremental Multi-stage Parameter estimation algorithm referred to as IMP by the author. Decomposition components are found progressively in decreasing order of magnitude. Figure 2 shows a progressive decomposition of simulated data from a sixteen element linear array (20 frames) in a non isotropic background. Successive difference spectra each represent a least mean squares modelling residue at a given signal model order or rank. The maximum in the spectrum at each stage is regarded as the indicating the most likely next decomposition component which is then included in the signal model. All simulated emitters have been located in this way. The final spectrum (hatched) uses the corresponding signal blocking matrix to check, against a threshold, that dominant spectral components do not remain. The filled diamond symbols indicate estimates of emitter power using signal extraction filters defined by $[\underline{A}_m^h.\underline{W}_0.\underline{W}_0^h.\underline{A}_m]^{-1}.\underline{A}_m^h.\underline{W}_0.\underline{W}_c^h$.

The effects of leakage (sidelobes) cannot be *completely* suppressed via the signal blocking transforms until one or more signals have been located *accurately*. We realise that the parameter estimates *initially* available at a given model order, m, are generally subject to significant residual bias due to this leakage. The largest remaining signal component is least affected and the *corresponding* principal maximum in the spectrum should correspond closely to the required maximum. Therefore, immediately after the model order has been incremented to 'm', the 'IMP' algorithm is set up to perform a localised (unimodal) maximum likelihood search involving small iterative adjustments to the parameters of each signal — before recomputing $\underline{C}_m$ and proceeding to the m+1 stage. It is essential that this iterative optimisation be allowed to converge sufficiently in order to ensure that, at stage 'm+1', residual sidelobe leakage is adequately suppressed relative to the smaller, as yet unidentified, 'm+2' emitter. The priority is to avoid mis-directing the future path of the search towards a sub maximum.

4.2 Model order control.

The IMP algorithm makes available separately optimised maximum likelihood solutions at each model order — this presents a multiple hypothesis situation in its own right. The choice of a suitable model order should depend directly on 'a priori' input. This may simply take the form of threshold on the final spectrum but clearly, for each candidate signal model variations in the estimated values of individual spatial positions and/or waveforms can be derived and examined. Candidate signal components can, in principle, be included or excluded from the model on a frame by frame basis. This approach potentially offers a significant advance on current adaptive procedures in which state variables and model order are heavily filtered.

Improved stability obtained by such means should enable parameter values, μ_m, to be tracked more accurately. These estimates, together with statistical properties, can be converted back to a likelihood function form and can then be combined recursively with incoming data to give 'less noisy' updates to the likelihood spectra. (The lower model order stages of IMP can also be bypassed given initial estimates of μ_m). Since

track behaviour of the values of μ_m can be monitored, the values at the new time can be be predicted before their use as 'a priori' estimates. The effective integration period can then be extended since the usual constraint that parameters must be stationary within a block of data can be relaxed. The technique for increasing integration aperture is analogous to that of the extended Kalman filter with similar potential performance advantages in difficult scenarios. In addition the restrictive constraints of fixed model order and slow track acquisition are alleviated by use of the directed search concept.

We realise that, since the search is multi-parameter we can, in principle, use an extended array manifold which includes a model of potential calibration errors. We can then optimise the parameters at each stage of the processing. We may update slowly changing parameters less frequently or on demand.

Since the parameters of a model are generally not independent, a parametric optimisation procedure is often highly iterative but, given appropriate 'a priori' models and a reasonable algorithmic routine based on a directed or progessive search, convergence is normally reasonably rapid. Computational efficiency can be improved by scheduling parameter updates according to rate of drift. Sensor calibration, for example, would need to be updated relatively infrequently compared to the parameters of a fleeting target.

5. CONCLUSIONS.

It is concluded that 'a priori' knowledge is essential to optimising high discrimination algorithms and that single pass algorithms, such as MUSIC, are inherently suboptimal due to residual sidelobe leakage. Guidelines can be followed which allow computationally efficient algorithms to be developed based on the principles of maximum likelihood and data fusion. An important conclusion reached is that, if 'a priori' likelihoods can be generated, then the order of search chosen can directly affect both the result and the computational load. It is suggested that this approach is currently a much undervalued method of exploiting 'a priori' knowledge.

A robust 'near optimal' Maximum Likelihood algorithm, IMP, based on the computationally efficient directed search, has been developed. The technique eliminates the well known limitations on resolution caused by sidelobe leakage. The basic concept contrasts with that of existing techniques which do not allow for the inherent variability of sensor calibration. The challenge is to develop the methodology and evolve complimentary hardware and software for real applications.

REFERENCES.

1   Schmidt RO. Multiple emitter location and spectral parameter estimation, Proc RADC Spectrum Estimation workshop, pp 243–258, 1979.
2   Clarke IJ. Robustness of eigen based analysis techniques versus iterative adaptation, RADAR 87 IEE Conference Publication No. 281, pp 84–88, 1987.
3   Clarke IJ. High discrimination detection bound and model order control. SPIE Conference Proceedings, Vol. 975, San Diego, 1988.
4   Mather JL. A Monte Carlo performance analysis of accelerated SVD-based high discrimination algorithms, Memo no 4083, RSRE, Malvern, England.
5   Nickel U. Angle estimation with adaptive arrays and its relation to super-resolution, IEE PROC H, 134, pp 77–82, 1987.
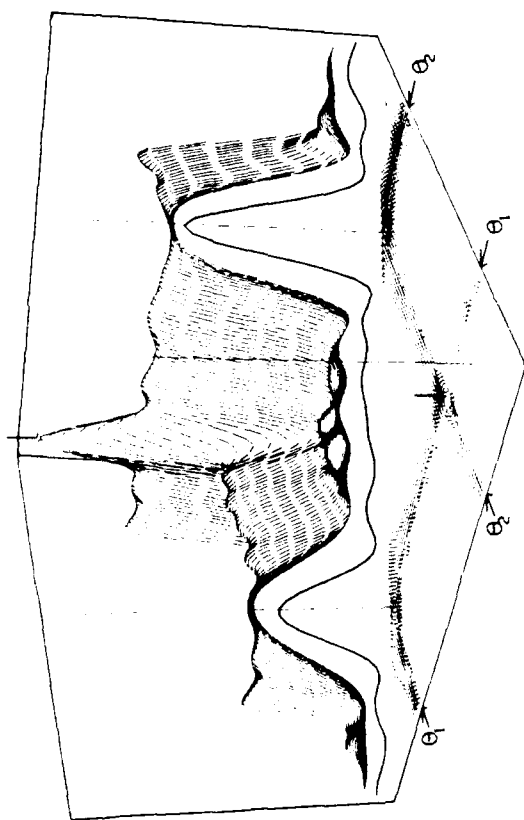
Figure 1. Example of a rank two spectral estimate, where the vertical scale corresponds to S_{md} and is linear in the weighted squares metric. θ_1 and θ_2 are emitter parameters used in generating simulated data (10 frames) from a linear antenna array.
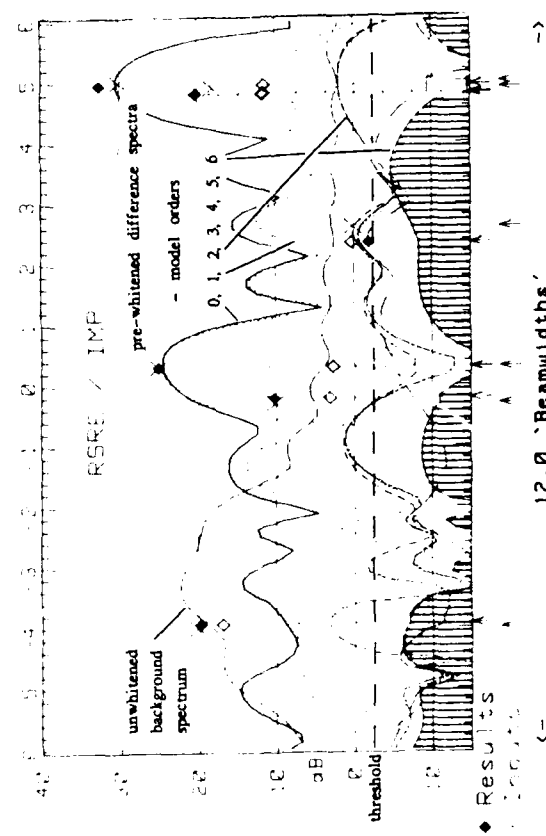

Figure 2. Weighted least mean squares residue spectra at model orders 0,1...6 as used in the IMP incremental multistage parametric decomposition algorithm showing the progressive whitening process.

BISPECTRAL ANALYSIS OF THE EEG IN DEVELOPING RATS

Taikang Ning and Joseph D. Bronzino

Department of Engineering and Computer Science,
Trinity College, Hartford, CT 06106

Abstract:

Bispectral analysis was applied to the electroencephalogram (EEG) recorded from the frontal cortex and hippocampus of the rat brain to examine the presence of quadratic phase coupling, as well as its deviation from Gaussian distribution during different vigilance states. Bispectra of these EEGs were computed for normally developing rats at different ages. At almost all ages it was found that significant phase coupling occurred within the hippocampal formation during REM sleep between the frequency components associated with theta rhythm. It was also observed that deviations from Gaussianity of the cortical EEGs follow a consistent ordering with cortical EEGs recorded during slow wave sleep having greater deviations from Gaussianity than quiet waking and REM sleep.

Introduction:

In recent years, the utilization of higher order spectra has increased in such diverse fields as radar, sonar, geophysics, and biomedicine, to extract useful information not obtainable form the second order spectrum (power spectrum). Of particularmportance in higher order spectral analysis is the third order spectrum (bispectrum) [1]-[5], which by definition is the Fourier transform of the third order cumulant sequence. The theoretical background, computing algorithms and application perspectives of bispectrum has been well documented in the literature [1].

Currently, most quantitative methods for EEG analysis implicitly assume that the underlying random process follows a Gaussian distribution based on studies using the Kolmogorov-Smirnov test, chi-square goodness of fit test, and skewness and kurtosis [10]-[12]. In this study we utilized bispectrum to examine deviations from Gaussian distribution for EEGs collected from the hippocampus and the frontal cortex of rats at different ages during various vigilance states.

Although bispectrum serves many purposes it was computed and utilized in our study 1) to quantify any vigilant-state dependent deviations from Gaussianity and 2) to detect and quantify the presence of any quadratic phase coupling. Because a stationary Gaussian process has a zero bispectrum, the amplitude of the estimated bispectrum provides a quantitative measure of the degree of deviation from Gaussianity, In addition, the bispectrum is also capable of detecting the quadratic phase coupling, and its significance level can be further quantified using a bicoherence index, i.e., a normalized bispectrum. Recently in our laboratory we reported in using bispectral analysis of the hippocampal EEG during REM sleep that a strong phase coupling exists between frequency components associated with theta rhythm [8]. These studies provide important insights into the frequency content of the EEG obtained from different brain structures during various vigilance states.

Bispectrum Computation

Bispectra of the EEGs were computed using the direct approach of conventional methods [1].

a) divide the EEG of each vigilance state into epoch of 1024 samples $\{x^l(n):$
$n=1,\ldots1024,\ 1=1,\ldots L\}$ (1 indicate the eth epoch).

b) compute the FourierMtransform of $\{x_1(n)\}$ to obtain $\{X_1(w)\}$.

c) estimate bispectrum

$$B(\omega_1,\omega_2) = \frac{1}{L}\sum_{l=1}^{L} X_l(\omega_1)X_l(\omega_2)X_l^*(\omega_1+\omega_2) \tag{1}$$

where * denotes the complex conjugate. Because of the utilization of FFT in step

b), the computation time is much shorter when compared against the indirect approach. If peaks (possible presence of quadratic phase coupling) were observed in the estimated bispectra, a bicoherence index was computed to indicate their significance levels. The index is a function consisting of bispectrum, B(w1,w2), and the power spectrum, P(w), i.e.,

$$bic(\omega_1,\omega_2) = \frac{B(\omega_1,\omega_2)}{P(\omega_1)P(\omega_2)P(\omega_1+\omega_2)} \quad (2)$$

To quantify the non-Gaussianity of the EEGs, the sum of the magnitudes of the estimated bispectrum was adopted as a measure, i.e.,

$$D = \sum_{(\omega_1,\omega_2)} |B(\omega_1,\omega_2)| \quad (3)$$

Results and Discussion

EEGs were recorded from the hippocampus and the frontal cortex of chronically implanted, freely moving rats during the following vigilance states: quiet waking (QW), slow-wave sleep 1 and 2 (SWS-1, SWS-2), and rapid-eye-movement (REM) sleep (see Fig. 1). These EEGs were sampled at 128 Hz and digitized into 8 second epochs and each epoch was manually scored by experts as one of four different vigilance states mentioned above. During the study, EEGs were collected from normally developing rats at five different ages, i.e., 14, 18, 22, 30 and 45 days old, respectively. Thirty two epochs of each vigilance state were scored and analyzed for each animal.

Using the deviation measure defined in equation (3), the bispectra revealed that the EEGs collected from the frontal cortex at all the ages mentioned above show a consistent ordering with respect to its deviation from a Gaussian distribution (see Table 1), that is

SWS-2 > SWS-1 > QW > REM

This observation was consistent with the results reported for adult rats in [8]. There was only one expection to the rule. For the 14 days old rat the EEG shows, a slightly larger deviation from Gaussianity during REM sleep than QW, although the difference was small. Bispectra measures also show that hippocampal EEGs in general deviate from Gaussian distribution during SWS more than that of QW and REM sleep (see Table 2). Thus, the bispectrum approach provides a quantitative approach to differentiate the relative nature of the distributions of the EEGs obtained during above vigilance states in the developing animals.

Our results also showed that the bispectra of hippocampal EEGs during REM sleep exhibit a significant phase coupling between frequencies in the theta range (5 to 8 Hz) at all ages except one (see Fig. 2). The computed bicoherence index at those observed peaks were summarized in Table 3. The phase coupling occurred for hippocampal EEG during REM sleep may indicate that the theta rhythms generated at the sites of CA1 and dentate gyrus in the hippocampus interacted and produced higher frequency components.

In conclusion, the results indicate that the bispectral analysis of the EEG can reveal extra information not obtainable from the power spectrum and may provide insights regarding the formation of the EEG within different brain structures during various vigilance states as the animal matures.

REFERENCES

[1] C. L. Nikias and M. R. Raghuveer, "Bispectrum Estimation: A Digital Signal Processing Framework," Proc. IEEE, vol.75, pp.869-891, July 1987.

[2] M. R. Raghuveer and C. L. Nikias, "Bispectrum Estimation: A Parametric Approach," IEEE Trans. Acous. Speech, Sig. Proc., vol. ASSP-33, no.5, pp.1213-1230, 1985.

[3] M. Rosenblatt and J. W. Van Ness, "Estimation of the Bispectrum," Ann. Math. Stat., vol.36, pp.1120-1136, 1965.

[4] J. W. Van Ness, "Asymptotic Normality of Bispectral Estimates," Ann Math. Stat., vol.37, pp.1257-1272, 1966.

[5] D. R. Brillinger, "An Introduction to Polyspectra," Ann. Math. Stat., vol.36, pp.1351-1374, 1965.

[6] P. J. Huber, B. Kleiner, T. Gasser, and G. Dumermuth, "Statistical Methods for Investigating Phase Relations in Stationary Stochastic Process," IEEE Trans. Audio and Electroacoustics, vol.AU-19, pp.78-86, 1971.

[7] T. Ning and J. D. Bronzino, "Bispectral Analysis of the EEG during Various Vigilance States," Proc. of the Ninth Annual IEEE-EMBS Conf., vol.2, pp.943-944, 1987.

[8] T. Ning and J. D. Bronzino, "Bispectral Analysis of the Rat EEG During Various Vigilance States," IEEE Trans. Biomed. Eng., vol.36, no.4, pp.497-499, 1989.

[9] G. Dumermuth, "Fundamentals of Spectral Analysis in Electroencephalography," in A Didactic Review of Methods and Application of EEG Data Processing, edited by A. Remond, Elsevier/North-Holland Biomedical Press, pp.83-105, 1977.

[10] J. A. McEwen, and G. B. Anderson, "Modeling the Stationarity and Gaussianity of Spontaneous Electroencephalographic Activity," IEEE Trans. Biomed. Eng. , vol. BME-22, pp.361-369, 1975.

[11] J. Persson, "Comments on Estimations and Tests of EEG Amplitude Distributions," Electroenceph. Clin.JNeurophysiol., vol.37, pp.309-313, 1974.

[12] H. Sugimoto, N. Ishii, A. Iwata, and N. Suzumura, "On the Stationarity and Normality of the Electroencephalographic Data During Sleep Stages," Computer Programs in Biomedicine, vol.8 pp.224-234, 1978.

[13] M. Grewal, T. Ning and J. D. Bronzino, "Coherence Analysis of EEG via Multichannel AR Modeling," Proc. of the 14th Northeast Bioengineering Conference, Durham, N.H. March, 1988.
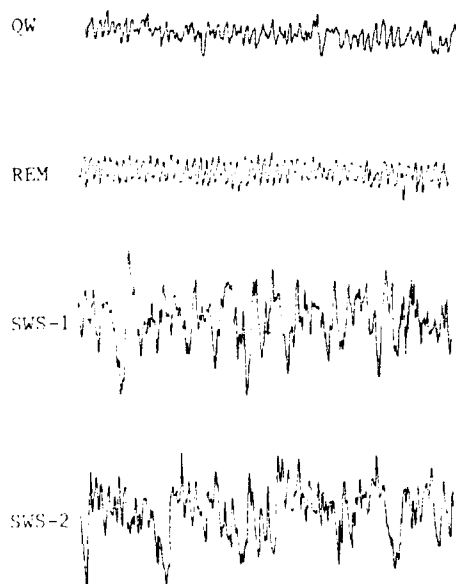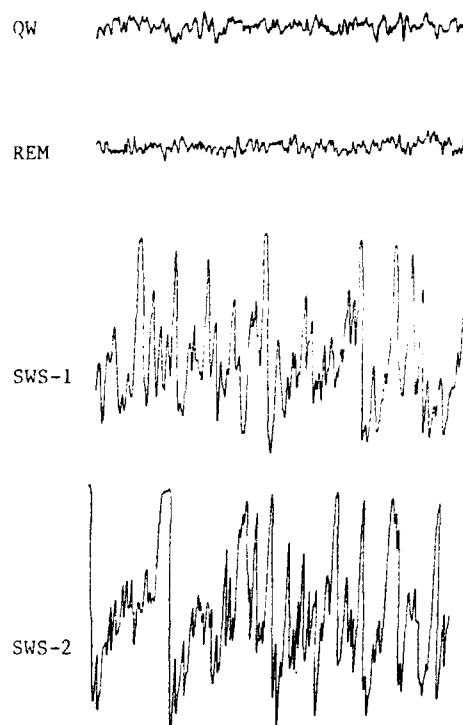
Figure 1.b: Cortical EEG
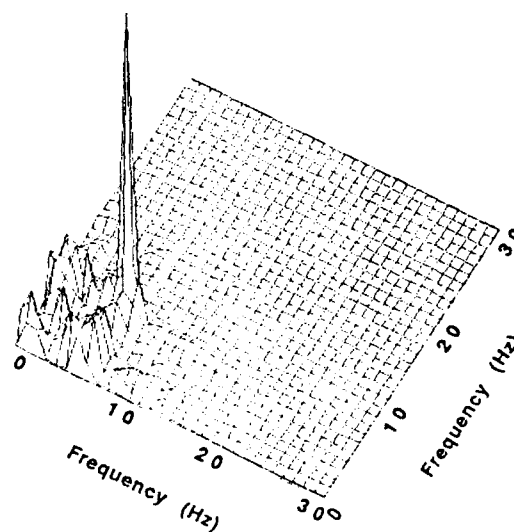

Figure 1.a:Hippocampal EEG

Figure 2: Bispectrum of Hippocampal EEG during REM Sleep

237

Table 1. Deviation from Gaussianity of the Cortical EEG

vig. \ ages	REM	QW	SWS-1	SWS-2
14	.899E+3	.587E+3	.938E+3	.118E+4
18	.215E+3	.640E+3	.230E+4	.395E+4
22	.104E+3	.327E+3	.176E+4	.446E+4
30	.135E+2	.353E+2	.344E+3	.662E+3
45	.228E+2	.155E+3	.439E+4	.638E+4

Table 2. Deviation from Gaussianity of the Hippocampal EEG

vig. \ ages	REM	QW	SWS-1	SWS-2
14	.236E+3	.345E+3	.411E+3	.386E+3
18	.214E+3	.167E+4	.314E+4	.304E+4
22	.559E+3	.505E+3	.896E+3	.812E+3
30	.135E+3	.116E+3	.455E+3	.389E+3
45	.573E+2	.863E+2	.286E+3	.397E+3

Table 3. Bicoherence Index for Hippocampal EEG during REM Sleep

ages \ dg. coup.	14	18	22	30	45
freq. pair	(5,5)	None	(6,6)	(7,7)	(7,7)
bicoherence	.42	None	.85	.73	.64

STOCHASTIC IMAGE MODELING USING CUMULANTS
WITH APPLICATION TO PREDICTIVE IMAGE CODING

T.E. Hall, and S.G. Wilson

Department of Electrical Engineering
University of Virginia
Charlottesville, VA 22901

Abstract

Stochastic image representation techniques traditionally rely upon second-order image statistics to determine the model parameters. This paper reports on the use of third-order cumulant statistics to implement non-causal, phase sensitive ARMA image models. A novel, linear equation based 2-D MA parameter estimation algorithm is extended from an existing 1-D algorithm, for modeling colored prediction-error residuals, and is used in conjunction with a non-causal 2-D ARMA parameter estimation algorithm. A weighted least-squares MA approach is also developed as has been done in the 1-D case. Application of cumulant-based stochastic image representations to predictive image coding is discussed and preliminary results using causal and noncausal ARMA predictors are presented.

1. Introduction

Stochastic image representations have found application in many areas of image processing such as data compression, restoration, spectral estimation, texture analysis and synthesis, and classification [9,p.190]. These representations characterize the image as a random field, which is modeled as the output of a 2-D linear system whose input is a random noise field, either white or colored. Depending on the nature of the input noise, stochastic image representations are categorized as minimum variance (MVR), white noise driven (WNDR), or autoregressive moving average (ARMA) [9,p.207]. Current parameter estimation techniques use the first- and second-order statistics of images so that the representation realizes the covariance properties of the process, or equivalently, its spectral density function. The associated normal equations are employed to solve for the coefficients of the model [1-3]. But autocorrelation statistics fail to convey complete phase information and cannot provide an adequate statistical description of non-Gaussian linear processes.

Recent research has shown that higher- than second-order statistics, which are phase sensitive, can be used to estimate general non-minimum phase and asymmetric non-causal parametric image models, [7,8]. These techniques attempt to match the image model to higher-order spectra of the process

rather than just the power spectrum, and as such they can be used to model a much broader class of image representations. In particular, predictive image coding is based upon the use of 2-D stochastic linear image representations to construct image predictors with which to remove redundancy from an image. The design of a predictive coding system is basically a parametric modeling problem, and higher-order statistics can be used to derive linear predictors which take into account the phase characteristics and non-causal dependencies among the pixels of an image.

This paper reviews and extends the 2-D modeling results of [7] and [8], and illustrates the potential application of third-order statistics for differential pulse code modulation (DPCM) predictive image coding (see also [12]). Section 2 describes the parameter estimation algorithms of the cumulant-based stochastic image representations. A novel 2-D MA parameter estimation algorithm is described in 2.2, by extending the 1-D algorithm described in [10]. In section 2.3, a weighted least-squares version of the 2-D MA algorithm is developed along the lines of [11], where the 1-D case was considered. Section 2.4 reviews the non-causal ARMA algorithm presented in [7], and discusses how it can be used in conjunction with the MA algorithms of sections 2.2 and 2.3 to reduce the numerical sensitivity of the parameter estimation. Section 3 outlines the implementation of cumulant-based stochastic image representations as linear predictors in both closed-loop and open-loop DPCM image coding systems. Section 4 provides simulation results.

2 Stochastic Image Modeling Using Cumulants

Let $y(m) = y(m,n)$ represent a zero-mean real-valued stationary random field, given by

$$y(n) = -\sum_{\substack{k \in N_a \\ k \neq (0,0)}} a(k) y(n-k) + \sum_{k \in N_b} b(k) w(n-k) \qquad (1)$$

$$N_a = [-M_1^a, M_2^a] \times [-N_1^a, N_2^a], \quad N_b = [-M_1^b, M_2^b] \times [-N_1^b, N_2^b].$$

It will be assumed that the input excitation $w(m)$ is zero mean, non-Gaussian and i.i.d. and that the model is exponentially

stable. Then the second, third, and fourth-order cumulants of $y(m)$ are given by

$$C_{2y}(i) \equiv E[y(m)y(m+i)], \tag{2}$$

$$C_{3y}(i,j) \equiv E[y(m)y(m+i)y(m+j)], \tag{3}$$

$$C_{4y}(i,j,k) \equiv E[y(m)y(m+i)y(m+j)y(m+k)]$$
$$- C_{2y}(i)C_{2y}(j-k) - C_{2y}(j)C_{2y}(k-i) - C_{2y}(k)C_{2y}(i-j). \tag{4}$$

Given a finite record of the 2-dimensional process, $y(n)$, $n \in N_y$, sample estimates of cumulants are obtained by replacing the expectation operator by sample averaging (ergodicity is implicitly assumed); thus,

$$\hat{C}_{3y}(m,n) = (n\{N_y\})^{-1} \cdot \sum_i y(i)y(i+m)y(i+n) \tag{5}$$

where $n\{N_y\}$ is the number of samples in the segment N_y. In this paper, we will focus on parameter estimation algorithms employing third-order cumulants.

2.1. Causal AR Parameter Estimation

If the model of (1) is causal, then the AR parameters satisfy the following recursions for both autocorrelation and third-order cumulants [7],

$$\sum_{k \in N_a} a(k)C_{2y}(k-m) = 0, \quad m \notin N_b. \tag{6}$$

$$\sum_{k \in N_a} a(k)C_{3y}(k-i,k-j) = 0, \quad i \notin N_b \text{ and/or } j \notin N_b. \tag{7}$$

Therefore, the $a(k)$'s can be obtained as the solution to an overdetermined system of equations using (6) and/or (7). The inclusion of the cumulant-based AR parameter solution allows for all-pass factors in the transfer function of the image model. As in the correlation-based 2-D case, the solution is not guaranteed to be stable in practice, and models of increasing orders are computed to find a stable one.

2.2. MA Parameter Estimation

In order to estimate the MA parameters of the ARMA image representation, the estimated AR parameters are used to compute the residual (i.e., AR compensated) image

$$y(m) - \sum_{i \in N_a} a(i)y(m-i) = \sum_{i \in N_b} b(i)w(m-i). \tag{8}$$

The AR compensated image is now considered as a 2-D MA process and the 2-D extension of the equations in [10] (see also [11]), yield (see Appendix A)

$$\sum_{i \in N_b} b(i)b(i+m_0)C_{2y}(m-i) + \sum_{i} b(i)C_{3y}(m-i,m+m_0-i), \tag{9}$$

$$m \in [-M^b, 2M^b] \times [-N^b, 2N^b], \quad m_0 \in [-M^b, M^b] \times [-N^b, N^b]$$

$$= \frac{E[w^3(m)]}{E[w^2(m)]}, \quad M^b = M_1^b + M_2^b, \quad N^b = N_1^b + N_2^b$$

To obtain estimates of the unknown parameters, an overdetermined system of linear equations can be constructed by con-

catenating (9) for each $m \in [-M^b, 2M^b] \times [-N^b, 2N^b]$. In order to simplify computation, the term m_0 is chosen to be 0 so that only diagonal moments are used. The novelty of the above algorithm is that it can estimate the parameters of a non-minimum phase 2-D MA process with non-Gaussian excitation. Note that the equations are over-parameterized, since $b^2(i)$ appears in the solution vector of (10) as a free parameter. Finally, the algorithm can provide an MA characterization for the colored residuals normally associated with MVR's, [7].

2.3. Weighted Least Squares MA Parameter Estimation

The matrix equation in (9) can expressed in the form,

$$[A(s)]\theta = b(s).$$

where θ is the unknown parameter vector and s is a vector consisting of the statistical moments,

$$s^t = [C_{2y}(n) \cdots C_{3y}(m,m) \cdots].$$

$$n \in [0,M^b] \times [0,N^b], \quad m \in [-M^b,M^b] \times [-N^b,N^b]$$

and $A(s)$ and $b(s)$ are matrix and vector functions of s respectively. The weighted least squares (WLS) estimate of θ is

$$\hat{\theta}^{(W)} = ([A(\hat{s})]^T W [A(\hat{s})])^{-1}[A(\hat{s})]^T W b(\hat{s}), \tag{10}$$

where $\hat{s}$ is the vector of sample moments. The weighting matrix which achieves the minimum variance estimate of θ among the class of estimates $\hat{\theta}^{(W)}$ is given by [11].

$$W = [\hat{D}\,\hat{\Sigma}\,\hat{D}^T]^{-1}$$

where $\hat{D}$ is a matrix whose i-th column is,

$$[\hat{D}]_i = \frac{\partial b(s)}{\partial s_i} - \frac{\partial A(s)}{\partial s_i}\hat{\theta}^{(I)}$$

and $\hat{\Sigma}$ is a consistent estimate of asymptotic normalized covariance matrix if $\hat{s}$. The initial parameter estimate $\hat{\theta}^{(I)}$ is found by solving (10) for $W = I$.

2.4. Non-causal ARMA Parameter Estimation

In deriving (6) and (7), it was necessary to assume that the representation was causal. But causality is not inherent in the structure of the image itself, and a non-causal support region (N_a arbitrary) would be appropriate for a more general image representation. Therefore, for non-causal parameter estimation, the algorithm described in [7] is used. Briefly, it can be shown that,

$$\sum_{i,j \in N_a} a(i,j)C_{3y}(m-i,n-j) = \gamma_{3w}\beta(m,n), \tag{12}$$

$$= 0 \quad \text{if } m \notin N_\beta \text{ or } n \notin N_\beta, \tag{13}$$

where

$$N_a = [-M^d, M^d] \times [-N^d, N^d], \quad N_\beta = [-M^b, M^b] \times [-N^b, N^b],$$
$$M^d = M_1^d + M_2^d, \quad N^d = N_1^d + N_2^d,$$

and,

$$\alpha(m;n) = \sum_{i \in N_a} a(i)a(i+m)a(i+n),$$ (14a)

$$\beta(m;n) = \sum_{i \in N_b} b(i)b(i+m)b(i+n).$$ (14b)

A system of linear equations can be constructed from (13), and used to solve for the unknown $\alpha(m,n)$ parameters. After having determined the $\alpha(m,n)$'s, (12) can be used to solve for the $\beta(m,n)$ terms. Then, the non-causal ARMA parameters can be obtained in closed form as

$$a(n) = \frac{\alpha(p,n)}{\alpha(p,0)}, \quad b(n) = \frac{\beta(q,n)}{\beta(q,0)},$$ (15)

$$p = (M^a, N^a), \quad q = (M^b, N^b).$$

The closed form expressions for the AR (MA) parameters in (15) make use of only the cumulants that are part of the p-slice (q-slice) of the region of support N_α (N_β), of the AR (MA) parameter cumulants. But the solutions of (12) and (13) provides the parameter cumulants over the entire regions of support, respectively. It was observed in [7] that any consistent MA parameter identification algorithm may be used to estimate the AR and MA parameters from (14a) and (14b). Therefore, if the MA estimation algorithm of Section 2.2 is used, the parameter estimates will be based upon the parameter cumulant samples over the entire support region, rather than just one slice. The 1-D counterpart of this approach is described in [13]. The advantage of this method over the closed form expressions of (15) is that all the parameter cumulant samples are utilized by the estimation algorithm. This helps to reduce the numerical sensitivity of the algorithm and provides improved esimates if the sample cumulants are noisy. In addition, the optimal WLS MA estimation algorithm previously described could be used to further refine the AR and MA estimates with respect to the parameter cumulants.

4. Application to predictive image coding

This section deals with the potential application of cumulant-based 2-D modeling approaches to predictive image coding. Linear predictors are constructed using the ARMA model of (1) where $w(n)$ is now considered a prediction-error residual. It is expected that the phase sensitive cumulant-based predictors will characterize the image redundancy better than their 2nd order counterparts. These predictors are used in two different DPCM image coding systems, depending whether the model is causal or non-causal. The first scheme uses a causal ARMA model in a closed loop DPCM system shown in Figure 1. Since the predictor is inside the feedback loop with the quantizer, it is well known that the reconstruction error $r(n)$ is equal to the quantization error $q(n)$, i.e.,

$$r(n) = x(n) - \hat{x}(n) = w(n) - \hat{w}(n) = q(n).$$

In the second scheme, the AR part of the ARMA model is non-causal and therefore it is necessary to use the more general

open-loop DPCM system shown in Figure 2. This also means that the AR part of the reconstruction filter in the encoder must be implemented by truncation. Assuming the trucation error is negligible, then the following Z-domain relationship can be readily established between the reconstruction and quantization error,

$$R(z_1,z_2) = Q(z_1,z_2) \frac{B(z_1,z_2) - F(z_1,z_2)}{A(z_1,z_2)}.$$

where $A(z_1,z_2)$ and $B(z_1,z_2)$ are the Z-transforms of the AR and MA parameters respectively, and $F(z_1,z_2)$ is the transfer function of the quantization error feedback filter. Suppose now that $A_c(z_1,z_2)$ is the spectrally equivalent minimum phase (SEMP) model of $A(z_1,z_2)$. Then if $F(z_1,z_2)$ is defined to be,

$$F(z_1,z_2) = B(z_1,z_2) - A_c(z_1,z_2).$$

it follows that,

$$S_{2r}(u,v) = S_{2q}(u,v),$$

where $S_{2r}(u,v)$ and $S_{2q}(u,v)$ are the spectral densities of $r(n)$ and $q(n)$ respectively. Therefore, by appropriate filtering of the quantization error, an equivalence can be established between the spectra of the reconstruction and quantization errors in an open-loop DPCM system, even though pointwise the two errors are no longer necessarily equal.

5. Simulations

In order to demonstrate the usefulness of cumulant-based image modeling, we generated a 256×256 ARMA image by using zero mean, i.i.d. noise from an exponential distribution with parameter $\lambda = 0.2$, as input to a system with the following transfer function, [12],

$$H(z_1,z_2) = \frac{1}{(1-0.6z_1^{-1})(1-0.9z_2^{-1})} \times \frac{1-1.25z_1^{-1}}{1-0.8z_1^{-1}}$$

$$= \frac{1-1.25z_1^{-1}}{1-1.4z_1^{-1}-0.9z_2^{-1}+1.26z_1^{-1}z_2^{-1}+0.432z_1^{-2}z_2^{-1}+0.48z_1^{-2}}.$$

Note that the transfer function is separable and contains an all-pass factor. The parameters of the image model are estimated using both autocorrelation-based and cumulant-based parameter estimation procedures and displayed in Table 1. The autocorrelation-based procedure (7) identifies the minimum phase part of the model but fails to characterize the all-pass factor. In contrast, the cumulant-based procedure (8), followed by the MA parameter estimation algorithm of the AR compensated image, estimates the true non-minimum phase transfer function.

Parameter estimation was also performed on images generated from causal ARMA(8,3) and non-causal AR(8), ARMA(8,3) image models, as described in the previous paragraph. The support regions for these models is shown in Figure 3. The results of these simulations, shown in tables 2-4,

indicate reasonably close agreement between the estimated parameters and the true values. Table 3 also illustrates the advantage of using the 2-D MA estimation algorithm on all the sample parameter cumulants, rather than the closed form expressions (15) of Section 2.4. In this case, the generated image was 128×128 and the cumulant estimates were noisier due to reduced sample averaging.

Finally, the image models of Figure 3 were used as the bases for estimating the linear predictor coefficients of a real-world image, the 256×256 "Lena" image with 8 bits/pixel resolution. The coefficients were derived by modeling the image in turn with causal/non-causal AR(8) and causal ARMA(8,3) image models. Predicted images were then generated by using the true pixel values in the AR part of the model (1). For comparison, a predicted image using an autocorrelation-based MVR is also displayed. It can be seen that the cumulant-based predictions are subjectively sharper, with better definition of edge detail than the autocorrelation-based prediction. Although the cumulant-based predictions are not optimal in the mean-square error sense, it is well known that this is not necessarily a valid measure of image fidelity.

6. Conclusions

Cumulant statistics can be used to provide phase sensitive, asymmetric non-causal, and non-Gaussian image representations. A novel, linear equation based MA parameter estimation algorithm is described which is potentially useful for modeling colored prediction error residuals. A WLS version of the MA algorithm was presented has minimum asymptotic variance in the class of WLS algorithms. The use of this algorithm in conjunction with the non-causal ARMA estimation algorithm of [7] provides more efficient parameter estimation. The application of third-order cumulant-based stochastic image models to predictive coding was discussed and preliminary results using causal and non-causal ARMA predictors were presented. Further investigation is necessary to assess the potential for cumulant-based non-causal, non-minimum phase ARMA modeling for purposes of predictive image coding.

Acknowledgement: The author would like to thank Dr. Georgios Giannakis and members of his research group for helpful discussions. The support provided by the National Science Foundation and Harry Diamonds Labs contract 5-25227 was also greatly appreciated.

REFERENCES

[1] N. S. Jayant and Peter Noll, *Digital Coding of Waveforms*, Chapter 6, Prentice-Hall, 1984.

[2] C W. Therrien, T. F. Quatieri, and D. E. Dudgeon, "Statistical Model-Based Algorithms for Image Analysis," *Proc. IEEE*, vol. 74, pp.532-551, April 1986.

[3] A. K. Jain, "Advances in Mathematical Models for Image Processing," *Proc. IEEE*, v. 69, pp.502-528, May 1981.

[4] C. L. Nikias and M. R. Raghuveer, "Bispectrum Estimation: A Digital Processing Framework," *Proc. IEEE*, vol. 75, pp.869-891, July 1987.

[5] A. L. Kok, D. G. Manolakis, and V. K. Ingle, "Efficient Algorithms for 1-D and 2-D Noncausal Autoregressive System Modelings," *Proc. ICASSP*, pp. 1977-1980. Dallas, April 1987.

[6] A. V. Oppenheim and J. S. Lin, "The Importance of Phase in Signals," *Proc. IEEE*, vol. 69, pp.529-541, 1981.

[7] A. Swami, G.B. Giannakis, and J.M. Mendel, "Modeling of Multidimensional Non-Gaussian Processes Using Cumulants," submitted to *Proc. IEEE*, Special Issue on Multidimensional Signal Processing, Jan. 1989.

[8] G.B. Giannakis, "Cumulants In Identification of Causal and Non-Causal 1-D (time series) and 2-D (image) ARMA Models," *Proc. of Conf. on Information Sciences and Systems*, Johns Hopkins Univ., Baltimore, MD., 1987

[9] A.K. Jain, *Fundamentals of Digital Image Processing*, Prentice-Hall, 1989.

[10] G.B. Giannakis, and J.M. Mendel, "Identification of Non-Minimum Phase Systems using Higher-Order Statistics," *IEEE Trans. ASSP*, v. 37, pp. 360-377, 1989.

[11] B. Friedlander and B. Porat, "Optimal estimates of MA and ARMA parameters of non-Gaussian processes from higher-order cumulants," *Proc. 4th ASSP Workshop on Spec. Est. & Model.*, pp. 208-212, Minneapolis, MN., 1988.

[12] T.E. Hall, G.B. Giannakis, and S.G. Wilson, "Predictive Image Coding Using Cumulant- Based Causal and Non-Causal AR/ARMA Models," *Proc. of Conf. on Information Sciences and Systems*, Johns Hopkins Univ., Baltimore, MD., 1989

[13] M. Rangoussi and G.B. Giannakis, "On The Use of Second- and -Higher-Order Inverse Statistics," *Proc. of Workshop on Higher-Order Spectral Analysis*, Vail, Colorado, 1989

Appendix A. 2-D MA Parameter Estimation

In this appendix we derive the 2-D extension of the MA parameter estimation algorithm of [10]. Let $y(n)$ be the output of a linear shift-invariant, causal, exponentially stable, 2-D system $h(i)$, which is driven by an i.i.d. random input $w(n)$ with 3rd-order cumulant γ_{3w} and variance σ^2, i.e.,

$$y(n) = \sum_{i \in N_n} h(i)w(n-i)$$

where N_n is the nonsymmetric half-plane. Then, [7],

$$C_{3y}(m_1, m_2) = \gamma_{3w} \sum_i h(i)h(i+m_1)h(i+m_2). \qquad (A1)$$

In the Z-domain,

$$S_{3y}(z_1, z_2; m_2) = \gamma_{3w} \sum_{m_1} \left[\sum_i h(i)h(i+m_1)h(i+m_2) \right] z_1^{-m_1} z_2^{-m_1}$$

$$= \gamma_{3w} \sum_i h(i) \left[\sum_{m_1} h(i+m_1)h(i+m_2)z_1^{-(i+m_1)} z_2^{-(i+m_1)} \right] z_1^i z_2^i$$

$$= \gamma_{3w} H(z_1^{-1}, z_2^{-1}) H_2(z_1, z_2; m_0). \qquad (A2)$$

where $m_0 = m_2 - m_1$, and

$$H_2(z_1, z_2; m_0) = \sum_n h(n)h(n+m_0)z_1^{-n} z_2^{-n_2}$$

$$= H(z_1, z_2) ** z_1^{m_{o1}} z_2^{m_{o2}} H(z_1, z_2)$$

and ** denotes 2-D complex convolution. The counterparts for 2-D autocorrelation and spectrum are,

$$C_{2y}(\mathbf{m}_1) = E[y(i)y(i+\mathbf{m}_1)] = \sigma^2 \sum_i h(i)h(i+\mathbf{m}_1). \quad (A3)$$

and

$$S_{2y}(z_1, z_2) = \sigma^2 H(z_1^{-1}, z_2^{-1}) H(z_1, z_2). \quad (A4)$$

Combining (A2) with (A4) and letting $\varepsilon = \dfrac{\sigma^2}{\gamma_{3w}}$,

$$S_{2y}(z_1, z_2) H_2(z_1, z_2; \mathbf{m}_0) = \varepsilon H(z_1, z_2) S_{3y}(z_1, z_2; \mathbf{m}_2), \quad (A5)$$

In the case of a linear shift-invariant 2-D MA model, the impulse response is finite and corresponds to the MA coefficients. Then the time-domain version of (A5) for the MA process may be written,

$$\sum_{i \in N_b} \beta(i, \mathbf{m}_0) C_{2y}(\mathbf{m}_1 - i) = \varepsilon \sum_{i \in N_b} h(i) C_{3y}(\mathbf{m}_1 - i, \mathbf{m}_2 - i)$$

where

$$\beta(i, \mathbf{m}_0) = h(i) h(i + \mathbf{m}_0).$$

FIGURE 1

C - causal
NC - noncausal
SEC - spectrally equiv. causal

ENCODER

DECODER

FIGURE 2

ENCODER

DECODER
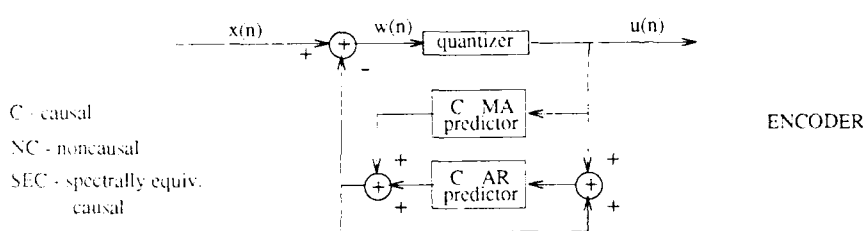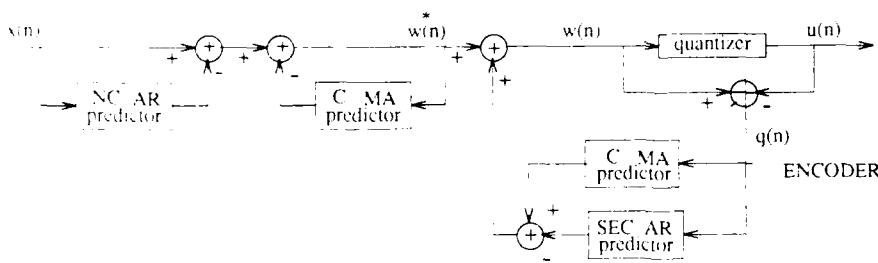
Table 1

ARMA (5,1) image model					
	AR coef.				MA coef.
True	-1.400	-0.900	1.260	-0.432	0.480	-1.250
$\hat{C}$	0.589	-0.894	0.526	-0.001	0.002	...
$\hat{C}$	-1.361	-0.897	1.217	-0.439	0.474	-1.213

Table 2

Causal ARMA(8,3) Parameters		
Coeff.	True	Est.
AR(8)	-0.800	-0.770
	1.000	1.025
	-0.700	-0.733
	0.300	0.264
	-0.380	-0.359
	0.150	0.214
	-0.250	-0.319
	0.200	0.260
MA(3)	-1.250	-1.177
	1.800	1.720
	-1.700	-1.552

Table 3

Non-Causal AR(8) Parameters		
True	Estimated	
	Clsd. Frm.	MA Alg.
-0.273	-0.417	-0.257
0.137	0.291	0.138
-0.356	-0.421	-0.347
0.164	0.122	0.150
-0.520	-0.417	-0.516
0.274	0.222	0.255
-0.425	-0.465	-0.425
0.103	0.146	0.081

Table 4

Non-Causal ARMA(8,3) Parameters		
Coeff.	True	Est.
AR(8)	-0.273	-0.295
	0.137	0.167
	-0.356	-0.326
	0.164	0.120
	-0.520	-0.500
	0.274	0.294
	-0.425	-0.333
	0.103	0.067
MA(3)	-1.000	-1.084
	3.000	4.342
	-2.000	-2.261

FIGURE 3

Causal AR(8)   Non-causal AR(8)   Causal MA(3)
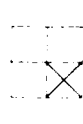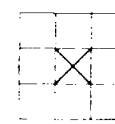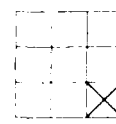
= Current pixel (m,n)

FIGURE 4

Original Image

Cumulant-Based ARMA(8,3) Model

Autocorrelation-Based AR(8) Model

Cumulant-Based Non-Causal AR(8) Model

Cumulant-Based AR(8) Model

ASYMPTOTICALLY OPTIMAL ESTIMATION OF MA AND ARMA PARAMETERS OF NON-GAUSSIAN PROCESSES FROM HIGH-ORDER MOMENTS

Benjamin Friedlander
Signal Processing Technology, Ltd.
703 Coastland Drive
Palo Alto, CA 94303
USA

Boaz Porat
Technion-Israel Institute
of Technology
Dept. of Electrical Engineering
Haifa 32000, Israel

Abstract

An asymptotically minimum-variance algorithm for estimating the MA and ARMA parameters of non Gaussian processes from sample high-order moments is described. The algorithm uses the statistical properties (covariances and cross-covariances) of the sample moments explicitly.

1. Introduction

Recent interest in parameter estimation of non Gaussian processes has led to some new parameter estimation algorithms, both batch-type and recursive. These algorithms use the third- (or fourth-) order sample cumulants, in addition to the sample covariances, to achieve several goals, such as: a) improve the accuracy of the estimated parameters; b) reduce the sensitivity to additive Gaussian noise; c) enable the estimation of non-minimum phase and/or non-causal processes. Some recent works on batch-type algorithms for parametric time-series are [1]–[4]. Examples of recursive algorithms are [5], [6].

The statistical accuracy of algorithms based on high-order statistics depends on the way in which the additional information is used. In [7], the statistical efficiency of some existing algorithms was explored. It was found that the algorithms discussed in [3] and [5] are not very efficient, in the sense that their asymptotic variance is rather high, compared to a certain lower bound. The paper [7] also showed, in principle, how the information in the high-order cumulants can be optimally exploited to attain asymptotically this lower bound.

The present work further expands the basic ideas presented in [7]. The statistical properties of the high-order cumulants are used to construct batch-type estimation algorithms for MA and ARMA processes. These algorithms are asymptotically minimum variance, in the class of algorithms based on the high-order moments.

In [8] we also describe algorithms of weighted least-squares type, with an optimal weight matrix. These algorithms do not achieve minimum variance performance,

but are computationally simpler than the minimum variance algorithms.

2. Minimum Variance Estimation Using the High-Order Moments

In this section we present some general results on the estimation of the parameters of stationary time series from high-order moments. In particular, we present an asymptotically minimum variance estimator, and discuss its statistical properties.

Let $\{y_t\}$ be a stationary and ergodic linear process, given by

$$y_t = \sum_k h_k u_{t-k} \quad , \qquad (2.1)$$

where $\{u_t\}$ is an i.i.d., non-Gaussian sequence of random variables. The impulse response sequence $\{h_k\}$ is assumed to depend on a parameter vector θ of fixed dimension. The impulse response is further assumed to be absolutely summable, i.e. $\sum_k |h_k| < \infty$.

Let us denote the moments of $\{u_t\}$ by

$$\gamma_k = Eu_t^k, \quad k \geq 1, \quad -\infty < \gamma_k < \infty. \qquad (2.2)$$

We assume that $\gamma_1 = 0$ for convenience.

Let $\mu_m(k_1, ..., k_{m-1})$ be the m-th order moment of y_t,

$$\mu_m(k_1, ..., k_{m-1}) = E\{y_t \prod_{i=1}^{m-1} y_{t+k_i}\}. \qquad (2.3)$$

Under the above assumptions, the moments of y_t of all orders are finite.

Assume we are given measurements of $\{y_t\}$ in the range $1 \leq t \leq N + K$, where K is a fixed integer. Let the m-th order sample moment $\hat{\mu}_m(k_1, ..., k_{m-1})$ be defined by

$$\hat{\mu}_m(k_1, ..., k_{m-1}) = \frac{1}{N} \sum_{t=1}^{N} (y_t \prod_{i=1}^{m-1} y_{t+k_i}), \qquad (2.4)$$

$$0 \leq k_{m-1} \leq ... \leq k_1 \leq K.$$

Each of the sample moments is an unbiased estimate of the corresponding statistical moment. This estimate

is also known to be consistent both in the mean-square and with probability one, i.e.

$$\lim_{N \to \infty} \hat{\mu}_m(k_1, ..., k_{m-1}) = \mu_m(k_1, ..., k_{m-1}) \quad \text{a.s.}$$
(2.5a)

$$\lim_{N \to \infty} E[\hat{\mu}_m(k_1, ..., k_{m-1}) - \mu_m(k_1, ..., k_{m-1})]^2 = 0.$$
(2.5b)

Let $\hat{s}$ denote a vector consisting of a fixed subset of sample moments as in (2.4), and let s be the corresponding vector of statistical moments as in (2.3). The problem we are concerned with is the estimation of the parameter vector θ from the vector $\hat{s}$, i.e.

$$\hat{\theta} = g(\hat{s}).$$
(2.6)

The asymptotic statistical properties of estimates of this type were discussed in detail in [7]. As was shown there, these properties depend on the asymptotic normalized covariance matrix of $\hat{s}$, given by

$$\Sigma(\theta) = \lim_{N \to \infty} N \cdot \left[E\left\{ \hat{s}\hat{s}^T \right\} - ss^T \right]$$
(2.7)

In particular, the asymptotic covariance of $\hat{\theta}$ was shown in [7] to be bounded from below as follows [7, Theorem 2]

$$\lim_{N \to \infty} N \cdot \text{cov}\{\theta\} \geq \left[\left(\frac{\partial s(\theta)}{\partial \theta} \right)^T \Sigma^{-1}(\theta) \left(\frac{\partial s(\theta)}{\partial \theta} \right) \right]^{-1}.$$
(2.8)

Furthermore, the lower bound (2.8) is asymptotically tight, i.e., there exists an estimate $\hat{\theta}$ whose asymptotic normalized covariance matrix satisfies (2.8) with equality. Such an estimate can be constructed as follows. For each vector x in the domain of θ, let

$$V(x) = [s(x) - \hat{s}]^T \Sigma^{-1}(x)[s(x) - \hat{s}].$$
(2.9)

Let $\hat{\theta}$ be the value of x for which $V(x)$ attains a global minimum (if a global minimum exists). This particular estimate achieves the lower bound (2.8) as $N \to \infty$ [7, Theorem 3].

Estimates obtained through minimization of (2.9) are difficult to implement. The main source of difficulty is the need to compute the matrix $\Sigma(x)$ as a function of the process parameters, at each iteration of the minimization procedure. Closed-form expressions for the entries of $\Sigma(x)$ were developed in [7], for the case where only $\hat{\mu}_2(k_1)$ and $\hat{\mu}_3(k_1, k_2)$ appear in $\hat{s}$. These expressions are very complicated, and would be considerably more complicated when the higher order moments are included. This difficulty essentially renders the algorithm based on the minimization of (2.9) impractical.

An alternative approach, is to replace $\Sigma(x)$ in (2.9) by an *estimate of this matrix, directly computed from the data*. Let $\hat{\Sigma}$ be such an estimate, and define

$$\hat{V}(x) = [s(x) - \hat{s}]^T \hat{\Sigma}^{-1}[s(x) - \hat{s}].$$
(2.10)

Let $\hat{\theta}$ be the value of x for which $\hat{V}(x)$ attains a global minimum (if a global minimum exists). Let us further assume that $\hat{\Sigma}$ is a consistent estimate of $\Sigma(\theta)$, θ being the *true* parameter vector. Then we have the following theorem.

Theorem 1: Under some regularity conditions on $\hat{\Sigma}$ (specified in [8]), the estimate $\hat{\theta}$ obtained through global minimzation of (2.10) has the asymptotic covariance given by the right-hand side of (2.8).

Proof: See [8].

Summing up, an asymptotically minimum variance estimate $\hat{\theta}$ can be obtained through global minimization of $\hat{V}(x)$ given in (2.10). For such an estimate to be possible, it is necessary to be able to compute a consistent estimate of $\Sigma(\theta)$, $\hat{\Sigma}$, from the measurements.

The estimation of $\Sigma(\vartheta)$ is discussed in the Appendix where an algorithm for computing $\hat{\Sigma}$ from the measurements is presented. Based on this estimate we derived practical algorithms for parameter estimation of MA and ARMA processes from high-order moments. Due to space limitations we defer many of the details to [8].

The Minimum Variance MA Algorithm

The estimation procedure involves the minimization of (2.10) using an iterative Gauss-Newton procedure. Having estimated $\hat{\Sigma}$ from the data, it remains to compute $s(x)$ and $\frac{\partial s(x)}{\partial x}$ (the latter is needed for the iterative update of x).

For MA processes we have

$$\mu_2(k) = \gamma_2 \sum_i b_i b_{i+k} ; \quad \mu_3(k, k) = \sum_i b_i b_{i+k}^2 ;$$

$$\mu_3(k, 0) = \gamma_3 \sum_i b_i^2 b_{i+k}$$
(2.11)

where the summations include all non-zero terms. Hence we get

$$\frac{\partial \mu_2(k)}{\partial b_\ell} = \gamma_2(b_{\ell+k} + b_{\ell-k});$$

$$\frac{\partial \mu_3(k, k)}{\partial b_\ell} = \gamma_3(b_{\ell+k}^2 + 2b_\ell b_{\ell-k});$$
(2.12a)

$$\frac{\partial \mu_3(k, 0)}{\partial b_\ell} = \gamma_3(b_{\ell-k}^2 + 2b_\ell b_{\ell+k})$$

246

$$\frac{\partial \mu_2(k)}{\partial \gamma_2} = \frac{\mu_2(k)}{\gamma_2}; \qquad \frac{\partial \mu_3(k,k)}{\partial \gamma_3} = \frac{\mu_3(k,k)}{\gamma_3};$$

$$\frac{\partial \mu_3(k,0)}{\partial \gamma_3} = \frac{\mu_3(k,0)}{\gamma_3}.$$

$$(2.12b)$$

The Minimum Variance ARMA Algorithm

As in the MA case, we need to compute $s(x)$ and $\frac{\partial s(x)}{\partial x}$ as functions of the ARMA parameters at each iteration. The paper [7] discusses how to do this for the second- and third-order moments. These quantities are then used in a Gauss-Newton procedure to find the value of x which minimizes (2.10).

3. Numerical Examples

In this section we illustrate the algorithms given in this paper by some examples, and compare the simulation results to analytic results, obtained by the methods described in [7]. All the examples involve MA processess, and the algorithms based on the third-order cumulants. The driving noise $\{u_t\}$ was taken as exponentially distributed, with $\gamma_1 = 0, \gamma_2 = 1, \gamma_3 = -2$. For each test case we performed 100 Monte-Carlo runs, and tested the Giannakis-Mendel (GM) algorithm, the weighted least-squares (WLS) algorithm (see [8] for details), and the minimum-variance (MV) algorithm.

The numerical results for the four test cases are given in Tables 1 through 4. The first test case uses a MA(1) process with zero inside the unit circle. The second uses a MA(2) process, with two complex zeros inside the unit circle. The third test case uses a MA(2) process with two real zeros, one inside the unit circle and one outside it. The fourth test case uses a MA(3) process, with two complex zeros outside the unit circle, and a real zero inside the unit circle.

The following conclusions can be drawn from the numerical results:

(i) The GM algorithm performs very close to what is predicted by the analysis. A similiar conclusion was drawn in [7].

(ii) The MV algorithm performs only slightly worse than what is predicted by the analysis. The reader is reminded that this algorithm uses the estimated matrix $\hat{\Sigma}$ rather than $\Sigma(\theta)$, so the slight degradation in performance is not surprising. In any case, the MV algorithm performs considerably better than the GM algorithm.

(iii) The WLS algorithm does not quite achieve the performance predicted by the analysis. We explain this behavior by the fact that this algorithm is relatively sensitive to the initial estimate obtained from the

Table 1. Results for $b(z) = 1 + 0.6z^{-1}$, $N = 1000$

Alg.	Par.	True Value	Monte-Carlo Mean	Monte-Carlo Std. Dev.	Analytic Standard Deviation
GM	b_1	0.6	0.5993	0.1066	0.1108
WLS	b_1	0.6	0.5913	0.0588	0.0656
MV	b_1	0.6	0.5950	0.0626	0.0646

Table 2. Results for $b(z) = 1 - 1.8z^{-1} + 0.95z^{-2}$, $N = 2000$

Alg.	Par.	True Value	Monte-Carlo Mean	Monte-Carlo Std. Dev.	Analytic Standard Deviation
GM	b_1	-1.80	-1.7853	0.3365	0.3545
	b_2	0.95	0.9418	0.0692	0.0550
WLS	b_1	-1.80	-1.7993	0.1668	0.0540
	b_2	0.95	0.9528	0.0607	0.0539
MV	b_1	-1.80	-1.8094	0.0593	0.0405
	b_2	0.95	0.9540	0.0510	0.0377

GM algorithm (via the matrix $D(\theta_0)$ — see [8]). Even so, the WLS algorithm appears to offer an improvement over the GM algorithm.

4. Conclusions

We presented several algorithms for estimating the parameters of MA and ARMA non-Gaussian processes from sample high-order moments. These algorithms use explicitly the second-order statistics of the sample mo-

Table 3. Results for $b(z) = 1 - 2.05z^{-1} + z^{-2}$, $N = 5000$

Alg.	Par.	True Value	Monte-Carlo Mean	Monte-Carlo Std. Dev.	Analytic Standard Deviation
GM	b_1	-2.05	-2.0418	0.1333	0.1631
	b_2	1.0	0.9938	0.0501	0.0477
WLS	b_1	-2.05	-2.0598	0.0752	0.0874
	b_2	1.0	1.0014	0.0455	0.0477
MV	b_1	-2.05	-2.0555	0.0452	0.0374
	b_2	1.0	1.0004	0.0339	0.0296

Table 4. Results for
$b(z) = 1 + 0.9z^{-1} + 0.385z^{-2} - 0.771z^{-3}$, $N = 1000$

Alg.	Par.	True Value	Monte-Carlo Mean	Monte-Carlo Std. Dev.	Analytic Standard Deviation
GM	b_1	0.900	0.8399	0.2080	0.2498
	b_2	0.385	0.3734	0.1022	0.0853
	b_3	-0.771	-0.7437	0.0930	0.1163
WLS	b_1	0.900	0.8617	0.1212	0.0705
	b_2	0.385	0.3905	0.0967	0.0794
	b_3	-0.771	-0.7573	0.0750	0.0678
MV	b_1	0.900	0.8905	0.0842	0.0529
	b_2	0.385	0.3850	0.0938	0.0591
	b_3	-0.771	-0.7767	0.0781	0.0502

ments (the matrix Σ) which is estimated from the measurements.

The asymptotically minimum variance algorithms were shown, by numerical simulations, to perform close to theoretical predictions. The optimal weighted least-square algorithms did not reach their theoretical performance, but still offered some improvement over simpler algorithms that do not use the Σ matrix.

From computational point of view, most of the load is taken by the computation of the high-order moments and the matrix $\hat{\Sigma}$. This load is approximately proportional to the cube of the model order per data point. Since the computational load for the minimum variance algorithm is similar to the weighted least-squares algorithm, while its statistical acuracy is considerably higher, this algorithm is preferable to the weighted least-squares for most applications. The main disadvantage of the minimum variance algorithm is its more complex implementation (programming), especially the need for iterative optimization procedure.

Interesting topics for future research include: i) developement of recursive/adaptive versions of the algorithms given in this paper; ii) performance analysis of the algorithms based on the fourth-order moments, similar to the one done in [7] for the third-order moments.

References

[1] G. B. Giannakis, "Cumulants: A Powerful Tool in Signal Processing", *IEEE Proceedings*, Vol. 75, No. 9. pp. 1333-1334, September 1987.

[2] M. S. Raghuveer and C. L. Nikias, "Bispectrum Estimation: A Parameter Approach", *IEEE Trans. Acoustics, Speech and Signal Processing*, Vol. ASSP-33, No. 4, pp. 1213-1230, October 1985.

[3] G. B. Giannakis and J. M. Mendel, "Identification of Non-Minimum Phase Systems Using Higher Order Statistics", *IEEE Trans. Acoustics, Speech, and Signal Processing*, Vol. 37, No. 3, pp. 360-377, March, 1989.

[4] G. B. Giannakis, "A Kronecker Product Formulation of the Cumulant Based Realization of Stochastic Systems", *Proc. Automatic Control Conference*, Atlanta, GA, June 1988.

[5] B. Friedlander and B. Porat, "Adaptive IIR Algorithms Based on High-Order Statistics", *IEEE Trans. Acoustics, Speech and Signal Processing*, Vol. 37, No. 4, pp. 485-495, April, 1989.

[6] A. Swami and J. M. Mendel, "Adaptive System Identification Using Cumulants", *Proc. Int'l Conf. Acoustics, Speech and Signal Processing*, New York City, NY, April 1988.

[7] B. Porat and B. Friedlander, "Performance Analysis of Parameter Estimation Algorithms Based on High-Order Moments", *Int. J. Adaptive Control and Signal Processing*, to appear.

[8] B. Friedlander and B. Porat, "Optimal Estimation

of MA and ARMA Parameters of Non-Gaussian Processes from High-Order Moments", *IEEE Trans. Automatic Control*, to appear.

[9] G. B. Giannakis and J. M. Mendel, "ARMA Order Determination via High-Order Statistics", submitted for publication.

[10] K. S. Lii and M. Rosenblatt, "Deconvolution and Estimation of Transfer Function Phase and Coefficients for Non-Gaussian Linear Processes", *Annals of Statistics*, vol. 10, no. 4, pp. 1195-1208, 1982.

Appendix: Estimation of the Covariances of the Sample Moments

In this appendix we derive a procedure for estimating the covariances of the sample moments of stationary and ergodic time series. We first assume that the given process is pure MA, and later extend the procedure to more general processes.

Let $\{y_t\}$ be a MA(q) process, and let $\mu_m(k_1, ..., k_{m-1})$ and $\hat{\mu}_m(k_1, ..., k_{m-1})$ be its statistical and sample moments, defined by (2.3) and (2.4) respectively. We have

$$E\{\hat{\mu}_m(k_1, ..., k_{m-1})\hat{\mu}_n(\ell_1, ..., \ell_{n-1})\}$$

$$= E\left\{\frac{1}{N^2}\sum_{s=1}^{N}\sum_{t=1}^{N} y_s y_t \left(\prod_{i=1}^{m-1} y_{s+k_i}\right)\left(\prod_{j=1}^{n-1} y_{t+\ell_j}\right)\right\}$$

$$= E\left\{\frac{1}{N^2}\sum_{s=1}^{N}\sum_{t=1}^{N} y_0 y_{t-s} \left(\prod_{i=1}^{m-1} y_{k_i}\right)\left(\prod_{j=1}^{n-1} y_{t-s+\ell_j}\right)\right\}$$

$$= \frac{1}{N}\sum_{t=-(N-1)}^{N-1}\left(1 - \frac{|t|}{N}\right)$$

$$E\left\{y_0 y_t \left(\prod_{i=1}^{m-1} y_{k_i}\right)\left(\prod_{j=1}^{n-1} y_{t+\ell_j}\right)\right\} \qquad (a.1)$$

Hence,

$$\text{cov}\{\hat{\mu}_m(k_1, ..., k_{m-1}), \hat{\mu}_n(\ell_1, ..., \ell_{n-1})\}$$

$$= \frac{1}{N}\sum_{t=-(N-1)}^{N-1}\left(1 - \frac{|t|}{N}\right) E\left\{\left[y_0 \left(\prod_{i=1}^{m-1} y_{k_i}\right)\right.\right.$$

$$\left. -\mu_m(k_1, ..., k_{m-1})\right]$$

$$\left.\cdot\left[y_t \left(\prod_{j=1}^{n-1} y_{t+\ell_j}\right) - \mu_n(\ell_1, ..., \ell_{n-1})\right]\right\} \qquad (a.2)$$

Now, since $\{y_t\}$ is a MA(q) process, the product $y_0\left(\prod_{i=1}^{m-1} y_{k_i}\right)$ is statistically independent of the product $y_t\left(\prod_{j=1}^{n-1} y_{t+\ell_j}\right)$ for $t > k_1 + q$, and for $t < -(q + \ell_1)$. Therefore (a.2) can be written as

$$\text{cov}\{\mu_m(k_1, ..., k_{m-1}), \mu_n(\ell_1, ..., \ell_{n-1})\}$$

$$= \frac{1}{N}\sum_{t=-(\ell_1+q)}^{k_1+q}\left(1 - \frac{|t|}{N}\right) E\left\{\left[y_0 \left(\prod_{i=1}^{m-1} y_{k_i}\right)\right.\right.$$

$$\left. -\mu_m(k_1, ..., k_{m-1})\right]$$

$$\left.\cdot\left[y_t \left(\prod_{j=1}^{n-1} y_{t+\ell_j}\right) - \mu_n(\ell_1, ..., \ell_{n-1})\right]\right\} \qquad (a.3)$$

The expression (a.3) is exact, and is, in fact, a generalization of the results in [10]. Using the stationarity and ergodicity properties of the given process, we can consistently estimate the expectation in the right-hand side of (a.3) by

$$E\left\{\left[y_0 \left(\prod_{i=1}^{m-1} y_{k_i}\right) - \mu_m(k_1, ..., k_{m-1})\right]\right.$$

$$\left.\cdot\left[y_t \left(\prod_{j=1}^{n-1} y_{t+\ell_j}\right) - \mu_n(\ell_1, ..., \ell_{n-1})\right]\right\}$$

$$\approx \frac{1}{N}\sum_{s=1}^{N}\left[y_s \left(\prod_{i=1}^{m-1} y_{s+k_i}\right) - \hat{\mu}_m(k_1, ..., k_{m-1})\right]$$

$$\cdot\left[y_{s+t} \left(\prod_{j=1}^{n-1} y_{s+t+\ell_j}\right) - \hat{\mu}_n(\ell_1, ..., \ell_{n-1})\right] . \qquad (a.4)$$

Finally we substitute (a.4) in (a.3) to get the following estimate

$$N \cdot \text{cov}\{\hat{\mu}_m(k_1, ..., k_{m-1}), \hat{\mu}_n(\ell_1, ..., \ell_{n-1})\}$$

$$\approx \frac{1}{N}\sum_{t=-(\ell_1+q)}^{k_1+q}\left(1 - \frac{|t|}{N}\right)\left\{\frac{1}{N}\sum_{s=1}^{N}\left[y_s \left(\prod_{i=1}^{m-1} y_{s+k_i}\right)\right.\right.$$

$$\left. -\hat{\mu}_m(k_1, ..., k_{m-1})\right]$$

$$\left.\cdot\left[y_{s+t} \left(\prod_{j=1}^{n-1} y_{s+t+\ell_j}\right) - \hat{\mu}_n(\ell_1, ..., \ell_{n-1})\right]\right\} . \qquad (a.5)$$

Next we wish to extend the result (a.5) to a broader class of processes. Let us assume that $\{y_t\}$ is the linear process given in (2.1) and that the impulse response $\{h_k\}$ is exponentially stable, *i.e.*

$$|h_k| < A e^{-\alpha|k|} \qquad (a.6)$$

for some $A > 0, \alpha > 0$. In this case, the product $y_0\left(\prod_{i=1}^{m-1} y_{k_i}\right)$ is approximately independent of $y_t\left(\prod_{j=1}^{n-1} y_{t+\ell_j}\right)$ whenever $t > k_1 + q_0$ or $t < -(q_0 + \ell_1)$, and q_0 is large enough. In other words, (a.5) holds as an approximation when q is replaced by q_0. The parameter q_0 represents the "effective MA order" of the process, or the separation beyond which the data are approximately

independent. We propose, therefore, to use (a.5), (a.6) and (a.7) for processes satisfying the above condition (ARMA processes in particular), while replacing q by q_0.

To make (a.5) a consistent estimate, we need to vary q_0 as a function of N. It can be shown that any weakly increasing function is sufficient for this purpose, *i.e.* a function satisfying

$$\lim_{N \to \infty} q_0(N) = \infty \quad ; \lim_{N \to \infty} \frac{q_0(N)}{N} = 0 \qquad (a.7)$$

For example, $q_0 = \log N$ is a reasonable choice.

When the number of data points is fixed, the notion of consistency is meaningless. Rather, one needs a practical procedure for determining the effective MA order q_0 from the measurements. To do this we note that, if the effective order is q_0, then $\hat{\mu}_2(q_0 + 1)$ is approximately normal with zero mean and variance given approximately by

$$\mathrm{var}\{\hat{\mu}_2(q_0 + 1)\} \approx \sum_{t=-(2q_0+1)}^{2q_0+1} \left(1 - \frac{|t|}{N}\right)$$

$$\left\{\frac{1}{N} \sum_{s=1}^{N} [y_s y_{s+q_0+1} - \hat{\mu}_2(q_0 + 1)] \right.$$

$$\left. \cdot [y_{s+t} y_{s+t+q_0+1} - \hat{\mu}_2(q_0 + 1)] \right\} . \qquad (a.8)$$

Therefore we can determine q_0 by the following procedure.

(i) Let $q_0 = 0$.

(ii) Compute $\hat{\mu}_2(q_0 + 1)$ by (2.4) and $\mathrm{var}\{\hat{\mu}_2(q_0+1)\}$ by (a.8).

(iii) Compute $\hat{\tau} = \hat{\mu}_2(q_0+1)/\sqrt{\mathrm{var}\{\hat{\mu}_2(q_0 + 1)\}}$ and compare to a threshold τ_0. The threshold is determined by the required probability of error and the standard normal distribution.

(iv) If $\hat{\tau} < \tau_0$ stop, else increase q_0 by 1 and goto step (ii).

This procedure has to be carried out prior to the computation of cov $\{\hat{\mu}_m(\kappa_1, ..., \kappa_{m-1}), \ \hat{\mu}_n(\ell_1, ..., \ell_{n-1})\}$ via (a.5). Alternatively, methods described in [9] can be used for the same purpose.

So far we have shown how to compute the entries of the matrix $\hat{\Sigma}$. An additional computational step will generally be required, because $\hat{\Sigma}$ is not guaranteed to be positive definite. Indefinite matrices are not allowed in the algorithms described in [8, Section 4], because they would lead to non-positive cost functions. Nevertheless, positive semidefinite matrix $\hat{\Sigma}$ is legitimate and can be accomodated, as explained in [8, Section 4]. Therefore, we propose to compute the final $\hat{\Sigma}$ as the minimum-norm positive semidefinite approximation of the matrix obtained above. This is done by computing the eigenvalue/eigenvector decomposition of $\hat{\Sigma}$, and replacing all negative eigenvalues by zeros. The eigenvector matrix Q and the modified eigenvalue matrix Λ are used by the algorithms described in [8, Section 4] in lieu of the matrix $\hat{\Sigma}$.

250

SIGNAL RECONSTRUCTION OF SONAR AND OPTICAL IMAGES
BY MULTISPECTRAL TECHNIQUES

A. C. Dubey, R. C. Manning, and E. Moritz

Naval Coastal Systems Center, Code 2230
Panama City, Florida

ABSTRACT

A computationally efficient identification procedure for non-Gaussian white noise driven linear, time-invariant, non-minimum phase systems was evaluated for use on sonar and optical images. The procedure which was proposed by Pan and Nikias [1] is based on the idea of computing the complex cepstrum of higher order cumulants of the system output. In particular, the differential cepstrum parameters of the non-minimum phase impulse response are estimated directly from higher order cumulants via a two-dimensional FFT operation. Individual scan lines from sonar images were processed and significant noise suppression was observed. The usefulness of the procedure as a method for the enhancement of sonar and optically acquired images was verified.

INTRODUCTION

In many Navy applications, one is faced with the need to perform detection and classification operations on data presented in image format. Examples of applications abound in beamformed sonar displays and passive and active optically acquired images. Typically these images contain a considerable amount of noise. For sonars, these noise sources may be environmental sea state noise, impulsive biologically generated noise sources (such as snapping shrimp), and boundary reverberations in the form of bottom or surface backscattering. In optical systems, one may be faced with the problem of glint, turbidity, and other interference sources. In order to perform the detection and classification tasks accurately, one desires to work with the best possible images. To this end, we are exploring alternative signal processing approaches to aid in image enhancement. Based on the progress of theoretical and algorithmic developments in the field of higher order spectral signal processing, it became apparent that investigation of higher order spectral signal processing on real images of interest was warranted.

In this paper, we report on the application of bispectrum/bicepstrum techniques to representative components of sonar generated imagery. This data is representative of a variety of image data including optically generated data. The approach taken in this paper is to work with individual scan lines of image data, as opposed to entire images. This makes the problem computationally simpler by transforming the 2-D filtering problem into a 1-D filtering problem. While this approach is not the ultimately desired complete 2-D formulation and test of the higher order spectral techniques, results of the work demonstrate the merit of using the higher order spectral techniques for signal enhancement.

BACKGROUND AND THEORY

In most cases (moderate depth) the noise in sonar is of a random nature and is Gaussian distributed over short time periods [3]. Phase relationships due to transient signals or signals generated by quadratic nonlinear mechanisms are described by their bispectrum [4]. Gaussian noise does not contribute to the bispectrum because the bispectrum is sensitive not just to the magnitude but also to the phase relationships of the frequency components of the signal. Thus, if a transient or non-Gaussian signal is present in a Gaussian noise environment, it is possible to suppress the noise and improve the signal to noise ratio via bispectrum approach. The method has been used in astronomy and in other areas [5, 6, 7].

The problem we are faced with is to develop a means for enhancing images that are contaminated with noise. To cast the problem into higher order spectral representation, images are translated into a collection of one dimensional signals (horizontal scan lines). The translation rule transforms the intensity of a given pixel such that it is regarded as an output sequence $\{X(k)\}$ of an Auto Regressive Moving Average (ARMA) process. This allows the use of multispectral techniques developed by Nikias et al[1, 2]. The objective now becomes the reconstruction of the phase and magnitude response for an output data sequence $\{X(k)\}$.

It is assumed that the output sequence $\{X(k)\}$, $K = 1, 2, ..., L$ is formed by the linear superposition of a zero-mean Gaussian, white noise process $\{W_G(k)\}$, and an ARMA process described by

$$X(k) - W_G(k) = -\sum_{i=1}^{L_1} d_i X(k-i) + \sum_{i=-L_1}^{L_2} u_i W_{NG}(k+i),$$

where $\{W_{NG}(k)\}$ is a zero-mean non-Gaussian, white noise process.

An estimate of the third order moment sequence $\hat{R}_x(m, n)$ is made by segmenting X(k) into N_L records of M samples such that

$$Y_j^{(i)} = x(j + (i - 1)M)$$

$$i = 1, 2, ..., N_L. \qquad j = 1, 2, ..., M.$$

The third order moment for each segment is generated by

$$r_x^{(i)}(m, n) = \frac{1}{M} \sum_{j=S_1}^{S_2} Y_j^{(i)} Y_{j+m}^{(i)} Y_{j+n}^{(i)} \qquad i = 1, 2, ..., N_L$$

$$S_1 = \max \{1, -m, -n\}, \qquad S_2 = \min \{M, M - m, M - n\}.$$

The estimate $\hat{R}(m, n)$ of the third order moment sequence for the input data {X(k)} is calculated by averaging over all the segments as follows:

$$\hat{R}(m, n) = \frac{1}{N_L} \sum_{i=1}^{N_L} r_x^{(i)}(m, n)$$

The cepstrum coefficients {$A^{(k)}$} and {$B^{(k)}$} are computed using the FFT method of reference 1.

Using the following recursion equations, the minimum phase $\hat{i}(n)$ and maximum phase $\hat{o}(n)$ impulse responses are calculated:

$$\hat{i}(n) = -\frac{1}{n} \sum_{k=2}^{n+1} i_d(k) \hat{i}(n - k + 1) \qquad n = 1, 2, 3, ...,$$

$$\hat{o}(n) = -\frac{1}{n} \sum_{k=n+1}^{0} o_d(k) \hat{o}(n - k + 1) \quad n = -1, -2, -3, ...,$$

$$and \quad \hat{i}(0) = \hat{o}(0) = 1$$

An FFT is performed to obtain the corresponding frequency responses.

$$\hat{I}(\omega) = \sum_{n=0}^{N_1} \hat{i}(n) e^{-j\omega n}$$

and

$$\hat{O}(\omega) = \sum_{n=-N_2}^{0} \hat{o}(n) e^{-j\omega n}$$

The overall system frequency response is defined by

$$\hat{H}(\omega) = \hat{I}(\omega) \cdot \hat{O}(\omega).$$

The recursion equation for $\hat{i}(n)$ is terminated at n = N_1 where $|\hat{i}(n)| < \gamma$ (very small) for all n = N_1. Recursion equation for $\hat{o}(n)$ is terminated at n = -N_2 where $|\hat{o}(n)| < \gamma$ for n < -N_2.

The recursion equation for $\hat{i}(n)$ is terminated at n = N_1 where $|\hat{i}(n)| < \gamma$ (very small) for all n = N_1. Recursion equation for $\hat{o}(n)$ is terminated at n = -N_2 where $|\hat{o}(n)| < \gamma$ for n < -N_2.

APPLICATION TO SONAR

Figures 1(a) through 1(d) are for a data sequence with noise only and figures 2(a) through 2(d) are for a data sequence with signal plus noise. In figure 2(a), the presence of the signal is apparent due to the occurrence of a shadow zone.

Figures 1(b) and 1(c) show the minimum and maximum phase impulse responses for the sequence with noise only. Figures 2(b) and 2(c) are the corresponding minimum and maximum phase impulse responses for the sequence which contains signal plus noise. Though there is no easily discernible difference between figures 1(b) and 2(b), there is a noticeable difference between figures 1(c) and 2(c). This is expected if the noise is Gaussian and the signal is the result of ARMA process described above.

When we compare figures 1(d) with 2(d) we notice a significant difference between the two. These two figures are the reconstructed non-minimum phase impulse responses for the sequences 1(a) and 2(a), i.e., noise vs. signal. The non-minimum phase impulse response of the signal is clearly evident.

CONCLUSIONS

For backscattered data acquired in real sonar environments, with a characteristic low signal to noise ratio (SNR), the process of computing the complex cepstrum of higher cumulants of the system output is an efficient approach for:

(1) Suppressing the ambient noise contamination of the sonar data.

(2) Estimating the non-minimum phase impulse response of the backscattering medium.

(3) Verifying the Gaussian and non-Gaussian characteristics of the individual components within the sonar data.

The results from this study suggest that the bispectrum/bicepstrum approach may be useful for enhancing the detection and classification capability of active sonar and optical imaging systems.

ACKNOWLEDGEMENTS

REFERENCES

[1] R. Pan and C. L. Nikias, "The Complex Cepstrum of Higher Order Cumulants and Nonminimum Phase System Identification," IEEE Trans. Acoust. Speech, Signal Processing, ASSP-36, pp 186-205 (1988).
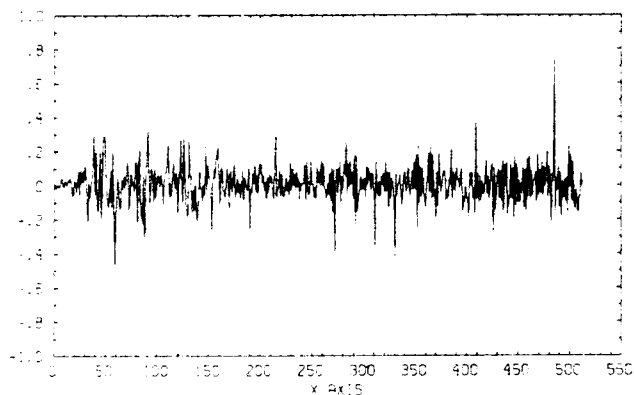
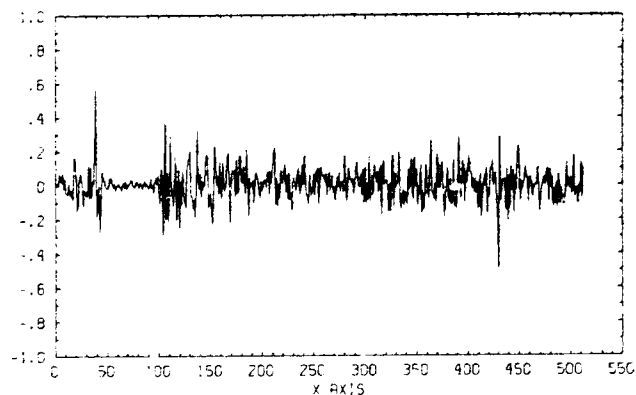Figure 1(a). The figure shows the data with noise only.

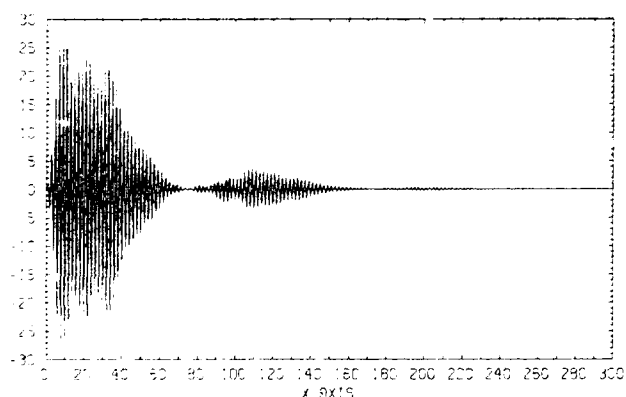Figure 2(a). Data with signal pulse noise.

Figure 1(b). Minimum phase impulse response
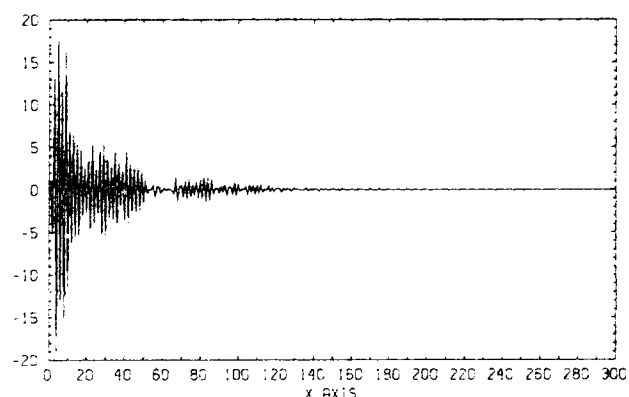$\hat{i}(n)$ of input sequence in Figure 1(a).

Figure 2(b). Minimum phase impulse response
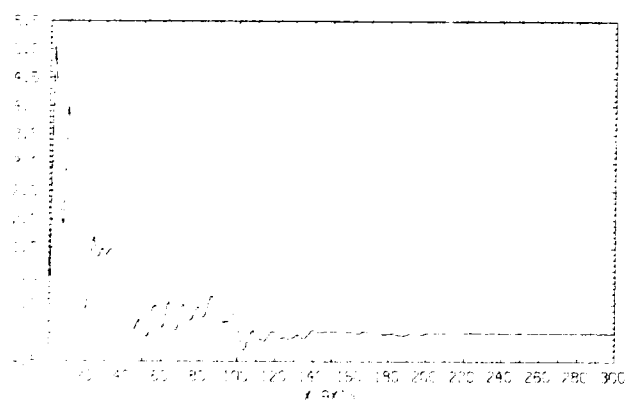$\hat{i}(n)$ of input sequence in Figure 2(a).

Figure 1(c). Maximum phase impulse response
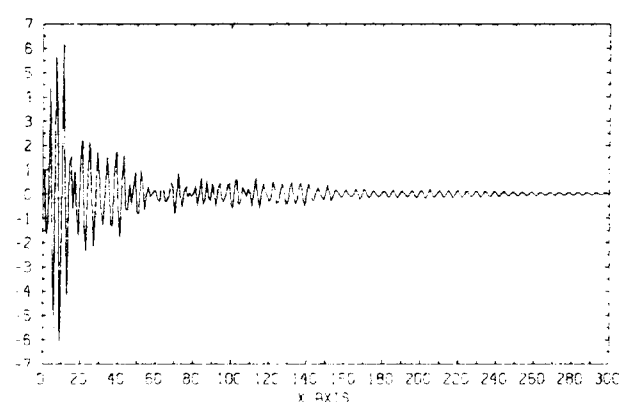$\hat{o}(n)$ of input sequence in Figure 1(a).

Figure 2(c). Maximum phase impulse response
$\hat{o}(n)$ of input sequence in Figure 2(a).

[2] C. L. Nikias and M. R. Raghuveer, "Bispectrum Estimation: A Digital Signal Processing Framework," Proc. IEEE, vol. 75, pp. 869-891, July 1987.

[3] R. J. Urick, "Principles of Underwater Sound," McGraw-Hill, 1975.

[4] Gary R. Wilson, ARL, The University of Texas at Austin, personal communication.

[5] A. W. Lohmann and B. Wirnitzer, "Triple Correlations," Proc. IEEE, vol. 72, pp. 889-901, July 1984.

[6] H. Bartelt, et al, "Phase and Amplitude Recovery from Bispectra," Applied Optics, vol. 23, no. 18, pp. 3121-3129, 15 Sep 1984.

[7] M. J. Hinich, et al, "Bispectrum of Ship Radited Noise," Jour. Acous. Soc. Am., vol. 85, no. 4, pp. 1512-1517, March 1989.
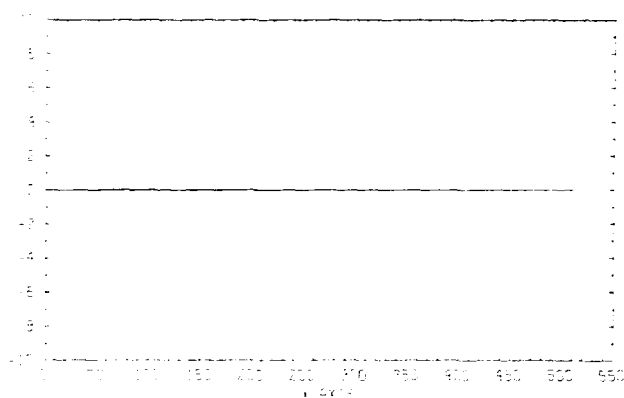
Figure 1(d).   Reconstructed impulse response (via complex cepstrum technique) of input sequence in Figure 1(a).
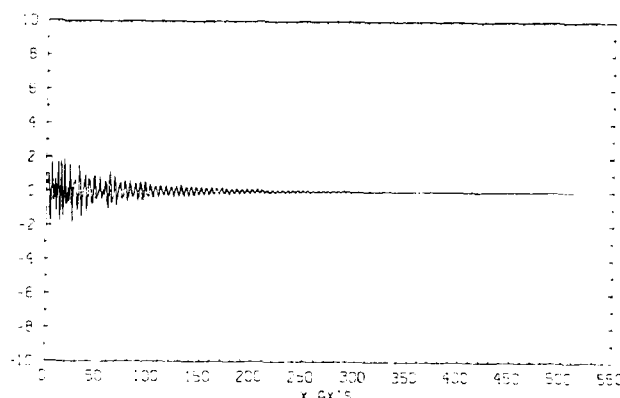

Figure 2(d).   Reconstructed impulse response (via complex cepstrum technique) of input sequence in Figure 2(a).